Aircraft Measurement of Chemical Processing and Export Fluxes of Pollutants over the United Kingdom

Debbie Polson

Doctor of Philosophy

The University of Edinburgh

2008

Acknowledgements

I would like to thank my supervisors from the Centre for Ecology and Hydrology, Edinburgh, Prof. David Fowler and Dr. Eiko Nemitz, who have both been extremely helpful and generous with their time and advice. Also my supervisors from the University of Edinburgh, Dr. John Moncrieff and Dr. Keith Weston for guiding me through some of the hardest parts of my Ph.D. There are many people from the Centre for Ecology and Hydrology, Edinburgh who have helped me in my work. I'd particularly like to thank all those involved in the AMPEP, Alan McDonald, Dr. Daniela Famulari, Dr. Chiara Di Marco, Dr. Ute Skiba and Dr. Ivan Simmons whose efforts during the flight campaign were essential to the success of the project. I'd also like to thank Dr. Ulli Dragosits and Dr. Ute Skiba for providing me with the emissions data crucial for all the modelling work and Jennifer Muller for her help with the oxidation work. The Atmospheric Dispersion group from the Met Office were incredibly welcoming during my short stays down in Exeter and I'm extremely grateful for all their advice and help in running the NAME model. Dr. Alistair Manning, Helen Webster and Mark Hamilton provided me with much needed ongoing help and support and I truly appreciate their time and guidance. The teams from the University of East Anglia, the University of Manchester and FAAM have been wonderful to work with and I'd especially like to thank Dr. Debbie O'Sullivan for the Halocarbon data, Dr. Dave Stewart for the NO_{xy} data and Jonny Crosier for the AMS data. Finally thanks to my friends and family who have all been incredibly supportive throughout my studies, and in particular thanks to Jude for putting up with me during it all.

Abstract

The current scientific and political attention to issues of climate change make scrutiny of country scale emissions and trends with time a very high priority. The United Kingdom is a signatory to the Kyoto protocol and has committed to a 13% reduction of six key Greenhouse gases from 1990 levels by the year 2010 and is required to report annual emissions of these gases. Furthermore the United Kingdom Government announced in November 2007 plans to introduce a bill committing the UK to a 60 % reduction target by the year 2050. The methodology for calculating national emissions is set by the Intergovernmental Panel on Climate Change (IPCC) and uses statistical activity data and emissions factors in a 'bottom up' approach. Annual UK emissions of N_2O, CO_2, CH_4 and the anthropogenic emissions marker CO are currently provided by the National Atmospheric Emissions Inventory (NAEI) (Baggott, 2004) using this 'bottom up' approach which involves summing the contribution for sources across the UK using source numbers, activity data and emission factors. This approach relies on assumptions that sources within the same sector have the same emissions factor and requires sufficient knowledge of source numbers and activity data. The NAEI also produce mapped emissions at 1 km resolution for the UK for the total emissions and for each source sector.

In this study an alternative 'top-down' approach was used to provide direct measurement of the net UK flux of greenhouse gas emissions at the UK scale, using aircraft sampling of the entire plume of GHG emissions downwind of the UK. An atmospheric mass budget over the country was established for each experimental flight and a direct calculation of the UK budget made from concentration measurements upwind and downwind of the UK (Gallagher, 1994; Fowler, 1998; Chou, 2002). Using atmospheric transport models (ATM), the spatially disaggregated emissions of the NAEI were validated by comparing the measured outflow concentrations to the predicted outflow of the models. The model outflow for each source sector could be used to derive the annual UK emissions using an iteration technique to alter total emissions from each sector such that the modelled outflow concentrations became consistent with the measured outflow concentrations. Using an inverse modelling approach, the spatially disaggregated emissions could also be

derived from the measured concentrations and could be used to further validate the NAEI total and mapped emissions. Measurement of Halocarbon species allowed mapped inventories to be produced for these species using the same inverse modelling approach. Sulphur and Nitrogen compounds were measured in both the gas and particle phase and the oxidation rates of SO_2 and NO_x calculated for urban and industrial plumes.

The measurements reveal annual UK emissions of CO of 2400 kT yr^{-1} and CO_2 of 514 MT yr^{-1}, within 10% of the NAEI emissions of 2400 kT yr^{-1} for CO and 555 MT yr^{-1} for CO_2. However, estimates of N_2O (330 kT yr^{-1}) and CH_4 (3300 kT yr^{-1}) emissions are significantly larger than inventory estimates of 130 kT yr^{-1} and 2400 kT yr^{-1} respectively. This suggests that there are potentially important sources of N_2O and CH_4 not currently included in the inventory, that the strength of some sources is underestimated or a combination of the two. The inverse modelling approach further validated the NAEI CO and CO_2 emissions while providing further evidence that the NAEI emissions underestimate the UK emissions for N_2O and CH_4. The mapped Halocarbon emissions produced source locations consistent with localised industrial sources. The oxidation analysis showed oxidation rates tend to be consistent for individual plumes between flights with greater variation between different plumes reflecting the differing nature of the plume sources. The average oxidation rate for NO_x for a power station plume is 1.4 ± 0.66 % N hr^{-1} compared to 4.4 ± 3.95 % N hr^{-1} for an urban plume and the average oxidation rate for SO_2 for a power station plume is 4.8 ± 0.76 % S hr^{-1} compared to 6.5 ± 5.71 % S hr^{-1} for an urban plume. The average oxidation rate for the whole UK was estimated as 3.2 ± 2.38 % N hr^{-1} for NO_x and 5.3 ± 1.80 S % hr^{-1} for SO_2.

Uncertainties in the method of measurement are small relative to the magnitude of the differences between the inventory and measurements for individual flights, but extrapolation from the 14 flights to provide annual budgets is an important source of uncertainty for N_2O emissions, which show considerable temporal variability in emissions. These new data provide a viable approach to estimate annual country scale UK emissions to test the quality of the existing inventory and to verify the progress of the emission reductions with time.

Contents

Abstract i

Chapter 1 Background and Theory 13

1.1 Introduction 13

1.2 Description of the Pollutants and Greenhouse Gases 17

1.2.1 Carbon Monoxide 17

1.2.2 Carbon Dioxide 18

1.2.3 Methane 19

1.2.4 Nitrous Oxide 20

1.2.5 Halocarbons 21

1.2.6 Sulphur and Nitrogen Compounds 22

1.3 Emissions Estimates 23

1.3.1 Bottom-Up Estimates 23

1.3.2 Top-Down Validation of Emissions Inventory 25

1.4 Boundary Layer Budget Approach to Estimate Pollutant Emissions 28

1.5 The Atmospheric Boundary Layer 30

1.6 Ideal Meteorology for UK Boundary Layer Budget Study 34

1.7 Review of Previous Boundary Layer Budget Studies 35

1.7.1 Measurements of Methane Fluxes from UK Wetlands 35

1.7.2 Measurement of Regional Methane Fluxes from Agriculture 39

1.7.3 Inverse Modelling to Derive Methane Emissions from Agriculture 42

1.7.4 Measurement of Methane Fluxes from Northern Britain 43

1.7.5 Calculating of Net UK Fluxes for CO_2, CO, CH_4 and N_2O 44

1.7.6 Trace Gases Regional Scale Fluxes Using Bayesian Inverse Analysis 50

1.7.7 Regional CO_2 Budget – CarboEurope Experiment Strategy 52

1.8 Objectives of this Work 54

1.8.1 Motivation for the Aircraft Measurements of Chemical Processing and Export Fluxes of Pollutants Over the UK Project (AMPEP) 54

1.9 Overview of the AMPEP Project 55

1.9.1 AMPEP Objectives 55

1.9.2 AMPEP Methodology 56

1.9.3 Thesis Objectives 62
1.10 Conclusions 63
Chapter 2 Models 65
2.1 Requirements of Models 65
2.2 FRAME - Fine Resolution Atmospheric Multi-Pollutant Exchange 67
2.3 NAME - Numerical Atmospheric Modelling Environment 69
2.4 Analysis of Previous Flight Data with FRAME and NAME 74
2.4.1 Model Setup 74
2.4.2 Results for Previous Round Britain Flight on 28th January 1997 75
2.4.3 Results for Previous Round Britain Flight on 22nd May 1998 77
2.4.4 Results for Previous Round Britain Flight on 7th July 1998 79
2.4.5 Conclusion 81
2.5 Inclusion of Biogenic CO_2 Signal in NAME 81
2.5.1 Photosynthesis 82
2.5.2 Respiration 86
2.5.3 Implementation of Biogenic CO_2 Flux in NAME 88
2.5.4 Results of Biogenic CO_2 Flux in NAME 88
2.5.5 Conclusion 90
2.6 Summary 91
Chapter 3 Review of Flights 93
3.1 Description of each Flight 96
3.1.1 Flight B92 96
3.1.2 Flight B97 99
3.1.3 Flight B102 102
3.1.4 Flight B111 104
3.1.5 Flight B112 107
3.1.6 Flight B113 109
3.1.7 Flight B118 112
3.1.8 Flight B119 114
3.1.9 Flight B126 116
3.1.10 Flight B130 119
3.1.11 Flight B132 122

3.1.12 Flight B134 124
3.1.13 Flight B136 127
3.1.14 Flight B244 129
3.2 Summary of Campaign and Data 132
Chapter 4 NAME Analysis of Flights 135
4.1 Introduction 135
4.2 Results of NAME Simulations of Individual Flights 136
4.2.1 Flight B92 09/05/05 136
4.2.2 Flight B97 25/05/05 139
4.2.3 Flight B102 14/06/05 141
4.2.4 Flight B111 14/07/05 144
4.2.5 Flight B112 19/07/05 147
4.2.6 Flight B113 20/07/05 150
4.2.7 Flight B118 03/08/05 152
4.2.8 Flight B119 04/08/05 155
4.2.9 Flight B126 07/09/05 157
4.2.10 Flight B130 19/09/05 159
4.2.11 Flight B132 21/09/05 161
4.2.12 Flight B134 26/09/05 164
4.2.13 Flight B136 29/09/05 166
4.2.14 Flight B244 19/09/06 169
4.3 Conclusion 172
Chapter 5 Deriving UK Budgets from 'Round-Britain' Observations 174
5.1 Box Model Method 174
5.2 NAME Iteration Technique 178
5.3 Estimating Uncertainty in F_{emit} 184
5.3.1 Uncertainty in Box Model Budget 184
5.3.2 Uncertainty in Model Iteration Technique 185
5.4 Bayesian Calibration 186
5.5 Results of Budget Analysis 191
5.5.1 UK Emission Estimates 191
5.5.2 Sector Analysis 195

5.6 Discussion and Conclusion 200
Chapter 6 Inversion 202
6.1 Introduction 202
6.2 Theory 202
6.3 Back Runs 204
6.4 Fitting Procedure 205
6.5 Assessment of Model Parameters 206
6.5.1 Noise Factor 206
6.5.2 Limiting Grid Boxes 207
6.5.3 Fitting Function 208
6.6 Results for Each Flight 210
6.6.1 CO 214
6.6.2 CO_2 218
6.6.3 CH_4 224
6.6.4 N_2O 231
6.6.5 Halocarbons 238
6.7 Uncertainties 241
6.8 Discussion & Conclusion 242
Chapter 7 Oxidation Rates of Urban and Power Station Plumes 245
7.1 Introduction 245
7.2 Methods 249
7.3 Results 256
7.3.1 Oxidation Rates for Flight B92 256
7.3.2 Oxidation Rates for Flight B97 257
7.3.3 Oxidation Rates for Flight B102 258
7.3.4 Oxidation Rates for Flight B111 259
7.3.5 Oxidation Rates for Flight B113 261
7.3.6 Oxidation Rates for Flight B118 262
7.3.7 Oxidation Rates for Flight B126 264
7.3.8 Oxidation Rates for Flight B130 265
7.3.9 Oxidation Rates for Flight B132 266
7.3.10 Oxidation Rates for Flight B136 268

7.4 Summary and Conclusion 269
Chapter 8 Discussion and Recommendations 275
8.1 Overview 275
8.1.1 Boundary Layer Budget 277
8.1.2 Inverse Modelling 283
8.1.3 Oxidation 286
8.2 Future Work 288
Appendix 1 290
Appendix 2 298
Appendix 3 306
Appendix 4 310
Appendix 5 315
Appendix 6 330
References 336

List of Symbols

Roman Alphabet

A	activity data of a source sector used to compile emission inventories	
A_{ds}	scaling constant to convert from MJ m^{-2} day^{-1} to J m^{-2} s^{-1}	
A_{Sin}	area of the inflow surface	(m^2)
A_{Sout}	area of the outflow surface	(m^2)
a_R	empirically derived constants for calculating radiation	
b	empirical parameter for calculating radiation	
b_R	empirically derived constants for calculating radiation	
$\boldsymbol{c}$	vector of measured air concentrations for inversion	(g m^{-3})
$\boldsymbol{C}$	influence matrix giving fraction of air from each grid box to arrive at observation	(m^{-3} s)
C	concentration of pollutant	(g m^{-3})
C_{bg}	background concentration	(g m^{-3})
C_{m}	concentration of sample m	(g m^{-3})
$C(\underline{x},t)$	concentration at location $\underline{x}$ at time t	(g m^{-3})
$C(\underline{x}_r,t_r)$	receptor concentration for receptor sites x_r at time t_r	(g m^{-3})
$C(z)$	concentration of pollutant at height z in boundary layer	(g m^{-3})
$\boldsymbol{C}_{io}$	NAME model concentration at grid box i for observation o for reverse transport of air	(g m^{-3})
C_{mod}	modelled concentration	(g m^{-3})
C_o	universal constant	
C_{obs}	observed concentration	(g m^{-3})
$C_{s,t}$	concentration resulting from each source s for each time t	(g m^{-3})
C_{mn}	modelled concentration for sample m for sector n	(g m^{-3})
d	data	
$\boldsymbol{D}_{io}$	dosage at the grid box i for observation o	(g m^{-3}s)
D_t	day length	(hours)
e	emission factor of a particular source sector to compile emission inventories	(g m^{-2} s^{-1} $source^{-1}$)

$\boldsymbol{E}$	model NAME emissions from inversion	($g\ s^{-1}$)
$f(\underline{x}_r, t_r \mid \underline{x}, t)$	footprint function for the receptor sites x_r at time t_r linking to the upwind source locations x at time t	
F_{antht}	anthropogenic flux of CO_2	($g\ m^{-2}\ s^{-1}$)
F_{dc}	rate of change due to chemical conversion	($g\ s^{-1}$)
F_{dep}	deposition flux in boundary layer budget	($g\ s^{-1}$)
F_{eco}	net ecosystem flux of CO_2	($\mu mol\ m^{-2}\ s^{-1}$)
F_{emit}	emitted flux in boundary layer budget	($g\ s^{-1}$)
F_{ent}	entrainment flux in boundary layer budget	($g\ s^{-1}$)
F_{in}	import flux in boundary layer budget	($g\ s^{-1}$)
F_n	original total emissions for sector n	($g\ s^{-1}$)
F^*_n	altered total emissions for sector n	($g\ s^{-1}$)
F_{out}	export flux in boundary layer budget	($g\ s^{-1}$)
F_{photo}	photosynthesis flux of CO_2	($\mu mol\ m^{-2}\ s^{-1}$)
F_{resp},	respiration flux of CO_2	($\mu mol\ m^{-2}\ s^{-1}$)
F_s	emission factor from source s	
F_∞	flux at saturating photosynthetic photo flux density	($\mu mol\ m^{-2}\ s^{-1}$)
H	local sensible heat flux	($W\ m^{-2}$)
H_s	surface heat flux	($W\ m^{-2}$)
j	eastwards, northwards or vertical direction	(m)
i_d	day of year	
$I(\underline{x}_r, t_r \mid \underline{x}, t)$	influence function which links the downwind concentrations at the receptor sites x_r at time t_r to the upwind source locations x at time t	
I_E	estimated radiation	($MJ\ m^{-2}$)
I_P	potential radiation	($MJ\ m^{-2}$)
k	von Karman's constant	
K_z	vertical diffusivity	($m^2\ s^{-1}$)
$K(z)$	eddy diffusivity	($m^2\ s^{-1}$)
ℓ	distance between the coast and inland experiment sites	(m)
L	Monin-Obukhov length	(m)
m	measured sample	
n	source sector	

N	number of observations	
$N(x,\sigma_x)$	distribution of variable x with standard deviation σ_x and mean value μ_x	
o_t	observation at Mace Head	(g m^{-3})
$P(\theta/d)$	probability of model parameter θ given data d	
$P(\theta)$	probability density function of model parameter θ	
$P(d/\theta)$	likelihood function of data d given model parameter θ	
$p(\underline{x},t\|\underline{x}_0,t_0)$	probability density function with respect to x and t	
$P_{s,t}$	concentration from each source s for each time t	(g m^{-3})
P_t	sum of the concentration from all sources for each time t	(g m^{-3})
Q	photosynthetic photo flux density	(μmol $s^{-2}m^{-2}$)
Q_E	upward latent heat flux out of top	(W m^{-2})
Q_G	molecular heat flux into the ground	(W m^{-2})
Q_H	upward sensible heat flux out of top	(W m^{-2})
Q_s	net upward radiation flux at the surface	(W m^{-2})
$-\Delta Q_s$	storage of internal energy	(W m^{-2})
$r(z)$	(molar) mixing ratio at height z	
R	dark respiration	(μmol m^{-2} s^{-1})
$R(T)$	temperature dependent respiration	(μmol m^{-2} s^{-1})
R_{NOx}	the oxidation rate of NO_x	(% N $hour^{-1}$)
R_{SO2}	the oxidation rate of SO_2	(% S $hour^{-1}$)
r_t	random Gaussian variable of zero mean and variance of 1	
s	emission source	
$S(\underline{x}_0,t_0)$	source strength at location $\underline{x}_0$ at time t_0	(g m^{-3} s^{-1})
S_c	body source term for processes not already included in flux calculation such as chemical reactions	(g m^{-3} s^{-1})
S_{CH4}	CH_4 source term	(g m^{-3} s^{-1})
S_t	hours since sunrise	(hours)
S_{out}	outflow surface	
t	time	(s)
t_r	duration of the release in backwards NAME model runs	(s)
Δt	model timestep	(s)
T	temperature	(°C)

$T_{R=0}$	temperature at which respiration totally stops	(°C)
T_f	wind fields	(hours)
tt	transmissivity	
tt_{clear}	clear sky transmissivity	
tt_{doy}	transmissivity of day	
T_{max}	daily air max temperature	(°C)
T_{min}	daily air min temperature	(°C)
T_{nc}	empirical parameter for calculating radiation	
$u(x_t)$	wind velocity vector	(m s^{-1})
$u'(x_t)$	turbulent velocity vector	(m s^{-2})
$u'_t(x_t)$	velocity vector for low frequency horizontal meandering	(m s^{-2})
$u(z)$	wind speed at height z	(m s^{-1})
u_*	friction velocity	(m s^{-1})
u_d	deposition velocity	(m s^{-1})
u_e	vertical component of air motion through top of the boundary layer	(m s^{-1})
U_j	component of wind speed in direction j	(m s^{-1})
u_{x0} and u_{xi}	wind speeds at x_0 and x_i	(m s^{-1})
W_t	weight factor	
$\underline{x}$	position vector	
x_j	distance in direction j	(m)
$\underline{x}_r$	receptor location	
z	height	(m)
z_A	height of the boundary layer	(m)
z_B	height surface layer	(m)
z_{BL}	boundary layer height averaged across the outflow region	(m)
z_{max}	maximum height of the aircraft	(m)

Greek Alphabet

α	apparent quantum yield	
ε	dissipation rate of TKE	(m^2 s^{-3})

γ	ratio of the molecular weight of CH_4 to the apparent molecular weight of dry air	
$\phi_M(\xi)$	dimensionless shear stability correction function	
ϕ_{lat}	latitude	(°)
ϕ_{dec}	declination	(°)
λ	set of parameters that surface flux is dependent on	
μ_x	mean value of variable x	
μ_{new}	new mean value of variable x	
θ	model parameter to be fitted using Bayesian Calibration technique	
θ_o	mean temperature in the layer of air	(K)
$\rho(z)$ I	density of dry air at height z	(g m^{-3})
σ_{bg}	uncertainty in measured background concentration	(g m^{-3})
σ_{BL}	uncertainty in the boundary layer height	(m)
$\sigma_{m,}$	measurement uncertainty	(g m^{-3})
σ_{map}	standard deviation in inversion maps of 10 models runs for each domain size	(g s^{-1})
σ_{para}	standard deviation of the average inversion maps for each set of parameters	(g s^{-1})
σ_u^2	vertical turbulence velocity variances	(m^2 s^{-2})
σ_ω^2	vertical turbulence velocity variances	(m^2 s^{-2})
$\sigma_{v,l}^2$	horizontal velocity variance for low frequency fluctuations	(m^2 s^{-2})
σ_x	standard deviation of variable x	
τ	time between the upwind and downwind measurements	(s)
τ_ω	vertical Lagrangian timescale	(s)
τ_u	horizontal Lagrangian timescales	(s)
ν_c	molecular diffusivity of pollutant	(m^2 s^{-1})
ω_*	convective velocity	(m s^{-1})
Ω_s	ensemble of all source locations	

Chapter 1 Background and Theory

1.1 Introduction

In the past two centuries industrialisation and population growth has led to a dramatic increase in anthropogenic emissions of air pollutants. The burning of fossil fuels, fertilisation of agricultural land, population increases of domestic animals, biomass burning and deforestation as well as numerous other sources are having a significant impact on the environment and the climate system. These effects include global increases in air and sea temperature resulting in melting of glaciers and arctic sea ice leading to rising sea level. Evaporation and precipitation are expected to increase globally with increases and decreases seen at regional scales leading to increases in incidents of flooding and drought. Overall extreme weather events are expected to become more common (Berger, 2002).

Radiatively active gases absorb the infrared radiation emitted by the Earth's surface and atmosphere. This trapping of radiation by the atmosphere is the greenhouse effect and as the concentration of these gases increase, so the trapping increases. As the greenhouse effect intensifies, the global temperature must increase in order to maintain the equilibrium at the top of the atmosphere. This leads to feedback effects and warming at the surface (Berger, 2002). The major radiatively active trace gases that have increased due to anthropogenic activity are carbon dioxide (CO_2), methane (CH_4) and nitrous oxide (N_2O) (IPCC, 2001). Figure 1 shows the components to climate forcing (IPCC, 2007).

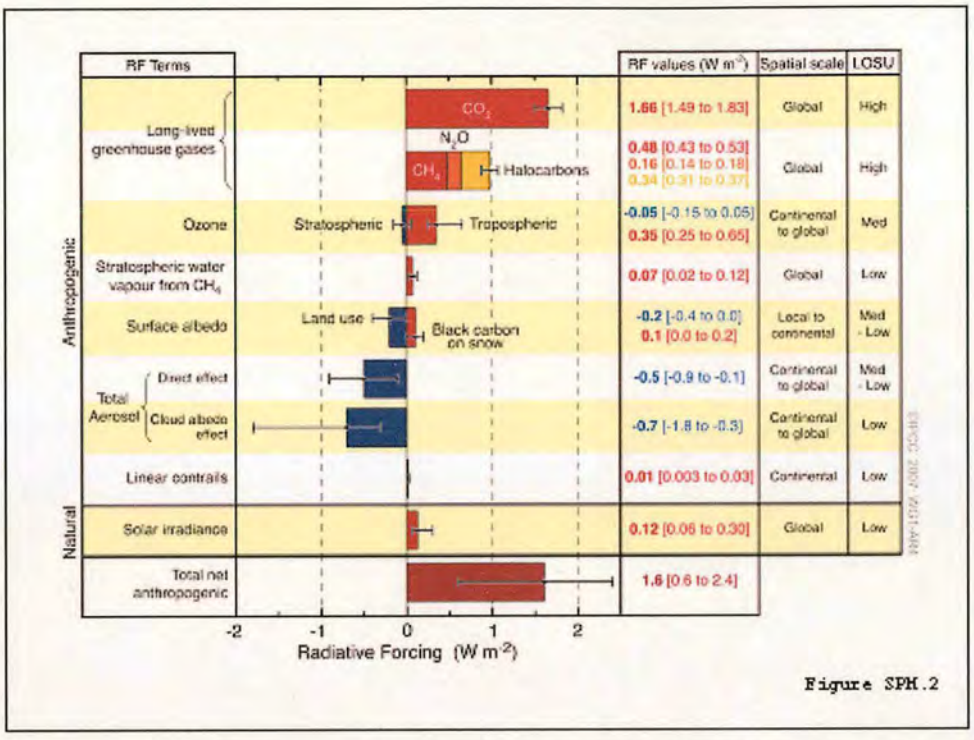

Figure 1. Global average radiative forcing (RF) estimates and ranges in 2005 for anthropogenic carbon dioxide (CO_2), methane (CH_4), nitrous oxide (N_2O) and other important agents and mechanisms, together with the typical geographical extent (spatial scale) of the forcing and the assessed level of scientific understanding (LOSU). The net anthropogenic radiative forcing and its range are also shown. (IPCC, 2007).

Other chemical species emitted by anthropogenic sources such as carbon monoxide also have an indirect effect on the climate through reactions with other trace gases. CO is the major sink for the hydroxyl radical (OH) which would otherwise react with CH_4 and O_3 resulting in a decrease in concentration of both species. Emissions of CO can therefore have an indirect radiative forcing effect (Crutzen, 2002). Other effects of anthropogenic pollution, such as sulphur and nitrogen oxides, include acidification and eutrophication of ecosystems and the formation of tropospheric ozone. Ozone is harmful to vegetation and human health and is the fourth most important greenhouse gas. Aerosols formed from these species have a negative radiative forcing effect by absorbing incoming solar radiation and increasing the cloud albedo (Moller, 2002).

In an attempt to stabilise greenhouse gas concentrations, many developed countries have agreed to reduce emissions of key greenhouse gas species and have signed up to the United Nations Framework Convention on Climate Change (UNFCCC). As part of this agreement the United Kingdom has committed to reducing emissions of six

key greenhouse gas species including CO_2, CH_4 and N_2O by 13% from 1990 levels by the year 2010 (Baggott, 2004). Furthermore, the UK is required to report annual emissions of these species and regularly update and submit emission inventories to the United Nations Commission for Europe (UN/ECE).

The major greenhouse gas is CO_2 which has increased from pre-industrial concentrations of 280 ppm to 379 ppm in 2005. CH_4 and N_2O have also increased significantly from pre-industrial levels with an increase from 715 ppb to 1774 ppb in 2005 for CH_4 and from 270 ppb to 319 ppb in 2005 for N_2O (IPCC, 2007). The largest anthropogenic sources of CO_2 are fossil fuel burning and deforestation (IPCC, 1994). Carbon monoxide is produced mainly through combustion processes and through oxidation of volatile organic compounds (VOC). It has a chemical life-time of 60 days and the non-anthropogenic sources are small relative to anthropogenic sources (Baggott, 2004). It can therefore act as a marker of anthropogenic emission at the local scale. Taking into account differences in chemical lifetime and specific warming potential, CH_4 and N_2O have a global warming potential (GWP) of 20 and 300 times respectively of CO_2 over a 100 year period (Baggott, 2004). While much work has been done to quantify CO_2 emissions, CH_4 and N_2O emissions in particular remain less well understood. The bulk of anthropogenic N_2O emissions come from microbial de-nitrification in agriculture soils, in particular due to fertiliser application. Thus, emissions of N_2O are especially hard to quantify as they depend strongly on environmental factors such as rainfall and temperature. Anthropogenic CH_4 emissions are dominated globally by rice cultivation, landfills and emissions from ruminant animals. Within the UK landfill and livestock emissions are the major sources. Table 1 gives the breakdown of the relative contribution of each source sector to the total UK emissions as reported by the NAEI for all four chemical species.

Table 1. Breakdown of source sectors and relative contribution to UK emissions for CO, CO_2, CH_4 and N_2O (NAEI, 2005).

CO	CO_2	CH_4	N_2O
Agriculture < 1%	Agriculture < 1%	Wetlands – 4%	Traffic – 8%
Road transport – 57%	Road transport – 22%	Gas pipes leaks – 15%	Livestock – 21%
Non-road transport – 13%	Non-road transport – 2%	Landfill – 42%	Rivers < 1%
Industrial combustion < 1%	Industrial combustion – 6%	Livestock – 31%	Estuaries < 1%
Industrial processes < 1%	Industrial processes < 1%	Open mines < 1%	Industry – 13%
Residential, commercial and institutional combustion – 7%	Residential, commercial and institutional combustion - 21%	Deep mines – 8%	Nitrogen Deposition - 4%
Energy production < 1%	Energy production < 1%		Fertiliser – 52%
Waste < 1%	Waste <1%		
Point sources – 23%	Point sources – 47%		
	Nature – 2%		
	Biogenic uptake < 1%		

The methodology for calculating emissions is prescribed by the IPCC and uses a combination of statistical activity data and emissions factors in a 'bottom up' approach. This approach assumes that sources within the same sector will emit at equal rates and that all sources are fully accounted for using statistical activity data. UK emissions are currently compiled by the National Atmospheric Emissions Inventory (NAEI) (Baggott, 2007) using a combination of statistical activity data using the IPCC methodology and reported emissions from regulatory bodies. Emissions are reported for sector totals as well as national totals and spatially disaggregated maps produced for certain species. The 2005 UK totals as reported by the NAEI are shown in Table 2.

Table 2. NAEI total UK emissions (kt yr^{-1}) for CO, CO_2, N_2O and CH_4 and associated uncertainty (Baggott *et al.*, 2007).

	NAEI UK totals (2005) kt yr^{-1}	Uncertainty (%)
CO	2400	20
CO_2	555000	2
N_2O	130	230
CH_4	2400	21

1.2 Description of the Pollutants and Greenhouse Gases

1.2.1 Carbon Monoxide

Carbon monoxide affects climate mainly through its effect on ozone and methane rather than affecting climate directly. It is toxic and also contributes to the formation of tropospheric ozone, which is harmful to human health and vegetation and also acts as a greenhouse gas. The lifetime of CO in the atmosphere is only a few months with background concentrations of less than 200 ppb. It is produced mainly through incomplete combustion of fossil fuels and its total global emission is around 2 orders of magnitude smaller than CO_2. In the UK, road transport is by far the largest source of CO accounting for around 45 % of emissions in 2005 (Baggott *et al.*, 2007). Other significant sources include non-road transport and industrial combustion. The dominance of road transport over emissions means that CO emissions are centred around urban areas and road networks.

UK emissions of CO were estimated at 2400 kt in 2005, a decrease of 71% from 1990 levels. Most of this decrease comes from the increased use of catalytic converters in cars. The increased popularity of diesel vehicles at the expense of petrol driven vehicles has also contributed to this reduction (Baggott *et al.*, 2007).

The uncertainty in emissions was calculated using a technique similar to Monte Carlo Simulation. Probability distribution functions are assigned to each emission factor and activity rate with a mean and variance value. Each pdf was sampled 10000 times and the emission calculated to produce a converged distribution which could be analysed to find the total uncertainty. In the main the activity data is considered to be more reliable with the uncertainty primarily caused by emission factor uncertainties for all species (Salway, 1998).

The uncertainty in the total UK CO emissions is estimated at 20%. This is mainly the result of uncertainty in road transport emissions which are based on relatively small number of measurements for a highly variable sector. The emissions from other combustion processes can also be highly variable, depending as they do on the specific conditions. The emission factors used are derived from relatively few types of boiler and so the uncertainty in the CO emissions from these sources is also

relatively high (Dore *et al.*, 2005). However, additional uncertainty is introduced by the spatial disaggregation of the emissions.

1.2.2 Carbon Dioxide

Carbon dioxide is produced mainly by burning of fossil fuels for energy and transport. Burning biomass is also an important global source of CO_2 but is harder to quantify as it includes natural fires as well as agricultural burning and is not a major UK source. CO_2 concentrations in the atmosphere have increased from 280 ppmv 200 years ago to 379 ppmv in 2005 (IPCC, 2007) and it has an atmospheric lifetime of 100 years. 20000 years ago CO_2 concentrations were believed to be only ~200 ppmv.

Natural emissions of CO_2 which arise from recently photosynthesised carbon are excluded from the NAEI are these are not permanent. The major sources of CO_2 in the UK are fossil fuel combustion for energy generation and transport. Domestic and industrial fossil fuel combustion are also significant sources. The source sectors are predominantly in urban areas and road networks making these areas the dominant CO_2 sources.

Emissions of CO_2 from the UK decreased by 6.4 % between 1990 and 2005 with CO_2 emissions at 555 Mt in 2005. Much of this decrease results from the move away from coal generated electricity to gas generation. Increases in efficiency have also contributed to the decrease in CO_2 emissions. The switch from coal and oil to natural gas has also resulted in a decrease in emissions from the domestic sectors. Emissions from transport have increased only slightly since 1990 levels despite the increased use of private motor cars due to greater fuel efficiency and the increasing popularity of diesel cars (Jackson *et al.*, 2007, Baggott *et al.*, 2007).

Land-use change can result in a net emission or absorption of CO_2 and can vary considerably from year to year. However, the net effect is small compared with the total CO_2 emissions for the whole year. The biogenic flux of CO_2 for England and Wales is estimated at 28 Mt yr^{-1} net uptake for all vegetation classes (Milne *et al*, 2006). Even accounting for the absence of the Scottish and Northern Irish flux, the biogenic flux is small compared to the anthropogenic emissions.

Uncertainty in the anthropogenic CO_2 budget is estimated at 2%. The low level of uncertainty for CO_2 reflects the fact that CO_2 emissions are dominated by fuel combustion which is related to the carbon content of the fuel. This can be easily measured and is well known (Jackson *et al.*, 2007, Baggott *et al.*, 2007).

1.2.3 Methane

Methane has an atmospheric lifetime of around 10 years and exists in much smaller concentrations of ~1.8 ppmv (Pacyna, 1994) than CO_2. However it has a Global Warming Potential (GWP) 21 times that of CO_2 at the 100 year horizon. The major global sources of methane are natural wetland followed by animals, rice cultivation and biomass burning. At a UK level, landfills and agriculture (ruminant animals and animal waste), are the two largest source sectors. Leaks from gas pipes and coal mines also contribute significantly to the total CH_4 emission. The levels of emission are hard to quantify because of the complex and diverse nature of the sources, which can depend on highly variable biological systems. Emissions from landfills for example are derived using a model based on anaerobic digestion of waste material. The diverse nature of the sources also means that CH_4 emissions are more evenly spread between urban and rural areas compared with CO and CO_2.

NAEI estimates show that annual UK emissions of CH_4 decreased by 52 % from 1990 to 2005 levels of 2400 kt. This reduction is mainly due to the decrease in coal mining and increases in the recovery of CH_4 from landfills. Reductions in animal numbers, particularly dairy cattle, have also contributed to a decrease in CH_4 emissions. Emissions from gas distribution systems have decreased significantly in recent years as old pipes are gradually replaced (Jackson *et al.*, 2007, Baggott *et al.*, 2007).

The estimated uncertainty in the CH_4 emission is 21 %. The quality of the data used to estimate CH_4 is poor compared with CO_2 resulting in a higher uncertainty. The main sources are themselves more variable depending on complex biological systems (Jackson *et al.*, 2007, Baggott *et al.*, 2007).

1.2.4 Nitrous Oxide

Nitrous oxide (N_2O) has an atmospheric lifetime of approximately 170 years with current concentrations of around 0.31 ppmv. Although concentrations of N_2O are significantly smaller than CO_2, the GWP of N_2O is 310 times that of CO_2 over a 100 year period. Globally, the largest contributors are biogenic sources such as natural soils and oceans. There are however a large number of anthropogenic sources such as fertiliser application and emissions resulting from ruminant animals as well as a host of minor sources such as post-burn effects of fossil fuel combustion and waste incineration. In the UK, agriculture is the major source from the application of mineral fertilizers and manure to land. Energy generation and industrial processes also contribute to emissions. N_2O emissions are therefore dominated by rural emissions with high levels from some industrial point sources.

NAEI estimates put the 2005 emission of N_2O from the UK at 130 kt, less than 38% of 1990 levels. These reductions are mainly due to abatement in the production processes of nylon and nitric acid or relocation of industry to other European countries. Emissions from road transport have increase significantly since 1990 due to increased numbers of motor vehicles with catalytic converters, where N_2O is a by-product of incomplete reduction of NO. However the contribution of road transport to the total UK emissions is small (Jackson *et al.*, 2007, Baggott *et al.*, 2007).

The uncertainty associated with N_2O is 230 % (Baggott *et al.*, 2007). This is a result of the dependence of N_2O emissions on environmental factors such as rainfall and temperature with bacterial activity in soils dominating the emissions. The bulk of N_2O emissions are from agriculture, in particular fertiliser application. However the resulting N_2O emissions depend on the type of fertiliser and the way in which it is applied. Water content, temperature of the soil and the type of soil all greatly influence emissions. This results in emissions which are very variable in time and space (Jackson *et al.*, 2007, Baggott *et al.*, 2007).

The agricultural component of the N_2O and CH_4 NAEI emissions inventory are compiled by CEH using the methodology of the IPCC. However the team responsible for the N_2O emissions at CEH also use an alternative method to the IPCC methodology for emissions of N_2O from soils due to the application of mineral

fertiliser. This method accounts for the water content of the soil and soil temperature in addition to the Nitrogen content of the fertiliser applied (Skiba *et al.*, 2001) which is the only factor in the IPCC method and produces an annual emission estimate of 165 kt yr^{-1}.

1.2.5 Halocarbons

Halocarbons are a family of chemical species containing carbons bonded to halogens such as bromine, fluorine and chlorine. They include the chlorofluorocarbons (CFCs), the hydroflurocarbons (HFCs), the hydrochlorofluorocarbons (HCFCs), methylhalides, carbon tetrachloride (CCl_4), carbon tetrafluoride (CF_4)), and the halons (bromide species). All species are powerful greenhouse gases. However, the role of the CFCs in depleting stratospheric ozone tends to offset their warming potential as ozone is itself a greenhouse gas.

Halocarbons are produced by anthropogenic sources though some such as the methylhalides do have natural sources. CFCs were produced as refrigerator compressor fluid and aerosol propellant. On discovering their harmful effects on the ozone layer, their use has been controlled under the Montreal Protocol and they have since been largely replaced by HCFCs and HFCs.

HFCs are one of the six species whose emissions the UK is required to report to the UNFCCC. UK emissions of HFCs are mainly from refrigeration and air conditioning equipment, aerosols and manufacturing of HCFCs and HFCs. Emission of HFCs have fallen by 40 % from their 1995 levels (Jackson *et al.*, 2007, Baggott *et al.* 2007) with emissions for 2005 estimated at 9206 kt CO_2 equivalent yr^{-1}. Increased use of HFCs in aerosols and refrigeration produced a large increase in emissions between 1990 and 1998. Since 1998 emissions have fallen mostly due to improved abatement processes at HCFC and HFC manufacturing plants.

1.2.6 Sulphur and Nitrogen Compounds

Emissions of SO_2 and NO_x (NO and NO_2) are oxidised in the atmosphere to the acidifying compounds H_2SO_4 and HNO_3 respectively, the deposition of which is damaging to fresh water systems, vegetation and buildings (NEGTAP, 2001). The oxidation of NO_x also contributes to the formation of troposheric ozone which is harmful to human health. Oxidation occurs in the gas phase (homogenous reactions), in atmospheric aerosol, or in cloud and rain droplets (heterogeneous reactions). The oxidation process of SO_2 and NO_2 are shown in Figure 2. SO_2 and NO_2 can also be deposited directly to the surface by dry deposition which can also acidify soils.

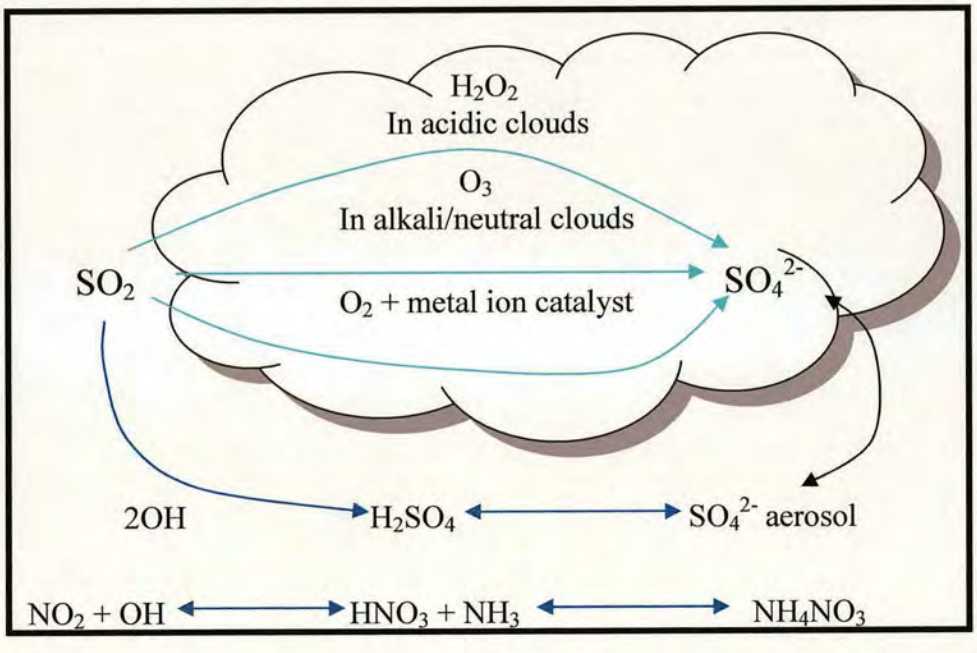

Figure 2. Sulphur dioxide and nitrogen dioxide oxidation processes (NEGTAP, 2001).

S and N species are emitted primarily from the combustion of fossil fuels in power generation and transportation and as such are emitted primarily from urban sources. The UK is committed to reducing acidifying gas and ozone precursor emissions and has signed a number of international agreements to this effect. The EU National Ceilings Directive sets ceilings for emissions for each member state. The UK ceiling for SO_2 is currently set at 585 kt yr^{-1} and the NO_x ceiling is set at 1167 kt yr^{-1} (Baggott *et al*, 2005).

The NAEI produces emission estimates for SO_2 and NO_x for the UK. SO_2 emissions are relatively easy to derive as they are based on the sulphur content in fuel and fuel consumption data, both of which are easily known from DTI fuel consumption data and data published on the sulphur content of coal. NO_x emissions are harder to derive as the NO_x emissions from combustion processes depend on the conditions of combustion, particularly the temperature and excess air ratio. The NO_x emissions are therefore less reliable than SO_2, depending on relatively few measurements where emissions can vary widely given apparently similar combustion plants.

1.3 Emissions Estimates

1.3.1 Bottom-Up Estimates

The United Kingdom is committed to a 12.5% reduction of global warming potential (GWP) of six key Greenhouse gases from 1990 levels by 2008-2012. Annual UK emissions are currently compiled as part of the National Atmospheric Emissions Inventory (NAEI) (Baggott, 2007) provided by the National Environmental Technology Centre (NETCEN) and all emission data given here comes from the NAEI. The NAEI emission data is submitted to the United Nations Commission for Europe (UN/ECE) and the United Nations Framework Convention on Climate Change (UNFCCC). The UK is required to publish regularly updated emission inventories using guidelines from the Intergovernmental Panel on Climate Change (IPCC). The species reported include the direct greenhouse gases CO_2, CH_4 and N_2O and the indirect greenhouse gas CO.

The current UK inventory is calculated using a combination of reported emissions from various regulatory bodies and statistical activity data using the equation

$$F_{emit} = Ae \tag{1.1}$$

where F_{emit} is the emission of the pollutant (g m^{-2} s^{-1} $source^{-1}$), A is the activity data (e.g. source number) and e is the emission factor (g m^{-2} s^{-1} $source^{-1}$).

The emission factors are calculated using measurements from a number of sources regarded as representative of the whole source sector. Some sectors include individual industrial point sources which are required to report annual emissions to regulatory bodies. The Environment Agency of England and Wales collects emissions from around 2000 large point sources, estimated by the plant operators, as part of the requirements under the European IPPC (Integrated Pollution Protection and Control) regulation, which are then incorporated separately into the NAEI. Likewise in Scotland and Northern Ireland where the Scottish Environmental Protection Agency and the Northern Ireland Department of Environment perform a similar function.

Where emissions from point sources are not available, emissions are estimated using activity data and an emission factor. The activity data can be fuel consumption, production of product, number of animals or some other statistical data which relates directly to the emissions. There are eleven sectors in the NAEI emission estimates which correspond to the classification from UNECE/CORINAIR SNAP 97. These are listed in Table 3.

Table 3. UNECE.CORINAIR SNAP 97 sector classification used by NAEI for UK emissions.

Combustion in Energy Production and Transformation
Combustion in Commercial, Institutional and Residential and Agriculture
Combustion in Energy
Production Processes
Extraction and Distribution of Fossil Fuels
Solvent Use
Road Transport
Other Transport and Mobile Machinery
Waste Treatment and Disposal
Agriculture Forestry and Land Use Change
Nature

For the combustion emissions, activity statistics are taken from the Digest of UK Energy Statistics (DUKES), (DTI, 2004). The statistical data for non-combustion emissions varies between the different activities; e.g. population data for emissions

from farm animals and process output for industrial processes. Other sectors require a more complex methodology to capture the complexity of the emissions. Emissions from road transport for example depend on the fuel type, vehicle type and age, average speed and a number of other factors. The road transport emissions are therefore calculated using a different model than the simple one described by equation (1.1). From the national totals, spatially disaggregated emission inventories at 1 km resolution are also produced for many species (King, 2006). Point source data for large industrial sources is included separately with the mapping of area source sectors based on the specific spatial statistics for that sector. Typical examples of the statistic used include population, fuel use, land use and employment figures. In some cases the distribution of a pollutant is based on the emission estimates of another species by allocating the national total to sites based on their share of a different pollutant.

1.3.2 Top-Down Validation of Emissions Inventory

Ryall *et al* (2000) attempted to validate the NAEI estimates using the atmospheric transport model, the Numerical Atmospheric Modelling Environment (NAME) (Ryall *et al*, 1998) and long term measurements from Mace Head in Ireland. NAME is a Lagrangian dispersion model which simulates the emissions and transport of pollutants using three-dimensional meteorology from the Met Office Unified Model (see Section 2.3). The Mace Head site is on the west coast of Ireland where the prevailing westerly winds bring relatively unpolluted air from the Atlantic. Around 20-30% of the time, the wind flow brings polluted air from continental Europe or the UK to the Mace Head site. Gas chromatography and chromatograph-mass spectrometer measurements have been used to collect high-frequency radiatively active trace gas and halocarbon data as part of the Global Gases Experiment (GAGE/AGAGE) since 1994 (Manning, 2003).

To determine the origin of the air and to eliminate the effect of local sources, the NAME model was used in backwards mode to estimate the contributing source regions to the Mace Head observations. The model was then run in forward mode with emissions released across Europe at a constant rate to predict the concentration

at Mace Head every 15 minutes. The model time-series was compared with the measured time series having removed baseline observations. The total concentration at Mace Head from all sources, P_t (g m^{-3}), is the sum of the concentration resulting for each source for each time in the time-series. Therefore, the concentration from each source for each time, $P_{s,t}$, multiplied by the actual emissions from that source, F_s, equalled the observation at Mace Head, o_t, creating a set of simultaneous equations equal to the number of times in the time-series. To simplify the problem and make it possible to solve, the emissions were assumed to be equal for all sources. The emissions were therefore equal to the observation divided by the total concentration at Mace Head.

$$F_t = \frac{o_t}{P_t} \tag{1.2}$$

To obtain F_i, weighted mean of F_t was used.

$$F_s = \frac{\sum_{t=1}^{T} W_t o_t / P_t}{\sum_{t=1}^{T} W_t} \tag{1.3}$$

The weighting factor, W_t, was set to P_s,t. This placed most emphasis on the times when the signal from source s was strongest.

This approach produced alternative estimates for the UK emissions N_2O, CH_4, CO, methylene dichloride and methyl chloroform for the years 1995, 1996, 1997 and 1998. Table 4 shows the NAME estimates compared to the NAEI estimates for the same year. The NAME estimates are broadly speaking in good agreement with the NAEI estimates for those years with the notable exception of methyl chloroform emissions which were found to be much lower than the inventory estimates for those years.

Table 4. NAME and NAEI UK totals (kt yr^{-1}) of selected species for the years 1995-1998 (Ryall *el al.*, 2000).

year	CH_4 NAME	CH_4 NAEI	CO NAME	CO NAEI	N_2O NAME	N_2O NAEI	Methy-lene Di-chloride NAME	Methy-lene chloride NAEI	Methyl Chloro-form NAME	Methyl Chloro-form NAEI
1995	3144	3751	6096	4939	143	183	10.8	14.84	1.7	15.9
1996	2917	3712	5822	4645	140	189	13.0		0.8	
1997	2871	2907	5716	5734	162	196	7.8		0.3	
1998	2724	2744	2854	5278	146	187	10.8		1.7	

A more sophisticated method was developed to produce estimates of the UK emissions using the Mace Head data and the NAME model (Manning *et al*, 2006). The NAME model was run in backwards mode to derive the origin of the air arriving at Mace Head for every hour between 1995 and 2005 inclusive. Using the observations from Mace Head and the air origin maps, an inversion technique was used to produce spatially disaggregated emission maps for continental Europe and the UK. An iterative approach was used, simulated annealing, to produce a best-fit emission map for the Mace Head observations. A full description of the inversion technique can be found in Chapter 6.

The results of the inversion technique for CO, CH_4, N_2O, HFC-134a and HFC-152a for the years 2001-2005 inclusive are shown in Table 5. While the inversion technique showed generally good agreement with the NAEI inventory, it should be noted that for CH_4, while the NAEI shows a gradual decrease in emissions over the 10 year period, the inversion showed a constant and possibly increasing trend.

Table 5. Inversion and NAEI UK totals (kt yr^{-1}) of selected species for the years 2001-2005 (Manning, 2006).

year	CH_4 INV	CH_4 NAEI	CO INV	CO NAEI	N_2O INV	N_2O NAEI	HFC-134a INV	HFC-134a NAEI	HFC-152a INV	HFC-152a NAEI
01-02	2600	3000	2700	3900	113	133	1.3	3.1	0.1	0.18
02-03	3000	2800	2900	3300	107	129	2.1	3.4	0.2	0.18
03-04	2500	2500	2400	2900	108	128	2.0	3.7	0.1	0.18
04-05	2700	2500	2700	2700	141	128	2.1		0.1	

Recent work by Peter Bergamaschi of the European Commission Joint Research Centre suggests that the UK is underestimating CH_4 emissions significantly (Bergamaschi, 2005). By measuring concentration differences at sites across the

globe and tracking the air movements, he was able to make a 'top down' estimate of emissions from individual countries. The CH_4 emissions for 2004 were estimated to be 4210 kt, nearly twice the reported emissions of 2190 kt.

1.4 Boundary Layer Budget Approach to Estimate Pollutant Emissions

In a boundary layer budget study, it is assumed that the total flux emitted can be measured directly by measuring the inflow and outflow fluxes across all sides of the box and calculating the difference. The components of the budget are shown in Figure 3.

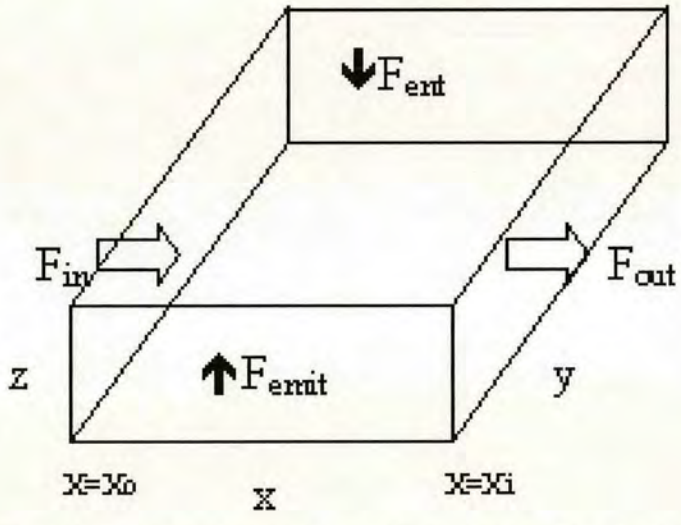

Figure 3. Boundary Layer Budget Components. F_{emit} is the emitted flux, F_{out} is the export flux, F_{in} is the import flux, F_{ent} is the entrainment flux, x_o is the x coordinate of the inflow surface and x_i is the x coordinate of the outflow surface, y is the length of the outflow surface and z is the height of the box (i.e. the boundary layer depth).

The flux emitted between x_0 and x_i is the difference between the flux through each surface into and out of the box. For reactive species this may include a deposition flux and chemical conversion flux.

$$F_{emit} = F_{out} - F_{in} + F_{ent} + F_{dc} + F_{dep} \tag{1.4}$$

where F_{emit} is the emitted flux (g s^{-1}), F_{out} is the export flux, F_{in} is the import flux, F_{ent} is the entrainment flux, F_{dc} is the rate of change due to chemical conversion and F_{dep} is the deposition flux.

$$F_{dc} = \int\int\int \frac{\{dC(x,y,z)\}}{dt} dxdydz \tag{1.5}$$

$$F_{dep} = \int\int -u_d C(x,y) dxdy \tag{1.6}$$

$$F_{out} = \int\int u_{xi}(y,z) C(y,z) dydz \tag{1.7}$$

$$F_{in} = \int\int u_{x_0}(y,z) C(y,z) dydz \tag{1.8}$$

$$F_{ent} = \int\int u_e(x,y) \Delta C(y,z) dydz \tag{1.9}$$

where C is the concentration (g m^{-3}), u_{x0} and u_{xi} are the wind speeds (m s^{-1}) at x_0 and x_i in the direction perpendicular to y, u_d is the deposition velocity (m s^{-1}) and u_e is the vertical component of air motion through top of the boundary layer (m s^{-1}).

For some species such as methane, which is a conserved trace gases, F_{dc} and F_{dep} are set to zero because its lifetime in the atmosphere is much longer than the timescale for crossing the UK. Therefore F_{emit} becomes

$$F_{emit} = F_{out} - F_{in} - F_{ent} \tag{1.10}$$

The flux entrained (F_{ent}) through the top of the atmosphere is assumed to be negligible compared with the other fluxes. However, in using a mass balance approach it is still preferable to take it into account. This has been done as described in chapter 5 giving a typical value of F_{ent} of around two orders of magnitude smaller than the flux emitted.

1.5 The Atmospheric Boundary Layer

The boundary layer (ABL) is the part of our atmosphere that reacts directly to processes at the Earth's surface such as the emission of pollutants. Unlike the free troposphere above, it shows a strong diurnal signature as it responds to changing heat flux from the surface. Typically it can be up to 2 km over land in the UK in the middle of the day, but perhaps only a few 10's of metres deep at night. As the sun heats the ground increasing the surface temperature, transport processes carry changes through the boundary layer. The latent and sensible heat flux from the Earth's surface provides most of the atmosphere's energy and generates turbulence, mainly in the form of convection. Turbulence is the main process responsible for transport of constituents upwards through the boundary layer and can also be produced by frictional drag and wakes caused by obstacles on the air flowing over the surface. The mean wind flow is primarily responsible for transport in the horizontal direction and turbulence is largely responsible for the transport in the vertical (Stull, 1989).

It is the heating of the Earth's surface by the sun that drives many of the processes which alter the depth of the boundary layer. In the bottom quasi-laminar sublayer, (typically a few mm think), molecular processes transport heat, momentum and tracers between the surface and the atmosphere. Above this sublayer, turbulence transports these constituents up through the atmosphere. The heat budget for an infinitesimally thin layer just above the Earth's surface is shown below

$$Q_s = Q_H + Q_E + Q_G + \Delta Q_s \tag{1.11}$$

where Q_s is the net radiation flux at the surface, Q_H is the sensible heat flux out of the top, Q_E is the latent heat flux out of the top, Q_G is the molecular heat flux into the ground and (ΔQ_s) is the storage of internal energy. For an infinitesimally thin layer ΔQ_s becomes zero since there is no mass within the layer to store the heat (Stull, 1989). During the day over land there tends to be more downward and longwave solar radiation entering the layer than upwards radiation leaving.

The components of the atmospheric boundary layer and its evolution are shown in

Figure 4 taken from Stull (1989). As the surface warms during the day, convection increases and the boundary layer grows to heights of up to 3000 m. Early in the morning the boundary layer grows as the turbulence slowly entrains material in a stable nocturnal boundary layer created the previous night when the surface cooled and became colder than the air above. Above this stable layer is the residual layer where the mean states of variables have been preserved overnight from the previous day. The top of the stable layer is poorly defined, merging into the residual layer above. The two layers are significantly different, however, with the stable layer of statically stable air where the less dense air lies above denser air below. This suppresses turbulence resulting in very little vertical mixing. The residual layer is neutrally stratified with turbulence that is equal in all directions. This tends to produce dispersal of constituents equal in the vertical and horizontal. When the boundary layer reaches the residual layer it begins to grow rapidly until it reaches a more stable layer of air where once its growth slows as it gradually entrains material. Late in the afternoon, the heat flux decreases and the boundary layer shrinks. As the surface cools at night below the temperature of air above, the temperature gradient reverses, a stable layer develops and turbulence is suppressed causing the nocturnal boundary layer to shrink to depths as low as 50 m.

In high-pressure regions, the daytime boundary layer can be divided roughly into 3 parts. The lowest part of the atmosphere is the surface layer where the turbulent fluxes are within 10% of their surface values. Above uniform surfaces, this layer is characterized by logarithmic profiles in wind speed, temperature and pollutant concentrations. Above this is the well-mixed layer (ML). Within this layer, turbulence, driven mainly by convection, causes intense mixing. This tends to leave conserved variables mixed uniformly in the vertical so, for example, pollutant concentration will be constant with height. At the top of the mixed layer is a capping stable layer that can act as a lid to rising thermals. It is here that entrainment from the free troposphere into the boundary layer takes place when the rising thermals overshoot the top of the boundary layer and become negatively buoyant, sinking back down and carrying air from the free troposphere with them. However because there is little turbulence in the free troposphere, the air in the thermals is not mixed into the surrounding air and so any constituents in the thermals are carried back down into the

boundary layer. If the absolute temperature increases with height, then this third part of the boundary layer is referred to as the inversion layer.

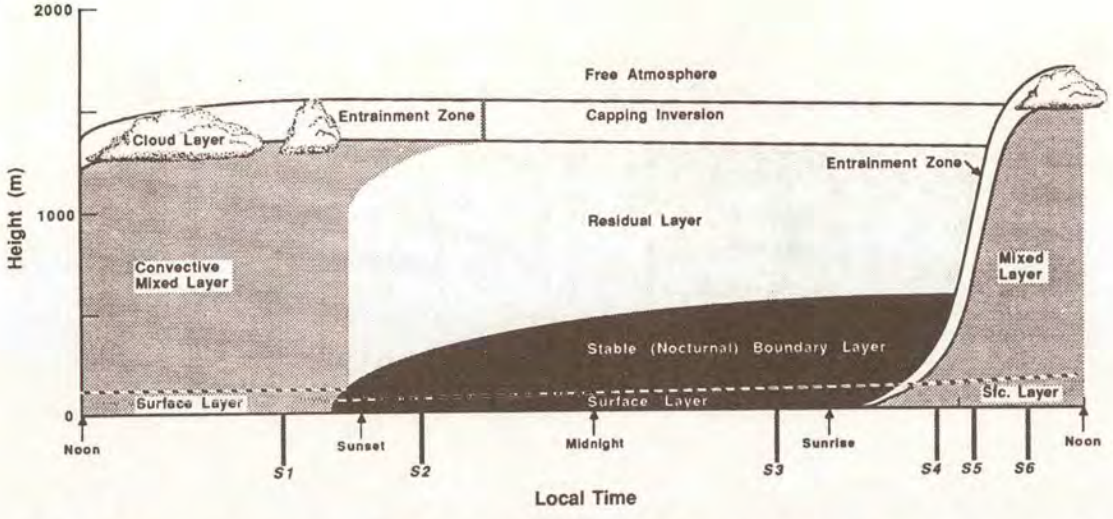

Figure 4. Diagram taken from Stull (1989) shows the atmospheric boundary layer as it evolves over the day. It consists of the turbulent mixed layer, less-turbulent residual layer and nocturnal boundary layer.

With few exceptions, anthropogenic emissions are produced at or near the Earth's surface. When a temperature inversion is present at the top of the boundary layer, the thermals are trapped within the boundary layer and therefore the pollutants they carry are also trapped.

The state of the boundary layer can be described quantitatively by equations of motion and a set of conservation equations for mass, momentum, moisture and heat. For a boundary layer budget study the quantity of interest is the concentration of a pollutant. This is a scalar quantity and can be described by the following mass conservation equation (Stull, 1989)

$$\frac{\partial C}{\partial t} + U_j \frac{\partial C}{\partial x_j} = \nu_c \frac{\partial^2 C}{\partial x_j^2} + S_c \qquad (1.12)$$

where C is the concentration (g m^{-3}), t is the time (s), U_j is the wind speed in direction j (m s^{-1}) where j is eastwards, northwards or vertical, x_j is distance (m) in direction j, ν_c is the molecular diffusivity (m^2 s^{-1}) of pollutant and S_c is the body source term for

processes not already included such as chemical reactions (g m^{-3} s^{-1}).

It is not possible to solve this equation analytically as the motion of the air in the boundary layer is too complex. Instead an approximate solution can be found by splitting Equation (1.12) into mean and turbulent parts with

$$U_j = \overline{U_j} + u' \tag{1.13}$$

and

$$C = \overline{C} + c' \tag{1.14}$$

where the overbar denotes the mean component and the prime denotes the perturbation due to turbulence. Equation (1.12) then becomes

$$\frac{\partial \overline{C}}{\partial t} + \frac{\partial c'}{\partial t} + \frac{\overline{U_j}\partial \overline{C}}{\partial x_j} + \frac{\overline{U_j}\partial c'}{\partial x_j} + \frac{u_j'\partial \overline{C}}{\partial x_j} + \frac{u_j'\partial c'}{\partial x_j} = \frac{\nu_c \partial^2 \overline{C}}{\partial x_j^2} + \frac{\nu_c \partial^2 c'}{\partial x_j^2} + S_c \tag{1.15}$$

Equation (1.15) can be given in terms of the mean variables with the turbulence converted into flux form (Stull, 1989).

$$\frac{\partial \overline{C}}{\partial t} + \frac{\overline{U_j}\partial \overline{C}}{\partial x_j} = \frac{\nu_c \partial^2 \overline{C}}{\partial x_j^2} + S_c - \frac{\partial(\overline{u_j'c'})}{\partial x_j} \tag{1.16}$$

The first and second terms on the left hand side represent the mean storage of tracer C and the advection of C by the mean wind. The first term on the right hand side represents the mean molecular diffusion of C. The last term on the left hand side represents the divergence of turbulent tracer flux. The molecular diffusion term is several orders of magnitude smaller than the other terms and so can be neglected so Equation (1.16) becomes

$$\frac{\partial \overline{C}}{\partial t} + \frac{\overline{U_j}\partial \overline{C}}{\partial x_j} = S_c - \frac{\partial(\overline{u_j'c'})}{\partial x_j} \tag{1.17}$$

This equation implies that the change in the mean concentration of a virtual control volume with time is the sum of the difference of the advective concentration fluxes in and out of this volume and the divergence from turbulent flux plus a contribution from any other forcings (emissions, chemistry).

1.6 Ideal Meteorology for UK Boundary Layer Budget Study

The UK is ideally suited to a boundary layer budget study. Being an island means that the inflow and outflow flux can be easily identified. The UK is situated at the Eastern boundary of the Atlantic and, with the exception of Ireland whose emissions are small compared to the United Kingdom, there is little inflow from neighbouring countries given a westerly or northerly wind flow. Therefore the background concentration should be relatively constant over the whole inflow region.

For a boundary budget study over the whole country, a steady, well-coupled and relatively constant wind flow is required, with a uniform background concentration, making it easier to identify the inflow and outflow regions and calculate the imported and exported flux. To limit the flux through the top of the boundary layer, a temperature inversion is required to trap pollutants within the boundary layer. Thus conditions with deep convection need to be avoided.

To achieve these conditions, a high-pressure region over the Atlantic to the west or south west of the UK would be ideal. Subsidence should cause a temperature inversion to develop as when sinking air is compressed it increases in temperature. Anticyclonic winds should bring clean Atlantic air into the UK and produce a well coupled westerly or northerly wind flow across the country. High pressure should also prevent rain clouds from forming preventing wash-out of particles and water soluble trace gases.

1.7 Review of Previous Boundary Layer Budget Studies

1.7.1 Measurements of Methane Fluxes from UK Wetlands

Aircraft measurements have been used in several studies to calculate emissions using a boundary layer budget technique. In the UK much of this work has been aimed at calculating landscape scale CH_4 fluxes from wetlands which are mainly the result of biogenic activity in anoxic soils. The first of these, reported by Gallagher *et al.* (1994), was aimed at determining if it would be possible to measure fluxes directly at a landscape scale using aircraft measurements. The site chosen was the Strathy Bog peatland in Northern Scotland situated approximately 50 km from the west coast, 30 km from the east coast and 10 km from the north coast. The remoteness of the site ensured anthropogenic emissions did not significantly influence the measurements. The site would normally consist of flooded pools, however during the first half of the campaign period which lasted from 18 July to 4th August 1992, conditions were very dry with no rain recorded during the previous 2 months. The average temperature during July was 1.5 °C higher than normal. The site was therefore uncharacteristically dry suggesting that CH_4 fluxes were smaller than average during this period. During the second half of the campaign, rainfall increased, returning anoxic conditions to most of the site. Some parts of the site were visibly wetter throughout the campaign period with pools of standing water to the west of the site. For much of the campaign, the atmospheric boundary layer was dominated by neutral stability by day with convective conditions increasing towards the end of the campaign resulting in the increased rainfall during this period. Wind flow was mainly westerly throughout the campaign.

For this study air was sampled into stainless steel canisters and Tedlar bags from a small propeller aircraft, to be analysed later on the ground using a gas chromatography technique. The canister samples took 60-90s to fill which corresponded to a horizontal distance of 3-4 km given the aircraft flying speed.

Samples were collected upwind, downwind and above the main surface measurement site where continuous measurements of CH_4 were made. In addition, samples were collected at a number of heights within the ABL and the free troposphere to provide profile information with canister and Tedlar bag samples also taken at the surface.

The CH_4 concentration was determined as a function of height and distance along the air trajectory at a given height.

To determine flux estimates from the measurements a simple one-dimensional Lagrangian diffusion model was developed. This assumed constant CH_4 concentration with height upwind of the source region and constant upward flux of CH_4 from the ground. Aircraft measurements supported the assumption of constant upwind CH_4 concentration with height and although the upward flux is not constant at small scales, because the aim was to measure the average over larger scales, assuming constant upward flux could be considered valid.

In the model an air column containing 3 layers is advected across the landscape and the diffusion equation solved. The general continuity equation for each layer of the model can be derived from Eq. (1.12). As the column is moving with the wind, the second term on the left hand side, which describes the concentration change due to the wind flow, becomes zero. This may be presented as

$$\frac{\partial C(z)}{\partial t} = -K(z)\frac{\partial^2 C(z)}{\partial z^2} + S_{CH4}(z=0) \tag{1.18}$$

where $K(z)$ is the eddy diffusivity for methane ($m^2\ s^{-1}$), S_{CH4} is the source term ($g\ m^{-3}\ s^{-1}$) and $C(z)$ is the concentration ($g\ m^{-3}$) for a given height z (m). In the lowest 100 m of the air parcel, K is defined by

$$K(z) = \frac{ku_* z}{\phi_M(\xi)} \tag{1.19}$$

where k is von Karman's constant, u_* is the friction velocity ($m\ s^{-1}$) and $\phi_M(\xi)$ is a dimensionless shear stability correction function derived from surface layer measurements approximated by

$$\phi_M(\xi) = 1 + 4.7\xi \qquad \text{for } \xi>0 \text{ (stable stratification)} \tag{1.20}$$

$$= 1 \qquad \text{for } \xi=1 \text{ (neutral stratification)} \tag{1.21}$$

$$= [1-15\xi]^{-0.25} \qquad \text{or } \xi<0 \text{ (unstable stratification)} \tag{1.22}$$

with $\xi = z/L$ where L is the Monin-Obukhov dimensionless length scale defined by

$$L = \frac{-\rho\theta_0 u_*^3}{KgH} \tag{1.23}$$

where θ_o is the mean temperature in the layer (K) and H is the local sensible heat flux (W m^{-2}); L is a measure of the atmospheric stability.

During the aircraft campaign simultaneous measurements of surface flux were measured within the sample area. At the Strathy Bog experimental site, tower-based sonic anemometers were used to measure L. It was also measured by a 100 m path length laser scintillometer and these measurements allowed corrections for atmospheric stability to be made which confirmed the analysis of aircraft soundings which showed nearly constant potential temperature profiles in the boundary layer.

In the second, or well-mixed layer, the diffusivity was extrapolated from the top of the surface layer using a number of parameterisation schemes e.g. Stull (1989). These included constant diffusivity and the cubic polynomial parameterisation from O'Brien (1970) where the diffusivity declines with height from a maximum within the boundary to zero at the top of the boundary layer.

$$K(z) = \frac{[(z-z_A)^2]}{\Delta z^2}\{K_B - K_A + (z-z_B)[K'_B + \frac{2(K_B - K_A)}{\Delta z}]\} \tag{1.24}$$

where z_A and z_B are the heights of the boundary layer and surface layer respectively and $\Delta z = z_A - z_B$. Primes denote differential with respect to z. K_A is set to zero and $K_{max} \sim (4/27).(K_A + z_A K'_B)$ at $z = 1/3 z_A$.

Aircraft measurements of dew point profiles were used to define the third layer, the top 100m of the boundary layer. Within this layer diffusivity was assumed to decline linearly to zero at the top of the boundary layer.

Compared to errors in the measurements, the sensitivity of the model to the parameterisation scheme was small. The diffusivity equation was solved for the air column as it was advected across the landscape using a simple finite difference technique to give the methane concentration. The surface flux was altered until the

concentration increase across the site matched that measured by the aircraft both at the surface and at higher altitudes. In this way the mean source strength for the site was determined.

The main source of error in this approach came from uncertainty in the upwind concentrations where ground based measurements were used on some occasions to represent the whole boundary layer. The assumption that the upwind concentration will be constant for the whole upwind region can lead to uncertainties in the measured enhancement. To minimise the effect of loss on emissions to the free troposphere, only days with a well-defined boundary layer top were used.

Comparison of the CH_4 flux predicted by the model and continuous ground based measurements made during the campaign show that the fluxes produced by the model were between 2 and 4 times larger than the fluxes measured at the ground. This was partly due to the dryness of the bog near the ground based site and the natural variation in CH_4 emissions across the region. The CH_4 flux was also compared to fluxes measured at other similar bogs in Scotland using enclosure techniques. These were found to be in reasonable agreement. Overall it was found that the enhancement to the CH_4 concentration was readily measurable and that this technique produced reliable estimates of landscape scale emissions with a mean for the daytime flux of 0.91 ± 0.51 $\mu g\ m^{-2}\ s^{-1}$. This was between 2 and 4 times larger than fluxes measured at the site using curvette techniques at the surface.

A similar study was carried out in a wetland in the Loch More area in Northern Scotland in 1993 (Choularton *et al.*, 1995). Using the same experimental approach as in the Strathy Bog study, CH_4 fluxes were measured using both ground based methods and aircraft measurements with the aircraft flying a race track pattern upwind, above and downwind of the site at several different altitudes. As with the Strathy Bog experiment, the site was unusually dry for most of the campaign period, with increasing rainfall towards the end. The fluxes predicted using the aircraft data and the modelling technique previously described were slightly larger than the Strathy Bog fluxes. The fluxes measured at the ground by eddy covariance using tunable diode laser absorption spectroscopy (Choularton *et al.*, 1995) peak at a value of roughly a factor of 2 smaller than the aircraft fluxes which had typical daytimes values of 100 $\mu mol\ m^{-2}\ h^{-1}$. This is probably due to the dryness of the site around the

ground based measurements. During 1994, further ground based measurements were made at the Loch More site (Fowler *et al.*, 1994) in a range of areas that were expected to produce the anoxic conditions required for higher CH_4 fluxes. The flux measurements were found to be highly dependent on sector chosen with wetter conditions leading to larger fluxes more consistent with the landscape scale fluxes measured by the aircraft.

At the same time as the UMIST Cessna aircraft made measurements close to the main site, the C-130 Hercules UK research aircraft operated by the UK Met Office made measurements over the sea around Northern Scotland. The aim of these flights was to measure the landscape scale CH_4 flux with the Cessna and regional scale flux with the C-130. A large concentration enhancement was measured of around 100 ppbv between the upwind and downwind sections of the flight. The same modelling technique was used as before and the estimated flux found to be very similar to that found in the Strathy Bog experiment for the wetter areas.

Overall this study confirmed the conclusions from the Strathy Bog experiment that aircraft measurements could be used to calculate fluxes at the landscape scale and in this case, regional scale ranging from an area of 10^3-10^4 km^2.

1.7.2 Measurement of Regional Methane Fluxes from Agriculture

Wratt *et al.* (2001) used aircraft measurements to estimate regional CH_4 fluxes from agriculture in New Zealand, which are dominated by enteric fermentation from sheep and cattle. Aircraft measurements upwind and downwind of pastoral land were used to calculate the CH_4 flux from the region using a boundary layer box model method. Ten flask samples were collected at a range of heights from near ground to 1500 m at a distance of 5 km off the coast downwind of the study area. Similarly, samples were collected 30 km inland from the coast over the study region at a range of heights in order to determine vertical profiles for CH_4. The samples were later analysed on the ground using gas chromatography techniques. The flasks were filled at the collection rate set so that each flask corresponded to a horizontal distance greater than the horizontal scale of convective turbulent plumes of around 200 m (Stull, 1989). This ensured that high-frequency variations in the CH_4 concentration were smoothed out.

Flight days were chosen when meteorological conditions provided steady onshore winds. Balloon soundings launched at noon and midnight by the Meteorological Service of New Zealand provided the wind, temperature and humidity data with hourly wind data available at a height of 10 m.

The budget method used to estimate emissions assumes a box placed over the study area with sides parallel to the coast and a height of hundreds of metres as described in Section (1.4). Methane is assumed to be a conserved tracer and so the concentration changes within the box are determined by the net flow through the sides of the box including through the top and bottom. The mass balance within the box is given by

$$\int_V \frac{\partial \overline{C}}{\partial t} dV = -\int_S \overline{C}\,\overline{U} dS - \int_S \overline{U'C'} dS \tag{1.25}$$

where C is the concentration (g m^{-3}). $C = \overline{C} + C'$ where $\overline{C}$ is the time-averaged concentration and C' is the fluctuating component. U is the wind velocity made up of similar time-averaged and fluctuating components and S is a surface. The left hand term represents the rate of change of CH_4 mass in the box. The first term on the right-hand side is net transport into the box by the mean flow and the second term represents net transport into the box by turbulent fluxes through the box sides and top and the net source through the bottom of the box. Assuming that the concentration at the upwind and downwind sites is constant with time, that the wind speed and direction at a given height is constant throughout the box, that there is no transport through the top of the box and no transport of CH_4 parallel to the coast, Eq. (1.25) can be simplified to

$$\overline{F_{emit}} = \frac{\gamma}{\ell}\left(\int_0^{z_{max}} \overline{u}\,\overline{\rho}_{x_{inland}}\,\overline{r}_{x_{inland}} dz - \int_0^{z_{max}} \overline{u}\,\overline{\rho}_{x_{coast}}\,\overline{r}_{x_{coast}} dz \right) \tag{1.26}$$

where F_{emit} is the CH_4 source flux (g m^{-2} s^{-1}), z_{max} is the maximum height of the aircraft (m), $u(z)$ is the wind speed (m s^{-1}) at height z, $r(z)$ is the (molar) mixing ratio at height z and $\rho(z)$ is the density of the dry air (g m^{-3}) at height z. The overbar represents the average across the box between sample sites at the coast, x_{coast}, and

inland. γ is the ratio of the molecular weight of CH_4 to the apparent molecular weight of dry air and ℓ (m) is the distance between the coast and inland site. This equation allows for the increase in boundary layer depth from the coastal site to the inland site as long as the maximum height of the aircraft H is above the top of the boundary layer.

A second technique was used to estimate the CH_4 source flux using a priori estimates of the CH_4 emissions at 5 km resolution. Using the Eulerian mesoscale meteorological model RAMS to simulate the transport and dispersion of the emissions, allowed the measured mixing ratios to be compared to the modelled mixing ratios based on the *a priori* estimates. Meteorological data were provided by meteorological forecast models such as the Met Office Unified Model. Any systematic difference between the modelled and measured values could be used to improve the *a priori* emissions.

The results of two case studies, where wind conditions were ideal with uniform, steady wind flow across the region, showed that the daytime fluxes for both techniques were in reasonable agreement with the emissions inventory. The simplified budget scheme tended to produce larger estimates than the modelling technique, yet the current inventory values were within the uncertainty of the estimates for both techniques suggesting that regional emissions from agriculture could be estimated using this approach. However the CH_4 profiles indicate the existence of a CH_4 rich layer above the boundary layer which could result in a downwards flux of CH_4 through the top of the boundary layer through entrainment. This would invalidate the assumption of zero flux through the top of the box resulting in higher estimates for the source flux for these days.

Flights on the 25 May 1995 and the 8 June 1995 show the limitations of this technique when conditions are not ideal. The wind speed on these days was too low at around 2.5 m s^{-1} with the result that the wind flow was too complex across the region making the calculation of the emissions impossible with the simplified budget box model scheme. In theory, the emissions could still be derived using the modelling technique. However the RAMS model was unable to simulate the fine-scale spatial wind changes requiring higher resolution meteorological data.

The results from this study show the importance of a dispersion model in the analysis for times when conditions are non-ideal. Modelling the transport over such a small region requires a comprehensive set of local meteorological data either from measurements or higher resolution forecast model data. Modelling the transport over the country-scale should not require such high resolution data as the concentrations measured will result from the integration of sources over a much larger area and so should not be so affected by such fine-scale, local phenomena. However, high resolution data would be required to capture local effects such as a sea-breeze which could significantly affect the measured concentration. Therefore samples should correspond to several kilometres horizontally to help mitigate local effects. The assumption of negligible flux through the top of the boundary layer may not be valid and so entrainment must also be accounted for in the budget calculations. Any dispersion model used must therefore also include entrainment.

1.7.3 Inverse Modelling to Derive Methane Emissions from Agriculture

In the New Zealand study (Wratt *et al.*, 2001) discussed previously, the data from the flights in June 1995 and April 1997 were used in combination with an inverse modelling technique to determine the CH_4 emissions (Gimson *et al.*, 2003). The RAMS model was used in combination with a Lagrangian particle dispersion (LPD) model to derive the influence function, $I(\underline{x}_r,t_r|\underline{x},t)$, which links the downwind concentrations at the receptor sites x_r at time t_r to the upwind source locations x at time t. The influence function, $I(\underline{x}_r,t_r|\underline{x},t)$, is effectively a weighting which describes the influence a source location has on the enhancement to the concentration measured at the downwind receptor location. The influence function is derived by running the LPD backwards using the reverse meteorology from the RAMS model with particles released from the receptor traced backwards in time.

Using prior estimates for the emissions flux and uncertainty and the uncertainty in the concentration enhancement, a Bayesian inversion approach (Tarantola, 1988) can be used to obtain the emissions flux which optimises the fit between the modelled and measured concentration change across the sample area. This has the advantage of estimating the combined uncertainty in the final flux estimate from measurement

error, *a priori* flux estimates error and modelling errors. By combining prior flux estimates with the inverse modelling approach, uncertainty in the flux estimate should be smaller than the uncertainty in either of the individual estimates. For these two case studies, the CH_4 emission fluxes were found to be 54 ± 32 and 56 ± 54 mg m^{-2} d^{-1} which were consistent with estimates based on animal populations and per-animal emission rates.

1.7.4 Measurement of Methane Fluxes from Northern Britain

A study using the Hercules C-130 aircraft operated by the NERC Scientific Services Atmospheric Research Support Facility tried to measure the CH_4 flux for the whole of Northern Britain from anthropogenic sources as well as natural wetland emissions (Beswick *et al*, 1998). The flight took place on the 29th of November 1994 round the Northern Coastline of the British Isles to capture emissions from Scotland and Northern England. The meteorological conditions were ideal with a well-coupled westerly wind flow producing low, uniform background concentrations. Tedlar bag samples were collected from a typical altitude of 150 m with 15 profiles taken at regular intervals at heights of 15, 90, 150 and 300 m. The bag samples were later analysed on the ground using Tunable Diode Laser Absorption Spectroscopy (TDL).

The same one-dimensional diffusion model was used as in the Strathy Bog and Loch More Studies. In this case the land track for the air parcel came from the Met Office back-trajectory model using the grid references for the air parcel at 3 hour intervals. Ten tracks were calculated across Northern Britain transecting the country from west to east ranging in length from 125 to 305 km and the mean wind speed calculated for each input into the model. The boundary layer height was estimated from the temperature profile from the Hercules aircraft. The model was initialised with the CH_4 flux from the Strathy Bog and Loch More studies and adjusted until the downwind concentration matched the measured concentration.

The model was then altered to account for agricultural emissions. Because NAEI did not provide spatially disaggregated emission inventories of CH_4 at the time, a spatially disaggregated emission inventory based on the distribution of cattle, sheep, pigs and poultry and emission factors for enteric fermentation and manure

management was compiled by Sutton *et al.* (1996). The agricultural emissions were mapped onto 20 km grid squares and the CH_4 flux for each square added successively to the initial wetland flux estimate. The non-agricultural flux was then adjusted until the model concentration matched the measured concentration.

The non-agricultural emissions for Northern Scotland should be almost entirely the result of wetland emissions. Comparison with estimates from the Strathy Bog and Loch More studies found a CH_4 flux of 2-3 times and 1.5 times smaller, respectively. The bulk of the difference was attributed to two factors. Firstly, the Strathy Bog and Loch More fluxes represent a peak value with flights taken place in mid-afternoon when emissions should be at a maximum. The flux estimated in this study represents an average over a much larger area and much longer time. Secondly, the flight took place in November when emissions would be expected to be smaller due to the lower temperature.

The largest fluxes were found for Northern England where anthropogenic emissions should dominate. Model results predict that agricultural emissions should contribute as much as 12% in this area. The main sources in these areas are likely to be landfill with gas leaks from pipes also being a significant factor, both associated with areas of high population density. Coal mines may also be significant contributors.

Overall, this study showed that it is possible to derive realistic estimates for CH_4 fluxes at large scales with the estimated flux comparable to earlier studies of similar areas. By including the agricultural emission inventory it was possible to estimate the contribution from other sources along the flight track. The inclusion of inventories for other source sectors should provide a way of producing a more sophisticated estimate of the flux by allowing the contribution from each source sector to be adjusted in such a way as to provide a best-fit between the modelled and measured concentrations.

1.7.5 Calculating of Net UK Fluxes for CO_2, CO, CH_4 and N_2O

The previously described boundary layer budget technique using aircraft data has also been applied to estimate net fluxes from the UK (Fowler *et al.* 1998, 2000). A total of five flights took place in November 1994, March 1996, January 1997, May 1998 and July 1998. The flight paths for each of the flights were unique, depending

on weather conditions on the days of the flights, but 3 of these flights, January 1997, May 1998 and July 1998, shown in Figure 5 (a), (b) and (c) respectively, allowed the total flux of the whole UK to be estimated.

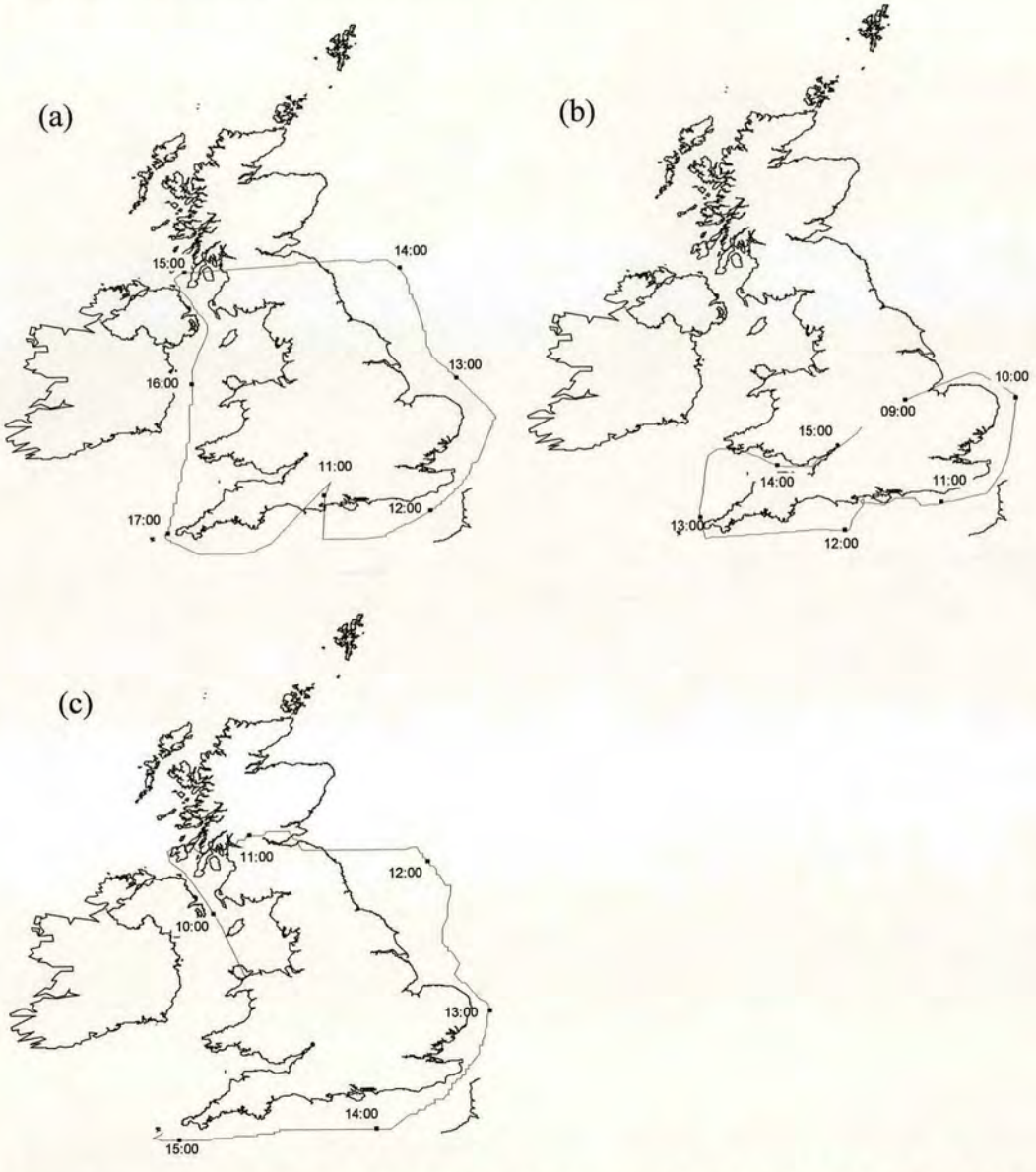

Figure 5. (a) Flight path for January 1997 flight. (b) Flight path for May 1998 flight. (c) Flight path for July 1998 flight (Fowler *et al.*, 2000).

Bag samples were collected and the sampling rate adjusted to give a sampling time of 20 s. This corresponded to a horizontal distance of approximately 2 km. Vertical profiles were taken every 100 km ranging from 50 m to 1300 m to ensure that two samples were taken from the free troposphere which was identified by the temperature and humidity profiles. These samples were then analysed on the ground using the TDL (CH_4 and N_2O), gas chromatography (CO) and an infrared gas

analyser (CO_2).

The winter flight on 28 January 1997 took place with a high pressure system centred over Northern Ireland bringing clean Atlantic air south over the UK, leaving the country over the Bristol Channel and Welsh coast. The C-130 Hercules aircraft was used to collect Tedlar bag samples that were later analysed on the ground for CO_2, CO, N_2O and CH_4. It was possible to observe the outflow from large industrial centres such as London with the main areas of outflow around the south of Wales.

The 22 May flight 1998 took place with a high pressure system centred over western Ireland producing a well-coupled northerly wind flow across the UK ideal for a boundary layer budget study. A smaller commercial aircraft operated by Air Atlantique was used for this flight partly to assess the use of a smaller, cheaper aircraft for 'round-Britain' studies. Due to the shorter flight time of the aircraft, a refueling stop at Bournemouth had to be included in the flight plan. Tedlar bag samples were collected for analysis later for 4 species, CO, CO_2, N_2O and CH_4, but technical problems with the TDL diode meant that the precision with which N_2O could be measured was not high enough to measure the N_2O enhancement from the country. Outflow was measured along the south coast with the outflow from London and Northern England identifiable as separate plumes over the English Channel.

The 7 July 1998 flight took place with a large high pressure system over the mid-Atlantic producing northerly winds over the UK with clean Atlantic air brought south over the country and outflow plumes observed over the south coast. Measurements of CO, CO_2, N_2O and CH_4 were possible for this flight allowing budget estimates to be made of all four species.

Ratios of CO/CH_4 and CO/N_2O were used as an indicator of pollution source. As described in Section (1.2.1) above, emissions of CO are dominated by fossil fuel combustion in urban areas. Rural emissions are much more significant for CH_4 and N_2O with enteric fermentation in ruminant animals and microbial activity in soils significant sources for CH_4 and N_2O respectively. Highly significant correlations ($p<0.001$) between CO and CO_2 and CO and CH_4 were observed for the January 1997 flight and May 1998 flight. Only the January 1997 produced a significant correlation between CO and N_2O. The July 1998 showed no correlation between CO and any of the 3 other species. This was caused by strong point sources for these gases with high

summer temperatures increasing microbial production of CH_4 and N_2O from landfills and soils.

The CO/N_2O ratio along the flight path ranged from 163 to 7.4 with the lowest ratios associated with outflow from Teesside where N_2O emissions were dominated by an adipic acid plant and large areas of grassland for grazing in western parts of the country. CO/CH_4 ratios ranged from 2.4 to 0.3. The lowest ratios were observed during the May and July 1998 downwind of Devon and Cornwall where livestock is the main source of CH_4.

The vertical distributions within and above the boundary layer were combined with concentration differences upwind and downwind to obtain net surface emissions. Budget studies were performed along sample back trajectories where the upwind and downwind concentrations were taken to be an average of several bag samples and a simple one-dimensional diffusion model used to estimate the surface emission along the trajectory. These were scaled up to provide an estimate of the annual emission for the whole UK.

The outflow plumes from the UK were identified by analysing the back trajectories and the elevations in concentration. From the concentration enhancements in the outflow plumes, it was then possible to get a direct measurement of the net UK daily flux which was then scaled to give an annual flux.

This approach produced very similar CH_4 fluxes to those of National Atmospheric Emissions Inventory (Salway 1998) of 3917 kt yr^{-1} for the January 97 (4675 kt yr^{-1}) and the May 98 flight (3723 kt yr^{-1}), but was smaller than expected for the July 98 flight (1183 kt yr^{-1}). The N_2O measurements produced for the January 97 flight were surprisingly large for winter emissions at 195 kt yr^{-1}, which could possibly be attributed to larger than expected soil emissions in winter. For the July 98 flight the annual flux was 305 kt yr^{-1}, about twice that of the NAEI (189 kt yr^{-1}). The May 98 flux could not be estimated due to instrumentation problems. For CO the flights produced annual fluxes of between 4229 kt to 6680 kt compared to the NAEI flux of 4641 kt. For CO_2, the estimate of a regional flux has the added complication of biogenic release and soil and plant respiration as well as uptake by photosynthesis which is highly variable in space and time. The January 1997 flight allowed the flux estimated to be attempted when these complications are at a minimum since

photosynthesis could be assumed to be negligible and soil respiration at a minimum. The measurements produced a flux of 1048 Mt annually which is 70% larger than the Salway inventory (593 Mt). This result is however consistent with the higher energy demand statistics and so a direct measurement of CO_2 is possible. However the two other flights, which took place during the summer, also produced larger fluxes of CO_2 than the NAEI (891 Mt and 994 Mt). These elevated fluxes may indicate that some sources are not included in the emission inventory. It should also be noted, however, that the quality of the CO_2 analysis was somewhat compromised due to CO_2 diffusion into the Tedlar bags which were stored in the laboratory for up to two weeks before analysis. From this experience, it was clear that, to obtain satisfactory results, CO_2 analysis had to be conducted as soon as possible after the flight and that the bags had to be stored at ambient concentration. The results for each flight for all four chemical species are summarized in Table 6.

Table 6. Summary of UK emissions (kt yr^{-1}) for 3 'round-Britain' flights compared to NAEI estimate for 1998.

	NAEI (kt yr^{-1})	Jan 97 (kt yr^{-1})	May 98 (kt yr^{-1})	July 98 (kt yr^{-1})
CO	4641	6680	4975	4229
CO_2	593000	1048000	891000	994000
CH_4	3917	4675	3723	1183
N_2O	189	195		305

The surface fluxes of CH_4 were also calculated using the simple one-dimensional diffusion model which was solved for an air parcel advecting across the UK with a constant CH_4 source over land and zero surface flux over the sea. The parcel was divided into 3 layers as with the previous model with a different eddy diffusivity in each layer. Again, as with the previous model, the diffusivity tended towards zero at the top of the boundary layer, which was defined using radiosonde ascents, and so entrainment was not accounted for. For a transect of a few hours this approximation is reasonable for a boundary layer with a well-defined temperature inversion. The air parcel was initiated with an upwind concentration taken to be the average of several bag samples collected close to the start of the trajectory and the surface flux was allowed to iterate until the downwind concentration matched the measured concentration (also an average of several bag samples). For the January 1997 flight

the CH_4 fluxes for 10 back trajectories were calculated, averaged and scaled to give an average emission rate for the whole of the UK. This scaled to a daily value of 3249 kt yr^{-1}, consistent with the NAEI estimate and the simple boundary layer budget estimate. The largest emissions were found for trajectories crossing London and the south east England conurbation. This suggests that emissions from landfill from these areas are the likely source of the CH_4 emissions. For July 1998 the advection time for an air parcel across the UK was longer than 24 hours. This introduced complications as diurnal changes in the boundary layer had to be accounted for in the model. At night (9 pm to 5 am) a stable nocturnal boundary layer depth of 100 m was assumed. This broke down as the sensible heat flux increased following dawn and the CH_4 within it started to mix through the depth of the daytime boundary layer. The model was run with constant surface flux to find a total flux producing an average CH_4 flux for the country of 2.5 kt day^{-1}, which scales to 910 kt yr^{-1}. This was consistent with the simple boundary layer budget estimate. The fluxes for the western trajectories across Wales and the West Country were the largest in this day with emissions from livestock the likely source. Further east the predicted fluxes are smaller. The concentrations predicted by the agricultural emission are larger than those measured which suggests that the CH_4 concentration was being diluted by the exchange of boundary layer air with the free troposphere, a process not accounted for in the model.

The conclusion that can be drawn from this study is that the technique of estimating UK fluxes of pollutants using aircraft sampling of boundary layer air upwind and downwind is feasible, but improvements need to be made to the modelling to more fully describe the meteorological processes taking place and better simulate the spatial variability of the emissions rather than simply assuming a constant flux. Where summer flights are included it will also be important to include some contribution from biogenic sources and sinks to the CO_2 flux. While not able to draw any firm conclusions about the UK budgets of the species measured, these flights provided some evidence to suggest that the N_2O emissions and the CO_2 emissions may have been larger for these years than the NAEI inventory suggests.

1.7.6 Trace Gases Regional Scale Fluxes Using Bayesian Inverse Analysis

The CO_2 Budget and Rectification Airborne study (COBRA-2000) used in-situ CO_2 measurements by systems onboard the University of North Dakota's Cessna Citation II aircraft to derive regional scale surface CO_2 fluxes (Lin *et al.*, 2004). A modified non-dispersive infrared gas analyser onboard the aircraft was used to measure atmospheric CO_2 concentration in combination with measurements of CO_2 over a range of heights on a Tall Tower from a site in North Wisconsin.

The Stochastic Time-Inverted Lagrangian Transport (STILT) model was used to model the transport of parcels of air between the downwind receptor sites and upwind locations. The model was driven with forecast meteorology from the Eta model to derive the upwind sampling locations for receptor sites in North Dakota. Meteorology from the Eta Data Assimilation System (EDAS) was used in the post flight analysis.

A Bayesian inverse analysis technique was used to derive the surface flux using a combination of the measured upwind and downwind concentrations and influence and footprint functions obtained from the STILT model. Post flight, the STILT model was used to transport ensembles of particles backwards in time using the EDAS data, producing the influence function $I(\underline{x}_r,t_r|\underline{x},t)$ and the footprint function $f(\underline{x}_r,t_r|\underline{x},t)$ that links the receptor concentration $C(\underline{x}_r,t_r)$ to the upwind surface fluxes $F(\underline{x},y,t)$ and concentration at the upwind locations $C(\underline{x},t)$, where $\underline{x}$ is some upwind location at time t and $\underline{x}_r$ is the receptor location at time t_r.

$$C(\underline{x}_r,t_r) = \sum_{i,j,m} f(\underline{x}_r,t_r \mid x_i,y_i,t_m).F(x_i,y_i,t_m) + \sum_{i,j,k} I(x_r,t_r \mid x_i,y_j,z_k,t_0).C(x_i,y_j,z_k,t_0) \quad (1.27)$$

where $F(x_i,y_j,t_m)$ is the surface flux (g s^{-1}) at location (x_i,y_j) at time t_m and $C(x_i,y_j,z_k,t_0)$ is the initial concentration at time t_0. The first term in the right-hand side represents the concentration change at the receptor from the surface fluxes during time interval t_0 and t_r. The second term on the right-hand side of the equation represents the

contribution to the receptor concentration from advection of tracers from the initial upwind concentrations.

Expressed in matrix formulation where an underline denotes a vector and a double underline denotes a matrix, Eq. (1.27) becomes

$$\underline{C} = \underline{\underline{f}}\,\underline{F} + \underline{\underline{I}}\,\underline{C_{to}} \tag{1.28}$$

By measuring the concentration at the upwind locations, C_{to}, and the downwind receptor locations, $\underline{C}$, and using the STILT model to derive the footprint matrix $\underline{f}$ and the influence matrix $\underline{I}$, it is possible to constrain the surface flux $\underline{F}$. Dividing by the time between the upwind and downwind measurements, τ, gives a vector of footprint weighted fluxes, $\underline{fF}/\tau$, which is a direct estimate of the surface tracer flux if it is invariant within the footprint.

Alternatively, a Bayesian inverse analysis can be used to optimise the surface flux using a least squares approach such that the modelled concentrations are consistent with the observed concentrations. This approach can capture the variability of the flux in space and time. The surface flux is dependent on a number of parameters such as temperature, vegetation etc. These are included in the surface flux as a set of parameters $\underline{\lambda}$ so the flux $\underline{F}$ becomes $\underline{F(\lambda)}$. Assuming $\underline{F}$ is linearly dependent on $\underline{\lambda}$ then $\underline{F(\lambda)}$ equals $\underline{\Phi\lambda}$. Using prior estimates of the values of $\underline{\lambda}$ and their associated errors and the measurement error, a Bayesian method can be used to derive the posterior optimised estimates for $\underline{\lambda}$ and their related uncertainties.

For CO_2 the net flux can be separated into the flux from photosynthesis and respiration and the flux from fossil fuel burning. The flux from the fossil fuel burning can be derived using CO measurements to calculate the CO flux directly using Eq. 1.28 and dividing by the time between the upwind and downwind measurements. The flux for CO is then multiplied by the ratio of fossil CO_2:CO enhancements at the receptor square from the emissions inventories for North America. Since the fossil CO_2:CO emissions ratio vary very little spatially while the fossil CO_2 emissions can vary over very small spatial scales, using the CO measurements gives a better estimate of combustion than using the CO_2 inventory directly.

Having calculated the CO_2 flux from fossil fuel burning, the Bayesian method could then be used to calculate the flux from the biosphere. The flux was assumed to be the sum of temperature dependent respiration and radiation dependent photosynthesis with the prior estimates for the fitting parameters based on eddy covariance measurements.

The results for the biosphere CO_2 flux were compared to one-dimensional estimates that use vertical profiles over a single location to calculate the flux. These were taken over the same location as the 2 flights. The result for the first flight of -17.5 μmol m^{-2} s^{-1} was consistent with one-dimensional approach which produced a flux of -11.8 μmol m^{-2} s^{-1}. However the results of the second flight show a net uptake of -2.3 μmol m^{-2} s^{-1} while the one-dimensional method showed a net release of 0.97 μmol m^{-2} s^{-1}. This demonstrates the usefulness in using upwind and downwind observations to measure regional scale fluxes directly. They provide a useful constraint on regional fluxes when attempting to scale up from small scale experiments. By combining small-scale observations with the aircraft data using the Bayesian inverse technique, it was possible to significantly reduce the errors in the prior estimates for the daytime uptake of CO_2 derived using eddy covariance methods alone.

The COBRA study showed that it was possible to use aircraft measurements of upwind and downwind concentrations to calculate the CO_2 flux from a region but unlike CH_4 which can be treated as a conserved tracer, some account must be taken for the biogenic sources and sinks.

1.7.7 Regional CO_2 Budget – CarboEurope Experiment Strategy

The CarboEurope Regional Experiment Strategy (CERES) aimed to quantify the carbon sources and sinks of a region using both aircraft CO_2 concentration and flux measurements over the whole area and concentration and flux measurements at fixed stations (Dolman *et al*, 2006). In May and June of 2005 in Les Landes, France, concentration measurements were made both in and above the ABL using an aircraft platform over an area of 250 by 150 km which were coupled to flux measurements made at the surface using a modelling / data assimilation framework. The sample region was in the south west of France and is bounded on one side by the Atlantic

Ocean. It is predominantly plantation forest and agricultural land of both crop and grazing pastures.

Preliminary results were presented for four days when a strong anticyclone produced weak winds and a deep ABL. The aircraft attempted to follow a balloon that was released upwind of the region to obtain a Lagrangian flight path. The CO_2 concentration variation observed by the aircraft was assumed to be due to uptake and emissions because of weak wind flow. Measurements implied that agricultural land was a larger sink than forest. The surface stations near summer crop sites showed small surface fluxes while the CO_2 flux observed over the forest was larger than expected given the large CO_2 concentration observed.

The STILT model was used to provide trajectories and footprints for the air measured at the surface stations and provide a better understanding of the discrepancies between the fluxes and concentrations. This revealed that the air measured over the forest had been advected along the coast where there was little uptake of CO_2 producing larger concentrations while the air measured near to the crops had been advected over land with active vegetation areas resulting in air depleted in CO_2. Taking either the concentration measurements from the aircraft or the surface flux measurements on their own would have resulted in incorrect conclusions about the fluxes at the surface. Both land surface fluxes and regional scale measurements need to be taken into account along with consideration of the synoptic flow in order to make a correct interpretation.

The results of the CERES study show that taking either the concentration at several locations as representative of the regional flux or up-scaling from local flux measurements to regional estimates produced inaccuracies in the distribution of the sources and sinks and that the best results could be produced by taking both approaches into consideration.

1.8 Objectives of this Work

1.8.1 Motivation for the Aircraft Measurements of Chemical Processing and Export Fluxes of Pollutants Over the UK Project (AMPEP)

As discussed in Section 1.2, the current UK NAEI emission inventory is compiled using a 'bottom up' approach that involves summing the contribution from individual sources and using statistical activity data and estimated emission factors to compile the inventory. This approach relies on assumptions that sources within the same sector have the same emissions factor and requires sufficient knowledge of source numbers and activity data. These assumptions lead to inherent uncertainties in the annual emissions and very few attempts have been made to validate this approach using a 'top down' method to calculate the budget directly.

A boundary layer budget approach using aircraft measurements can provide a direct measurement of the emissions flux (Gallagher, 1994; Fowler, 1998). Upwind and downwind concentration measurements can be turned into inflow and outflow fluxes with the difference the flux emitted. With suitable conditions to minimise entrainment at the top of the boundary layer and and provide steady, well-coupled winds with a uniform background concentration; a simple box model can be used to calculate the emitted flux which scaled gives annual emissions. The flights discussed in section (1.6.5) demonstrated the suitability of the approach. However, a larger programme with an increased number of 'round-Britain' flights during different times of the year is required to provide a more robust top-down estimate of the annual emissions.

Further analysis with a Lagrangian particle dispersion model (the Numerical Atmospheric Modelling Environment, NAME) of the UK Met Office, and complete 3D meteorology from the Met Office Unified Model, would provide better validation of the emissions inventory and produce alternative estimates for the annual emissions.

In addition, the use of the better equipped new UK BAe-146 research aircraft operated by the Facility for Airborne Atmospheric Measurement, a joint venture between the UK Natural Environment Research Council and the UK Met Office, would provide measurements of a much larger range of compounds. In this way the budget work on the non-reactive radiatively active gases could be extended to reactive sulphur and nitrogen compounds, including aerosols.

1.9 Overview of the AMPEP Project

For this purpose the AMPEP project was initiated as a boundary layer budget study that uses a mass balance approach to quantify import, export and emission terms of a larger range of pollutants, using 108 flight hours. AMPEP was a collaboration between a number of partners including the Centre for Ecology and Hydrology (CEH) Edinburgh, the University of Manchester, the Met Office and FAAM. AMPEP was funded as part of the Polluted Troposphere (PT) directed Research Programme of the UK Natural Environmental Research Council (NERC).

1.9.1 AMPEP Objectives

In detail the objectives of AMPEP were:

a) To measure the gas/particle partitioning and oxidation state of S and N compounds in the emission plumes from UK source regions with different relative source strengths.
b) To measure the net export flux of S and N compounds from the UK under a range of atmospheric conditions as a test of the long-range transport, chemistry and deposition models in current use.
c) To deduce the spatially disaggregated and total UK source strength of the radiatively active gases CH_4 and N_2O directly from mass balance measurements in the UK boundary layer upwind and downwind of the UK coast.
d) To measure the UK and regional net emission, import and export fluxes of CO_2 and the seasonal variation directly from boundary layer flux studies, to quantify the combustion and biogenic components and their seasonal and spatial variation.
e) To measure the net UK emissions of a range of toxic metals (Pb, Cd, Zn, Cu, speciated Hg) in a range of surface conditions and seasons.
f) To interpret the measurements using atmospheric transport models to provide mass budgets and validate UK spatially disaggregated emission inventories.

A second project within PT, the Flux Experiment (FLUXEX) project run by the University of East Anglia (UEA), shared a similar experimental approach to AMPEP but focused on a different range of species including halocarbons, hydrocarbons, NO_x

and NO_y. It was therefore decided that the two projects would collaborate, sharing aircraft time and data.

1.9.2 AMPEP Methodology

The full range of species measured during the campaign is listed in Table 7 along with the equipment used and the institute responsible. A complete list of the data collected by FAAM as part of the core measurements including temperature, pressure and height can be found at http://www.faam.ac.uk/public/instrumentation.html.

Table 7. Species measured during the AMPEP campaign with the sampling method used and institute responsible for the collection.

Data	Instrument	Operating Institute
CO	AL5002 Carbon Monoxide instrument	FAAM
CO_2	Tedlar Bag / off-line IRGA analysis	CEH Edinburgh
CH_4	Tedlar Bag / off-line TDL analysis	CEH Edinburgh
N_2O	Tedlar Bag / off-line TDL analysis	CEH Edinburgh
CO_2, CH_4*	Tunable diode laser	Univ. of Cambridge / NPL
NO, NO_2, NO_x	TECO 42 chemiluminescence instrument	FAAM
Ozone	TECO 49 UV photometric instrument	FAAM
Aerosol Composition	Aerosol Mass Spectrometer	Univ. of Manchester
Aerosol Physics	PCASP, CPC	FAAM / Univ. of Manchester
Halocarbons	Whole Air Sampler (WAS) Bottle	UEA / Univ. of York
Hydrocarbons	Proton Transfer Reaction Mass Spectrometer	UEA
NO, NO_2, NO_y	NOxy 4 channel chemil-uminescence analyser	UEA
SO_2	SO_2 analyser	FAAM / CEH Edinburgh
Major ions, HNO_3, HCl, NH_3	Filters	CEH Edinburgh

* Instrument trials, data compromised and not yet made available.

Logistic constraints related to the aircraft operation meant that some of the AMPEP objectives could only be partly addressed:

i) The aircraft became available 18 months later than planned.
ii) Unforeseen costs in the certification of new equipment meant that several instruments that were originally planned could not be implemented on the aircraft, including an infrared gas analyser for CO_2, a TDL for NH_3 and a Hg analyser.
iii) Costs involved in the re-certification after each role change, meant that the AMPEP flights were confined to one main flight window between May and September 2005 and thus do not provide full annual coverage.

The main flight window for the AMPEP project was between May and September 2005 inclusive with a second shorter window in September 2006. During this period several other projects were also vying for time on the aircraft. With the aircraft based in Cranfield in Bedfordshire and the suitability of different projects very dependent on the weather the teams from the different projects worked on an 'on-call' basis ready to mobilise at very short notice when a particular project was given the go ahead. Weekly conference call meetings took place every Friday morning with the aim of drawing up a rota for the following week based on forecast data from the UK Met Office. In practice, decisions could often not be made so far in advance and the final decision was delayed to the day before the flight.

The particular conditions most suitable for an AMPEP flight were westerly winds to ensure a relatively constant background concentration with a well-coupled wind flow and a temperature inversion at the top of the boundary layer. Because the wider aims of the project included the measurement of aerosol species, it was also important that there was no or little rain over the country during the flights to prevent the wash-out of particles from the atmosphere. In practice it was difficult to get the ideal conditions so compromises had to be made on some occasions to ensure enough flights took place.

Once a project had been given the go ahead, a flight plan was submitted based on the meteorological conditions. Using forecast data from the Unified Model and the NAEI 1 km CO emissions; the locations of the main outflow plumes from the larger urban centres could be predicted using the NAME model. This allowed the selection of

profiles locations which would not interfere in capturing the main UK outflow. The flight plan could be altered during the flight if fuel reserves allowed. This typically meant that runs could be extended to better capture the outflow of air from the UK.

The flight time of the aircraft was around 5 hours, which was not long enough for a complete circumnavigation of the whole country. On several occasions the flight time was extended by stopping to refuel however there were still restrictions on how late the aircraft could return to Cranfield airport. To shorten the flight time and ensure that the main outflow from the UK was well characterised; the measurement of the background air was compromised. It was assumed that the background concentration would be constant across the whole inflow region and that by sampling only a section of the background air, the whole of the inflow could be captured. With a westerly wind flow this is a not unreasonable assumption given that air from the Atlantic should be clean and well-mixed. This approach does not account for Ireland, however emissions of all 4 species from Ireland are small compared to the UK and so should not significantly affect the budget estimates (McGettigan *et al.*, 2007).

Tedler bags (1 litre) were used to collect air samples at a frequency of 1 per minute during downwind sections of the flight path and 2 per minute upwind. The aircraft travels at a typical speed of around 400 km $hour^{-1}$, so the horizontal distance travelled per air sample is therefore approximately 3 - 4 km. The samples were analysed on the ground within 2 days of the flight. An infrared gas analyser (Model 7000, LICOR, Cambridge, UK) was used for CO_2 analysis and tunable diode laser absorption spectroscopy (TDLAS, Aerodyne Research Inc., Billerica, MA, USA) for N_2O and CH_4. The detection limit of the LICOR for CO_2 is 0.2 ppm and for the TDLAS for CH_4 and N_2O; 0.5 ppb and 0.1 ppb respectively. Therefore the enhancement to the background concentration is easily measurable for all 3 species. CO was measured onboard the plane at 1 Hz with an Aero-Laser GmbH AL5002 Fast Carbon Monoxide Monitor. This has a detection limit of < 2 ppbV which is within the acceptable limit to measure the CO enhancement.

The layout of the aircraft is shown in Figure 6. The bag filling took place at the rear port side of the aircraft at the aft core console with the Tedlar bag storage moved to the position of the baggage store shown in the diagram. Air from an inlet at the front of the aircraft as shown on Figure 7 was pumped to the rear bag filling position to

prevent contamination by exhaust from the engines. Figure 8 shows the inside of the aircraft as seen from the bag filling position.

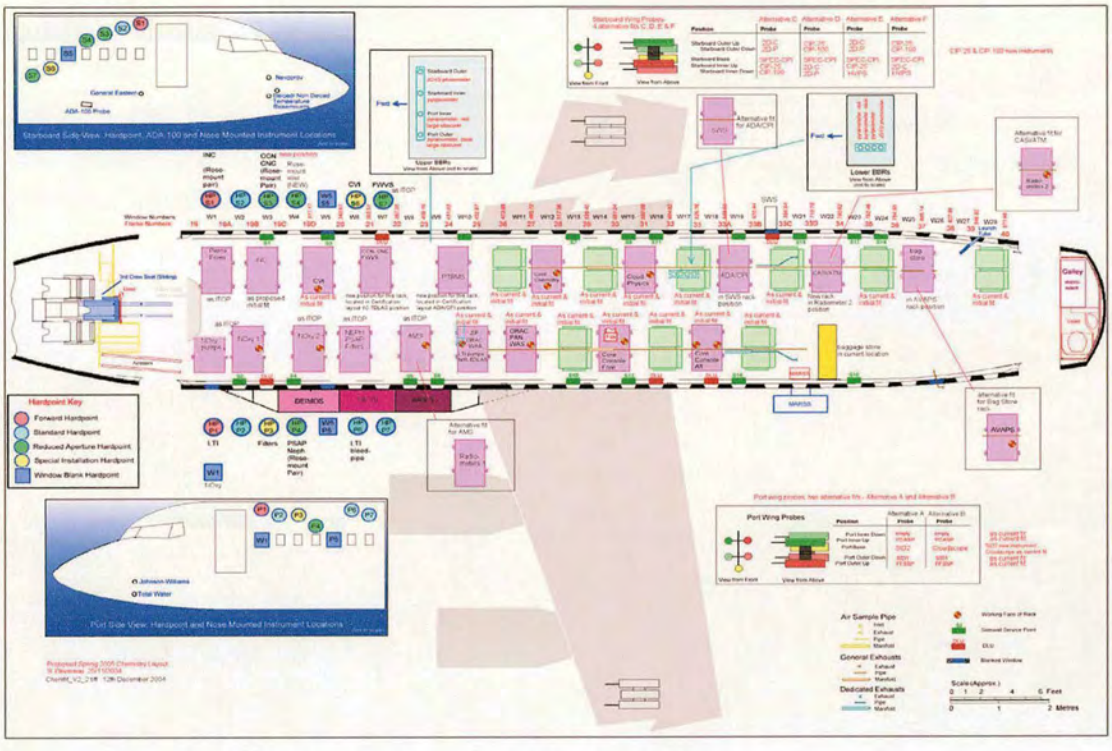

Figure 6. Layout of FAAM aircraft during AMPEP campaign.

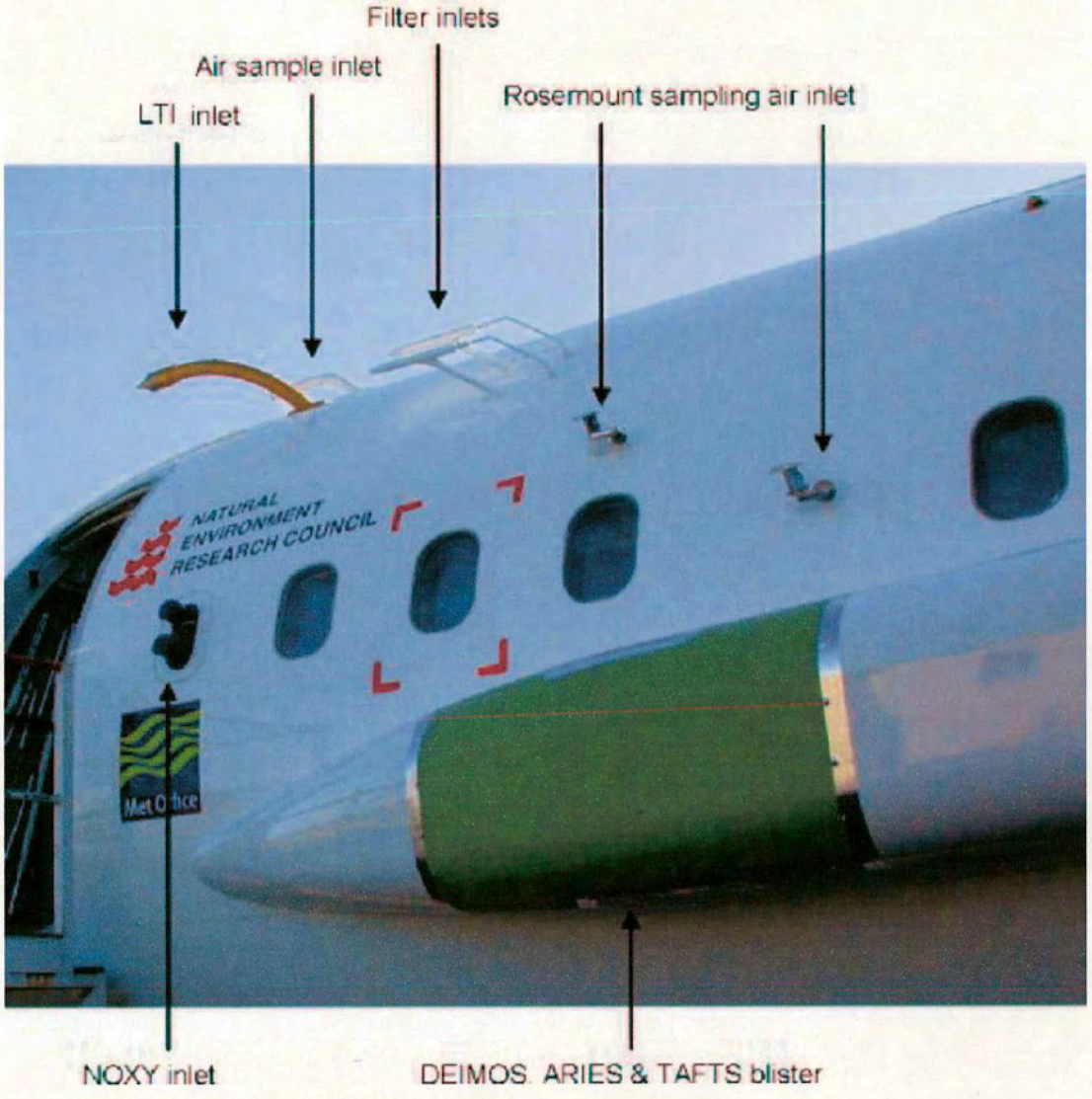

Figure 7. Sampling inlets on the upper port side of the aircraft.

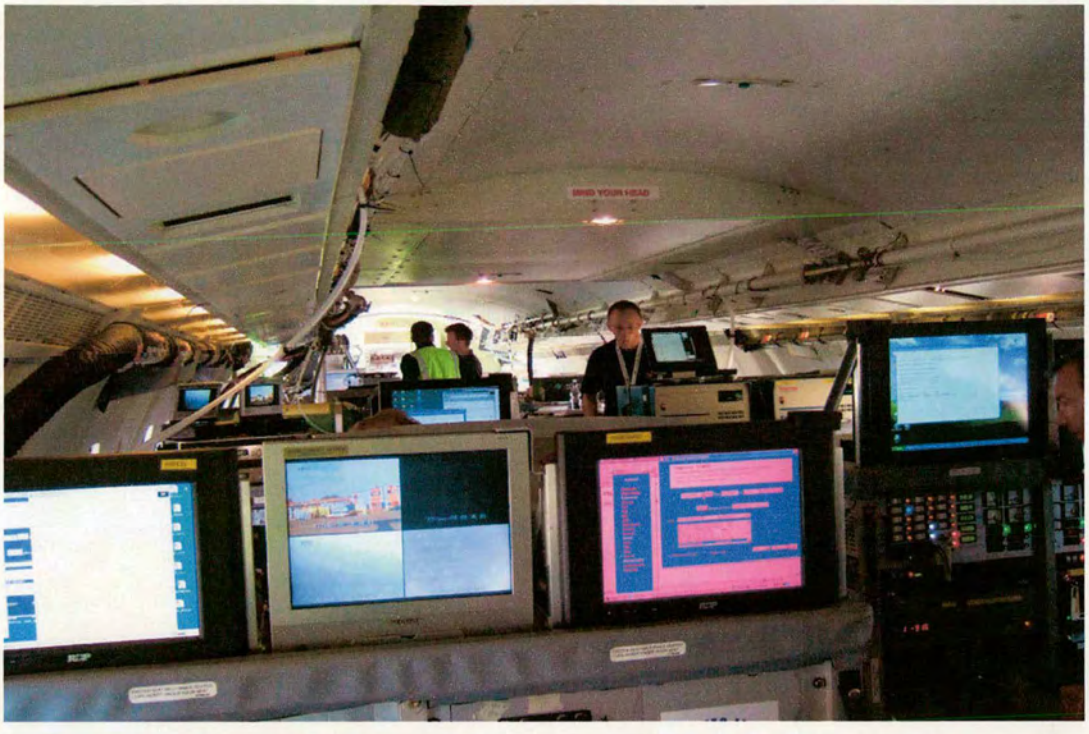

Figure 8. Inside of aircraft as seen from bag filling position.

1.9.3 Thesis Objectives

The work described in this thesis focuses on the analysis of four non-reactive species: CO, CO_2, CH_4 and N_2O and the gas/aerosol partitioning of SO_2/SO_4^{2-} and $NO/NO_2/HNO_3/NO_3^-$ systems to derive oxidation rates in UK plumes. The thesis also discusses work done in collaboration with UEA on estimating budgets and spatially disaggregated emissions for Halocarbon species. In detail the objectives of this thesis are:

i) to provide operational forecasting for plume transport for the 'round-Britain' flights by running an atmospheric transport model in forecasting mode for CO,
ii) to take Tedlar bag samples during 'round-Britain' flights and analyse these on the ground for CO_2, CH_4 and N_2O, in collaboration with other colleagues at CEH,
iii) to derive country emission budgets for CO, CO_2, CH_4 and N_2O using three different approaches: a simple boundary layer approach, a forward modelling approach and an inverse modelling approach, allowing for terrestrial sinks of CO_2,
iv) to assess the consistency between the split of emissions between sectors predicted by current emission inventories and implied by the 'round-Britain' flights,
v) to derive the spatial structures of the emissions of CO, CO_2, CH_4 and N_2O from the UK through inverse modelling and compare with current emission inventories,
vi) to analyse the gas / aerosol partitioning of SO_x and NO_x in industrial and urban plumes of the UK and to derive oxidation rates.

As such this work addresses the AMPEP objectives (c) and (d), using modelling techniques as described under objective (f), and partially addresses AMPEP objectives (a) and (b).

1.10 Conclusions

Current country-scale emissions, produced according to the globally used IPCC methodology, are derived using a 'bottom-up' approach which is open to uncertainties from under or over estimation of source numbers, incorrect emission factors and exclusion of unknown sources. The UK provides an opportunity to verify the IPCC methodology using a 'top-down' boundary layer budget technique to derive emissions. Using an aircraft to circumnavigate the UK in a westerly wind flow, measurements of greenhouse gases upwind and downwind of the country can be used to measure the emitted flux directly. By scaling up the daily flux totals and averaging the results of number of flights, an annual estimate is produced.

Previous work on boundary layer budgets of large regions demonstrated the ability of this technique to produce realistic flux estimates over large areas. In Fowler (2000), a technique used previously at a regional scale over wetlands by Gallagher *et al.* (1994), Choularton *et al.* (1995) and Beswick *et al.* (1998), was applied to the whole UK. The measurements from the flights were used to derive country-scale emissions for CO, CO_2, CH_4 and N_2O which were compared to the emissions derived using the bottom-up approach of the NAEI. For CO, CH_4 and N_2O the technique was shown to be successful, however CO_2 emission estimates were significantly larger than expected suggesting that errors were made in storing the samples over too long a period. For the AMPEP campaign is was therefore crucial that the analysis of the samples is carried out as soon as possible after the flights and samples are analysed within a day of collection.

In understanding the measurements it was also shown to be important to used 3-D meteorological atmospheric transport models which can track the flow of air over the country and help in understanding the origin of emissions (Wratt *et al.*, 2001 and Dolman *et al.*, 2006). The use of models help in identifying the outflow plumes and interpreting the measurements by revealing where complex meteorology may influenced measurements such as inflow or re-circulated air. The inclusion of emission inventories as input into the models can also distinguish between the different source sectors helping in understanding where emissions may be under or over estimated (Beswick *et al*, 1998).

Finally inverse modelling was shown to be a powerful technique for providing top-down flux estimates (Ryall *et al.*, 2000, Manning *et al.*, 2003, Manning *et al.*, 2006, Gimson *et al.*, 2003 and Lin *et al.*, 2004). Using 3-D Atmospheric transport models to determine the origin of sampled air and the relative influence on the measurement, iterative fitting techniques can by used to optimise the fit between the measured and modelled concentrations by altering the emissions from the source regions. This produces spatially disaggregated maps of the emissions and regional/country-scale emission estimates which can be compared to the NAEI 'bottom-up' maps.

Chapter 2 Models

2.1 Requirements of Models

An atmospheric transport model was needed in AMPEP to assist in the analysis of the data and pre-flight planning to forecast the location of the main outflow plumes to help determine the flight path. Post flight analysis included validation of the current emission inventories and making new estimates of the total budget for the UK. For this comparison, model derived concentrations based on the current inventory were required. The model was also used to estimate the current total budget by altering emissions from the current inventory to produce a best-fit between modelled and measured data.

The model therefore had to be able to simulate emissions at a high resolution using the current NAEI emissions as input data. It had to be able to simulate the mixing of the pollutant through the ABL and the capping inversion at the top of the ABL. It also had to be able to simulate the transport of the pollutant across the country based on the wind trajectory data for the day of the flight requiring input data from a weather prediction model such as the Met Office Unified Model.

The output from the model includes the concentration at the position and time of each bag sample collected on the aircraft. The resolution in both space and time had to be high enough to capture the characteristics of the outflow, i.e. at a resolution approximately equal to the horizontal distance of each Tedlar bag sample of 3-4 km.

For the analysis of the CO_2 data, the model had to include photosynthesis and respiration and therefore required land type data and meteorological data to determine the radiation flux. It also had to be able to cope with negative values for the concentration, i.e. concentration below the baseline value, in the event that the sink strength is greater than the source strength in some areas.

There are two possible types of model that would be suitable for this analysis; a Eulerian type model or a Lagrangian type model. A Eulerian model uses a fixed grid as a reference system while a Lagrangian model uses the moving system as a reference. A Lagrangian model follows the evolution of a particle over time and can be used to predict the dispersion of a pollutant in a known flow. This approach

assumes that the concentration at any one point results from the superimposition of all sources and sinks that could affect it and is described by equation (Thomson, 1987)

$$\overline{C(\underline{x},t)} = \int_{\Omega_s} S(\underline{x}_0,t_0)\,p(\underline{x},t \mid \underline{x}_0,t_0)\,d\underline{x}_0 dt_0 \qquad (2.1)$$

where $C(\underline{x},t)$ is the concentration (g m^{-3}) at a point and the overbar represents the ensemble average, not the time average. $S(\underline{x}_0,t_0)$ is the source strength (g m^{-3} s^{-1}) at location $\underline{x}_0$ at time t_0, $p(\underline{x},t|\underline{x}_0,t_0)$ is the probability density function with respect to x and t (m^{-1}), i.e. the probability that a particle passing $(\underline{x}_0,t_0)$ passes at $(\underline{x},t)$, and Ω_s is the ensemble of all source locations.

Ideally the model should be able to cope with complete three-dimesional meteorology and simulate not only the mixing in the ABL due to convection and turbulence but also entrainment at the top of the ABL. The UK Met Office Model, the Numerical Atmospheric Modelling Environment (NAME), a Lagrangian particle dispersion model, fitted the modelling requirements needed for AMPEP. NAME uses the complete three-dimensional meteorology from the UK Met Office Unified Model and is able to simulate emissions at 5km resolution. The Fine Resolution Atmospheric Multi-Pollutant Exchange (FRAME) model from CEH Edinburgh is a statistical Lagrangian dispersion model. It uses wind trajectory data from European Centre for Medium-Range Weather Forecasts (ECMWF) to transport single air columns with a fixed boundary layer height across the UK. FRAME is a statistical model that uses average wind trajectory data for a whole year to predict annual values and so had to be adapted to be able to model one-off events. It does not include any crosswind dispersion between the columns or complete three-dimensional meteorology but it does have a higher vertical resolution than NAME.

Both models were tested using data from previous 'round-Britain' flights to determine if they were able to simulate individual days adequately enough to reproduce the measured concentrations.

2.2 FRAME - Fine Resolution Atmospheric Multi-Pollutant Exchange

The atmospheric transport model FRAME (Fine Resolution Atmospheric Multi-Pollutant Exchange) transports a column of air across the model domain using a Lagrangian approach. It simulates emission, chemistry and wet and dry deposition within the air column as it travels across an 860 × 1220 km grid at 5 km resolution.

The air column contains 33 layers with top boundaries at 2, 4, 6, 10, 25, 50, 100, 150, 200 m, and thereafter at 100 m steps up through the mixing layer. Vertical diffusion through the layers is described by K-eddy diffusivity. The exchange of material through the layers is determined by the equation

$$\frac{\partial c}{\partial t} = -\frac{\partial}{\partial z}\left(K_z \frac{\partial c}{\partial z} \right) \tag{2.2}$$

where c is the concentration (g m^{-3}) and t is time (s). The vertical diffusivity K_z (m^2 s^{-1}) is a function determined by the stability of the mixing layer, the height in the mixing layer and the time of day. It is assumed to increase linearly up to a specified height and thereafter remain constant to the top of the ABL (Singles, 1996).

The daytime height of the boundary layer is calculated using the model of Carson (1973), which calculates the growth of the layer due to heat flux from the surface and the entrainment of stable air from above. The night-time height is calculated using Pasquill stability classes of the ABL.

FRAME was initially developed to assess the long-term annual mean NH_3 surface concentrations and NH_x deposition over the UK (Singles, 1996). It uses a statistical approach, using straight-line trajectories that cross the domain in a specified wind direction with an average wind speed, starting at different times of the day. The results are combined statistically to reflect the annual frequency of the wind flow from each direction. It includes parameterisations for deposition and sulphur and nitrogen chemistry. These aspects of the model are not needed for the analysis of the previous flight data as the species measured were non-reactive on the timescale considered here, however a full description can be found in Fournier *et al* (2004). The

model also allows conserved tracers CO, N_2O and CH_4 to be emitted into the column and mixed through the boundary layer without any chemistry or deposition.

The FRAME code was optimised and a parallel version developed using High Performance Fortran which took advantage of the fact that each trajectory runs independently of any other. This allows the trajectories to run simultaneously on different processors, significantly shortening the runtime of the model (Fournier *et al.*, 2002). However while this approach is suitable for a statistical model, it limits the model's ability to simulate one-off events as it makes it impossible to include any interaction between individual trajectories without significantly altering the structure.

For the purposes of this study, the model needed to be able to simulate the meteorological conditions of individual days. Straight-line trajectories were therefore not suitable and so the model was adapted to permit curving trajectories. A routine was added that would calculate in advance the path of the trajectory across the model domain based on back trajectory data for a point of interest at a particular time. The model was adapted to allow the column to spend varying amounts of time in each grid square to reflect changing wind speed and direction and allow the trajectory to start at a specified time. The boundary layer height could be set to a constant value derived from radiosonde data for the day of interest or some other source.

In order to calculate budgets every grid square in the domain must be covered by a column once and only once. This meant that the wind trajectory used had to remain constant across the whole model domain and travel in such a way that trajectories could run parallel to each other across the domain without passing through a grid square previously entered by another trajectory or missing out grid squares between 2 adjacent trajectories. Figure 9 (a) shows an example of a 2 parallel trajectories crossing over each other. A routine was developed to calculate a trajectory based on these criteria using the initial back trajectory data. The final trajectory is an approximation to the initial back trajectory that replicates the actual trajectory as closely as possible while still meeting the criteria required for budget estimates as shown in Figure 9 (b). This therefore means that the model is limited in how well it can simulate conditions of individual days requiring a well-coupled and relatively straight wind flow. Due to the constraints of the parallel structure of FRAME, it is also unable to simulate mixing of air between air columns.

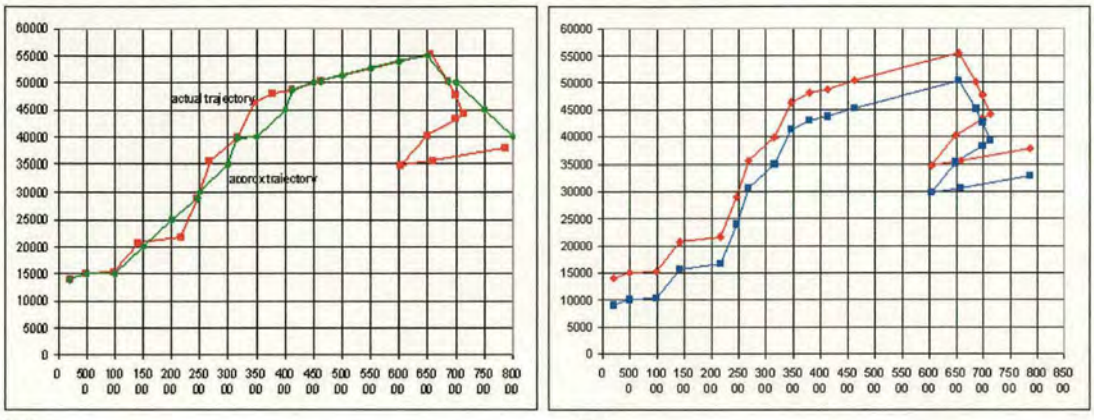

(a) (b)

Figure 9. (a) Plot showing the overlapping of parallel trajectories in FRAME domain. (b) Plot of approximate trajectory compared to actual trajectory.

2.3 NAME - Numerical Atmospheric Modelling Environment

NAME is a Lagrangian dispersion model, using three-dimensional synoptic meteorology from the Unified Model (Cullen, 1993) to transport 'particles' of air. It uses a random walk technique to move the particles taking account of the mean wind flow, the wind meander and turbulence using values based on empirical profiles of the real boundary layer. The wind data from the Unified Model is available at 3 resolutions from 3 versions of the model. Global at 6 hourly intervals at 90 km horizontal resolution, regional at 3 hourly intervals at 50 km horizontal resolution and mesoscale at 1 hourly intervals and 16 km horizontal resolution.

The NAME model can run in backwards or forwards mode. In forwards mode particles are transported across the model domain simulating the motion of air over a defined time period. The particles in the model can represent passive tracers which simulate un-reactive pollutants which are carried by the model unchanged or can represent non-passive tracers which can be altered by chemical and deposition processes resulting in a change in the characteristics of the particles.

In the model setup, a number of parameters are defined to customise the model run to the particular conditions of the time frame being simulated. These include the window of the model run and the meterological input files, the emission sources

which for the AMPEP runs are the NAEI emissions maps and the timestep of the model which is chosen to be small compared to the Lagrangian timescale τ_ω.

At the start of each time-step in the model, a set of particles is released for each emission source. The NAME sources file containing the source details can define multiple releases with each source defined separately. Parameters include the x, y and z coordinates and dimensions of the source, the start and end time of release, the release rate and weighting for winter or summer traffic cycle. It is also possible to define the shape of the release; either ellipsoid, cuboid or point source. To account for the shape of the release, a random perturbation is added to the x, y, and z coordinates of the particles. The function used to calculate the perturbation depends on the shape of the source, ensuring that the new particles are spread throughout the whole source volume.

For each particle, including particles released in previous timesteps, the model loops through a number of schemes to apply any changes to the particle characteristics. For example changes in mass due to deposition or radioactive decay or changes in position due to convective cloud systems. The particles are then advected according to the meteorological conditions defined in the setup files, turbulence profiles based on conditions in the boundary layer, empirically derived parameters and random perturbations. Collectively these represent the mean wind velocity, turbulence and, taking the form (Ryall *et al.*, 1998)

$$x_{t+\Delta t} = x_t + [u(x_t) + u'(x_t) + u_t'(x_t)]\Delta t \tag{2.3}$$

where x is the particle position vector (m), $u(x_t)$ the wind velocity vector (m s^{-1}), $u'(x_t)$ the turbulent velocity vector, $u_t'(x_t)$ the velocity vector for low frequency horizontal meandering and Δt the timestep (s). For the turbulence and meander the expression for the horizontal velocity component is

$$u'_{t+\Delta t} = u'\left(1 - \frac{\Delta t}{\tau_u}\right) + \left(\frac{2\sigma_u^2 \Delta t}{\tau_u}\right)^{\frac{1}{2}} r_t \tag{2.4}$$

where σ_u^2 is the horizontal turbulence velocity variance (m s^{-1}), τ_u, the horizontal Lagrangian timescales (s) and r_t is a random Gaussian variable of zero mean and variance of 1. This expression represents the previous motion of the particle and a new random perturbation to the velocity vector. The turbulence vertical velocity component is

$$\varpi'_{t+\Delta t} = \varpi'\left(1-\frac{\Delta t}{\tau_\varpi}\right)+\left(\frac{2\sigma_\omega^2\Delta t}{\tau_\varpi}\right)^{\frac{1}{2}} r_t + \frac{\Delta t}{\sigma_\varpi}\frac{\partial \sigma_\varpi}{\partial z}\left(\sigma_\varpi^2+\varpi_t'^2\right) \tag{2.5}$$

where σ_ω^2 is vertical turbulence velocity variance and τ_ω is the vertical Lagrangian timescales. The vertical velocity component includes a term to prevent particles collecting at levels of small σ_ω where the turbulence varies with height (Ryall *et al.*, 1998).

For turbulence, the vertical profiles of σ and τ are determined from empirically derived expressions combined with the meteorological data from the Unified Model of boundary layer depth z_i (m), friction velocity, u_* (m s^{-1}), convective velocity ω_* (m s^{-1})and surface heat flux, H_s (W m^{-2}). The Monin-Obhukov length, L, is used to determine the stability of the atmosphere with the stable boundary layer velocity variances calculated using

$$\sigma_u = \sigma_v = 2.0u_*\left(1-\frac{z}{z_i}\right) \tag{2.6}$$

$$\sigma_\omega = 1.3u_*\left(1-\frac{z}{z_i}\right) \tag{2.7}$$

and the Lagrangian timescale by

$$\tau_u = \tau_v = 0.07\frac{z_i}{\sigma_v}\left(\frac{z}{z_i}\right)^{\frac{1}{2}} \tag{2.8}$$

For an unstable boundary layer the velocity variance is calculated using

$$\sigma_u = \sigma_v = \left[0.4\omega_*^2 + \left(5 - 4\frac{z}{z_i} \right) u_*^2 \right]^{\frac{1}{2}} \tag{2.9}$$

$$\sigma_\omega = \left[1.2\omega_*^2 \left(1 - 0.9\frac{z}{z_i} \right) \left(\frac{z}{z_i} \right)^{\frac{2}{3}} + \left(1.8 - 1.4\frac{z}{z_i} \right) u_*^2 \right]^{\frac{1}{2}} \tag{2.10}$$

and the Lagrangian timescale by

$$\tau_{u,v,\omega} = 2\sigma_{u,v,\omega}^2 / C_o \varepsilon \tag{2.11}$$

where C_o is a universal constant and ε is the dissipation rate of turbulent kinetic energy ($m^2\ s^{-3}$). In a convectively unstable boundary the turbulence profiles are non-Gaussian so the stochastic equation

$$\omega'_{t+\Delta t} = \omega_t + at + \left(C_o \varepsilon \Delta t \right)^{\frac{1}{2}} r_t \tag{2.12}$$

is used to account for the skewed velocity distribution. The coefficient a represents the drift and is a function of σ_ω and ε both of which are measurable. The term $(C_o\varepsilon)^{1/2}$ represents the diffusion.

For the meander, the velocity variances are calculated using estimates from observational data from the Met Research Unit at Cardington (Maryon, 1997)

$$\sigma_v^2 = \sigma_u^2 = 2\kappa u_{10} T_f \tag{2.13}$$

where u_{10} is the 10 min wind and κ is a constant which depends on the time interval between wind fields T_f. The turbulence in the free troposphere is constant with values of: σ_u, = 0.25 m s^{-1}, σ_ω = 0.1 m s^{-1}, τ_u =300 s and τ_ω=100 s to represent low turbulence.

The advection scheme also includes a parameterisation for entrainment between the boundary layer and the free troposphere. If the turbulent vertical velocity in the boundary layer is sufficiently large compared to the variance and the variance in the boundary layer is sufficiently large compared the variance in the free troposphere a particle will cross into the free troposphere. That is if the quantity Arg^2 is negative a particle will not cross into the free troposphere and if Arg^2 is positive it will, where

$$Arg^2 = \frac{\omega'^2_{old}}{\sigma^2_{\omega,old}} + ln\frac{\sigma^2_{\omega,new}}{\sigma^2_{\omega,old}} \tag{2.14}$$

and *old* and *new* represent past and present values. A particle may also be transported into the free troposphere by a convective cloud system if the cloud base is below 300hPa. The simplified scheme in NAME randomly reassigns a particle somewhere between the surface and cloud top with a probability $(\Delta t/3600)$ × convective cloud fraction (Ryall *et al,* 1998).

Once all the particles have been advected, the model loops through other selected schemes such as chemistry. This requires the mass of particles in each grid square in each layer of the model to be converted into concentrations. The model applies any changes due the selected process and the newly calculated concentrations in each grid square and layer are assigned back to particles. The model moves onto the next time step, looping through the same process until the model run is complete outputting selected parameters such concentration at the spatial and temporal resolution defined in the model setup.

In backwards mode the transport of the particles is reversed. The loss processes can not be simulated in backwards mode so all chemistry and deposition processes are switched off. For a sample location of interested, particles are released at a constant rate for a time period reflecting the length of the sample window. The particles are then transported across the model domain using the same expressions as the forward mode but with the mean wind velocity components reversed. The output is a footprint showing where the air measured originated and the relative influence of each grid square on the measured air sample.

2.4 Analysis of Previous Flight Data with FRAME and NAME

In order to determine the suitability of the models for the analysis of the AMPEP data, both were tested with the data from a previous 'round-Britain' study (Fowler, 2000) as described in section (1.6.5). Data from 3 flights on the 28th January 1997, 22nd May 1998 and 7th July 1998 was used and the models were tested using emission inventories of CO, CH_4 and N_2O. The model concentrations were compared to the measured values to determine how well the model could simulate the transport of emissions across the country on these 3 days. Only the results for CO are shown below as this is the most reliable inventory and the species that the models should perform best with.

2.4.1 Model Setup

For FRAME, for each bag sample location, a 30-minute resolution back trajectory was obtained from the European Centre for Medium-Range Weather Forecasts (ECWMF) through the British Atmospheric Data Centre (BADC). The emissions for N_2O and CO are from the National Atmospheric Emissions Inventory (Salway, 2000) at 5km resolution. The CH_4 emissions are from the Centre for Ecology and Hydrology Edinburgh.

The model domain is covered for each trajectory producing a concentration map that is an average of the results for the wind trajectory for each sample location. The boundary layer height is an average value derived from Met Office radiosonde data from across the country on the day of the flight. The concentration at the bags sample locations are those for the relevant trajectory at the appropriate grid square and height.

NAME ran with mesoscale meteorological data from the UM at 16 km spatial resolution and 1 hour temporal resolution for the 5 days up to and including the day of the flight. The emissions for CO and N_2O were also from the NAEI and the CH_4 data from CEH Edinburgh. The time step in the model was set to 900 s to minimise the run time and the position of each sample requested as hourly time-series for the entire model run at heights of 200, 400, 600, 900, 1400, 1600, 1900 and 3000 m.

From these time-series, the concentration to the nearest hour could be obtained for each sample as an average over the appropriate vertical layer.

2.4.2 Results for Previous Round Britain Flight on 28th January 1997

The outflow plume on this day is between Wales and Devon (Figure 10 (a) and (b)). Air entering the northwest is swept back over the country and exits on the southwest.

The two models perform very differently. FRAME is very restricted in its ability to approximate the wind direction and here the wind trajectories curve too much for the model. We therefore see the outflow on the south west coast (Figure 10 (a)). This is shown in Figure 11(a) as the small peak between 17:00 and 17:45. We can also see FRAME has grossly underestimated the concentrations of this flight.

NAME performs much better. From Figure 11 (a) we can see how the model reproduces the flow across the country. There is a small peak to the south of London which the model fails to capture. It also fails to predict the peak off the north east of England, where the plume does not reach as far into the North Sea as the measurements suggest. However it does manage to reproduce the main outflow, although it underestimates the southern half of the plume from 16:40 to 17:00 (Figure 11 (a)) and slightly overestimates the northern half from 16:10 to 16:40.

The scatter plot (Figure 11 (b)) shows the concentrations predicted by the model against the measured concentration. It is clear that NAME is far better at reproducing concentrations measured in the bag samples than FRAME with FRAME greatly underestimating the concentration in the outflow plume. The correlation coefficient for FRAME and the measured concentration is 0.11 while for NAME it is 0.62.

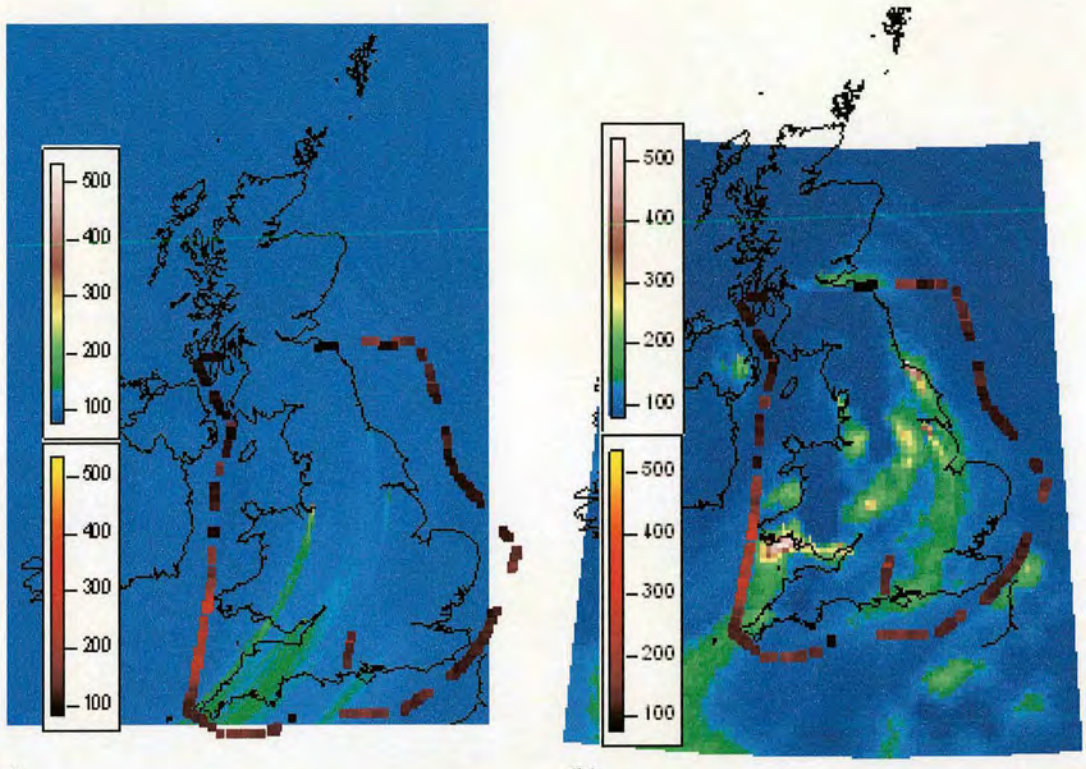

(a) (b)

Figure 10. (a) CO concentration (ppb) output from FRAME model for 28/01/97. Overlaid are the measured CO concentrations (ppb) for each Tedlar bag sample at the sample position on flight path. (b) CO concentration (ppb) output from NAME model for 28/01/97. Overlaid are the measured CO concentrations (ppb) for each Tedlar bag sample at the sample position on flight path. Upper scale is model concentration, lower scale is measured concentration.

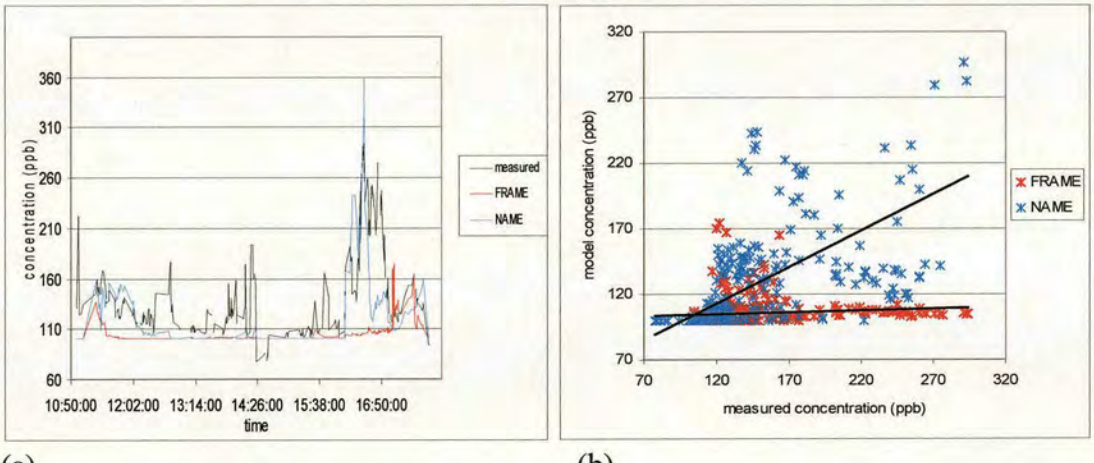

(a) (b)

Figure 11. (a) CO Measured, FRAME and NAME concentrations (ppb) for 28/01/97. (b) CO model against measured concentrations (ppb) for 28/01/97.

2.4.3 Results for Previous Round Britain Flight on 22nd May 1998

The outflow is spread across the south coast with a small outflow plume from the southwest between Devon and Wales (Figure 12 (a) and (b)). There is a large peak in the plume towards the southeast with a larger peak to the west of this peak. There is a peak slightly to the east. FRAME predicts the outflow across the south coast (Figure 12 (a)) managing to capture the location of the main peak between 11:00 and 11:30 (Figure 13 (a)) but overestimating the concentration.

From the NAME concentration maps (Figure 12 (b)) we can see that much of the air from the north east of England appears to be advected across the UK and is being exported largely from the south west. The small peak in the concentration to the southeast measured on the day of the flight is reproduced by NAME (Figure 13 (a)) though it fails to capture the width of this plume. NAME captures the most easterly of the peaks but underestimates the larger peak to the west. NAME manages to capture the peaks to the west of the Devon.

Figure 13 (b) shows the modelled concentration plotted against the measured concentration. It can be seen that FRAME significantly overestimates the concentration while NAME is better able to reproduce the measured data. The correlation coefficient between the measured and modelled concentrations for FRAME is 0.11 and for NAME is 0.49. Again NAME outperformed FRAME appreciably, managing to broadly reproduce the structure of the outflow.

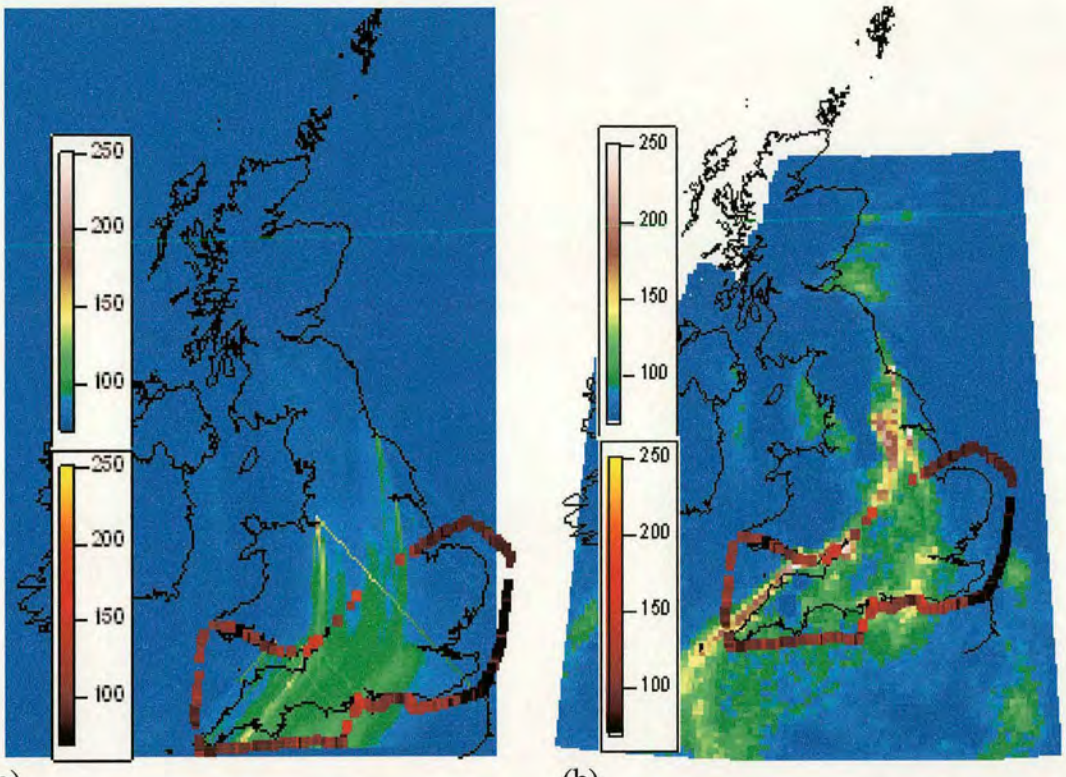

(a) (b)

Figure 12. (a) CO concentration (ppb) output from FRAME model for 22/05/98. Overlaid are the measured CO concentrations (ppb) for each Tedlar bag sample at the sample. (b) CO concentration (ppb) output from NAME model for 22/05/98. Overlaid are the measured CO concentrations (ppb) for each Tedlar bag sample at the sample position on flight path. Upper scale is model concentration, lower scale is measured concentration.

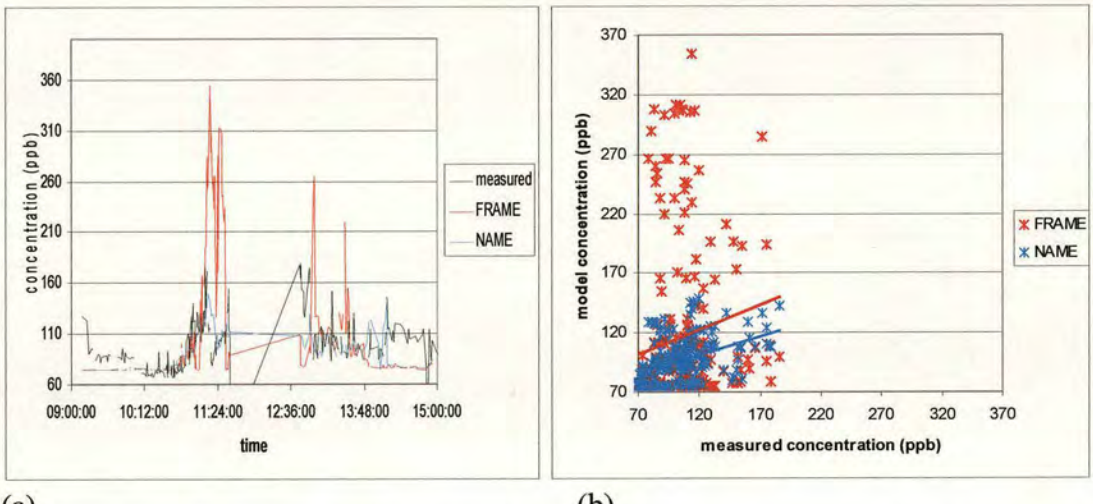

(a) (b)

Figure 13. (a) CO measured FRAME and NAME concentrations (ppb) for 22/05/98. (b) CO model against measured concentrations (ppb) for 22/05/98.

2.4.4 Results for Previous Round Britain Flight on 7th July 1998

The outflow plume is concentrated to the south west of the country, with a small peak south of London. FRAME produces a broad outflow plume across the south coast (Figure 14 (a)). This plume captures part of the outflow though it misses the main peak. NAME (Figure 14 (b)) reproduces the westerly peak in the outflow but not the peak to the east. It predicts a slight enhancement at the London outflow but this is much smaller than the measured enhancement. The concentration plots of NAME reveal the air advecting across from the south east of England and being exported out of the south west with some enhancement to the concentration to the south of London. This broadly matches the measured profiles.

Figure 15 (b) shows the modelled concentrations against the measured concentrations and shows that NAME is better able to reproduce the measured concentrations. The correlation coefficient between the measured and FRAME concentrations is 0.19 and for NAME is 0.54. NAME performs significantly better than FRAME at reproducing the outflow plumes from the UK.

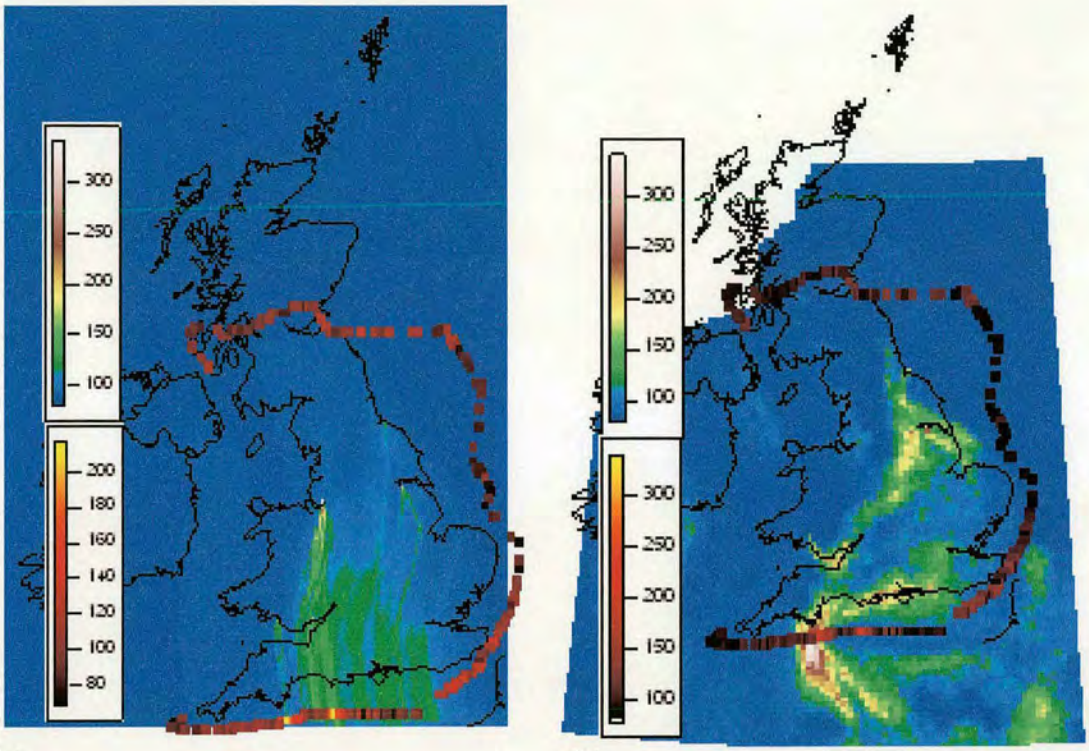

(a) (b)

Figure 14. (a) CO concentration (ppb) output from FRAME model for 07/07/98. Overlaid are the measured CO concentrations (ppb) for each Tedlar bag sample at the sample position on flight path. (b) CO concentration (ppb) output from NAME model for 07/07/98. Overlaid are the measured CO concentrations (ppb) for each Tedlar bag sample at the sample position on flight path. Upper scale is model concentration, lower scale is measured concentration.

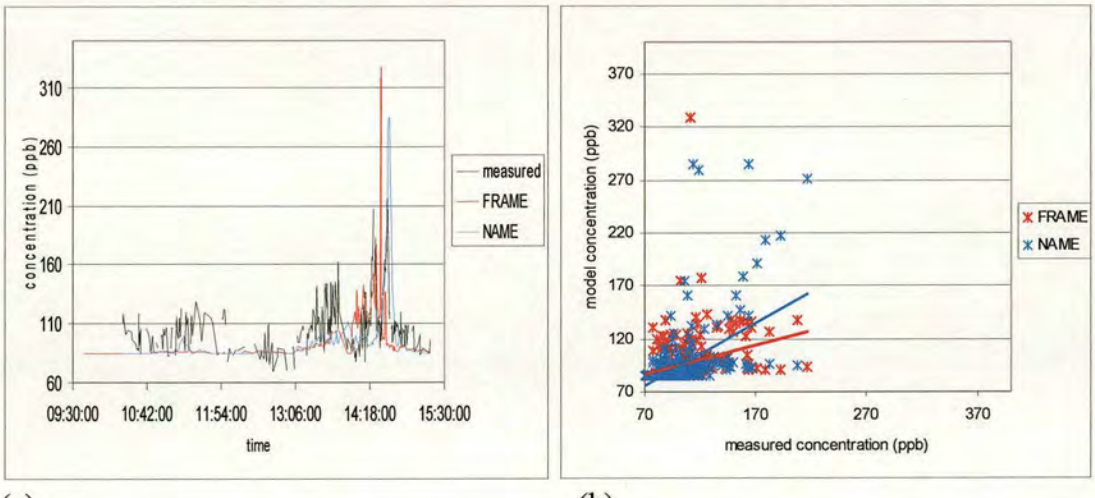

(a) (b)

Figure 15. (a) CO measured, FRAME and NAME concentrations (ppb) for 07/07/98. (b) CO FRAME and NAME model against measured concentrations (ppb) for 07/07/98.

2.4.5 Conclusion

Both FRAME and NAME manage to broadly reproduce the outflow for the May 1998 and July 1998 flight. For the 28th of January 1997, FRAME is unable to cope with curvature in the wind trajectories and so fails to even predict the region of the main UK outflow. The lack of cross wind dispersion in the model is a major problem, resulting in 'streaks' in the concentration maps where emissions from a particularly large source are forced to remain within a single 5km x 5km column of air as it travels across the county.

NAME performs significantly better overall, managing to capture much of the structure in the outflow plumes for CO. The model itself is far better suited to analysing one-off events as it uses complete three-dimensional meteorology and also allows for loss of the tracer to the free troposphere.

The approximate meteorology approach used by FRAME was unable to model individual days satisfactorily and so it was decided that only NAME would be used for the analysis of the AMPEP data. While the chemistry and vertical resolution of FRAME would have made it useful in analysing reactive species, it failed to simulate the transport of emissions well enough to justify its use.

2.5 Inclusion of Biogenic CO_2 Signal in NAME

The flights for the AMPEP campaign took place over the spring and summer months of 2005/2006. It was therefore important to include some estimate of the biogenic sources and sinks for CO_2. The CO_2 flux from a plant canopy is a balance of a positive flux (source) from respiration and a negative flux (sink) from photosynthesis. Photosynthesis is proportional to the photosynthetic photon flux density (PPFD) up to some saturating value which is controlled by the photosynthetic capacity producing an asymptotic response function. In a canopy, less radiation reaches lower leaves, leaving them PPFD limited when leaves at the top of the canopy have already reached a saturating level of PPFD. The response of the CO_2 flux to PPFD is therefore less rapid than would be the case for a single leaf. The respiration is a combination of

respiration from leaves, shoots, roots and from microorganisms in the soil. In practice, it can be difficult to measure these fluxes separately with respiration included in the overall net CO_2 flux. Respiration however occurs even when no photosynthetically active radiation is available. This is known as dark respiration which can be measured separately at night. Combining the dark respiration term with the photosynthetic response function produces a response function of CO_2 flux to PPFD that is a rectangular hyperbola (Ruimy *et al.* 1995).

2.5.1 Photosynthesis

To calculate the photosynthesis rate an empirical function is used which uses the photosynthetic photon flux density and parameters derived for measured data for three classes of vegetation, forest, grassland and crops (Ruimy *et al.*, 1995).

The first step is to calculate the photosynthetic photon flux density. The Campbell-Donatelli (Donatelli *et al.*, 1998) model calculates global radiation using atmospheric transmittance and potential radiation.

$$I_{E\,doy} = tt_{doy} I_{p\,doy} \tag{2.15}$$

Where I_{Edoy} is the estimated radiation for day of the year measured in (MJ m^{-2}), I_{Pdoy} is the potential radiation for day of the year (MJ m^{-2}), and tt_{doy} is the transmissivity for day. The transmissivity of day is calculated from temperature data (from UM) and a set of parameters taken from the RadEst 3.00 model specific to a location using the equation (Donatelli *et al.*, 1998).

$$tt_{doy} = tt_{clear}[1 - exp(-bf(T_{avg})\Delta T_{doy}^{2} f(T_{min}))] \tag{2.16}$$

Where tt_{clear} is the clear sky transmissivity, T_{max} is the maximum temperature (°C), T_{min} is the minimum temperature, T_{avg} is measure of the average temperature over the day calculated using $(T_{max} + T_{min})/2$, ΔT is a measure of the variation in temperature

over the next two days calculated using $T_{max,doy} - (T_{min,doy} + T_{min,doy+2})/2$ and $f(t_{avg})$ and $f(T_{min})$ are functions of T_{avg} and T_{min} respectively where

$$f(T_{avg}) = 0.017 \exp(\exp(-0.053 T_{avg})) \tag{2.17}$$

and

$$f(T_{min}) = \exp(\frac{T_{min,doy}}{T_{nc}}) \tag{2.18}$$

where T_{nc} and b are empirical parameters where the values depend on location. Their effect on I_E is small compared to latitude so average values for the UK are used.

The potential radiation is a product of the location and the day of year.

$$I_P = \frac{1}{\pi}\{117.5(1 + 0.033\cos(0.017 i_d - 0.055))$$

$$(h_s \sin(\phi_{lat})\sin(\phi_{dec}) + \cos(\phi_{lat})\cos(\phi_{dec})\sin(h_s))\} \tag{2.19}$$

where ϕ_{lat} is the latitude, ϕ_{dec} is the declination angle where

$$\phi_{dec} = a\sin(0.398 \sin^* 4.87 + 0.017 i_d + 0.033 \sin(6.224 + 0.017 i_d)) \tag{2.20}$$

and

$$h_s = a\cos(-\tan(\phi_{dec})\tan(\phi_{lat})) \tag{2.21}$$

where i_d is day of year (Donatelli *et al.*, 2001).

A simple sin function is used to turn the radiation for the day into hourly values

$$I_{EH} = A_{ds} \frac{\pi I_{Ei}}{2 D_t} \sin(\frac{\pi S_t}{D_t}) \tag{2.22}$$

where I_{EH} is the hourly radiation, D_t is the day length, S_t is hours since sunrise and A_{ds} is a scaling constant to convert from MJ m^{-2} day^{-1} to J m^{-2} s^{-1}. A conversion factor of 2.07 is used to convert from J m^{-2} s^{-1} to μmol m^{-2} s^{-1} (Ting, 1987). This assumes that 45% of the available solar radiation is suitable for photosynthesis and a conversion factor of 4.6 to convert from W m^{-2} to μmol s^{-1} m^{-1}.

Figure 16 shows the hourly radiation values predicted by the model compared to data measured at 54 Met Office stations in the UK. The correlation coefficient between the two series is 0.73. Although the model is able to broadly reproduce the measured data, as can be seen from Figure 16, it tends to underestimate the radiation, particularly at larger values. Table 8 shows the correlation coefficients between the model and measured radiation for each flight day. The model better predicts the measured values towards the end of the flight window when the days are shorter and peak radiation value is lower. The model performs better at lower radiation and so tends to underestimate the photosynthesis at peak times.

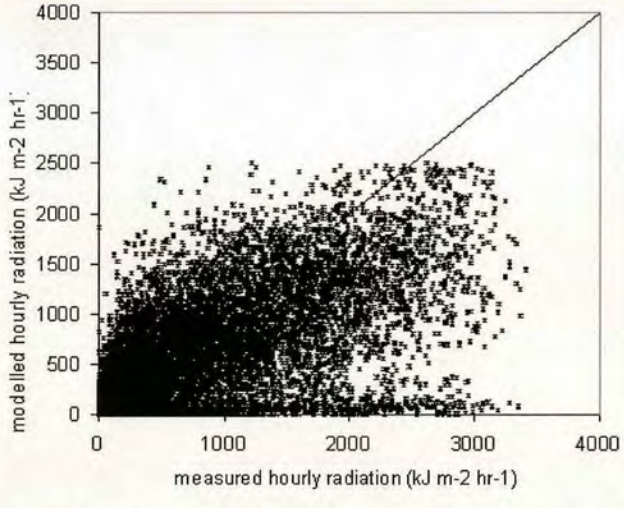

Figure 16. The modelled hourly radiation values (kJ m^{-2} s^{-1}) for locations of 54 MetOffice stations against the Metstation data.

Table 8. Correlation between UK MetOffice station hourly radiation data model prediction.

Date	correlation
05/05/2005	0.73
25/05/2005	0.72
14/06/2005	0.70
14/07/2005	0.78
19/07/2005	0.74
20/07/2005	0.72
03/08/2005	0.63
04/08/2005	0.83
07/09/2005	0.84
19/09/2005	0.47
21/09/2005	0.82
26/09/2005	0.78
29/09/2005	0.85

Ruimy and Jarvis (1995) suggest a hyperbolic response function to radiation. They collected together CO_2 flux data over canopies from a large number of data sets for different vegetation classes. The data sets were grouped together according to the conditions in which the data was collected and were required to satisfy certain criteria. For the NAME model, instantaneous data sets, i.e. data in half hour or hourly average values, were most suitable. The photosynthetic flux response was modelled using the following formula;

$$F_{eco} = \frac{\alpha Q F_{\infty}}{\alpha Q + F_{\infty}} - R \qquad (2.23)$$

where F_{eco} is the net ecosystem flux (μmol s^{-2} m^{-2}), Q is the photosynthetic photo flux density (μmol s^{-2} m^{-2}), α is the apparent quantum yield (i.e. df/dQ at $Q = 0$), R is the dark respiration ($F = 0$) (μmol s^{-2} m^{-2}), and F_{∞} is F_{eco} at saturating Q (Q =1800 μmol s^{-2} m^{-2}).

Statistical regression analysis was applied to the radiation response curves for the data sets for different vegetation classes and the above model fitted to the data with the constraints that $0< \alpha<1$, $F_{\infty} > 0$, $R > 0$. The non-linear coefficient of determination, r^2, was calculated using an iterative procedure to produce the best fit. The mean values of grouped instantaneous data sets of α, F_{∞} and R for the three vegetation classes; forest, grassland and crops, are used in combination with land

cover data from Land Cover Map 2000 (LCM2000) to estimate the net photosynthetic flux.

Once incorporated into NAME, the model underestimated the draw down on concentration due to photosynthesis with the decrease in concentration in the measured data not reproduced by the model. Therefore the values of α, F_∞ and R calculated for the upper 10% of flux values were used instead. That is the largest 10 % of CO_2 flux values in eight equal size classes of PPFD which were analysed using the same technique as before. The model concentrations were found to better match the measured concentrations. The values of α, F_∞ and R used in NAME for each land class, are shown in Table 9.

Table 9. Values of α, F_∞ and R used in NAME for 3 land classes, forests, grasslands and crops.

Land Class	A	F_∞	R
Forest	0.071	47.66	0.00
Grassland	0.044	70.09	2.90
Crops	0.084	57.30	0.084

Data from the Land Cover Map 2000 from CEH Edinburgh gives the percentage of each land class in 1km x 1km grid squares. The rate in each grid square from each vegetation type is calculated and the sum used as the net flux in each grid square.

2.5.2 Respiration

The respiration term in the flux equation is a constant value. Respiration from the soil is dependent on microbial activity and increases with increasing temperature. Several empirically derived equations have been suggested to represent the increase of in soil respiration with temperature. Fang *et al.* (1999) investigated the fit between several types of equations and respiration data from incubated soil samples collected from farmland and sitka spruce sites in Scotland. They suggest an equation of the form

$$R(T) = a_R (T - T_{R=0})^{b_R} \tag{2.24}$$

where $R(T)$ is the temperature dependent respiration (μmol s^{-2} m^{-2}), a_R and b_R are empirically derived constants and $T_{R=0}$ is a temperature (°C) at which respiration totally stops. Only samples from forest and farmland are used and so the grassland respiration rate is calculated using parameters for farmland.

The equation for the photosynthetic flux is an empirical fit and the dark respiration term a combination of soil and plant respiration. In order to ensure that the temperature dependent respiration improves the CO_2 flux calculation, the model was run with both constant and temperature dependent R. The correlation coefficient between the modelled and measured data for constant R and $R(T)$ are compared in Table 10. The average correlation coefficient using $R(T)$ is slightly larger than the correlation coefficient for constant R and so it was therefore decided to use the temperature dependent respiration.

Table 10. Correlation coefficient for modelled and measured data for constant respiration and temperature dependent respiration

Flight	*R*	*R(T)*
B92	0.47	0.43
B97	-0.13	0.43
B102	0.31	0.35
B111	0.30	0.10
B112	0.66	0.67
B113	0.50	0.12
B118	0.65	0.66
B119	0.25	0.30
B126	0.26	0.38
B130	0.35	0.35
B132	0.24	0.31
B134	0.32	0.48
B136	0.30	0.21
B244	0.50	0.53
Average	0.39	0.50

It is assumed that the growing season lasts from March to October and therefore, photosynthesis is turned on in all of the AMPEP flights.

2.5.3 Implementation of Biogenic CO_2 Flux in NAME

An option is included in the NAME model to allow photosynthesis to be included. In this event, the radiation for each hour of the model run, for each grid box, is calculated before the start of the main loop using temperature data from the Unified Model.

After each time step, the masses of the model 'particles' in each grid square are summed and converted into the concentration in each grid square, in each layer of the model. The net biogenic flux is calculated in each grid box using the radiation data for the appropriate time and the percentage of each vegetation class in the grid square. This flux is converted into a change in concentration in the bottom layer of the model only. This is then added to the existing concentration, where a net uptake of CO_2 due to photosynthesis is a negative flux, and a net emission from respiration is a positive flux. Once the new concentration in each grid square has been calculated, the total mass in the square is assigned back to model 'particles'. If the concentration in the square is negative due to a net uptake of CO_2, then the mass is transported by the model as a positive value in the particle but tagged as a negative. When the concentration in each grid box is again calculated, the mass of negative value particles can be subtracted from the total to give the correct concentration. An option to assign the background concentration is included so that the output concentration in each grid box is the total concentration rather than the difference from the background. This prevents negative values for the concentration.

2.5.4 Results of Biogenic CO_2 Flux in NAME

Figure 17 (a) and (b) show the biogenic CO_2 flux across the UK as predicted by the NAME model at noon for 2 days, the 14th of June 2005 and the 29th September 2005 respectively. These represent the 2 extremes of the AMPEP data set with maximum PPFD for the June flight and minimum PPFD for the September flight. The difference between the 2 days is obvious with very little photosynthesis or respiration on 29th September making the net biogenic signal from the UK almost zero. For 14th June, the areas of peak radiation are around the agricultural areas of the south of England

where high levels of PPFD and large areas of crops and particularly grassland for grazing result in a net uptake of CO_2. Kielder Forest in Northumbria also shows up as a strong sink. Respiration from arable land along the east coast shows up as a net source of CO_2, although the strength of the source is small compared to the uptake of CO_2 in other areas.

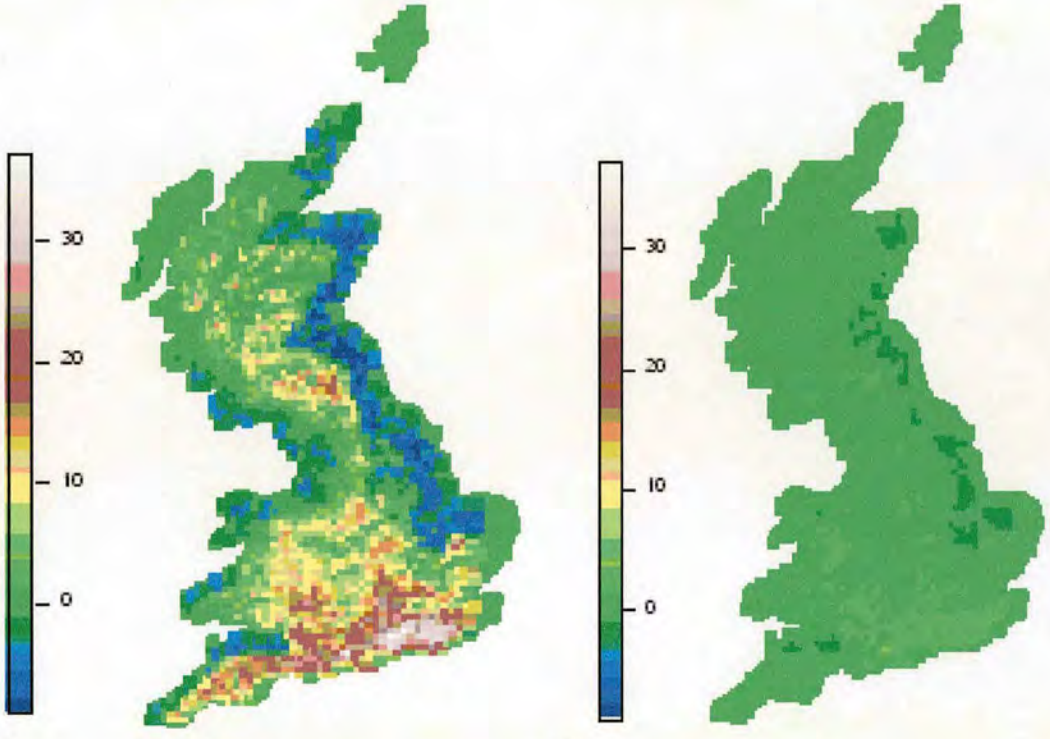

(a) (b)

Figure 17. (a) CO_2 flux (μmol m^{-2} s^{-1}) from photosynthesis and respiration in NAME model across the UK for 14/06/05 (flight B102) at noon. Positive flux represents a net sink. (b) CO_2 flux (μmol m^{-2} s^{-1}) from photosynthesis and respiration in NAME model across the UK for 29/09/05 (flight B136) at noon. Positive flux represents a net sink.

The total flux of CO_2 due to photosynthesis and respiration for the duration of the model run is also calculated. The total CO_2 flux for each flight is shown in Table 11. The average value, based on the average of monthly values is a net uptake of CO_2 of 1800 kt yr^{-1}. This is based only on the months of May to September inclusive and does not include the winter months when photosynthesis is switched off and respiration is at a minimum. Current estimates put the net annual biogenic flux at approximately 28000 kt yr^{-1} net uptake (Milne *et al.*, 2006).

Table 11. CO_2 flux for each flight scaled to yearly values (kt yr^{-1}). Negative values represent a sink and positive terms represent a source. The average is weighted to reflect the data quality of each flight. Flights are combined to give monthly values for the CO_2 flux weighted also by the data quality for each flight and the average value represents the average flux between the months of May and September.

Flight	CO_2 flux (kt yr^{-1})	Month	Monthly Average (kt yr^{-1})
B92	-220000	May	-178000
B97	-64000	May	
B102	-20900	June	-20900
B111	-400	July	42200
B112	65800	July	
B113	53800	July	
B118	42300	August	38700
B119	29200	August	
B126	168400	September	109000
B130	137600	September	
B132	113000	September	
B134	35400	September	
B136	62500	September	
B244	219600	September	
Average	33600 ± 106900		-1800 ± 108700

2.5.5 Conclusion

The biogenic flux of CO_2 varies greatly between flight days with large net uptake predicted for May (Spring) and large net emissions predicted for September (Autumn). However the uptake in the summer months is less than might be expected given the larger flux of solar radiation expected during these months with a net source predicted for July and August. The simplified scheme used to calculate the biogenic flux depends only on the temperature and the type of vegetation and the higher temperatures in the summer months produces larger respiration than photosynthesis rates. This results in net emissions when biogenic uptake should be at a peak. The scheme was chosen for speed of implentation and a more advance approach would significantly improve the biogenic flux calculation. As it is largely empirical, a sensitivity study of the parameters used could also significantly improve the flux estimates by calibrating the scheme to UK conditions.

2.6 Summary

Work was done to analyse the effectiveness of two atmospheric transport models using data from a previous round-Britain boundary layer budget study, Fowler (2000). The first model analysed was the FRAME model, a statistical Lagrangian model which transports columns of air over the UK on a fixed trajectory. Despite adaptations to the model to allow for more flexible trajectory paths, the inability of the model to mix air between columns and the limited nature of the trajectories over the UK meant the model was unable to cope with simulating individual days sufficiently well for the needs of the AMPEP campaign and was therefore not used in any of the AMPEP analysis.

The second model analysed was the NAME model of the UK Met Office which used complete 3-D synoptic meteorology of the Unified Model. By transporting individual particles of air, the model was able to capture the outflow from the UK with much greater accuracy than FRAME as it could simulate the cross-wind dispersion and complex wind flow patterns. NAME also includes a scheme to simulate entrainment and convective mixing into the free troposphere allowing the flux at the top of the box to be estimated. It was therefore decided that NAME would be used to analyse the AMPEP data.

In order to estimate all terms in the budget calculation for CO_2, it was necessary to include a scheme to calculate the biogenic flux in NAME. The scheme chosen used relatively simple formulae based on the radiation flux, temperature and a simple parameristation for CO_2 flux using three categories of plant type; grass, crops and forest. This approach allowed the scheme to be implemented in a relatively short time-scale however it was understood that a more sophisticated approach would have allowed for better estimation of the biogenic flux. The scheme used did manage to simulate uptake from photosynthesis and emissions from respiration however as it was largely dependent on temperature for calculating the radiation flux and the respiration, it was found that the uptake was underestimated in the summer months with higher temperatures resulting in disproportionally larger respiration flux than photosynthesis flux. Given sufficient time, a full sensitivity analysis would have allowed for the parameters to be calibrated to UK conditions, however despite the

failure of the scheme to sufficiently calculate the uptake, it was an improvement on the existing model which ignored the biogenic flux completely.

Chapter 3 Review of Flights

Seventeen flights were flown in total during the campaign. The majority were flown in the first flight window from April – September 2005. Two flights were flown during a second window in September 2006. Three flights have been excluded from the analysis due to unsuitable conditions. Flight B91 was flown during a south-easterly wind flow which brought inflow from continental Europe into the UK. This made the background concentration profile too complex for this study which required uniform background concentrations for reliable measurement of UK emissions only in the outflow plumes. Flight B133 was flown in a south-westerly wind flow but with stagnant air over the south east and too much influence from Continental air to reliably identify the outflow from the UK. The final flight, B247, was aimed at accurately describing the outflow from London and so does not give a picture of the whole UK. All other flights were adequate for further analysis. Table 12 gives a brief summary of the weather conditions and flight path of each flight and Table 13 summarises the species measured during the flight and the quality of the data.

Table 12. Summary of all 15 flights during the AMPEP campaign from April 2005 to September 2006.

Flight	Wind Direction	Flight Path	Comments
B91 – 21/04/05	SE	Clockwise circumnavigation of England, Wales and Southern Scotland	
B92 – 09/05/05	NNW	Clockwise circumnavigation – south and east coasts	Convective day, showers encountered during flight. Sea breeze in western Channel
B97 – 25/05/05	SW	Anticlockwise coastal transect of South and East coast of England	
B102 – 14/06/05	SW	Anticlockwise coastal transect of South and East coast of England	Showers encountered near Newcastle
B111 – 14/07/05	SW	North then Southbound transect of East Coast of England and Scotland	Background concentration estimated from northern part of leg off the Moray Firth
B112 – 19/07/05	W	North then Southbound transect of East coast of England and south Scotland	East Channel congested; shipping may be large source of pollutants. Light rain near Durham southbound.
B113 – 20/07/05	NW	Anticlockwise coastal transect of South and East coast of England	Cloudy with rain showers throughout day.
B118 – 03/08/05	W	Anticlockwise coastal transect of South and East coast of England	Brief sea-breeze observed NE of Dover. Brief showers on East coast, rain observed inland
B119 – 04/08/05	W	North then Southbound transect of East coast of England and south Scotland	
B126 – 07/09/05	SW	Anticlockwise coastal transect of South and East coast of England	
B130 – 19/09/05	SW	Anticlockwise coastal transect of South and East coast of England	Air masses encounter in English Channel and South East influenced by Continental air
B132 – 21/09/05	SSW	Anticlockwise coastal transect of South and East coast of England	Air masses encounter in English Channel and South East influenced by Continental air.
B133 – 22/09/05	SSW	Anticlockwise coastal transect of South and East coast of England	Air masses encounter in English Channel and South East influenced by Continental air.
B134 – 26/09/05	SW	Anticlockwise coastal transect of South and East coast of England	
B136 – 29/09/05	NW	Clockwise circumnavigation of Great Britain	
B244 – 19/09/06	SW	Anticlockwise coastal transect of South and East coast of England	
B247 – 29/09/06	SW	Transects back and forth Norfolk coast	Flight aimed to measuring outflow from Lond Flew transects through London plume.

Table 13. Summary of species measured on each flight. 1- satisfactory, 0 - poor/not available. ? data not yet analysed. Data quality was assessed first qualitively to decide if further analysis was suitable. Where quality was considered border-line (1/0), the decision to include the data in further analysis was based on a number of factors taking into account the standard deviation of bags analysed repeatedly (measurement uncertainty), correlation with other species and variation in data quality throughout the flight. Where the uncertainty in the measurements was greater than 1 % the baseline concentration, the data was typically border-line quality.

	Core Chemistry						Tedlar Bags			AMS	NOxy		WAS
Flight	CO	NO_2	NO_x	NO	O_3	SO_2	CO_2	CH_4	N_2O	Aerosol	NO_x	NO_y	Halocarbon
B91	1	1	1	1	0	1	1	1/0	1/0	1	0	0	1
B92	1	1	1	1	0	1	1	1/0	1/0	1	1	1	1
B97	1	1	1	1	0	1	1	1	1/0	1	1	1	1
B102	1	1	1	1	0	1	1	0	1/0	1	1	1	1
B111	1	1	1	1	0	0	1	1/0	1	1	1	1	1
B112	1	1	1	1	0	1	1	1/0	1	1	1	1	0
B113	1	1	1	1	0	1	1	1/0	1/0	1/0	0	0	0
B118	1	1	1	1	1	0	1	0	1	1	1	1	1
B119	1	1	1	1	1	0	1	0	1	1	0	0	0
B126	1	1	1	1	1	0	1	1/0	1/0	1	1	1	1
B130	1	1	1	1	1	0	1	1/0	1	1	1	1	1
B132	1	1	1	1	1	0	1	1	1	1	1	1	0
B133	1	1	1	1	1	0	1	1	1	1	1	0	0
B134	1	1	1	1	1	0	1	1	1	1	1	0	1
B136	1	1	1	1	1	1	1	1/0	1	1	1	0	1
B244	1	1	1	1	1	1	1	1	1/0	1	1	?	0
B247	1	1	1	1	1	1	1	1	1/0	1	1	?	0

	Filters							
	Gases				Aerosol			
Flight	NH_3	HCL	HNO_3	H_2SO_4	NO_4	Cl	SO_4	HM
B91	1	1	1	?	?	?	?	?
B92	1	1	1	?	?	?	?	?
B97	1	0	0	0	0	0	0	?
B102	1	1	1	?	?	?	?	?
B111	1	1	1	?	?	?	?	?
B112	0	1	1	?	?	?	?	?
B113	1	1	1	?	?	?	?	?
B118	1	1	1	?	?	?	?	?
B119	1	1	1	?	?	?	?	0
B126	1	1	1	?	?	?	?	?
B130	1	1	1	?	?	?	?	?
B132	1	1	1	?	?	?	?	?
B133	1	1	1	?	?	?	?	?
B134	1	1	1	?	?	?	?	?
B136	1	1	1	?	?	?	?	?
B244	?	?	?	?	?	?	?	?
B247	?	?	?	?	?	?	?	?

3.1 Description of each Flight

The following section gives a detailed description of the 14 flights used in the boundary layer budget study. For each flight, a full list of the species measured can be found in Table 13. Only the species used for the boundary layer budget study are described in the following section.

3.1.1 Flight B92

Flight B92 was the first flight flown which was suitable for a boundary layer budget analysis. It took place on 09/05/05 in a north-westerly wind flow with an average ABL wind speed from UM data was about 11 m s^{-1} and the average wind direction 335°. The synoptic chart is shown in Figure 18 (a). The conditions on this day were quite convective for mid flight and not ideal for a boundary budget layer type study. A sea-breeze was also encountered in the western half of the English Channel. Due to a mismatch between the original flight plan and fuel consumption, the flight had to be cut short and a refuelling stop at Cardiff was necessary. Figure 18 (b) shows the CO concentrations measured along the flight path with the main outflow plumes from London identifiable off the south east of England. Of the species measured for the boundary layer budgets CH_4 and N_2O were consider border-line satisfactory for this flight. The measured concentration of CO, CO_2, CH_4 and N_2O are shown in Figure 19 (a), (b), (c) and (d) respectively.

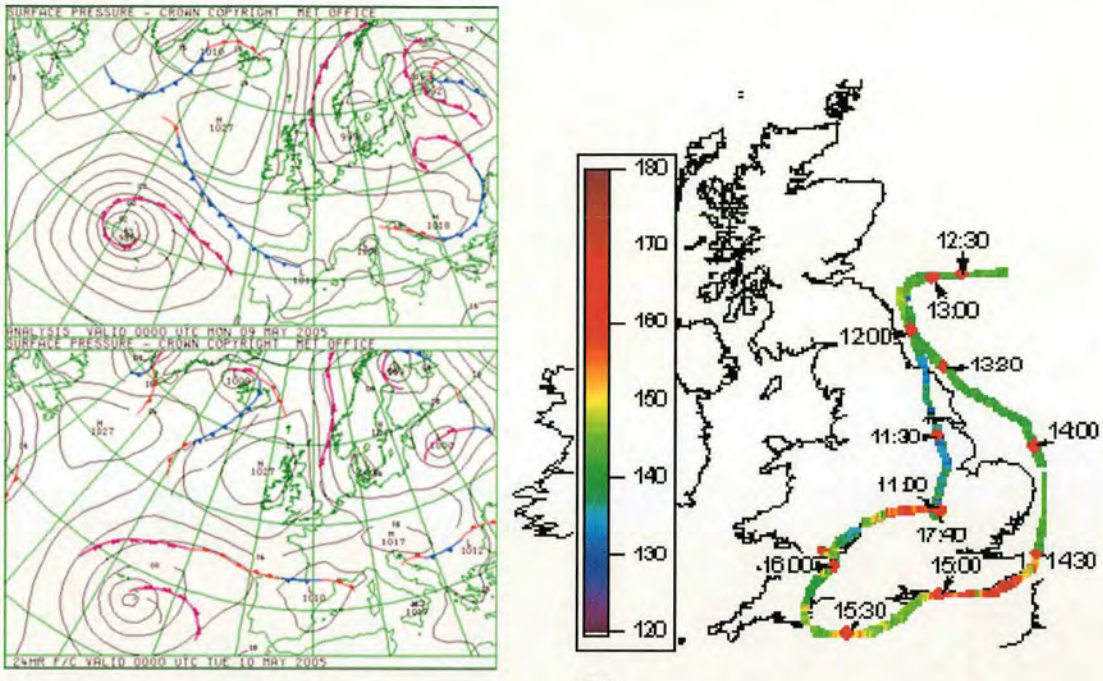

(a) (b)

Figure 18. (a) Synoptic chart for 00:00 09/05/05 and 00:00 10/05/05. (b) Flight path of flight B92 with measured CO concentrations (ppb).

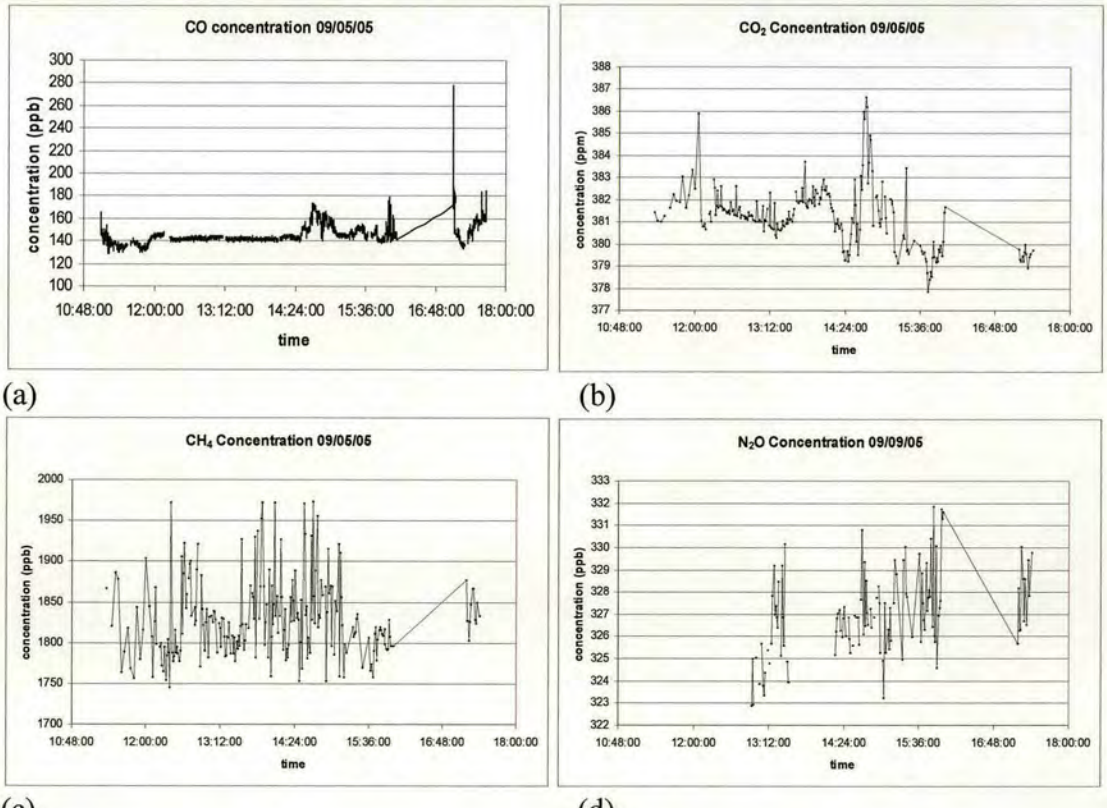

(a) (b)

(c) (d)

Figure 19. Concentration measured during flight B92. (a) CO concentration (ppb). (b) CO_2 concentration (ppm). (c) CH_4 concentration (ppb). (d) N_2O concentration (ppb).

The CO concentration and temperature of three profiles flown during the flight (Figure 20 (a) and (b)) show little evidence of a temperature inversion at the top of the ABL in the downwind section of the flight. In the upwind section there is evidence of a capping inversion from temperature profile 2 which shows an increase in temperature at around 1000 m. It is likely that a significant proportion of the UK emissions will be lost by venting through the top of the boundary layer for this flight with the result that the budgets will be underestimated for this day. Work done by Helen Dacre, modelling the convection in the boundary layer on this day, suggests that as much of 50% of the UK emissions may be vented to the free troposphere by this process (Dacre *et al.* 2007)

.

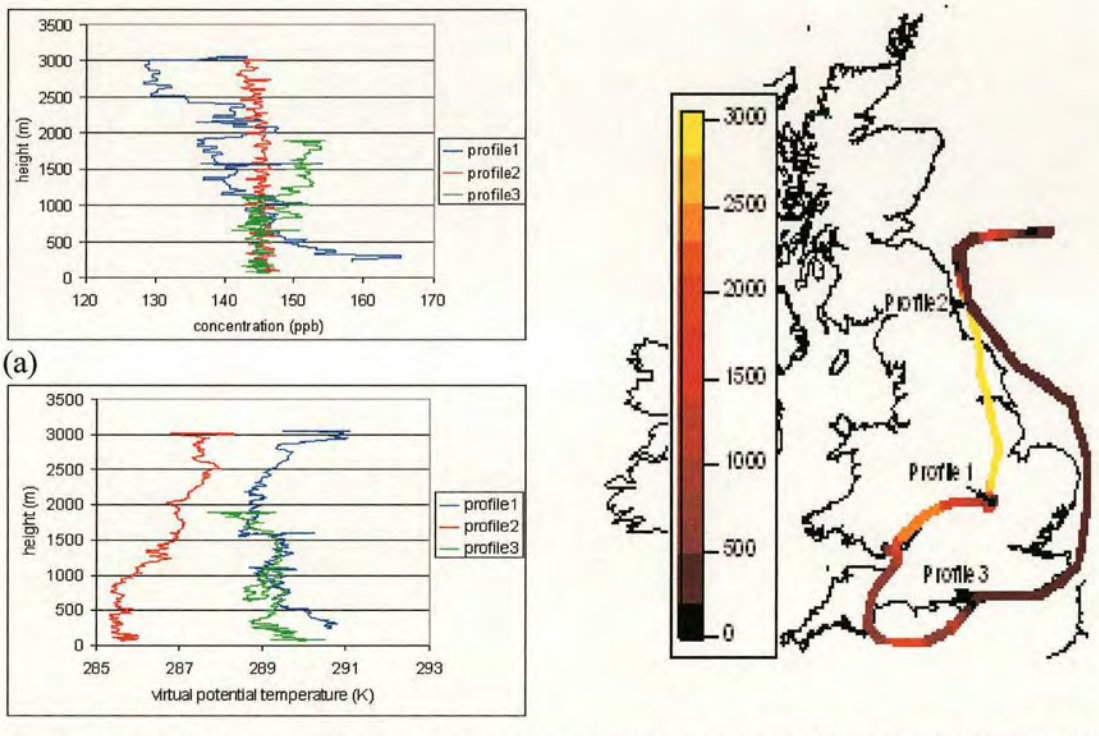

Figure 20. (a) CO Concentrations profiles of 3 profiles from flight B92. (b) Virtual Potential Temperature (K) of profiles from flight B92. (c) Height of plane and location of profiles from flight B92.

3.1.2 Flight B97

Flight B97 was flown on 25/05/05. There was a south westerly wind flow with an average wind speed of about 12 m s^{-1} and direction of 223°. The synoptic chart is shown in Figure 21 (a) and the flight path is shown in Figure 21 (b). Figure 21 (b) also shows the CO concentration along the flight path. The measured concentrations of CO, CO_2, CH_4 and N_2O are shown in Figure 22 (a), (b), (c) and (d) respectively. Of the species used for boundary layer budgets, only N_2O is considered border-line satisfactory, all others are satisfactory. The concentrations in the English Channel are slightly enhanced compared to the concentrations in the Bristol Channel for all 4 species. This is likely to be due to emissions from northern France. This makes the background concentration for this flight more uncertain.

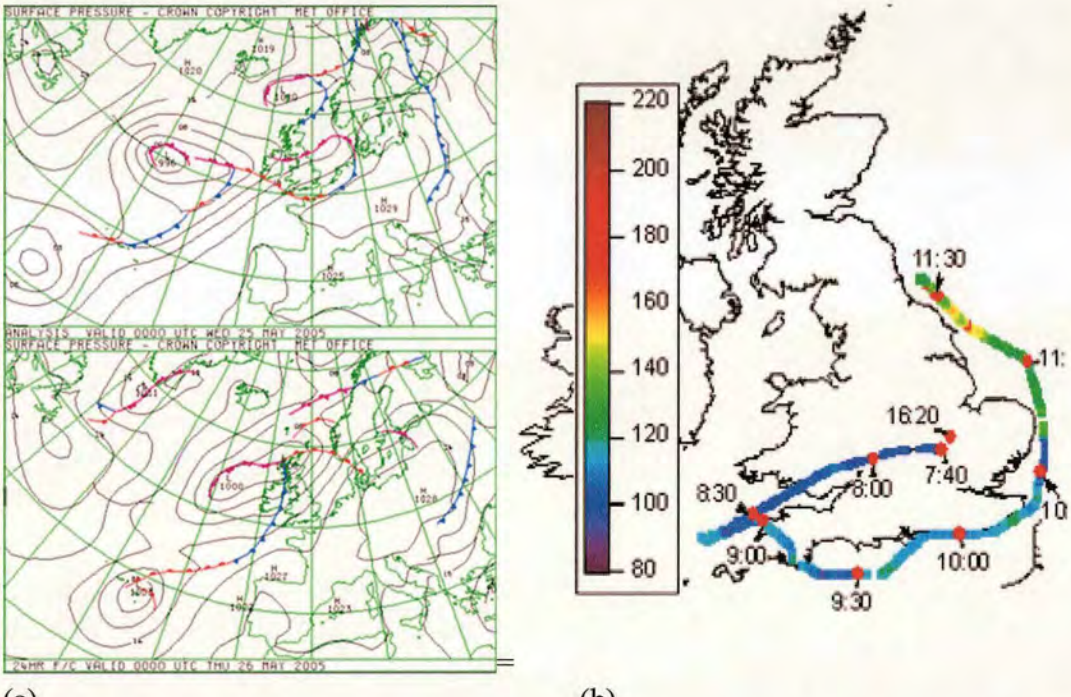

(a) (b)

Figure 21. (a) Synoptic charts for 00:00 25/05/05 and 00:00 26/05/05. (b) Flight path for flight B97 with measured CO concentrations (ppb).

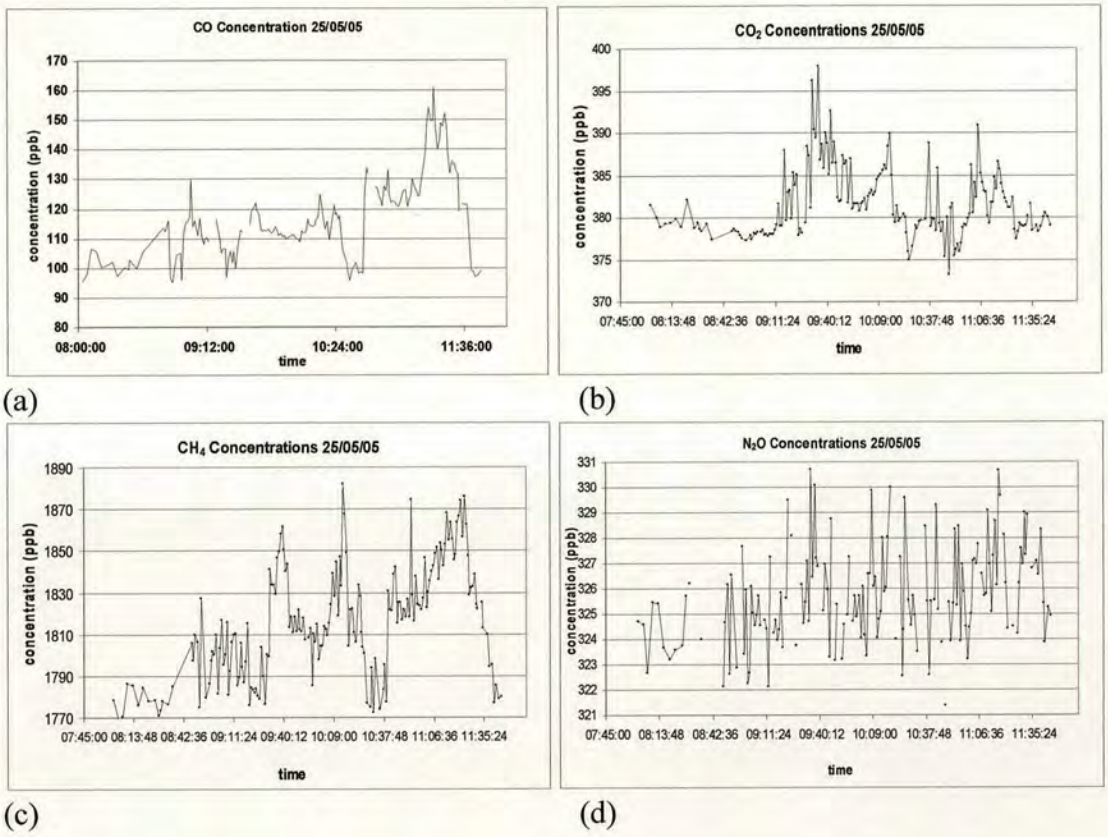

Figure 22. Concentrations measured during flight B97. (a) CO concentration (ppb). (b) CO_2 concentration (ppm). (c) CH_4 concentration (ppb). (d) N_2O concentration (ppb).

Figure 23 (a) shows the CO concentration of three profiles flown during flight B97 and Figure 23 (b) shows the temperature profiles. The height of the aircraft during the flight and the location of the three profiles are shown in Figure 23 (c). Profile 1 shows a sudden reduction in the CO concentration at about 900 m while the temperature profile is more complex with an increase in temperature at 600 m and a decrease at around 1300 m with a second increase at 1500 m. The concentration profile suggests an ABL height of around 900 m while the temperature profile suggests a capping inversion at 600 m with the plane flying through a layer of colder air between 1300 and 1500 m. The two downwind profiles both show a steady decline in concentration with height except for a spike in profile 2 at about 500 m which is likely the result of a nearby source rather than the structure of the ABL. The decline continues to around 1200 m at which point both profiles show a more rapid decrease and then a levelling off of the CO concentration. This suggests that the ABL has grown to around 1200 m by midday. This is confirmed by temperature profile 2 which shows a sudden increase in temperature at around the same height.

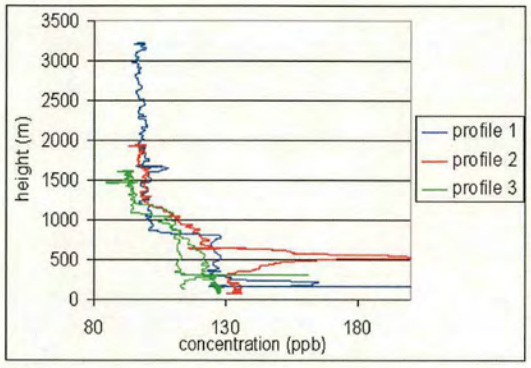

(a)

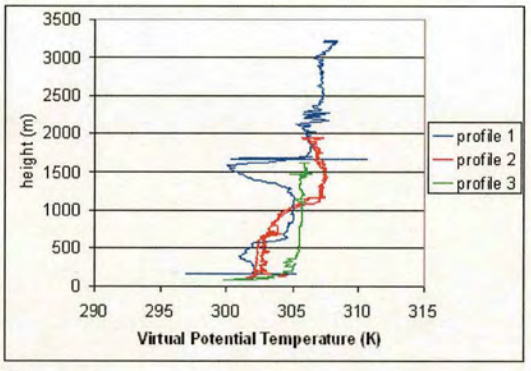

(b)

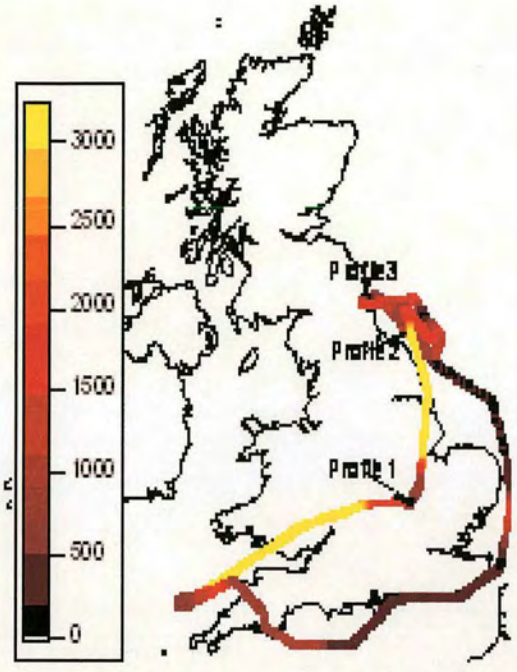

(c)

Figure 23. (a) CO concentration (ppb) profiles from flight B97. (b) Virtual Potential Temperature (K) of profiles from flight B97. (c) Height of plane (m) during flight B97 with locations of profile.

3.1.3 Flight B102

Flight B102 took place on 14/06/05. The wind flow was south westerly with an average speed of about 9 m s^{-1} and direction 251°. Figure 24 (a) shows the synoptic chart for 00:00 14/06/05 and 00:0 15/06/05. The flight path is shown in Figure 24 (b) along with the measured CO concentrations and the location of the aircraft at half hour intervals. Samples were taken at low level in the Bristol Channel to get an estimate of the background concentration. Of the species used for the boundary layer budget analysis, CH_4 was very poor on this flight due to a stability problem with the TDL diode and could not be used to calculate a UK flux. N_2O was border-line between poor and satisfactory and so a boundary layer analysis was attempted for it. The concentrations of CO, CO_2, CH_4 and N_2O are shown in Figure 25 (a), (b), (c) and (d). Rain showers were encountered near Newcastle where the plane stopped to refuelling before sampling back down the East coast and returning to Cranfield.

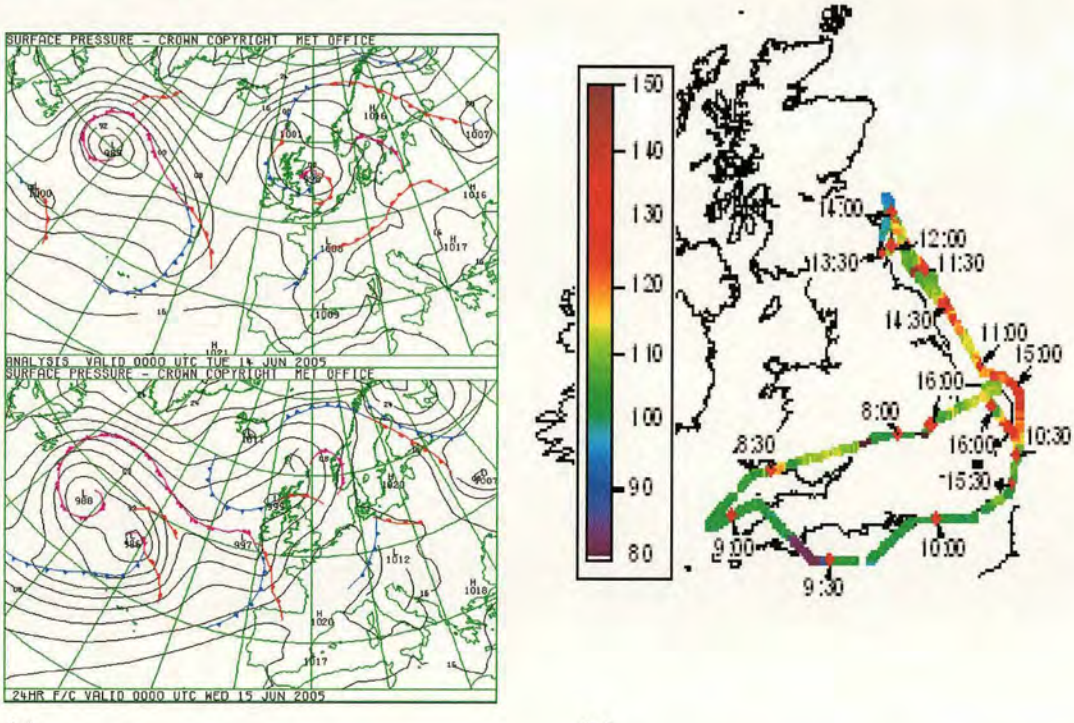

(a) (b)

Figure 24. (a) Synoptic chart for 00:00 14/06/05 and 00:00 15/06/05. (b) CO concentration (ppb) along flight path of flight B102. The location of the plane at half hour intervals is plotted along the flight path.

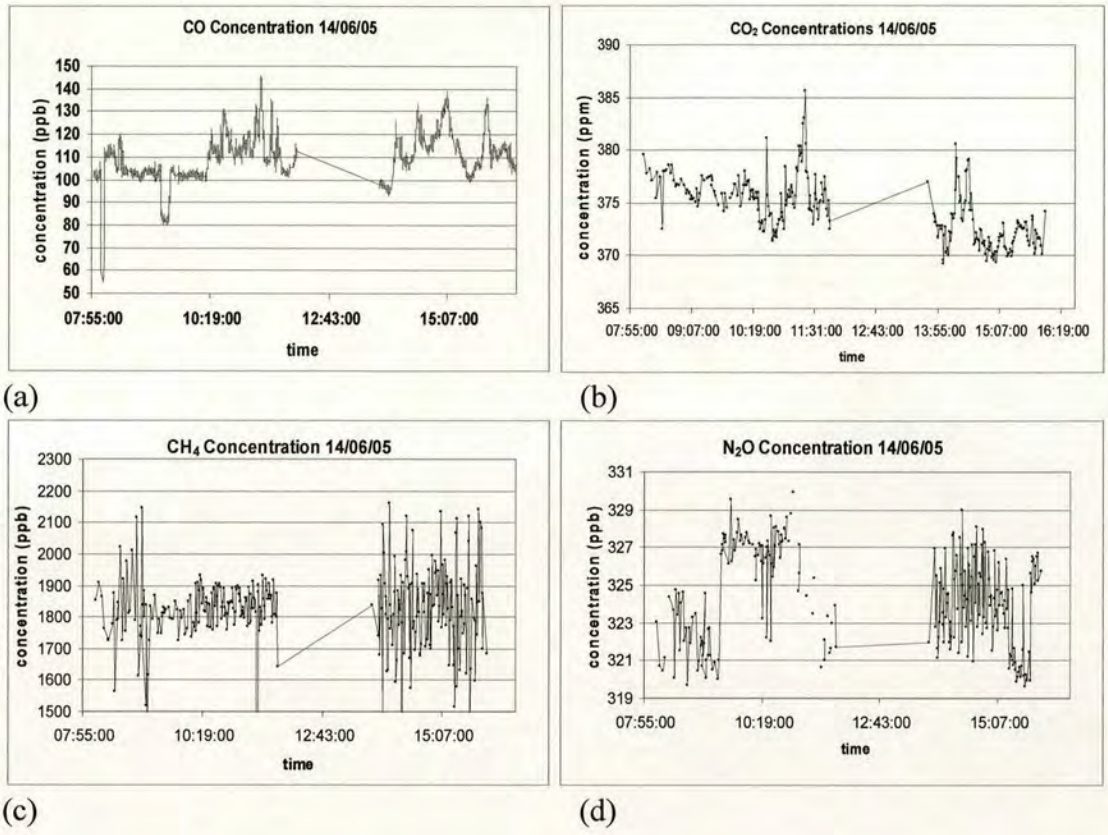

Figure 25. Concentrations measured during flight B102. (a) CO concentration (ppb). (b) CO_2 concentration (ppm). (c) CH_4 concentration (ppb). (d) N_2O concentration (ppb).

The CO concentrations for four profiles from the flight are shown in Figure 26 (a), the temperature profiles are shown in Figure 26 (b) and the locations of the profiles along with the flight path of the aircraft are plotted in Figure 26 (c). Only profiles 1 and 4 extend from low level to above 1500 m. Temperature profile 1 shows evidence of a temperature inversion at the top of the boundary layer at a height of 1500 m. Profile 4 was taken as the aircraft climbed on final transit back to Cranfield and during the profile the aircraft is moving inland. As the aircraft climbs, there is an increase in CO concentration up to 1500 m where there is a sudden decrease. It is possible that the increase is due to flying over or near to sources as the plane flies inland and this is responsible for the increase up to 1500 m where the aircraft encounters the top of the ABL. The temperature profile does show an increase at around the same height as the decrease in CO concentration, however as the profile does not extend above this it is not possible to know if higher temperatures continue above this height.

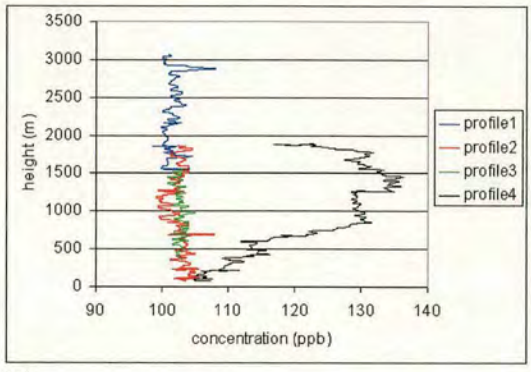

(a)

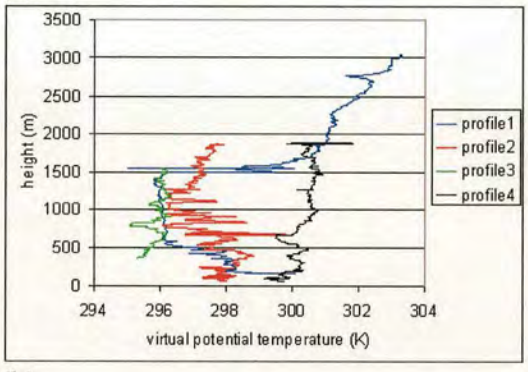

(b)

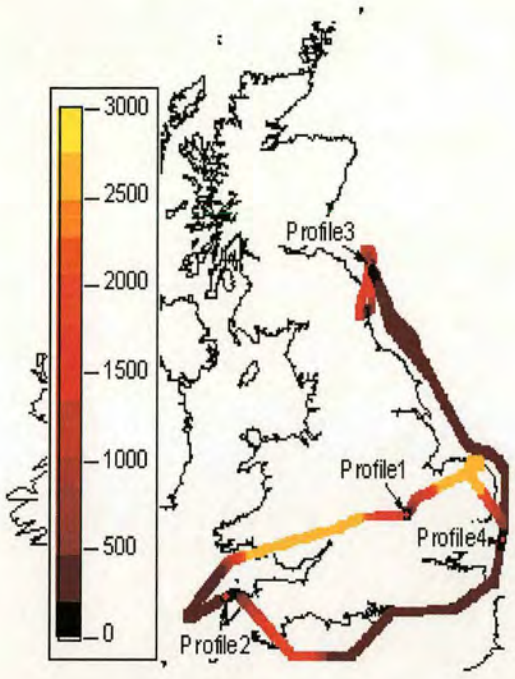

(c)

Figure 26. (a) CO concentration (ppb) of 4 profiles from flight B102. (b) Virtual Potential Temperature (K) profiles from flight B102. (c) Height (m) of plane during flight B102 and location of 4 profiles.

3.1.4 Flight B111

Flight B111 took place on the 14/07/05 in a south westerly wind flow with an average wind speed of about 5 m s^{-1} and direction of 226°. The synoptic charts for 00:00 14/07/05 and 00:00 15/07/05 is shown in Figure 27 (a). Figure 27 (b) shows the flight path and times for the flight with the CO concentration measured around the country. Of the boundary layer budget species, all were satisfactory except CH_4 which was border-line between satisfactory and poor. The concentrations of CO, CO_2, CH_4 and N_2O are shown in Figure 28 (a), (b), (c) and (d) respectively. The wind flow on this days was uncoupled with air in the southern half of the outflow plume originating over continental Europe and the air in the northern half originating over the Atlantic. Because of this, the budget calculated for this flight was not included in the final estimate.

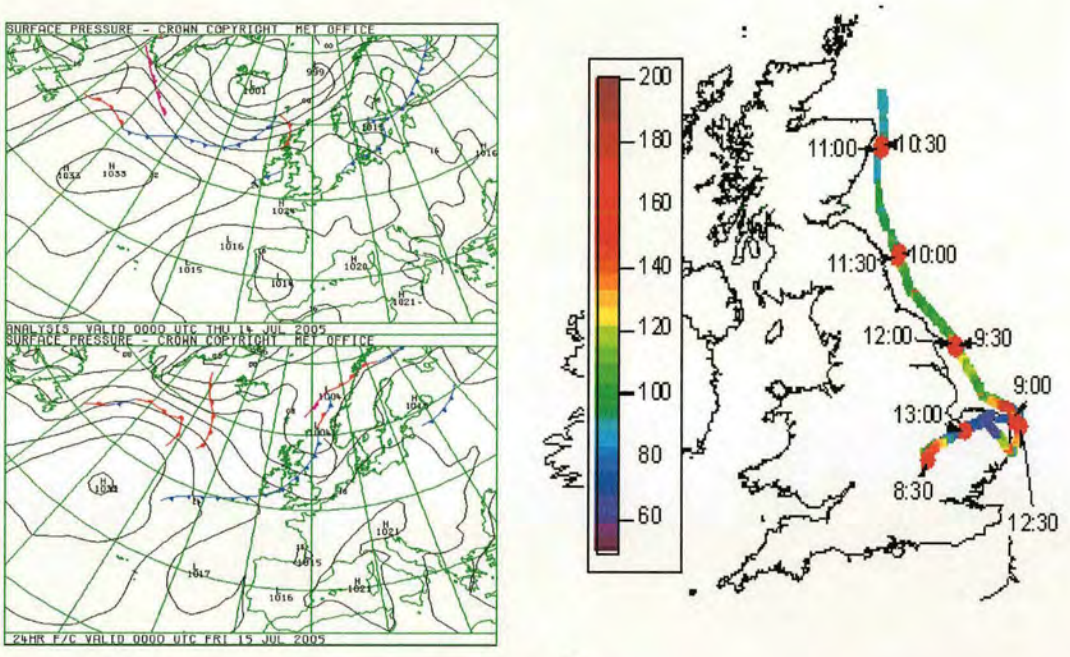

(a) (b)

Figure 27. (a) synoptic chart for 00:00 14/07/05 and 00:00 15/07/05. (b) CO concentration (ppb) measured along path of flight B111 on 14/07/05 with the position of plane at half hourly intervals marked.

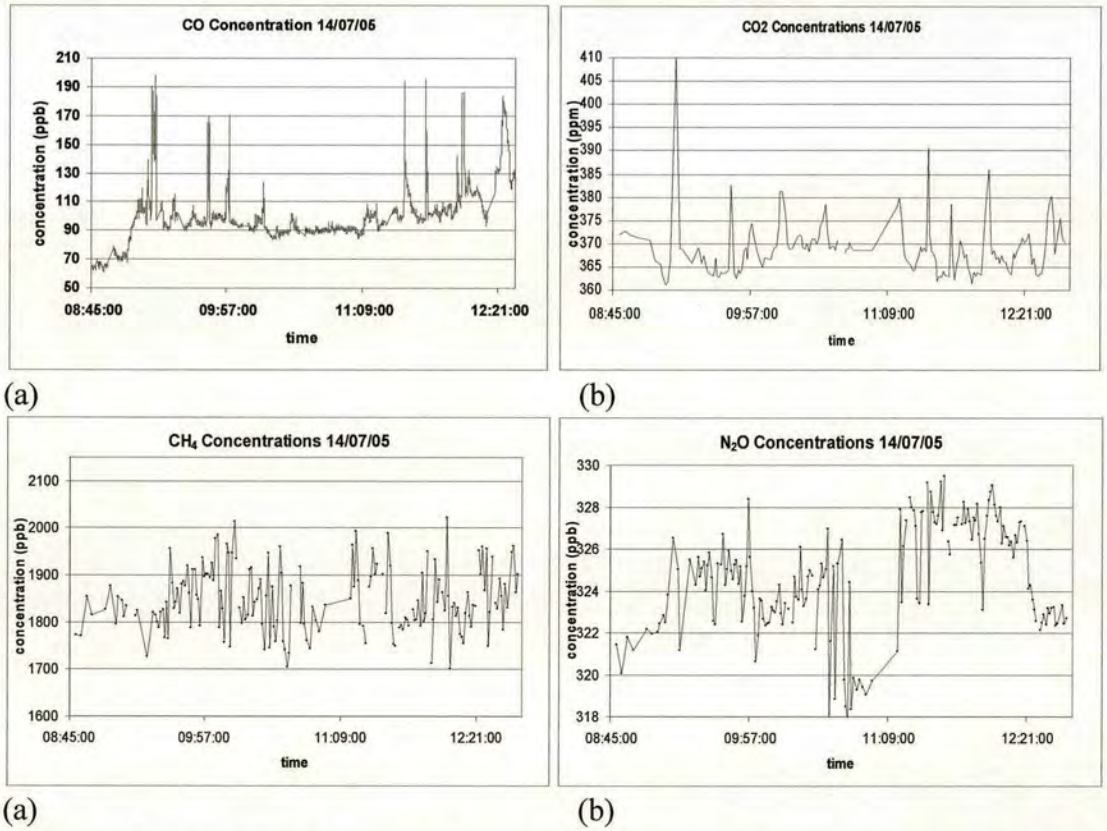

(a) (b)

Figure 28. Concentrations measured during flight B111. (a) CO concentration (ppb). (b) CO_2 concentration (ppm). (c) CH_4 concentration (ppb). (d) N_2O concentration (ppb).

The CO concentrations and temperatures for 5 profiles flown during the flight are shown in Figure 29 (a) and (b) respectively. The locations of the aircraft at the start of the profiles are shown in Figure 29 (c). All 5 profiles show a gradual decrease in CO concentration with height except profile 4. Profile 4 has almost constant concentration with height with a small decrease at around 1400 m which is consistent with background air with the same CO concentration above and below the ABL. Temperature profile 4 shows a temperature inversion at 1000 m. Concentration profile 2 shows a sharp decrease at around 1400 m and a second decrease at 2000 m. This is matched by temperature increases at the same heights. The complexity of profile 2 may be partly explained by plane travelling over land and out to sea with the height of the ABL dependent on location. Profiles 1 and 5 also show very complex structure with the temperature and concentration fluctuating with height. As both profiles are also taken over land these fluctuations may represent changes in the ABL with position above the surface rather than height.

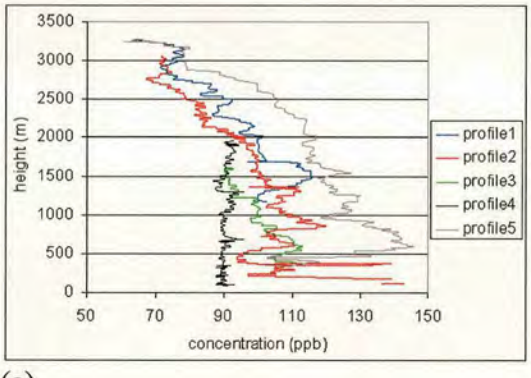

(a)

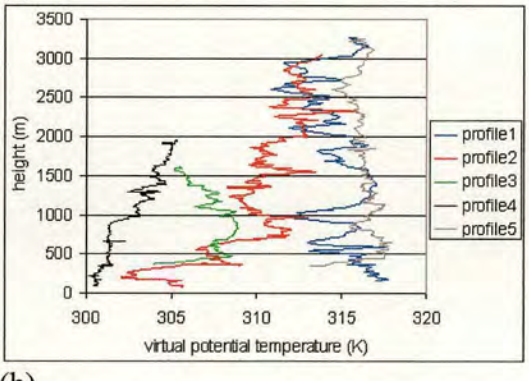

(b)

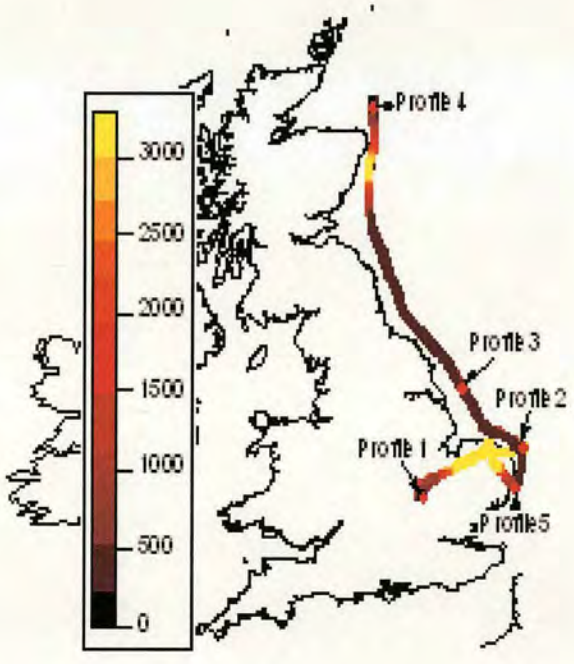

(c)

Figure 29. (a) CO concentration (ppb) during 5 profiles from flight B111. (b) Virtual potential temperature (K) of profiles. (c) Height of plane during flight B111 and locations of profiles 1-5.

3.1.5 Flight B112

Flight B112 took place on 19/07/05 in a westerly wind flow with an average wind speed of about 11 m s^{-1} and direction of 268°. The synoptic chart for 00:00 19/07/05 and 00:00 20/07/05 is shown in Figure 30 (a) and the flight path and CO concentration are shown in Figure 30 (b). Of the boundary layer budget species, all were considered satisfactory except CH_4 which was border-line satisfactory but still considered good enough for a budget calculation. The concentrations of CO, CO_2, CH_4 and N_2O are shown in Figure 31 (a), (b), (c) and (d) respectively. During the flight a slight sea breeze was encountered in the east of the English Channel and light rain was encountered off the north west of England.

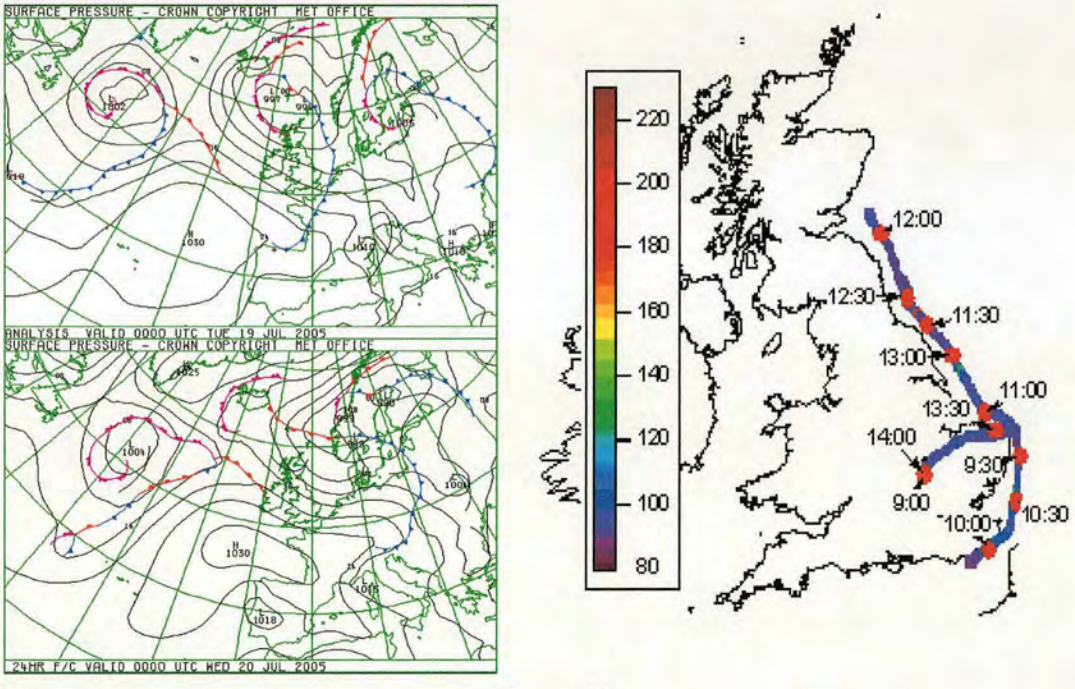

(a) (b)

Figure 30. (a) Synoptic charts for 00:00 19/07/05 and 00:00 20/07/05. (b) CO concentration (ppb) measured along path of flight B112 on 19/07/05 with the position of plane at half hourly intervals marked.

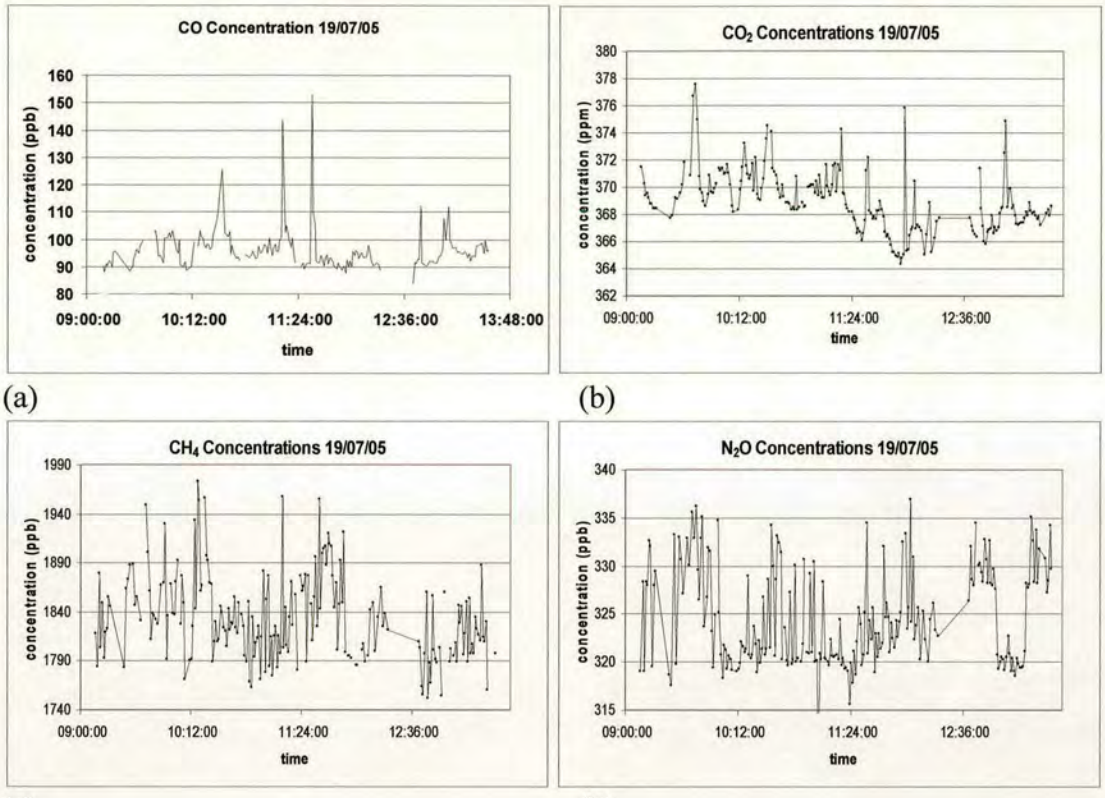

Figure 31. Concentrations measured during flight B112. (a) CO concentration (ppb). (b) CO_2 concentration (ppm). (c) CH_4 concentration (ppb). (d) N_2O concentration (ppb).

Figure 32 (a) and (b) show the CO concentration and temperature profiles respectively of three profiles flown during flight B112. Profiles 1 and 2 show a decrease in concentration at about 1400 m. Profile 3 shows a decrease at about 1500 m. Both profiles 1 and 3 show an increase in concentration above this up to around 2500 m. In both cases the aircraft is over land during this part of the profile and this may explain the increase in concentration up to this height indicating that over the sea the ABL height is around 1400-1500 m and around 2500 m over land. This is consistent with profile 2 which is entirely over sea. Temperature profile 2 shows an increase at a similar height suggesting a capping inversion at this height. Temperature profile 1 shows an increase from 1500 m upwards with a more sudden increase at 2500 m, similar to profile 3.

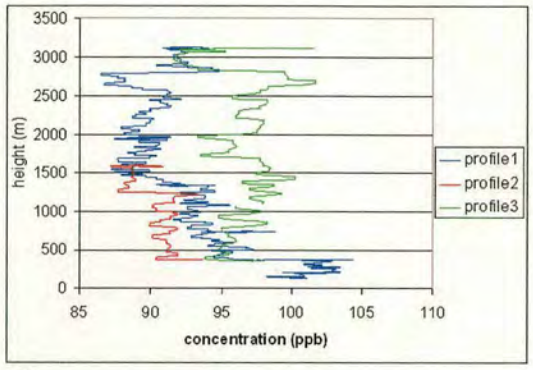

(a)

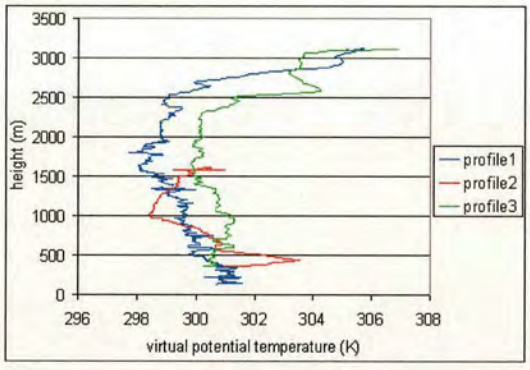

(b)

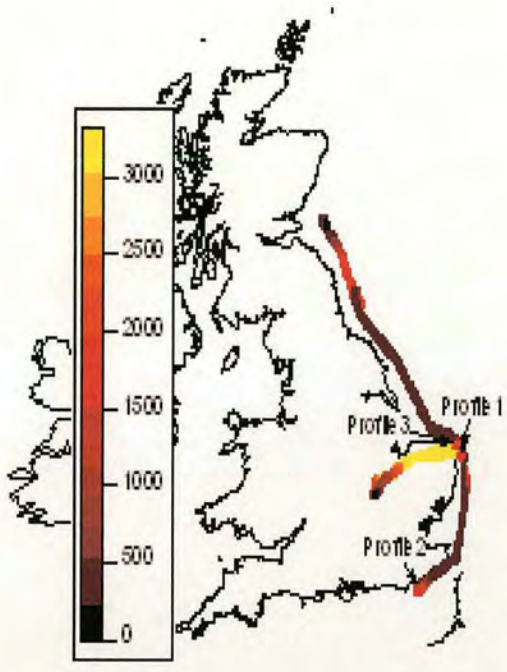

(c)

Figure 32. (b) CO concentration (ppb) of 3 profiles from flight B112. (b) Virtual Potential Temperature of profiles from flight B112. (c) Height (m) of plane during flight B112 and locations of 3 profiles.

3.1.6 Flight B113

Flight B113 took place on 20/07/05 in a north westerly wind flow with an average wind speed of about 14 m s^{-1} and direction of 287°. The synoptic chart for 00:00 12/07/05 and 00:00 21/07/05 is shown in Figure 33 (a) and the flight path and CO concentration are shown in Figure 33 (b). Of the boundary layer budget species, all were considered satisfactory except CH_4 which was border-line but still considered good enough for a budget calculation. The concentrations of CO, CO_2, CH_4 and N_2O are shown in Figure 34 (a), (b), (c) and (d) respectively. Scattered showers were encountered throughout the flight.

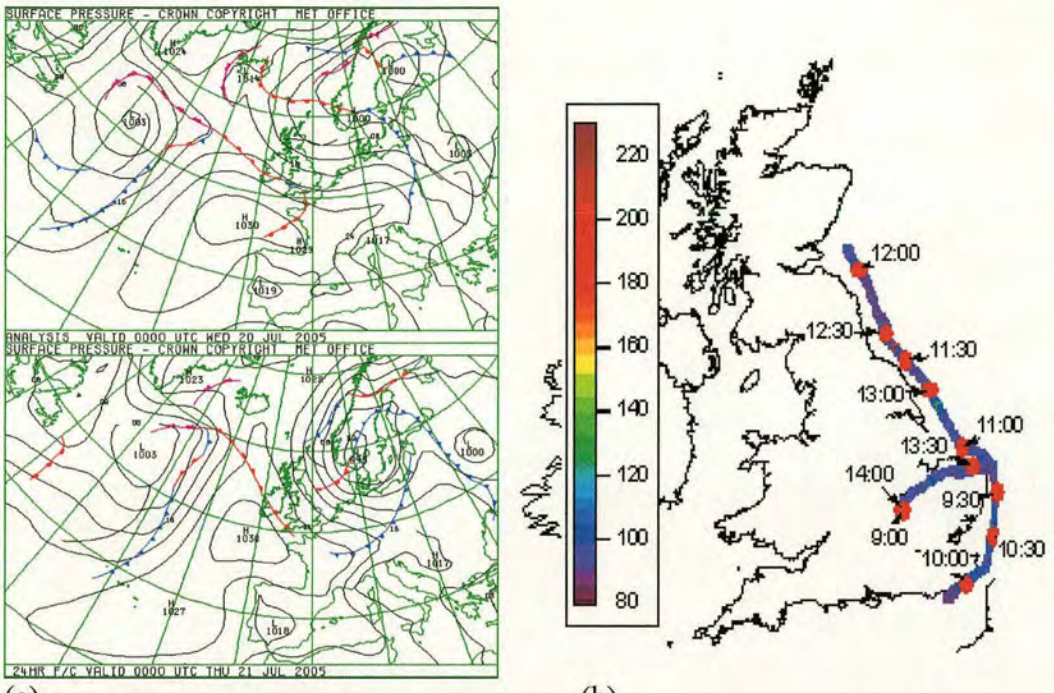

Figure 33. (a) Synoptic charts for 00:00 20/07/05 and 00:00 21/07/07. (b) CO concentration (ppb) measured along path of flight B113 on 20/07/05 with the position of plane at half hourly intervals marked.

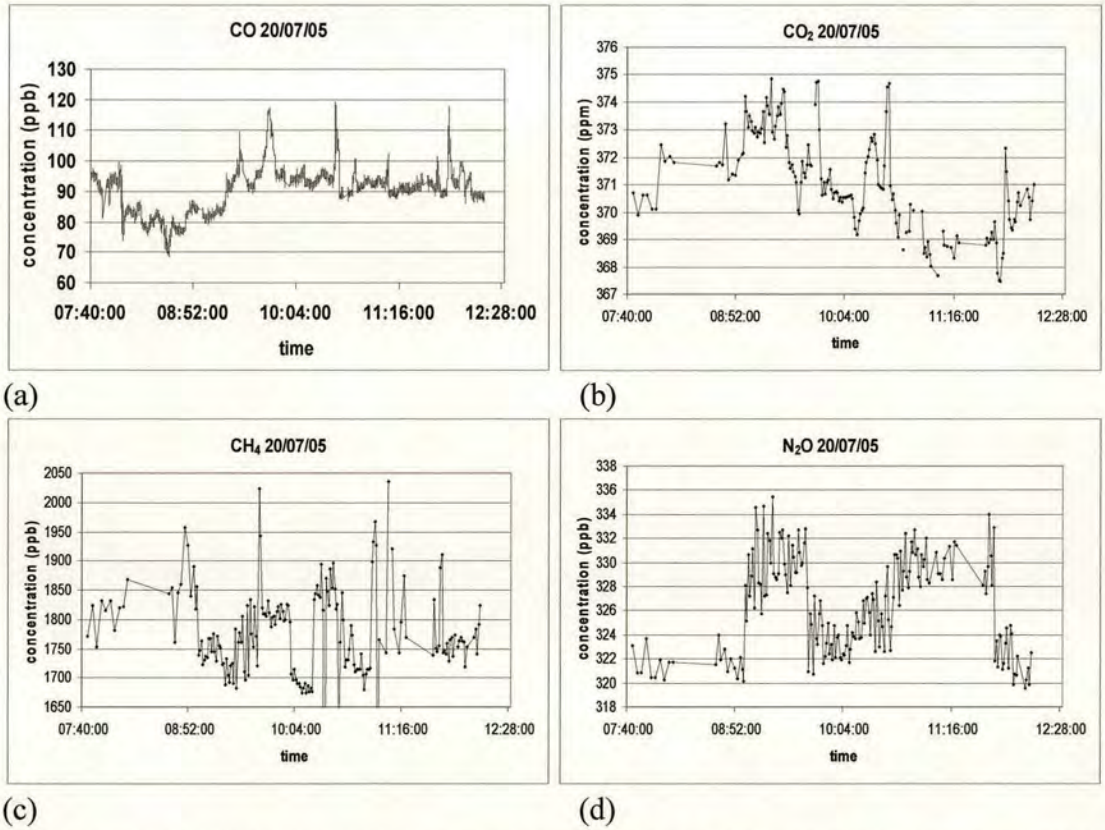

Figure 34. Concentrations measured during flight B113. (a) CO concentration (ppb). (b) CO_2 concentration (ppm). (c) CH4 concentration (ppb). (d) N_2O concentration (ppb).

Figure 35 (a) and (b) show the CO concentration and temperature profiles respectively of four profiles flown during flight B113. Concentration profile 1, taken during take off as shown in Figure 35 (c), does not show any evidence of an inversion at the top of the ABL. However the temperature profile shows a strong temperature inversion at around 1600 m. Profile 2 is taken in background air and shows a strong temperature inversion at 2000 m. The concentration of profile 2 does not change significantly above this height as expected for background air where the concentration is the same above and below the ABL. Profile 4 shows good evidence of a temperature inversion at around 1600 m with the concentration decreasing at a height of around 1400 m.

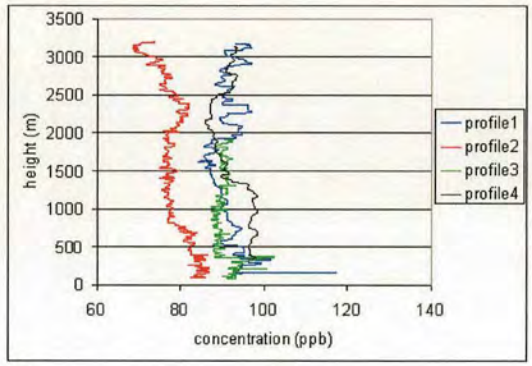

(a)

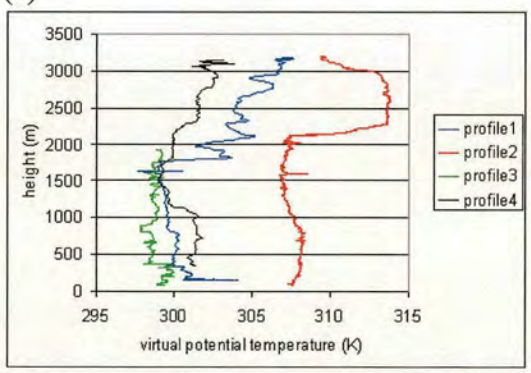

(a)

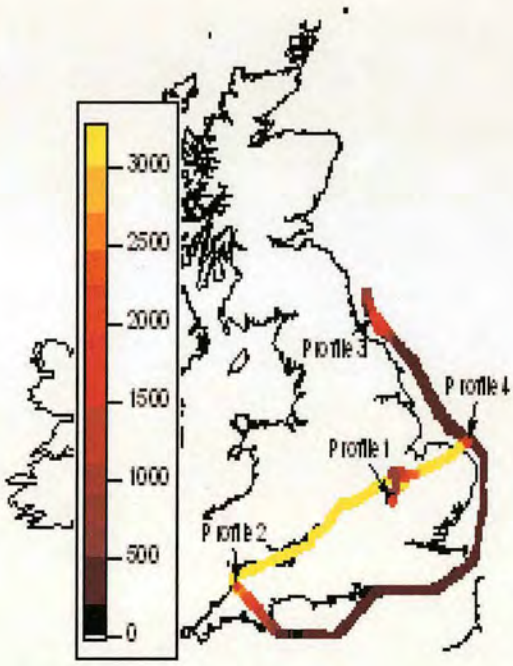

(b)

Figure 35. (a) CO concentration (ppb) of 4 profiles from flight B113. (b) Virtual Potential Temperature (K) from flight B113. (c) Height (m) of plane during flight B113 and locations of 4 profiles.

3.1.7 Flight B118

_Flight B118 took place on 03/08/05 in a westerly wind flow with an average wind speed of about 9 m s^{-1} and direction of 278°. The synoptic chart for 00:00 03/08/05 and 00:00 04/08/05 is shown in Figure 36 (a) and the flight path and CO concentration are shown in Figure 36. Of the boundary layer budget species, CH_4 was considered too poor quality for a boundary layer budget. The concentrations of CO, CO_2, CH_4 and N_2O are shown in Figure 37 (a), (b), (c) and (d) respectively. During the flight a slight sea breeze effect was observed to the north east of Dover and brief showers encountered on the east coast leg. Heavier rain was observed inland to the west.

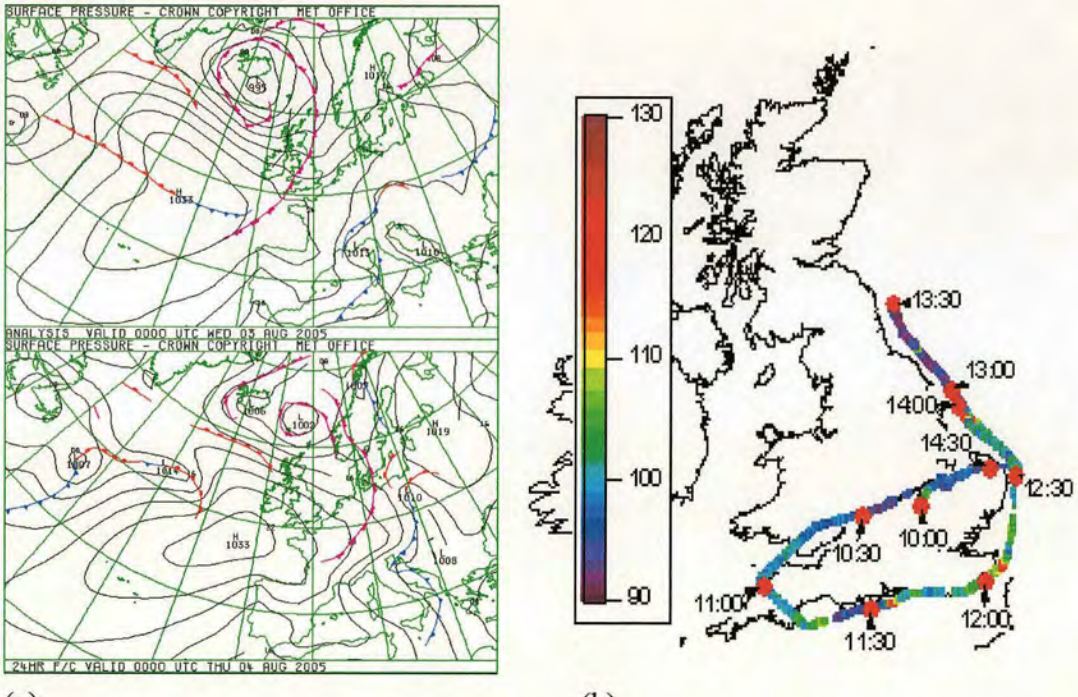

(a) (b)

Figure 36. (a) Synoptic charts for 00:00 03/08/05 and 00:00 04/08/05. (b) CO concentration (ppb) measured along path of flight B118 on 03/08/05 with the position of plane at half hourly intervals marked.

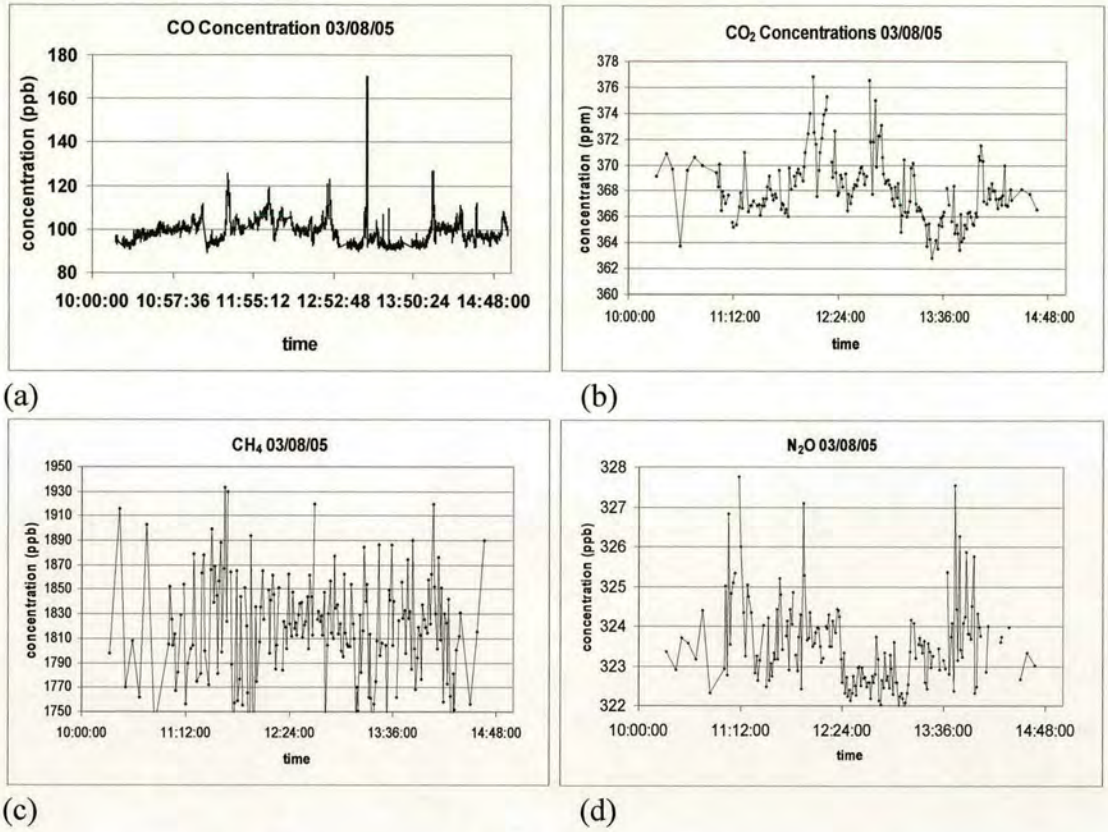

Figure 37. Concentrations measured during flight B118. (a) CO concentration (ppb). (b) CO_2 concentration (ppm). (c) CH_4 concentration (ppb). (d) N_2O concentration (ppb).

Figure 38 (a) and (b) show the CO concentration and temperature of three profiles flown during flight B118. Profile 1 is taken during the transit over Cornwall as shown in Figure 38 (c). Profile 1 shows a decrease in temperature up to 2000 m and a temperature inversion at this height. The concentration profile also shows a decrease in concentration at this height. Profile 3 is taken as the aircraft ascends to make the final transit back to Cranfield and crosses from land to sea. The temperature profile shows a temperature inversion at around 2000 m. The concentration is quite variable up to around 1500 m and decreases steadily thereafter. The variation in the lower part of the profile is perhaps due to the aircraft flying close to sources inland.

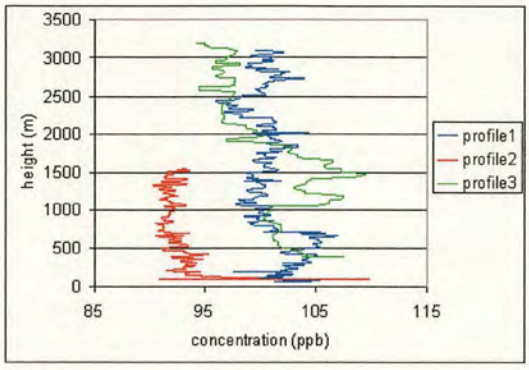

(a)

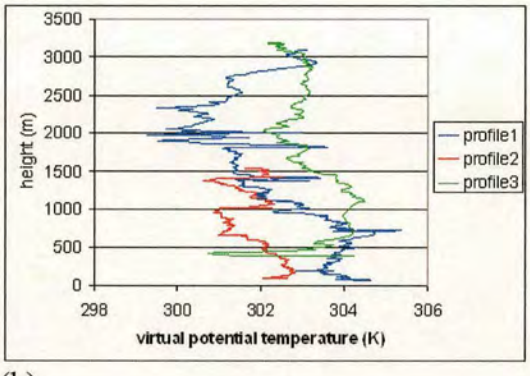

(b)

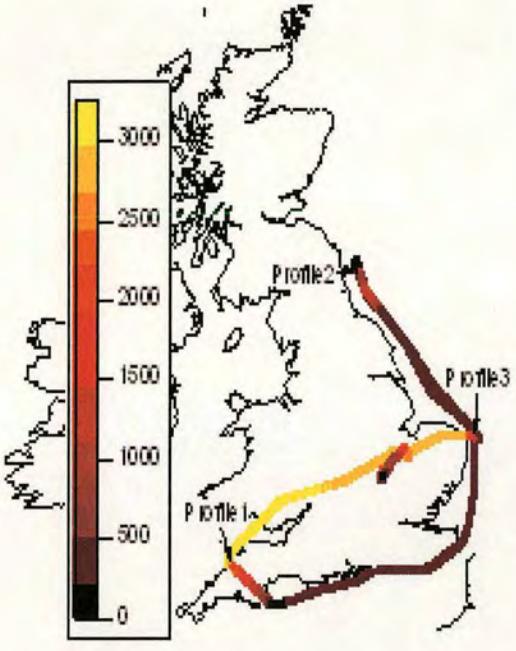

(c)

Figure 38. (a) CO concentration (ppb) of 3 profiles from flight B118. (b) Virtual Potential Temperature (K) profiles from flight B118. (c) Height (m) of plane during flight B118 and locations of 3 profiles.

3.1.8 Flight B119

_Flight B119 took place on 04/08/05 in a westerly wind flow with an average wind speed of about 10 m s^{-1} and direction of 275°. The synoptic charts for 00:00 04/08/05 and 00:00 05/08/05 are shown in Figure 39 (a) and the flight path and CO concentration are shown in Figure 39 (b). Of the boundary layer budget species, CH_4 was considered too poor quality to attempt a boundary layer budget. The concentrations of CO, CO_2, CH_4 and N_2O are shown in Figure 40 (a), (b), (c) and (d) respectively.

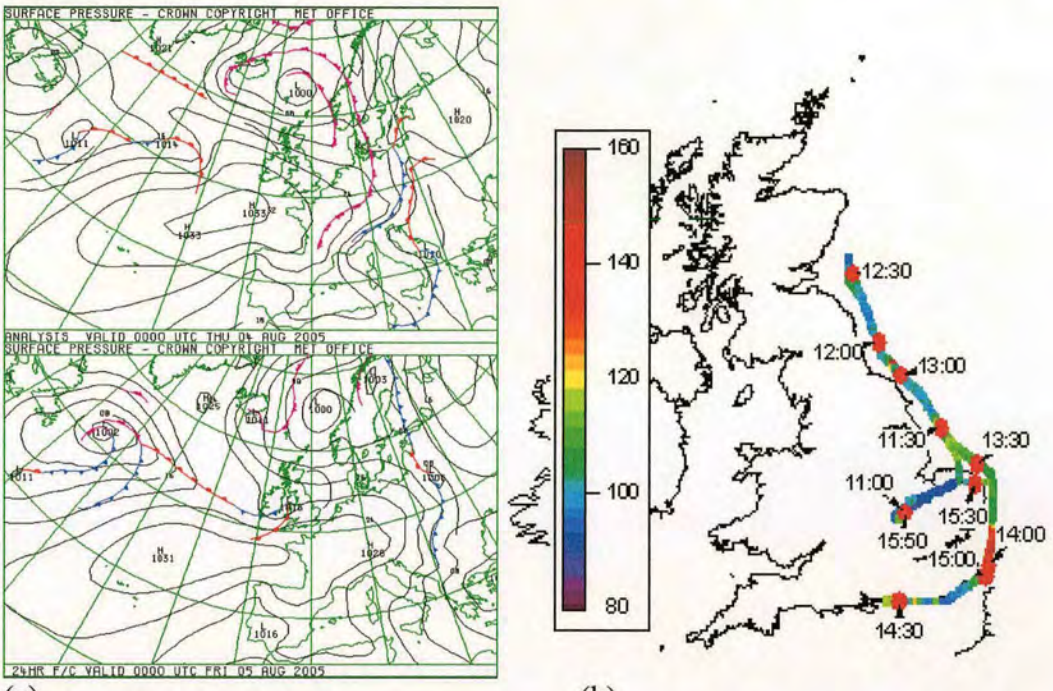

(a) (b)

Figure 39. (a) Synoptic charts for 00:00 04/08/05 and 00:00 05/08/05. (b) CO concentration (ppb) measured along path of flight B119 on 04/08/05 with the position of plane at half hourly intervals marked.

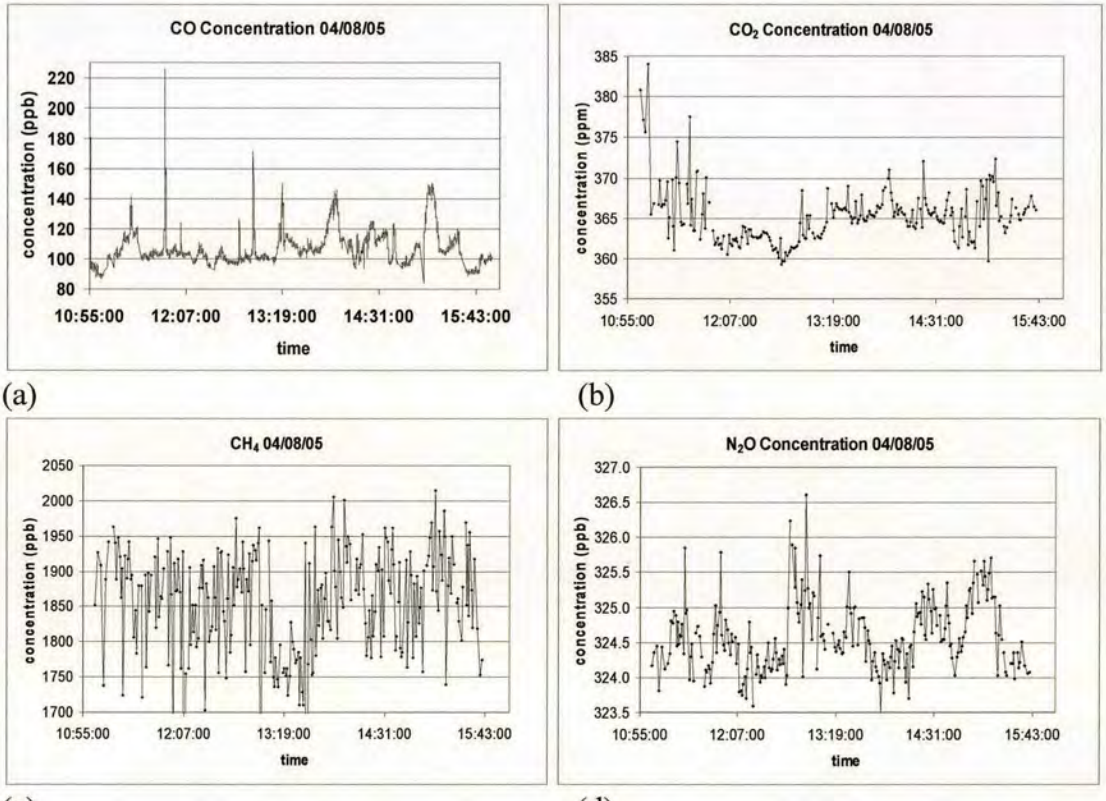

(a) (b)

(c) (d)

Figure 40. Concentrations measured during flight B119. (a) CO concentration (ppb). (b) CO_2 concentration (ppm). (c) CH_4 concentration (ppb). (d) N_2O concentration (ppb).

Figure 41 (a) and (b) show the CO concentration and temperature respectively of three profiles flown during flight B119. Profile 1 has relatively constant concentration but the temperature shows a dramatic increase at around 2000 m. Profiles 2 shows an increase in concentration up to around 700 m then a rapid decrease with a temperature inversion at the same height. There is a second temperature inversion at around 2000 m. As profile 2 was taken as the aircraft descended over land and out to sea, this suggests that the ABL height is around 2000 m over land and 700 m over the sea.

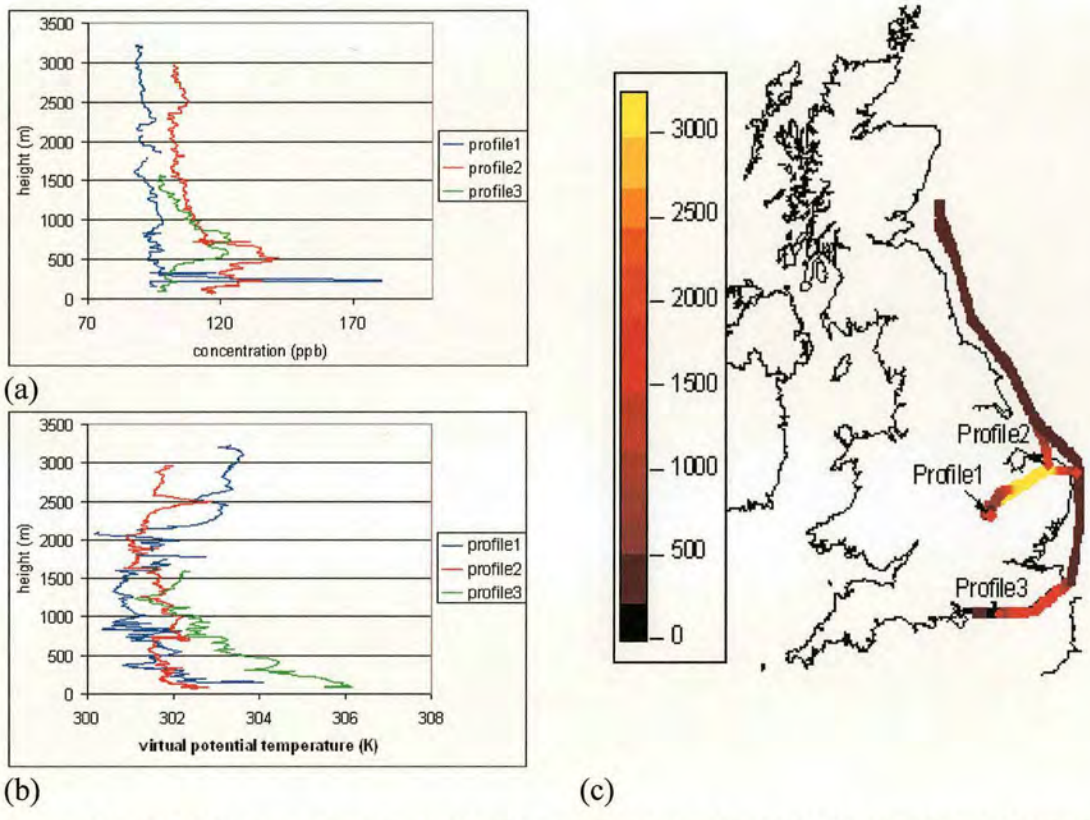

Figure 41. (a) CO concentration (ppb) of 3 profiles from flight B119. (b) Virtual Potential Temperature (K) pf profiles from flight B119. (c) Height (m) of plane during flight B119 and locations of 4 profiles.

3.1.9 Flight B126

Flight B126 took place on 07/09/05 in a south westerly wind flow with an average wind speed of about 9 m s^{-1} and direction of 234°. The synoptic chart for 12:00 07/09/05 is shown in Figure 42 (a) and the flight path and CO concentration are

shown in Figure 42 (b). Of the boundary layer budget species, CH_4 and N_2O were both border-line in quality but were considered satisfactory for a boundary budget estimate. The concentrations of CO, CO_2, CH_4 and N_2O are shown in Figure 43 (a), (b), (c) and (d) respectively.

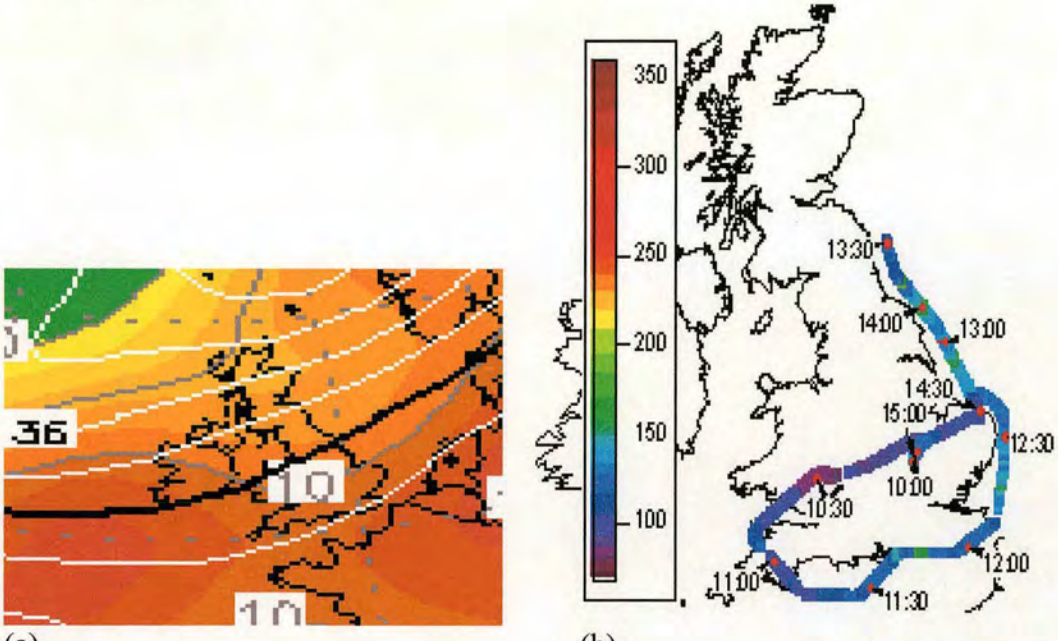

(a) (b)

Figure 42. (a) Synoptic charts for 12:00 07/09/05. (b) CO concentration (ppb) measured along path of flight B126 on 07/09/05 with the position of plane at half hourly intervals marked.

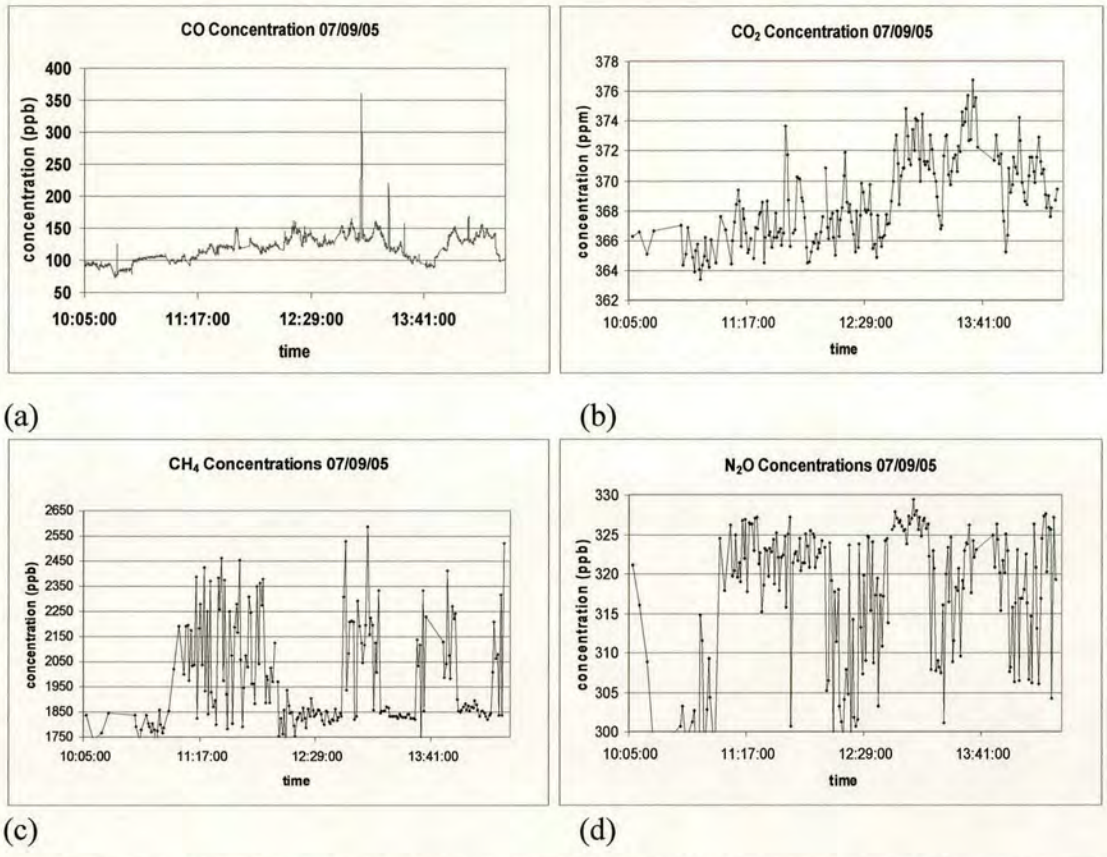

Figure 43. Concentrations measured during flight B126. (a) CO concentration (ppb). (b) CO_2 concentration (ppm). (c) CH_4 concentration (ppb). (d) N_2O concentration (ppb).

Figure 44 (a) and (b) show the CO concentration and temperature respectively of four profiles flown during flight B126. Profiles 1 and 2 are both taken over land as shown in Figure 44 (c) and show a sudden drop in concentration at around 2500 m suggesting the ABL of this depth. Temperature profiles 1 and 2 both show a gradual increase in temperature from around 1000 m with a more sudden increase also at 2500 m. Profile 4 was taken as the aircraft headed inland for the final transit to Cranfield. It shows a decrease in concentration at around 1200 m and a second decrease at around 3000 m. Where the concentration decreases at around 1000 m, the temperature also decreases with a temperature inversion at the same height as the second concentration decrease at 3000 m. This suggests that at the start of the flights the ABL height is 2500 m growing to 3000 m later in the day.

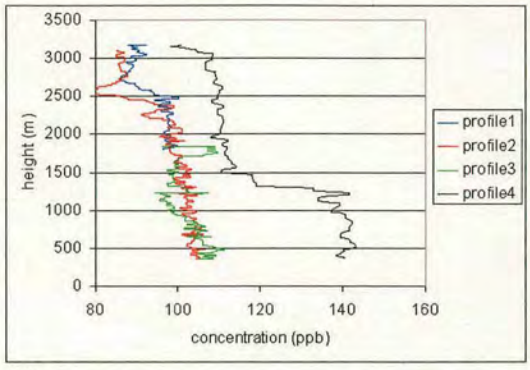

(a)

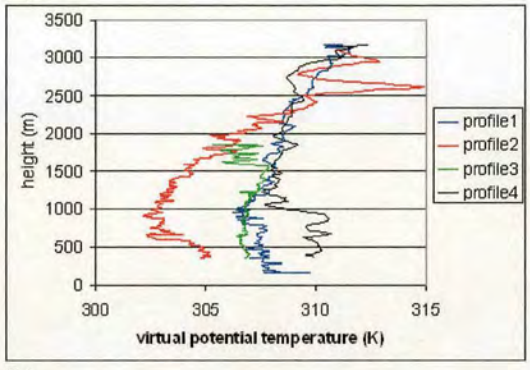

(b)

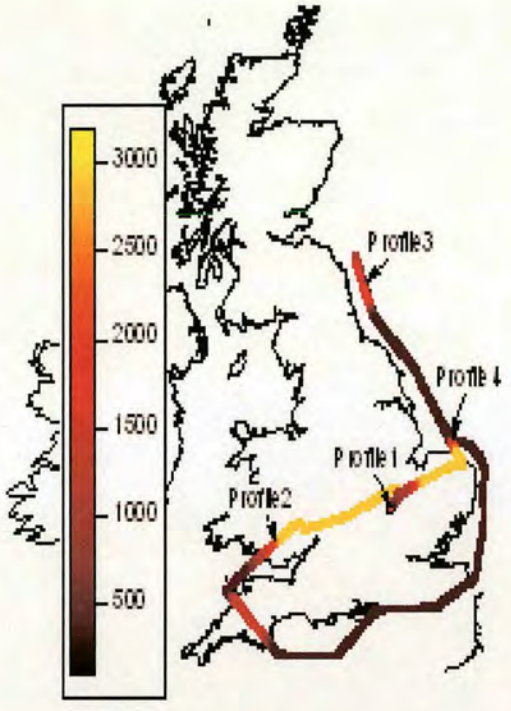

(c)

Figure 44. (a) CO concentration (ppb) of 4 profiles flown during flight B126. (b) Virtual Potential Temperature (K) pf profiles from flight B126. (c) Height (m) of plane during flight B126 and locations of 4 profiles.

3.1.10 Flight B130

Flight B130 takes place on the 19/09/05 in a south westerly wind with an average wind speed of about 9 m s^{-1} and direction of 214°. Figure 45 (a) shows the synoptic chart for 12:00 19/09/05 and Figure 45 (b) shows the flight path and CO concentration. Of the boundary layer budget species, CH_4 was considered border-line quality but adequate for a budget estimate. All other species were satisfactory. The concentrations of CO, CO_2, CH_4 and N_2O are shown in Figure 46 (a), (b), (c) and (d) respectively. Air masses encountered in the English Channel and off south east coast of England were influenced by continental air.

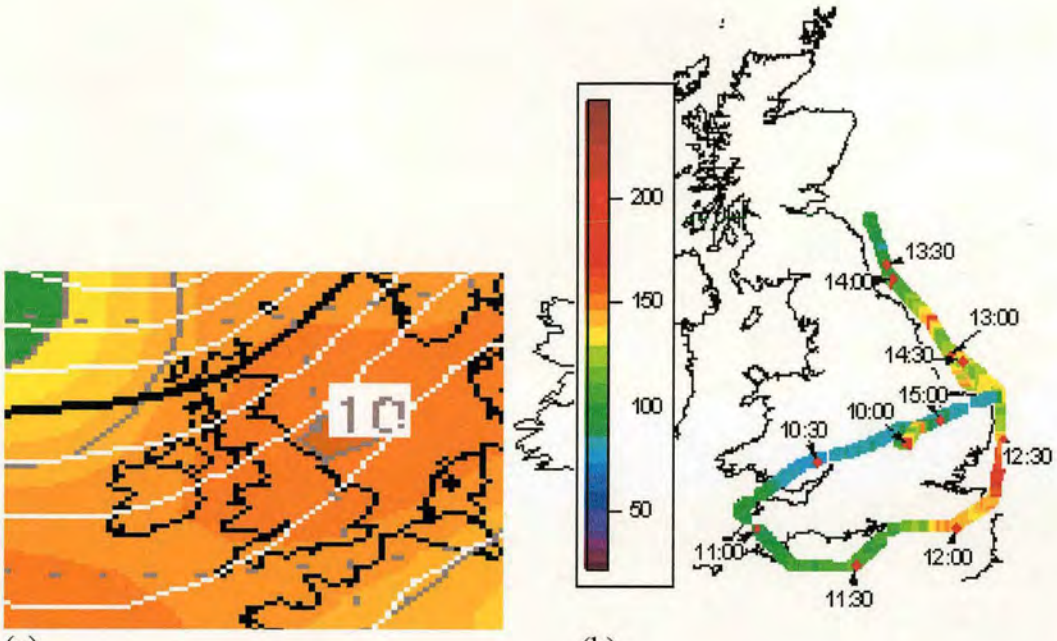

(a) (b)

Figure 45. (a) Synoptic charts for 12:00 19/09/05. (b) CO concentration (ppb) measured along path of flight B130 on 19/09/05 with the position of plane at half hourly intervals marked.

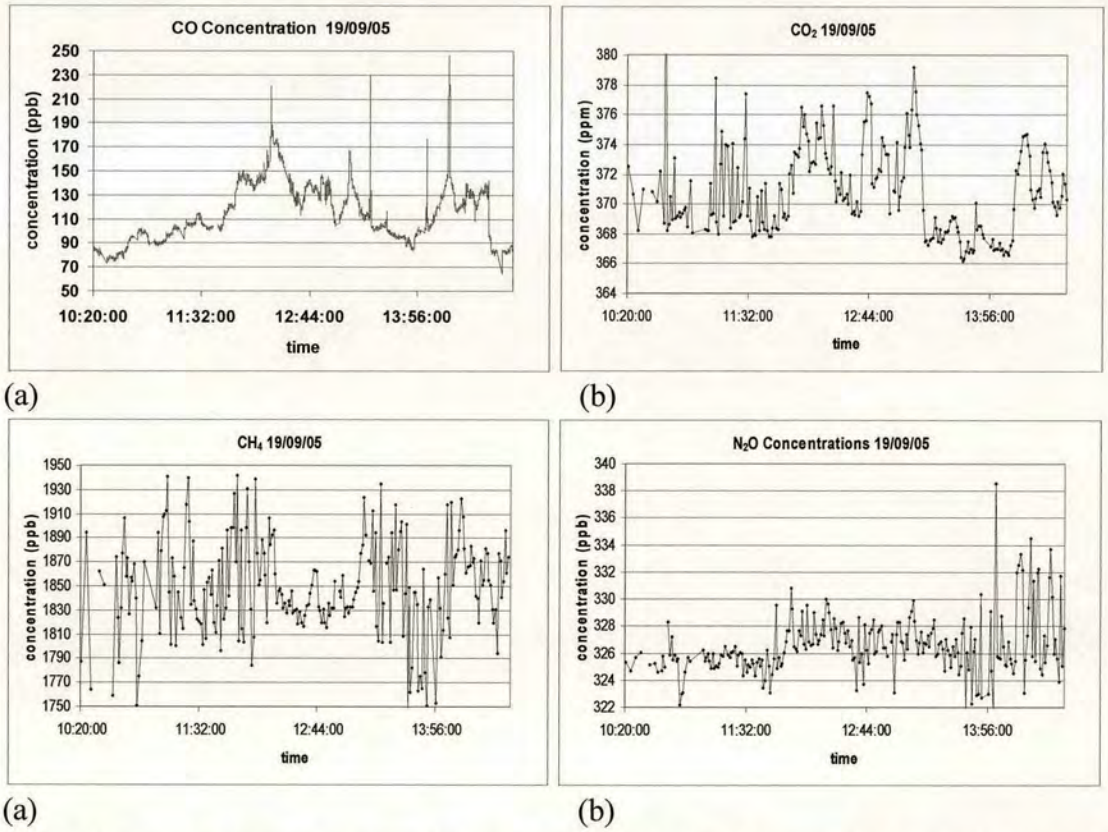

(a) (b)

(a) (b)

Figure 46. Concentrations measured during flight B130. (a) CO concentration (ppb). (b) CO_2 concentration (ppm). (c) CH_4 concentration (ppb). (d) N_2O concentration (ppb).

Figure 47 (a) and (b) show the CO concentration and temperature respectively of five profiles flown during flight B130. Profile 1 was taken over land as shown in Figure 47 (c) and shows an ABL height of around 1500 m. Profile 5 was also taken over land as the aircraft headed inland for the final transit to Cranfield. It shows a decrease in concentration at around 1500 m also. The temperature profiles both show a temperature inversion at around the same height suggesting that over land the ABL height was around 1500 m.

Profile 2 and 3 were both taken in background air. Profile 2 shows a steady but slight decrease in concentration throughout the whole profile while the temperature increases at around 1500 m suggesting that the background concentration is the same above and below the ABL. Profile 3 shows constant concentration up to 1000 m and then a slight decrease with a temperature inversion at about the same height suggesting the ABL is only 1000 m at this location. Profile 4 shows a temperature inversion at around 1600 m not matched in the downwind section of the flight.

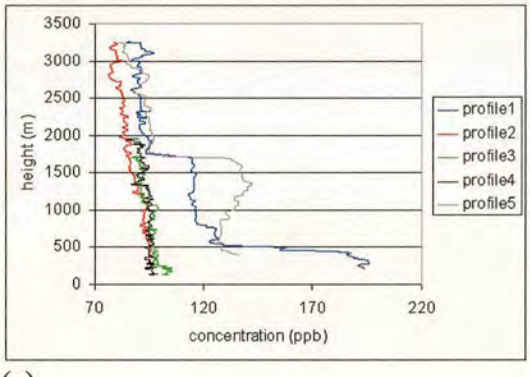

(a)

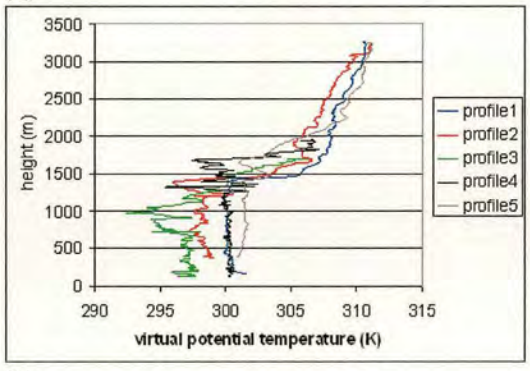

(b)

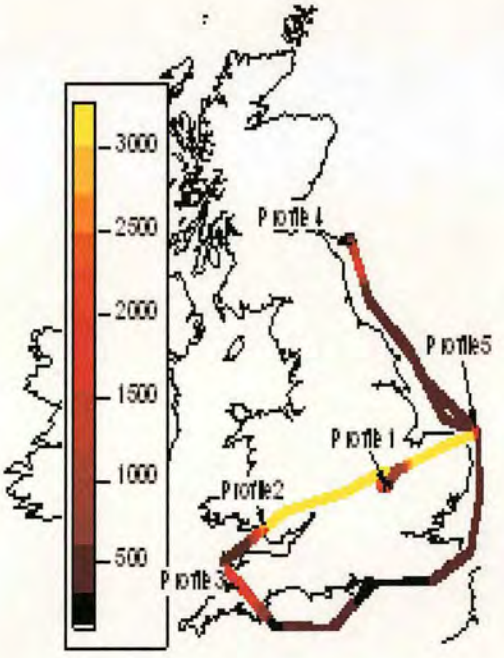

(c)

Figure 47. (a) CO concentration (ppb) of 5 profiles flown during flight. (b) Virtual Potential Temperature (K) of profiles from flight B130. (c) Height (m) of plane during flight B130 and locations of 4 profiles.

3.1.11 Flight B132

Flight B132 takes place on the 21/09/05 in a south westerly wind with an average wind speed of 6 m s^{-1} and direction of 195°. Figure 48 (a) shows the synoptic charts for 00:00 21/09/05 and 00:00 22/09/05. Figure 48 (b) shows the flight path and CO concentration. Of the boundary layer budget species, all were satisfactory. The concentrations are shown in Figure 49 (a), (b), (c) and (d) respectively. Air masses encountered in the English Channel and off south east coast of England were influenced by Continental air.

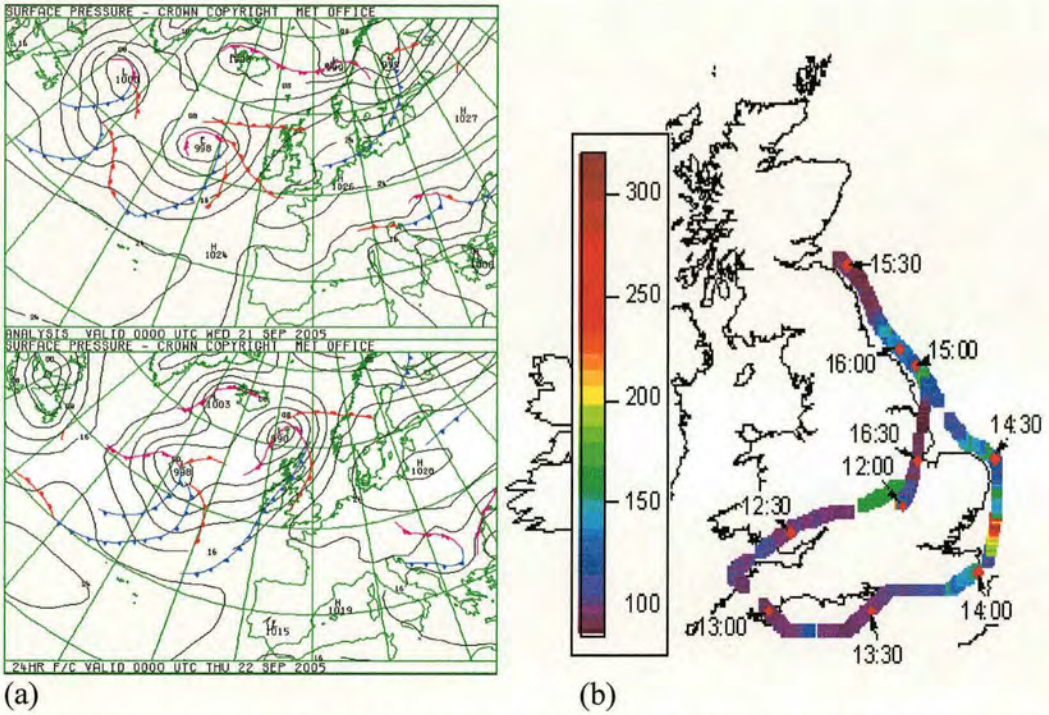

(a) (b)

Figure 48. (a) Synoptic charts for 00:00 21/09/05 and 00:00 22/09/05. (b) CO concentration (ppb) measured along path of flight B132 on 21/09/05 with the position of plane at half hourly intervals marked.

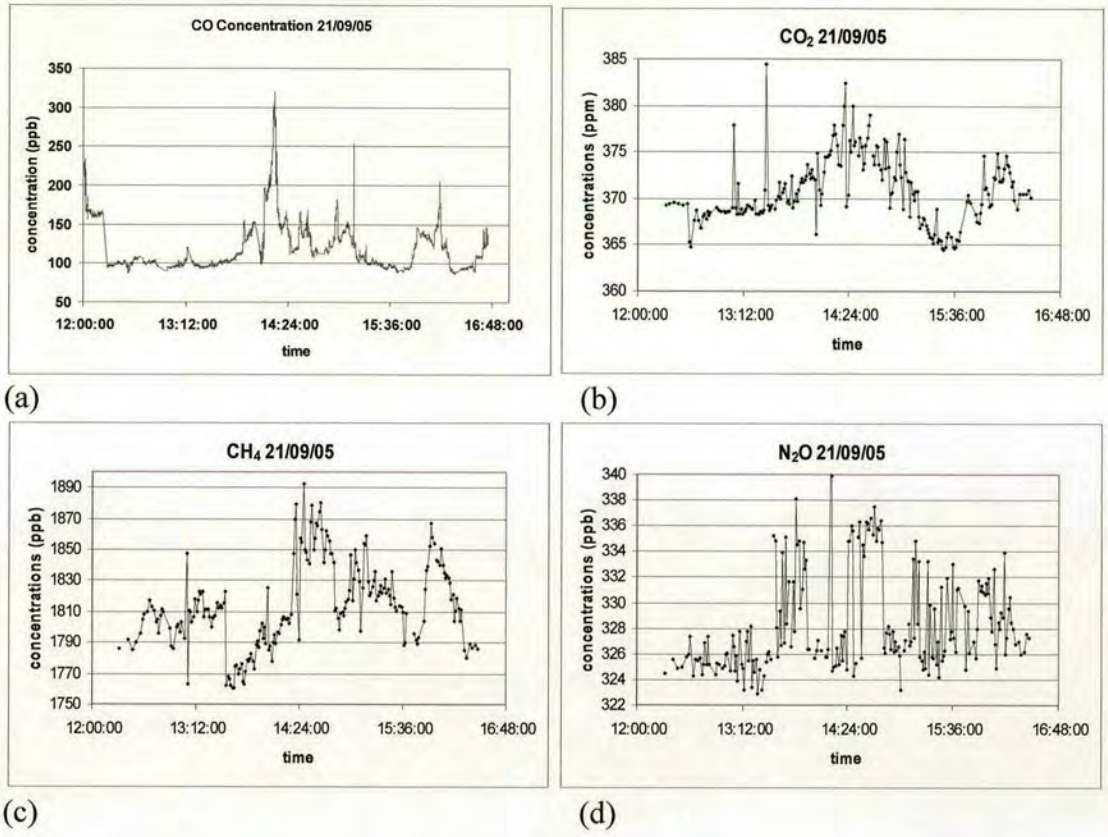

Figure 49. Concentrations measured during flight B132. (a) CO concentration (ppb). (b) CO_2 concentration (ppm). (c) CH_4 concentration (ppb). (d) N_2O concentration (ppb).

Figure 50 (a) and (b) show the CO concentration and temperature respectively of five profiles flown during flight B132. Profile 1 shows much larger concentrations than the other profiles probably because it was taken over land closer to CO sources. It shows a sharp decrease in concentration at around 1100 m suggesting the ABL reaches this height over land. Profiles 2 and 3 are in background air and only profile 2 shows evidence of the ABL top with a slight decrease in concentration at around 1900 m. Temperature profile 3 does not ascend to this height; however there is a temperature inversion at around 1000 m. Profiles 4 and 5 are both in the upwind section of the flight. Profile 5 shows evidence of a temperature inversion at 1500 m with a corresponding decrease in concentration at the same height. Temperature profile 4 shows evidence of a temperature inversion at 1300 m with a slight decrease in concentration at this height. The profiles suggest the ABL reaches to a maximum height of 2000 m during the day in the upwind section of the flight and reaches a height of 1500 m during the downwind section.

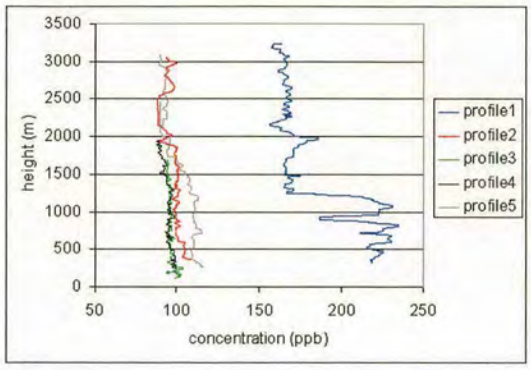

(a)

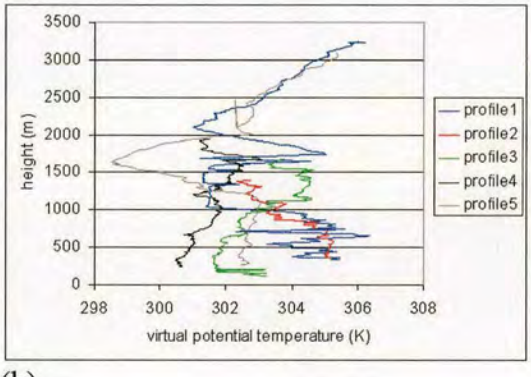

(b)

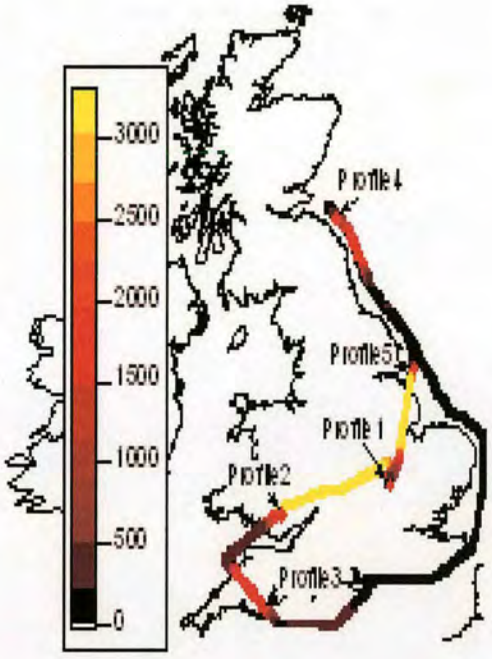

(c)

Figure 50. (a) CO concentration (ppb) of 5 profiles flown during flight B132. (b) Virtual Potential Temperature (K) of profiles from flights B132. (c) Height (m) of plane during flight B132 and locations of 5 profiles.

3.1.12 Flight B134

Flight B134 took place on the 26/09/05 in a south westerly wind with an average wind speed of about 11 m s^{-1} and direction of 215°. Figure 51 (a) shows the synoptic charts for 00:00 26/09/05 and 00:00 27/09/05. Figure 51 (b) shows the flight path and CO concentration. All the boundary layer budget species were satisfactory. The concentrations of CO, CO_2, CH_4 and N_2O are shown in Figure 52 (a), (b), (c) and (d) respectively.

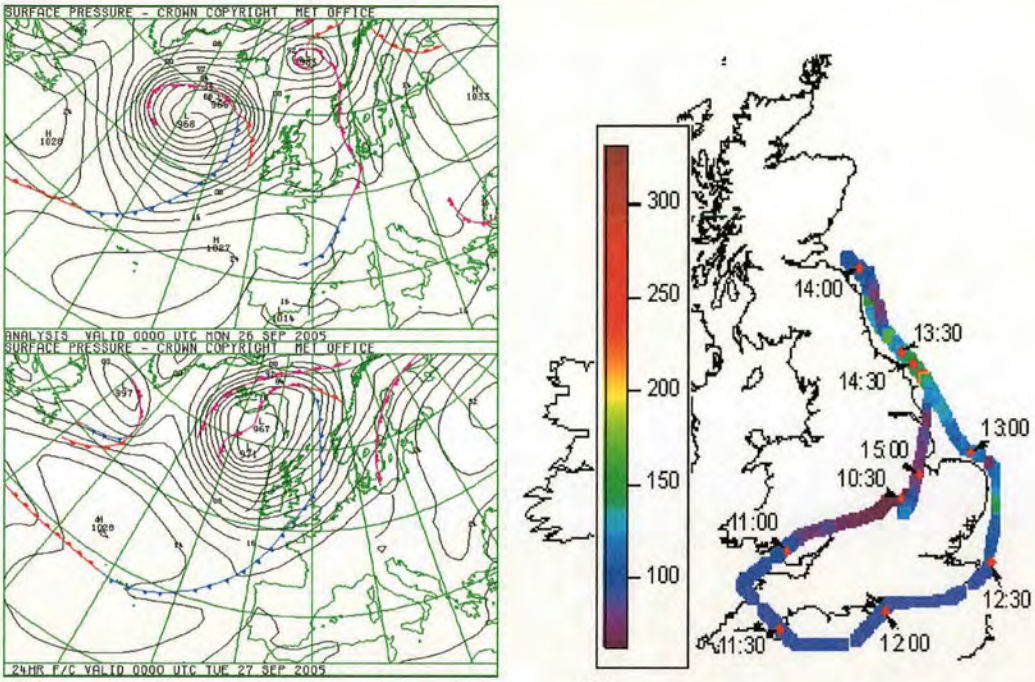

(a) (b)

Figure 51. (a) Synoptic charts for 00:00 26/09/05 and 00:00 27/09/05. (b) CO concentration (ppb) measured along path of flight B134 on 26/09/05 with the position of plane at half hourly intervals marked.

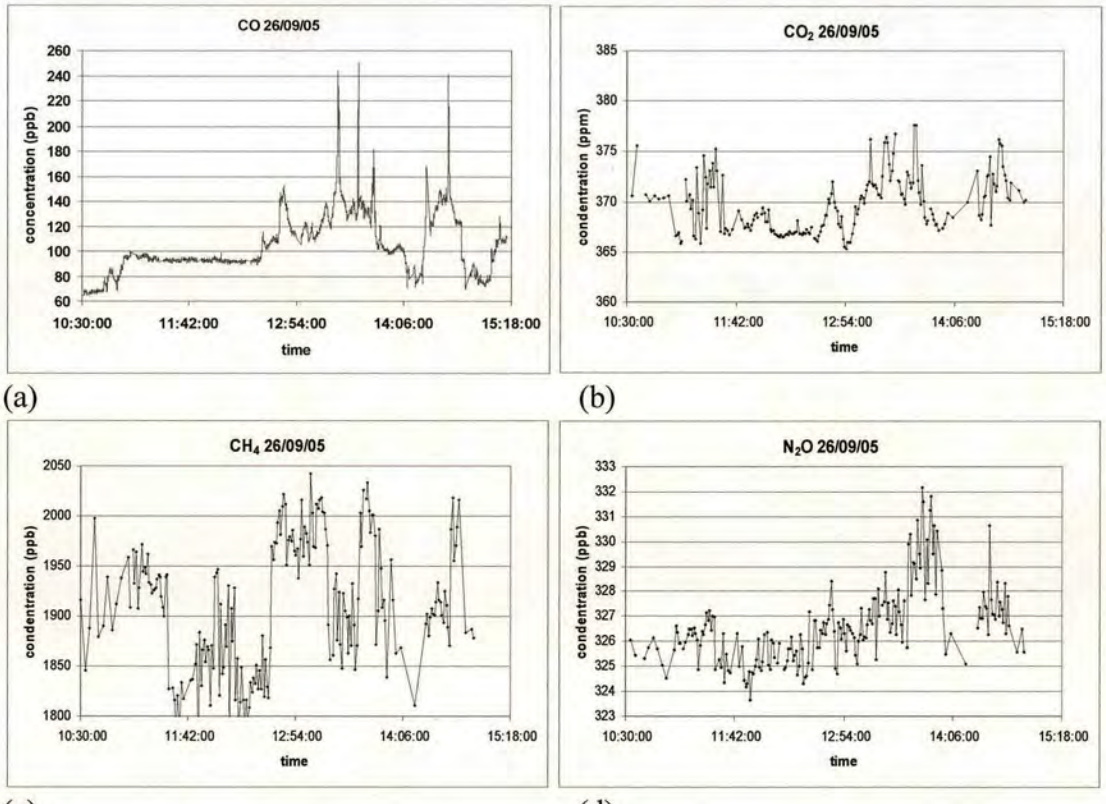

(a) (b)

(c) (d)

Figure 52. Concentrations measured during flight B134. (a) CO concentration (ppb). (b) CO_2 concentration (ppm). (c) CH_4 concentration (ppb). (d) N_2O concentration (ppb).

Figure 53 (a) and (b) show the CO concentration and temperature respectively of five profiles flown during flight B134. The best evidence for the ABL height comes from profiles 1 and 5 which both show a steep decrease in concentration at around 1000 m suggesting a capping inversion at this height. Temperature profile 5 shows a temperature inversion at this height. Profile 4 also shows a decrease in concentration at around 1000 m and a temperature increase at around the same height. Profiles 2 and 3 are in background air and so the concentration remains constant with height despite the presence of a temperature inversion at around 1300 m.

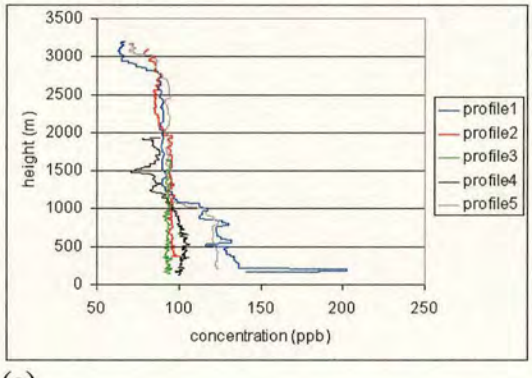

(a)

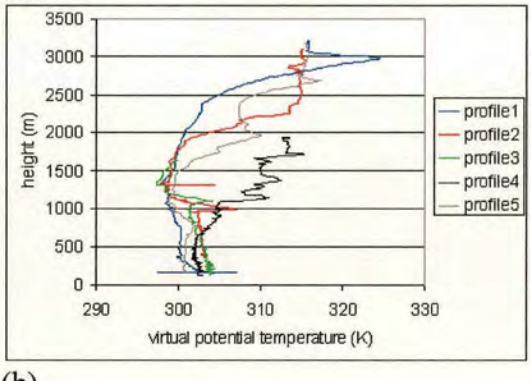

(b)

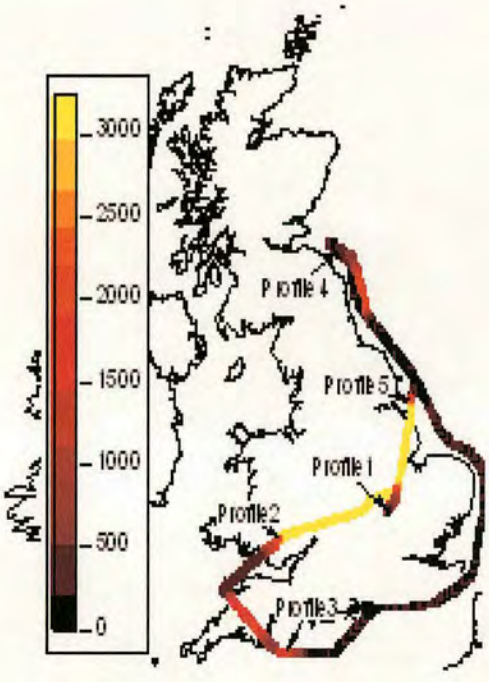

(c)

Figure 53. (a) CO concentration (ppb) of 5 profiles flown during flight B134. (b) Virtual Potential Temperature of profiles form flight B134. (c) Height (m) of plane during flight B134 and locations of 5 profiles.

3.1.13 Flight B136

Flight B136 took place on the 29/09/05 in a north westerly wind with an average wind speed of about 11 m s^{-1} and direction of 292°. Figure 54 (a) shows the synoptic charts for 00:00 29/09/05 and 00:00 30/09/05. Figure 54 (b) shows the flight path and CO concentration. Of the boundary layer budget species, all were satisfactory except CH_4 which was border-line but still good enough to attempt a budget estimate. The concentrations of CO, CO_2, CH_4 and N_2O are shown in Figure 55 (a), (b), (c) and (d) respectively. This is the only flight with a complete circumnavigation of the whole country.

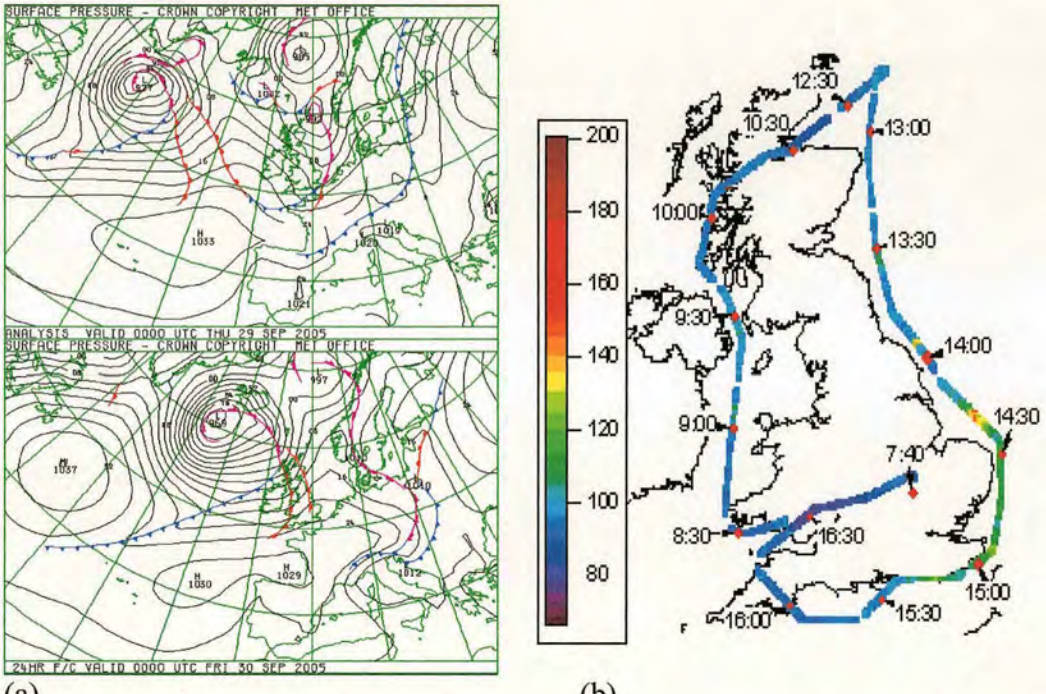

(a) (b)

Figure 54. (a) Synoptic charts for 00:00 29/09/05 and 00:00 30/09/05. (b) CO concentration (ppb) measured along path of flight B136 on 29/09/05 with the position of plane at half hourly intervals marked.

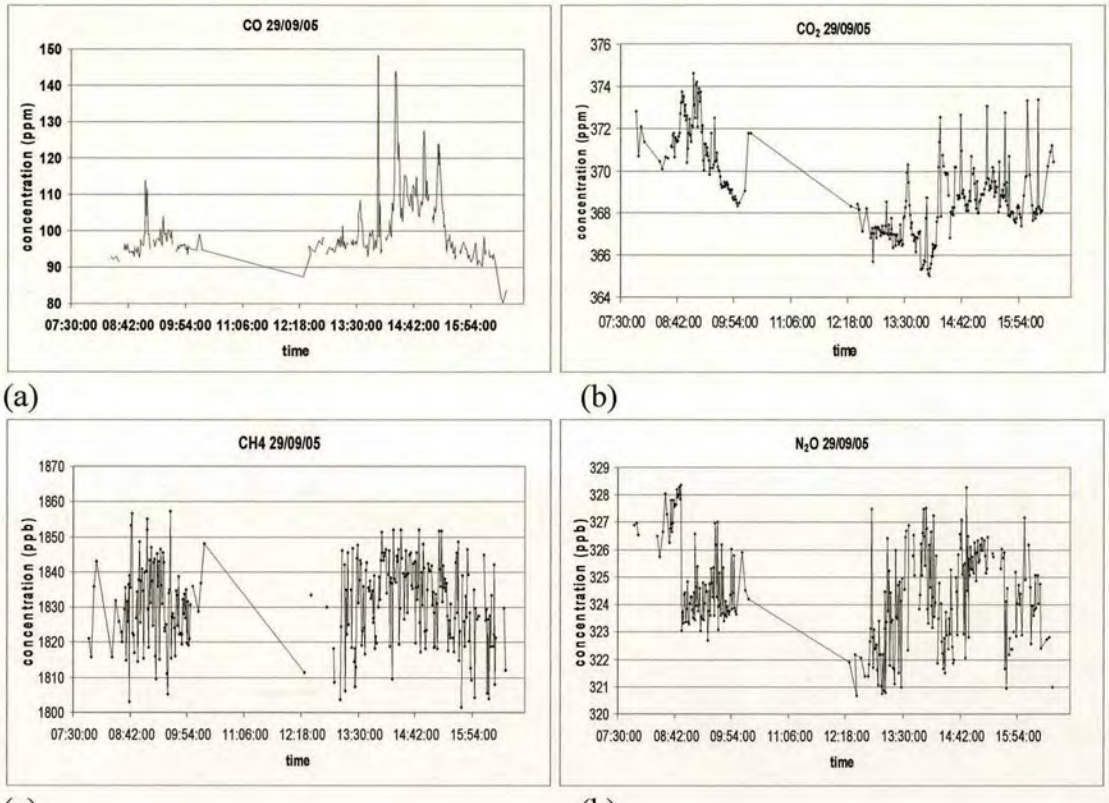

Figure 55. Concentrations measured during flight B136. (a) CO concentrations (ppb). (b) CO_2 concentration (ppm). (c) CH_4 concentration (ppb). (d) N_2O concentration (ppb).

Figure 56 (a) and (b) show the CO concentration and temperature of four profiles flown during flight B136. Profile 2 shows a temperature inversion at 2000 m though the concentration remains relatively constant with height as the profile is in background air. Profile 2 shows the concentration decreasing at around 1500 m with the temperature increasing slightly from around 1000 m. Profile 4 shows the best evidence of a temperature inversion with a sharp temperature increase at 1500 m accompanied by a concentration decrease at around 1700 m. This suggests that the ABL reaches to about 1500 – 2000 m with a temperature inversion at the top trapping the CO emissions below this height.

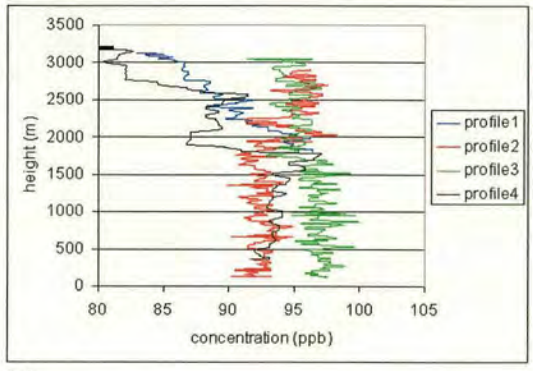

(a)

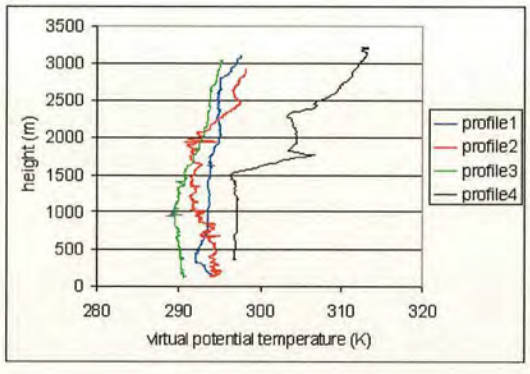

(b)

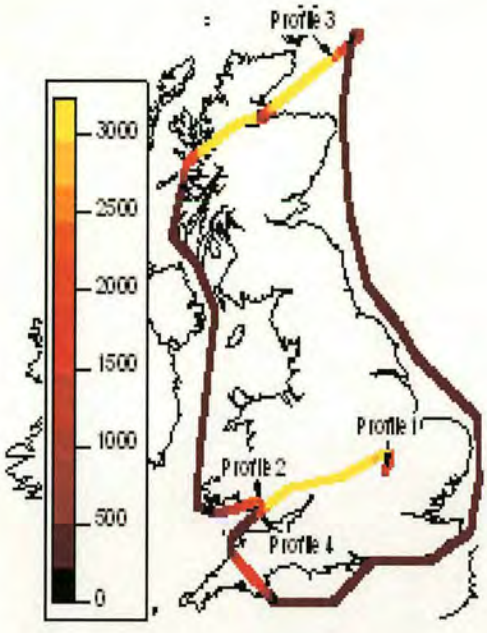

(c)

Figure 56. (a) CO concentration (ppb) of 4 profiles flown during flight B136. (b) Virtual Potential Temperature (K) of profiles from flight B136. (c) Height (m) of plane during flight B136 and locations of 5 profiles.

3.1.14 Flight B244

Flight B244 took place on the 19/09/06 in a westerly wind with an average wind speed of about 14 m s^{-1} and direction of 257°. Figure 57 (a) shows the synoptic charts for 00:00 19/09/06 and 00:00 20/09/06. Figure 57 (b) shows the flight path and CO concentration. Of the boundary layer budget species, all were satisfactory except N_2O which was border-line but still good enough to attempt a budget estimate. The concentrations of CO, CO_2, CH_4 and N_2O are shown in Figure 58 (a), (b), (c) and (d) respectively.

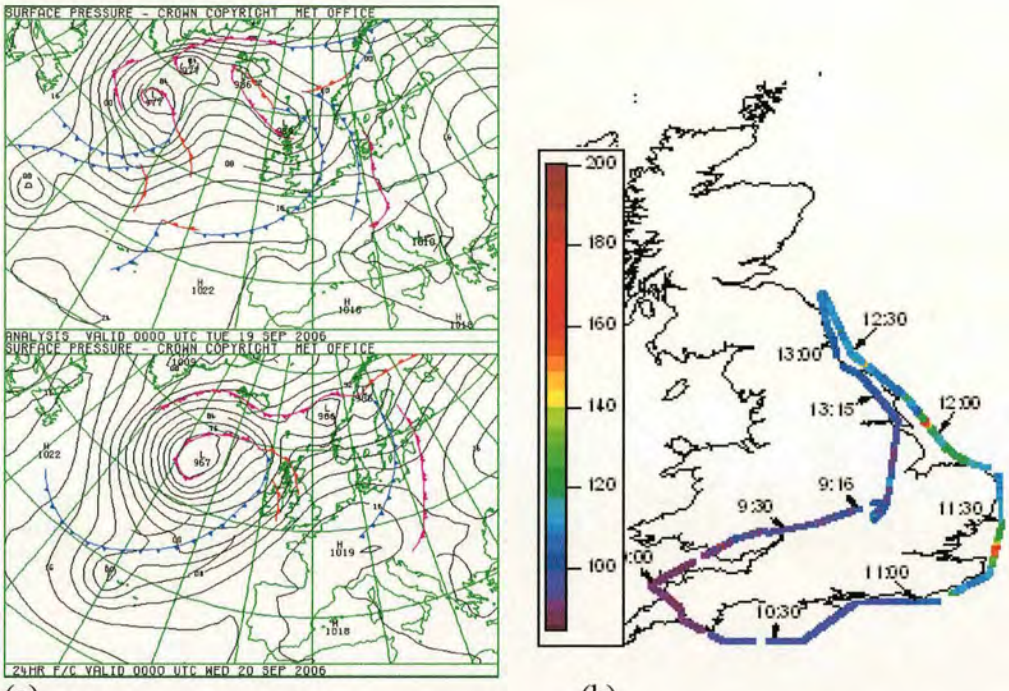

(a) (b)

Figure 57. (a) Synoptic charts for 00:00 19/09/06 and 00:00 20/09/06. (b) CO concentration (ppb) measured along path of flight B244 on 19/09/06 with the position of plane at half hourly intervals marked.

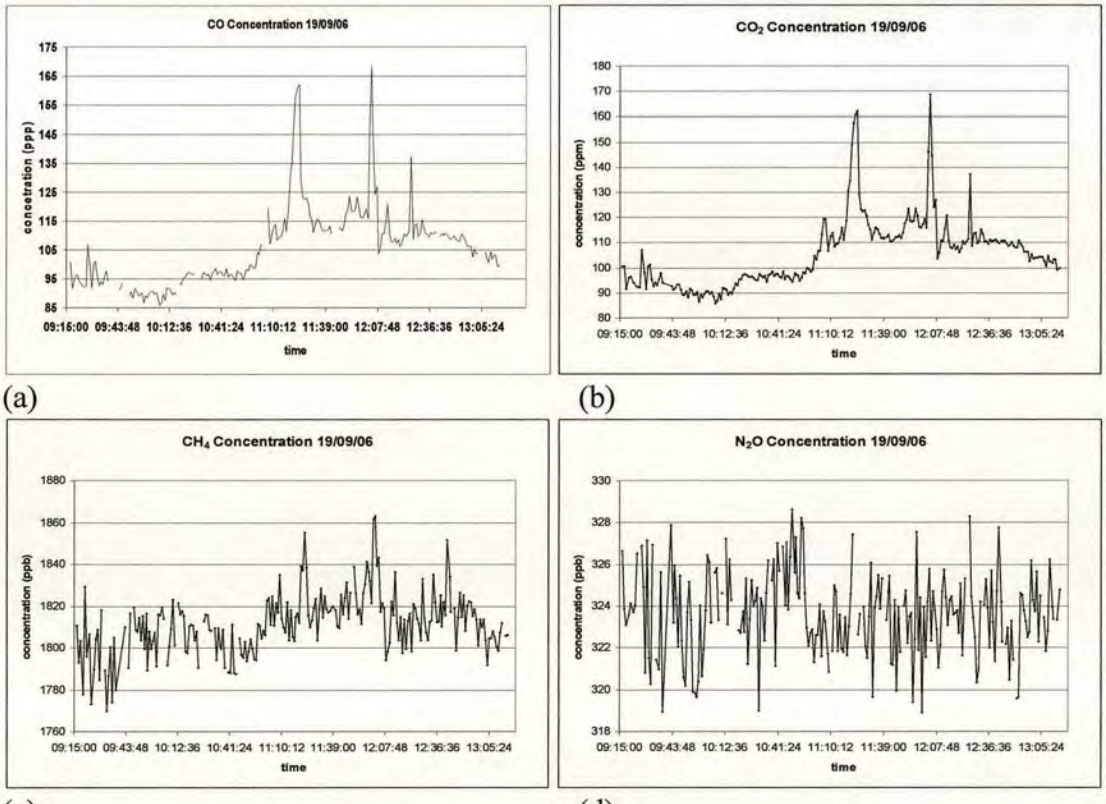

(a) (b)

(c) (d)

Figure 58. Concentrations measured during flight B244. (a) CO concentration (ppb). (b) CO_2 concentration (ppm). (c) CH_4 concentration (ppb). (d) N_2O concentration (ppb).

Figure 59 (a) and (b) show the CO concentration and temperature of four profiles flown during flight B244. Profile 1 shows a gradual decrease in concentration as the aircraft takes off up to a height of around 800 m where the concentration levels off. Its is possible that the decrease seen up to this height is the plane flying away from a local source and not a result of the structure of the boundary layer. At a height of 2000 m the concentration decreases quickly suggesting a capping inversion at this height with the temperature increasing from 2100 m. Profile 2 is taken as the plane descends to measure the background air in the Bristol Channel as seen in Figure 59 (c). The variation in concentration in this profile particularly the larger spike at around 1400 m is more likely due to flying in close proximity to CO sources rather than due to the structure of the ABL. At around 1700 m there is a decrease in concentration with a temperature inversion from around 2000 m. Above 1700 m there is an increase in concentration from 2300 m to 2800 m. This may be the residual boundary layer from the previous day. We see a similar structure in profile 1, though the increase is less dramatic. Profile 4 shows relatively constant concentration throughout with a slightly drop at around 2000 m with a temperature inversion at around 2300 m. This suggests that the ABL reaches at height of 2300 m in the downwind section of the flight.

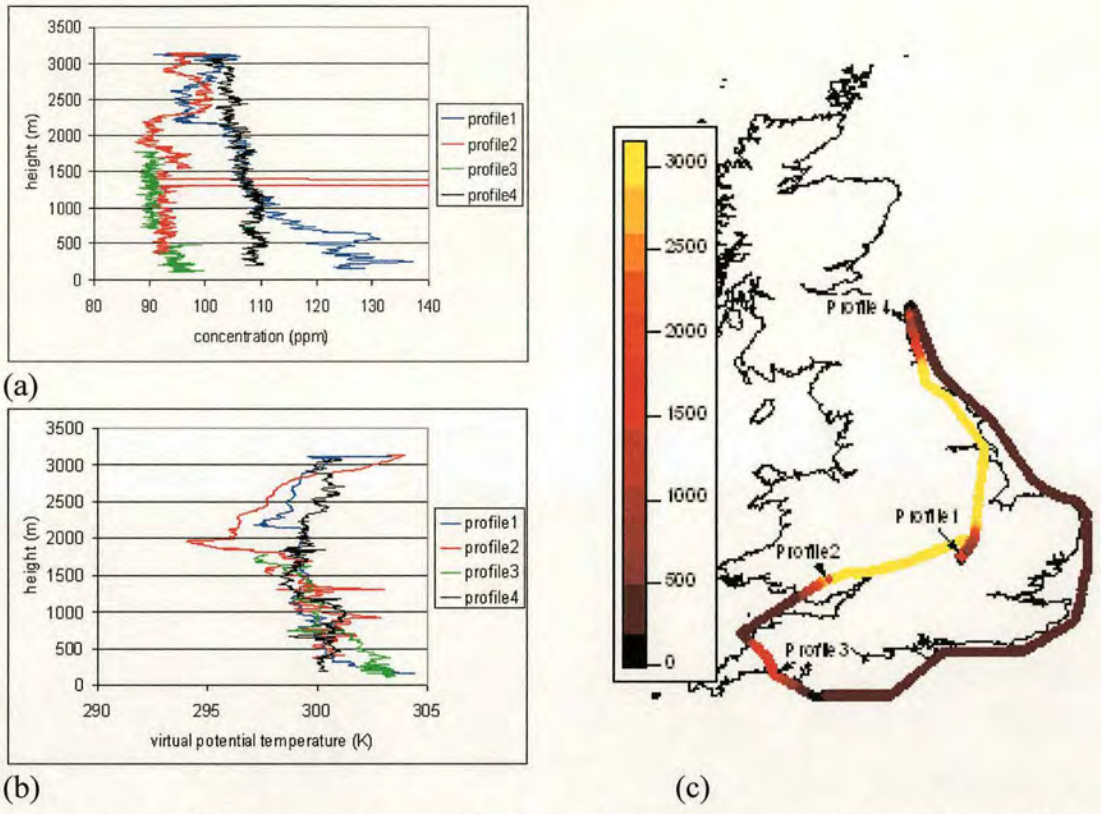

Figure 59. (a) CO concentration (ppb) of 4 profiles flown during flight B244. (b) Virtual Potential Temperature (K) of profiles from B244. (c) Height (m) of plane during flight B244 and locations of 5 profiles.

3.2 Summary of Campaign and Data

Conditions on 14 of the flights were suitable for a boundary budget analysis providing data for May to September. All flights had evidence of a temperature inversion at the top of the ABL trapping UK emissions, permitting the use of the boundary layer budget method. Relatively constant concentration with height provided good evidence that a uniform background concentration could be applied to the upwind air with the concentration remaining constant below and above a temperature inversion at the top of the ABL. Relatively constant concentration with height up to the top of the ABL in the downwind section of the flights suggests that measurement in the mid boundary layer were representative for the whole depth of the ABL. However flying profiles over land tended to complicate the measurement of the structure of the ABL. This is a

result to flying close to sources and the potential for changing ABL height with position, particularly when a profile is flown partly over land and partly over sea.

No instrument problems were encountered for CO or CO_2 providing consistent and high quality data for both species for all flights. The CO data can therefore be used as a basis for determining the suitability of a day for a boundary layer budget type analysis as all major sources are anthropogenic allowing UK plumes to be easily identified. Furthermore the analysis of the CO data can be used to determine the success of the NAME model and the NAEI emissions inventory in simulating the UK outflow as there should be no biogenic signal to interfere with the interpretation of the measurements. This allows a baseline which the other species with relatively more complex sources and greater uncertainty in the emissions and / or measurements can be compared to.

Problems with the TDL diode resulted in loss of CH_4 and N_2O data for some flights and greater variability in data quality. While certain flights produced high quality data for either N_2O or CH_4, only flight B134 produced high quality data for both species. N_2O was less affected by diode problems producing nines days of high quality data with CH_4 data only consider high quality on 5 flights. However by weighting the flights according to measurement noise and background concentration uncertainty, data from days where the data is noisy but still showing a strong outflow signal, can be included in the analysis greatly increasing the number of observations in the data set.

A factor that also needs to be considered is the bias in the data set towards the summer months. While this should not be a significant factor for CO or CH_4 it should be noted that CO_2 emissions will be lower in the summer with energy use at a minimum. However the relative difference in winter and summer energy consumption will depend on the temperatures over the winter and summer months with relatively warmer winters resulting in less energy consumption due to lower heating demands and hotter summers resulting in more energy consumption with greater demand for air conditioning. N_2O is also affected by seasonal variations as microbial activity in soils is very dependent on temperature. Emissions will broadly expected to be lower in winter months however dry summer months may act to suppress emissions as microbial activity is also strongly dependent on water content. Anthropogenic factors

will also alter emissions with application of mineral fertilisers expected to significantly increase emissions. This would be expected to peak in the spring prior to the start of the AMPEP campaign. Therefore annual emissions calculated from the AMPEP data are subject to two opposing factors with winter emissions expected to be smaller than those during the AMPEP campaign and spring emissions expected to be larger. It should also be noted the summer of 2005 was drier than normal and so the summer emissions of N_2O are therefore expected to be smaller than for a typical year.

Chapter 4 NAME Analysis of Flights

4.1 Introduction

Each flight was analysed using the NAME model and the current emission inventories. The NAME model was run in forward mode using the analysed Unified Model data at 16 km spatial resolution and 1 hour temporal resolution. The source data in the model are the mapped emissions data of the NAEI for 2004 for CO, CO_2 and N_2O and the CEH Edinburgh spatially disaggregated emissions from 1994 for CH_4. The CO, N_2O and CH_4 emissions were put into a 5 km × 5 km resolution grid with each grid square emitting from the entire model run at a constant rate (g s^{-1}) representing an average of the annual emitted flux. The CO_2 emissions were put into a 10 km × 10 km grid as a 5 km resolution would have required additional memory to track significantly more particles. Traffic emissions are included separately as the emitted flux is weighted to reflect day of the week and hour of the day.

The model ran for each chemical species individually using meteorology for the three days preceding the flight allowing the model to spin-up and for the day of the flight itself. The model timestep was set at 900 s with new particles released at the start of each time-step. All new and existing particles were then transported using the mean wind, turbulence and meander terms. CO, CH_4 and N_2O are passive tracers and so no further processing is carried out the particles at the end of each timestep. For CO_2, the total particle mass in each grid box is converted into a concentration, the biogenic flux is then calculated and the concentration updated accordingly. The total mass in each grid box is then assigns back to particles and the model proceeds with the following timestep.

The location for each bag sample is defined in the model setup and an hourly time-series output for each observation. Taking the model concentration at the hour nearest to the time of the actual observation produces a concentration series along the outflow for comparison with the measured data.

By comparing the model and measured concentrations it is possible to validate the emission inventories. The correlation between the two series indicates the accuracy of the spatial disaggregation of the emissions and can be used to compare the accuracy

of the inventories of the different chemical species. Comparing the absolute values of the concentrations for the two series can indicate whether the emissions are over or underestimated. The concentration maps produced by NAME can also be used to determine the source of the outflow plumes helping to identify which areas of the inventory are accurate and which are not with source location also acting as an indicator of source sector. As an example Figure 60 shows the outflow plumes for fight B112 for CO with the source area of each plume labelled.

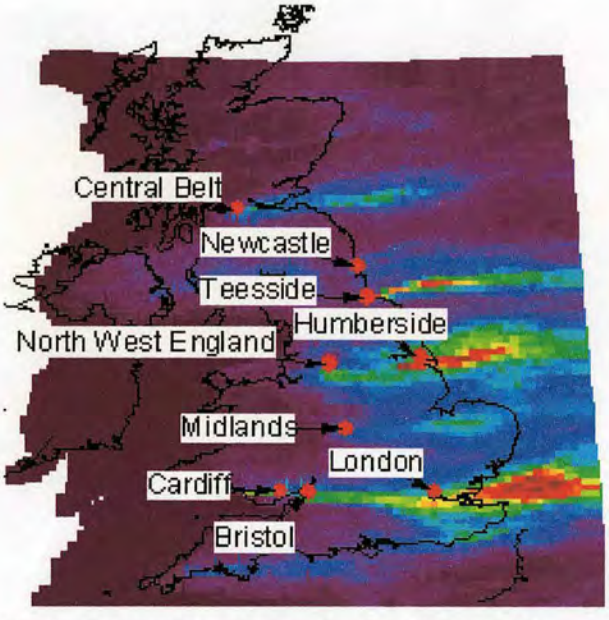

Figure 60. Outflow plumes for CO flight B112.

4.2 Results of NAME Simulations of Individual Flights

4.2.1 Flight B92 09/05/05

Flight B92 took place in a north westerly flow. CO, CO_2 and N_2O were analysed using the NAME model, (CH_4 was too poor). The NAME concentration maps for CO, CO_2 and N_2O for 12:00 09/05/05 are shown in Figure 61 (a), (b) and (c) respectively. Figure 61 (a) shows the NAME and observed CO concentrations. The main outflow is in the south east with smaller plumes to the south west. CO is a marker of urban anthropogenic sources and outflow plumes from London, North West England and Teesside are identifiable on the NAME map. The location of the outflow predicted by NAME matches the measured plumes. Similarly for CO_2 shown in Figure 61 (b), the

model predicts the location of the main outflow. From Figure 61 (c) for N_2O the measurements indicate that the main outflow is along the east coast while NAME predicts it to be along the south coast.

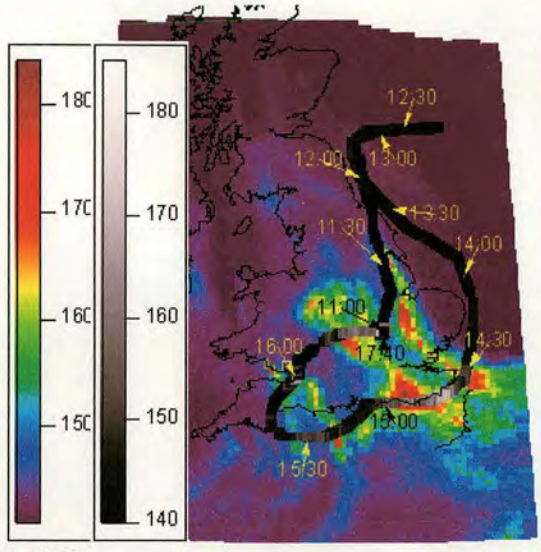

(a) CO

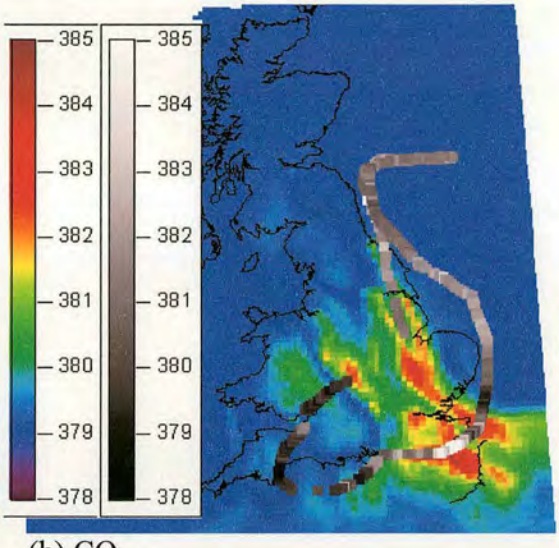

(b) CO_2

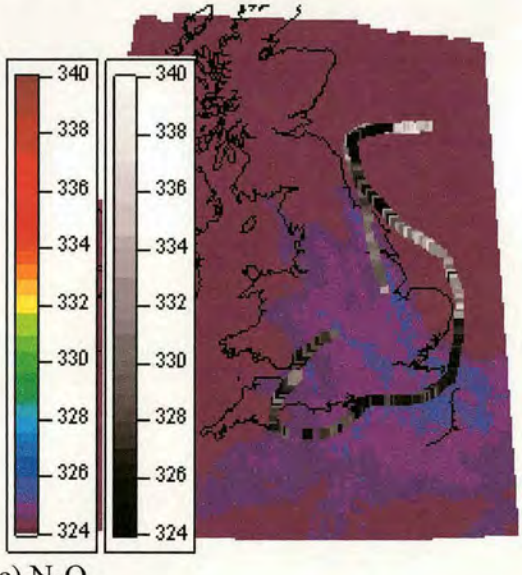

(c) N_2O

Figure 61. NAME concentration map for 12:00 09/05/05 (rainbow) with sample concentration (grey) overlaid. (a) CO (ppb) with aircraft times. (b) CO_2 (ppm). (c) N_2O (ppb).

Figure 62 (a), (b) and (c) show the modelled and measured concentrations for CO, CO_2 and N_2O respectively. The CO modelled concentrations are in very good agreement with the measured concentrations with a highly significant (p-value < 0.01) correlation between the two series with a correlation coefficient (R) of 0.71. The CO_2

concentrations are also in good agreement ($R = 0.43$, p-value < 0.01) with the model capturing the main outflow plume well. However the measurements show larger concentrations along the east coast which the model does not predict, possibly from sources not included in the inventory such as coastal shipping and oil and gas platforms in the North Sea. Overall both CO and CO_2 show good agreement between modelled and measured concentrations suggesting their emission inventories are accurate and that given accurate emissions, NAME is able to capture the outflow pattern.

The N_2O measurements are relatively poor for this day and several samples have been excluded from the analysis as they were considered too unreliable. These samples were taken mostly along the east coast and account for the large concentrations in this area. The remaining data is still relatively poor quality compared to other flights, however the measurements indicate fairly broad plumes along the south coast, consistent with rural emissions over large areas. The model does predict a small plume in the south east but massively underestimates the concentrations. The correlation between the modelled and measured concentration is poor and is not statistically significant. This is likely due to a combination of poor quality data and inaccuracies in the emission inventory.

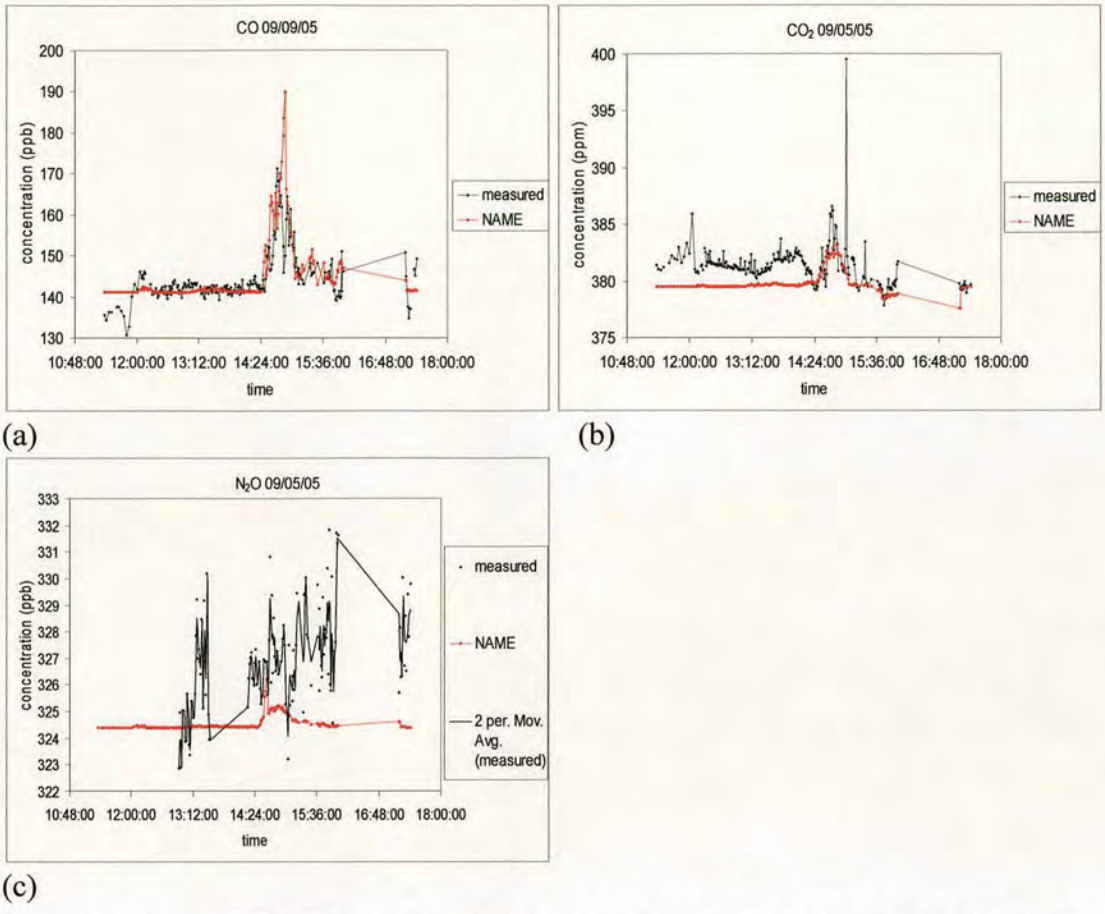

Figure 62. Measured (black) and NAME (red) sample concentration for flight B92. (a) CO (ppb). (b) CO_2 (ppm). (c) N_2O (ppb) with moving average applied to measured data.

4.2.2 Flight B97 25/05/05

Flight B97 took place in a south westerly flow. All four chemical species were analysed with NAME although the N_2O data is very noisy. Figure 63 (a), (b), (c) and (d) show the NAME and measured concentrations for CO, CO_2, CH_4 and N_2O respectively. From Figure 63 (a), the outflow plumes from urban sources are clearly visible along the east coast with a particularly large point source on the north east. The CO_2 concentrations are enhanced along the English Channel which the model does not predict, however it does manage to reproduce the location of the main outflow plumes from the UK from London and Humberside. Figure 63 (c) shows the CH_4 plume along the east coast as a broader structure incorporating emissions from larger, more rural areas as well as some urban emissions. The plume also seems to mostly originate from larger area sources with large emissions from the midlands.

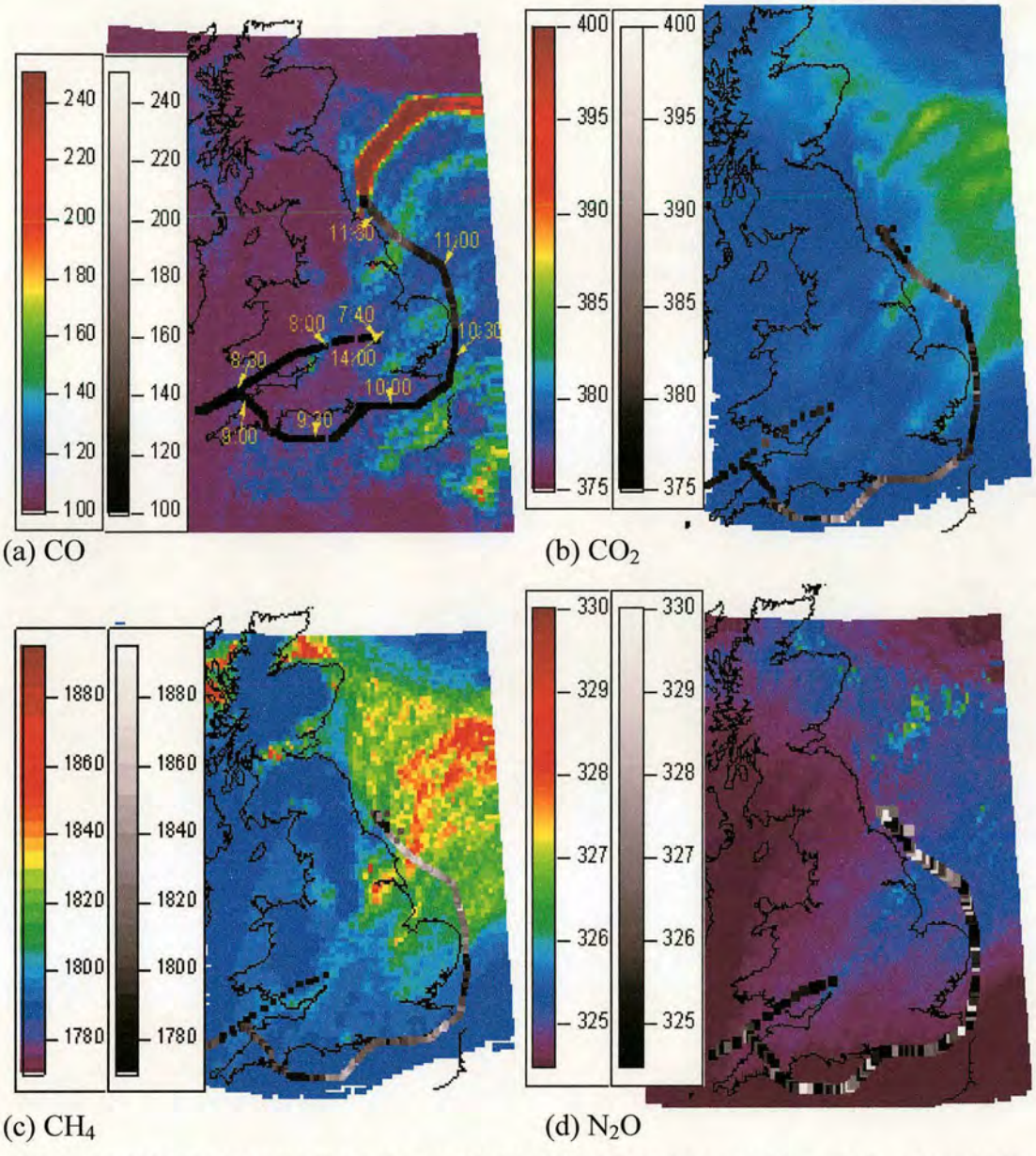

(a) CO (b) CO_2

(c) CH_4 (d) N_2O

Figure 63. NAME concentration map for 12:00 25/05/05 (rainbow) with sample concentration (grey) overlaid. (a) CO (ppb) and aircraft times. (b) CO_2 (ppm). (c) CH_4 (ppb). (d) N_2O (ppb).

Figure 64 shows the modelled and measured concentration of each sample for each chemical species. The measured series show large concentrations for samples in the English Channel which are mostly due to emissions from the Continental Europe and so are not captured by the model. The outflow plumes for CO and CO_2 and CH_4, shown in Figure 64 (a), (b) and (c), the model is able to reproduce accurately while the N_2O measurements, though very noisy, do show much larger concentrations where the model suggests the main outflow plume should be. The correlations between the modelled and measured outflow for CO, CO_2 and CH_4 are all statistically

significant (R = 0.70 for CO, R = 0.43 for CO_2 and R = 0.69 for CH_4). For N_2O the correlation is not statistically significant.

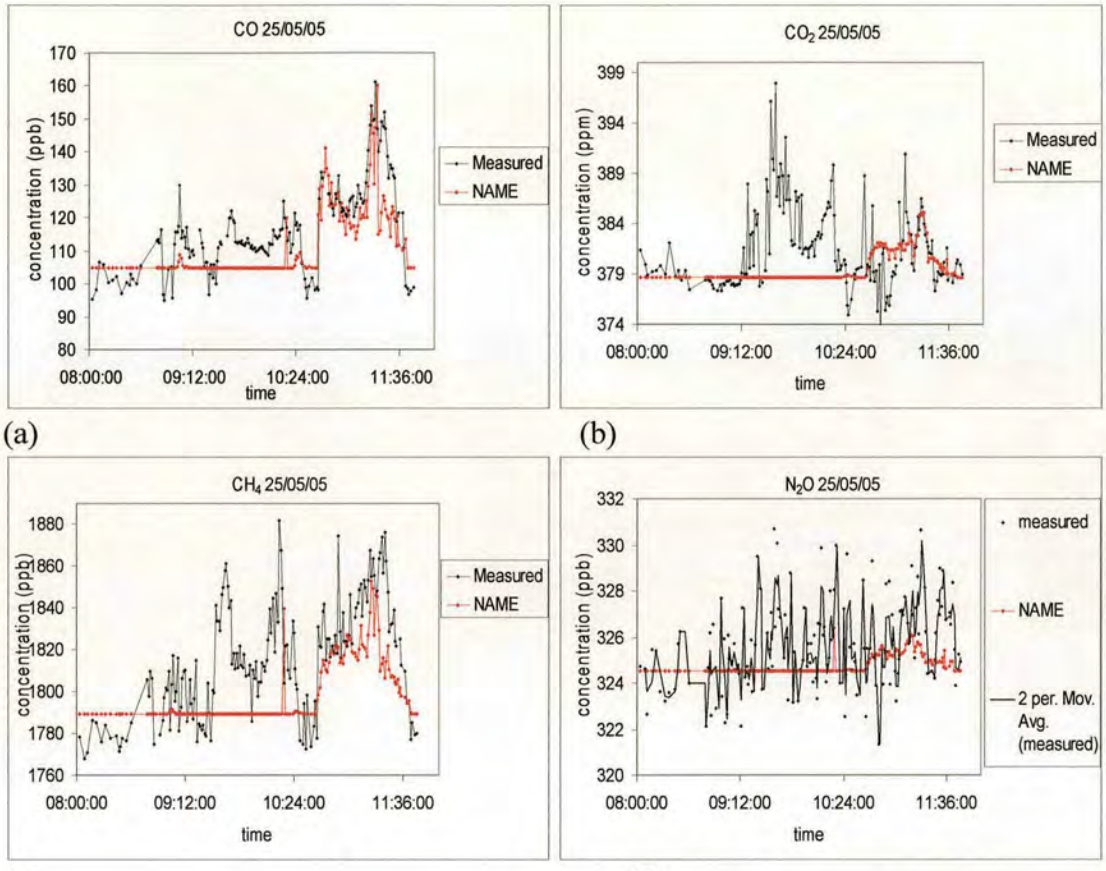

Figure 64. Measured (black) and NAME (red) sample concentration for flight B97. (a) CO (ppb). (b) CO_2 (ppm). (c) CH_4 (ppb). (d) N_2O (ppb) with moving average applied to measured data.

4.2.3 Flight B102 14/06/05

Flight B102 took place in a westerly flow. The CO, CO_2 and N_2O were analysed with NAME while the CH_4 data was considered too poor. Figure 65 (a), (b) and (c) show the modelled and measured concentrations for CO, CO_2 and N_2O respectively. Figure 65 (a) shows the CO plumes as predicted by NAME along the east coast corresponding well with the measured outflow. Figure 65 (b) shows the CO_2 outflow plumes along the east coast from the north west of England, Humberside and Teesside which the model is able to reproduce. However the CO_2 concentrations are elevated

all along the English Channel which the model does not predict. Figure 65 (c) shows the N_2O modelled plumes also along the east coast. The measured concentrations are larger along this stretch of the flight however the largest concentrations are in the English Channel which have not been reproduced by the model.

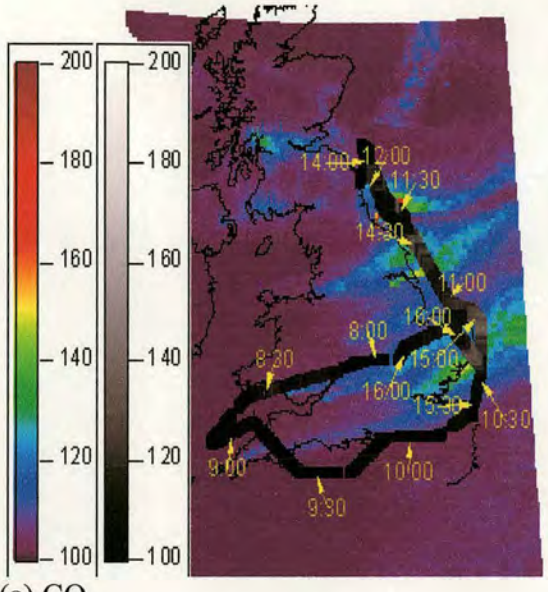

(a) CO

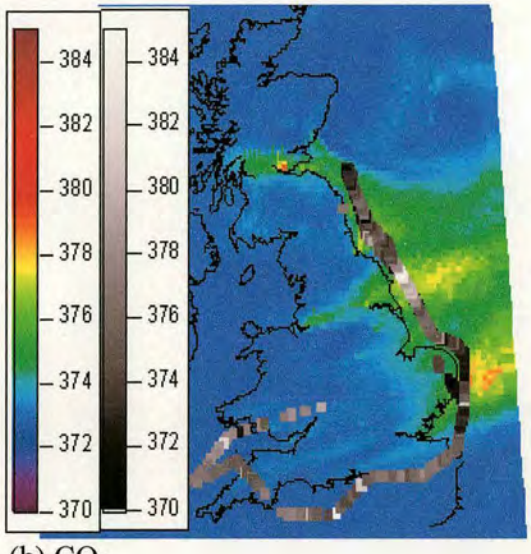

(b) CO_2

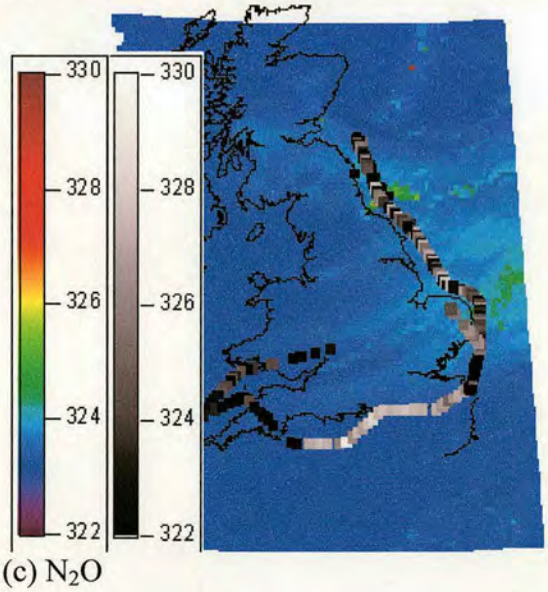

(c) N_2O

Figure 65. NAME concentration map for 12:00 14/06/05 (rainbow) with sample concentration (grey) overlaid. (a) CO (ppb) and aircraft times. (b) CO_2 (ppm). (c) N_2O (ppb).

Figure 66 (a), (b) and (c) show the modelled and measured concentrations of each sample for CO, CO_2, and N_2O. For CO, the NAME model is able to predict the outflow very accurately with meteorology producing ideal conditions with a low,

uniform background concentration and no complexity introduced by inflow or stagnant air. For CO_2, there is a distinct decrease in concentration over time particularly when comparing the same plumes from the northbound and southbound legs. The model is able to reproduce much of the outflow, however there are enhanced concentrations observed over the English Channel which are not reproduced by the model. It is unlikely that these are due to shipping in the Channel as the CO concentrations are not enhanced. The N_2O concentrations are also enhanced along this leg of the flight suggesting that the source of the CO_2 enhancement is respiration from agricultural land in the south west of the country from the previous night. The origin of each plume has been labelled on both the CO and CO_2 plots. It is clear that while the CO outflow concentration remains relatively constant between the northbound and southbound legs, the CO_2 concentration decreases significantly. As the CO concentrations do not change between the legs, the decrease in CO_2 concentration is most likely the result of photosynthesis. This biogenic signal is only evident on a small number of flights and flight B102 is the clearest example. The flight takes place in mid June, when photosynthesis would be expected to be high. The take-off time for this flight is also slightly earlier than usual and may explain why the biogenic signal is much stronger on this day with larger concentrations earlier in the flight from air advected across the country mostly overnight and smaller concentrations later in the flight from air that travelled across the country after photosynthesis has started.

The N_2O data is much noisier than either the CO or CO_2 data but it is possible to identify outflow plumes along the east coast. However the concentrations measured in the outflow are much larger than the modelled concentrations. The measurements also show large concentrations along the English Channel which are not reproduced by the model. It is unlikely that this is due to inflow from elsewhere and the most likely explanation for these enhanced concentrations are emissions from agricultural land in the south west of England that are not present in the current inventory.

The modelled and measured data for CO are highly correlated with $R = 0.59$. For CO_2, the whole time-series is not correlated with $R = -0.03$. This is due to the enhanced concentrations along the Channel. Looking at only the outflow, the modelled and measured data are correlated to a statistically significant level with $R = 0.35$. The N_2O model data is correlated with the measured data to a statistically

significant level, but the correlation is still weak with R = 0.23, reflecting the fact the enhancement in the English Channel is not reproduced by the model. Overall the concentrations predicted by the model are much smaller than those measured suggesting the emission inventory is significantly underestimating N_2O emissions on this day.

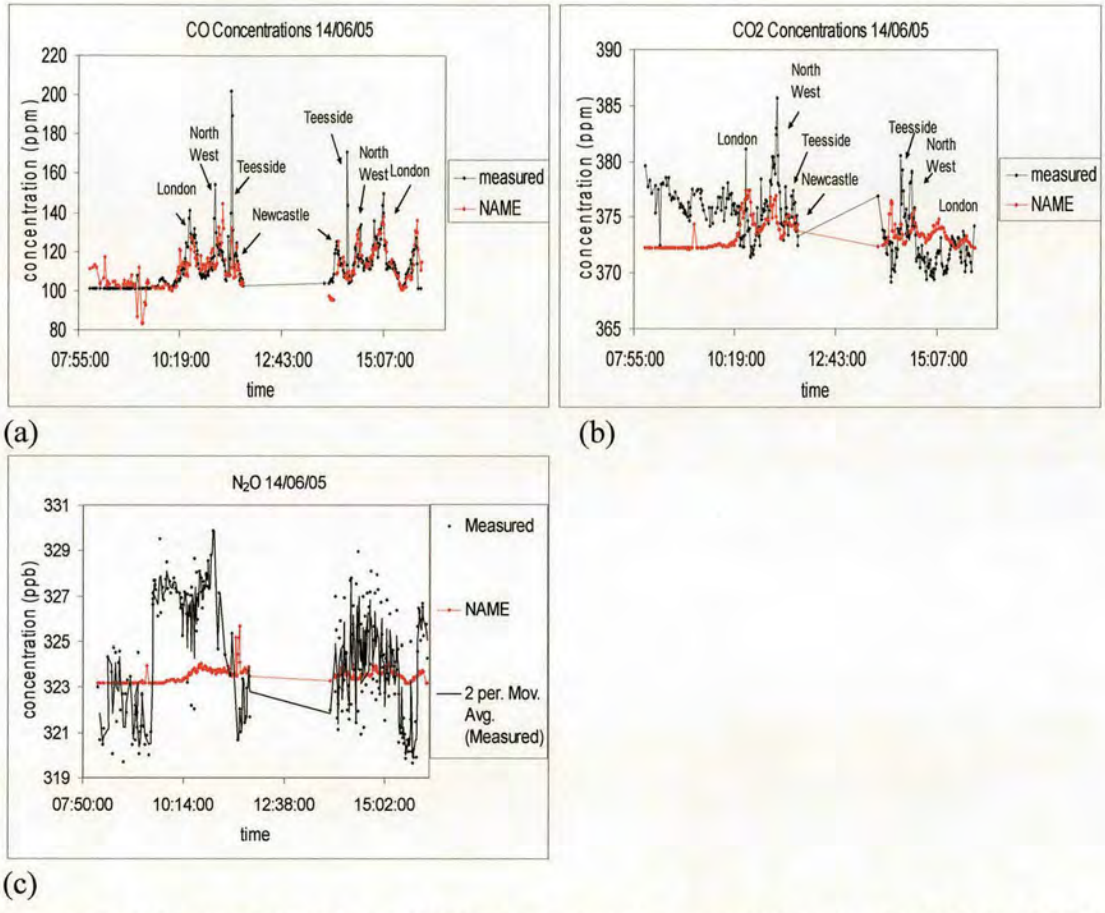

(a) (b)

(c)

Figure 66. Measured (black) and NAME (red) sample concentration for flight B102. (a) CO (ppb). (b) CO_2 (ppm). (c) N_2O (ppb) with moving average applied to measured data.

4.2.4 Flight B111 14/07/05

The wind flow on this day was more complex than for a typical flight with divergent wind flow in the south of the country and inflow from Europe overlapping with the outflow from the UK. Outflow Plumes from London, Humberside and Teesside are still evident along the east coast for CO shown in Figure 67 (a), however they sit on

top of a plume from Europe making the enhancement from the UK hard to quantify. The CO_2 outflow, shown in Figure 67 (b), shows plumes from the north west of England and Humberside and Teesside between 9:30 and 9:50 which the model is able to predict however there are also enhanced concentrations off the east coast of Scotland around 11:00 that do not correspond to any emissions from the UK. The N_2O outflow, shown in Figure 67 (c), shows enhanced concentrations all along the east coast with small plumes corresponding to the Midlands and Teesside.

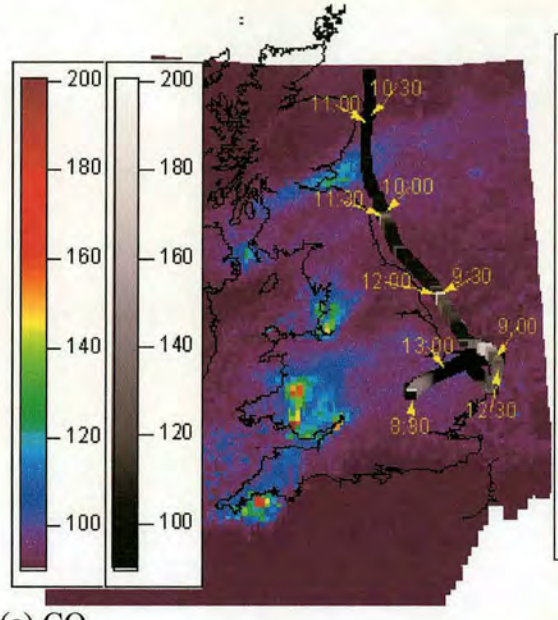

(a) CO

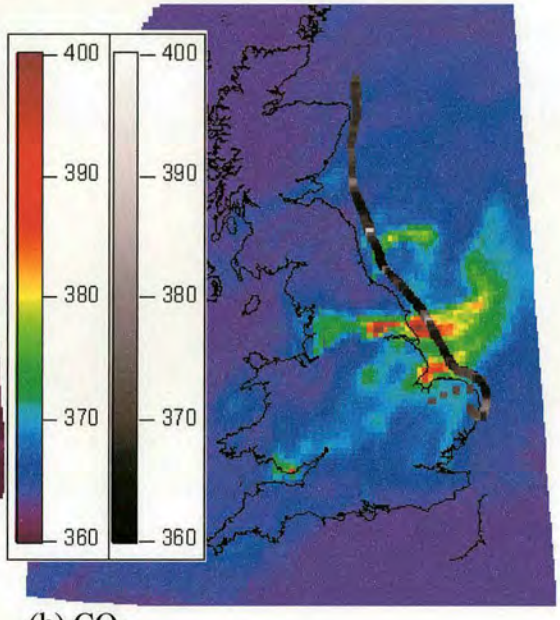

(b) CO_2

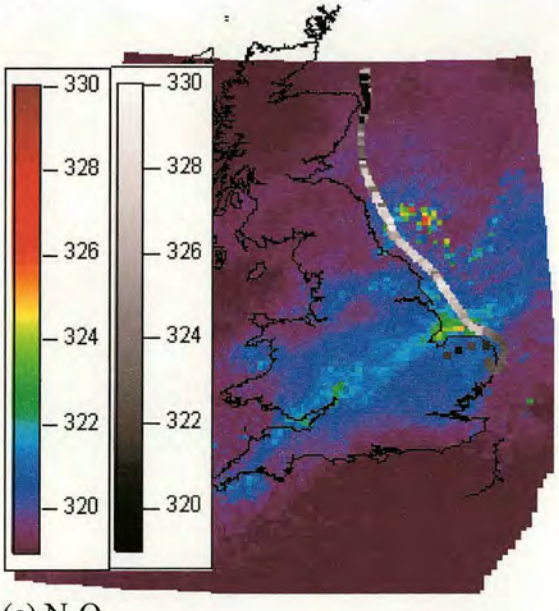

(c) N_2O

Figure 67. NAME concentration map for 12:00 14/07/05 (rainbow) with sample concentration (grey) overlaid. (a) CO (ppb) and aircraft times. (b) CO_2 (ppm). (c) N_2O (ppb).

Despite the complex wind flow, the NAME model is able to reproduce the CO concentrations, shown in Figure 68 (a), with R = 0.61. For CO_2, shown in Figure 68 (b), the model is able to reproduce the outflow from London and the Midlands but underestimates the concentration from the north of England. Along this stretch of the flight, the wind speed decreases resulting in stagnant air and enhanced CO_2 concentrations from the industrial sources in the north of the England which the model is unable to reproduce. The model also fails to capture the plumes from northern Scotland. The absence of CO plumes from this area suggest that the CO_2 source is not a typical anthropogenic combustion source so the enhanced concentrations may be due to respiration from forests from the previous night. The result is that there is no correlation between the modelled and measured series for CO_2 (R = 0.10). For N_2O, shown in Figure 68 (c), the enhancement measured along the east coast is greatly underestimated by the model. However the background concentration is estimated from concentration off the north of Scotland and with the complex meteorology on this day, these may not represent the real background concentration. The correlation between the modelled and measured data is statistically significant though small (R = 0.36) suggesting that the model is able to broadly predict the structure of the outflow plumes though it significantly underestimates their scale suggesting that N_2O emissions are much larger on this day.

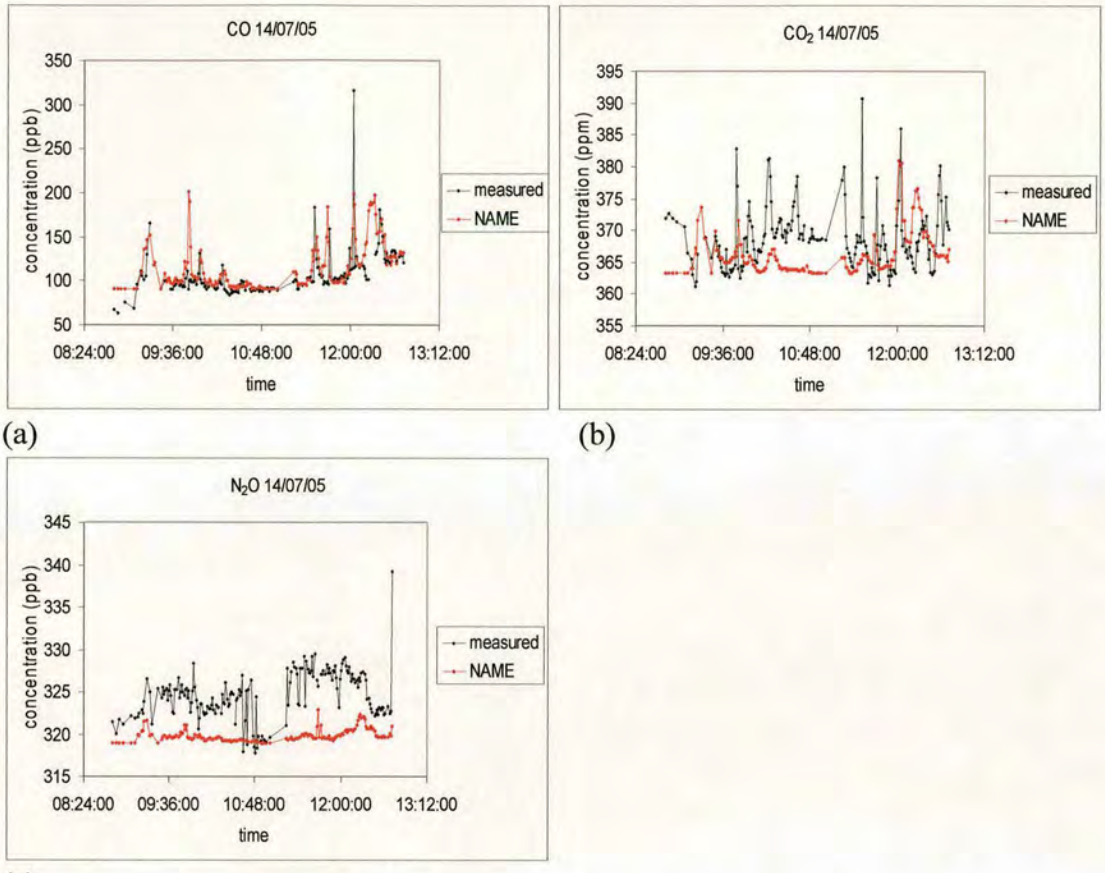

Figure 68. Measured (black) and NAME (red) sample concentration for flight B111. (a) CO (ppb). (b) CO_2 (ppm). (c) N_2O (ppb).

4.2.5 Flight B112 19/07/05

Flight B112 took place in a generally westerly wind flow. Figure 69 (a) and (b) show the modelled and measured CO and CO_2 concentrations respectively. The locations of the modelled outflow plumes from the major urban centres correspond well with the measured plumes. For CH_4, shown in Figure 69 (c), the measured concentrations show broader outflow plumes than those from the model, particularly the north east and London plumes. The model also seems to underestimate the outflow particularly from a plume with large concentrations from the south east of the country. The model N_2O outflow, shown in Figure 69 (d), greatly underestimates the measured concentrations. The measurements show large plumes from London, the Midlands and a broad plume from Teesside and the north east of England.

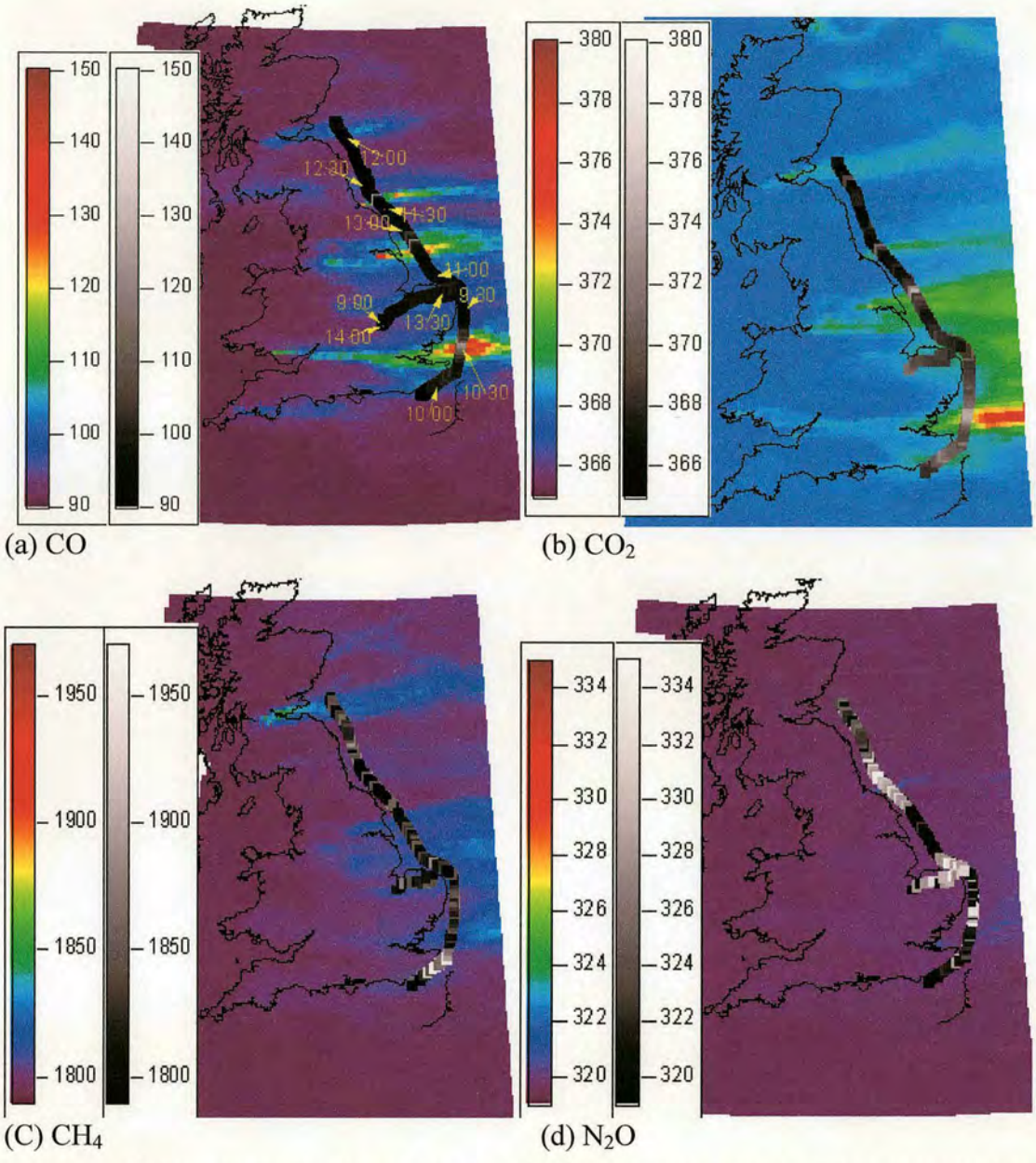

(a) CO (b) CO_2

(C) CH_4 (d) N_2O

Figure 69. NAME concentration map for 12:00 19/07/05 (rainbow) with sample concentration (grey) overlaid. (a) CO (ppb) and aircraft times. (b) CO_2 (ppm). (c) CH_4 (ppb). (d) N_2O (ppb).

Figure 70 (a), (b), (c) and (d) show the modelled and measured concentrations for CO, CO_2, CH_4 and N_2O respectively. For CO and CO_2, the model has been able to capture the outflow well with a statistically significant correlation between the modelled and measured data with R = 0.45 for CO and R = 0.67 for CO_2. CO_2 shows some evidence of photosynthesis with the concentration decreasing to below the background value at around 12:00. This decrease in concentration takes place in an air mass that has travelled over Kielder Forest in Northumbria making photosynthesis the

likely source of the decrease. Although the CO_2 plumes from Teesside and the north west of England are slightly smaller on the return leg, the CO plumes are also smaller on the return leg of the flight, suggesting that photosynthesis is not responsible for the decrease in concentration. The modelled and outflow for both CH_4 and N_2O, shown in Figure 70 (c) and (d) respectively, significantly underestimate the measurements. Neither CH_4 nor N_2O show any correlation between the modelled and measured data, partly due to the noisiness of the data. However the measurements of both CH_4 and N_2O show much larger and broader plumes than those predicted by the model, particularly from the north west of England and Teesside between 11:30 and 12:14 on the northbound leg of the flight.

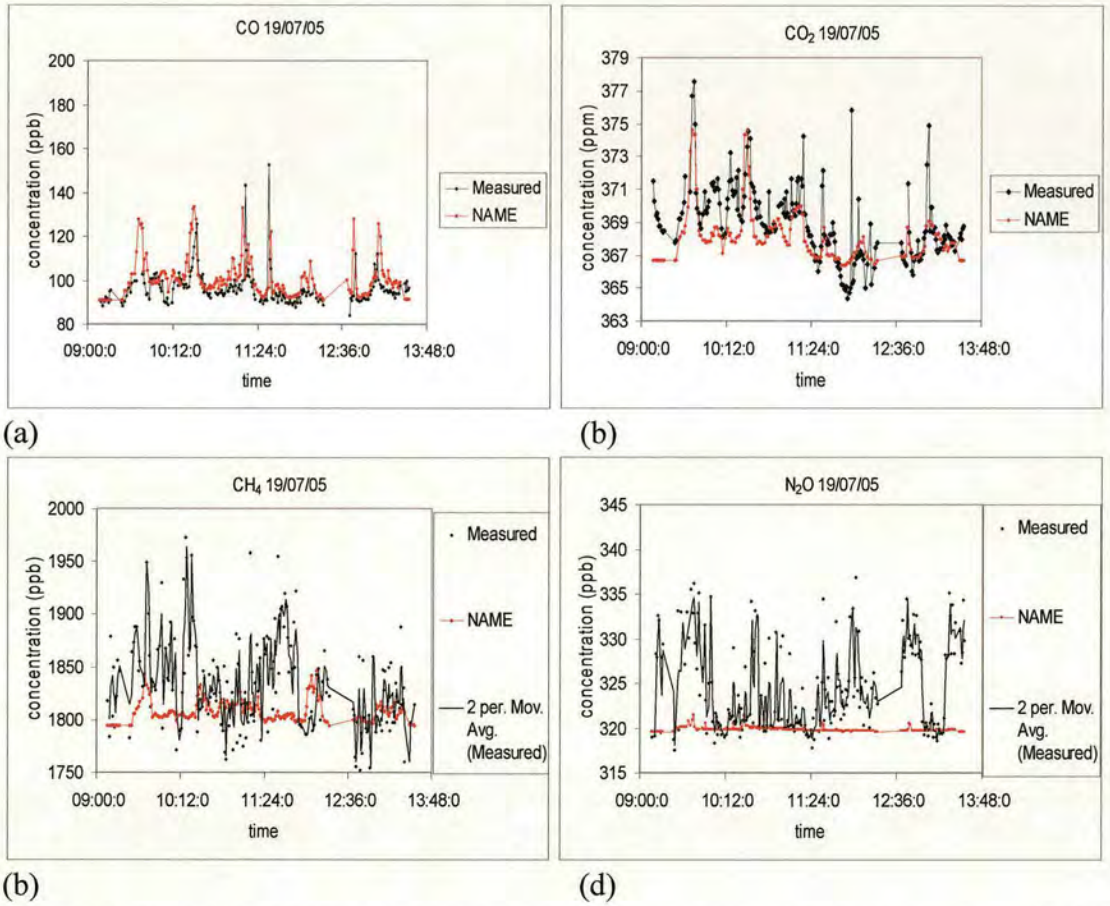

Figure 70. Measured (black) and NAME (red) sample concentration for flight B112. (a) CO (ppb). (b) CO_2 (ppm). (c) CH_4 (ppb) with moving average applied to measured data. (d) N_2O (ppb) with moving average applied to measured data.

4.2.6 Flight B113 20/07/05

Flight B113 took place in a generally north westerly wind flow. Figure 71 (a), (b), (c) and (d) show the modelled and measured concentrations of CO, CO_2, CH_4 and N_2O respectively. The CO and CO_2 modelled outflow manages to capture the location of the main urban outflow plumes from London and Humberside. The plume from the north west of England is superimposed over the plume from Humberside, while the plume from Bristol/Cardiff is evident as a distinct plume on the south coast rather than being integrated in the Midlands plume as is the case for most flights. The CH_4 and N_2O modelled outflow seems to underestimate the actual plumes with broader plumes of larger concentration measured. This is particularly the case for N_2O which has very large concentrations all along the English Channel which have not been captured by the model.

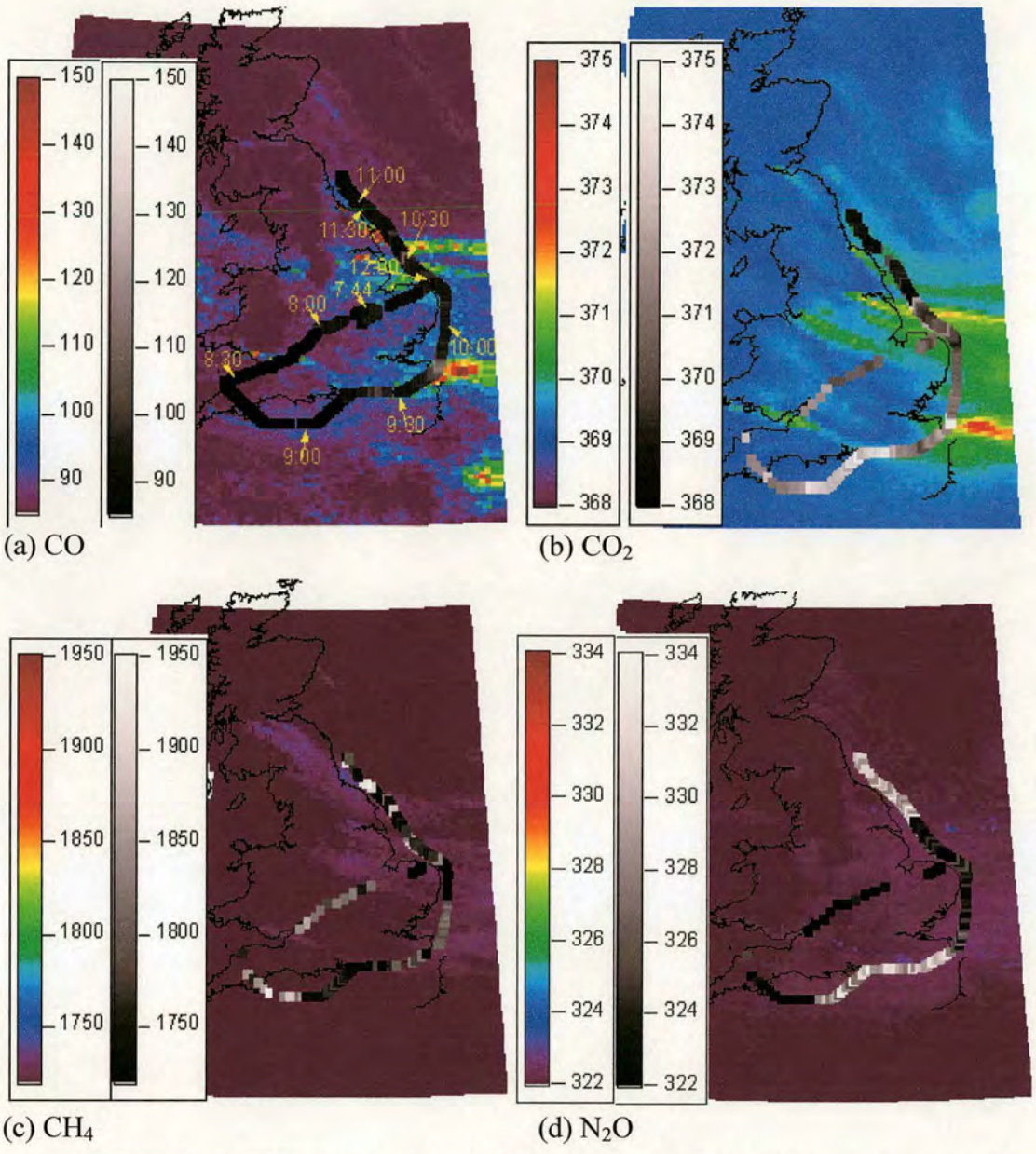

(a) CO (b) CO_2

(c) CH_4 (d) N_2O

Figure 71. NAME concentration map for 12:00 20/07/05 (rainbow) with sample concentration (grey) overlaid. (a) CO (ppb) and aircraft times. (b) CO_2 (ppm). (c) CH_4 (ppb). (d) N_2O (ppb).

Figure 72 (a), (b), (c) and (d) show the modelled and measured concentrations for CO, CO_2, CH_4 and N_2O respectively. The model is able to reproduce much of the structure in the CO and CO_2 measurements. However the CO_2 measurements show much larger concentrations at high level during the transit out to Bristol Channel and over the West Country at around 8:45 resulting in no correlation between the CO_2 model and measured series. Given the enhanced CH_4 and N_2O concentrations over the West Country but the absence of a CO enhancement, the likely source is agriculture

with CO_2 emissions from the previous night from respiring grassland used to graze livestock. The CO modelled concentrations are correlated with the measurements, R = 0.66. The CH_4 model concentrations significantly underestimate the measurements and the two series are not correlated. The N_2O measurements for this flight are poor quality and the model and measurement series are not correlated.

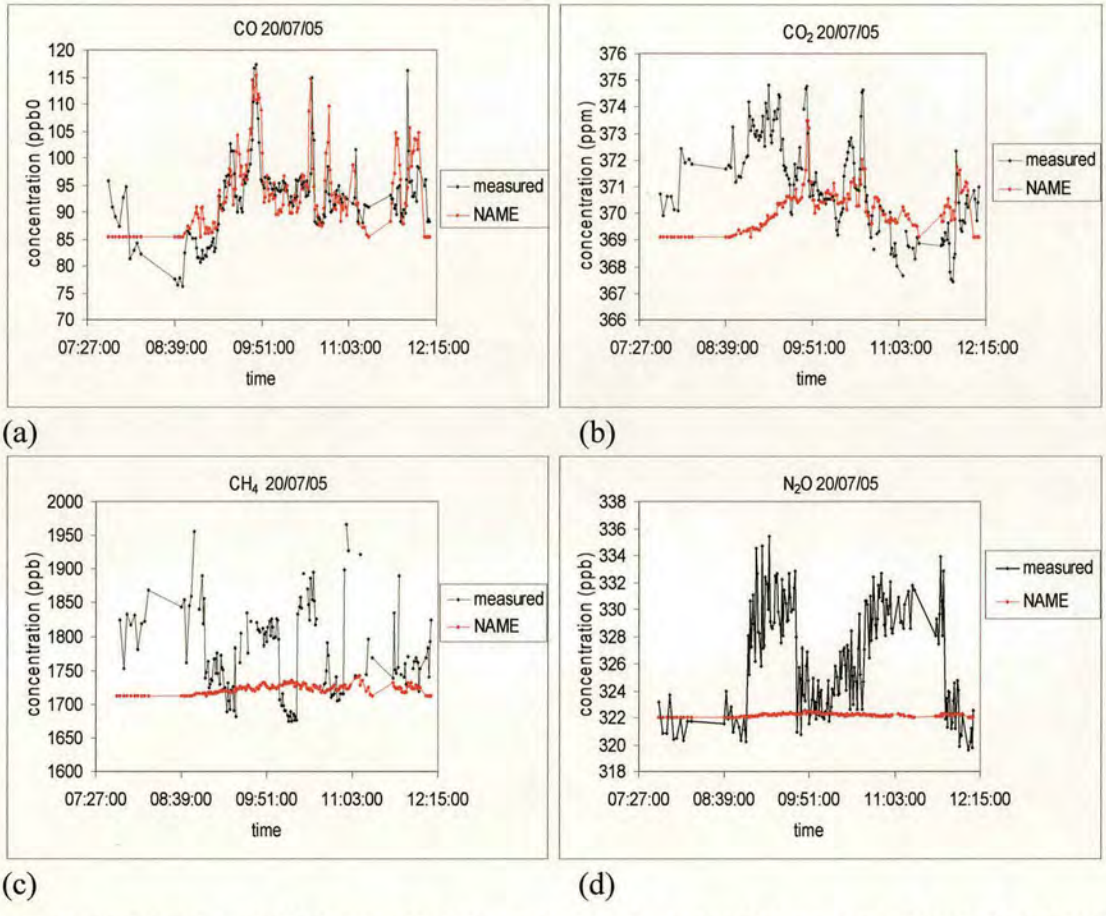

Figure 72. Measured (black) and NAME (red) sample concentration for flight B113. (a) CO (ppb). (b) CO_2 (ppm). (c) CH_4 (ppb). (d) N_2O (ppb).

4.2.7 Flight B118 03/08/05

Flight B118 took place in a generally westerly wind flow. Figure 73 (a) shows the CO modelled and measured concentrations. The model is able to correctly predict the locations of the outflow plumes from the main urban centres for CO and CO_2 with distinct plumes from London, the north west of England and Teesside along the east

coast and a plume from Bristol/Cardiff on the south coast. The model is also able to broadly reproduce the measured outflow for N_2O (Figure 73 (c)) with the largest plumes from London and Teesside. However there are plumes in the measured outflow not predicted by the model from the West Country and North West of England.

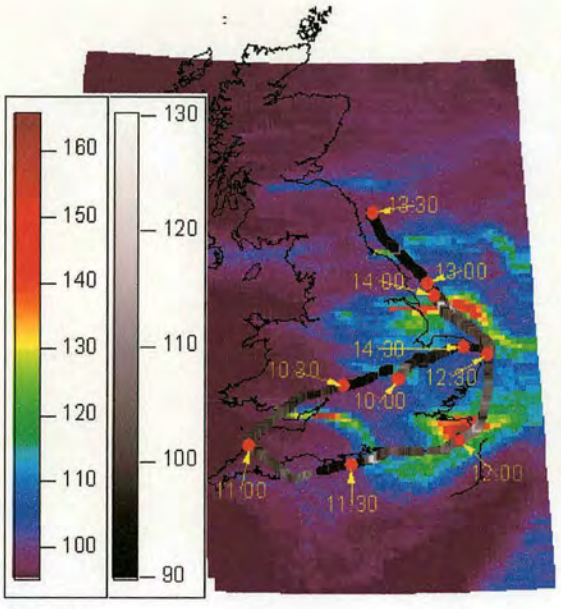

(a) CO

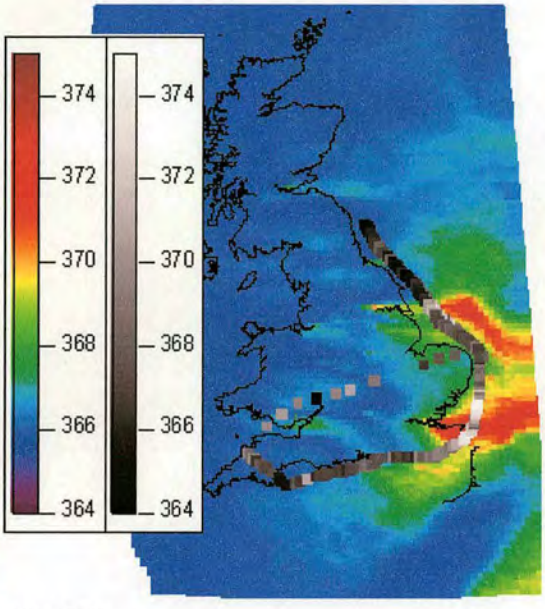

(b) CO_2

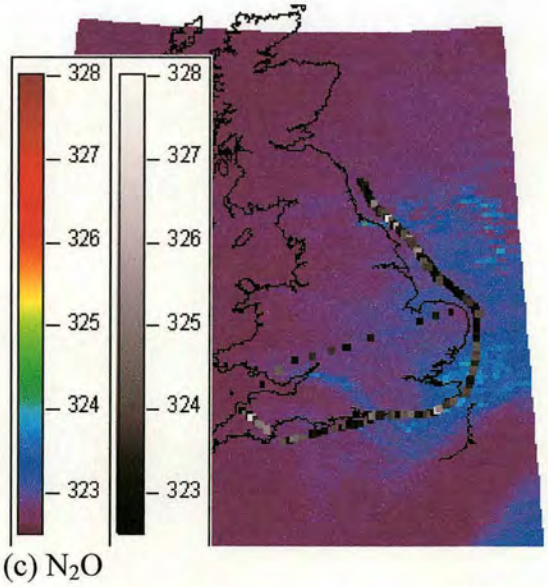

(c) N_2O

Figure 73. NAME concentration map for 12:00 03/08/05 (rainbow) with sample concentration (grey) overlaid. (a) CO (ppb) and aircraft times. (b) CO_2 (ppm). (c) N_2O (ppb).

Figure 74 (a), (b) and (c) show the modelled and measured concentration series for CO, CO_2 and N_2O respectively. The model CO concentrations significantly overestimate the measured values and there is no correlation between the modelled and measured series. The CO_2 modelled concentrations predict the measured outflow well with a correlation between the two series of 0.66. The N_2O modelled measured concentration underestimate the measured values and the two series are not correlated with the model failing to predict large plumes from the West Country and the North West of England.

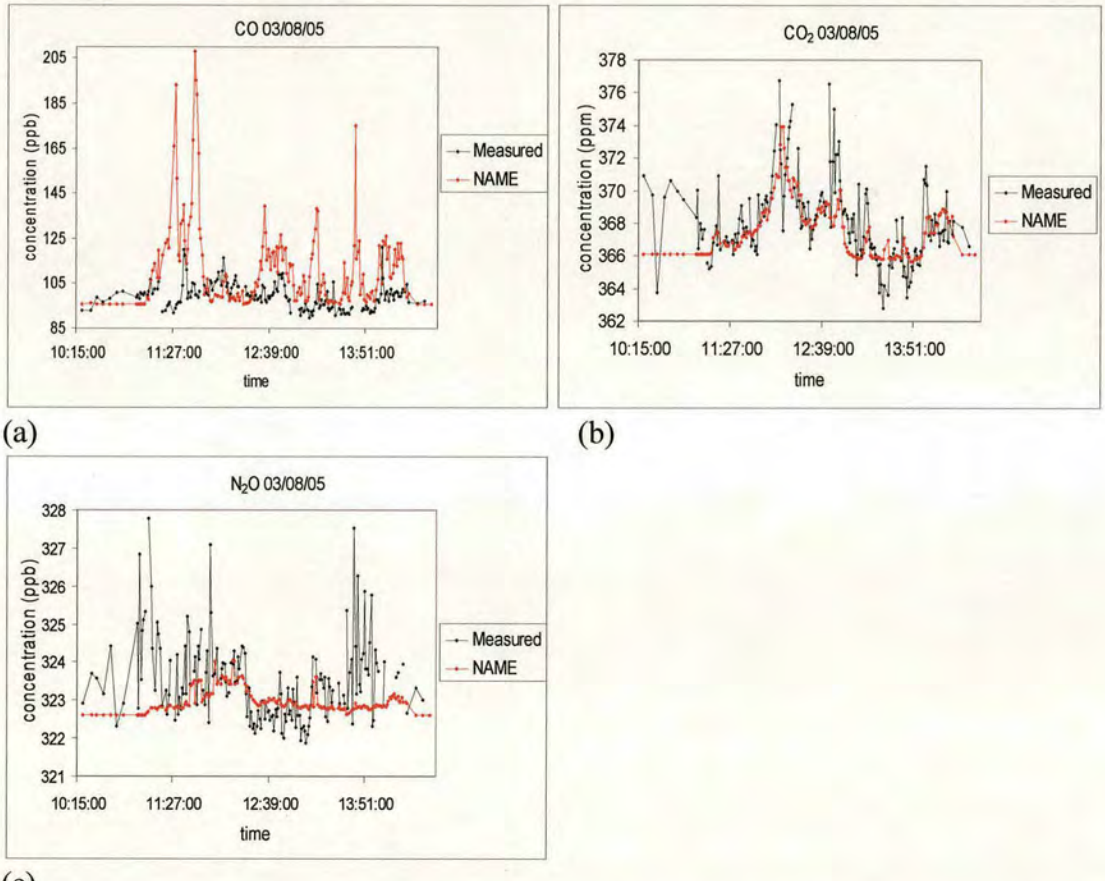

Figure 74. Measured (black) and NAME (red) sample concentration for flight B118. (a) CO (ppb). (b) CO_2 (ppm). (c) N_2O (ppb).

4.2.8 Flight B119 04/08/05

Flight B119 took place in a westerly wind flow. Figure 75 (a) shows the modelled and measured CO concentrations with distinct plumes from London, Humberside, Teesside and the Central Belt of Scotland along the east coast. Similarly for CO_2, (Figure 75 (b)), NAME correctly predicts the outflow of the main urban plumes. The measured N_2O plumes (Figure 75 (c)) are broader that the CO plumes, particularly the London and Teesside plumes off the south east and north east of England

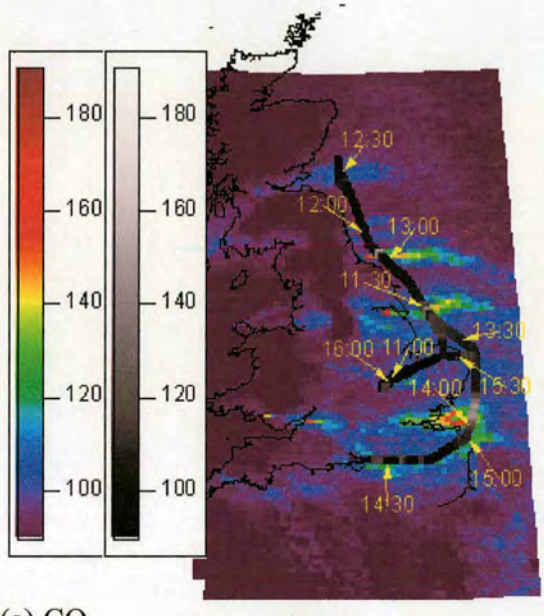

(a) CO

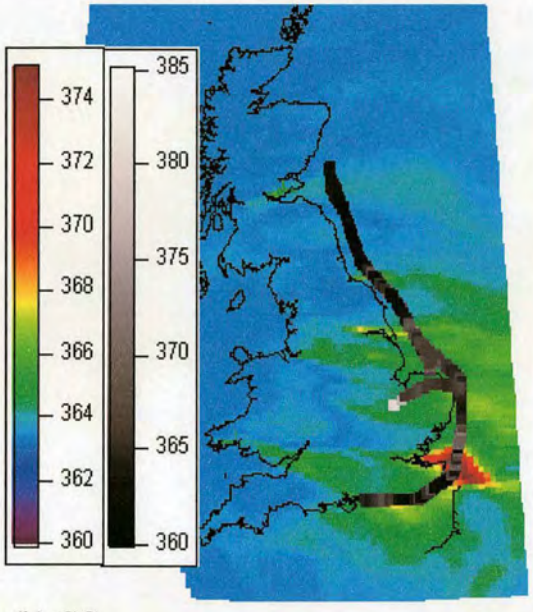

(b) CO_2

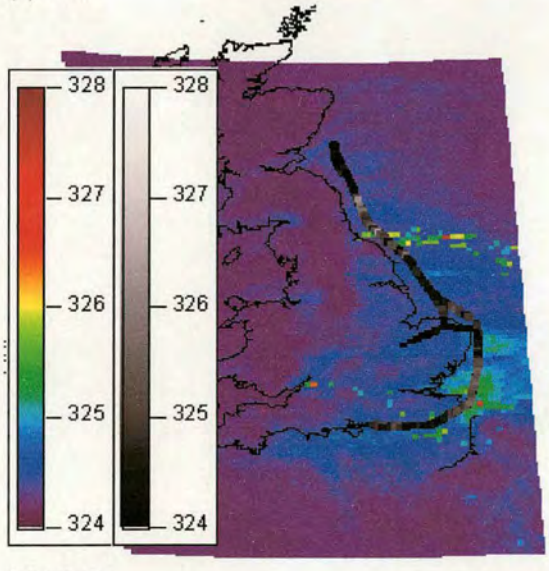

(c) N_2O

Figure 75. NAME concentration map for 12:00 04/08/05 (rainbow) with sample concentration (grey) overlaid. (a) CO (ppb) and aircraft. (b) CO_2 (ppm). (c) N_2O (ppb).

The NAME model is able to broadly reproduce the measured outflow for all three chemical species as can be seen in Figure 76 (a), (b) and (c) which shows the modelled and measured concentrations for CO, CO_2 and N_2O respectively. The model series is correlated with the measurements for both CO and CO_2 (R = 0.58 for CO and R = 0.30 for CO_2). For CO_2, the model is able to reproduce the outflow, however during transit over East Anglia, the measured concentrations show a large enhancement possibly from flying over local sources which the model fails to reproduce. There is also a decrease in concentration at 12:45 due to photosynthesis from Kielder Forest that the model fails to reproduce fully and these combine to lower the correlation between the model and measured data compared to CO. For N_2O, despite the model broadly reproducing the structure of the outflow, there is no correlation between the modelled and measured data. In particular the model underestimates the large Teesside plume particularly on the southbound leg between 12:45 and 13:00 and also fails to capture a plume off the south east English Channel between 14:15 and 14:46 which is most likely from the Bristol and the West Country.

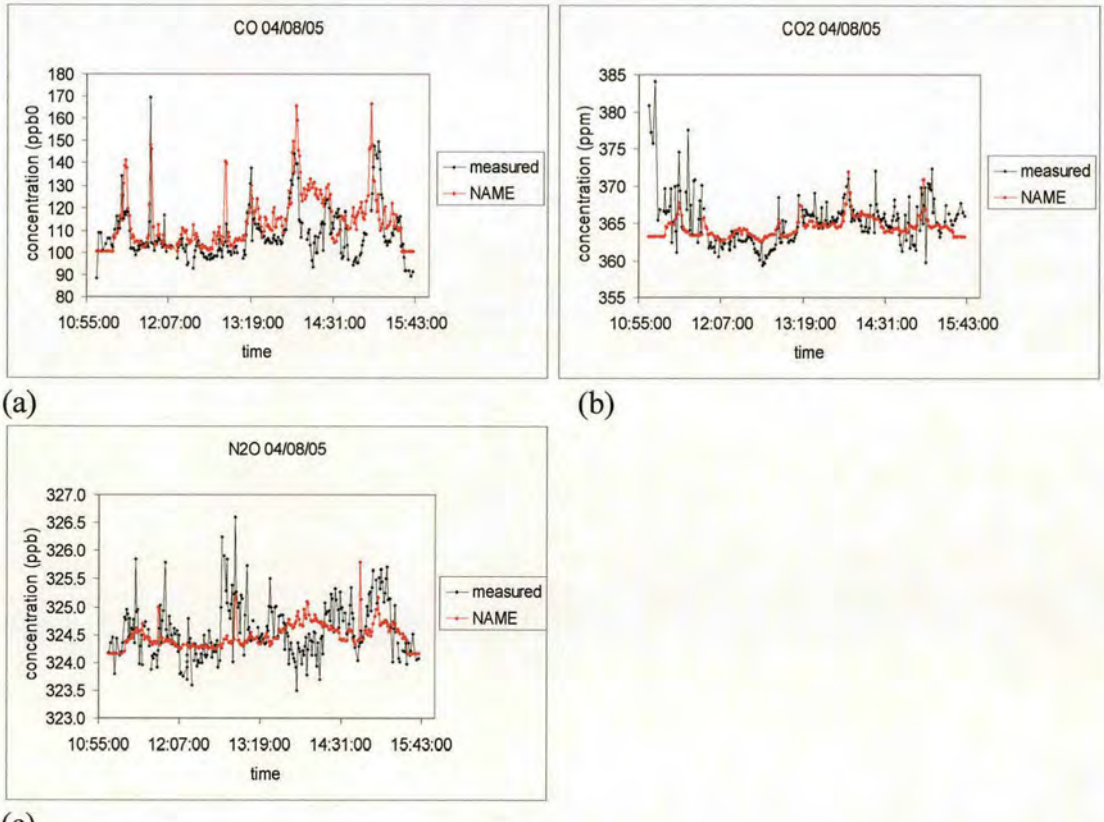

Figure 76. Measured (black) and NAME (red) sample concentration for flight B119. (a) CO (ppb). (b) CO_2 (ppm). (c) N_2O (ppb).

4.2.9 Flight B126 07/09/05

Flight B126 took place in a generally south westerly flow. This produces less distinct plumes compared to westerly conditions with plumes from Bristol, Cardiff, Midlands and Humberside integrated as seen in the CO NAME concentration map and measured outflow in Figure 77 (a). For CO_2, shown in Figure 77 (b), the model simulates the outflow from the north west of England and the Midlands however the measurements show a plume from the north of England which the model does not predict. The CH_4 measurements, shown in Figure 77 (c), show large concentrations to the west of the Channel, the origin of which is uncertain. The measurements also show more distinct plumes of larger concentrations than those modelled. The N_2O measurements, shown in Figure 77 (d), are much larger than the modelled values with large values in the Channel and broad plumes along the east coast.

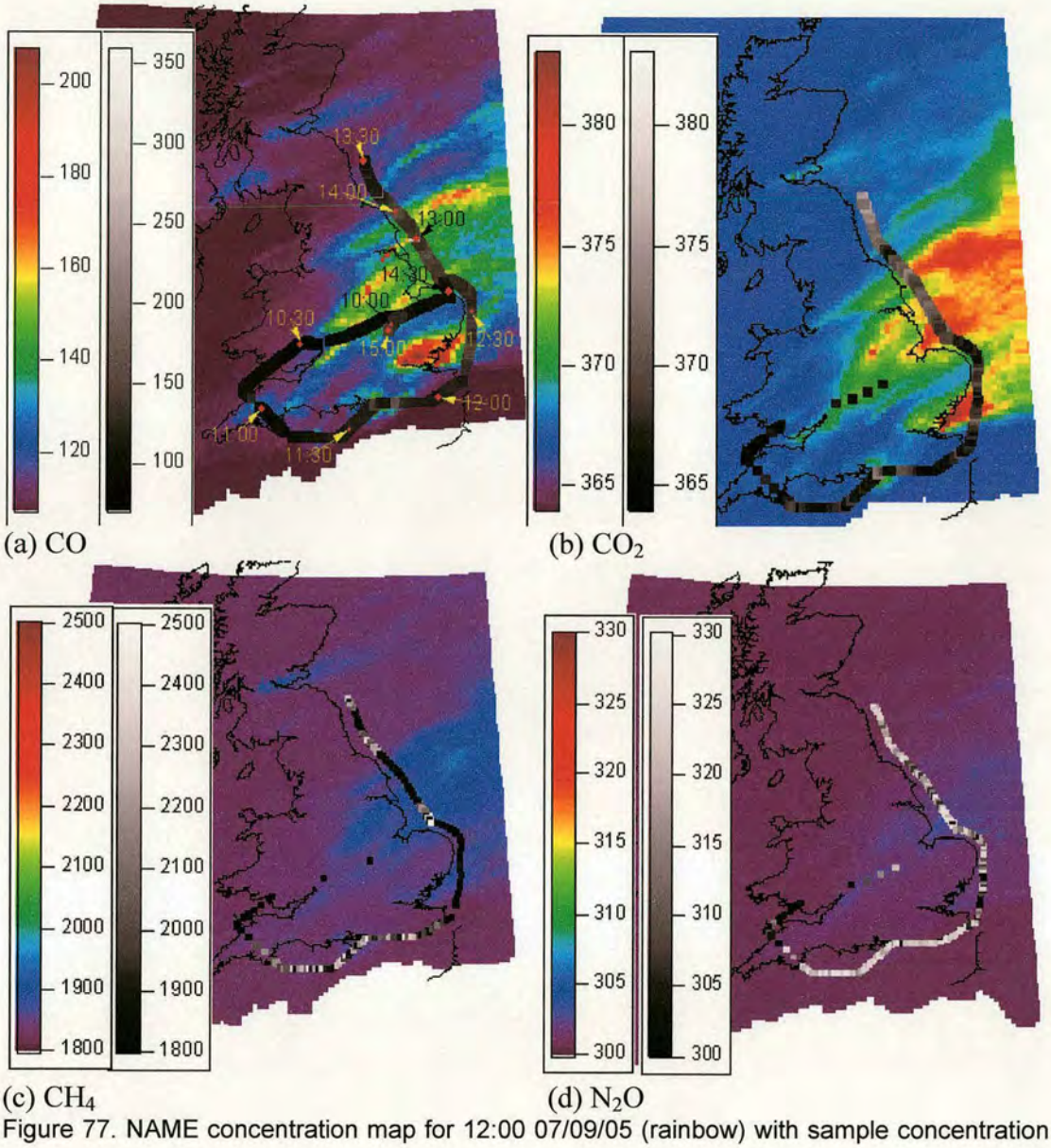

(a) CO (b) CO_2

(c) CH_4 (d) N_2O

Figure 77. NAME concentration map for 12:00 07/09/05 (rainbow) with sample concentration (grey) overlaid. (a) CO (ppb) and aircraft times. (b) CO_2 (ppm). (c) CH_4 (ppb). (d) N_2O (ppb).

Figure 78 (a), (b), (c) and (d) show the modelled and measured concentrations along the flight path for CO, CO_2, CH_4 and N_2O respectively. The model is able to mostly reproduce the outflow for CO but fails to capture the structure of the CO_2 outflow fully resulting in a lower correlation between the modelled and measured data for CO_2 ($R = 0.38$) than CO ($R = 0.69$). For both CH_4 and N_2O the model significantly underestimates the measured concentrations neither does it capture structure of the broad outflow plumes resulting in no correlation between the modelled and measured data for these two species.

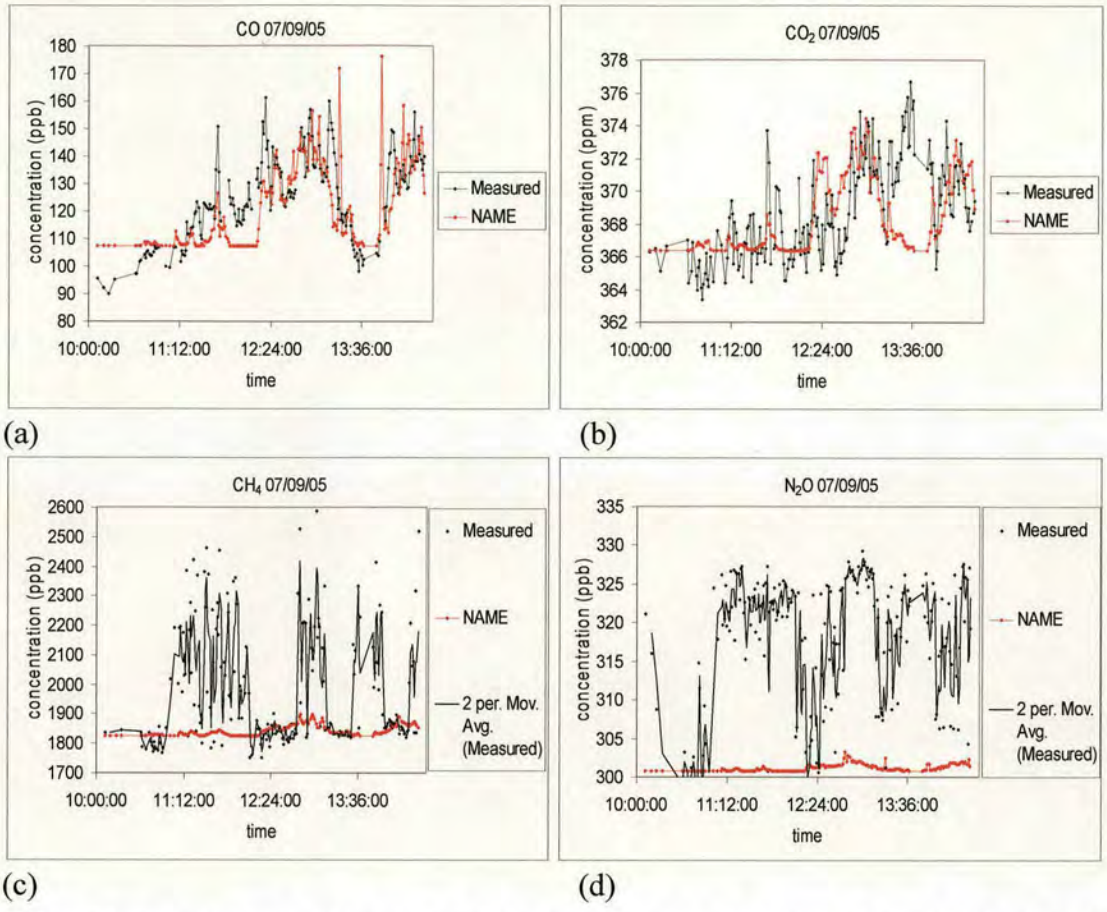

Figure 78. Measured (black) and NAME (red) sample concentration for flight B126. (a) CO (ppb). (b) CO_2 (ppm). (c) CH_4 (ppb) with moving average applied to measured data to smooth data. (d) N_2O (ppb) with moving average applied to measured data to smooth data.

4.2.10 Flight B130 19/09/05

Flight B130 took place in a mainly south westerly wind flow, however stagnant air in the south east resulted in some air recirculation and produced interference from European air in the UK outflow plumes. In Figure 79 (a), (b), (c) and (d) which show the modelled and measured concentrations for CO, CO_2, CH_4 and N_2O respectively, the large concentrations in the English Channel are the result of recirculation of outflow from the UK from the previous days. The measurements for all four chemical species show large concentrations in the south east as a result of inflow from Europe and recirculation of UK outflow. Further up the east coast, the wind flow becomes less complex producing more distinct plumes from the UK and because the flow is south westerly, most of the outflow from the UK can still be identified.

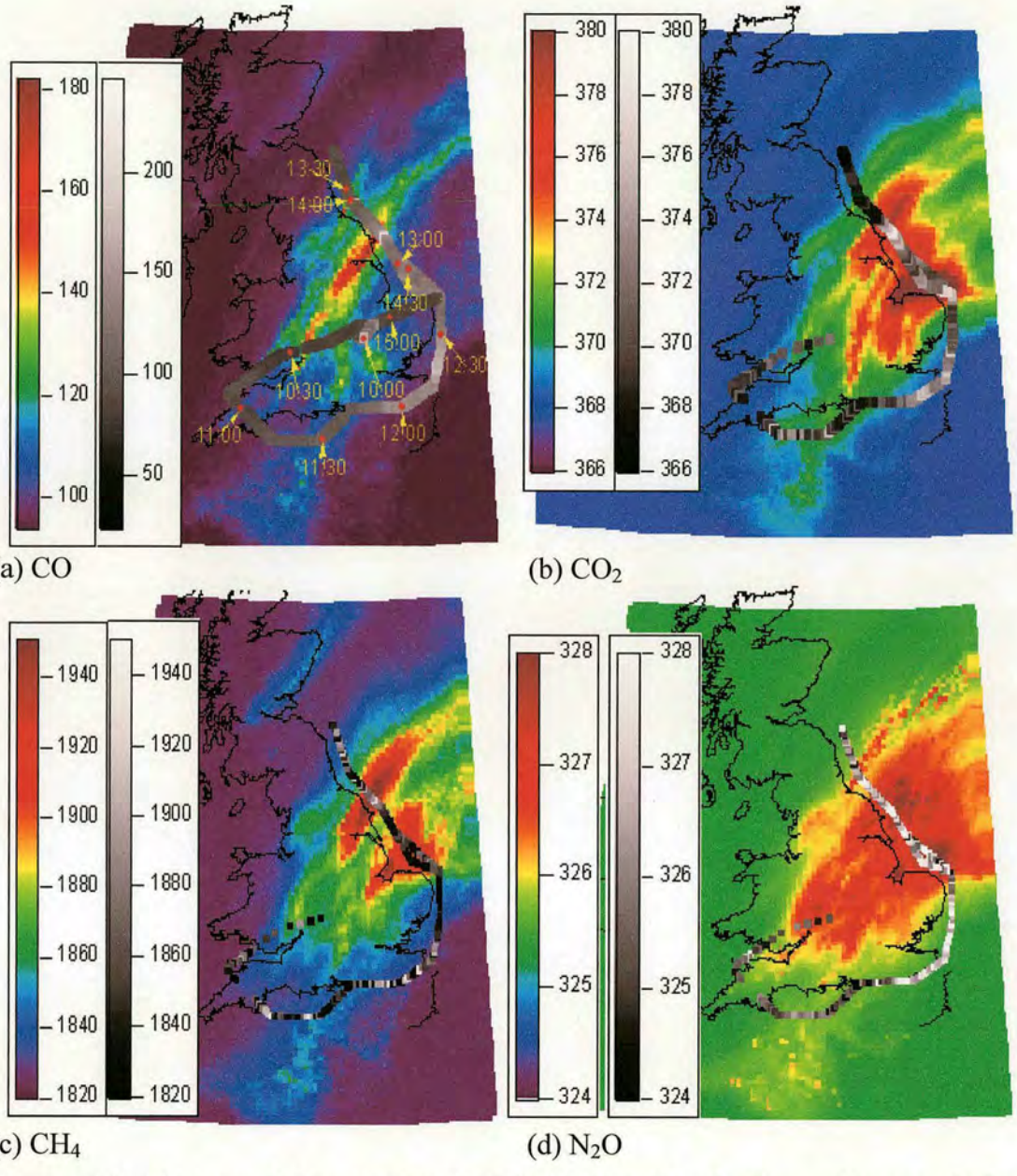

Figure 79. NAME concentration map for 12:00 19/09/05 (rainbow) with sample concentration (grey) overlaid. (a) CO (ppb) and aircraft times. (b) CO_2 (ppm). (c) CH_4 (ppb). (d) N_2O (ppb).

Figure 80 (a), (b), (c) and (d) show the modelled and measured concentrations for CO, CO_2, CH_4 and N_2O. All four plots show large measured concentrations between 11:30 and 12:20 corresponding to the inflow in the south east which the model does predict. Further up the east coast, the model is able to reproduce much of the outflow from the UK for all four species although it underestimates the N_2O concentrations from the Midlands and Humberside on the southbound leg. The correlation between the modelled and measured data is weak for CO, CO_2 and N_2O with R = 0.34, R =

0.35 and R = 0.34 respectively. There is no correlation at all between the modelled and measured CH_4 data.

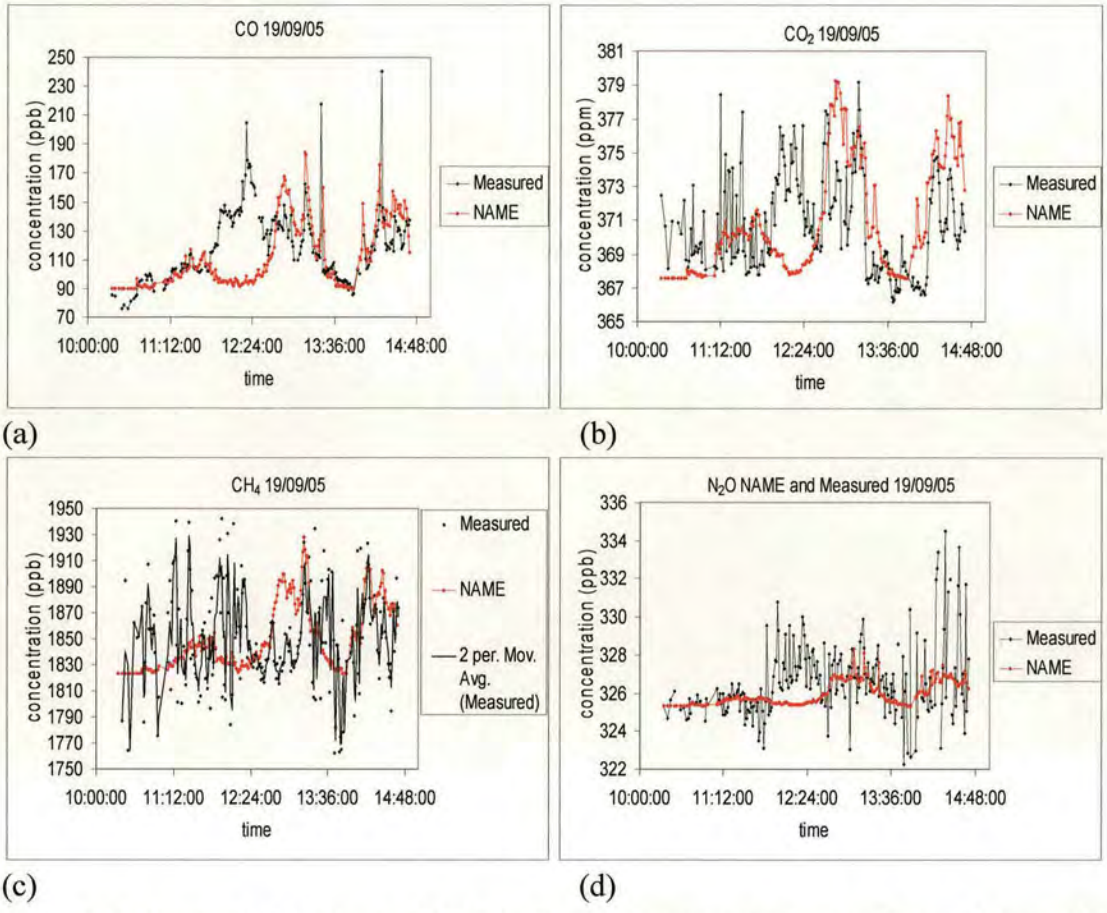

Figure 80. Measured (black) and NAME (red) sample concentration for flight B130. (a) CO (ppb). (b) CO_2 (ppm). (c) CH_4 (ppb) with moving average applied to measured data to smooth data. (d) N_2O (ppb).

4.2.11 Flight B132 21/09/05

Flight B132 took place in similar conditions to flight B130, however the wind flow was less complex and with less recirculation of air and inflow from continental Europe. Figure 81 (a), (b), (c) and (d) show the modelled and measured concentrations for CO, CO_2, N_2O and CH_4 respectively. The model is able to correctly predict the main outflow plumes from the north west of England, the Midlands and London for all four species.

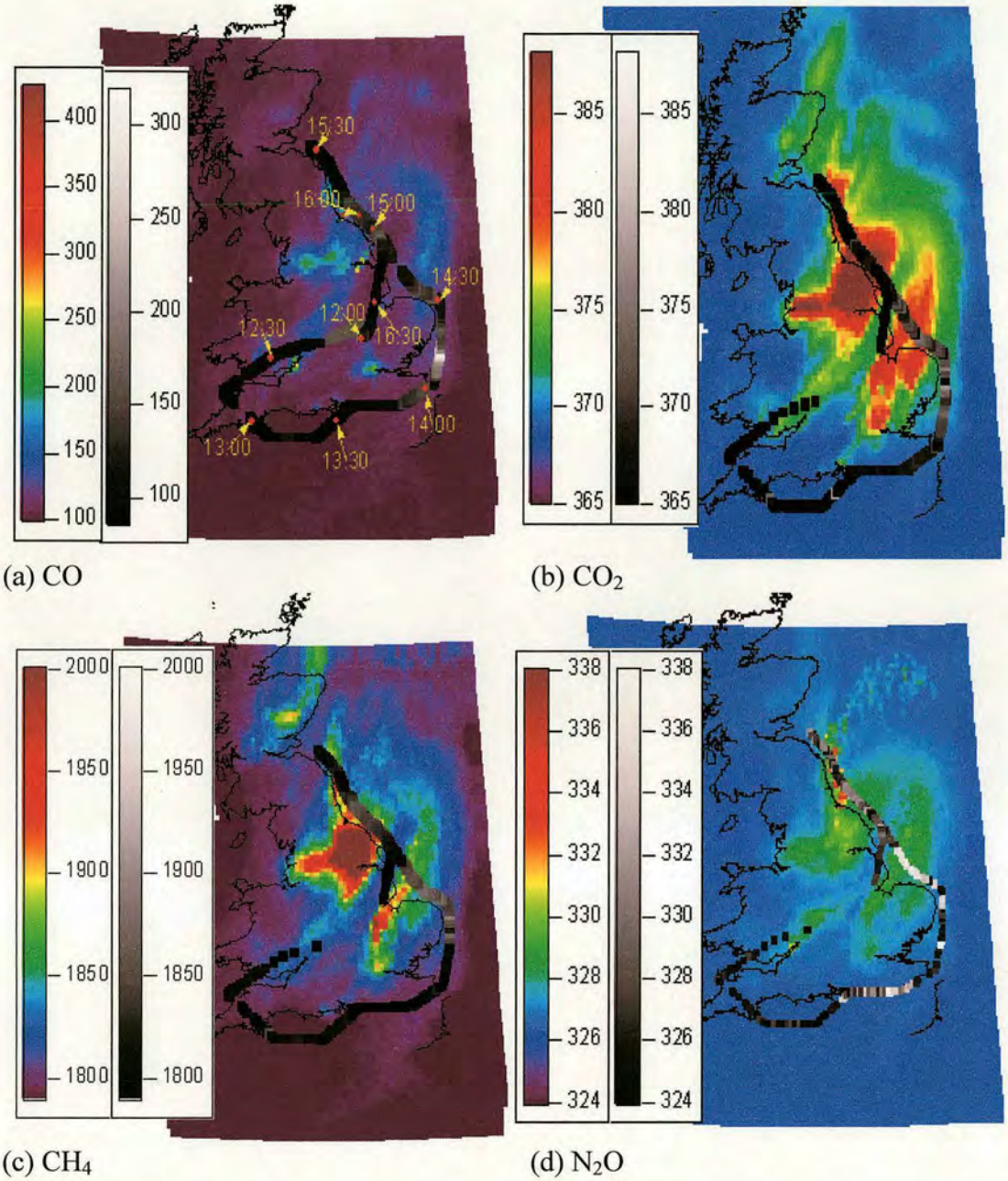

(a) CO (b) CO_2

(c) CH_4 (d) N_2O

Figure 81. NAME concentration map for 12:00 21/09/05 (rainbow) with sample concentration (grey) overlaid. (a) CO (ppb) and aircraft times. (b) CO_2 (ppm). (c) CH_4 (ppb). (d) N_2O (ppb).

As with flight B130, there are large measured concentrations in the south east for all four species which are not reproduced by the model as can be seen in Figure 82 (a), (b), (c) and (d) for CO, CO_2, CH_4 and N_2O respectively. The model is able to reproduce the outflow of CO accurately with a correlation between the two sets of data of 0.36. For CO_2, the model tends to overestimate the outflow concentrations though this may partly be due to an overestimation of the background concentration.

The two sets of data are still correlated with R = 0.31. For CH_4, the model tends to overestimate the outflow concentrations but the two sets of data are well correlated with R = 0.52. The concentrations in the English Channel and around the south east of the country are lower for CH_4 suggesting less interference from continental and re-circulated air for this species, resulting in a higher correlation than CO and CO_2. Despite overestimating the outflow concentrations, the model was able to reproduce the relative heights of the outflow plumes. For N_2O R = 0.30. The large concentrations in the Channel and around the south coast lower the correlation while the structure of the outflow has been reasonably well simulated by the model. However the model underestimates the concentration in the outflow plumes.

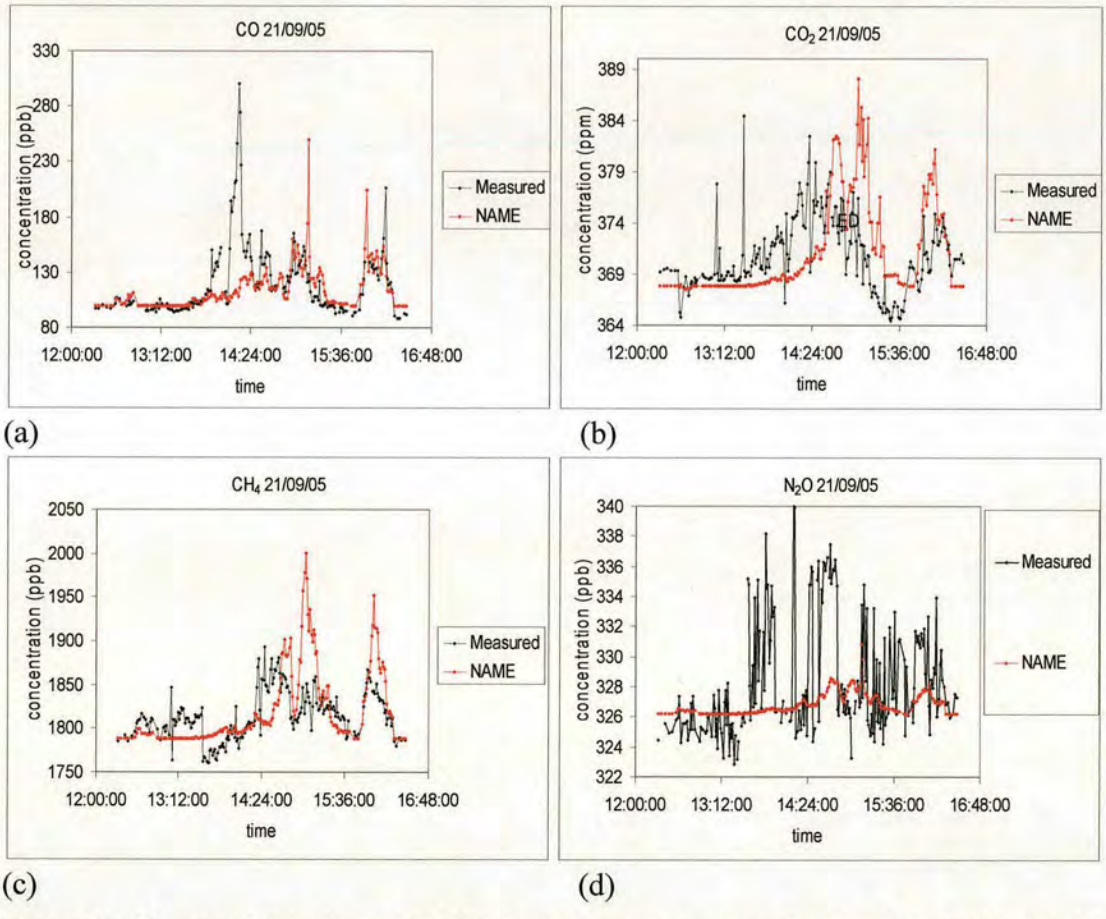

Figure 82. Measured (black) and NAME (red) sample concentration for flight B132. (a) CO (ppb). (b) CO_2 (ppm). (c) CH_4 (ppb). (d) N_2O (ppb).

4.2.12 Flight B134 26/09/05

Flight B134 took place in a south westerly flow. Figure 83 (a), (b), (c) and (d) show the modelled and measured concentrations for CO, CO_2, CH_4 and N_2O respectively. All four show the outflow along the east coast which is reproduced by the model. However for CO_2, CH_4 and N_2O the measurements show large concentrations over the West Country not reproduced by the model. Given the nature of the sources in this area and lack of CO, the likely sources are rural with CH_4 emissions from livestock and N_2O emissions from the soil. The source of CO_2 could be respiration from the previous night from grassland used for grazing livestock.

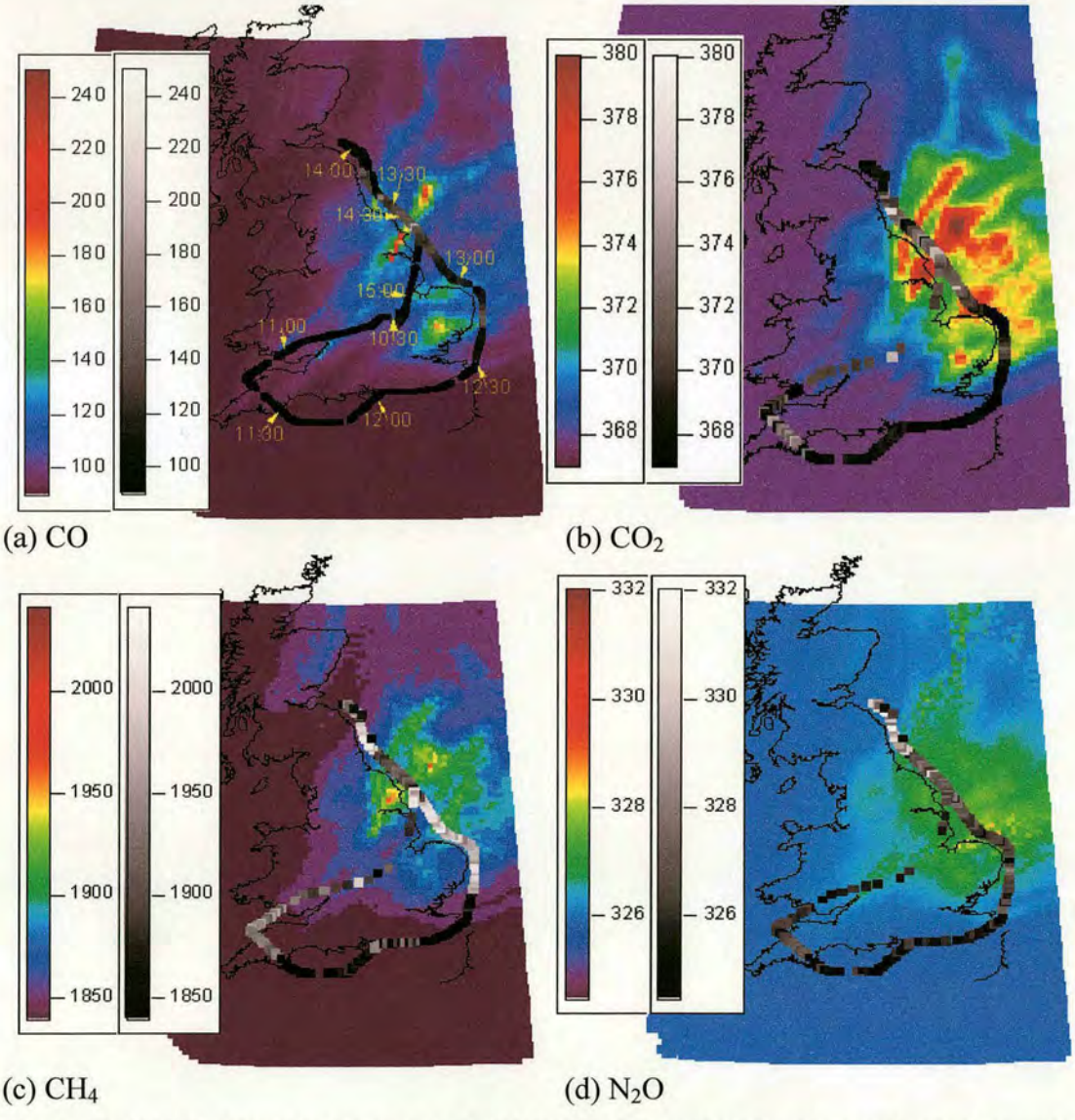

(a) CO (b) CO_2

(c) CH_4 (d) N_2O

Figure 83. NAME concentration map for 12:00 26/09/05 (rainbow) with sample concentration (grey) overlaid. (a) CO (ppb) and aircraft times. (b) CO_2 (ppm). (c) CH_4 (ppb). (d) N_2O (ppb).

Figure 84 (a), (b), (c) and (d) show the modelled and measured concentrations for CO, CO_2, CH_4 and N_2O respectively. The model captures the CO outflow very well with a strong correlation of R = 0.84. For CO_2 the model captures the general structure of the outflow with a correlation of R = 0.48. The model predicts a broader plume all along the east coast while the measurements show London as a distinct plume at around 12:45. The measurements also show large concentrations between 11:15 and 11:30 as the plane flew over Devon not captured by the model. The CH_4 measurements show broad plumes along the east coast from London up to the Midlands with a separate distinct plume from the north west of England merged with the plume from the north east. The enhancement from this plume is much larger than predicted by the model and the model also failed to capture large concentrations over Devon. The correlation between the modelled and measured concentrations is relatively weak compared to CO and CO_2 with R = 0.31. The N_2O measurements are reasonably well simulated by the model except for a large, broad plume from the north east of England. The correlation between the modelled and measured data for N_2O is also relatively weak compared to CO and CO_2 with R = 0.29.

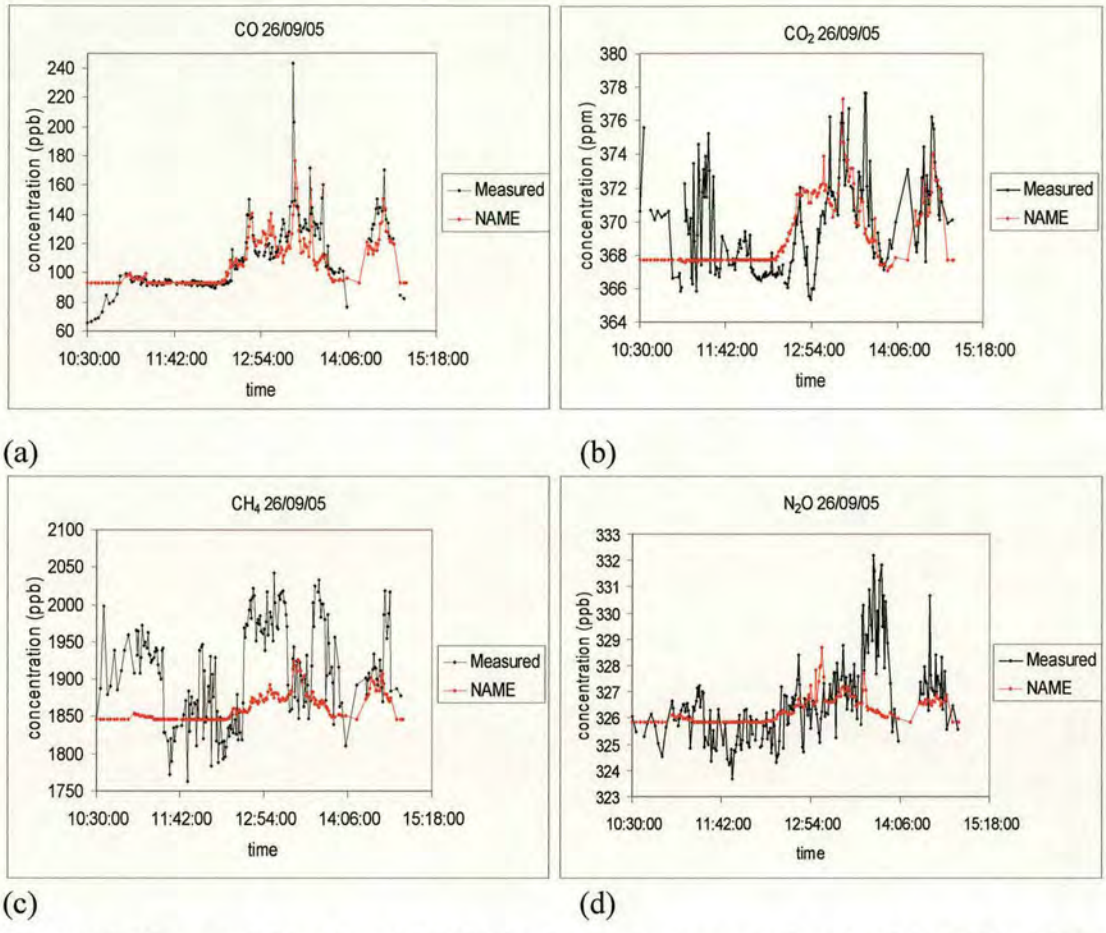

Figure 84. Measured (black) and NAME (red) sample concentration for flight B134. (a) CO (ppb). (b) CO_2 (ppm). (c) CH_4 (ppb). (d) N_2O (ppb).

4.2.13 Flight B136 29/09/05

Flight B136 took place in a generally north westerly flow. Most of the outflow is from the south east of the country as can be seen in Figure 85 (a) which shows the modelled and measured concentrations for CO. There are also smaller plumes from central Scotland and north east of England which the model is able to reproduce for CO and CO_2. The CH_4 and N_2O plots, Figure 85 (c) and (d) respectively, show enhanced concentrations all along the east coast which the model is able to mostly reproduce for CH_4 but not N_2O. This broader outflow suggests that the emission for CH_4 and N_2O originate from larger areas unlike the mainly urban emissions of CO and CO_2 which produce distinct outflow plumes.

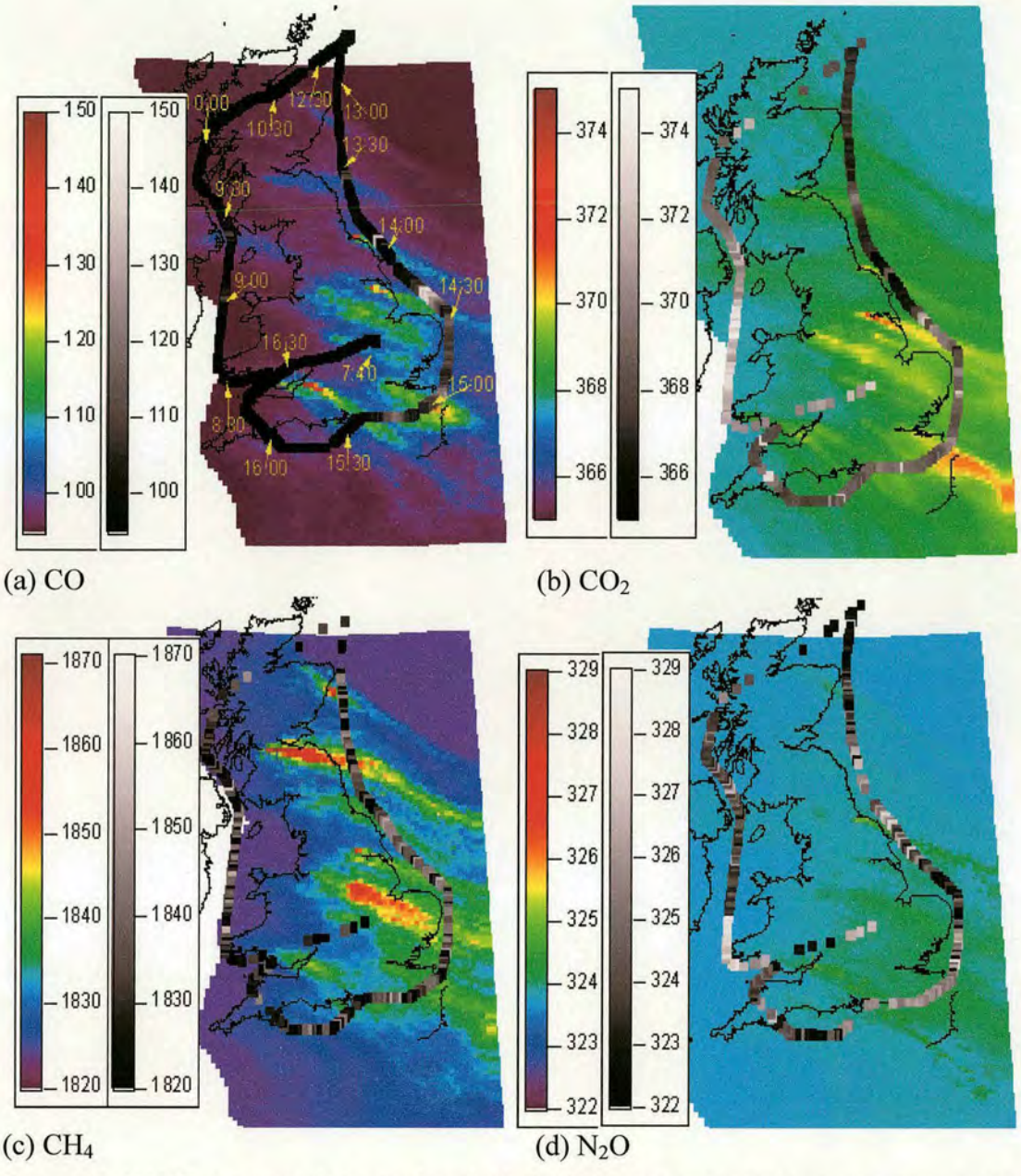

(a) CO (b) CO_2

(c) CH_4 (d) N_2O

Figure 85. NAME concentration map for 12:00 29/09/05 (rainbow) with sample concentration (grey) overlaid. (a) CO (ppb) and aircraft times. (b) CO_2 (ppm). (c) CH_4 (ppb). (d) N_2O (ppb).

Figure 86 (a), (b), (c) and (d) show the modelled and measured concentrations for CO, CO_2, CH_4 and N_2O respectively. This flight is the only one where emissions from Ireland are measured separately from the UK plume. For CO, the measurements show how small the Irish emissions are compared to the UK with a very small plume. The model is able to capture most of the UK outflow well with a statistically significant correlation between the two series with R = 0.66. The CO_2 measurements show much larger concentrations from Ireland compared to the UK than CO. As CO_2 is mainly

from similar urban sources to CO, it is unlikely that anthropogenic Irish CO_2 emissions are proportionally much larger than CO compared to the UK so it is likely that the decrease in concentration in the UK outflow is partly due to photosynthesis. Flight B136 started earlier in the morning than was typical and so the sampling of Irish air took place before photosynthesis had time to significantly affect the outflow concentration. In the outflow from the UK there is also evidence of a draw down of CO_2 from Kielder forest with a decrease in concentration at around 14:00. Overall there is no correlation between the modelled and measured data, however comparing only UK outflow, a weak correlation ($R = 0.21$) is found between the two data sets. The CH_4 measurements are relatively noisy for this flight, however they show a distinct plume from Ireland and a broad plume for the UK which is relatively well simulated by the model. The CH_4 emissions from Ireland are larger relative to the UK emissions compared to CO due to large numbers of livestock in Ireland. There is no correlation between the model and measured concentrations for the whole data set, however there is weak correlation for the UK outflow with $R = 0.25$. The N_2O measurements also show larger concentrations from Ireland compared CO which fits with proportionally higher levels of agriculture. The outflow from the UK seems to be in two distinct broad plumes, one from the north east of England and one off the south east coast which is a merger of plumes from the north west of England, the Midlands and London. There is also a small plume over the West Country. Overall the model underestimates the outflow and there is no correlation between the model and measured data. For the UK outflow only, a weak correlation between the two data sets of $R = 0.38$ is found.

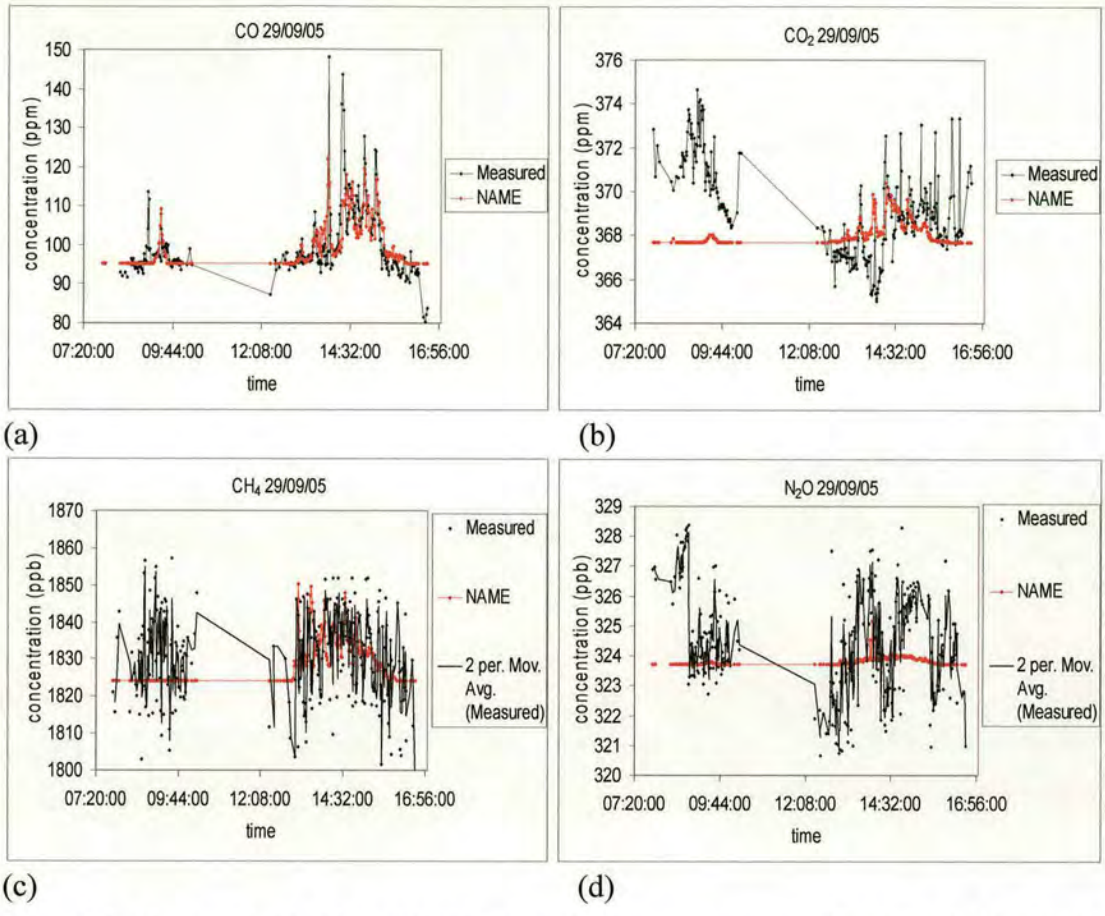

Figure 86. Measured (black) and NAME (red) sample concentration for flight B136. (a) CO (ppb). (b) CO_2 (ppm). (c) CH_4 (ppb) with moving average applied to measured data. (d) N_2O (ppb) with moving average applied to measured data.

4.2.14 Flight B244 19/09/06

Flight B244 took place in a generally westerly flow. Figure 87 (a) and (b) show the distinct urban plumes from London, the Midlands and the north west of England for CO and CO_2 respectively in both the modelled and measured concentrations. The CH_4 measurements, shown in Figure 87 (c), show a broad outflow plume along the east coast with larger concentrations corresponding to a plume from London and the north west of England.

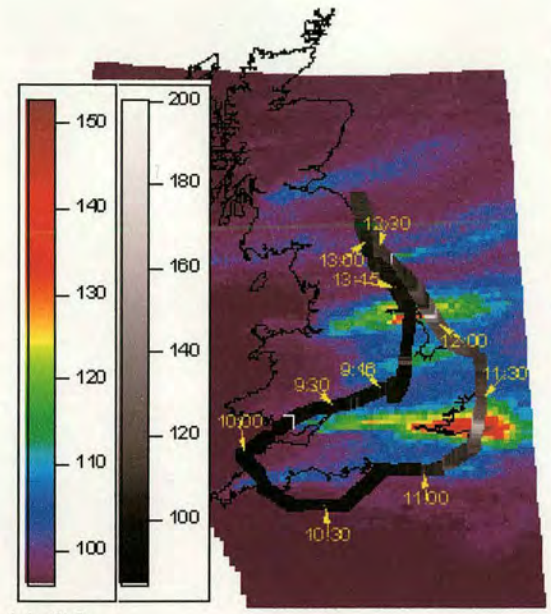

(a) CO

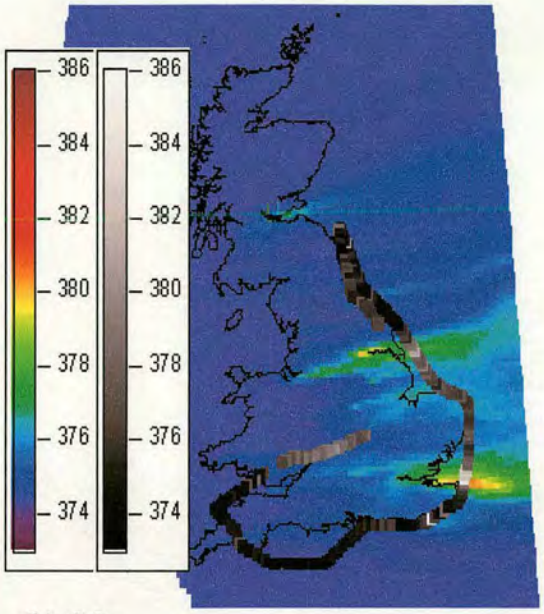

(b) CO_2

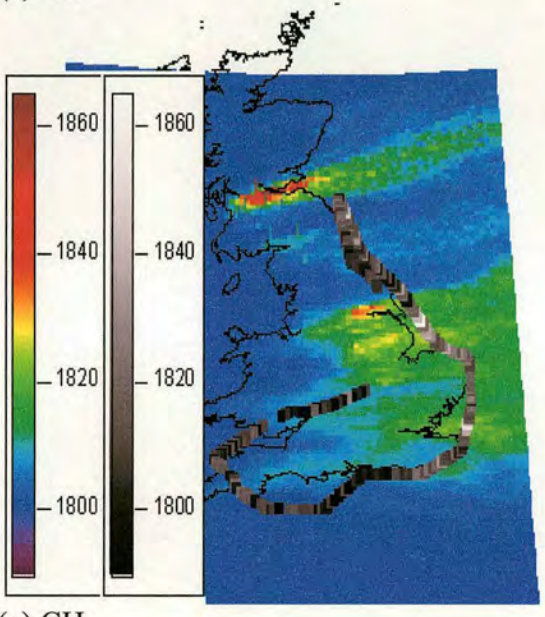

(c) CH_4

Figure 87. NAME concentration map for 12:00 19/09/06 (rainbow) with sample concentration (grey) overlaid. (a) CO (ppb) and aircraft times. (b) CO_2 (ppm). (c) CH_4 (ppb).

Figure 88 (a), (b) and (c) show the modelled and measured concentrations for CO, CO_2 and CH_4 respectively. The model is able to simulate the CO outflow well with a strong correlation between the modelled and measured data (R = 0.83). The model is also able to simulate the CO_2 outflow well however the enhanced concentrations during the transit out and over the West Country are not reproduced which results in a weaker correlation between the modelled and measured data (R = 0.53) than for CO.

The CH_4 measurements also show enhanced concentration from the West Country which the model does not simulate. The model is able to simulate the bulk of the outflow from London up to the north west of the country, however the model underestimates the outflow from the north east up to central Scotland. The overall correlation between the modelled and measured data is good compared to other flights with R = 0.47 but weak compared to CO and CO_2.

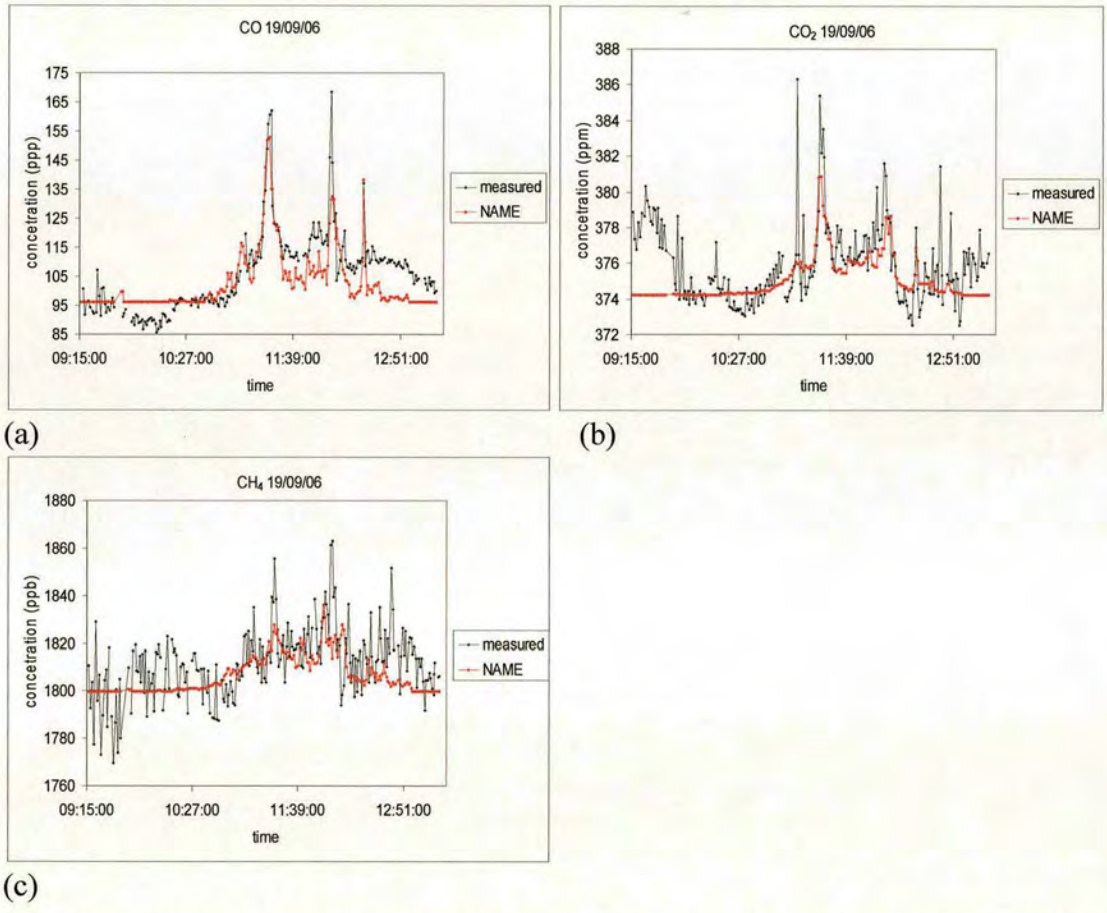

Figure 88. Measured (black) and NAME (red) sample concentration for flight B244. (a) CO (ppb). (b) CO_2 (ppm). (c) CH_4 (ppb).

4.3 Conclusion

Using the NAME model in forward mode to simulate the emissions and transport of air over the UK for each species for each flight allowed the NAEI mapped emission inventories to be validated against a set of independent measurements. Overall the NAME model is able to successfully reproduce the measured CO concentrations such that the correlation between the modelled and measured data is statically significant (p-value < 0.01) for 13 of the 14 flights. It is also able to reproduce the CO_2 concentrations in 12 of the 14 flights though the correlation between the modelled and measured data is typically weaker for CO_2 than CO due to the added complications of the biogenic flux and larger than expected concentrations at high levels on the transit out to the Bristol Channel and over Devon and Cornwall. For both CO and CO_2 it seems that the current NAEI inventory is accurate both in total emissions and spatially and combined with the NAME model, can be used to successfully predict the UK outflow.

For CH_4, the model is only able to reproduce the outflow to a statistically significant level in 5 of the 14 flights. Partly this is due to the poorer quality CH_4 data with 6 flights excluded because of unsatisfactory measurements. However the model also tends to underestimate the size of the outflow plumes for a number of flights suggesting that the emissions are underestimated for those days. As CH_4 is treated identically to CO in the model, as a passive tracer, NAME should be able to predict the CH_4 concentrations as accurately as the CO concentrations given an equally accurate emission inventory. As this is not the case, it seems likely that the CH_4 mapped emissions are not accurate enough to successfully predict the CH_4 outflow from the UK. This is as expected given that the emission inventory for CH_4 dates back to 1994. However the 1994 emissions are larger than the current NAEI estimate for 2004 so the model would be expected to overestimate the outflow concentration. In fact the opposite happens, with the outflow underestimated by the model on a number of flights suggesting that the current inventory underestimates the real CH_4 emissions.

For N_2O, the correlation between the model and measured data is generally very weak and only statistically significant for five flights while the absolute values the

model concentrations tend to significantly underestimate the measured concentrations. In addition there are occasions where the model fails to predict the presence of a plume at all where a large plume was measured (e.g. flight B134). Overall the model tends to significantly underestimate the outflow concentrations and as with CH_4, N_2O is treated identically to CO by the NAME model. The poor performance of the model for N_2O must therefore be the result of inaccuracies in the emission inventory, with the current inventory significantly underestimating the actual emissions for most of the flights. When scaling the daily flux up to an annual estimate it might be expected that the summer estimates produced by the AMPEP data will overestimate the real annual average as winter emissions are expected to be lower due to the colder temperatures which suppress the microbial activity in soils. However peak emissions would be expected earlier in the year during the spring when farmers fertilise their fields. Therefore the largest emissions were not captured during the AMPEP campaign where outflow concentrations are already measured to be consistently significantly larger than those produced using current inventory estimates. This would suggest significantly larger N_2O emissions from the UK than currently accounted for in the NAEI.

Chapter 5 Deriving UK Budgets from 'Round-Britain' Observations

5.1 Box Model Method

Using the technique described in section 1.4, the total UK budget of a conserved chemical species may be quantified using a simple box model. For a boundary layer budget study it is assumed that the total flux emitted can be measured directly by measuring the inflow and outflow fluxes across a region and calculating the difference. The components of the boundary layer budget over the UK are shown in Figure 89. If there is an inversion at the top of the boundary layer the exchange between the BL and the free troposphere (FT) is restricted and for this technique we assume the ABL to FT exchange is negligibly small. However it is clear that this assumption requires testing. If we also assume that the boundary layer is well mixed then the measurements made at the mid BL are representative of the concentration through the whole ABL depth. This assumption is tested with profile ascents.

With these assumptions a 'simple box model' approach may be applied in which a virtual box is placed over the country and assumes that the area through which air enters the UK is the same as the air leaving. The flux out of the country must therefore equal the flux entering plus the flux emitted.

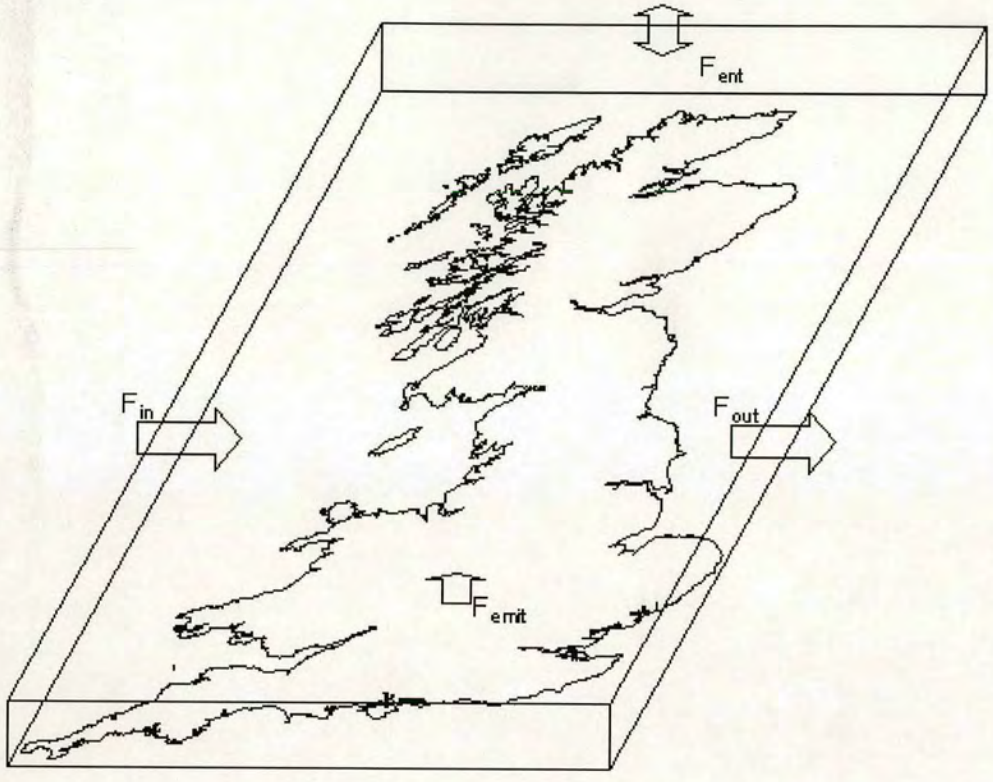

Figure 89. Boundary Layer Budget Components for a box model budget study of the UK.

The terms in the budget are

$$F_{emit} = F_{out} - F_{in} + F_{ent} \tag{5.1}$$

Where F_{emit} is the flux emitted (g s^{-1}), F_{out} is the export flux, F_{in} is the import flux and F_{ent} is the entrained flux through the top of the boundary layer. Assuming the wind speed is constant

$$F_{out} = \int \int u_{out}(y,z)C(y,z)dydz \tag{5.2}$$

and

$$F_{in} = \int\int u_{in}(y,z)C(y,z)dydz \tag{5.3}$$

where C is the concentration (g m^{-3}), $u(y,z)$ is the wind speed (m s^{-1}) through the inflow flow surface (*in*) and the outflow surface (*out*) at distance y (m) along the

northwards direction perpendicular to the direction of the wind flow and height z (m). The entrained flux (F_{ent}) was taken directly from the NAME model. The net loss to the Free Troposphere was calculated by summing the mass of each 'particle' in the model that crossed from the ABL to the Free Troposphere. For any particles that crossed back into the ABL from the Free Troposphere, the mass was subtracted from the total. The total mass was summed for the whole country from the time the sampled air entered the UK to the time it left. It was found that $F_{ent} << F_{out} - F_{in}$ and so could be neglected. For CO, the average value of F_{ent} for the flights is 15 kt yr^{-1} with a maximum value of 47 kT yr^{-1} for flight B111. This is two orders of magnitude smaller than $F_{out} - F_{in}$.

For the simple box model method it is assumed that the wind speed, u, and direction remained constant across the country throughout the height of the ABL. The inflow and outflow surfaces are assumed to be perpendicular to the direction of the wind flow and the areas of the inflow and outflow surfaces equal. The height of the surface is the boundary layer height, z_{BL}, averaged across the outflow region.

The average wind speed and direction were calculated from UM data, averaged across the UK from the time the air sampled in the outflow first entered the UK. The boundary layer was also calculated from the UM data but was taken to be the average value over the outflow flight path. The average standard deviation for the wind speed for the flights is < 1 % compared to an average standard deviation for the ABL height of 36 %. Therefore the accuracy of the boundary layer height will have the greater affect on the final budget estimate and so the model values for z_{BL} were validated by comparing with estimates from radiosonde data and the flight profiles. Figure 90 shows z_{BL} predicted by the model compared to the height estimated from the sonde and flight profile data. The model z_{BL} matches the flight profile z_{BL} better with a correlation coefficient of 0.79 between the two compared to a correlation coefficient of 0.47 between the model z_{BL} and the sonde z_{BL}. This is most likely to be because model estimates for the boundary layer height are an average over a 16 km grid square. Most of the sonde release sites are near to the coast so the relevant model grid square will incorporate both sea and land. The model z_{BL} tends to underestimate the sonde z_{BL} for these sites suggesting that while the sonde data is giving an estimate for z_{BL} over land, the model value is essentially for a marine boundary layer. The flight

profiles on the other hand tend to be either well inland during take-off and landing, or well over the sea, resulting in a much better fit between the model and flight values of z_{BL}.

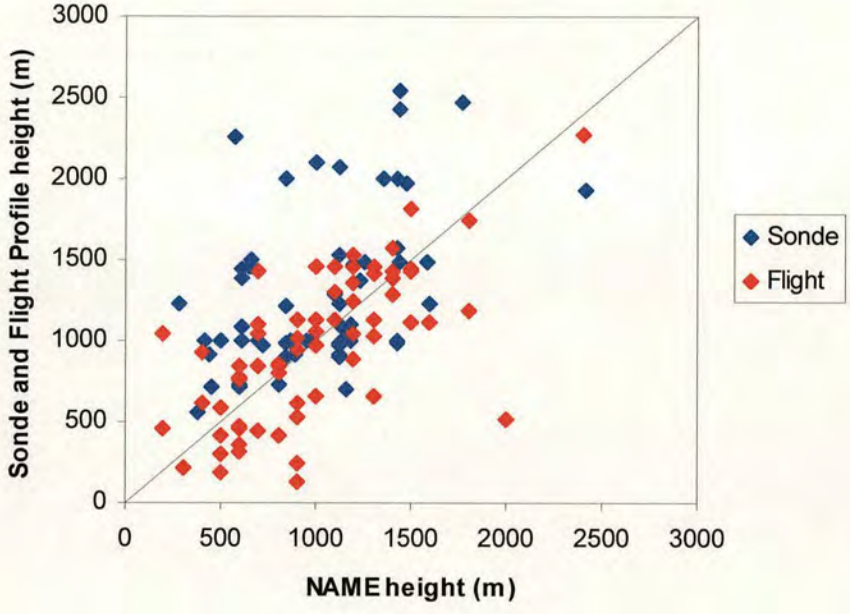

Figure 90. Height of the boundary layer (z_{BL}) as estimated from radiosonde and flight profiles against the NAME model estimate.

The outflow was calculated by defining an outflow surface, S_{out}, perpendicular to the average wind direction for the length of the enhanced outflow from the country. The concentrations, C_m (g m^{-3}), for each sample m, within the boundary layer in the outflow were then projected onto this surface producing a plot of C versus distance along S_{out} (m^2). The software IGOR was used to calculate the area under the plot to give the total concentration in the outflow, C_{out} (g m^{-3}). The export flux, F_{out} (g s^{-1}) , was calculated using

$$F_{out} = u \int_m C_m z_{BL} \partial x \tag{5.4}$$

The import flux, F_{in} (g s^{-1}), could be calculated by averaging the upwind concentrations but was in fact taken from the value found using the iteration technique described in section 5.2. The background concentration, C_{bg} (g m^{-3}), was

assumed to be constant across the whole inflow region and the area of the inflow surface, A_{Sin}, was assumed to equal the area of A_{Sout} (m). F_{in} could then be calculated using

$$F_{in} = C_{bg} A_{S_{out}} u \tag{5.5}$$

F_{emit} could then be calculated by subtracting F_{in} from F_{out}.

This is a relatively simple approach to calculating the UK budget. It fails to capture any of the complex meteorology such as divergent or converging wind flow and changing wind speed however as long as the conditions on the day in question are relatively simple such that our assumptions are reasonable, then it should produce a realistic estimate for the total emissions for that day. The advantage of this approach is that it is not necessary to sample the whole inflow region as F_{in} can be calculated from a few upwind samples and by applying the same conditions to the inflow as the outflow.

5.2 NAME Iteration Technique

An alternative method was also used to estimate annual UK emissions using the NAME model and an iteration technique which optimised the fit between the modelled and measured concentrations by altering the annual emissions. To infer annual emissions for each species, the spatially disaggregated emissions were divided into individual source sectors using the UNECE sectors reported in the NAEI. The model was run for each sector using the same set of parameters as the total source runs and enhancements summed to produce the total enhancement in concentration. The source sectors for each species are shown in Table 14.

Table 14. Source sectors for CO, CO_2, CH_4 and N_2O and contribution to total annual UK emissions for each chemical species from the NAEI.

CO	CO_2	CH_4	N_2O
Agriculture < 1%	Agriculture < 1%	Wetlands – 4%	Traffic – 8%
Road transport – 57%	Road transport – 22%	Gas pipes leaks – 15%	Livestock – 21%
Non-road transport – 13%	Non-road transport – 2%	Landfill – 42%	Rivers < 1%
Industrial combustion < 1%	Industrial combustion – 6%	Livestock – 31%	Estuaries < 1%
Industrial processes < 1%	Industrial processes < 1%	Open Mines < 1%	Industry – 13%
Residential, commercial and institutional combustion – 7%	Residential, commercial and institutional combustion - 21%	Deep Mines – 8%	Nitrogen Deposition - 4%
Energy production < 1%	Energy production < 1%		Fertiliser – 52%
Waste < 1%	Waste <1%		
Point sources – 23%	Point sources – 47%		
	Nature – 2%		
	Net Biogenic uptake < 1%		

Figure 91 (a), (b), (c) and (d) show the model concentrations for CO, CO_2, CH_4 and N_2O respectively for each source sector for flight B134.

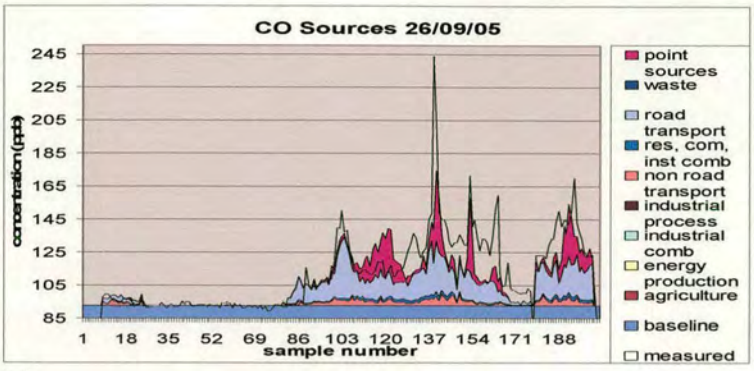

(a)

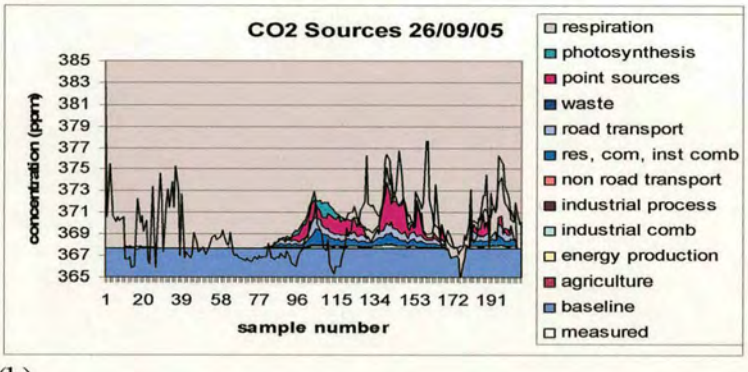

(b)

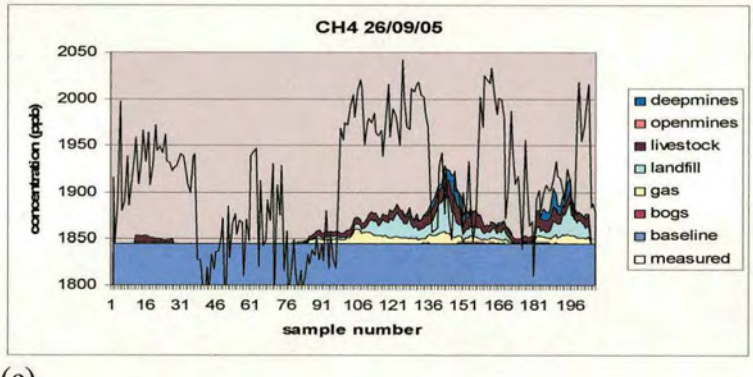

(c)

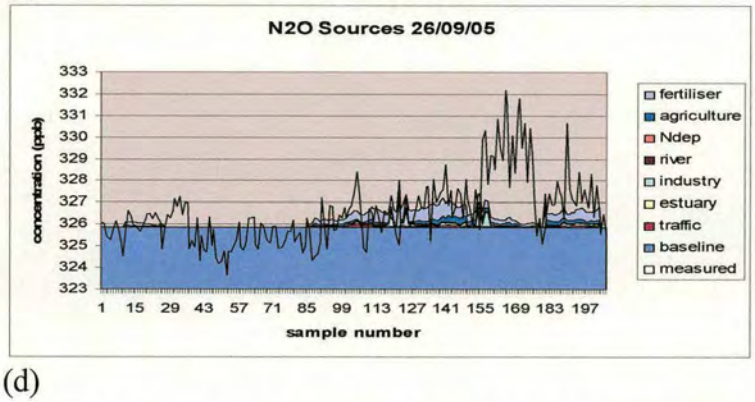

(d)

Figure 91. NAME concentration for each sample source sector and measured concentration for flight B134. (a) CO (ppb), (b) CO_2 (ppm) (NB respiration flux is negative), (c) CH_4 (ppb) and (d) N_2O (ppb).

To calculate the total annual emissions an iteration technique was used. Emissions from each sector were changed systematically and using least squares fitting, a best-fit between the total modelled and measured concentrations yielded the best estimate of emissions from each sector. The total modelled concentration, C_m, for sample m was calculated using the equation

$$C_m = \sum_j C_{mn}\left(\frac{F_n^*}{F_n}\right) + C_{bg} \tag{5.6}$$

where C_{mn} is the modelled concentration for sample m for sector n (g m^{-3}), F^*_n is the altered total emissions for sector n (kt yr^{-1}), F_n is original total emissions for sector n (kt yr^{-1}) and C_{bg} is the background concentration (g m^{-3}). The altered total emissions, F^*_n, and background concentration, C_{bg}, were allowed to vary until the model concentrations became consistent with the measured concentrations. The background concentration, C_{bg}, was allowed to take any value while F^*_j was allowed to take any value greater than 50% of F_j. This was to prevent the emissions from each sector becoming unrealistically small. Any sectors that did not contribute to more than 5% of the UK emissions were fixed at F_n. These sectors at no point contributed enough to C_m to significantly affect the overall fit and so it was unrealistic to expect the iteration technique to fit these sectors.

For CO_2 the biogenic flux was taken directly from the NAME model and was not allowed to change. For N_2O the modelled enhancements were generally much smaller than the measured enhancements. Therefore C_{bg} was set to fixed value calculated by averaging the upwind concentrations. This prevented the fitting procedure from setting C_{bg} to some average value of the measured concentrations which was well above the background.

The total emissions from the UK, F_{emit} (kt yr^{-1}), for each chemical species was calculated by summing the sector emissions F^*_n (kt yr^{-1}).

$$F_{emit} = \sum_n F_n^* \tag{5.7}$$

Figure 92 (a), (b), (c) and (d) show the altered concentrations for each source sector for CO, CO_2, CH_4 and N_2O respectively for flight B134. From Figure 93 (a), (b), (c) and (d) which show the original and altered NAME concentration with the measured concentration for CO, CO_2, CH_4 and N_2O respectively for flight B134, we can see that while CO and CO_2 change very little suggesting that the original emissions are accurate, the altered concentrations of CH_4 and N_2O are significantly larger than the original emissions suggesting that they have been underestimated. Figure 92 (c) suggests that CH_4 emissions from gas pipe leaks have been significantly increased by the iteration technique. Figure 92 (d) shows an increase in emissions from livestock (i.e. manure) for N_2O. By combining the information for all the flight days it is possible not only to estimate the total annual emissions but also build up a picture of which source sectors are likely to be underestimated.

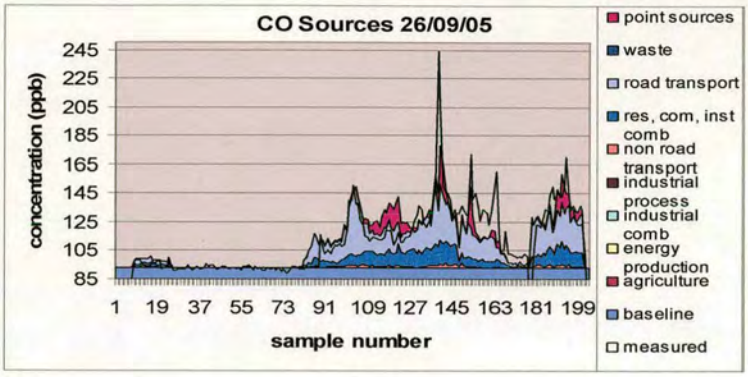

(a)

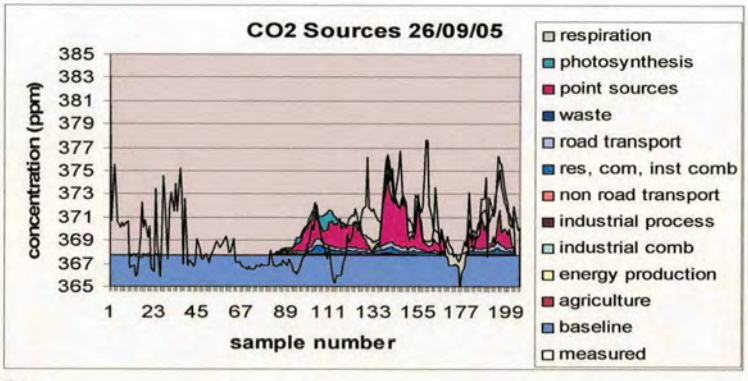

(b)

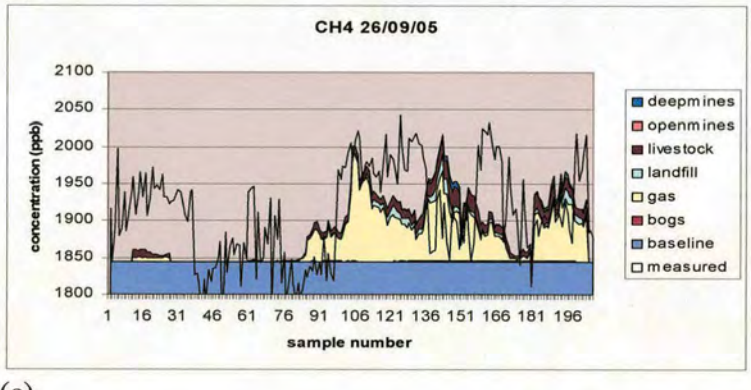

(c)

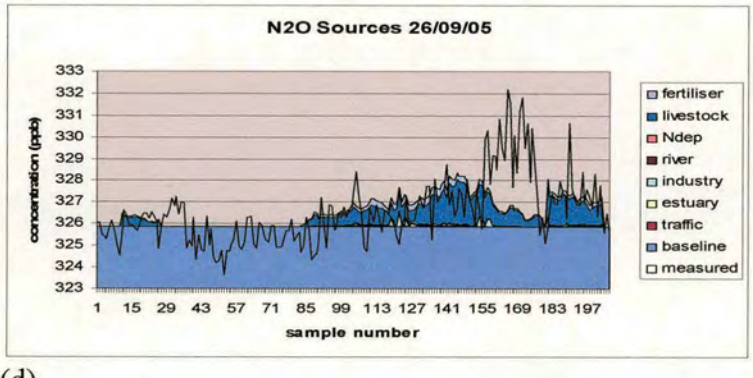

(d)

Figure 92. Altered NAME concentration for each sample source sector and measured concentration for flight B134. (a) CO (ppb), (b) CO2 (ppm) (NB respiration flux is negative), (c) CH4 (ppb) and (d) N2O (ppb).

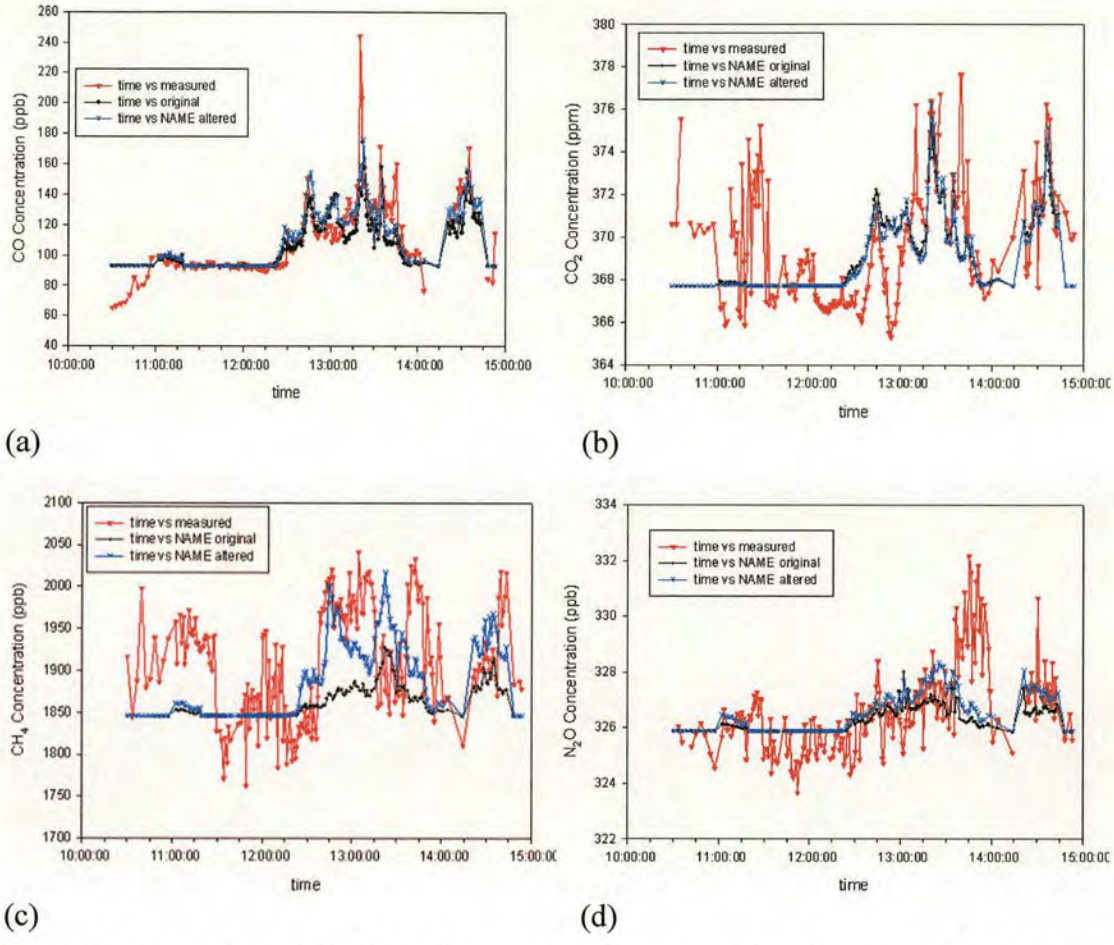

Figure 93. Original and altered NAME concentrations and measured concentration at time of sample. (a) CO, (b) CO2, (c) CH4 and (d) N2O.

5.3 Estimating Uncertainty in F_{emit}

5.3.1 Uncertainty in Box Model Budget

The main sources of error in the box model estimate of F_{emit} are the measurement error, σ_m, the error in C_{bg}, σ_{bg}, and the error in the z_{BL}, σ_{BL}. The relative errors in wind speed and wind direction are negligibly small in comparison, typically < 1%, and so were ignored in the error calculation.

The measurement error, σ_m, was estimated using the average standard deviation of bag samples that were analysed more than once for each flight. For CO_2 there were 4 flights where this method was not applicable and so the average error for the other days was used. For CO which was measured on the aircraft, it was assumed that

background air sampled over a short time period should have the same concentration. The measurement error, σ_m, was estimated by calculating the standard deviation of samples over 10 second periods (at a sample rate of 1 s^{-1}) for samples taken over 10-20 minutes in background air. The average was used as the measurement error. The background error, σ_{bg}, was estimated by averaging the concentration of samples believed to be of background air and taking the standard deviation of this value and the model iteration value for C_{bg}. Typically the σ_{bg} was smaller than the σ_m and so to avoid double counting σ_m, the background error was taken to be σ_m only. Otherwise σ_{bg} was used as it should include σ_m. The ABL height error, σ_{BL}, was taken to be the standard deviation of the ABL height across the outflow.

The error in F_{emit} was then calculated using standard propagation of errors techniques.

5.3.2 Uncertainty in Model Iteration Technique

Uncertainty in fluxes has been estimated using a two stage process, firstly estimating very approximately the expected range in uncertainty which is then used in a more rigorous approach by Bayesian methods.

To estimate the range in F_{emit}, a technique was devised to calculate the range of possible emissions taking the extremes of the upwind and downwind concentrations. The two main sources of error were the measurement errors and the error in the background concentration. The same values of σ_m and σ_{bg} were used as in the simple box model method.

To calculate an upper and lower limit for F_{emit}, C_{bg} was forced to the lower then upper limit of σ_{bg} and the upwind and downwind concentrations to the lower and upper limits of the σ_m. The iteration was then performed again with the measurements and C_{bg} alternately forced to their upper and lower limits producing the extreme upper and lower values for F_{emit}.

This technique does not produce an estimate of the uncertainty in F_{emit}, only giving a range which will be far larger than the real uncertainty. In order to calculate the uncertainty a Bayesian Calibration technique was used as described in the section below.

5.4 Bayesian Calibration

To estimate the uncertainty in the iteration technique, a Bayesian calibration approach was used. The basis of this approach is Bayes Theorem

$$P(\theta/d) = \frac{P(\theta)P(d/\theta)}{\int_{-\infty}^{\infty} P(\theta)P(d/\theta)d\theta} \tag{5.8}$$

where $P(\theta/d)$ is the probability of parameter θ given data d and is effectively a probability density function. $P(\theta)$ is the probability density function of θ and $P(d/\theta)$ is the likelihood function, i.e. the likelihood of data d given parameter θ. The denominator is the integral between -∞ and ∞ and is a scaling constant.

To estimate the uncertainty in the iteration technique firstly an estimate of $P(\theta)$ is required. In this case θ is the scaling parameter used to alter the modelled concentrations, i.e. F^*/F. Assuming that $P(\theta)$ is a normal distribution with a mean value of F^*/F where F^* is the best-fit value as estimated using the iterative technique. The standard deviation of the $P(\theta)$ is harder to define. A value of 10% was chosen for CO and CO_2 as both species are well defined. The uncertainty in the NAEI emissions for CO and CO_2 is 20% and 2% respectively. Because the CO and CO_2 emissions should be relatively constant throughout the year and because the range estimated for CO and CO_2 using the iteration technique is typically within 10% of the estimated value, an uncertainty of 10% was chosen for both CO and CO_2. For CH_4 and N_2O a value of 30% was chosen. A larger value was chosen than for CO and CO_2 because emissions for both species are less well defined and N_2O in particular is more variable throughout the year.

To calculate the likelihood function the normal approach would be to perform thousands of runs of the model with different values of θ and using a Monte Carlo approach, gradually refine the estimate of θ to produce a best-fit between the model and measured data. The data in this case refers to the enhancement to the concentration from UK emissions and not the absolute concentration. The resulting values from the many model runs can then be plotted to produce a pdf of the data

given parameter θ, i.e. $P(d/\theta)$. As the fit between the model and measured data is refined, the model data will tend towards the values for the best-fit value of parameter θ and so the pdf of the data should tend towards the likelihood function $P(d/\theta)$ where θ is the best-fit value. However due to time constraints this approach could not be used with the NAME model and a shortcut approach was taken.

It was already assumed that the concentrations produced by the model will scale linearly with the emissions. The iterative technique assumes that the concentration at a particular observation point is the sum of the concentration produced by each source sector multiplied by some scaling factor for each source sector. The parameter θ is simply the sum of the scaling factors for each sector. For this approach it is assumed that the concentration will scale with the total scaling factor. This is a reasonable assumption as can be seen from Figure 94 which shows the model concentrations for the sources scaled by the sources scaling factors separately then summed against the model concentrations for the sources summed and then scaled by the total scaling factor. The correlation coefficient of the two series is 0.99.

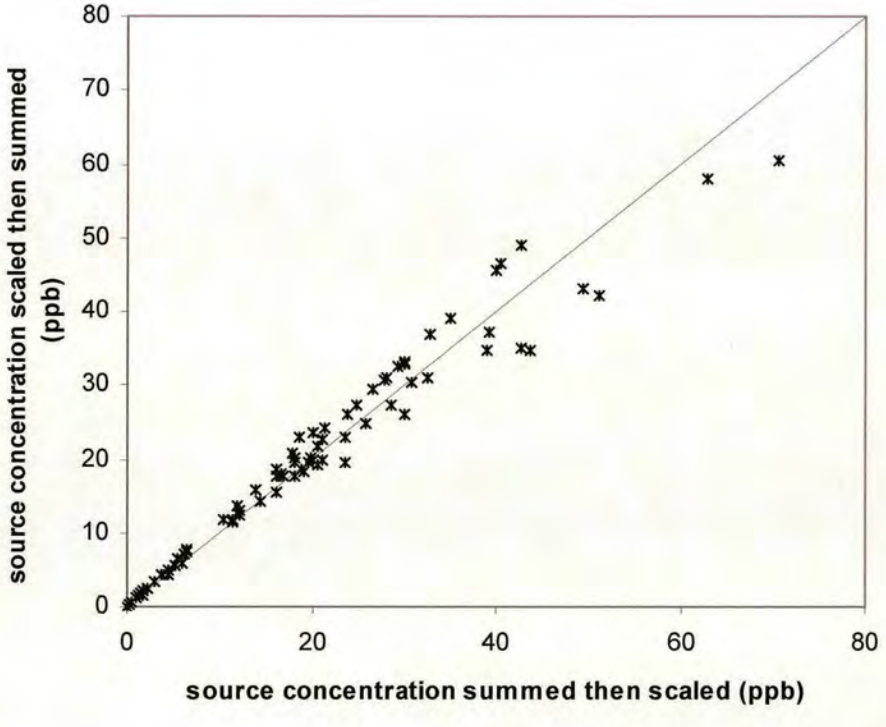

Figure 94. CO concentration (ppb) for flight B97 for source concentration scaled separately and sum against source concentration summed then scaled (R = 0.99).

Assuming linearity allows the likelihood function to be estimated in terms of the scaling factor. That is, it is assumed that for a scaling factor of θ_n, the modelled concentration C_{mod} will be

$$C_{mod}(\theta_n) = C_{mod}(\theta = 1)\theta_n \tag{5.9}$$

For the best-fit value of the parameter θ, the model values C_{mod} should equal the observed values, C_{obs}, where the background concentration has been subtracted from the absolute values measured during the flight to get the enhancement. The likelihood function should then simply be the distribution of the measured data. The best fit data in terms of the scaling factor is then

$$\theta = \frac{C_{obs}}{C_{mod}(\theta = 1)} \tag{5.10}$$

We would expect the data to be approximately normally distributed with a mean at the mean value of the data and a standard deviation of the uncertainty in the data but with a slight tail towards larger values. The uncertainty in the data comes from both uncertainty in the background and the measurements.

This would be the case if our measurements were a random sample and the sample set was large enough. However the measurements are not a random sample of the concentrations around the country, but are biased to the larger concentrations in the outflow plumes. So instead of simply taking the uncertainty in the data as the standard deviation, the distribution was plotted and a normal distribution fitted to the data using the software IGOR. Plotting the distribution of the data in terms of the scaling parameter gives a distribution of the form shown in Figure 95 (a). This shows the distribution of data for CO for flight B97. B97 is the smallest data set due to the shorted flight path and the relatively large number of observations in background air which are not captured by the model. Even for this small dataset the distribution takes the form of a normal distribution. Figure 95 (b) shows the distribution of data for N_2O. This is an example of a poor quality dataset and shows that even when the data

is poor, a normal distribution is still the best assumption for the form of the distribution.

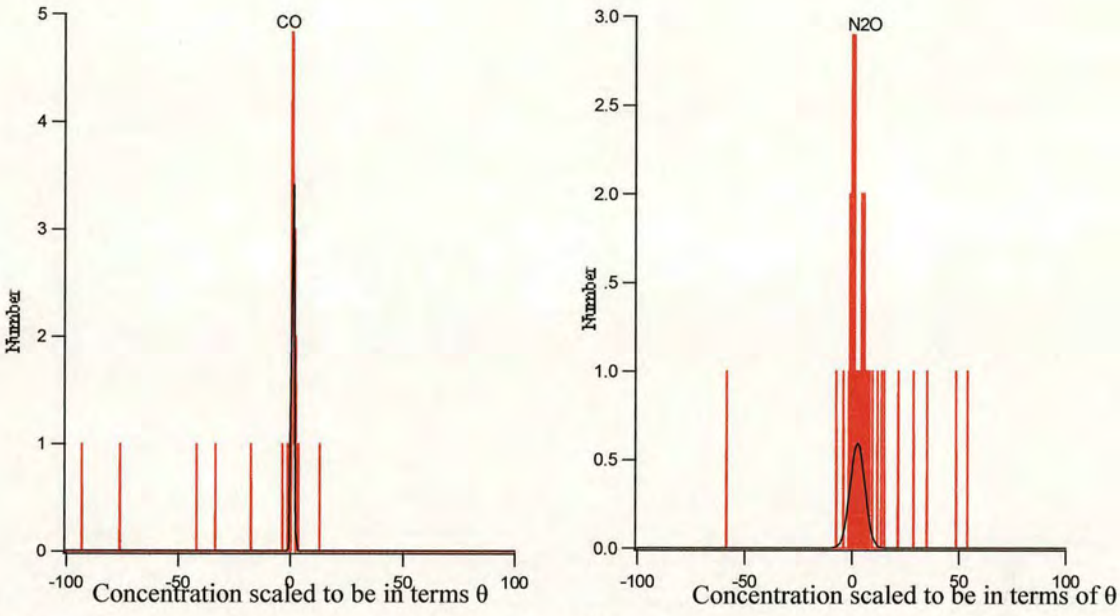

(a) (b)

Figure 95. (a) Distribution of CO data for flight B97 scaled to be in terms of emissions parameter with normal distribution fitted. B97 has smallest dataset of all flights but can still be approximated as a normal distribution. (b) Distribution of N_2O data for flight B97 scaled to be in terms of emissions parameter with normal distribution fitted. This is an example of a poor quality dataset but it still takes approximated form of normal distribution.

$P(\theta/d)$ is then the product of two normal distributions which is itself also a normal distribution and allows us to determine the mean value and standard deviation very simply. If we take a normal distribution

$$N(x,\sigma_x) = \frac{1}{\sigma_x\sqrt{2\pi}}\exp[-\frac{1}{2}(\frac{x-\mu_x}{\sigma_x})^2] \tag{5.11}$$

where $N(x,\sigma_x)$ is distribution of variable x with standard deviation σ_x and mean value μ_x.

If we say

$$B = \frac{1}{2\sigma_x^2} \tag{5.12}$$

then equation (5.12) becomes

$$N(x,\sigma_x) = \sqrt{\frac{B}{\pi}} exp[-B(x-\mu_x)^2] \tag{5.13}$$

If we define a second normal distribution as

$$N(y,\sigma_y) = \sqrt{\frac{S}{\pi}} exp[-S(y-\mu_y)^2] \tag{5.14}$$

This is the likelihood function for variable y given x where

$$S = \frac{1}{2\sigma_y^2} \tag{5.15}$$

where σ_y is the standard deviation of variable y and μ_y is the mean values of y.
Multiplying equations (5.13) and (5.14) we get

$$N(x,\sigma_x)N(y,\sigma_y) = \frac{\sqrt{BS}}{\pi} exp[-B(x-\mu_x)^2 - S(y-\mu_y)^2] \tag{5.16}$$

To get the scaling constant in Bayes Theorem we need to take the integral of equation (5.16) between -∞ and ∞.

$$\int_{-\infty}^{\infty} N(x,\sigma_x)N(y,\sigma_y) = \sqrt{\frac{BS}{\pi(B+S)}} exp[-\frac{BS}{(B+S)}(\mu_y-\mu_x)^2] \tag{5.17}$$

Dividing equation (5.16) by equation (5.17) gives

$$N(x/y) = \sqrt{\frac{B+S}{\pi}} exp[-(B+S)(\frac{B\mu_x + S\mu_y}{B+S} - x)^2] \tag{5.18}$$

This is the probability density function of x given y and is a normal distribution from which we can get the mean and standard deviation.

The mean value is

$$\mu_{new} = \frac{B\mu_x + S\mu_y}{B+S} \tag{5.19}$$

and the new standard deviation is

$$\sigma_{new} = \sqrt{\frac{\sigma_x^2\sigma_y^2}{\sigma_x^2+\sigma_y^2}} \tag{5.20}$$

Replacing x with parameter θ and y with concentration data C where C has been rescaled to be given in terms of scaling parameter θ produces the predicted mean and uncertainty of the scaling factor θ given data C.

5.5 Results of Budget Analysis

5.5.1 UK Emission Estimates

The emissions estimated by the box model method and the model iteration technique for each flight are shown in Table 15 and Table 16 respectively along with the inventory estimates. To get the average annual emission, each flight was weighted to reflect the measure of uncertainty in each from σ_m and σ_{bg}.

For CO, the average total UK emissions as calculated by the simple box model method are 2900 ± 880 kt yr^{-1}. This compares to an iteration method estimate of 2400 ± 250 kt yr^{-1}. The NAEI estimate for CO is 2400 kt yr^{-1} for 2005 with an uncertainty of 20%. Both the box model method and model iteration method produce estimates well within the uncertainty of the NAEI emissions and are a very good agreement with the NAEI total. This suggests that UK CO emissions are well understood as was expected and validates both the box model and model iteration techniques as a

method of estimating annual UK emissions, at least within the uncertainty discussed earlier.

For CO_2, the box model method emissions are quoted as the initial flux estimate, F_{emit}, and also as the anthropogenic emissions only by subtracting the biogenic flux calculated by the NAME model. If uptake by photosynthesis, F_{photo}, is considered a negative flux and release by respiration, F_{resp}, a positive flux, then the total anthropogenic flux, F_{anht}, will be

$$F_{anth} = F_{emit} - F_{resp} + F_{photo} \tag{5.21}$$

The average biogenic flux for all the flights is small compared to the emissions but including the biogenic flux results in a slightly lower estimate for F_{anth} as the flights are slightly biased towards the end of the summer when F_{photo} is much smaller than F_{resp}. The model iteration method already takes account of the biogenic flux as this is included in the model concentrations.

The average annual UK anthropogenic emissions as calculated by the box model method are 689 ± 282 Mt yr^{-1}. The model iteration method produces an annual estimate of 514 ± 65 Mt yr^{-1}. The NAEI estimate for CO_2 for 2005 is 555 Mt yr^{-1} with an uncertainty of only 2%. The box model method emissions are larger than the NAEI emissions by 24% while with model iteration method emissions are 7% smaller than the NAEI. The NAEI emissions are however within the uncertainty of the estimates of both methods and all three methods are in good agreement.

The N_2O emissions as predicted by the box model methods are 300 ± 216 kt yr-1. The model iteration method emissions are 330 ± 105 kt yr^{-1}. The NAEI estimate for 2005 was only 130 kt yr^{-1}, less than half of the 'round-Britain' estimates. The uncertainty in the NAEI emissions is very large (230 %), so the box model and model iteration estimates are within the uncertainty of the NAEI emissions. The uncertainty for the box model method is also very large in this case, however by including a Bayesian calibration in the model iteration analysis, the uncertainty for this technique has been significantly reduced making this estimate the most reliable. Although this estimate is based on relatively few days and only covers part of the year, the time at which we were sampling was not expected to be the peak time for emissions. This

should have been earlier in the spring at the time when farmers were applying mineral fertilisers to their fields. N_2O emissions are also significantly affected by rainfall with wetter soils increasing emissions. With the exception of August, all months during the period of sampling were drier than average suggesting emissions should have in fact been smaller than normal during this period. It is therefore likely that the NAEI estimate significantly underestimates the real UK N_2O emissions. Due to the limited nature of this study and the variable nature of N_2O emissions, as can be seen from the variation between flights, it is not possible to say for definite how well the total of 330 kt yr^{-1} reflects the actual annual emissions but it is strong evidence that UK emissions are significantly underestimated.

The CH_4 emissions are based on fewer days and more variable data quality. Some flights such as B97 and B244 produced good quality CH_4 data while others such as B102 were very poor. For this reason some flights have been ignored in the analysis. By weighting the flights based on the quality of the data, the annual average should still be a reasonable estimate. CH_4 is not expected to vary greatly throughout the year as N_2O does, so having fewer days on which to base the estimate should not affect our estimate too greatly. However it should be noted that the CH_4 emission estimate is not as reliable as the estimates for the other three chemical species.

The box model estimate for CH_4 is 3900 ± 2100 kt yr^{-1}. The model iteration estimate is 3300 ± 1000 kt yr^{-1}. Both are larger than the NAEI estimate of 2400 kt yr^{-1} and outside the NAEI uncertainty of 21 %. The NAEI estimate is however within the uncertainty of both the box model and model iteration estimates. Although based on fewer flights, the 'round-Britain' estimate suggests that the UK may be underestimating CH_4 emissions. Peter Bergamaschi, (Bergamaschi *et al.*, 2005) has suggested that UK emissions for 2004 were actually 4210 kt yr^{-1}, very similar to the estimate produced by the box model method and further evidence supporting this claim.

Table 15. Total annual emissions (kt yr^{-1}) for CO, CO_2, N_2O and CH_4 using the simple box model method. The average value is weighted according to the relative error of the measurements for each flight and the boundary layer height on that day. * - not included in average budget because of suspicious data quality, **** - data not available for this flight.

	CO kt yr^{-1})	CO_2 (kt yr^{-1})	CO_2 (kt yr^{-1}) With biogenic flux	N_2O (kt yr^{-1}	CH_4 (kt yr^{-1})
NAEI (2005)	2400	555000		130	2400
B92	2500 ± 700	735000 ± 236000	955000 ± 236000	750 ± 413	*7700 ± 6530
B97	3700 ± 1470	398000 ± 175000	462000 ± 175000	330 ± 320	3600 ± 1600
B102	1800 ± 920	241000 ± 208000	262000 ± 208000	240 ± 238	*****
B111	*1000 ± 610	*399000 ± 266000	*399000 ± 266000	*430 ± 298	*****
B112	2100 ± 740	557000 ± 365000	491000 ± 365000	2670 ± 112	8300 ± 4020
B113	2900 ± 1200	1134000 ± 455000	1080000 ± 455000	2670 ± 907	11900 ± 7240
B118	830 ± 370	884000 ± 372000	841000 ± 372000	190 ± 166	*****
B119	1600 ± 870	493000 ± 296000	463000 ± 296000	110 ± 99	*****
B126	4400 ± 1550	861000	693000 ± 358000	4240 ± 432	7100 ± 7400
B130	4000 ± 1310	689000 ± 262000	587000 ± 262000	350 ± 166	2300 ± 1100
B132	1500 ± 560	295000 ± 227000	182000 ± 227000	370 ± 243	1700 ± 650
B134	6000 ± 920	779000 ± 175000	744000 ± 175000	450 ± 239	11400 ± 5510
B136	2600 ± 830	257000 ± 251000	195000 ± 251000	460 ± 566	*1700 ± 2140
B244	6800 ± 1220	1122000 ± 299000	903000 ± 299000	780 ± 1282	3600 ± 1810
AVERAGE	2900 ± 880	689000 ± 281500	662000 ± 281500	300 ± 216	3900 ± 2100

Table 16. Total annual emissions (kt yr^{-1}) for CO, CO_2, N_2O and CH_4 using the Bayesian calibration technique. The average value is weighted according the relative errors in the measurements for each flight. * - not included in average budget because of suspicious data quality, **** - data not available for this flight.

	CO (kt yr^{-1})	CO_2 (kt yr^{-1})	N_2O (kt yr^{-1})	CH_4 (kt yr^{-1})
NAEI (2005)	2400	555000	130	2400
B92	2900 ± 190	406000 ± 23600	1150 ± 255	*9800 ± 2530
B97	3700 ± 360	168000 ± 56100	430 ± 158	4500 ± 360
B102	2700 ± 270	531000 ± 31200	790 ± 179	*****
B111	2500 ± 300	518000 ± 139000	880 ± 265	*****
B112	1300 ± 180	404000 ± 65000	1560 ± 577	5200 ± 2760
B113	2700 ± 260	438000 ± 87000	2870 ± 848	13000 ± 3670
B118	500 ± 80	499000 ± 71600	200 ± 95	*****
B119	1400 ± 180	450000 ± 96600	180 ± 56	*****
B126	3200 ± 320	846000 ± 89700	3420 ± 1041	6000 ± 2320
B130	2300 ± 230	166000 ± 45600	160 ± 61	1500 ± 550
B132	1500 ± 160	298000 ± 54400	210 ± 114	1500 ± 430
B134	3800 ± 460	498000 ± 62800	230 ± 91	4700 ± 1700
B136	2400 ± 290	690000 ± 48400	870 ± 185	*2900 ± 750
B244	4300 ± 550	900000 ± 108500	670 ± 260	3500 ± 1130
AVERAGE	2400 ± 250	514000 ± 65000	330 ± 105	3300 ± 1000

5.5.2 Sector Analysis

The model iteration technique gives an indication as to which sectors in the NAEI estimates may be inaccurate. Looking at the new estimates for the annual emission for each source sector can act as a pointer. However it should be noted that the distribution of the emissions between the sectors may not be accurate as only 2 or 3 sectors tend to dominate the outflow and therefore the fitting. If a sector is significantly underestimated such that it does not contribute significantly to the outflow, then the model iteration technique will not refit the emissions from that sector. Also the total for the mapped UNECE sectors do not necessarily equal those reported in the NAEI total emissions. The NAEI is updated every year and emissions for previous years are updated to reflect the latest methodology. The mapped emissions are only compiled for the latest year and so are not necessarily consistent with the latest total emissions. While the totals from each sector may be different, the distribution of sources should not change significantly. As the iteration technique is trying to fit the total emissions, it should not matter if these are slightly wrong as the fitting should bring the emissions more into line with current estimates if these are indeed correct.

For CO the original and altered emissions for each sector are shown in Figure 96. The NAEI emission estimate seems to be very accurate and so we would not expect a great deal of change between the pre-iteration and post-iteration emissions. The mapped NAEI emissions for 2004 are larger than the current NAEI total at 3300 kt yr^{-1} compared to 2400 kt yr^{-1} and the iteration technique has the affect of lowering the emissions overall compared to the mapped total. Figure 96 shows the emissions from both road and non-road transport to be reduced by 20% and 35% respectively. Emissions from point sources have also decreased by 40%. Emissions from residential, commercial and institutional combustion have doubled although they are a relatively small part of the total and so this does not affect the total emissions significantly. Overall it seems that the iteration technique has acted to lower the total emissions, bringing them more inline with the current NAEI estimate for that year.

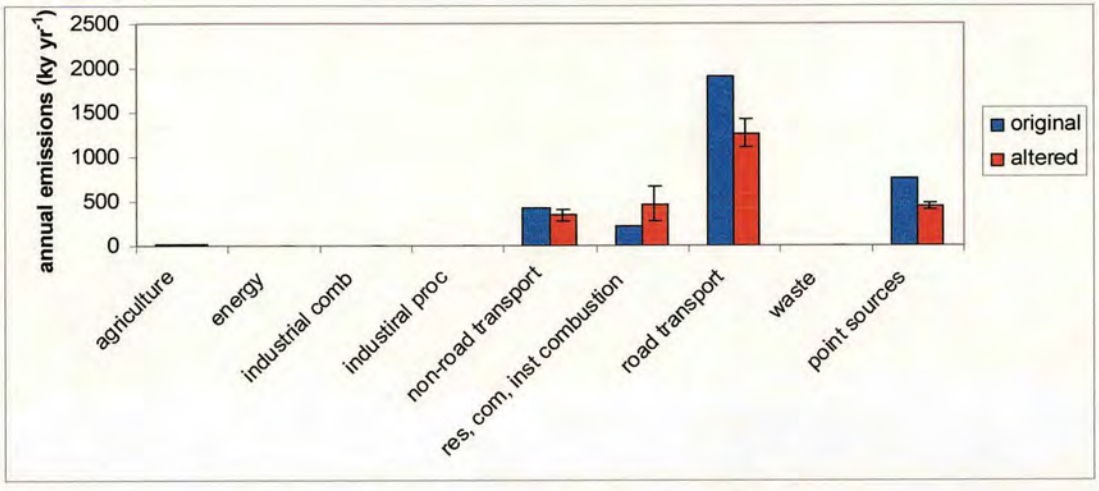

Figure 96. CO annual UK emissions (kt yr^{-1}) before and after fitting with MIT.

The CO_2 sector emissions are shown in Figure 97. The mapped emissions for CO_2 for 2004 are 98% of the current NAEI estimate. The iteration technique increases the mapped total CO_2 emissions by 15%, slightly above the current NAEI estimate. The major changes are non-point source industrial combustion which increases by 560% and point sources which decreases by 32%. These sectors are closely linked with the point sources representing industrial and energy sources large enough to be reported independently. Therefore these sectors can be considered together resulting in an overall increase in industrial and energy generation combustion emissions of 30%. There is also an increase in non-road transport emissions of 30% which is mostly offset by a decrease in residential, commercial and institutional combustion of 23 %.

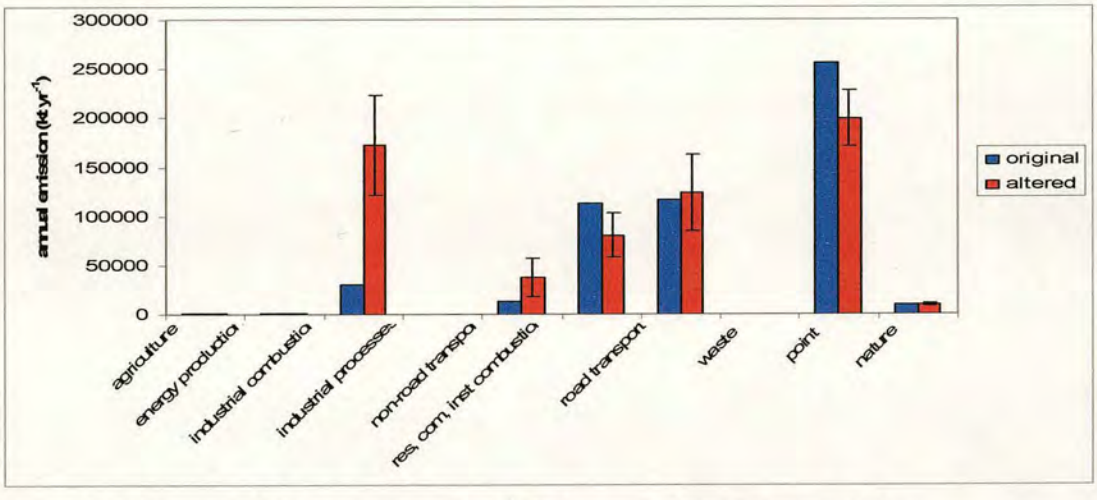

Figure 97. CO_2 annual UK emissions (kt yr^{-1}) before and after fitting with MIT.

The CH_4 sector emissions are shown in Figure 98. The mapped CH_4 emissions do not come from the NAEI and are a combination of agricultural emissions for 2004 and an old emissions inventory compiled by CEH Edinburgh for 1994 for all other sectors. While the totals from these sectors will have changed over the years, the distribution should not have changed significantly and so should still be valid. The mapped inventory total is 10 % larger than the current NAEI estimate yet the model concentrations still tend to underestimate the concentrations. Figure 98 shows an increase in emissions from all sectors except landfill emissions which fall by 50%. The major increase is in livestock emissions which increase by 160%.

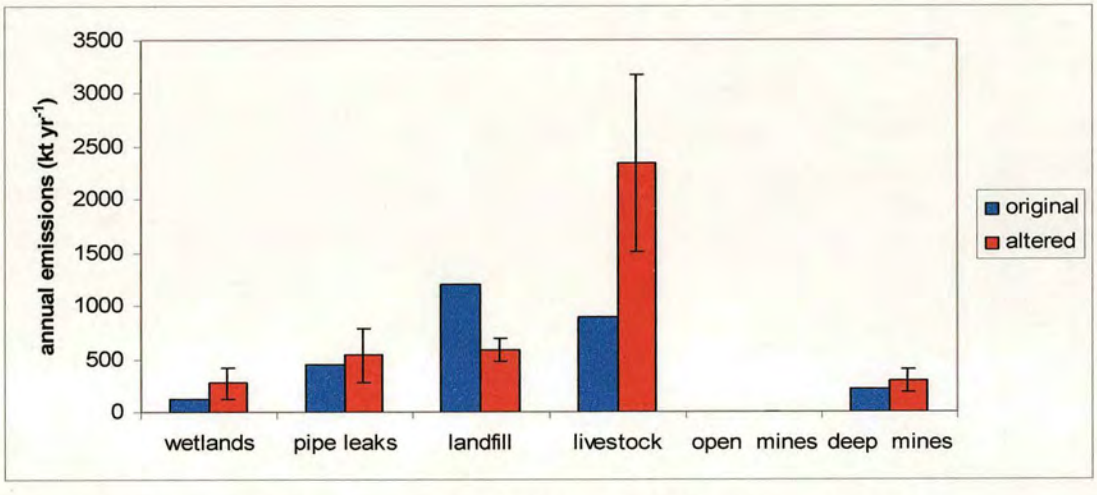

Figure 98. CH_4 annual UK emissions (kt yr^{-1}) before and after fitting with MIT.

The N_2O sector emissions are shown in Figure 99. The mapped emissions used for the modelling come directly from the team responsible for compiling the emissions for NAEI at CEH Edinburgh but uses an improved method of calculating emissions for soils fertilised with mineral fertiliser. This increases the annual total from 130 kt yr^{-1} as in the NAEI, to 165 kt yr^{-1}. The model concentrations using this inventory still underestimate the observed concentrations significantly and the effect of the inversion is to increase emissions overall by 170% compared to the NAEI. Although there is a 90% increase in traffic emissions, this is a small fraction of the total and the bulk of the increase is due to increased emissions from livestock with a 470% increase from this sector. As with CH_4, the N_2O emissions are dominated by two sectors, in this case livestock and mineral fertiliser. Both are predominantly emissions from soil after the addition of Nitrogen either through mineral fertiliser or manure and so are dominated by rural emissions. They do however reflect emissions from different areas of the country with livestock farming concentrated more in the west and arable farming more in the east. For a westerly wind flow the emissions will tend to be mixed by the time the outflow is observed along the east coast, however the iteration technique tends to consistently increase the livestock emissions in favour of the mineral fertiliser emissions and for the two days where a north westerly wind produces distinct plumes along the south coast, the iteration increases the livestock emissions in both cases suggesting that it is indeed livestock emissions that are underestimated.

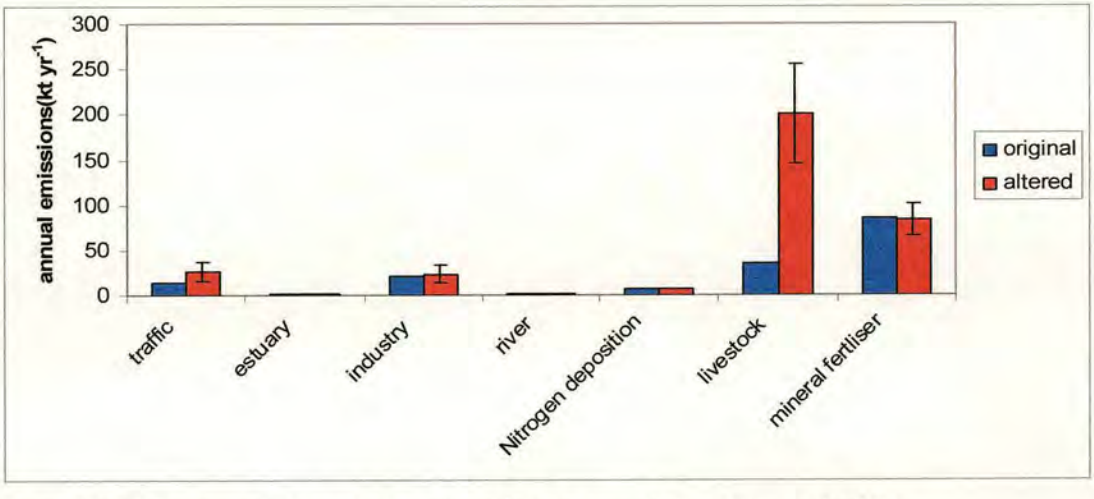

Figure 99. N_2O annual UK emissions (kt yr^{-1}) before and after fitting with MIT.

It should also be noted that the changes to the emissions from each sector are an average for all the flights and do not necessarily reflect a consistent pattern over all. We would not necessarily expect the emissions from each sector to be the same comparatively between flights as they can change depending on a number of factors including weather conditions (e.g. N_2O emissions from soil), time and day of the week (e.g. traffic) and other miscellaneous factors such as production rates from factories. So while a consistent pattern may provide further evidence of a real pattern, the lack of a consistent change does not exclude the possibility that the observed changes are real. However it is important to be careful in making any definite conclusions as the estimates are based on relatively few days of data. Inverse modelling techniques can provide clues to the emission sector distribution by providing a map of emissions since knowing the spatial distribution of the emissions can help identify the possible source sectors.

5.6 Discussion and Conclusion

Two techniques were used to derive annual emissions from the AMPEP measurements. The first was a simple boundary layer budget box model technique which assumes that all emissions from the UK are trapped inside a box over the country with the emitted flux then calculated directly from the difference in the upwind and downwind pollutant concentrations. The second method uses the atmospheric transport model NAME and the NAEI spatially disaggregated emissions to simulate the emission and transport of air from each source sector for each species. A model iteration technique is then used to alter the emissions from each sector such that the fit between the predicted model and observed concentrations is optimised. A Bayesian calibration technique is then applied to fine tune the emission estimate and determine the uncertainty.

Overall the simple box model method and iteration technique produce very similar estimates for the total annual UK emissions for CO and CO_2 as the NAEI. The model iteration (MIT) combined with the Bayesian calibration technique is a more robust method than the simple box model with the box model estimate acting as a verification of the iteration technique estimate. Taking the iteration technique estimate as the final value, the 'round-Britain' flights produce an annual emission of 2400 ± 250 kt yr^{-1} for CO, 514000 ± 65000 kt yr^{-1} for CO_2, 3300 ± 1000 kt yr^{-1} for CH_4 and 330 ± 105 kt yr^{-1} for N_2O with the estimates from the simple box model method all within the uncertainty of the iteration and Bayesian estimates. For CO and CO_2 the MIT estimates are within the uncertainty of the NAEI estimates, and verify the current estimates for the total emissions. As the CO and CO_2 emissions are expected to be accurate, the success in the technique in reproducing the current inventory demonstrates the ability of the 'round-Britain' flights approach to produce reliable estimates for the total annual UK emissions.

For CH_4, the MIT estimate for the total annual UK emissions was within the uncertainty of the simple box model method estimate but was larger than the NAEI estimate by 38%, larger than the uncertainty in the NAEI estimate of 21 %. The quality of the CH_4 data was very variable between flights compared to CO and CO_2 and the NAEI estimate is within the MIT uncertainty of 1000 kT yr^{-1}, however the

annual emissions suggests that the UK may be underestimating the real CH_4 emissions, a conclusion verified by an independent study (Bergamaschi *et al.*, 2005). The sector analysis suggests that the source of the unaccounted for emissions may be livestock.

For N_2O, the MIT estimate is within the uncertainty of the simple box model method. Both are significantly larger than the current inventory estimate with the MIT emissions over twice the NAEI value. Emissions of N_2O are expected to be very variable between flights as they are highly dependent on soil moisture and temperature. The summer emissions measured during the AMPEP campaign should therefore be larger than the winter emissions which if included would produce a smaller annual average more consistent with the NAEI estimate. However three important factors need to be considered when assessing significance of the AMPEP results in relation to the NAEI findings. Firstly the 'round-Britain' flights took place after N_2O emissions are expected to peak. The application of mineral fertilizers by farmers during the Spring months should significantly increase N_2O emissions from agricultural soils and had the AMPEP campaign included this time period, even larger estimates for annual N_2O emissions would have been calculated. Secondly rainfall during the summer of 2005 was lower than average. This would have acted to reduce summer emissions compared to a typical year with lower water content in soils reducing the anaerobic microbial activity. Thirdly the annual estimate calculated from the AMPEP data is over twice the NAEI estimate. Therefore even with zero emissions for the rest of the year, the values calculated using the 'top-down' technique will still exceed the estimate produced using the 'bottom-up' methodology of the IPCC. The AMPEP data therefore provides strong evidence that the UK is significantly underestimating the annual N_2O emissions with the sector analysis suggesting that the livestock emissions are the major source of accounted emissions, similar to the results of the CH_4 analysis.

Chapter 6 Inversion

6.1 Introduction

This chapter outlines an inverse modelling technique to estimate spatially disaggregated emissions and its application to the AMPEP data using the NAME model. In inverse modelling, observed data is used to derive the values of model parameters as previously discussed in Chapter 1. The AMPEP data set describes the enhancement to ABL concentrations from UK emissions at locations downwind of the UK coast. Using the upwind concentrations, an estimate of the background concentration is made which can be subtracted from the downwind concentrations to derive the enhancement from the UK. The NAME model is run in backwards mode to derive the origin of the air at each sample location. Knowing the contribution to the sample concentration from the predefined grid squares across the UK and the enhancement due to the emissions from those grid squares, a best-fit iteration technique can then be used to derive the emissions from each square that best describes the overall dataset.

6.2 Theory

To use NAME to calculate the history of the air measured at each observation location, the model is run in backwards mode with a source at the location and time of each sampling point on the flight track. In backwards mode, particle transport is reversed to determine where the air measured at the observation point originated. The model is run until all the emitted particles have left the domain, producing a map of the total concentration (dosage=time integrated concentration) to pass through each surface grid square. The atmospheric transport is assumed to be reversible and thus the concentration at each receptor grid box can be derived assuming each grid box in the domain is a source (with strength 1 g s^{-1}) for the duration of the model run.

$$C_{io} = D_{io} / t_r \tag{6.1}$$

where $\boldsymbol{C}_{io}$ is the concentration from grid box i at observation o, $\boldsymbol{D}_{io}$ is the dosage at the grid box and t_r is the duration of the emission. Combining $\boldsymbol{C}_{io}$ for all grid boxes and observations into a single matrix and dividing by the initial release rate (g s^{-1}) gives an influence matrix, $\boldsymbol{C}$, which gives the fraction of air at each observation point from each grid square. This matrix, $\boldsymbol{C}$, can be used to convert emissions in g s^{-1} ($\boldsymbol{E}$) across the domain, to air concentrations in g m^{-3} ($\boldsymbol{c}$) at the receptor.

$$\boldsymbol{C.E} = \boldsymbol{c} \tag{6.2}$$

where $\boldsymbol{C}$ represents the fraction of air that arrives from each surface grid box in the domain at the location and time of the observation.

Assuming the air entering the UK has a constant background concentration, the enhancement to the concentration from the UK emissions can be calculated using the upwind observations. The observations are combined with the dilution matrices to derive the UK emissions using the best-fit iterative technique of 'simulated annealing'. In simulated annealing the current solution is replaced by some randomly chosen neighbouring solution based on a probability function. The probability function is chosen such that the solutions gradually tend to minimise some global parameter but also allow the global parameter to increase so as not to get stuck in some local minima. Given sufficient permutations, the solution will eventually tend to a good approximation of the optimum solution (Kirkpatrick et al., 1983). The initial emissions map is produced randomly by the inversion routine and a statistical score calculated using one of a variety of fitting functions (see below) which combines correlation coefficient, normalised mean square error and fraction within a factor of two. The emissions map is randomly altered and for each new map that produces a better score, the previous map is rejected and the new estimate accepted as an improvement. This process continues until eventually the best-fit is achieved.

6.3 Back Runs

The first step in the inversion process is to produce a dosage map for each observation which gives the contribution to the measured observation from each grid square. The NAME model is run in backwards mode which reverses the transports of particles. Particles are released from the observation point for 1 minute at the time the observation was made and then transported using the reverse of the mean wind velocity vector until all particles have left the model domain. Using the meteorology from the previous days, the particles are tracked as they are transported across the domain producing a footprint showing which grid boxes the observed air travelled through and their relative influence on the observed concentration. A 0.3° latitude × 0.18° longitude resolution grid was used and assuming that all emissions originate from the UK and Ireland, the domain was set to 44 grid boxes in the x direction and 64 grid boxes in the y direction as shown in the example in Figure 100. To produce sufficient particles in a 1 minute release window, a release rate of 10000 g s^{-1} was used. The same Unified Model 3-D synoptic mesoscale data of 16 km horizontal and 4 hourly temporal resolution was used as in the forward mode runs with a typical model run of 2 days allowing sufficient time to transport all particles out of the domain.

The resulting maps give the dosage (g m^{-3} s) in each grid box in the bottom 200 m of the boundary layer; summing the contribution from all particles to travel through each box during the time it took for all particles to exit the model domain. These dosage maps give the contribution from the surface emissions in each grid square to the final observation. The maps are combined into a single matrix containing the contribution to all the observations from each grid square in the domain. The size of the matrix equals no. of grid boxes × no. of observations, for a typical flight of around 200 observations, the matrix contains 112.64×10^6 separate values. Removing all zero values significantly reduces the size of the matrix by a factor of around 1000.

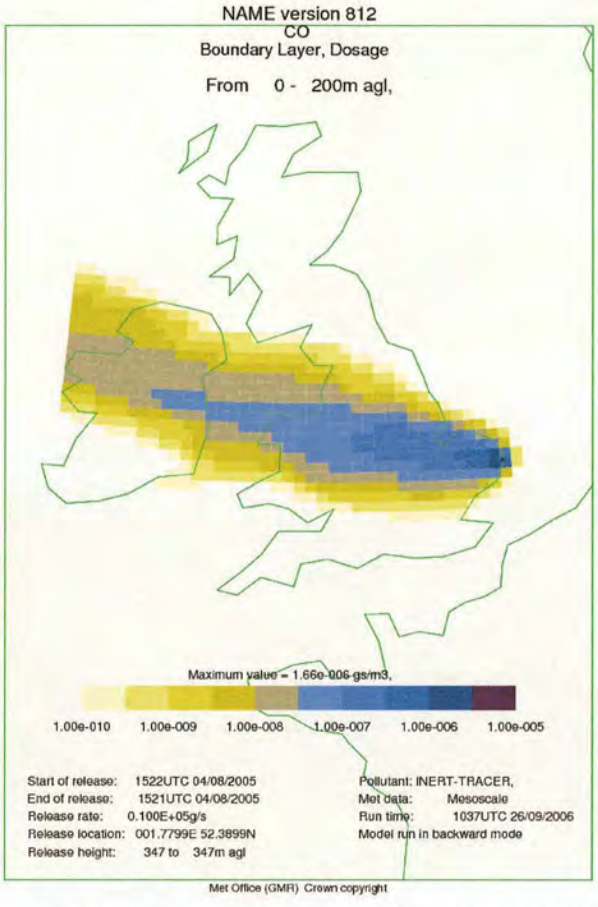

Figure 100. An example of a dosage map for one observation from flight B92.

6.4 Fitting Procedure

The inversion routine fits the dilution matrix (***C***) to the observations (***c***) by altering the emissions vector (***E***). The first emission vector is a random map produced by the routine. The map is gradually improved to maximise the fit between the observations and dosage matrix. Before each inversion the observations are randomly altered by a noise element with a prescribed mean and standard deviation. The mean is zero and the standard deviation is defined in 6.5.1. The noise factor was calculated as a multiple of the average uncertainty in the observations. Having produced the best fit, the inversion smoothes the map by randomly reassigning emissions from a grid box to adjacent boxes. For this process the fit between the observations and dosage matrix is allowed to degrade slightly within defined limits. In the model setup used, the degradation limit is set between 2 % and 4 % with the percentage of degradation

allowed to increase as the fit between the observations and the dosage matrix increases. The inversion is solved multiple times to estimate the uncertainty of the solution with respect to the noise.

To minimise the effects of under-prescribed grid boxes within the domain but predominantly around the edge, boxes that did not contribute to at least some minimum number of the observations, ($\sqrt{N}$, where N is the number of observations) were excluded from the inversion.

6.5 Assessment of Model Parameters

Each parameter was assessed using the CO observations for flight B92. CO was chosen for the reliability of the measurement data, the greater certainty in the NAEI emissions inventory, compared with N_2O and CH_4, and the absence of terrestrial emission / uptake, compared with CO_2. Flight B92 was chosen at it was one of the few flights where the whole of the UK was covered by the air history maps with a well-coupled wind flow and no inflow from Europe.

6.5.1 Noise Factor

The noise factor was chosen to be some multiple of the average measurement uncertainty in the observations and the uncertainty in the background concentration. To determine the sensitivity of the final emission map to the choice of scaling factor, three test values, (3, 4 and 5), were tried. For each factor, emission maps were produced at three spatial resolutions; 0.3° × 0.18°, the resolution of the back maps themselves, 0.6° × 0.36°, (2 × 2 grid boxes) and 01.2° × 0.72° (4 × 4 grid boxes). The emissions were either allowed to originate from anywhere in the model domain (land and sea) or were restricted to just the UK and Ireland (land only) with the assumption that all emissions originate from land based sources.

For each grid resolution and for each set of parameters, the inversion was performed 10 times. The standard deviation, σ_{box}, for each grid box between each of these 10 maps was calculated and the summed values of σ_{box} for the whole map, σ_{map}, and the

standard deviations between the average maps for each set of parameters, σ_{para} was used as a comparison of similarity between the different sets of parameters. Table 17 shows σ_{map} and σ_{para}. The difference between the average results derived for the 3 noise factors is smaller than the variation within the 10 re-runs using the same noise level. This indicates that the sensitivity to the choice of the noise level lies within the overall uncertainty of the inversion routine. It was therefore arbitrarily decided that a noise factor of 4 would be used.

Table 17. The average standard deviation (σ_{map}) between 10 maps for each noise level (*NL*) sampled at resolutions 1×1 grid box, 2×2 grid boxes and 4×4 grid boxes and the standard deviation between the average maps, σ_{para}, for each *NL*. The inversion routine alternately allows emissions in all grid boxes in the domain or restricts the emissions to the UK and Ireland (g m^{-3} s^{-1}).

Grid	σ_{para} between *NL*	σ_{map} between 10 runs		
		NL = 3	*NL* = 4	*NL* = 5
1×1	3.16E-08	6.22E-08	7.97E-08	9.96E-08
1×1 UK	4.02E-08	9.7E-08	1.10E-07	1.22E-07
2×2	5.16E-07	1.73E-06	5.24E-07	7.67E-07
2×2 UK	1.04E-07	1.23E-07	1.32E-07	4.24E-07
4×4	1.92E-08	6.29E-08	7.35E-08	7.57E-08
4×4 UK	3.54E-08	7.96E-08	1.08E-07	1.27E-07

6.5.2 Limiting Grid Boxes

The dosage matrix used in the final inversion was restricted to grid boxes which contributed to some minimum number of observations ($\sqrt{N}$). This limited the effects of under-prescribed grid boxes that contribute to only a small number of observations. To determine the sensitivity of the final emission map to the level of restriction, three limiting factors were tested with the model run 10 times for each factor using the same set of test conditions and parameters as with the noise factors. The level of difference between the 10 emissions maps was determined by calculating the standard deviation for each grid box and summing for the whole map. This standard deviation, σ_{map}, between the 10 models runs for each limiting factor was compared to the standard deviation, σ_{para}, between the '10 run average' map for each set of test parameters which included the limiting factor, grid resolution and land and sea or land only condition.

The three limiting factors chosen were no limit on grid boxes (factor 1), limiting to grid boxes that contributed emissions to more than $\sqrt{N}$ observations (factor 2), where N is the number of observations, and limiting to grid boxes that contributed emissions to more than $2\times\sqrt{N}$ observations, (factor 3). Table 2 shows σ_{map} and σ_{para} for each limit factor, resolution and the land and sea condition or land only condition.

The standard deviation for each set of parameters, σ_{para}, between maps produced using the unrestricted condition and the limited conditions is far greater than σ_{para} between maps produced using the two limited conditions. The difference between the 10 maps produced for each set of the same conditions is also far greater when no restriction was applied. This suggests that as long as a limit is imposed, the actual magnitude of this limit is of secondary importance. Limiting factor 2 was chosen to apply to the final inversion runs. This removed the most uncertain grid boxes from the domain while the difference between the average map for factor 2 and the average map for factor 3 is smaller than or similar to the difference between the 10 maps produced for each set of conditions.

Table 18. Standard deviation (□) of maps for an unlimited domain (factor 1), domain limited to boxes that contributed to over $\sqrt{N}$ (factor 2), and $2\times\sqrt{N}$ (factor 3).

Grid	σ_{para} betw factors 1, 2 and 3	σ_{para} between fact 2 and 3	σ_{map} between 10 runs		
			Factor 1	Factor 2	Factor 3
1×1	1.65E-07	6.93E-08	1.74E-06	3.33E-07	1.88E-07
1×1 UK	1.24E-07	1.28E-07	4.72E-07	1.18E-07	1.18E-07
2×2	2.68E-05	2.40E-07	7.46E-04	4.60E-06	1.05E-06
2×2 UK	5.64E-06	1.17E-07	2.35E-04	1.88E-07	9.35E-08
4×4	2.42E-05	6.56E-08	4.38E-04	2.71E-07	5.71E-08
4×4 UK	1.31E-06	1.00E-07	3.77E-05	2.70E-07	1.05E-07

6.5.3 Fitting Function

Several fitting functions were tested using the same conditions as before, with the chosen noise factor and limiting factor applied. The 5 functions tested are summarised in Table 3.

Table 19. Fitting functions used in inversion where *x* and *y* are the model and observed concentration enhancements respectively. *N* is the total number of observations, *X*2 is the total number of model values within a factor of 2 of the observations and *Y* is the total number of observations above the noise value.

Function	
F_1 correlation coefficient type method	$1.0-\frac{\sum(x-\bar{x})(y-\bar{y})}{\sqrt{\sum(x-\bar{x})^2\sum(y-\bar{y})^2}}$
F_2-least squares type method	$\frac{\sum(x-y)^2}{N}$
F_3	$9F_3+\frac{F_2}{xy}$
F_4	$10F_3+\frac{F_2}{xy}+4(1.0-\frac{X_2}{Y})$
F_5	$10F_3+2\frac{F_2}{xy}+4(1.0-\frac{X_2}{Y})$

The standard deviations, σ_{map}, between the 10 maps for each function are shown in Table 20. Function 1 leads to an extremely large standard deviation for the 4×4 resolution map and so was immediately discounted as the possible fitting function. The standard deviation, σ_{map}, of the 2×2 resolution maps of functions 2 and 3 were almost an order of magnitude larger than the functions 4 and 5 and so the choice was between functions 4 and 5. The standard deviation, σ_{map}, between the 10 runs at each resolution is very similar for both functions and σ_{para} between the 2 functions is smaller than the standard deviation between the 10 runs for each. The standard deviation, σ_{map}, of function 4 tends to be slightly smaller than function 5 and so function 4 was chosen as the fitting function for the final inversion. However function 5 would probably have been just as effective.

Table 20. Standard deviations (σmap) of 10 maps for 5 functions resolutions 1×1, 2×2 and 4×4 grid boxes. The inversion routine alternately allows emissions in any grid box in domain or restricts emissions to UK and Ireland (UK).

Grid	σ_{map} between 10 runs				
	F_1	F_2	F_3	F_4	F_5
1×1	5.60E-08	5.65E-08	4.26E-08	7.97E-08	7.04E-08
1×1 UK	4.92E-08	1.06E-07	8.85E-08	1.10E-07	1.21E-07
2×2	1.93E-02	9.32E-07	2.04E-06	5.24E-07	5.22E-07
2×2 UK	3.29E-04	3.35E-06	1.40E-06	1.32E-07	2.03E-07
4×4	1.51E+19	6.83E-08	4.05E-07	7.35E-08	7.26E-08
4×4 UK	5.04E+18	1.50E-07	1.83E-07	1.08E-07	1.33E-07

Table 21. σpara between functions 2,3,4,5 and σpara between functions 4 and 5 at resolutions 1×1, 2×2 and 4×4 grid boxes. The inversion routine alternately allows emissions in any grid box in domain or restricts emissions to UK and Ireland (UK).

Grid	σ_{para} between functions	
	F_2,F_3,F_4,F_5	F_4,F_5
1×1	3.61E-08	3.61E-08
1×1 UK	9.15E-08	4.55E-08
2×2	4.82E-07	1.99E-07
2×2 UK	7.60E-07	5.86E-08
4×4	1.08E-07	2.17E-08
4×4 UK	1.03E-07	3.54E-08

Function 4 takes into account the correlation between the two series, the difference between the absolute values of the two series and the number of extreme outlier points in the model series.

There are no published sensitivity studies for the parameters values used in the inversion methodology. The parameter values developed in the study are similar to those used in other inversion studies (Manning, Personal Communication).

6.6 Results for Each Flight

For each flight and chemical species the emission maps were produced for each of the three spatial resolutions with lower resolution producing greater skill in the maps. However this also produces a loss of detail and a tendency to produce larger values for the total UK emissions. The emissions are allowed either across the whole domain or restricted to the UK and Ireland and a small band of surrounding sea. Restricting the emissions to the UK and Ireland is a less reliable approach as this will tend to

increase total UK emissions. With the restricted approach, emissions which may have genuinely originated over the sea, such as shipping, are forced into the UK. Emissions may also have originated outside the prescribed domain resulting in varying background air concentration and uncertainties in the enhanced observation. Where this happens, the unrestricted approach will tend to allocate elevated emissions to the edge of the domain when the background air is above the chosen baseline value and depress emissions when the background air is below the baseline. This minimises the impact of the uncertainties on the UK emissions map and such grid boxes can generally be discounted as a product of the uncertainty in the data. However when the domain is restricted, the inversion is forced to reconcile any uncertainties in the data within the map of the UK and Ireland. The resulting UK emissions will therefore have greater uncertainty, particularly around the edge of the domain. An extreme example of this is shown in Figure 101 which compares the unrestricted and restricted CO emissions map for flight B130[1]. On this day, there was circulating air in the south east bringing inflow from Northern France. The unrestricted domain assigns the bulk of these emissions to Northern France and the eastern edge of the domain. However the restricted inversion assigns the emissions to Northern Scotland, the area which contributes least to the overall dosage map of this flight, resulting in far larger emissions in the UK. An alternative approach may be to use a hybrid map with emissions restricted to the UK and Ireland and a band around the edge of the domain.

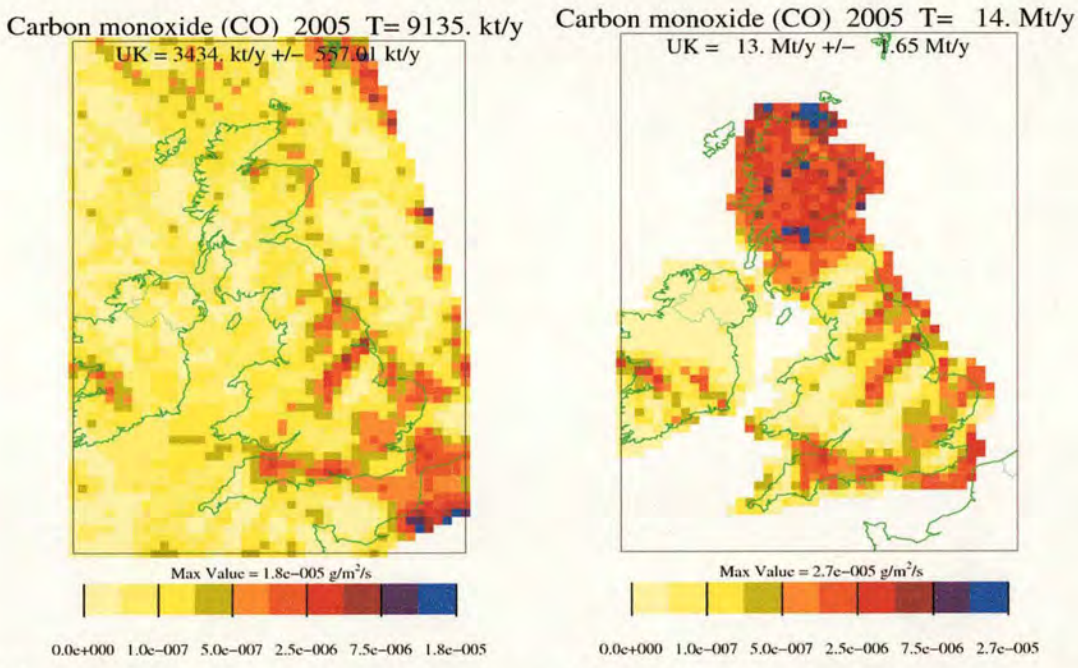

(a) (b)

Figure 101. (a) CO emissions for flight B130 at 1x1 resolution in an unrestricted domain. (b) CO emissions for flight B130 at 1x1 resolution in domain restricted to the UK and Ireland.

The final maps for each flight are an average of three inversion runs. By comparing the results for each run we can get an estimate of the uncertainty in the maps due to measurement, background and dispersion errors and the uncertainty due to the inversion itself. To test the robustness of each map, the inversion was repeated using only 90% of the observations that were randomly sampled. This reveals any areas where the inversion may depend on only a few observations. Figure 102 shows emissions produce for flight B130 using only 90 % of the observations. In virtually all flights the difference between the three runs is greater than the difference between the average maps using all observations and using 90% of the observations. In order to check which areas of the map contain the most skill, the standard deviation for each grid square has[1] been plotted alongside the emissions map and the total gives the overall difference in the UK budget for the three plots.

[1] NB contours are the same for all maps of the same species with the exception that the highest value is set to the highest value of each map.

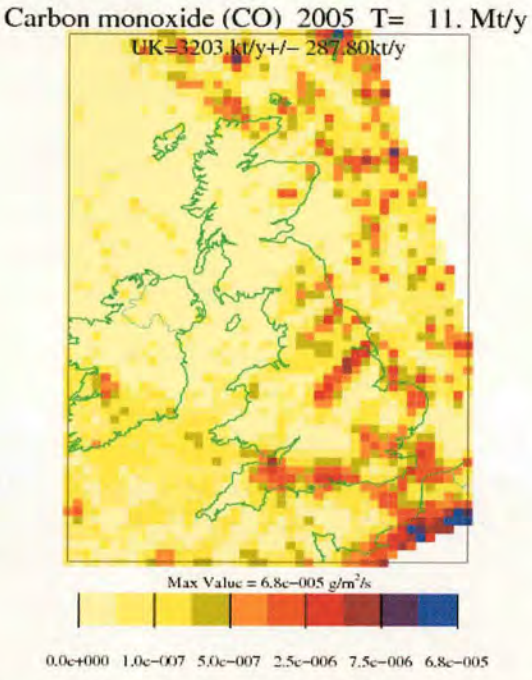

Figure 102. CO emissions for flight B130 at 1x1 resolution in an unrestricted domain using only 90 %of the observations.

The total budget for the UK is calculated by summing the emission in the grid boxes in the UK and for two squares around the UK map. This takes into account uncertainties in allocating the emissions and is also consistent with coastal shipping being counted as part of the national emission inventories. The standard deviation of the total budget is the standard deviation of the totals for the three maps.

Two approaches were taken to estimate the average emission for the whole year. Firstly, an average was taken of the maps produced for individual flights. This approach had the advantage that flights could be weighted to take account of the level of uncertainty in the measurements and the background concentration using the relative error in the measurements and background estimates. However the disadvantage of this approach is that there are fewer observations to constrain the inversion producing greater uncertainty in each of the individual emission maps.

Secondly, the observations for all flights were combined into a single data set taking account of the varying background between flights. The backruns of each of the individual samples from all flights were then combined into a single matrix and the inversion performed on the combined data set. This approach is much more tightly constrained than using the individual flights. The disadvantages of this approach are

that all flights are given the same weighting and uncertainties will be introduced when individual flights conflict. Due to the limited number of flights (14 at most), conflicts between individual days (e.g. a day of large emissions in one location and small emissions in another versus a second day showing the opposite) adds considerable conflict to the overall dataset. Rather than giving an average value for the two days, the inversion may find that the best solution is to put large emissions somewhere that it has less knowledge of and therefore has less affect on the skill of the map.

6.6.1 CO

The plots for CO for each flight are shown in Appendix 1. Figure 103 (a) shows the emissions derived by the inversion with all observations combined. Flights B111, B130 and B247 are not used in producing this average as these days do not have the ideal meteorology, with inflow from continental Europe. The weighted average of the solutions of all individual flights is shown in Figure 103 (c). Again, flights B111, B130 and B247 have been excluded. The figures shown below are for the highest 1×1 resolution; lower resolution plots are included in Appendix 6. For comparison, Figure 104 shows the NAEI emissions (Baggott *et al.*, 2005).

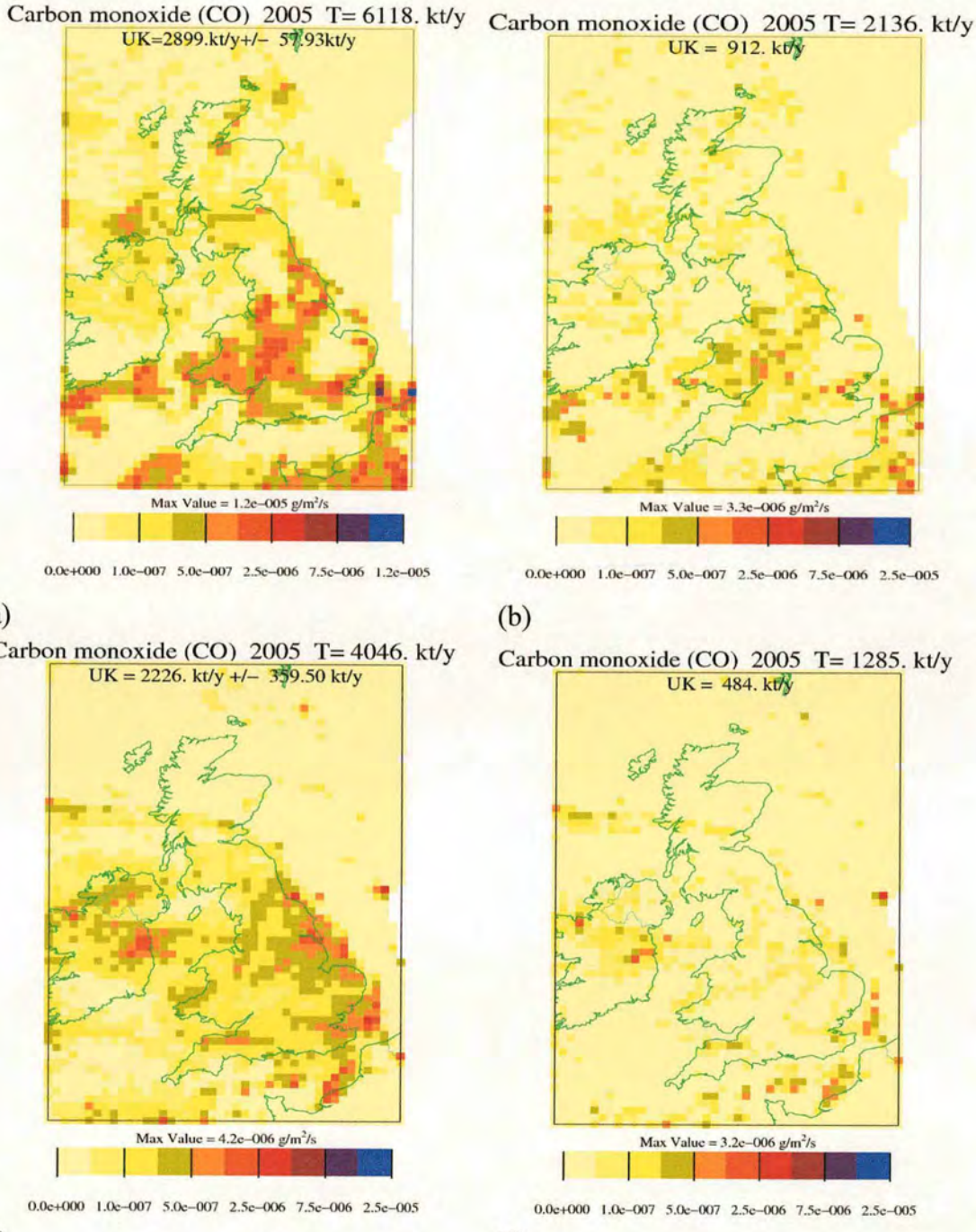

Figure 103. Average results for CO for all flights excluding B111, B130 and B247, at resolution 1×1 grid boxes. (a) Average CO emissions (g m^{-2} s^{-1}) of 3 inversion solutions using combined observations of all flights. T = total for whole domain, UK = total for UK ± standard deviation for total UK emissions from 3 inversion solutions. (b) Standard deviation for CO for 3 inversions solutions using combined observations of all flights. T = total standard deviation of all grid boxes in domain, UK = total standard deviation of all grid boxes in UK. (c) Emissions from weighted average technique. (d) Standard deviation for CO from weighted average technique.

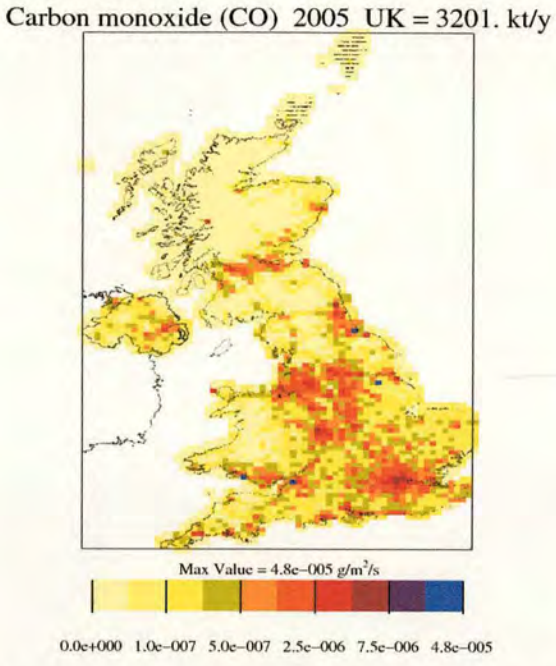

Figure 104. NAEI CO emissions at 10km resolution for 2004.

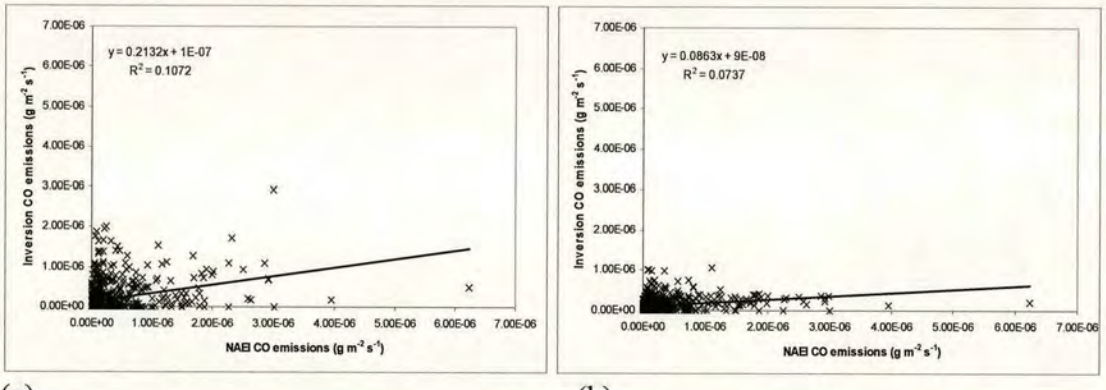

(a) (b)

Figure 105. (a) CO emissions for combined observations inversion technique v NAEI emissions (g m^{-2} s^{-1}) for resolution of 1×1 grid boxes and unrestricted domain (R2 = 0.33). (b) CO emissions from weighted average inversion technique v NAEI emissions (g m^{-2} s^{-1}) for resolution of 1×1 grid boxes and unrestricted domain. R=0.27. Re-scaled the estimated emissions onto the same grid as the NAEI emissions.

Comparison of Figure 103 (a) and (c) reveals that both approaches managed to limit emissions primarily to the UK and Ireland as expected and both produce realistic estimates for total UK emissions. However the spatial correlation between the emissions produced by the two methods and the NAEI emissions, (Figure 105 (a) and (b) for the combined observations and weighted average techniques respectively),

show that the combined observation technique produces emissions closer to the NAEI map than the weighted average approach. The correlation coefficients for the two approaches are 0.33 for the combined observation technique and 0.27 for the weighted average technique. Neither is particularly high partly due to a small number of outliers affecting the fit and partly because the inverse technique, while assigning emissions to broadly the same areas as the current inventory, does not necessarily assign emissions to exactly the same grid box as in the current inventory. By increasing the size of the grid boxes, the fit can be improved with correlation coefficients of 0.45 for the combined observation and 0.52 for the weighted average maps for the 4 × 4 maps and the NAEI emissions. However this will result in a loss of detail in the maps. The R^2 for the lower resolution maps and the NAEI map are shown in Table 22, showing the R^2 increasing with decreasing resolution.

Table 22 R^2 for each domain and resolution for weighted average and combined observations techniques.

	R^2 Combine observations	R^2 Weighted average
1×1	0.107	0.074
1×1 UK	0.063	0.072
2×2	0.135	0.168
2×2 UK	0.129	0.149
4×4	0.205	0.266
4×4 UK	0.279	0.239

The weighted average technique tends to produce larger emissions along the east coast. While it manages to attribute emissions broadly to the expected source areas around London and in the industrial areas along the east coast, it fails to reproduce the emissions in the north-west of England. It seems in general that emissions are pulled slightly to the east of where they might be expected, particularly in London where the emissions are concentrated just off the coast and in the Thames estuary. This is expected since the observations are concentrated along the east coast and emissions from sources along this area will have a proportionally higher impact on the observations than emissions from sources further away. This can result in these nearby sources effectively 'hiding' the signal of distant sources such as the emissions from the north-west of England.

The combined observations technique produces an emissions map which seems to reproduce the emissions from London, the north west of England and the Midlands accurately. By combining the flights, the problem of local sources masking the signal of distant sources seems to be largely overcome. Combining the data for varied wind direction and flight paths seems to counteract this effect. However, this approach continues to suggest emissions in Wales which are much larger than might be expected. This could be due to conflicts between flights with the result that the inversion is putting the emissions into an area it has less knowledge about. The nature of the inversion is that grid boxes further from the observations have increasingly less effect on the fit so they can be assigned much larger values without impacting the fit to any great extent. This can result in greater emissions than expected in the grid squares furthest from the observations. This problem is particularly pronounced for these AMPEP flights which tended to be conducted in similar conditions, under connected westerly flow, to improve the applicability of the budget technique to derive country budgets (Section 1.4.2). By contrast, for the inversion approach a range of conditions and trajectories would have been preferable.

Overall, the technique of combining the observations produces a closer fit to the NAEI emissions. From earlier work (Chapter 5) the NAEI CO inventory is expected to be accurate. That the inversion technique is able to reproduce it reasonably well provides further confirmation of the inventory's accuracy and shows that this technique is a viable means of producing a spatially disaggregated emissions inventory. The total budget for the UK estimated by this technique is 2900 kt yr^{-1} and is close to the current NAEI estimate of 2400 kt yr^{-1}, although it should be noted that the flights were conducted during the summer season (April to September), where average emissions should lie below the annual average due to lower energy consumption during the warmer summer months.

6.6.2 CO_2

For CO_2, the inversion technique was tried both with and without a sink term to represent a net uptake from photosynthesis and emissions from respiration by vegetation. For this purpose the inversion routine was adapted to allow grid boxes to

take on negative emission values, which represent a net sink. Figure 106 (a) shows the CO_2 emissions predicted using the combined observation approach and an unlimited domain with the sink term switched on. Figure 106 (b) shows the CO_2 emissions with the sink term switched off. For the UK, both produce a similar emissions pattern with large emissions from London, the Midlands, the North West of England and Humberside. This broadly matches the NAEI emissions shown in Figure 108. The correlation coefficient for the sink switched on and NAEI emissions is 0.12, very close to the value produced with the sink switched off (0.13). This lower correlation, compared with CO, is not entirely surprising because the NAEI only compiles the anthropogenic emissions without information on the terrestrial source / sink term.

Although both approaches produce similar estimates for the total emissions from the UK, the inversion with the sink produces far larger emissions overall. This is partly due to a slight di-poling effect in areas of the map where low emissions may be expected such as the seas around Scotland. The map with no sink is broadly consistent with this picture with emissions at almost zero except for some areas at the very edge of the domain. With the sink term switch on however, the solution contains grid boxes with net emissions next to grid boxes with net uptake. Although, these will average out to give an emission of approximately zero as seen by the observations, they add up to produce a much larger emission estimate for the total budget for the domain. In addition, the maximum emissions when the sink is allowed are over 100 times larger than the maximum emissions produced by using no sink. These large emissions are almost all from grid boxes in areas around the edge of the domain which are very uncertain due to reasons previously discussed and contribute to the much larger total emissions for the whole domain. Additionally this method does not allow the possibility for sources and sinks to be co-located within a single grid square. An alternative but more complicated method would be to model the loss process in the NAME back runs directly; however this in itself would lead to increased uncertainty.

In addition, both methods produce significantly larger emissions for Ireland than would be expected. These emissions may be partly explained by enhanced concentrations in the upwind sections of some flights during the transits over land to the Bristol Channel and over the West Country. The enhanced concentrations are

likely due to respiration from grassland from the previous evening which the inversion assigns to Ireland. As the grid boxes in Ireland tend to be further from the bulk of the observations, their influence on the overall statistical score of the map is small compared to the grid boxes in the UK and so these larger emissions are not corrected for.

The total CO_2 sink over the UK is in fact relatively small compared to the total budget as we would expect. Because of the similarity of the two maps for the UK, it is preferable to use the map with the sink as it is more realistic to represent photosynthesis in the inversion. Although allowing a sink produces a di-poling effect, this tends to be restricted to areas outside the UK and so can be ignored for the purposes of this study. Figure 107[2] shows the uncertainty associated with each grid square for the inversion with the sink included.

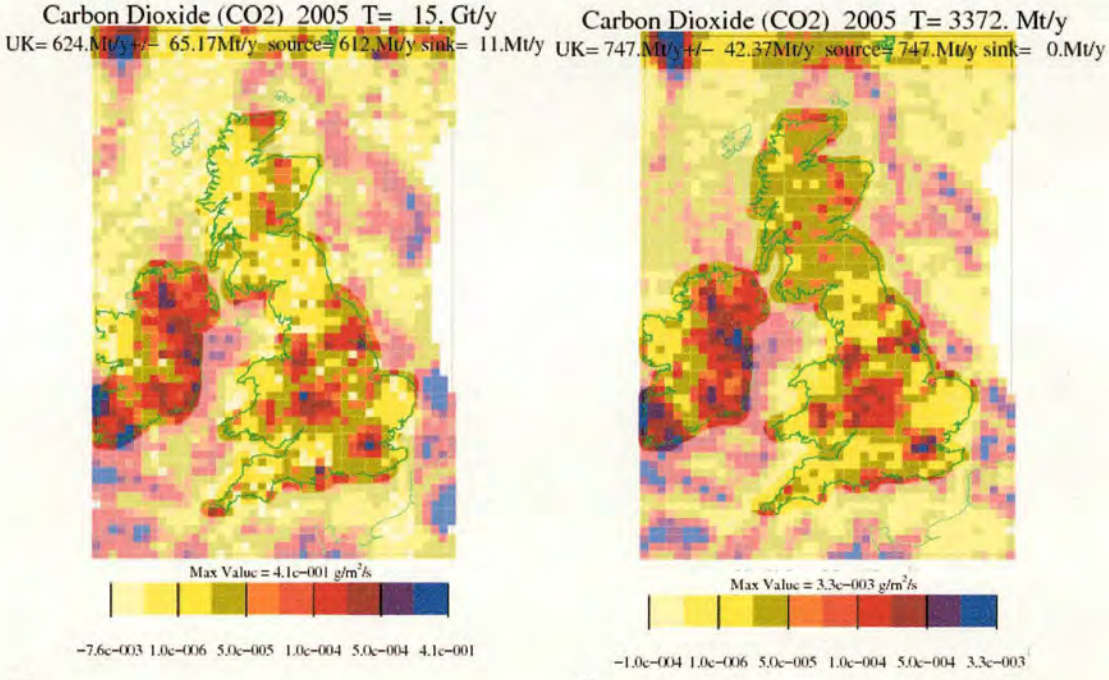

Figure 106. Average results for CO_2 for all flights excluding B111, B130 and B247, at resolution 1×1 grid boxes. (a) Average CO_2 emissions (g m^{-2} s^{-1}) of 3 inversion solutions using combined observations for inversion with sink. T = total for whole domain, UK = total for UK ± standard deviation for total UK emissions from 3 inversion solutions. (b) Average CO_2 emissions of 3 inversion solutions using combined observations for inversion with no sink.[2]

[2] NB the contours are the same scale on all maps, however where the minimum / maximum flux is below / above the min / max of the scale, they are reset to these values in order to show the minimum and maximum fluxes.

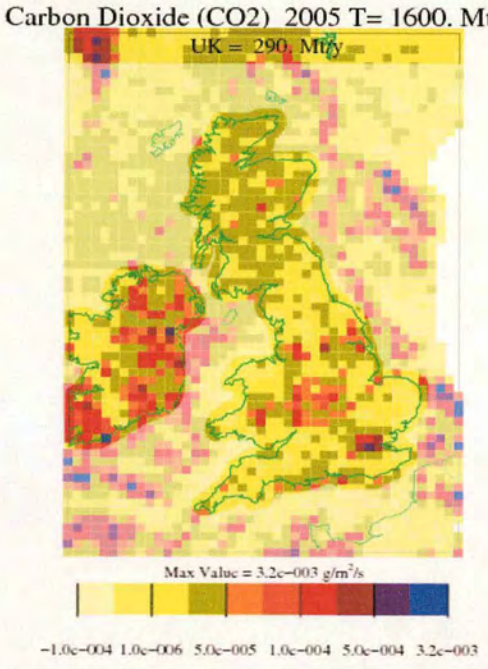

Figure 107. Standard deviation of 3 CO_2 inversion solutions (g m^{-2} s^{-1}) for combined observation with sink term switched on. UK = total standard deviation of all grid squares. T = total standard deviation of all grid boxes boxes in domain, UK = total standard deviation of all grid boxes in UK.

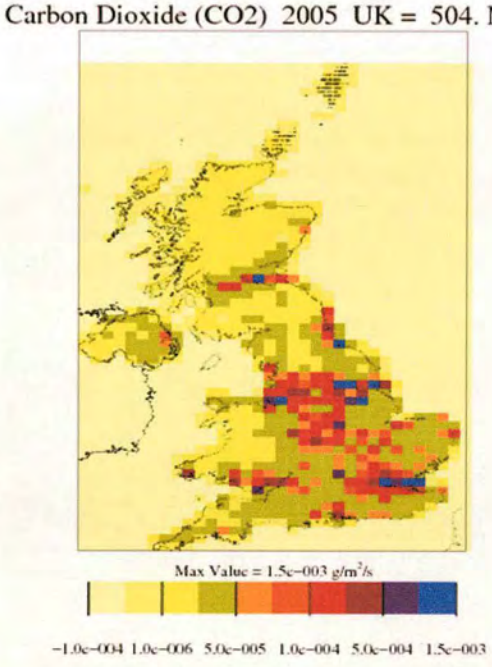

Figure 108.CO_2 emissions (g m^{-2} s^{-1}) from the NAEI from 2004.

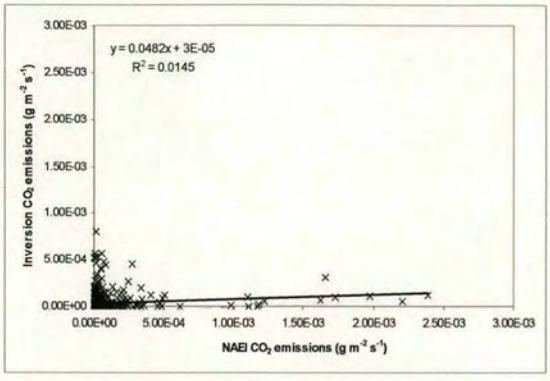

Figure 109. CO_2 emissions for combined observation inversion with unrestricted domain and sink against the NAEI emissions (g m^{-2} s^{-1}). R=0.12.

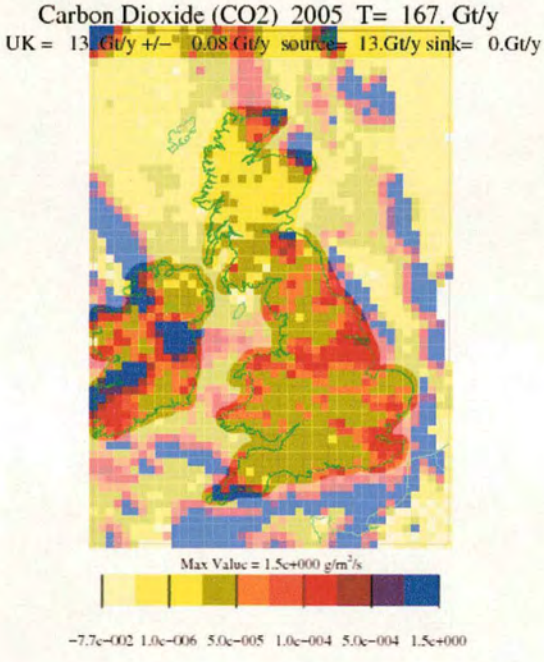

Figure 110. CO_2 emissions (g m^{-2} s^{-1}) using weighted average approach with unrestricted domain and sink term switched on. T = total for whole domain, UK = total for UK ± standard deviation for total UK emissions.

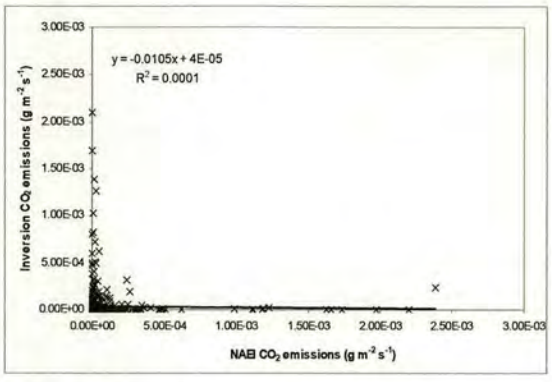

Figure 111. CO_2 emissions from weighted average technique with sink against NAEI emissions (g m^{-2} s^{-1}). R=-0.01

Figure 110 shows the emissions from the weighted average technique and Figure 111 shows these emissions against the NAEI emissions. The emissions predicted by this technique are very large and the correlation coefficient with the NAEI emissions negative. Including the sink term produces very large emissions around the edge of the domain from the individual flights as previously discussed. This results in large emissions around the UK, particularly around the East and South coasts, from flights where this effectively represents the edge of the domain due to the dosage maps. The combined observation map is therefore the one that should be used as the final estimate of the CO_2 emissions. The 2×2 and 4×4 grid box resolution maps can be found in Appendix 6. The correlation coefficients of the lower resolution maps with the NAEI emissions are higher than the 1×1 resolution map but lack the detail of the 1×1 grid box map as the variations between grid boxes are smoothed out.

Overall, the inversion technique seems able to assign the CO_2 emissions to broadly the same areas as in the current inventory although the correlation between the two is small. As with CO, this is partly due to a small number of outliers affecting the fit. CO_2 also seems to be more affected by inflow from Europe than CO. The total budget predicted by the inversion technique (including the terrestrial sink) for CO_2 is 620 Mt yr^{-1} with 610 Mt yr^{-1} from anthropogenic emissions and a biogenic sink of 10 Mt yr^{-1}, very similar to the current NAEI estimate of 555 Mt yr^{-1} with a biogenic sink of 28 Mt yr^{-1} (Milne *et al.*, 2006).

6.6.3 CH_4

For CH_4, the measurements for several of the flights were not of sufficient quality to produce reliable maps. For the final maps only flights B92, B97, B113, B132, B134, B136 and B244 were used. The maps shown here are for a resolution of 1×1 grid boxes, lower resolution maps are included in Appendix 6. Appendix 3 shows the maps for the individual flights for CH_4

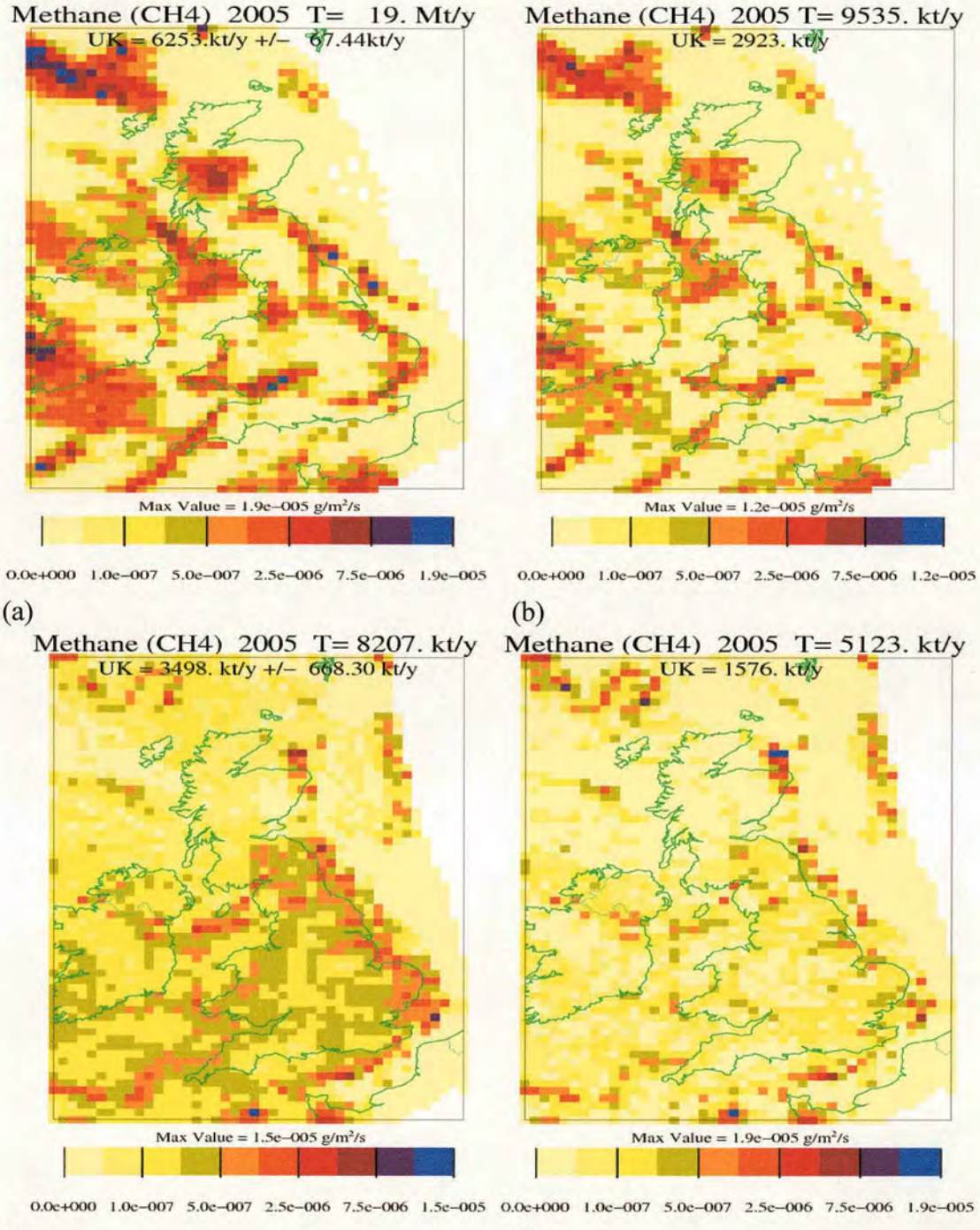

Figure 112. Average results for CH_4 using resolution of 1×1 grid boxes and unrestricted domain. (a) Average CH_4 emissions (g m^{-2} s^{-1}) of 3 inversion solutions from combined observation inversion. T = total for whole domain, UK = total for UK ± standard deviation for total UK emissions from 3 inversion solutions. (b) Standard deviation of CH_4 emissions for combined observations. T = total standard deviation of all grid boxes boxes in domain, UK = total standard deviation of all grid boxes in UK. (c) CH_4 emissions using weighted average approach. (d) Standard deviation of CH_4 emissions for weighted average technique.

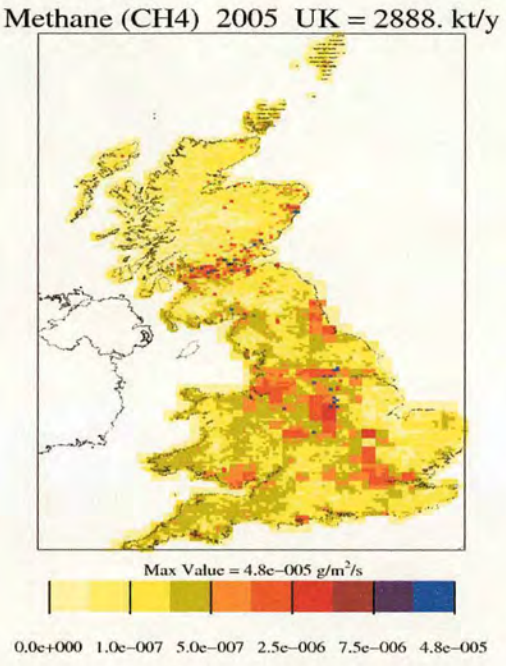

Figure 113. CEH-Edinburgh emissions (g m^{-2} s^{-1}) for CH_4 for 1994.

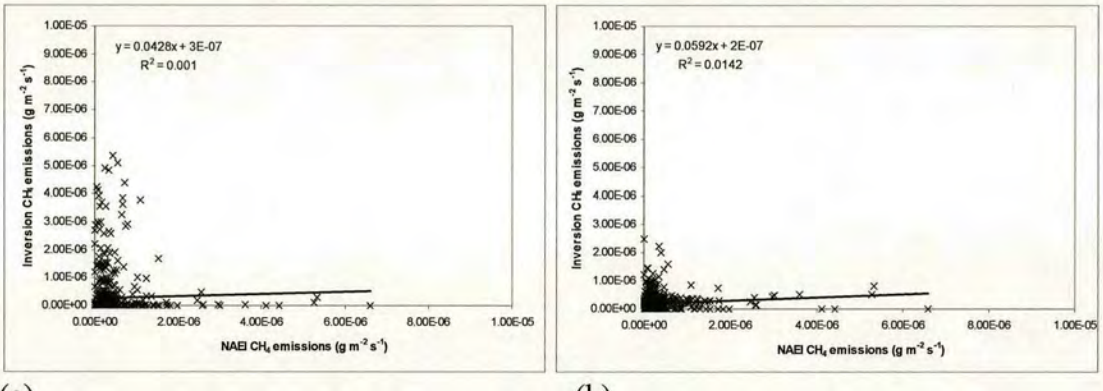

(a) (b)

Figure 114. (a) CH4 emissions for combined observations inversion technique v NAEI emissions (g m^{-2} s^{-1}) for resolution of 1×1 grid boxes and unrestricted domain. R = 0.03. (b) CH4 emissions for weight average inversion technique v NAEI emissions (g m^{-2} s^{-1}) for resolution of 1×1 grid boxes and unrestricted domain. R = 0.12.

The CH_4 maps are not as reliable as the CO and CO_2 maps as fewer days were used to produce the annual average. Also the quality of the measurements was in general poorer. However, as shown in Figure 112 (c) the inversion technique does manage to assign the bulk of the emissions to the UK and Ireland as expected for the weighted average approach. Unlike for CO and CO_2, for CH_4 the combined observations approach is less successful at assigning the emissions to the UK and tends to produce

far larger emissions to the western edge of the domain as shown in Figure 112 (a). The reason for this is likely to be the greatly varying quality of the observations. As all observations are given the same weighting in this approach, days with poorer quality measurements may conflict with the days with better quality data. These days, specifically B92, B113 and B136 (cf. associated Figures in Appendix 3) tend to overestimate the emissions. The inversion method, unable to accommodate these larger emissions within the areas of where it has the most information, will tend to put them in the areas of which it has less knowledge and which have a smaller effect on the statistical score of the map, i.e. to the far west of the domain. For this reason it seems that in this case, the weighted average approach gives a better estimate of the emissions. The weighed average technique tends to assign larger emissions to the east coast for reasons previously discussed for CO. Therefore the spatial disaggregation of the map is not as reliable as that produced by the combined observation approach. However the total UK emissions produced by this approach should be a fair representation of the emissions required to produce the observed outflow concentrations, and by allowing individual flights to be weighted, the weighted average technique should produce a good estimate for the total UK emissions. Figure 114 (a) and (b) show that for both techniques there is no correlation between the emissions derived by the inversion and the NAEI emissions with a correlation coefficient of 0.03 for the combined observation technique, compared with correlation coefficient of 0.12 for the weighted average technique. The uncertainty associated with each grid box is also much lower for the weighed average map than the combined observation map (Figure 112 (b) and (d)).

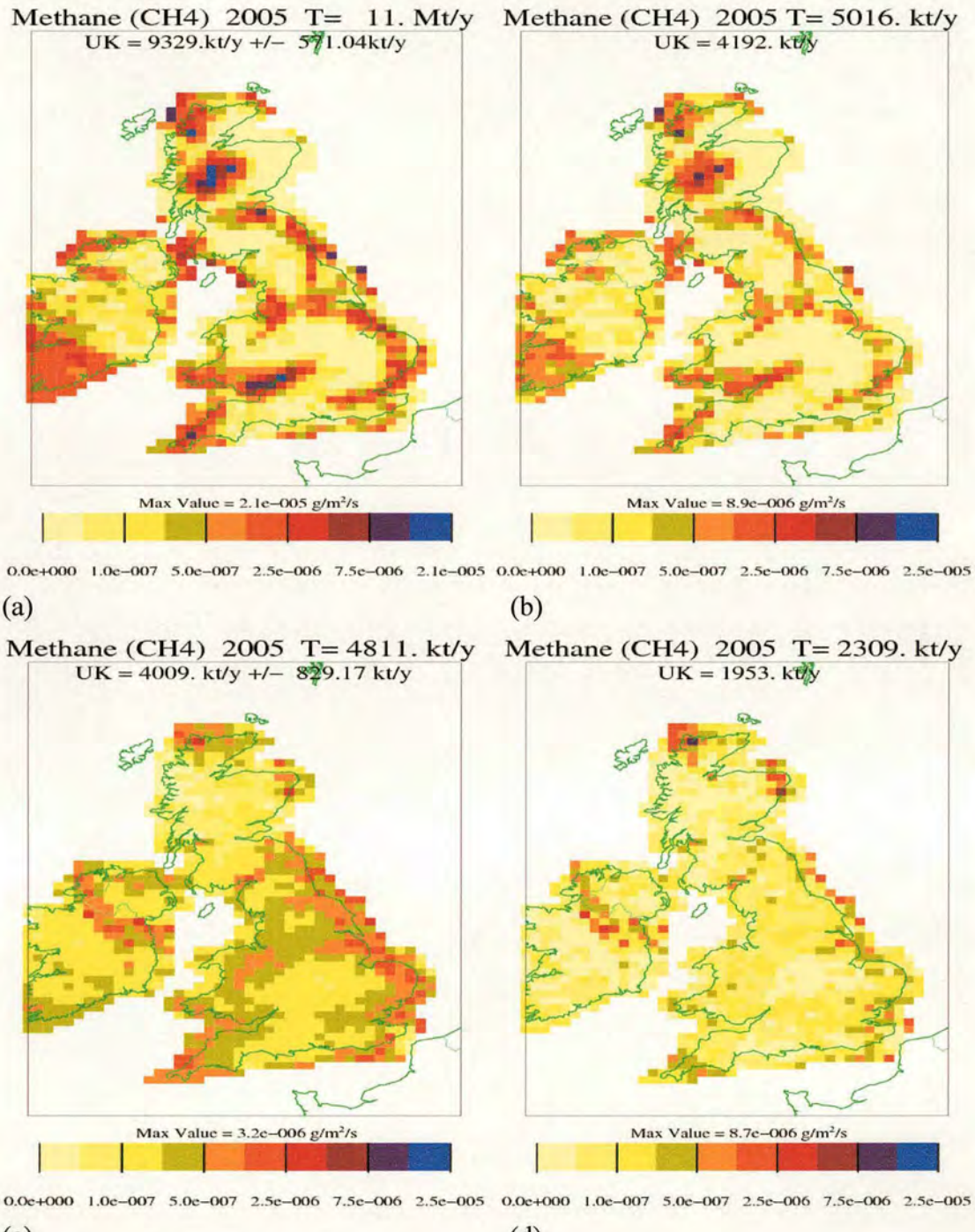

Figure 115. Average results for CH_4 for resolution of 1×1 grid boxes and restricted domain (a) Average CH_4 emissions (g m^{-2} s^{-1}) of 3 inversion solutions from combined observation inversion technique. T = total for whole domain, UK = total for UK ± standard deviation for total UK emissions from 3 inversion solutions. (b) Standard deviation of CH_4 emissions for combined observations. T = total standard deviation of all grid boxes in domain, UK = total standard deviation of all grid boxes in UK. (c) CH_4 emissions for weighted average technique. (d) Standard deviation of CH_4 emissions for weighted average technique.

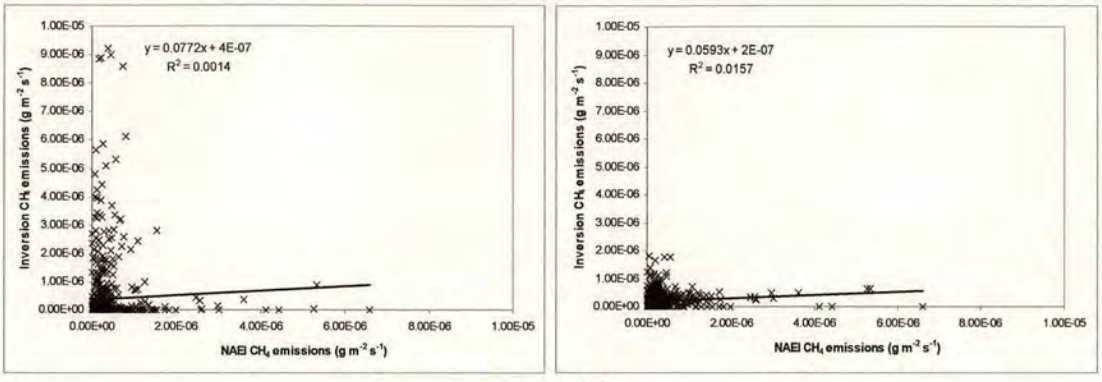

(a) (b)

Figure 116. (a) CH4 emissions for combined observations inversion technique v NAEI emissions (g m^{-2} s^{-1}) for resolution of 1×1 grid boxes and restricted domain. Correlation coefficient = 0.04. (b) CH4 emissions for weighted average technique against NAEI emissions (g m^{-2} s^{-1}) for resolution of 1×1 grid boxes and unrestricted domain. R=0.13.

Alternatively, the emissions can be forced to originate from the UK and Ireland only. This approach, however, has the disadvantage of tending to increase the total UK emissions. Emissions are forced into the restricted domain which otherwise may have originated from outside of the domain or are products of uncertainties in the observation data. This can be seen in the increase in the uncertainty in the map, particularly around the edges of the restricted domain, by comparing the uncertainty in the unrestricted map (Figure 112 (d)), to the uncertainty in the restricted map (Figure 115 (d)). The total uncertainty in the grid boxes within the UK in the restricted domain is around 2000 kt yr^{-1} compared with only 1600 kt yr^{-1} for the unrestricted domain. However, the correlation coefficients for the restricted maps of 0.04 (Figure 116 (a)) and 0.13 (Figure 116 (b)) for the combined observation and weighted average techniques, respectively, are slightly higher than for the unrestricted maps. This suggests that overall, restricting the domain gives a better estimate of the emissions. The best emission map to compare with the NAEI emissions comes from the weighted average technique using a domain restricted to the UK and Ireland and indeed the correlation coefficient of this map and NAEI emissions is the largest of all the maps.

Overall the CH_4 emissions as predicted by the inversion are about twice the current inventory values. However by restricting the domain for CH_4, the total emissions for the UK will be larger due to the uncertainties around the edges as has already been

discussed. The inversion estimate for the UK budget for CH_4 is around 4000 kt yr^{-1} for the restricted domain but 3500 kt yr^{-1} for the unrestricted domain, so restricting the domain increased the emissions by 500 kt yr^{-1} which is within the uncertainty of the emissions of both estimates. The emissions predicted by both methods are still significantly larger than the NAEI estimate.

While the combined observation technique does not produce a reliable estimate for the scale of the emissions, it can give an indication of the spatial disaggregation of emissions from which areas of the country tend to produce the largest emissions. The map produced by the weighted average technique may also give some indication of the spatial disaggregation. For both methods, the bulk of the increase in emissions is down the east coast and much of this may be due to local emissions masking the signal of emissions further to the west as discussed for CO above. In the case of the combined observation approach, large emissions from remote areas such as the north Scottish coast may be due to uncertainties in the data or conflicts between individual flights which inversion solves by assigning emissions to the area of the domain which has the least affect on the statistical score of the map. It is therefore difficult to pinpoint exactly which source sectors may be underestimated in the current emission inventory. If we assume that the larger emissions in the east are partly real, then the sources responsible are likely to be urban, mostly likely landfill or leakages from the gas supply network. In the north-east, emissions from abandoned coal mines are also a possible source of the extra emissions. Larger emissions than expected were derived for Wales and the South West. These are mainly rural, agricultural areas and so it is possible that these emissions are from livestock with the current inventory underestimating emissions from this source. The large emissions around the tip of Cornwall will be partly due to uncertainty associated with the edge of the domain.

Due to the small number of flights with high quality data, the emission map produced for CH_4 is not as reliable a prediction of the spatial disaggregation as the CO map, and thus it is not easy to draw conclusions about which source sectors are responsible for the larger than predicted emissions. However, although the distribution of the emissions may not be accurate, the total emissions should be a reliable estimate of the total UK budget which at around 3500 kt yr^{-1} is around 45 % larger than the current NAEI estimate, further corroborating the findings of the other techniques (Chapter 5).

6.6.4 N_2O

As with CH_4, the N_2O measurements for several of the flights were not good enough to produce reliable maps. The final maps were produced using flights B92, B102, B118, B119, B134, B136 and B244. The maps shown here are all for 1×1 grid box resolution, lower resolution maps are included on Appendix 6. Appendix 4 shows the maps for the individual flights for N_2O.

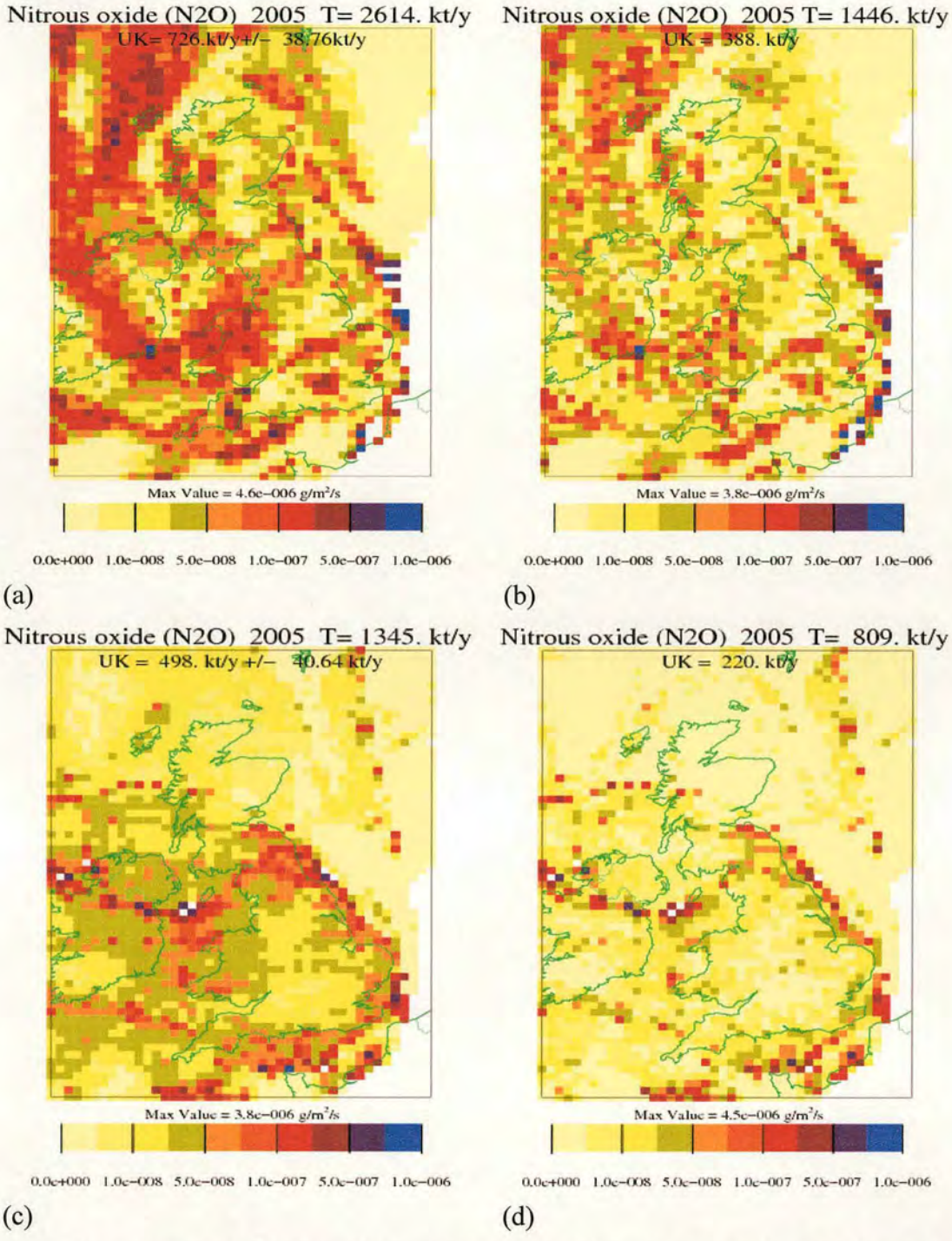

Figure 117. Average N_2O results for resolution of 1×1 grid boxes and unrestricted domain. (a) Average N_2O emissions (g m^{-2} s^{-1}) of 3 inversion solutions for combined observation inversion technique. T = total for whole domain, UK = total for UK ± standard deviation for total UK emissions from 3 inversion solutions. (b) Standard deviation of N_2O emissions for combined observation technique. T = total standard deviation of all grid boxes in domain, UK = total standard deviation of all grid boxes in UK. (c) N_2O emissions from weighted average technique. (d) Standard deviation of N_2O emissions from weighted average technique.

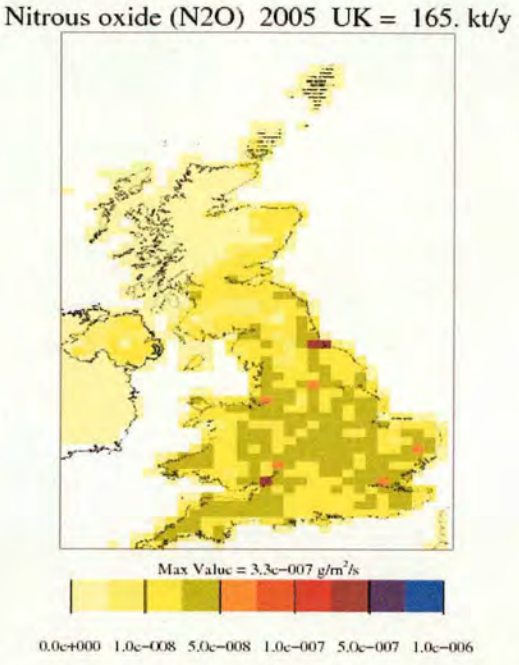

Figure 118. NAEI emissions (g m^{-2} s^{-1}). for N_2O.

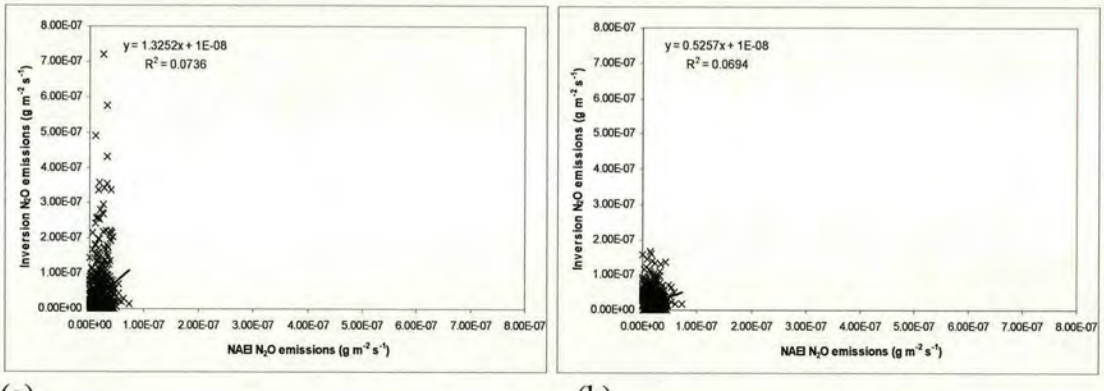

(a) (b)

Figure 119. (a) N2O emissions for combined observations inversion technique v NAEI emissions (g m^{-2} s^{-1}) for resolution of 1×1 grid boxes and unrestricted domain. R = 0.27. (b) N2O emissions for weighted average technique v NAEI emissions (g m^{-2} s^{-1}) for resolution of 1×1 grid boxes and unrestricted domain R=0.26.

Fewer days were used to produce the annual average and the resulting maps are not as good as CO and CO_2. As with CH_4, the quality of the data was in general poorer and N_2O is naturally more variable from day to day than say, CO. However, the inversion technique does manage to assign the bulk of the emissions to the UK and Ireland as expected for the weighted average approach as shown in Figure 117 (c). The combined observations approach is less successful at assigning the emissions to

the UK and, like CH_4, tends to produce far larger emissions at the western edge of the domain, (Figure 117 (c)). The reason for this is likely to be the greatly varying quality of the observations between flights and the variability of N_2O emissions from day to day as can be seen from the maps from individual flights in Appendix 4. As with CH_4, when there are conflicts between the information from individual flights, the inversion technique tends to assign emissions to areas of which it has the least knowledge and which therefore have least affect on the statistical score. Giving all flights equal weighting will also tend to result in overestimation of the emissions. The larger the uncertainty in the measurements, then the larger the variation between measurements and therefore the larger the emissions. The weighted average approach gives a better estimate of the total UK emissions as the variation in the data quality between flights is such that, without the weighting the total emissions will be overestimated. Figure 119 (a) shows the combined flights emissions against the NAEI emissions with a correlation coefficient of 0.27. Figure 119 (b) shows the weighted average emissions against the NAEI emissions with a correlation coefficient of 0.26. The correlation coefficients are very similar, though neither is very high. The uncertainty in each grid box is far less in the weighted average technique (Figure 117 (b)) compared with the combined observation technique (Figure 117 (d)). Therefore using the weighted average approach seems a more reliable method of calculating the emissions for N_2O in the absence of more reliable data.

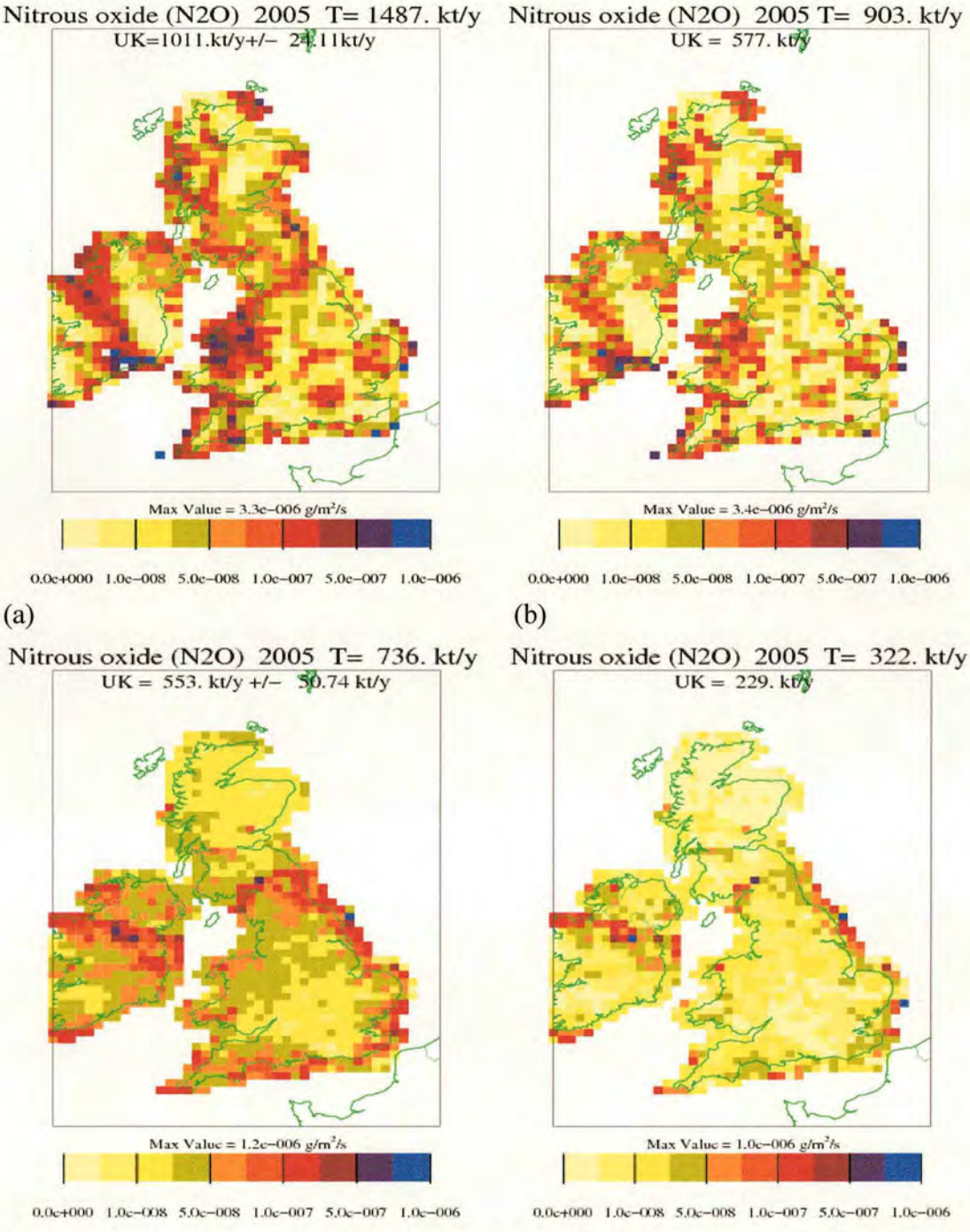

Figure 120. Average N_2O results for resolution of 1×1 grid boxes and restricted domain. (a) Average N_2O emissions (g m^{-2} s^{-1}) of 3 inversion solutions for combined observation inversion technique. T = total for whole domain, UK = total for UK ± standard deviation for total UK emissions from 3 inversion solutions. (b) Standard deviation of N_2O emissions for combined observation technique. T = total standard deviation of all grid boxes in domain, UK = total standard deviation of all grid boxes in UK. (c) N_2O emissions from weighted average technique. (d) Standard deviation of N_2O emissions from weighted average technique.

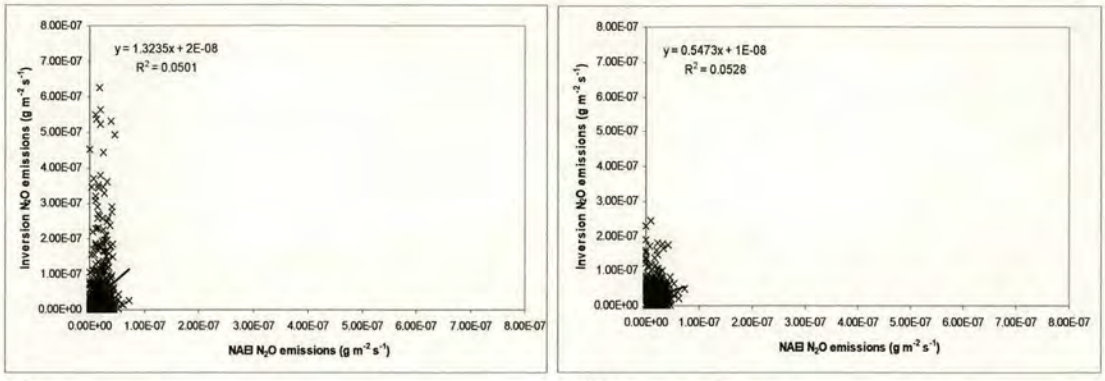

(a) (b)

Figure 121. (a) N2O emissions for combined observations inversion technique v NAEI emissions (g m^{-2} s^{-1}) for resolution of 1×1 grid boxes and restricted domain. R = 0.22. (b) N2O emissions for weighted average technique v NAEI emissions (g m^{-2} s^{-1}) for resolution of 1×1 grid boxes and restricted domain. R=0.23.

By restricting the domain to just the UK and Ireland, the fit between the combined observation emissions and the NAEI emissions worsens to a correlation coefficient of 0.22 as seen in Figure 121 (a). The total budget for the UK also increases as we would expect, with larger emissions around the coast of the UK and Ireland (the edge of the domain). The uncertainty associated with each individual grid square also significantly increases as seen in Figure 120 (b), which shows the uncertainty in each grid box in the restricted domain, compared with Figure 117 (b), which shows the uncertainty in each grid box in the unrestricted domain. Figure 120 (c) shows the map produced by the weighted average technique with a restricted domain. The total emissions produced by this technique are slightly larger than the total emissions from the unrestricted domain. However the uncertainty associated with each grid square in the UK is almost the same for the restricted domain (Figure 120 (d)) and the unrestricted domain (Figure 117 (d)). Both show the largest uncertainty to be around the east coast closest to the observations. However, the unrestricted domain shows higher levels of uncertainty in the English Channel where the inversion has placed air probably from Continental Europe which affects the accuracy of the background concentration estimate. Air from Europe will send the background concentration above the baseline value and the result will tend to be an increase in emissions in grid squares at the edge of the domain.

The weighted technique is better at calculating the emissions than the combined observation technique for N_2O. However it is hard to say whether restricting the domain offers any great improvement to the emission map. The unrestricted domain has a higher correlation coefficient with the NAEI emissions of 0.26 compared to 0.23 for the restricted domain (Figure 121), but the NAEI emissions are themselves very uncertain and so this is not a reliable indicator, and N_2O emissions are highly variable in time. Because of the fewer number of flights used, the greater measurement uncertainty and the greater variability in N_2O emissions; the best approach is to constrain the inversion as much as possible by restricting the domain and accept the greater uncertainty at the domain edges. Therefore Figure 120 (c) is taken as the best N_2O map.

Comparing Figure 120 (c) with the NAEI emissions in Figure 118, we see the inversion technique predicts much larger emissions for the total UK budget with emissions of 550 kt yr^{-1} for the restricted domain. The unrestricted domain produces emissions of around 500 kt yr^{-1} so restricting the domain causes an increase in emissions of around 50 kt yr^{-1} which is similar to the uncertainty of both emission estimates. As with CH_4, the combined observation map, Figure 120 (a), can be used in combination with weighted average, Figure 120 (c) to give an indication of the spatial disaggregation of the emissions. The weighted average map shows the same east coast effect as CH_4, however both Figure 120 (a) and (c) show larger than expected emissions from the Teesside area, most likely due to an industrial source. Comparing these maps to the NAEI emissions indicates that emissions from Wales and the South West of England, in areas associated with livestock farming, are larger than expected. Agricultural emissions are the most uncertain area of the N_2O budget as they depend on the levels of nitrogen added to the soil from mineral fertilizer and manure and on the weather condition, in particular rainfall (Bouwman, 1995). It is therefore not surprising to see that the areas of the country where N_2O emissions are much larger than in the current budget are rural, agricultural areas.

The observations are restricted to the summer months and so are not representative of the whole year. However peak emissions of N_2O are expected to be earlier in the year during the spring when mineral fertilisers are being applied by farmers. Also rainfall was below average for these months (www.metoffice.gov.uk) which should act to

suppress N_2O emissions from soils. Therefore the inversion emissions still suggest that annual emissions of N_2O are being underestimated in the current inventory.

6.6.5 Halocarbons

Using observation of 20 species of halocarbons (HCs) taken with whole air bottle samples (WAS) during flights B92, B102, B111, B118, B126 and B134, made by the Universities of East Anglia and York under the AMPEP sister project 'FLUXEX', it was possible to produce spatially disaggregated emissions for these species. There were fewer whole air bottle samples than Tedlar bag samples collected, typically 50% fewer per flight resulting in fewer observations with which to constrain the inversion. This greatly increases the uncertainty in the halocarbon maps. Because of the lack of data, flight B111 was included which had been excluded for the other species due to the complex meteorology. Two species are shown here as examples in Figure 122 and the rest are included in Appendix 5.

Because spatially disaggregated emissions do not currently exist for these species it is not possible to compare directly and thus this approach provides the first spatially disaggregated HC emission maps for the UK. The UK totals for these species are broadly what would be expected as are the source locations which are mainly centred around urban and industrial areas. Halocarbons emissions tend to originate from these areas because of their use industrial processes, building materials and consumer products (Manning *et al.*, 2003). Because so few days are used for the inversion, a bias of sources to the east coast is observed. However Figure 122 (a), which shows the emissions of $CHClCCl_2$, indicates emissions from localised sources around Cardiff, London and Teesside and Newcastle. Figure 122 (c) shows of emissions of C_2Cl_4 and also indicates localised sources around Cardiff, London, Teesside and Newcastle and a source in the North West of England.

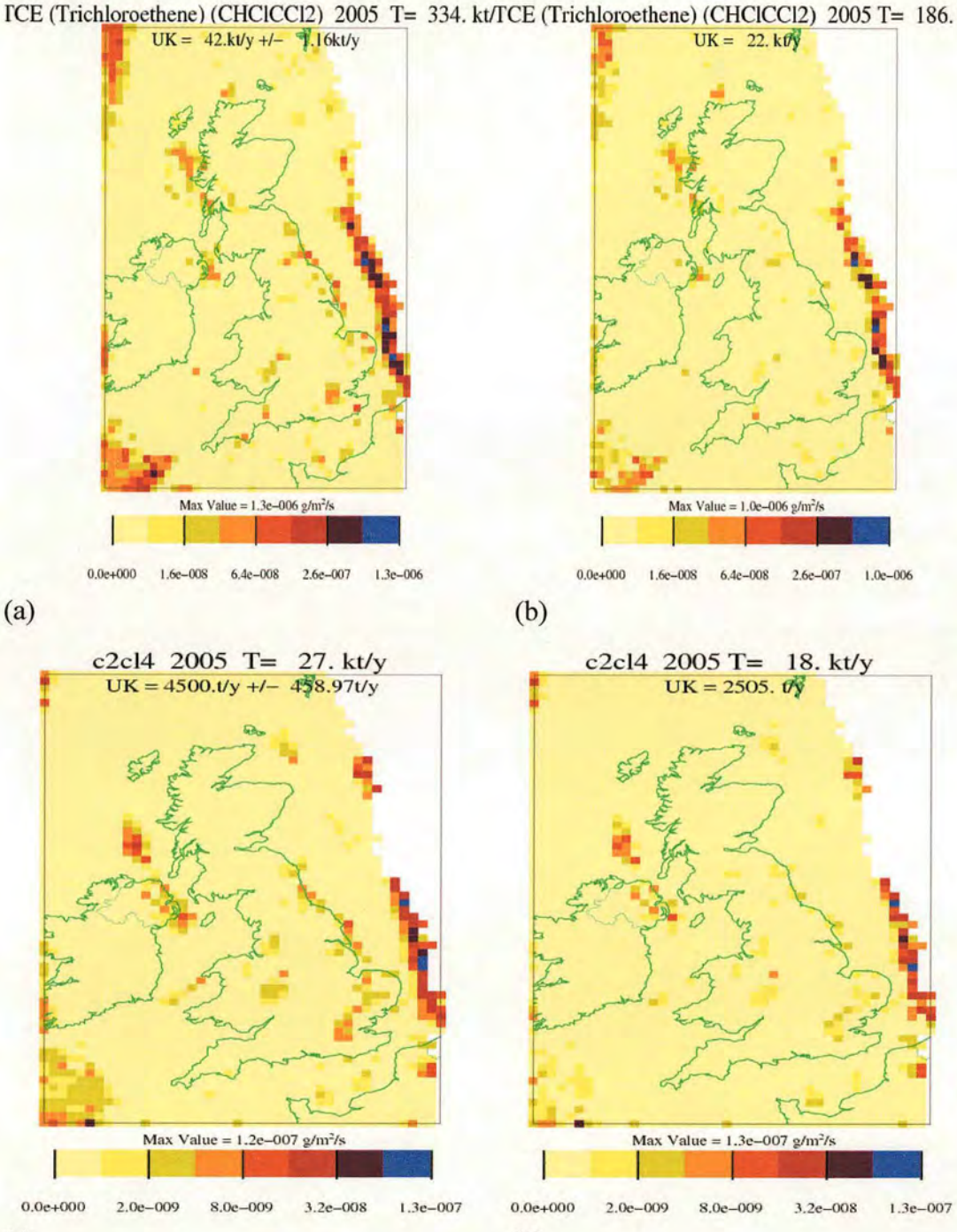

Figure 122. Average results for flights B92, B102, B111, B118 and B134 at 1×1 resolution and unrestricted domain using combined observation technique. (a) Average CHClCCl2 emissions (g m^{-2} s^{-1}) of 3 inversion solutions. T = total for whole domain, UK = total for UK ± standard deviation for total UK emissions from 3 inversion solutions. (b) Standard deviation of CHClCCl2 emissions of 3 inversions solutions. T = total standard deviation of all grid boxes in domain, UK = total standard deviation of all grid boxes in UK. (c) Average C2Cl4 emissions of 3 inversion solutions. (d) Standard deviation of C2Cl4 3 inversions solutions.

Total UK emissions for each species for the 1 × 1 grid box resolution maps with the unrestricted domain are shown in Table 23. The AMPEP emissions of selected species are compared to NAEI emissions and emissions derived using the NAME inversion technique and Mace Head data (Manning *et al.*, 2003 and Manning 2006) in Table 24. This shows that the AMPEP Halocarbon estimates are generally in good agreement with other estimates.

Table 23. Annual UK emissions (t yr^{-1}) for halocarbons from inversion maps for 1 × 1 grid box resolution, unrestricted domain.

Chemical Species	UK emission (t yr^{-1})	Chemical Species	UK emission (t yr^{-1})
C_2Cl_4	4500 ± 459	CFC-113	3230 ± 257
CCl_4	5340 ± 505	CFC-114	1190 ± 478
CH_2Br_2	120 ± 31	HCFC-21	75000 ± 13590
CH_2BrCl	20 ± 1	HCFC-22	3800 ± 469
CH_2Cl_2	20 ± 14	HCFC-123	20 ± 5
CH_3Br	910 ± 58	HCFC-124	120 ± 7
CH_3CCl_3	1570 ± 32	HCFC-141b	900 ± 253
CH_3Cl	16000 ± 2300	HCFC-142b	560 ± 97
$CHCl_2Br$	70 ± 13	HFC-134a	3090 ± 176
$CHCl_3$	640 ± 68	HFC-152a	370 ± 91
$CHClBr_2$	40 ± 19	Halon-1211	210 ± 68
$CHClCCl_2$	42000 ± 1160	Halon-1301	1080 ± 232
CFC-11	950 ± 177	Halon-2402	50 ± 7
CFC-12	9100 ± 68	npb	110 ± 36

Table 24. AMPEP derived emissions compared to inversion derived emissions using the NAME model and Mace Head data for mean of 1995-2000 (Manning *et al.*, 2003), for 2005 (Manning, 2006) and NAEI UK totals (kt yr^{-1}) of selected species.

year	AMPEP	Mace Head 1995-2000	Mace Head 2005	NAEI
HFC-134a	3.1		2.1	3.7 (2004)
HFC-152a	0.4		0.1	0.2 (2004)
Combined HFC	3.5			5.7 (2005)
CFC-11	1.0	1.4		
CFC-12	9.1	1.7		

6.7 Uncertainties

The uncertainty associated with the final map is a combination of the errors in the backward modelling from the meteorology and the transport parameterisations in NAME and in the observations. The inversion assumes that the emissions are constant and that all emissions originate within the model domain. Where the background air differs from the estimated value, emissions around the edge of the domain can be elevated or suppressed. Emission nearer to the observations will have a larger impact than emissions further away and may mask their signal. By combining the data from different flights this effect can be mostly overcome but as our dataset is biased to days with broadly westerly winds, there may still be some bias to the east in the final emissions maps.

The inversion routine begins with a random map which it improves to produce a best-fit. Because of this randomness, the best-fit map produced by the inversion can vary slightly between runs that use the same set of starting conditions. To account for any measurement errors and to some degree transport uncertainties, the observations are allowed to change by some multiple of the measurement uncertainty. This noise factor was set at 4. This can also contribute to variation between maps. The inversion was therefore run 3 times for each set of conditions and the average taken. This also provided a measure of the uncertainty in the map due to the inversion itself and the uncertainty in the observations.

The totals for the maps are more certain than their spatial disaggregation. The inversion may assign emissions to one of a number of adjacent grid boxes without significantly affecting the statistical score of the map. This can lead to variation between grid boxes for individual runs which we see in the standard deviation maps. However, although the placement of the emissions can vary, the total emissions assigned should vary much less. Therefore the uncertainty in the total budget is much less than the total uncertainty in the grid boxes. This can be seen in Figure 103 (a) and (b) which show the emissions and standard deviation for each grid box respectively for CO using the combined observation technique. The uncertainty of the total UK emissions is only 58 kt yr^{-1} (2 %) while the total uncertainty of all the UK grid boxes is 912 kt yr^{-1} (31 %). For CO_2 the uncertainty in the UK total is 10 % while the total

uncertainty of all the grid boxes is 46 %. For CH_4 and N_2O the weighted average technique was used to produce the final maps with the uncertainty calculated from the variation between individual flights. For N_2O the uncertainty in the total is 8 % while the total uncertainty of all the grid boxes is 44 %. For CH_4 the uncertainty in the total UK emissions is 27 % while the total uncertainty of all the grid boxes is 63 %. The Halocarbon maps are based far less data resulting in greater uncertainty in the emissions maps with the typical uncertainty in the total of around 15 %

6.8 Discussion & Conclusion

Using the NAME model in backwards mode, dosage maps were produced showing the relative influence of each grid box on an observation point. For each observation a map was produced and the results of all observations for each flight combined into a single matrix. When this matrix is multiplied by the emissions from each grid box, a predicted concentration at the observation location is calculated. Using the technique of 'simulated annealing', the emissions are optimised by maximising the fit between the measured and predicted concentrations of the observations. Using this inversion technique, a spatially disaggregated emission map is produced which can be used to validate the spatially disaggregated emissions of the NAEI. The results for each flight were combined in two ways to produce an average map of the annual emissions. The first method combined the observations and dosage map into a single inversion run to produce average annual spatially disaggregated emissions. The second method averaged the emission maps produced for each individual flight.

The result of the inversion for CO is very promising, showing that this technique can be used to produce spatially disaggregated emissions maps. By combining all the observations for each flight the inversion can be more tightly constrained than running the inversion for the individual flights. Combining data from different days also helps to overcome any biases in the data due to the focus on observations along the east coast. With only slightly differing windflow patterns for the different flights, the problem of sources near to the observations masking more distant sources can by largely overcome. The combined observation approach to the inversion therefore

produces a much more realistic emissions map for the annual emissions and is the favoured technique given consistent data quality over the campaign period. As the data for both CO and CO_2 was of a consistently high quality throughout the campaign it was this approach that was used to produce the final emission maps. The result suggests that the current NAEI emissions inventories for CO and CO_2 are accurate and the total UK emissions for both are well understood. The inversion estimate for the UK budget for CO is 2900 kt yr^{-1}, similar to the current estimate for 2005 of 2400 kt yr^{-1}. The inversion estimate for the UK budget for CO_2 is 620 Mt yr^{-1} with a sink term of 11 Mt yr^{-1}, similar to the current budget of 555 Mt yr^{-1} and a sink of around 28 Mt yr^{-1} (Milne et al., 2006).

For CH_4 and N_2O the data quality varied throughout the campaign. To produce the map of annual emissions the alternative approach was used which averaged the emission maps produced for each individual flight. This allowed the maps to be weighted to reflect the data quality giving greater weighting to days where the data quality was good. While this approach will estimate the total emissions from the UK accurately, it will not necessarily assign the emissions to the correct area of the country as a bias is introduced by the relatively greater number of observations along the east coast. The results for N_2O and CH_4 suggest that the current NAEI total emissions underestimate the actual total emissions. The inversion estimate for the UK budget for CH_4 is around 3500 kt yr^{-1}, 45 % higher than the NAEI estimate for 2005. The N_2O budget is around 500 kt yr^{-1} over 3 times the current budget.

While the spatial disaggregation of the emissions in the CH_4 and N_2O maps is not expected to be as accurate as for CO and CO_2, it can still give an indication of where the unaccounted for emissions may originate. For both N_2O and CH_4 the emission maps suggest larger emissions from rural areas suggesting agricultural sources are the likely origin. This is consistent with the work on the total budget using the model iteration technique and sector analysis (Chapter 5) which suggests significantly larger emissions from agriculture (livestock) for both CH_4 and N_2O. Given the location of the larger emissions in the inversion emission maps, the sector analysis which shows larger emissions from manure but not mineral fertiliser for N_2O and larger emissions for CH_4 for livestock; a consistent picture seems to be emerging with larger emissions

from the livestock but not arable farming resulting in significantly larger emissions of CH_4 and N_2O than currently accounted for in the NAEI estimates.

For this technique to be used to produce reliable annual emissions inventories at the resolution of the current NAEI inventory, many more flights would be required to give greater temporal coverage throughout the year to account for differences in agricultural activity and to constrain the inversion far more than the current number of observations allow. Taking more measurements upwind would allow better measurement of the background concentration and minimise the uncertainty around the edge of the model domain.

Other inversion studies by e.g. Manning *et al.*, (2006) and Bergamaschi *et al.*, (2005) are described in section 1.3.2. Manning *et al.*, (2006) found similar values for CO of 2700 kt yr^{-1} for the year 2004-2005 but lower emissions for CH_4 and N_2O at 2700 kt yr^{-1} and 141 kt yr^{-1} respectively. Although the CH_4 emission estimate was lower than the emissions found here it is greater than the NAEI emissions and the trend found over the 10 previous years suggests an increase in CH_4 emissions unlike the NAEI emissions which show a decrease. Peter Bergamaschi *et al.*, (2005) found CH_4 emissions of 4210 kt yr^{-1} for 2004, very similar to the value found here.

Chapter 7 Oxidation Rates of Urban and Power Station Plumes

7.1 Introduction

During the AMPEP project, measurement of NO_x, SO_2 and oxidation products HNO_3 and NO_3^- and SO_4^{2-} particles allowed oxidation rates in UK outflow plumes to be estimated for urban, industrial and power plants plumes. The major homogeneous oxidation pathway for both NO_x and SO_2 in the gas-phase is by reaction with the hydroxyl radical (OH). SO_2 oxidation in cloud is mainly in the heterogeneous phase; however cloudy conditions were avoided for the AMPEP flights. OH is formed in unpolluted air by the photolysis of O_3 and in polluted air by the photolysis of nitrous acid (HONO) and hydrogen peroxide (H_2O_2). Where air pollution is extreme, OH can be formed by the photolysis of a range of oxygenated organic compounds produced by incomplete combustion of fossil fuels (Hewitt, 2000).

Anthropogenic emissions of nitrogen oxides (NO_x), mainly in the form of NO and NO_2, are dominated by fossil fuel combustion and contribute to the formation of tropospheric ozone. Freshly emitted NO reacts rapidly with O_3 to form NO_2 which has a lifetime of less than one day against oxidation to nitric acid (HNO_3), HONO, peroxyacylnitrates (PAN) and other organic nitrates, referred to collectively as NO_z (Parrish, 2003). NO_2 can also photo-dissociate back to NO and $O(^3P)$ which in turn reacts with O_2 to form a new O_3 molecule with the NO reacting rapidly back to NO_2. The oxidation products HONO and PAN are likely to decompose to NO and NO_2 respectively and therefore do not necessarily represent a permanent removal of NO_x. HNO_3 and NO_2 can go on to form nitrate particles (NO_3^-).

Sulphur dioxide (SO_2) is emitted mainly from the combustion of fossil fuels and is converted by oxidation with OH to H_2SO_4 which reacts irreversibly with ammonia (NH_3), sea-salt particles and cloud droplets to form sulphate particles. Figure 123 shows the oxidation processes for both SO_2 and NO_2. Comparison of the SO_2 and SO_4^{2-} particle concentrations in the outflow plumes can be used with a knowledge of the sources to derive the oxidation rate of SO_2 (Bamber *et al*, 1984). Likewise,

comparison of NO_2 with oxidation products HNO_3 and NO_3^- can be used to estimate the NO_x oxidation rate.

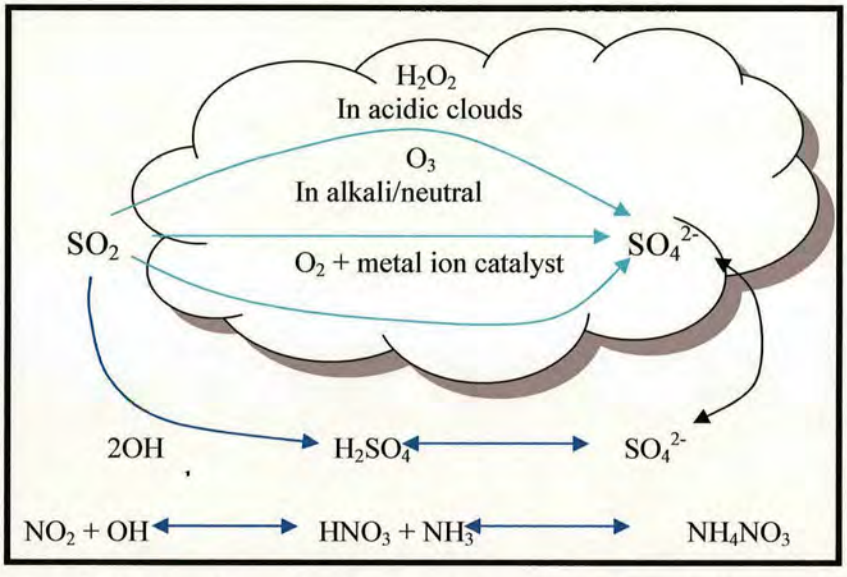

Figure 123. Sulphur dioxide and nitrogen dioxide oxidation processes (NEGTAP, 2001).

The oxidation rate of sulphur and nitrogen compounds in plumes from urban and industrial sources depends on a number of factors including the chemical composition of the polluted air both due to emissions and background air, the presence of cloud allowing for aqueous phase oxidation and the oxidising capacity of the air which in turn is dependent on the supply of radicals generated by solar radiation. It is important to measure the oxidation rate of outflow plumes in order to provide simple parameterisation for models and to validate existing chemistry schemes.

The oxidation rate of NO_x and SO_2 from urban sources may differ from the oxidation rate in plumes from industrial and power plant sources due to the differing composition of pollutants. Where NO_x emissions are high, the condition in the plumes near to the sources can result in the supply of NO_x exceeding the supply of OH as O_3 is depleted by consumption by NO. As the plumes travels away from the source, the supply of OH increases and eventually the supply of oxidants will overcome the supply of NO_x from the source (Milford *et al.*, 1989). Power plants produce very high emissions of NO_x resulting in NO_x saturated conditions (Sillman *et al.*, 1993; Hanna *et al.*, 1996). Near to the source, the high concentration of NO results in NO_x titration of O_3 forming NO_2. The absence of VOCs in power plant plumes which can provide an alternative means of O_3 production results in a decrease in O_3 concentrations at the

centre of the plume. In urban centres high NO_x also results in NO_x saturation (Lawson *et al.*, 1990; Drummond *et al.*, 1998; Williams and Grosjean, 1990; Sakugawa and Kaplan *et al.*, 1989; Sillman *et al.*, 1997) however urban pollution also comprises high CO and VOC emissions, distinguishing urban from power station plumes. The oxidation rates of urban plumes may therefore be quite different and exceed those of power station plumes due to larger concentrations of VOCs which increases oxidant supply (Hewitt, 2000).

A study of an isolated power plant plume (Springston *et al.*, 2005) in Texas on 10 September 2000 provided estimates of the oxidation rates of SO_2 and NO_x. The DOE G-1 aircraft made 12 downwind transects of a power plant plume measuring SO_2, sulphate aerosol, NO, NO_2 and total NO_y. The weather was clear with no precipitation and a capping inversion at the top of the boundary layer. There was some cloud visible but all at or above the top of the boundary layer. It was assumed that SO_2 and NO_x were oxidised primarily by OH resulting ultimately in aerosol SO_4^{2-} and HNO_3 with dry deposition of SO_2 and HNO_3. The air measured at each transect was assigned an age based on the distance from the power plant and average wind speed. The ratios of SO_2 to SO_4^{2-} and NO_x to NO_y with plume age were used to determine the oxidation rates. It was found that as the plume aged, the oxidation rate increased up to a rate of approximately 23 % N $hour^{-1}$ for NO_x for a plume age of around 3 hours and approximately 3 % S $hour^{-1}$ for SO_2 at around 4 hours from the source. Near the power plant, the high NO_x environment and low photochemistry suppressed oxidation which increased as the plume aged. After the plume had aged to approximately 3.5 to 4 hours, the oxidation rate began to decrease once more for both NO_x and SO_2.

In 1982, the Met Office Hercules C130 W M K 2 aircraft was used to measure the SO_2 oxidation rate of outflow plumes from the United Kingdom (Bamber *et al.*, 1984). In July, the aircraft made a circumnavigation of the UK within the boundary layer about 20 km offshore. A second aircraft (the Cranfield Institute of Technology Jetstream) flew flight tracks between the Isle of Man, Liverpool and Cranfield at different altitudes. Both aircraft intercepted westward moving plumes of SO_2 and NO_x with low level cloud intercepting the plumes over North Wales. A simple Gaussian model was used to model the spread of the plume with constant vertical diffusion, wind speed and boundary layer height. SO_2 emissions were estimated for low level

and high level (e.g. power plant) sources with dry deposition and oxidation parameters. For the Jetstream aircraft which intercepted plumes inland from the North West of England and the Midlands, an oxidation rate of 2 % S hr^{-1} was found to reproduce the observed SO_2 flux and enhancement to the SO_4^{2-} concentration. Further downwind, the Hercules aircraft which intercepted the plumes offshore required an oxidation rate of 4% S hr^{-1} to reproduce the observations. The air measured by the Hercules aircraft had encountered cloud over the North of Wales allowing aqueous phase oxidation and wet deposition over the higher ground in this area of the country. To account for the sulphate observed on the Hercules required an oxidation rate of 5.3 % S hr^{-1} between the Jetstream aircraft and the Hercules aircraft with wet deposition of SO_2 and SO_4^{2-} from the low lying cloud over North Wales.

A study applying a Gaussian trajectory transfer-coefficient model to a case study of Taichung City in Taiwan for November to December 1997 produced gas-particle conversion rates of NO_x and SO_2 as part of the model calibration (Tsuang *et al.*, 2003). Taichung City has a metropolitan population of 0.9 million with two fossil fuel power stations located nearby. Using existing emission inventories and observed pollutant concentrations a NO_x rate of 0.75 % N $hour^{-1}$ and SO_2 to sulphate rate of 7.8 % S $hour^{-1}$ was found.

Hewitt (2000) reviewed atmospheric chemistry of SO_2 and NO_x in power station plumes combining results from a number of studies. This work included publishing the SO_2 average oxidation rates found for a number of coal power stations plumes as well as urban plumes from three cities. The SO_2 oxidation rate for coal power stations ranged from almost zero to more than 16 % S $hour^{-1}$. A mean rate of 2.3 % S $hour^{-1}$ was calculated from the average rates published for each study. The urban plumes produced rates of 1 to 31 % S $hour^{-1}$ for plumes from St Louis (USA), Milwaukee (USA) and Budapest (Hungary). Average rates of 4 and 10 % $hour^{-1}$ were found for Milwaukee and Budapest respectively. Due to limited NO_x data, only a single NO_x oxidation rate was found of 27 % N $hour^{-1}$ for a coal fired power station (Luria *et al.* 1983).

A number of conclusions about the NO_x and SO_2 chemistry in power station plumes were drawn. These included the conclusion that in non-cloudy conditions the NO_x oxidation rate should be more rapid than the SO_2 oxidation rate with the reverse true

in cloudy conditions where aqueous phase chemistry provides an alternative pathway for SO_2 oxidation. The oxidation rates in the centre of a power station plume are expected to be lower than in the surrounding air due to suppressed oxidant formation with the rate dependent on a number of factors including the composition of a plume and background air and meteorological conditions. Sunny conditions should provide the highest rates with removal rate of NO_x (maximum ~30 % N $hour^{-1}$) expected to be larger than the SO_2 removal rates (maximum ~3 % S $hour^{-1}$) where oxidant supply is not limited.

7.2 Methods

In this study transects of plumes along the UK coast measured the polluted air from urban and industrial sources. This work combines data from the Aerodyne quandrupole-based Aerosol Mass Spectrometry (Q-AMS) on the FAAM aircraft data for NO_3^- and SO_4^{2-} and data of gas-phase NO, NO_2 and HNO_3 from a 4-channel chemiluminescence analyser with SO_2 data from the chemiluminescence analyser operated by the FAAM team, to derive average oxidation rates for urban and industrial plumes. For each flight, the concentration of N from NO_2 and combined N from HNO_3 and NO_3^- particles were plotted and the origin of each plume identified from the NAME CO maps produced by the NAME model (Chapter 4). Similarly, the SO_2 and SO_4^{2-} concentrations were plotted as S. A one minute running mean of the concentration was calculated and the one minute average concentration at the peak of the plume was used for the plume concentration.

The distance between the observation and the plume origin was calculated and the travel time between emission and measurement calculated using the average wind speed from the Unified Model meteorological data. The oxidation rate was estimated by calculating the ratio of N and S in the emitted NO_x and SO_2 to the oxidation products $HNO_3 + NO_3^-$ and SO_4^{2-} in the outflow plumes. It was assumed that all NO oxidised quickly to NO_2 so the NO_x oxidation rate was calculated using NO_2 data using the equation

$$R_{NO_x} = \frac{N(HNO_3 + NO_3^-)}{N(HNO_3 + NO_3^-) + N(NO_2)} \quad (7.1)$$

where R_{NOx} is the oxidation rate of NO_X (% N hour^{-1}), $N(NO_2)$ is the mass of nitrogen in the emitted pollutant NO_2 and $N(HNO_3 + NO_3^-)$ is the mass the nitrogen in the oxidation products $HNO_3 + NO_3^-$. Similarly the SO_2 oxidation rate is calculated using the equation

$$R_{SO_2} = \frac{S(SO_4^{2-})}{S(SO_4^{2-}) + S(SO_2)} \quad (7.2)$$

where R_{SO2} is the oxidation rate of SO_2 (% S hour^{-1}), $S(SO_2)$ is the mass of sulphur in the emitted pollutant SO_2 and $S(SO_4^{2-})$ is the mass of sulphur in the oxidation products SO_4^{2-}.

To determine the plume origin, the NAME concentration plots were used to locate the measured plumes as shown in Figure 125 and trace their source. Flight B112 is used as case study to demonstrate the method used as both the N and S species produced distinct plumes along the east coast. For all other flights the CO NAME concentrations plots from Chapter 4 were used to identify the anthropogenic plumes. Using the observed concentrations as shown in Figure 127 to get the time of the plume peak, the origin of the plume was established by comparing the location of the plane from Figure 126 with the outflow plume at that location and time. Often the plumes from near the east coast sat on top of the broader outflow plumes from the North West of England and the Midlands making it difficult to separate individual plumes. However a good indication of the plume origin is the shape of the plume, with a sharp spike indicating a localised source such as a power station and a broader, flatter plume indicating an urban plume with the emissions spread over a wider area. As can be seen from the plume in Figure 127 (a) between 11:08 and 11:22, there are sharp spikes superimposed on top of a broader plume. Using Figure 125 (a) which shows the NO_x outflow plumes and major urban sources and Figure 124 which shows the location of power stations, the broad plume is identified as originating from the North West of England mainly from the large cities of Manchester and Liverpool. The

spikes are likely to be from the large power stations in Humberside; Drax, Eggborough and Ferrybridge. Because the three Humberside power stations are so close together and are sitting in a line in the same direction as the wind flow for AMPEP flights, it can be difficult to distinguish which plume originates from which power station, but as Drax is the largest, producing twice as much energy as the other two, it is likely that the largest NO_x plume belongs to it. Drax has a SO_2 scrubber to reduce SO_2 emissions and so the SO_2 signal should be much smaller. Eggborough is also equipped with desulphurisation equipment so produces only small SO_2 emissions. The London plume tends to be very distinctive as it is generally isolated and has a broader shape making it easily identifiable as an urban plume. In Figure 127 (a) the large broad plume at around 10:32 is an excellent example of the London plume. Teesside and Newcastle tend also to be easily identified as they are generally isolated from other outflow. Teesside is mainly an industrial plume and tends to be a sharp plume as seen Figure 127 (a) at around 11:34. Newcastle produces a small plume which is mainly urban so has a broader structure as seen in Figure 127 (a) at around 11:43. Depending on wind direction, the Midlands plume can sometimes be isolated as seen in Figure 127 (a) at around 10:57 however there are power stations sitting in the plumes path which may be responsible for the spikes in the plume. The plume from the Central Belt of Scotland is complex with two power stations near to the East coast sitting in the outflow path of the urban sources which are concentrated nearer to the west around Glasgow.

Figure 124. Locations of UK coal power stations (UK Quality Ash Association www.ukqaa.org).

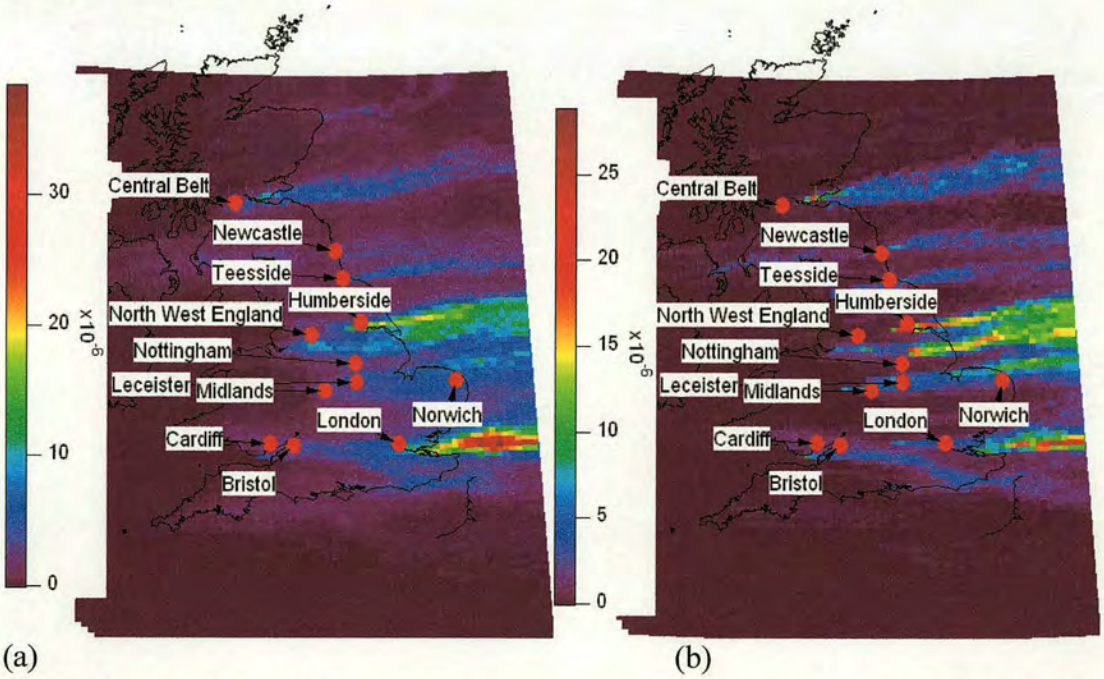

(a) (b)

Figure 125. (a) NAME NO_x outflow plumes (g m^{-3}) for flight B112. (b) NAME SO_2 outflow plumes (g m^{-3}) for flight B112.

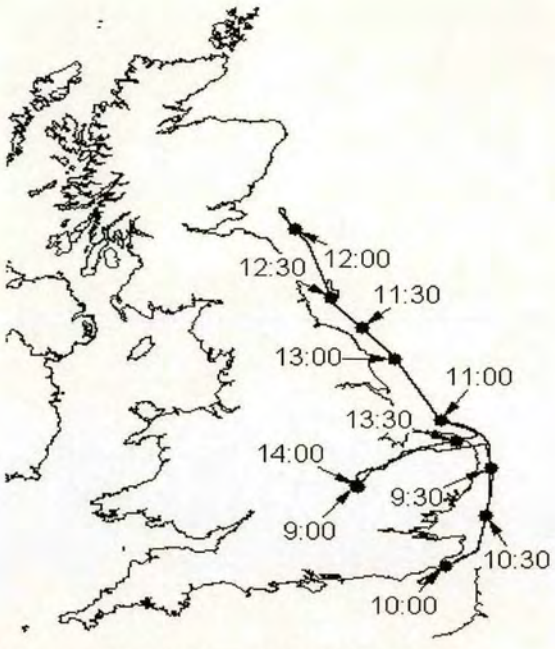

Figure 126. Flight path for flight B112.

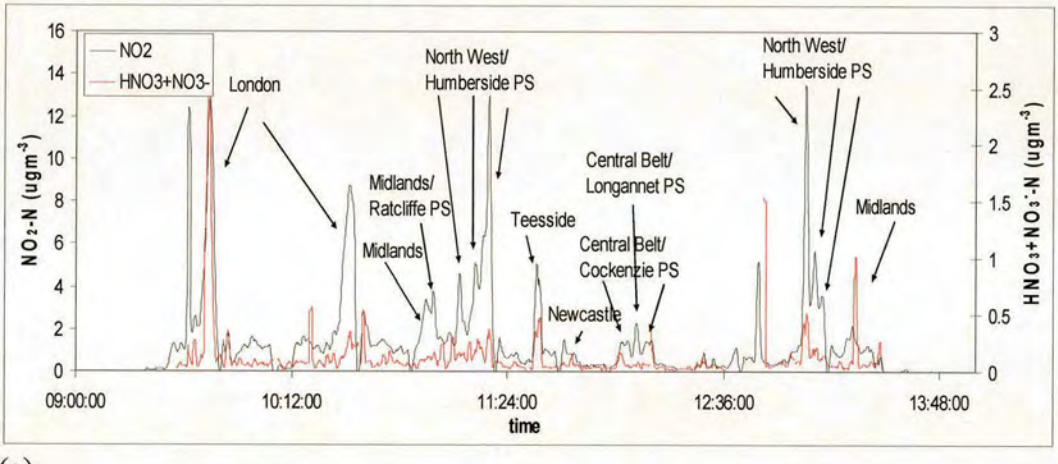

(a)

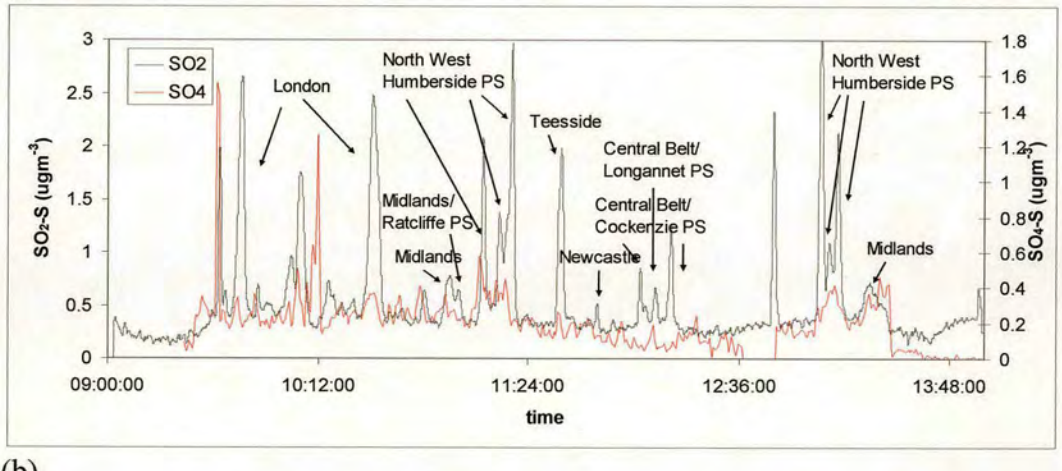

(b)

Figure 127. Flight B112 (a) NO_2 and $HNO_3+NO_3^-$ concentration (N μgm^{-3}). (b) SO_2 and SO_4^{2-} concentration (S μgm^{-3}).

The plane transected the London plume twice in the space of an hour as the aircraft headed south and north respectively. During the first transect, the NO_3 concentration is high giving a high oxidation rate of 6.35 % N $hour^{-1}$. However during the second transect, the HNO_3+NO_3^- concentration is much smaller giving an oxidation rate of only 1.18 % N $hour^{-1}$. This is not reflected in the SO_2 oxidation rate which is similar for both transects so the NO_3 (mainly in the form of HNO_3) must originate from a source with low SO_2 emissions. The next plume encountered originates from the Midlands but a spike in the plume at 10:59:40 is likely to be from Ratcliffe on Soar power station. The SO_2 oxidation rate is similar for the Midlands for both the northbound and southbound legs. The NO_x oxidation rate is only 0.62 % N $hour^{-1}$ on the northbound leg but increases to 5.94 % N $hour^{-1}$ on the southbound leg, again due to a spike in HNO_3. The aircraft then transects through the plumes from the power stations in Humberside which are superimposed on the plume from the North West of England. The SO_4 concentrations seem to show the peak of the plume from the North West at around the same point as the middle power plant plume. This may explain why the SO_2 oxidation rate is higher for this plume than the other two on both legs. The NO_x oxidation rates are similar for all the power plant plumes, though the rate for the middle plume on the northbound leg is slightly higher than for the other two. The Teesside and Newcastle plumes have similar rates for NO_x oxidation while the SO_2 oxidation rate is significantly higher for Newcastle than Teesside. The reason for this is not clear however it should be noted that the peak of the NO_x plume and the SO_2 plumes are slightly different suggesting different sources. At the northern end of the leg the plume transects the plume from the Central Belt on top of which sits the plumes from the power station near the east coast. The plume from Cockenzie has a significantly higher NO_x oxidation rate than Longannet suggesting that the Longannet plume is separated from the main urban outflow from Glasgow. Overall the plumes from the power plants tend to have lower oxidation rates than plumes from urban areas.

Table 25. Oxidation rate of NO_2 to HNO_3+NO_3^- of plumes for flight B112 for northbound leg. PS = power station.

	London		Midlands	Midlands Radcliffe on Soar PS	North West Humberside Power stations			Teesside	Newcastle
time	09:43:40	10:31:40	10:57:10	10:59:40	11:08:20	11:15:10	11:17:50	11:33:50	11:43:10
NO_2 (N µg m^{-3})	10.25	8.39	3.30	3.74	4.14	4.88	13.00	5.07	1.40
HNO_3+NO_3^- (N µg m^{-3})	2.48	0.33	0.11	0.15	0.13	0.21	0.37	0.32	0.06
Distance (m)	125000	129000	221000	155000	110000	89000	83000	50000	34000
Wind speed (m s^{-1})	11.36	11.36	11.36	11.36	11.36	11.36	11.36	11.36	11.36
% oxidised per hour	6.35	1.18	0.62	1.02	1.11	1.93	1.36	4.82	4.99

Table 26. Oxidation rate of NO_2 to HNO_3+NO_3^- of plumes for flight B112 for southbound leg.

	Central Belt Cockenzie PS	Central Belt Longannet PS	Central Belt Cockenzie PS	North West Humberside Power stations			Midlands
time	12:02:30	12:07:00	12:12:00	13:03:00	13:06:20	13:09:10	13:19:20
NO_2 (N µg m^{-3})	1.39	2.27	1.48	12.72	5.43	3.33	1.92
HNO_3+NO_3^- (N µg m^{-3})	0.10	0.05	0.22	0.32	0.20	0.14	0.83
Distance (m)	67000	104000	71000	84000	94000	101000	208000
Wind speed (m s^{-1})	11.36	11.36	11.36	11.36	11.36	11.36	11.36
% oxidised per hour	3.91	0.90	8.02	1.21	1.56	1.62	5.94

Table 27. Oxidation rate of SO_2 to SO_4 of plumes for flight B112 on northbound leg.

	London		Midlands	Midlands Ratcliffe PS	North West Humberside Power stations			Teesside	Newcastle
time	09:46:00	10:30:57	10:55:45	10:58:46	11:08:56	11:14:20	11:18:44	11:35:33	11:48:00
SO_2 (S µg m^{-3})	2.59	2.41	0.65	0.56	1.75	1.31	2.73	1.89	0.46
SO_4 (S µg m^{-3})	0.34	0.37	0.35	0.28	0.37	0.37	0.19	0.18	0.13
Distance (m)	122000	127000	226000	160000	110000	89000	82000	46000	41000
Wind speed (m s^{-1})	11.36	11.36	11.36	11.36	11.36	11.36	11.36	11.36	11.36
% oxidised per hour	2.27	4.30	6.32	8.47	6.54	10.11	3.21	7.77	22.15

Table 28. Oxidation rate of SO_2 to SO_4 of plumes for flight B112 on southbound leg.

	Central Belt Cockenzie PS	Central Belt Longannet PS	Central Belt Cockenzie PS	North West Humberside Power stations			Midlands
Time	12:02:30	12:06:45	12:12:55	13:04:20	13:08:50	13:10:00	13:21:30
SO_2 (S µg m^{-3})	0.77	0.53	1.16	2.82	1.13	2.01	0.68
SO_4 (S µg m^{-3})	0.07	0.19	0.08	0.26	0.41	0.31	0.45
Distance (m)	67000	110000	71000	88000	101000	106000	218000
Wind speed (m s^{-1})	11.36	11.36	11.36	11.36	11.36	11.36	11.36
% oxidised per hour	5.38	10.43	3.53	3.84	10.77	5.13	7.50

7.3 Results

7.3.1 Oxidation Rates for Flight B92

Figure 128(a) shows the concentration of NO_2 and HNO_3+NO_3^- for flight B92. Figure 128(b) shows the concentration of SO_2 and SO_4. Because the wind flow is northerly, the plumes are harder to identify as they are superimposed on top of one another. However five peaks were identified as plumes from London, the Midlands, the North West of England, Cardiff and a merged plume from the three Humberside power stations. Table 29 shows the NO_2 oxidation rates and Table 30 shows the SO_2 oxidation rates. The NO_2 oxidation rate ranged from 0.73 % N $hour^{-1}$ for the Humberside power stations to 9.40 % N $hour^{-1}$ for Bristol. The SO_2 oxidation rate ranged from 0.95 % S $hour^{-1}$ for Humberside power stations to 3.78 % S $hour^{-1}$ for the London. Overall the power station plumes have a smaller oxidation rate than the urban plumes for both NO_x and SO_2.

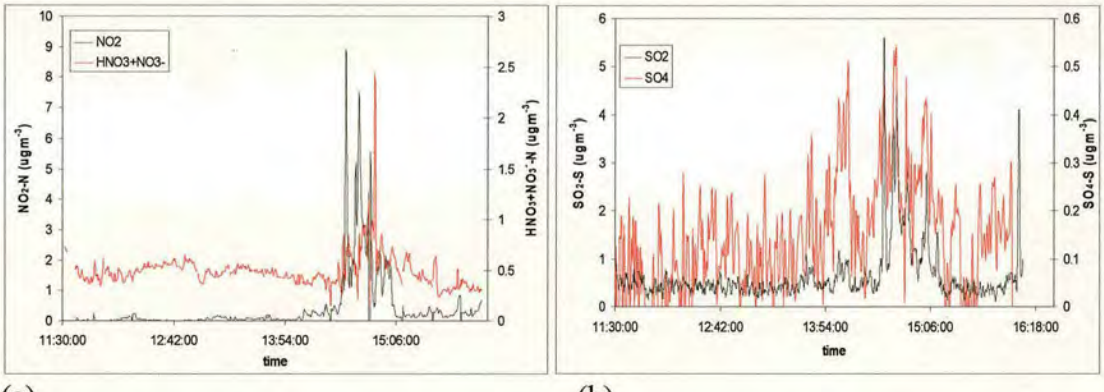

(a) (b)

Figure 128. Flight B92 concentrations averaged over 1 minute (a) NO_2 and HNO_3+NO_3^- concentration (N μgm^{-3}). (b) SO_2 and SO_4 concentration (S μgm^{-3}).

Table 29. Oxidation rate of NO_2 to HNO_3+NO_3^- of plumes for flight B92.

	Humberside PS	London	North West	Midlands	Cardiff
Time	14:33:20	14:42:00	14:49:00	15:01:00	15:47:00
NO_2 (N $\mu g\ m^{-3}$)	8.91	7.28	2.26	1.71	0.85
HNO_3+NO_3^- (N $\mu g\ m^{-3}$)	0.52	0.87	1.20	0.60	0.33
Distance (m)	302000	106000	342000	217000	120000
Wind speed (m s^{-1})	11.20	11.20	11.20	11.20	11.20
% oxidised per hour	0.73	4.06	2.33	4.82	9.40

Table 30. Oxidation rate of SO_2 to SO_4 of plumes for flight B92.

	Humberside	London	North West	Midlands
Time	14:34:00	14:43:00	14:49:16	15:04:45
SO_2 (S µg m^{-3})	5.56	3.92	2.21	1.22
SO_4 (S µg m^{-3})	0.43	0.42	0.48	0.29
Distance (m)	306000	104000	359000	215000
Wind speed (m s^{-1})	11.20	11.20	11.20	11.20
% oxidised per hour	0.95	3.78	2.00	3.63

7.3.2 Oxidation Rates for Flight B97

Figure 129(a) shows the concentration of NO_2 and HNO_3+NO_3^- for flight B97. Figure 129 (b) shows the concentration of SO_2 and SO_4. Six plumes were identified for NO_2 and five plumes for SO_2. Table 31 shows the NO_2 oxidation rates and Table 32 shows the SO_2 oxidation rates. The NO_2 oxidation rates range from 1.69 % N $hour^{-1}$ for London and 5.20 N % $hour^{-1}$ for Norwich. The SO_2 oxidation rate ranges for 2.01 % S $hour^{-1}$ for the West Burton power station plume which sits on top of a Midlands plume to 9.27 % S $hour^{-1}$ for Teesside.

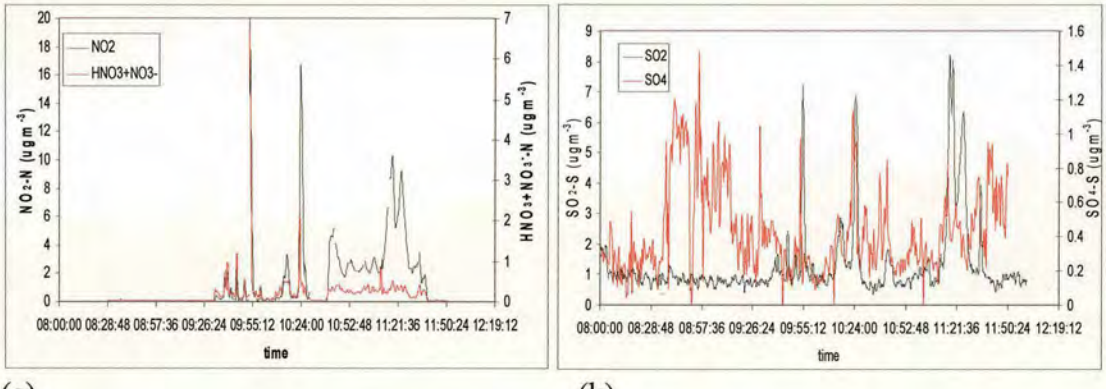

(a) (b)

Figure 129. Flight B97 concentrations averaged over 1 minute (a) NO_2 and HNO_3+NO_3^- concentration (N µgm^{-3}). (b) SO_2 and SO_4 concentration (S µgm^{-3}).

Table 31. Oxidation rate of NO_2 to HNO_3+NO_3^- for plumes of flight B97.

	London	Norwich	Leicester	Nottingham	Midlands West Burton PS	Midlands Humberside PS
time	10:43:00	10:54:20	11:02:40	11:08:00	11:18:30	11:23:50
NO_2 (N µg m^{-3})	4.66	2.87	2.54	3.03	10.37	9.07
HNO_3+NO_3^- (N µg m^{-3})	0.35	0.23	0.31	0.28	0.54	0.39
Distance (m)	170000	60000	196000	161000	100000	82000
Wind speed (m s^{-1})	11.54	11.54	11.54	11.54	11.54	11.54
% oxidised per hour	1.69	5.20	2.30	2.18	2.07	2.07

Table 32. Oxidation rate of SO_2 to SO_4 for plumes of flight B97.

	London	Midlands Cottam PS	Midlands West Burton PS	Midlands Humberside PS	Teesside
time	10:44:20	11:17:30	11:19:20	11:25:20	11:35:00
SO_2 (S μg m^{-3})	1.32	8.09	7.69	6.22	3.93
SO_4 (S μg m^{-3})	0.35	0.52	0.40	0.40	0.48
Distance (m)	165720	124000	100000	83000	48000
Wind speed ($m\ s^{-1}$)	11.54	11.54	11.54	11.54	11.54
% oxidised per hour	5.04	2.04	2.01	2.94	9.27

7.3.3 Oxidation Rates for Flight B102

Figure 130(a) shows the concentration of NO_2 and HNO_3+NO_3^- for flight B102. Figure 130 (b) shows the concentration of SO_2 and SO_4. Seven plumes were identified for NO_2 and SO_2. Table 33 shows the NO_2 oxidation rates and Table 33 shows the SO_2 oxidation rates. The NO_2 oxidation rates range from 0.62 % N $hour^{-1}$ for one of the Humberside power station plumes merged with the plume from the North West to 6.23 % N $hour^{-1}$ for Newcastle. The SO_2 oxidation rate ranges from 1.68 % S $hour^{-1}$ for one of the Humberside power station plumes merged with the North West plume to 6.16 % S $hour^{-1}$ for Newcastle. The oxidation rates of the Humberside power station plumes range from 0.62 % N $hour^{-1}$ to 2.85 % N $hour^{-1}$ for NO_x and 1.68% S $hour^{-1}$ to 5.80 % S $hour^{-1}$ for SO_2. As these plumes sit on top of the mainly urban plume from the North West of England, the oxidation rates will be affected by where in the North West outflow the power stations sit. The small SO_2 concentrations of the middle Humberside plume make it likely that this plume is from Eggborough. As Drax is the largest plant, the third Humberside plume, being the largest NO_x plume, is the source of the peak.

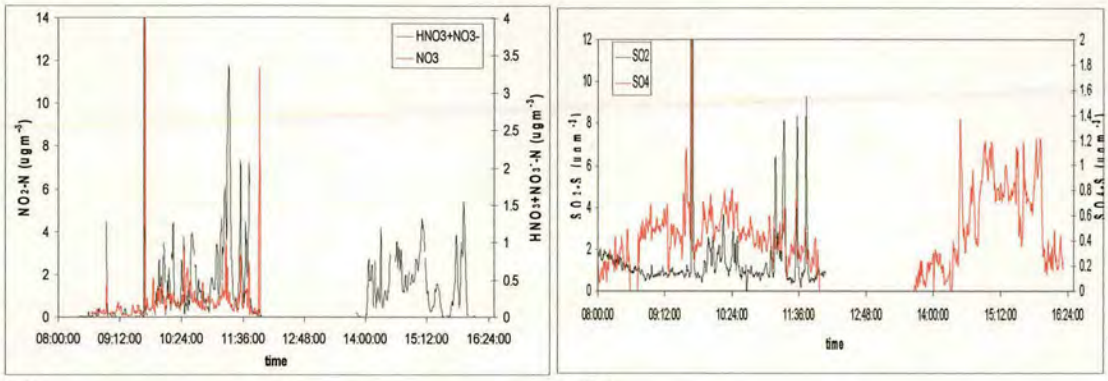

(a) (b)

Figure 130. Flight B102 concentrations averaged over 1 minute (a) NO_2 and HNO_3+NO_3^- concentration (N μgm^{-3}). (b) SO_2 and SO_4 concentration (S μgm^{-3}).

Table 33. Oxidation rate of NO_2 to HNO_3+NO_3^- for 3 plumes for northbound leg of flight B102.

	London	Midlands	North West Ferrybridge PS	North West Eggborough PS	North West Drax PS	Teesside	Newcastle
time	10:34:30	11:00:00	11:13:00	11:14:50	11:19:10	11:32:00	11:43:00
NO_2 (N $\mu g\ m^{-3}$)	2.78	1.73	3.24	6.12	11.81	3.76	5.54
HNO_3+NO_3^- (N $\mu g\ m^{-3}$)	0.57	0.22	0.28	0.33	0.20	0.26	0.67
Distance (m)	141000	201000	85000	83000	82000	62000	53000
Wind speed ($m\ s^{-1}$)	8.54	8.54	8.54	8.54	8.54	8.54	8.54
% oxidised per hour	3.71	1.73	2.85	1.91	0.62	3.22	6.23

Table 34. Oxidation rate of SO_2 to SO_4 for 4 plumes for Northbound leg of flight B102.

	London	Midlands	North West Ferrybridge PS	North West Eggborough PS	North West Drax PS	Teesside	Newcastle
time	10:31:46	11:00:00	11:10:52	11:14:45	10:20:03	11:34:00	11:44:00
SO_2 (S $\mu g\ m^{-3}$)	1.05	1.22	6.27	1.75	7.93	8.19	8.04
SO_4 (S $\mu g\ m^{-3}$)	0.38	0.41	0.33	0.33	0.46	0.42	0.36
Distance (m)	132000	201000	92000	83000	84000	61000	58000
Wind speed ($m\ s^{-1}$)	8.54	8.54	8.54	8.54	8.54	8.54	8.54
% oxidised per hour	6.16	3.86	1.68	5.80	2.02	2.44	2.27

7.3.4 Oxidation Rates for Flight B111

Figure 131 shows the concentration of NO_2 and HNO_3+NO_3^- for flight B111. There are no SO_2 data for this flight. Ten plumes were identified for NO_2 with four of the plumes sampled on both the northbound and southbound legs of the flight. Table 34

shows the NO_2 oxidation rates for the northbound leg of the flight and Table 36 shows the NO_2 oxidation rates for the southbound leg of the flight. The NO_2 oxidation rates range from 1.0 % N $hour^{-1}$ for a Humberside power station to 11.2 % N $hour^{-1}$ for Aberdeen. There seems to be a time delay in the response of the NOxy instrument to a drop in HNO_3 concentration however this should not affect the oxidation rates as the peak of the plumes are used for the calculations. The Humberside power station plumes produce lower oxidation rates than the urban plumes, however the power station plumes from the Central Belt produce high oxidation rates and are therefore likely to be more influenced by urban emissions concentrated to the west, around Glasgow.

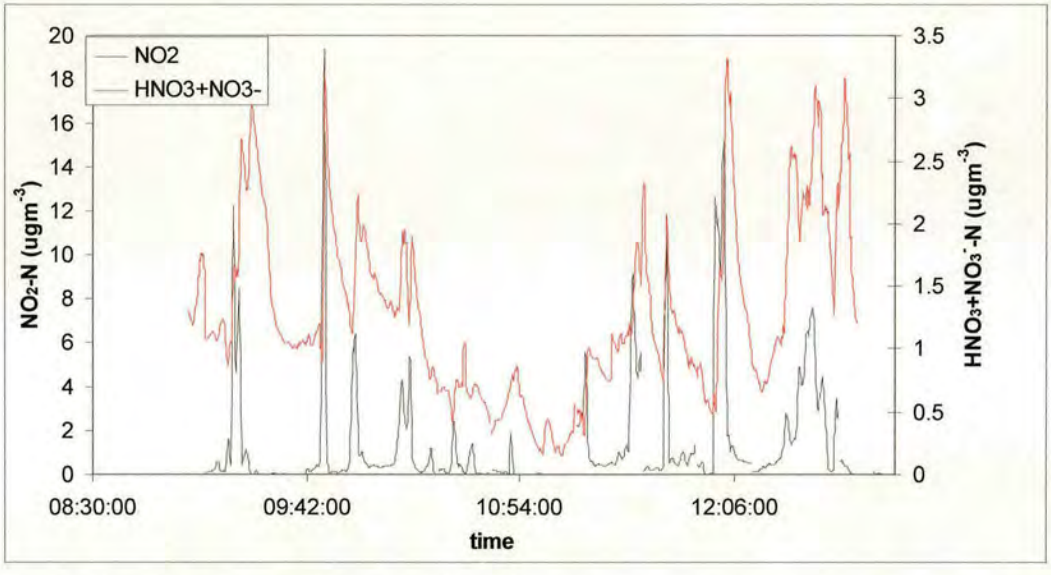

Figure 131. Flight B111 NO_2 and HNO_3+NO_3^- concentration averaged over 1 minute (N μgm^{-3})

Table 35. Oxidation rate of NO_2 to HNO_3+NO_3^- for 8 plumes for flight B111 for northbound leg.

	North West Humberside Power station		Teesside	Newcastle	Central Belt Cockenzie PS	Central Belt Longannet PS	Dundee	Aberdeen
time	09:17:20	09:19:10	09:47:40	09:58:10	10:14:20	10:16:50	10:24:00	10:31:30
NO_2 (N $\mu g\ m^{-3}$)	12.23	8.46	19.44	6.12	4.30	5.19	1.17	2.41
HNO_3+NO_3^- $\mu g\ m^{-3}$)	1.66	2.06	2.59	1.42	1.93	1.43	0.80	0.47
Distance (m)	139000	127000	45000	43000	75000	121000	80000	24000
Wind speed ($m\ s^{-1}$)	4.91	4.91	4.91	4.91	4.91	4.91	4.91	4.91
% oxidised per hour	1.73	2.73	4.60	7.79	7.36	3.16	8.98	11.77

Table 36. Oxidation rate of NO_2 to HNO_3+NO_3^- for 6 plumes for flight B111 for southbound leg.

	London	Midlands	North West Humberside PS	North West Humberside PS	Teesside	Newcastle
time	12:32:30	12:23:50	11:59:50	12:02:10	11:43:00	11:32:30
NO_2 (N µg m^{-3})	7.42	2.60	12.27	15.21	11.84	6.81
HNO_3+NO_3^- (N µg m^{-3})	2.73	1.99	0.59	2.10	1.95	1.63
Distance (m)	170000	233000	81000	84000	45000	38000
Wind speed (m s^{-1})	4.91	4.91	4.91	4.91	4.91	4.91
% oxidised per hour	2.80	3.29	1.00	2.57	5.60	8.97

7.3.5 Oxidation Rates for Flight B113

Figure 132 shows the concentration of SO_2 and SO_4 for flight B113. There are no HNO_3 data for flight B113. Nine plumes were identified for SO_2. Table 37 shows the SO_2 oxidation rates for the power station and industrial plumes and Table 38 shows the oxidation rates for the urban plumes. The rates range from 2.85 % S $hour^{-1}$ for London to 23.01 % S $hour^{-1}$ for Newcastle. Five power station plumes were sampled from the Trent Valley and Humberside. The two Trent Valley power station plumes seem to merge with the small plume from Norwich which may explain the high oxidation rates.

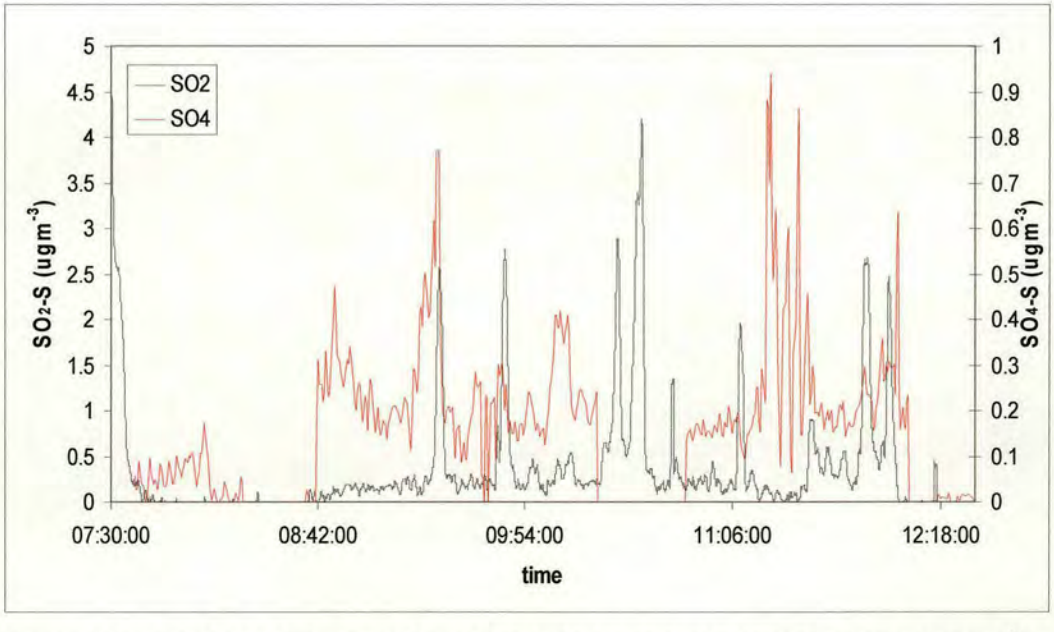

Figure 132. Flight B113 SO_2 and SO_4 concentrations averaged over 1 minute (S µgm^{-3}).

Table 37. Oxidation rate of SO_2 to SO_4 for power station and industrial plumes of flight B113.

	Norwich Cottam PS	Norwich West Burton PS	Teesside	Humberside Drax PS	Humberside Eggborough PS	Humberside Ferrybridge PS
time	10:05:30	10:10:40	11:39:30	11:52:50	11:59:00	12:00:15
SO_2 (S µg m^{-3})	0.45	0.49	0.54	2.60	0.73	2.34
SO_4 (S µg m^{-3})	0.38	0.21	0.18	0.24	0.27	0.28
Distance (m)	235000	198000	115000	128000	168000	182000
Wind speed ($m\ s^{-1}$)	13.81	13.81	13.81	13.81	13.81	13.81
% oxidised per hour	9.74	7.63	10.77	3.23	7.97	2.95

Table 38. Oxidation rate of SO_2 to SO_4 for urban plumes of flight B113.

	Cardiff/ Bristol	London	North West	Newcastle
time	09:24:30	09:47:00	09:58:30	11:35:15
SO_2 (S µg m^{-3})	2.34	2.68	0.32	0.56
SO_4 (S µg m^{-3})	0.40	0.20	0.17	0.19
Distance (m)	228000	120000	321000	55000
Wind speed ($m\ s^{-1}$)	13.81	13.81	13.81	13.81
% oxidised per hour	3.21	2.85	5.40	23.01

7.3.6 Oxidation Rates for Flight B118

Figure 133 shows the concentration of NO_2 and HNO_3+NO_3^- for flight B118. Ten plumes were identified for NO_2 with three sampled on both northbound and southbound legs. Table 39 and Table 40 show the NO_2 oxidation rates. The NO_2 oxidation rates range from 0.55 % N $hour^{-1}$ for the Trent Valley power stations to 16.09 % N $hour^{-1}$ for Norwich.

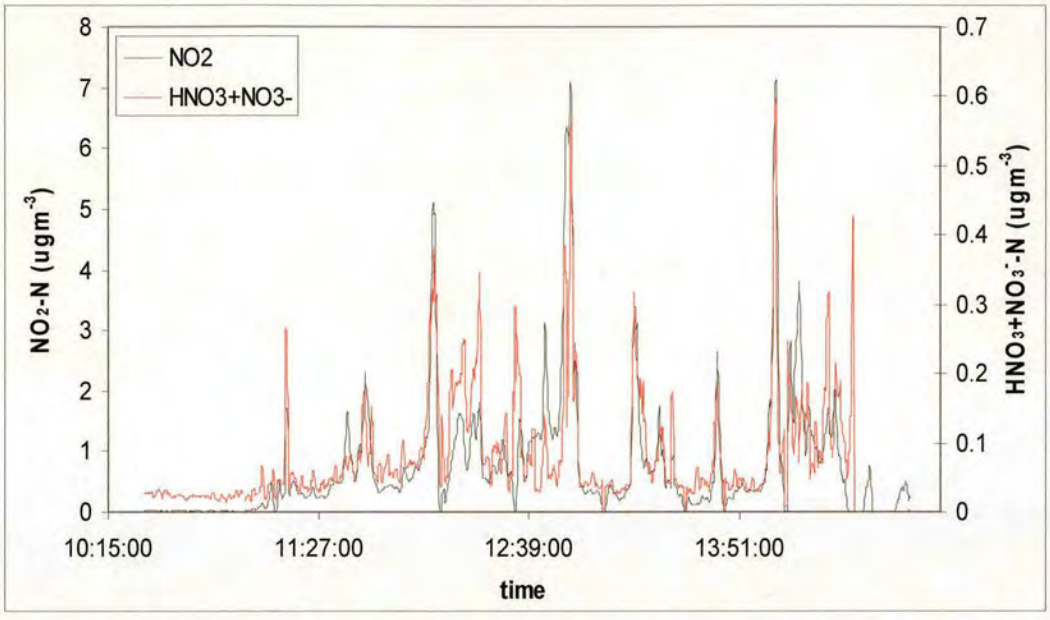

Figure 133. Flight B118 NO_2 and $HNO_3+NO_3^-$ concentrations averaged over 1 minute (N μgm^{-3})

Table 39. Oxidation rate of NO_2 to $HNO_3+NO_3^-$ for plumes of flight B118.

	Cardiff	Bristol	London	Midlands Leicester	Midlands Nottingham	Norwich	North West Trent Valley PS	North West Humberside PS
Time	11:37:00	11:43:00	12:06:40	12:16:30	12:22:20	12:31:40	12:45:00	12:53:40
NO_2 (N $\mu g\ m^{-3}$)	1.59	2.28	4.94	1.48	1.60	0.67	2.91	6.90
$HNO_3+NO_3^-$ (N $\mu g\ m^{-3}$)	0.06	0.13	0.33	0.24	0.30	0.14	0.12	0.57
Distance (m)	173000	158000	118000	222000	224000	36000	159000	117000
Wind speed ($m\ s^{-1}$)	9.41	9.41	9.41	9.41	9.41	9.41	9.41	9.41
% oxidised per hour	0.73	1.17	1.77	2.16	2.37	16.09	0.83	2.19

Table 40. Oxidation rate of NO_2 to $HNO_3+NO_3^-$ for plumes of flight B118.

	Teesside	Newcastle	Teesside	North West Humberside PS	North West Trent Valley PS
Time	13:15:30	13:24:00	13:44:00	14:03:10	14:11:40
NO_2 (N $\mu g\ m^{-3}$)	3.40	1.52	2.23	7.00	3.64
$HNO_3+NO_3^-$ (N $\mu g\ m^{-3}$)	0.28	0.12	0.12	0.56	0.10
Distance (m)	100000	146000	100000	116000	164000
Wind speed ($m\ s^{-1}$)	9.41	9.41	9.41	9.41	9.41
% oxidised per hour	2.61	1.63	1.71	2.16	0.55

7.3.7 Oxidation Rates for Flight B126

Figure 134 shows the concentration of NO_2 and HNO_3+NO_3^- for flight B126. There are no SO_2 data for flight B126. Eight plumes were identified for NO_2 with four sampled on both northbound and southbound legs. Table 41 and Table 42 show the oxidation rates for NO_2, the rates range from 0.94 % N $hour^{-1}$ for Liverpool to 7.66 % N $hour^{-1}$ for Norwich. During the transect of the London plume, two distinct peaks were observed, one with high HNO_3 concentrations and one with low HNO_3 concentrations producing radically different oxidation rates of 7.57 and 1.55 % N $hour^{-1}$. It is possible that the second peak at 12:29 is influenced by emissions from power stations on the Thames resulting in lower oxidation rates and less HNO_3.

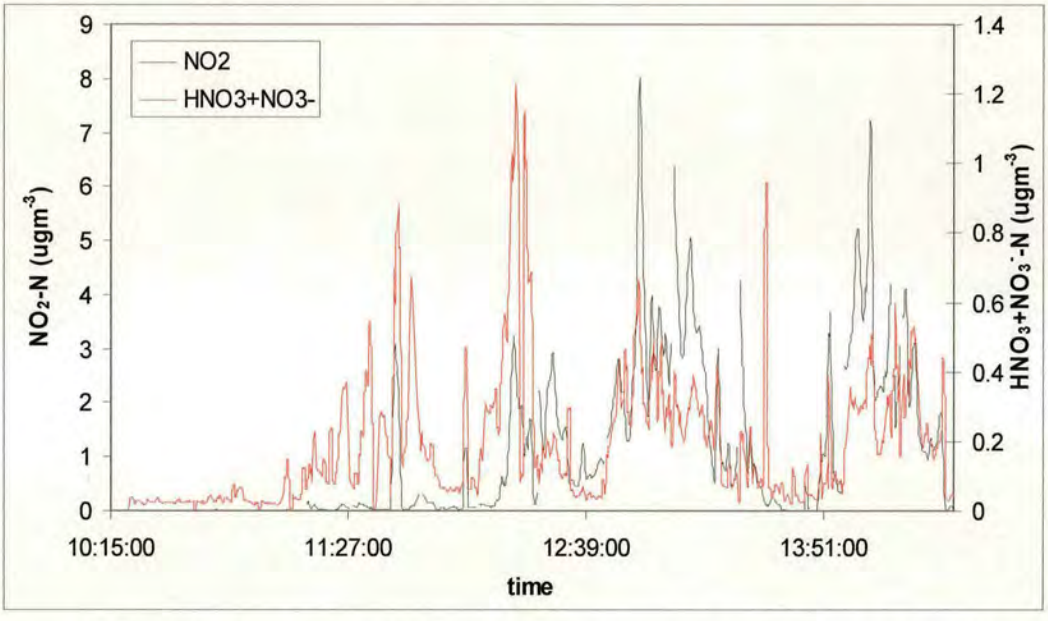

Figure 134. Flight B126 NO_2 and HNO_3+NO_3^- concentrations averaged over 1 min (N μgm^{-3}).

Table 41. Oxidation rate of NO_2 to HNO_3+NO_3^- for plumes of flight B126.

	London		Norwich	Bristol/ Cardiff	Midlands Drax PS	Midlands Eggborough PS	Midlands Ferrybridge F
Time	12:17:20	12:29:10	12:36:20	12:48:50	12:55:00	13:00:50	13:01:30
NO_2 (N $\mu g\ m^{-3}$)	2.96	2.70	0.47	2.75	8.00	3.78	3.65
HNO_3+NO_3^- (N $\mu g\ m^{-3}$)	1.23	0.22	0.04	0.44	0.63	0.40	0.45
Distance (m)	1241000	158000	35000	335000	105000	85000	83000
Wind speed ($m\ s^{-1}$)	8.90	8.90	8.90	8.90	8.90	8.90	8.90
% oxidised per hour	7.57	1.55	7.66	1.33	2.24	3.65	4.28

Table 42. Oxidation rate of NO_2 to HNO_3+NO_3^- for plumes of flight B126.

	North West Manchester	Teesside		North West Manchester	North West Liverpool	Midlands Ferrybridge PS	Midlands Eggborough PS
Time	13:10:40	13:19:00	13:52:30	14:01:10	14:04:50	14:11:10	14:15:50
NO_2 (N µg m^{-3})	4.94	3.03	3.20	5.23	7.24	4.22	3.81
NO_3 (N µg m^{-3})	0.33	0.37	0.39	0.29	0.48	0.25	0.33
Distance (m)	169000	107000	108000	169000	211000	87000	99000
Wind speed (m s^{-1})	8.90	8.90	8.90	8.90	8.90	8.90	8.90
% oxidised per hour	1.20	3.28	3.22	1.00	0.94	2.02	2.59

7.3.8 Oxidation Rates for Flight B130

Figure 135 shows the concentration of NO_2 and HNO_3+NO_3^- for flight B130. There are no SO_2 data for flight B130. Seven plumes were identified for NO_2 with four sampled on the northbound and southbound legs. Table 43 and Table 44 show the NO_2 oxidation rates which range from 2.68 % N $hour^{-1}$ for the power stations in the Trent Valley and the Midlands to 27.99 % N $hour^{-1}$ for Newcastle. Flight B130 is heavily influenced by continental air and so high background concentrations of the oxidation products from European outflow will have increased the estimated oxidation rates.

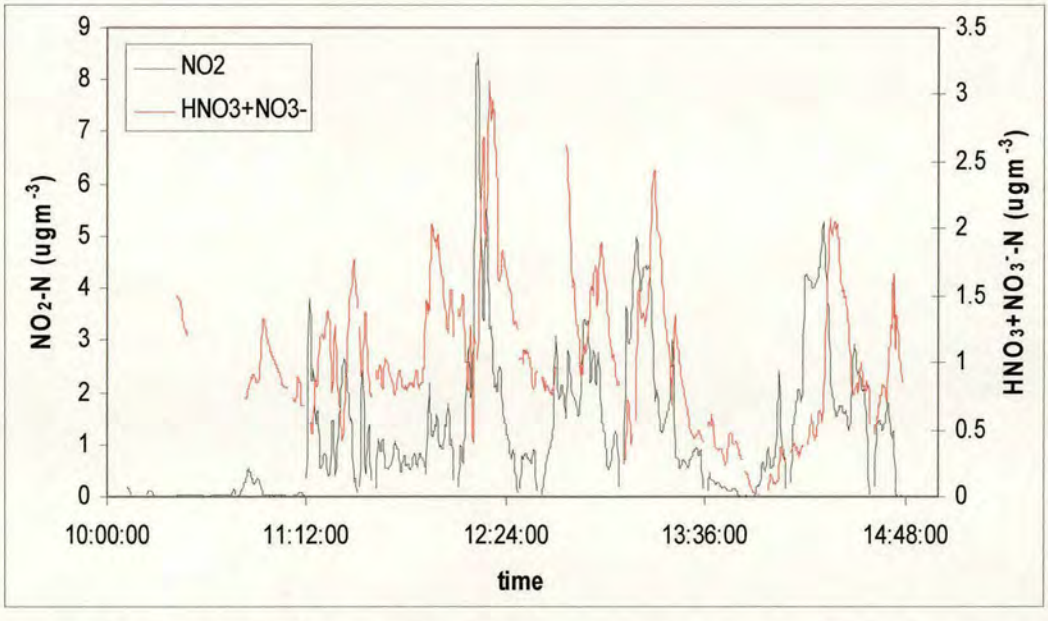

Figure 135. Flight B130 NO_2 and HNO_3+NO_3^- concentrations averaged over 1 min (N μgm^{-3}).

Table 43. Oxidation rate of NO_2 to $HNO_3+NO_3^-$ for plumes on northbound leg of flight B130.

	London	Midlands Trent Valley	Midlands Humberside Power stations			Teesside	Newcastle
Time	12:54:10	13:09:30	13:11:00	13:16:00	13:18:50	13:26:10	13:34:30
NO_2 (N µg m^{-3})	2.80	3.53	4.88	4.33	2.07	2.97	0.78
$HNO_3+NO_3^-$ (N µg m^{-3})	1.34	0.39	0.74	1.76	2.03	1.11	0.45
Distance (m)	200000	121000	80000	83000	90000	45000	43000
Wind speed ($m\ s^{-1}$)	9.12	9.12	9.12	9.12	9.12	9.12	9.12
% oxidised per hour	5.32	2.68	5.41	11.46	17.97	21.91	27.99

Table 44. Oxidation rate of NO_2 to $HNO_3+NO_3^-$ for plumes on southbound leg of flight B130.

	Teesside	Midlands Humberside Power stations			London
Time	14:02:20	14:11:00	14:13:50	14:20:40	14:30:10
NO_2 (N µg m^{-3})	2.16	2.25	4.18	3.04	2.76
$HNO_3+NO_3^-$ (N µg m^{-3})	0.15	0.39	0.52	2.00	0.82
Distance (m)	45000	82000	79000	83000	225000
Wind speed ($m\ s^{-1}$)	9.12	9.12	9.12	9.12	9.12
% oxidised per hour	4.64	5.90	4.62	15.60	3.34

7.3.9 Oxidation Rates for Flight B132

Figure 136 shows the concentration of NO_2 and $HNO_3+NO_3^-$ for flight B132. There are no SO_2 data for flight B132. Nine plumes were identified for NO_2. Table 45 shows the NO_2 oxidation rates of the power station and industrial plumes and Table 46 shows the oxidation rates for the urban plumes. The oxidation rates range from 0.86 % N $hour^{-1}$ for the Cottam power station plume to 1.99 % N $hour^{-1}$ for the Ferrybridge power station plume which sits on top of the plume from the North West of England.

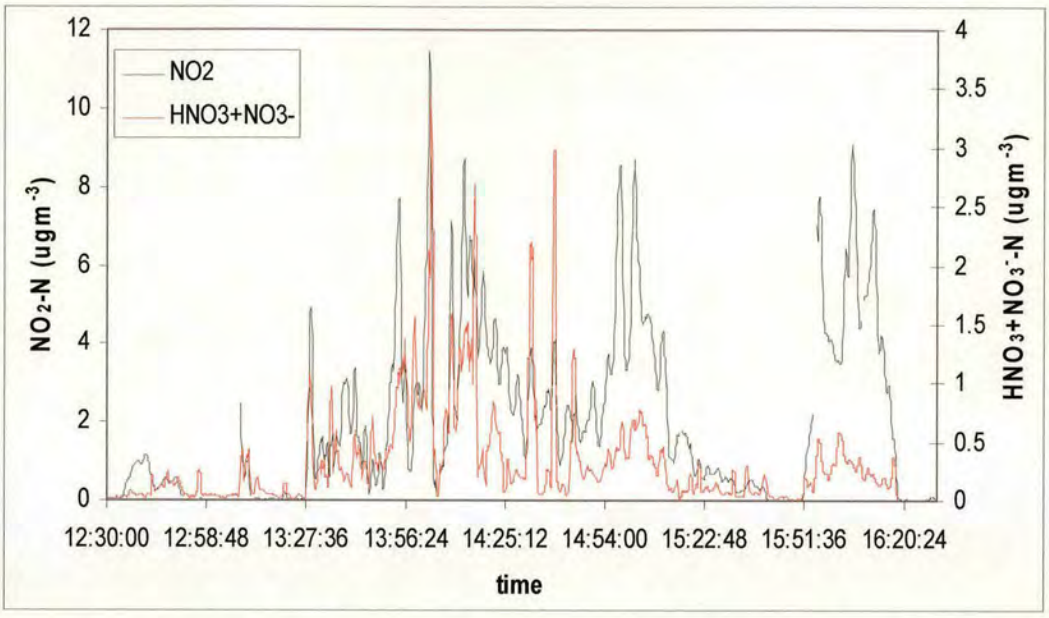

Figure 136. Flight B132 NO_2 and HNO_3+NO_3^- concentrations averaged over 1 min (N μgm^{-3}).

Table 45. Oxidation rate of NO_2 to HNO_3+NO_3^- for power station and industrial plumes of flight B132.

	Midlands Cottam PS	North West West Burton PS	North West Drax PS	North West Eggborough PS	North West Ferrybridge PS	North West Teesside
Time	14:50:40	14:56:30	14:58:30	15:02:30	15:07:00	15:10:40
NO_2 (N μg m^{-3})	2.96	3.78	8.37	8.73	4.60	4.35
HNO_3+NO_3^- (N μg m^{-3})	0.23	0.33	0.48	0.65	0.40	0.45
Distance (m)	174000	148000	100000	88000	83000	112000
Wind speed (m s^{-1})	5.77	5.77	5.77	5.77	5.77	5.77
% oxidised per hour	0.86	1.12	1.12	1.63	1.99	1.74

Table 46. Oxidation rate of NO_2 to HNO_3+NO_3^- for urban plumes of flight B132

	London	Midlands Bristol / Cardiff	Newcastle
Time	14:39:00	14:45:40	15:17:50
NO_2 (N μg m^{-3})	4.07	2.31	1.63
HNO_3+NO_3^- (N μg m^{-3})	2.97	1.22	0.19
Distance (m)	454000	402000	213000
Wind speed (m s^{-1})	5.77	5.77	5.77
% oxidised per hour	1.93	1.79	1.02

7.3.10 Oxidation Rates for Flight B136

Figure 137 shows the concentration of SO_2 and SO_4 for flight B136. There are no HNO_3 data for flight B136. Eight plumes were sample for SO_2. Table 47 shows the SO_2 oxidation rates which range from 0.17 % S hour^{-1} for the Central Belt to 6.37 % S hour^{-1} for London. The plumes from the power stations tend to produce lower oxidation rates than the urban plumes.

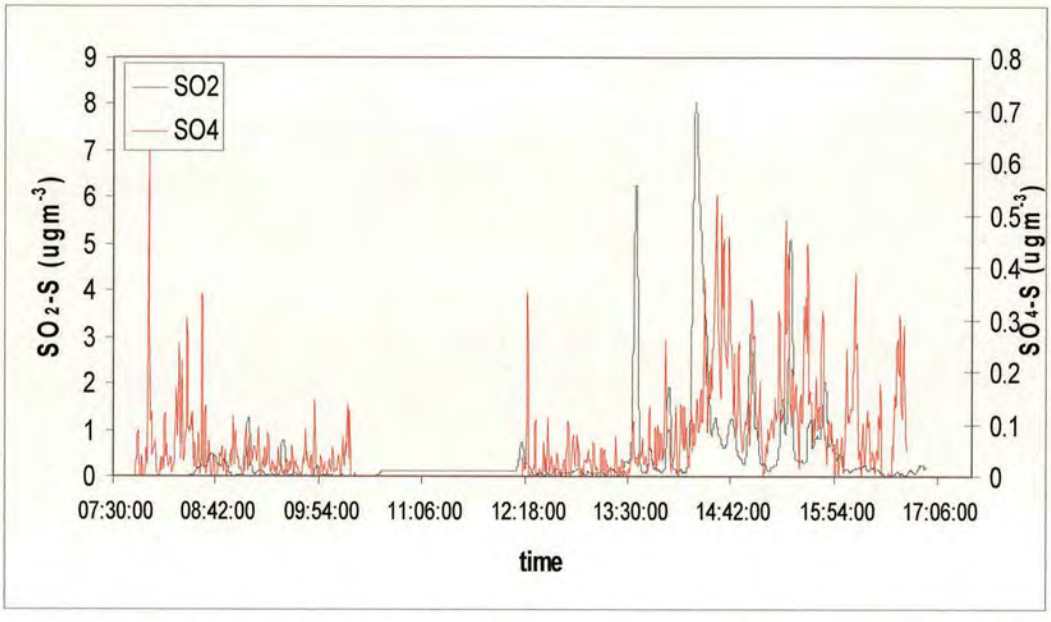

Figure 137. Flight B136 SO_2 and SO_4 concentrations averaged over 1 minute (S µgm^{-3}).

Table 47. Oxidation rate of SO_2 to SO_4^- for 8 plumes for flight B136.

	Central Belt	Teesside	Humberside PS	North West	Midlands	London	Bristol	Cardiff
Time	13:35:50	13:59:30	14:17:50	14:32:15	14:43:50	14:58:15	15:24:15	15:47:15
SO_2 (S µg m^{-3})	6.26	1.78	7.89	1.13	1.16	1.57	4.84	2.06
SO_4 (S µg m^{-3})	0.11	0.09	0.08	0.46	0.12	0.27	0.14	0.10
Distance (m)	145000	83000	147000	293000	261000	111000	145000	168000
Wind speed (m s^{-1})	11.45	11.45	11.45	11.45	11.45	11.45	11.45	11.45
% oxidised per hour	0.50	2.52	0.27	5.73	1.61	6.37	0.81	1.19

7.4 Summary and Conclusion

The oxidation rates of NO_x and SO_2 in urban, power station and industrial plumes were calculated by determining the travel time of the observed air and the relative concentrations of the emitted and oxidised pollutants. Table 48 shows the NO_2 oxidation rates for each flight for the power station and industrial plumes and Table 49 shows the rates for the urban plumes. Flight B130 is included in the table but has been excluded from the final analysis due the continental inflow. The NO_x oxidation rates range from 0.45 % N $hour^{-1}$ for a power station plume to 16.9 % N $hour^{-1}$ for the Norwich plume. Overall the plumes from power stations and industrial sources have smaller oxidation rates than urban plumes with plumes from power stations in the Trent Valley having the smallest average oxidation rate of 0.9 ± 0.56 % N $hour^{-1}$. Of the plumes measured on at least three flights, the Newcastle plume has the largest average oxidation rate of 5.1 ± 3.23 % N $hour^{-1}$.

Table 50 shows the SO_2 oxidation rates for each power station and industrial plume for each flight and Table 51 shows the urban plumes. The oxidation rates range from 0.3 % S $hour^{-1}$ to 23 % S $hour^{-1}$. Of the plumes measured on at least three flights, the Humberside power stations have the smallest average oxidation rate of 4.3 ± 3.17 % S $hour^{-1}$ and the Newcastle plume has the largest average oxidation rate of 15.8 ± 11.80 % S $hour^{-1}$.

The power station plumes tended to sit in the outflow from urban centres. Analysis of the Humberside power stations shows that when the plume was influenced by outflow from the Midlands, the NO_x oxidation rate tended to be higher at 2.8 ± 0.94 % N $hour^{-1}$ compared to when it was influenced by the plume from the North West of England which produced an average oxidation rate of 1.7 ± 0.65 % N $hour^{-1}$. On the single occasion where the power station plume was isolated from both the North West and Midlands plume the NO_x oxidation rate was significantly smaller at 0.7 % N $hour^{-1}$. Similarly for SO_2, when the power station plumes are influenced by urban outflow from the North West, the average oxidation rate is higher at 5.0 ± 3.33 % S $hour^{-1}$ compared to when the plumes are isolated with a rate of 3.1 ± 3.02 % S $hour^{-1}$. The plumes from the Humberside power stations produced an average NO_x oxidation rate of 1.8 ± 0.88 % N $hour^{-1}$ and SO_2 oxidation rate of 4.3 ± 3.17 % S $hour^{-1}$.

The Trent Valley power stations plume sat in the Midlands outflow on all except one occasion. Excluding this flight from the analysis produces a NO_x oxidation rate for the combined Trent Valley and Midlands plume of 1.0 ± 0.65 % N $hour^{-1}$. The SO_2 plumes from the Trent Valley power stations were influenced by the Midlands plume on one occasion and produced an average oxidation rate of 2.0 ± 0.02 % S $hour^{-1}$. When the plumes from the Trent Valley power stations mixed with the outflow from Norwich a much larger oxidation rate of 8.7 ± 1.49 % S $hour^{-1}$ was found.

The plumes from power stations in the Central Belt of Scotland were heavily influenced by the urban plume from Glasgow. This resulted in a significantly higher NO_x oxidation rate of 5.1 ± 3.94 % N $hour^{-1}$. However, a NO_x oxidation rate of 0.9 % N $hour^{-1}$ is found for a plume from the Longannet power station for flight B112 where the plume may be isolated from the urban outflow. SO_2 plumes from these power stations were identified on only one flight producing an oxidation rate of 6.5 ± 3.57 % S $hour^{-1}$, higher than the rates from the Humberside and Trent Valley power stations.

The Teesside plume is a mainly industrial plume. This plume was isolated for all the flights bar B136 where the plume from the North West mixes with the Teesside outflow. Excluding this plume from the analysis produces an average NO_x oxidation rate of 3.6 ± 1.28 % N $hour^{-1}$ and a SO_2 oxidation rate of 6.6 ± 3.87 % S $hour^{-1}$. Where the plume from the North West mixes with the Teesside plume, the NO_x oxidation rate falls to 1.4 ± 0.44 % N $hour^{-1}$.

The urban plumes produce larger average oxidation rates for NO_x of 4.4 ± 3.94 % N $hour^{-1}$ and SO_2 of 6.5 ± 5.71 % S $hour^{-1}$, than the power station and industrial plumes. The variation between plumes is greater with NO_x oxidation rates ranging from 0.6 to 16.1 % N $hour^{-1}$ and SO_2 oxidation rates ranging from 0.5 to 23 % S $hour^{-1}$. However with the exception of a few plumes which produced extremely small oxidation rates and may be mixed with power station or industrial plumes, the urban plumes produce larger oxidation rates than the power station plumes. The plume from London which is typically an isolated and easily identified plume was measured on a number of flights. The oxidation rates for both NO_x and SO_2 show more consistency between flights than some other less well defined plumes. The average NO_x oxidation rate for the London plume is 3.9 ± 2.91 % N $hour^{-1}$ and the average SO_2 oxidation rate is 4.6 ± 1.3 % S $hour^{-1}$. The Newcastle plume is also an easily identified and isolated plume.

The Newcastle plume has particularly high SO_2 oxidation rate of 15.8 ± 11.80 % S $hour^{-1}$. The NO_x oxidation rate of 5.1 ± 3.23 % N $hour^{-1}$ for the Newcastle plume is also larger than other urban plumes.

Larger oxidation rates in urban plumes than power station plumes are not unexpected due to differences in oxidant availability. Oxidant supply in power station plumes can be limited by the reaction of NO with O_3 in the core of the plume which suppresses oxidation. In urban areas, emissions of VOCs are an alternative source of O_3, increasing the supply of oxidants resulting in larger oxidation rates (Hewitt, 2000). This is consistent with the results of this work which show consistently larger oxidation rates for urban plumes than power station plumes for both NO_x and SO_2.

Analysis of the plume composition by comparing the NO_2/CO and SO_2/CO ratios of the power station and urban plumes shows that the urban plumes have smaller CO concentration relative to NO_2 and SO_2. Emissions of CO tend to be higher in urban areas due to incomplete combustion in car engines. The combustion process in power stations is more efficient producing relatively less CO. The ratios NO_2/CO and SO_2/CO are expected to be lower for urban plumes due to relatively larger CO emissions. The average NO_2/CO ratio for a power station plume is 1.4 compared to 0.7 for an urban plume and the average SO_2/CO ratio for a power station plume is 0.5 compared to 0.3 for an urban plume with smaller values for urban plumes as expected.

Table 48. Oxidation rates of NO_2 to $HNO_3+NO_3^-$ (% N oxidised per hour) of power station and industrial plumes with the average and standard deviation (σ) for each plume. * In North West England plume. ** In Midlands plume.

	Humberside Power Stations				Trent Valley Power Stations			Teesside	Central Belt of Scotland Power Stations	
	Drax	Egg	Ferry	Merged	Cottam	West Burton	Merged		Cockenzie	Longannet
B92				0.73						
B97				2.07**		2.07**				
B102	0.62*	1.91*	2.85*					3.22		
B111 N B111 S	1.73* 1.00*	2.73* 2.57*						4.6 5.6	7.36	3.16
B112 N B112 S	1.11* 1.62*	1.93* 1.56*	1.36* 1.218					4.82	5.89 8.02	0.90
B118 N B118 S				2.19* 2.16*			0.83* 0.55*	2.61 1.71		
B126 N B126 S	2.24**	3.65** 2.59**	4.28** 2.02**					3.28 3.22		
B130 N B130 S	5.41** 5.90**	11.46** 4.62**	17.97** 15.60**				2.68**	21.91 5.32		
B132 N B132 S	1.12* 0.60*	1.63* 0.79*	1.99* 1.27*		0.86** 0.50**	1.12** 0.45**		1.74* 1.12*		
Average	1.26	2.15	2.14	1.79	0.68	1.21	0.69	3.19	7.09	2.03
σ	0.57	0.83	1.11	0.71	0.25	0.81	0.20	1.47	1.09	1.60

Table 49. Oxidation rates of NO_2 to $HNO_3+NO_3^-$ (% N oxidised per hour) for urban plumes with the average and standard deviation (σ) for each plume.

	Cardiff	Bristol	London	Norwich	Midlands	NW England	Newcastle	Miscellaneous
B92	9.4		4.06		4.82	2.22		
B97			1.69			1.05		
B102			3.71		1.73		6.23	
B111 N B111 S			2.8		3.29		7.79 8.97	8.98 Dundee 11.77 Aberdeen
B112 N B112 S			1.18 6.35		0.62		4.99	
B118 B118	0.73	1.17	1.77	16.09			1.63	2.16 Leicester 2.37 Nottingha
B126 N B126 S	1.33	1.33	7.57 1.55	7.66		1.2 1, 0.94		
B130 N			17.97				27.99	
B132 N	1.79		1.93		1.79		1.02	
Average	3.31	1.25	3.26	11.88	2.45	1.44	5.11	
σ	4.08	0.11	2.18	5.96	1.63	0.68	3.23	

Table 50. Oxidation rates of SO_2 to SO_4 (% S oxidised per hour) of urban and industrial plumes with the average and standard deviation (σ) for each plume. * In North West England plume. ** In Midlands plume. *** In Norwich plume.

	Humberside Power Stations				Trent Valley Power Stations		Teesside	Central Belt of Scotland Power Stations	
	Drax	Egg	Ferry	Merged	Cottam	West Burton		Cockenzie	Longannet
B92				0.95					
B97				2.94**	2.04**	2.01**	9.27		
B102	2.02*	5.80*	1.81*	1.68*			2.44		
B112 N B112 S	6.54* 5.13*	10.11* 10.77*	2.57* 3.84*				7.77	5.38 3.53	10.43
B113	3.23	2.95	7.97		9.74***	7.63***	10.77		
B136							2.52		
Average	4.23	7.41	4.05	1.46	5.89	4.82	6.55	4.46	10.43
σ	2.00	3.70	2.75	1.14	5.44	3.97	3.87	1.31	

Table 51. Oxidation rates of SO_2 to SO_4 (% S oxidised per hour) for urban plumes with the average and standard deviation (σ) for each plume.

	Cardiff	Bristol	London	Midlands	North West England	Newcastle	Miscellaneous
B92			3.78	3.63	2		
B97			5.04				6.07 Leicester 7.00 Nottingham 17.51 Norwich
B102			6.16	3.86		2.16	
B112 N B112 S			3.89 4.30	6.32 7.5		22.15	
B113	3.21	3.21	2.85		5.4	23.01	
B136	1.19	0.81	6.37	1.61	5.73		0.5 Central Belt
Average	2.20	2.01	4.63	4.58	4.38	15.77	
σ	1.43	1.70	1.30	2.33	2.06	11.80	

Table 52 shows the average oxidation rates for NO_x and SO_2 for three other studies compared to the AMPEP oxidation rates for power station and urban plumes. Relatively little work has been done on NO_x oxidation rates compared SO_2 so the rates are based entirely on single plumes. Likewise, fewer studies have been done on the oxidation rates of urban plumes. The rates from Hewitt (2000) are from only two cities, Milwaukee and Budapest while the Bamber *et al.* (1984) SO_2 oxidation rate is for a single day for a plume from the North West of England and the Midlands.

The AMPEP SO_2 oxidation rate for urban plumes is consistent with rates found for urban plumes in other studies. However Hewitt (2000) concludes that the NO_x oxidation rate should exceed the SO_2 rate where aqueous chemistry does not provide an alternative pathway for SO_2 oxidation as should mostly be the case for AMPEP. The average NO_x oxidation rates for AMPEP are smaller than the SO_2 rates for both power station and urban plumes and significantly lower than the 23 % N hr^{-1} and 27

% N hr^{-1} for power station plumes from Springston *et al.* (2005) and Hewitt (2000) respectively. The AMPEP NO_x average oxidation rate for power plants plumes of 1.4 ± 0.66% N hr^{-1} is consistent with the rate of Tsuang *et al.* (2003) of 0.75 % N hr^{-1}.

Table 52. Oxidation rates of power station and urban plumes found in other studies compared to AMPEP oxidation rates for NO_x and SO_2.

	Power Station (Springston *et al.*, 2005)	Power Station (Hewitt, 2000)	Power Station (urban) (Tsuang *et al.*, 2003)	Power Station AMPEP	Urban (Bamber *et al.*, 1984)	Urban (Hewitt, 2000)	Urban AMPEP
SO_2 (% per hour)	3	2.3	7.8	4.8 ± 0.76	2 (5.3 cloud)	4, 10	6.5 ± 5.71
NO_x (% per hour)	23	27	0.75	1.4 ± 0.66			4.4 ± 3.95

For the purposes of atmospheric models, an average oxidation rate for the whole of the UK was calculated by weighting the average rate for the power station, urban and industrial plumes by the relative contribution of the sources to overall UK emissions. Urban emissions were assumed to be from traffic which contribute to 41 % of overall UK emissions for NO_x and 6 % for SO_2. Emissions from industrial sources contribute to 18 % of overall emissions for NO_x and 22 % for SO_2 and emissions from energy generation (power stations) contribute to 28 % of overall emissions for NO_x and 66 % for SO_2 (Baggott *et al.*, 2005). Emissions from other sectors are small in comparison to the three largest sources. The weighted average oxidation rate for NO_x is 3.2 ± 2.38 % N hr^{-1} and for SO_2 the weighted average oxidation rate is 5.3± 1.80 % S hr^{-1}.

Chapter 8 Discussion and Recommendations

8.1 Overview

"Warming of the climate system is unequivocal, as is now evident from observations of increases in global average air and ocean temperatures, widespread melting of snow and ice, and rising global average sea level" (IPCC AR4, 2007).

The issues of climate change make the quantification of greenhouse gas emissions of crucial importance. However the methodology as set out by the IPCC has yet to be formally verified. The UK provides an opportunity to validate the methods used to estimate annual emissions using a boundary layer budget approach which can produce a direct measurement of the emitted flux. The focus of the science is the degree to which this ambitious objective can be met for greenhouse gases. The technique used also allows for the measurement of a range of other species including sulphur and nitrogen compounds from which oxidation rates for outflow plumes can be estimated for use in atmospheric chemistry models.

The main aims of this project were to (1) determine the total UK emissions of CO, CO_2, CH_4 and N_2O using a 'top-down' approach as a means of validating the official estimates compiled by the National Atmospheric Emissions Inventory (NAEI) and (2) to derive oxidation rates of sulphur and nitrogen species in UK plumes. This was done by measuring the upwind and downwind concentrations of all four non-reactive species as well as SO_2, SO_4^{2-} and the NO, NO_2, HNO_3, NO_3^- using the Facility for Airborne Atmospheric Measurements (FAAM) aircraft. Using a boundary layer budget approach where it is assumed that all emissions from the UK are trapped within the boundary layer, it was possible to calculate the emitted flux directly from the difference between the upwind and downwind fluxes. Atmospheric transports models allowed for more sophisticated analysis, including validation of the mapped emissions inventories by forward and inverse modelling techniques.

The United Kingdom is ideally suited for the application of a boundary layer budget approach for calculating national emissions as shown in Figure 138. As an island located in the eastern Atlantic, a well-coupled westerly wind flow with a temperature inversion at the top of the boundary layer produces relatively uniform background conditions in upwind air against which the enhancement from the UK alone can be measured. The size of the UK allows for well-coupled air flow across the whole country with a travel time for an air parcel of only 1-2 days. This is essential to allow the outflow to be identified and measured and allows chemical processes to be neglected for CO, CO_2, CH_4 and N_2O as their reaction timescales in the atmosphere are much longer than the crossing timescale. The UK is also small enough that an aircraft can circumnavigate most of the country in a single day. Refuelling is necessary to achieve this and further lengthens the experiment.

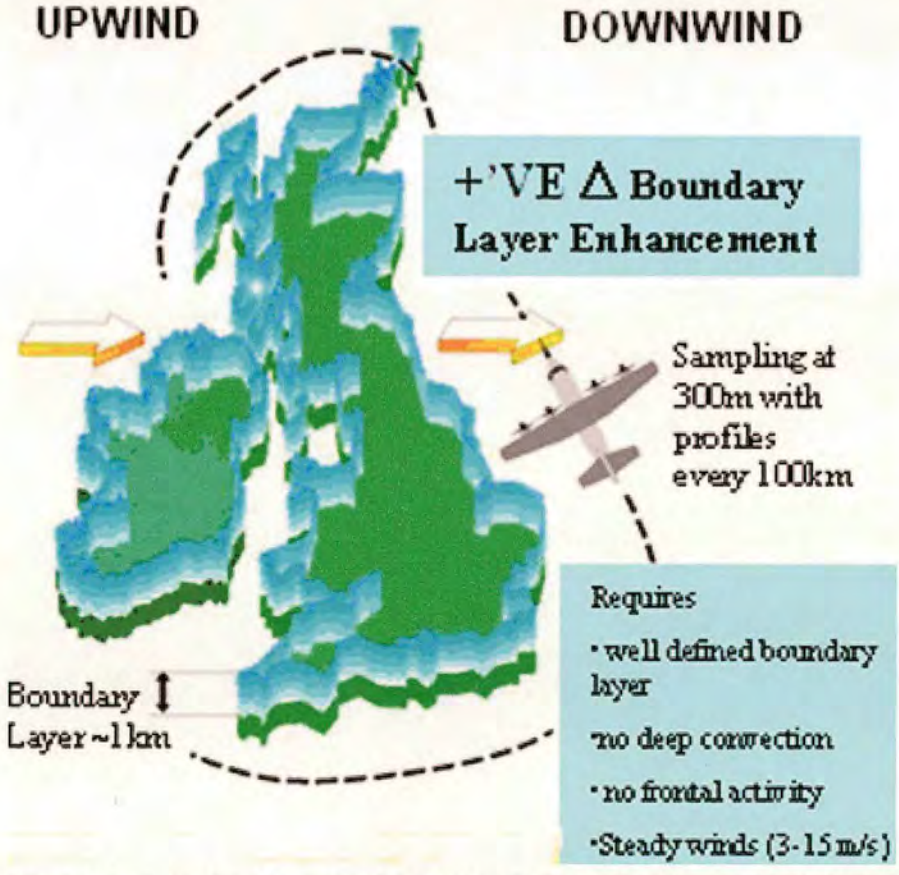

Figure 138. Boundary Layer budget approach for estimating total UK emissions.

8.1.1 Boundary Layer Budget

Given the necessary conditions, the background concentration could be estimated by sampling a small section of the upwind air assuming the background concentration was uniform in a westerly wind flow. The entire outflow was sampled and outflow concentration summed across the whole outflow region to given the total outflow mass. Assuming the size of the inflow region is equal to the size of the outflow region, the total inflow mass could also be calculated. It was assumed that in steady well-coupled condition the wind flow across the country was constant allowing an average wind speed and direction to be calculated from meteorological data from the Met Office Unified Model. This was then used to calculate the total UK emitted flux by subtracting the inflow flux from the outflow flux.

In total 14 viable days of data were collected. For CO and CH_4 scaling up from a small number of flights should provide a reasonable measurement for the total annual emissions as variation in source emissions between days should be relatively small. For CO_2, although a strong seasonal cycle is to be expected in the biogenic flux, the annual biogenic flux is considerably smaller than the anthropogenic flux. For N_2O, the relatively small number of days is bigger problem as N_2O is considerably more variable from day to day, depending strongly on rainfall and temperature. The N_2O estimates of annual emissions are therefore less reliable than for the other species.

To analyse the measured concentrations of GHG, a Lagrangian transport model, Numerical Atmospheric Modelling Environment, (NAME), of the UK Met Office was applied. To verify the NAEI spatially disaggregated emissions inventory for CO, CO_2, CH_4 and N_2O, the mapped emissions were used as the emissions data in the model and the predicted outflow compared with the measurements. It was also possible to use a more complex model iteration and Bayesian calibration technique to calculate the total UK emissions by iteratively fitting the UK emissions to produce a best-fit between the modelled and measured concentrations. Running NAME with the emissions for each source sector and summing the contribution for each sector produced the total UK outflow concentration as predicted by the emissions inventories. Assuming a linear relationship between the emissions and the outflow concentration allowed the concentration from each sector to be altered by multiplying

by some factor of the total emissions from that sector. This provided a means of fitting the modelled concentration to the measured concentration by altering the total emissions from each sector. The best fit emissions for each sector could then be summed to produce a new total for the total UK emissions. By using a Bayesian Calibration technique where the probability distribution for the estimated total emissions could be used in combination with the likelihood function for the emissions given the measured data, a pdf of the total UK emissions was produced which both fine-tuned the emission estimate and provided a measure of the uncertainty.

The results of the NAME modelling for CO show that the technique is both viable and that the CO emissions are well understood. Figure 139 shows the modelled and measured concentrations for flight B134 mapped with the outflow plumes for the NAME model coinciding with the peak concentrations in the measured samples. Figure 140 shows the modelled and measured concentrations along the flight path. The NAME model is able to accurately predict the CO outflow concentration for all flights. The mapped CO emissions are therefore likely to accurately represent the actual annual UK emissions and the NAME model using the NAEI mapped emissions and the Unified Model meteorological data is able to accurately simulate the transport of pollutants and predict the outflow concentrations. The results of the budget analysis for CO produced similar values for the total annual UK emissions for both the simple box model method and the model iteration technique. Both estimates are also similar to the current NAEI estimate for the annual emissions. The simple box model method estimate is 2900 ± 880 kt yr^{-1}. This compares to an iteration method estimate of 2400 ± 250 kt yr^{-1}. The NAEI estimate for CO is 2400 kt yr^{-1} for 2005 with an uncertainty of 20%. Given that the NAEI emissions have been shown to be accurate using the forward modelling, the similarity between the NAEI, simple boundary budget and model iteration estimates validates both approaches.

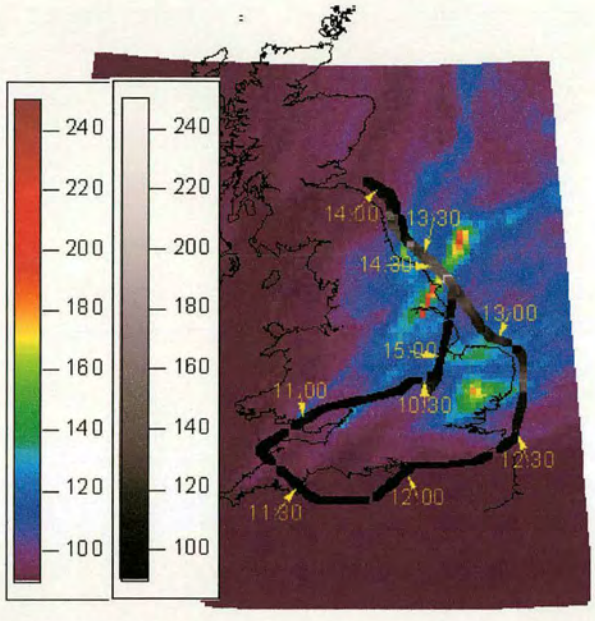

Figure 139. NAME concentration map (ppb) for flight B134 at 12:00 26/09/05 (rainbow) with sample concentration (grey) overlaid for CO (ppb) with aircraft times.

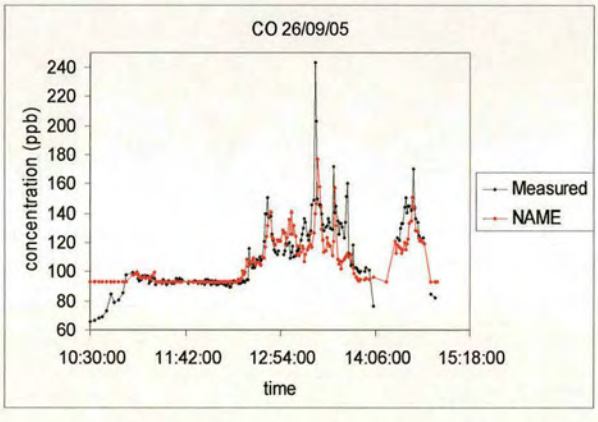

Figure 140 Measured (black) and NAME (red) sample concentration for flight B134 for CO (ppb).

For CO_2 the NAME model was adapted to include photosynthesis and respiration which allowed the biogenic flux to be estimated. This was found to be small compared to the anthropogenic flux with an average annual uptake of 1.8 Mt yr^{-1}. This is small compared to the expected annual uptake of CO_2 which is estimated at 28 Mt yr^{-1} (Milne *et al.* 2006). This is most likely due to a combination of the method used to estimate photosynthesis which is dependent on radiation flux and the small number of days for which the model was run. If the model predicted relatively low radiation flux for a few summer days as it did for July and August flights, then the uptake for the whole summer is underestimated resulting in an underestimation of the total annual uptake. For CO_2 the NAME model was able to accurately predict the outflow concentrations for most of the flights suggesting the mapped CO_2 and total annual emissions for CO_2 are accurate. The simple box model method produced an annual emission estimate of 689 ± 282 Mt yr^{-1}. The model iteration method produced an annual estimate of 514 ± 65 Mt yr^{-1}. The NAEI estimate for CO_2 for 2005 is 555 Mt yr^{-1} with an uncertainty of only 2%. Both methods produce estimates for the annual UK emissions within the uncertainty of estimate and the three estimates are in good agreement suggesting that the current CO_2 emissions are accurate.

For CH_4, the model concentrations tend to underestimate the measured outflow concentrations. The quality of the CH_4 data varied greatly between flights due to problems with the instrument, however even where the quality of the CH_4 is good, the NAME model still tends to underestimate the outflow as can be seen in Figure 141 which shows the CH_4 concentrations from flight B244 where the broad plume between 12:00 and 13:00 is significantly underestimated by the model. This suggests that the actual emissions are underestimated by the mapped emissions. Both the simple box model and model iteration methods produce estimates for the annual emissions that are significantly larger than the current NAEI estimate. The simple box model estimate was 3900 ± 2100 kt yr^{-1}. The model iteration estimate is 3300 ± 1000 kt yr^{-1}. Both are larger than the NAEI estimate of 2400 kt yr^{-1} and outside the NAEI uncertainty of 21 %. Due to the poorer data quality on many of the flights, the uncertainty in the estimates is larger than for CO and CO_2 for both methods. However given the agreement between the two methods and the underestimation of the outflow

concentration by the model, it seems likely that the current NAEI emissions underestimate the actual UK emissions on the flight days.

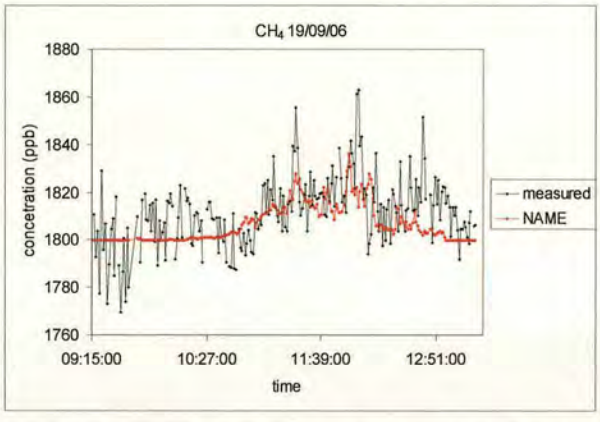

Figure 141. Measured (black) and NAME (red) sample concentration for flight B244 for CH_4 (ppb).

For N_2O, the data quality also varied between flights, though not to the extent of CH_4. The forward modelling in NAME also tended to underestimate the measured outflow suggesting that the mapped emissions did not accurately represent the actual UK emissions. The annual emissions calculated by the simple box model method of 300 ± 216 kt yr^{-1} are in good agreement with the model iteration method emissions of 330 ± 105 kt yr-1. Both estimates are significantly larger than the NAEI estimate for 2005 of 130 kt yr^{-1}. The uncertainty in the NAEI emissions is very large at 230 %. This is due to the variability of N_2O emissions due to their dependence on rainfall and temperature (Bouwman, 1995). Although the 'round-Britain' estimates for the N_2O emissions are significantly larger than the NAEI estimate, the time of year when sampling occurred was not expected to be during peak emissions. This was likely to be earlier in the year when farmers were applying mineral fertiliser. The rainfall during the summer of 2005 was also below average which should have suppressed emissions as the N_2O emissions from the bacteria in soil is larger when heavy rainfall creates anaerobic conditions. Therefore although N_2O emissions are very temporally variable and may be expected to be lower during the colder winter months, there is evidence that the annual UK emissions are underestimated in the current NAEI inventory.

Based on the results of CO and CO_2, the model iteration technique is the more accurate method and so the final AMPEP emissions estimates are the values derived using this approach. The final annual emissions as estimated from the AMPEP data are shown in Table 53 along with the NAEI emissions and estimates from Manning *et al.* (2006) and Bergamaschi (2005). For CO the AMPEP, NAEI and Manning estimates are all in good agreement as are the AMPEP and NAEI estimates for CO_2. However the CH_4 estimates are not in such good agreement with AMPEP, Manning and Bergamaschi all finding emissions larger than those in the current NAEI inventory, but of varying amounts. The AMPEP N_2O emissions are larger than both the NAEI and Manning estimates with the Manning emissions only slightly larger than those of the NAEI. Although the difference between the NAEI emissions and those found in other studies varies, the findings of Manning and Bergamaschi are consistent with the findings of AMPEP that suggests that the NAEI emissions for CH_4 and N_2O may underestimate the actual emissions.

Table 53. Annual UK emissions for 2005 as estimated from the AMPEP data, the NAEI methodology, Manning *et al.*, (2006) and Bergamaschi *et al.*, (2006) for 2004.

study	AMPEP	NAEI	Manning *et al.*, (2006)	Bergamaschi *et al.*, (2005)
year	2005	2005	2005	2004
CO (kt yr^{-1})	2400	2400	2700	
CO_2 (Mt yr^{-1})	514	555		
CH_4 (kt yr^{-1})	3300	2400	2700	4210
N_2O (kt yr^{-1})	330	130	141	

8.1.2 Inverse Modelling

An inverse modelling technique was used to derive spatially disaggregated emissions from the measured concentrations. This involved running the NAME model in backwards mode to reverse the transport of air and derive which grid boxes the measured air travelled through and what influence each box had on the measured air sample. By combining observations for each flight and iteratively fitting the modelled and observed concentrations by altering the emissions from each grid box, new emission maps were produced. To produce an average from all flights, the observations from all flights could be combined and the inverse performed for the combined dataset. Alternatively the inversion could be performed on individual flights and the maps averaged to produce the annual emission map. The advantage of the first approach is that by combining the observations for different days, the variety in the wind flow compensates for bias in the map produced by nearby sources masking the signal of sources far away. The disadvantage of this approach is that individual days can not be weighted to account for varying data quality between flights. For CO and CO_2 this was not a problem as data quality remained uniform for the campaign. For CH_4 and N_2O, weighting and averaging individual flights produced a better estimate for the total emissions due to the variety in data quality. The combined observation maps give an indication of where large emissions are expected, though the scale of the emissions is not accurate.

The results for CO and CO_2 show that this technique is viable and can be used to produce spatially disaggregated emissions. The map for CO emissions is shown in Figure 142 (a) and the NAEI mapped emissions are shown in Figure 142 (b).

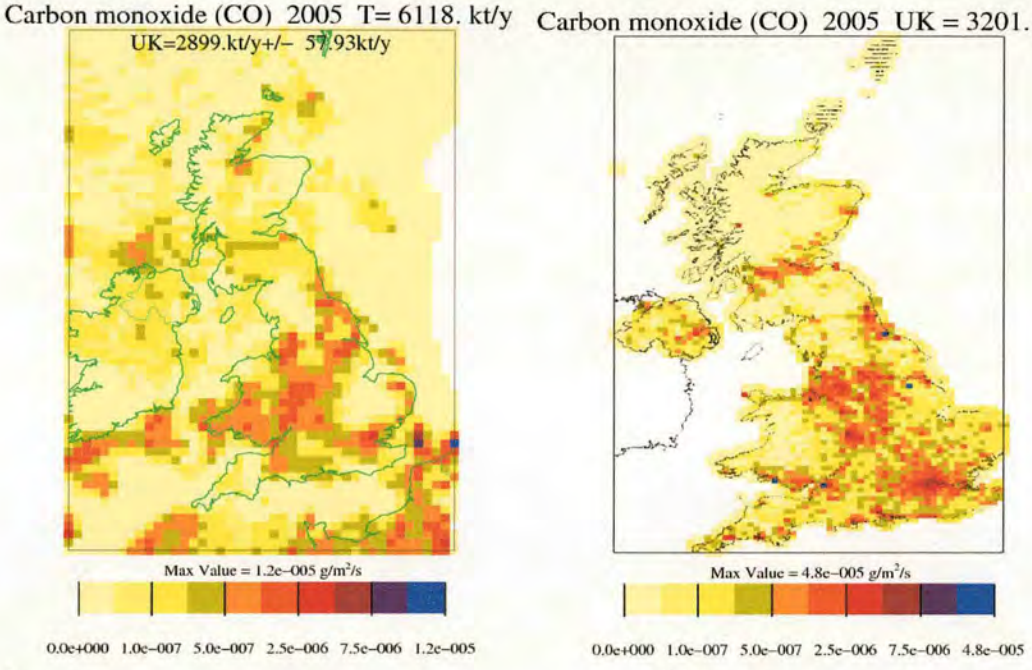

Figure 142. (a) Average CO emissions (g m^{-2} s^{-1}) of 3 inversion solutions using combined observations excluding flights B111, B130 and B247, at resolution 1×1 boxes and unrestricted domain. T = total for whole domain, UK = total for UK ± standard deviation for total UK emissions from 3 inversion solutions. (b). NAEI CO emissions at 10km resolution for 2004.

The inversion is able to capture the majority of the CO emissions from London, the Midlands, the North West of England and Teesside showing that given reliable data, a suitable number of flights and some variety in the wind direction, the inversion technique can be used to produce spatially disaggregated emissions. The total UK emissions produced by this method of 2899 kt yr^{-1} is also in good agreement with other estimates.

For CO_2 the inversion technique was altered to allow negative fluxes to represent photosynthesis. The inversion was able to produce spatially disaggregated emissions for CO_2 that are in good agreement with the current NAEI emissions maps with emissions concentrated around urban areas of London, the Midlands, the North West of England and Teesside. The total CO_2 emissions produced were 620 Mt yr^{-1} with a sink of 11 Mt yr^{-1}.

Due to the number of flights with poorer quality data for CH_4 and N_2O, the spatial disaggregation in the maps was less reliable than for CO and CO_2. The weighted

average technique was therefore used to produce the final maps, this however introduced a bias in the maps with larger emissions assigned to the east coast where the observations were concentrated. The total emissions for the UK are expected to be accurate as individual flights could be weighted to reflect the quality of the data.

For CH_4, the inversion was further constrained by forcing emissions into the land only. This resulted in an increase in emissions from the UK due to increased uncertainty within the UK grid boxes. However the increase of 500 kt yr^{-1}, from 3500 ± 668 kt yr^{-1} for the unrestricted domain to 4000 ± 829 kt yr^{-1} for the restricted domain, is within the uncertainty of the emission estimate of both estimates. The value of 3500 kt yr^{-1} for the unrestricted domain is a more accurate estimate for the total emissions and is in good agreement with the simple box model and model iteration method providing further evidence to indicate that the total UK emissions for CH_4 are underestimated in the current inventory.

Using the maps produced by the inversion and the sector analysis from the model iteration technique, the likely sources of the unaccounted emissions can derived. For CH_4 the sector analysis suggests that the source of the unaccounted emissions is mainly livestock. This agrees with the inversion technique which allocates larger emissions to the south west of England and Wales where livestock farming is concentrated. The sector analysis also allocates larger emissions to gas pipes leaks and mines. This agrees with the inversion analysis which allocates larger emissions to East (gas leaks) and North East England (mines).

For N_2O the weighted average and restricted domain approach was used to produce the best emission map to account for the varying data quality between flights. The total emissions predicted by the inversion technique for N_2O are 500 ± 40 kt yr^{-1}. This is larger than the estimates of the simple box model and model iteration techniques but also significantly larger than the current NAEI estimate, further evidence that the current inventory underestimates the real emissions. From the inversion maps there is a significant underestimation of emissions from rural areas in South West England and Wales. This agrees with the sector analysis from the model iteration which suggests that the sector that is most underestimated is livestock, i.e. the emissions from the soils of land used for grazing seem to be poorly understood. These are concentrated in west and south west England. Given the results of the AMPEP

analysis and the fact that emissions from soils are the most uncertain part of the N_2O budget, it is likely that this sector is underestimated in the current inventory.

The inversion technique was also used to produce emission maps for a number of Halocarbons species for the first time. Though the number of data points with which to attempt the inversion was far fewer, it was still possible to produce realistic maps with emissions concentrated in localized industrial areas as would be expected with national totals that were in good agreement estimates derived using independent data.

8.1.3 Oxidation

Using SO_2, SO_4^{2-} and the NO_2, HNO_3, NO_3^- concentration measurements and the NAME concentration maps, as shown in Figure 144 and Figure 143 respectively, it was possible to identify a number of outflow plumes and determine their origin. By using the average wind speed calculations from the Unified Model meteorological data, the travel time for the air samples from emissions to point of sampling could be estimated and using the ratio of emitted pollutant to oxidation product the oxidation rate (% oxidised $hour^{-1}$) was calculated.

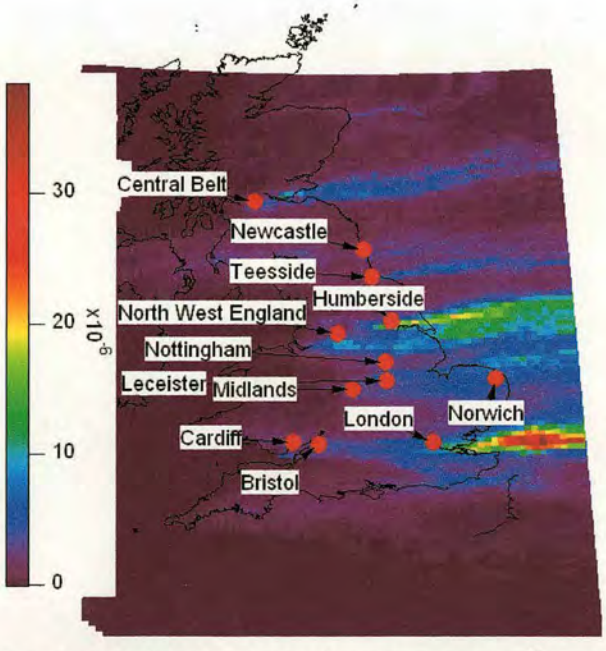

Figure 143. NAME NO_x outflow plumes (g m^{-3}) for flight B112.

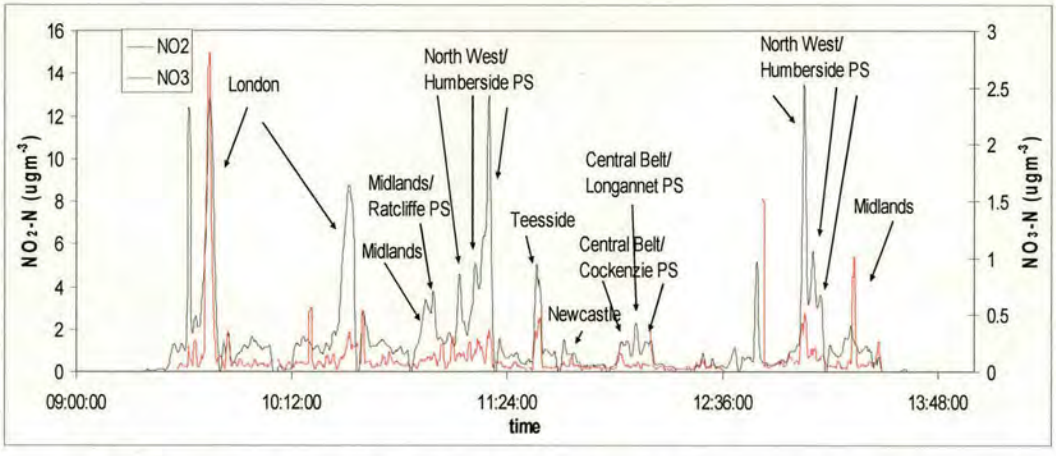

Figure 144. Flight B112 NO_2 and HNO_3+NO_3^- (HNO_3 and NO_3^-) concentration (N μgm^{-3}).

It was possible to produce oxidation rates for urban, industrial and power station plumes for both NO_x and SO_2. The oxidation rates for individual plumes tended to be fairly consistent between flights with an average oxidation rate for the whole UK of 3.2 ± 2.38 % $hour^{-1}$ for NO_x and 5.3± 1.80 % $hour^{-1}$ for SO_2. Overall the oxidation rates of power stations and industrial plumes were much smaller than the oxidation rates in urban plumes most likely due to the greater availability of oxidants in urban plumes. The average oxidation rate for NO_x for a power station plume was 1.4 ± 0.66 % N $hour^{-1}$ compared to 4.4 ± 3.95 % N $hour^{-1}$ for an urban plume and the average oxidation rate for SO_2 for a power station plume was 4.8 ± 0.76 % S $hour^{-1}$ compared to 6.5 ± 5.71 % S $hour^{-1}$ for an urban plume. The AMPEP SO_2 oxidation rate for the urban plumes was consistent with rates found for urban plumes in other studies (see Table 54) while the oxidation rate for power station was found to be approximately twice those found from most other studies (Hewitt (2000)). Few studies have been made of NO_x oxidation rates, of those the AMPEP NO_x oxidation rates for power stations was significantly smaller than rates found in two other studies (Hewitt (2000) and Springston *et al.* (2005)) but was similar to the rate found in one study (Tsuang *et al.* (2003)). Also the NO_x oxidation rates tended to be smaller than the SO_2 rates which contradicted the results of Hewitt (2000) and Springston *et al.* (2005) but confirmed the results of Tsuang *et al.* (2003).

Table 54. Oxidation rates of power station and urban plumes found in other studies compared to AMPEP oxidation rates for NO_x and SO_2 (% $hour^{-1}$).

	Power Station (Springston *et al.*, 2005)	Power Station (Hewitt, 2000)	Power Station (urban) (Tsuang *et al.*, 2003)	Power Station AMPEP	Urban (Bamber *et al.*, 1984)	Urban (Hewitt, 2000)	Urban AMPEP
SO_2 (% oxidised per hour)	3	2.3	7.8	4.8 ± 0.76	2 (5.3 in cloud)	4, 10	6.5 ± 5.71
NO_x (% oxidised per hour)	23	27	0.75	1.4 ± 0.66			4.4 ± 3.95

8.2 Future Work

With increasing attention given to climate change and the commitments given by the UK government to reduce greenhouse gas emissions, it is important to develop a means of validating the UK emission inventories. Aircraft measurements can provide a valuable method of validation as they provide a 'top-down' estimate which does not rely on assumptions on the nature or number of sources. Using sophisticated modelling techniques it is also possible not only to calculate a total budget but to investigate which areas of the inventory may be less well understood and to produce spatially disaggregated emission maps.

In addition to the points discussed in section (8.1), this work has also shown the importance of determining the temporal signal in UK flux, particularly for N_2O which is very dependent on soil conditions and is therefore very variable in time. Therefore to confirm whether the larger emissions of N_2O and CH_4 are real it is important to measure the flux during the winter months. Also, given the poorer quality of both N_2O and CH_4 measurements relative to CO and CO_2, additional flights are required to pin down the annual flux of both chemical species more accurately.

During the budget analysis and inversion work, the importance of being able to accurately determine the background concentration became apparent. Therefore during any future flights it would be advisable to sample the inflow region more fully in order to characterise the background concentration for the whole of the inflow air. Additionally, for the inverse modelling, it is important to be able to combine observations made in a range of conditions with wind flow from different directions. Attempts should therefore be made to conduct flights on days with northerly wind

flow which can provide the uniform background required while producing significantly different outflow pattern to the westerly conditions favoured during this campaign.

To increase the range of conditions in which flights can be made, the inclusion of an accurate convective boundary layer venting scheme in the NAME model would allow reliable budgets to be calculated for more convective conditions. Further improvements to the NAME model should include an improved scheme for the biogenic flux. Very little sensitivity analysis has been done on the parameters used for both photosynthesis and respiration, and a full analysis should improve the calculation of the biogenic sources and sink terms considerably.

To improve the inversion, an alterative mask could be used to the two tried in this analysis. Instead of allowing emissions to be allocated to the whole domain or to land only, the emissions could instead be restricted to the UK and Ireland with a band around the edge of the domain where emissions may also be assigned. This would hopefully reduce the emissions allocated to the sea while maintaining the accuracy of the emissions from the UK and Ireland.

Having demonstrated the power of the boundary layer budget approach to produce reliable estimates for annual emissions, it could also be applied to other suitable nations and regions as a means of validating their reported emissions which in turn could be used to validate the IPCC methodology used by all nations to calculate annual emissions. Potential countries where such an approach could be used include New Zealand, Japan, Ireland, Denmark, Norway and Scandinavia as a whole as well as any small island nation.

Appendix 1 NAME Inversion Emissions Maps for CO for Individual Flights

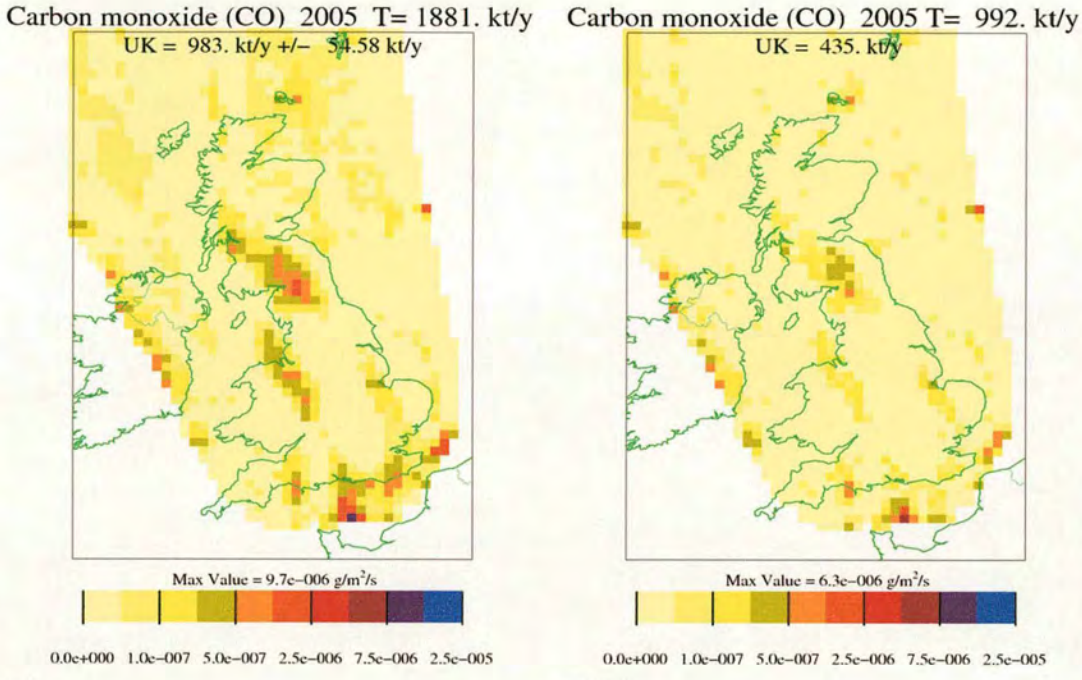

(a) (b)

Figure 145. (a) CO emissions (g m^{-2} s^{-1}) for flight B92 at resolution 1×1 boxes and unrestricted domain. (b) Standard deviation of CO emissions for 3 maps produced at resolution 1×1 boxes and unrestricted domain.

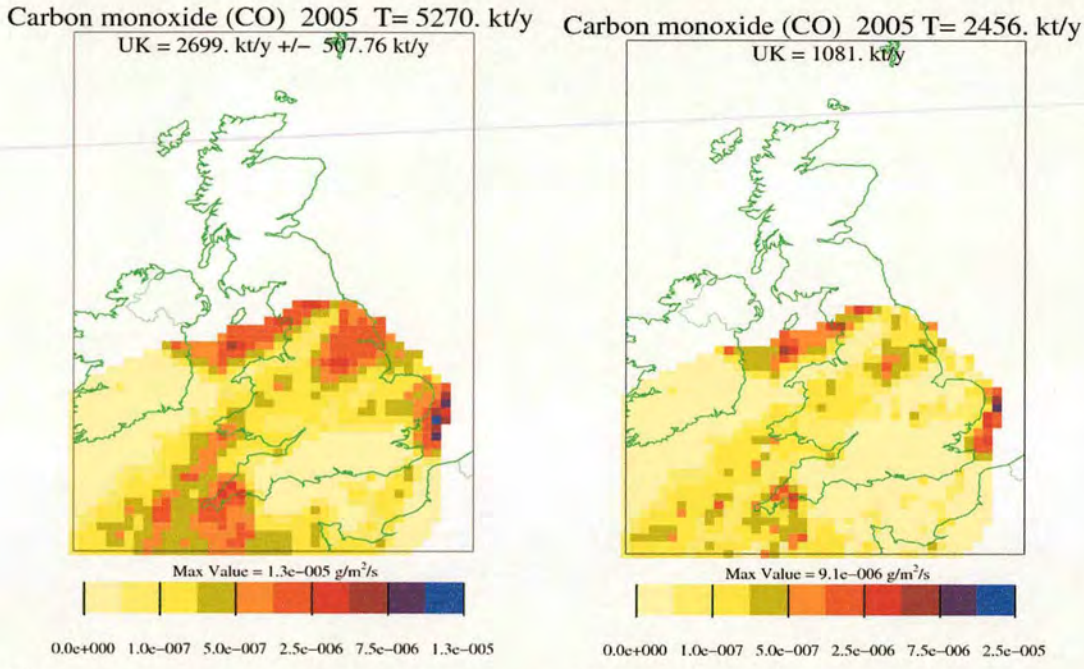

(a) (b)

Figure 146. (a) CO emissions (g m^{-2} s^{-1}) for flight B97 at resolution 1×1 boxes and unrestricted domain. (b) Standard deviation of CO emissions for 3 maps produced at resolution 1×1 boxes and unrestricted domain.

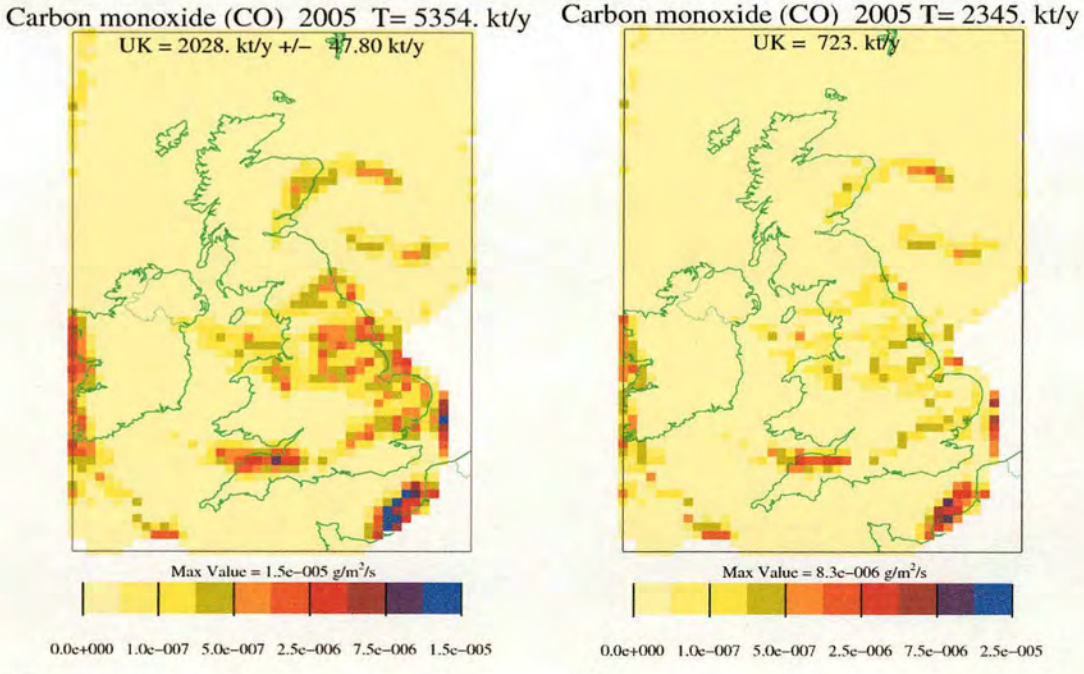

(a) (b)

Figure 147. CO emissions (g m^{-2} s^{-1}) for flight B102 at resolution 1×1 boxes and unrestricted domain. (b) Standard deviation of CO emissions for 3 maps produced at resolution 1×1 boxes and unrestricted domain.

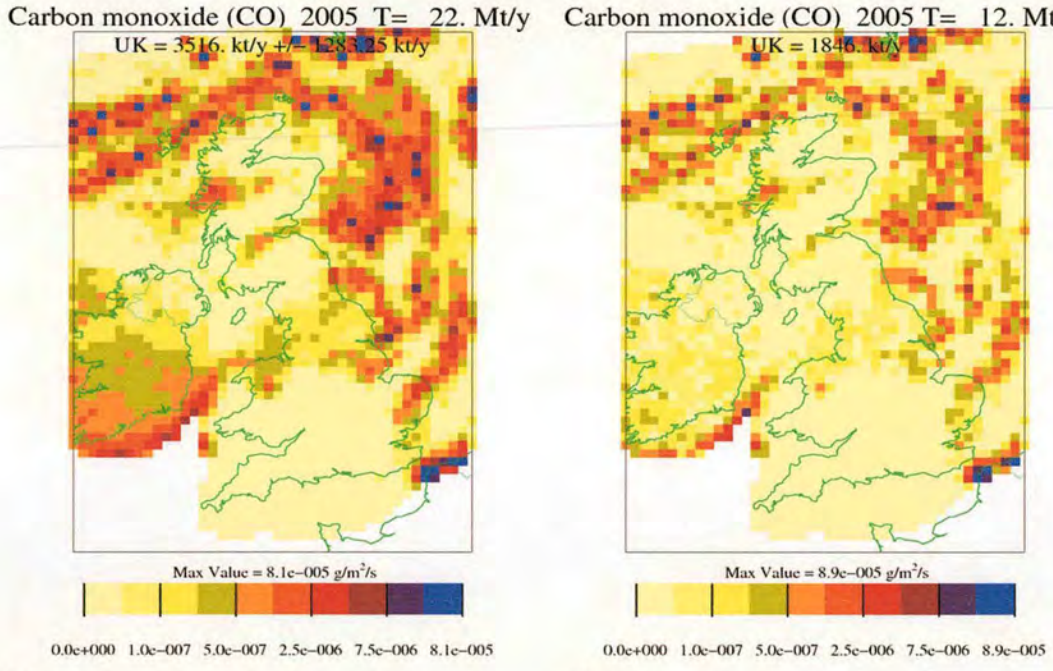

(a) (b)

Figure 148. CO emissions (g m^{-2} s^{-1}) for flight B111 at resolution 1×1 boxes and unrestricted domain. (b) Standard deviation of CO emissions for 3 maps produced at resolution 1×1 boxes and unrestricted domain.

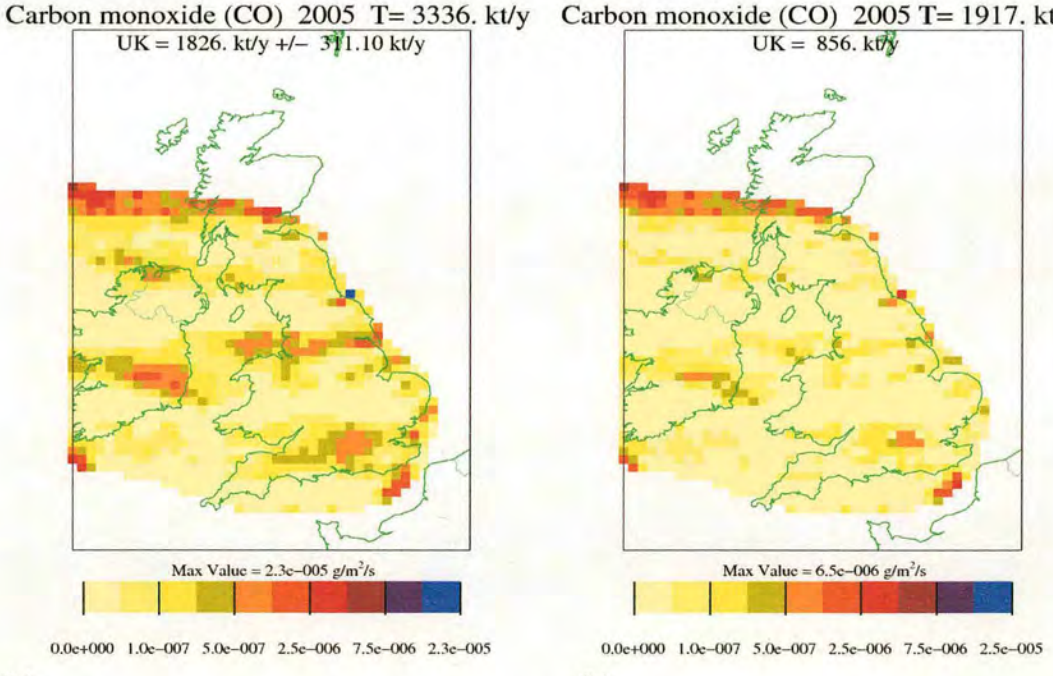

(a) (b)

Figure 149. CO emissions (g m^{-2} s^{-1}) for flight B112 at resolution 1×1 boxes and unrestricted domain. (b) Standard deviation of CO emissions for 3 maps produced at resolution 1×1 boxes and unrestricted domain.

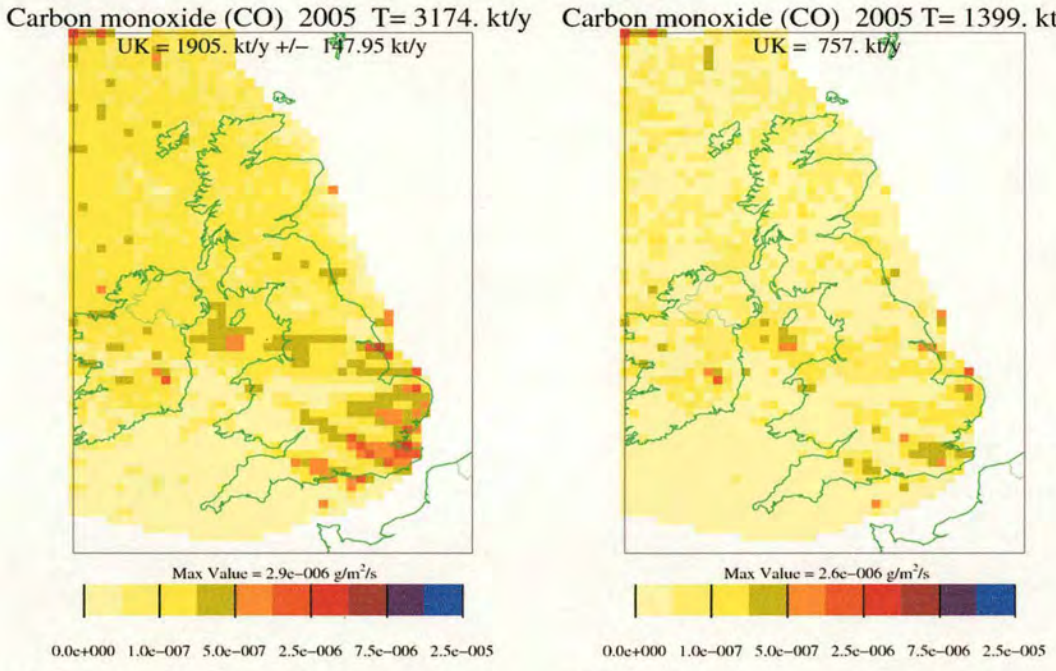

(a) (b)

Figure 150. CO emissions (g m^{-2} s^{-1}) for flight B113 at resolution 1×1 boxes and unrestricted domain. (b) Standard deviation of CO emissions for 3 maps produced at resolution 1×1 boxes and unrestricted domain.

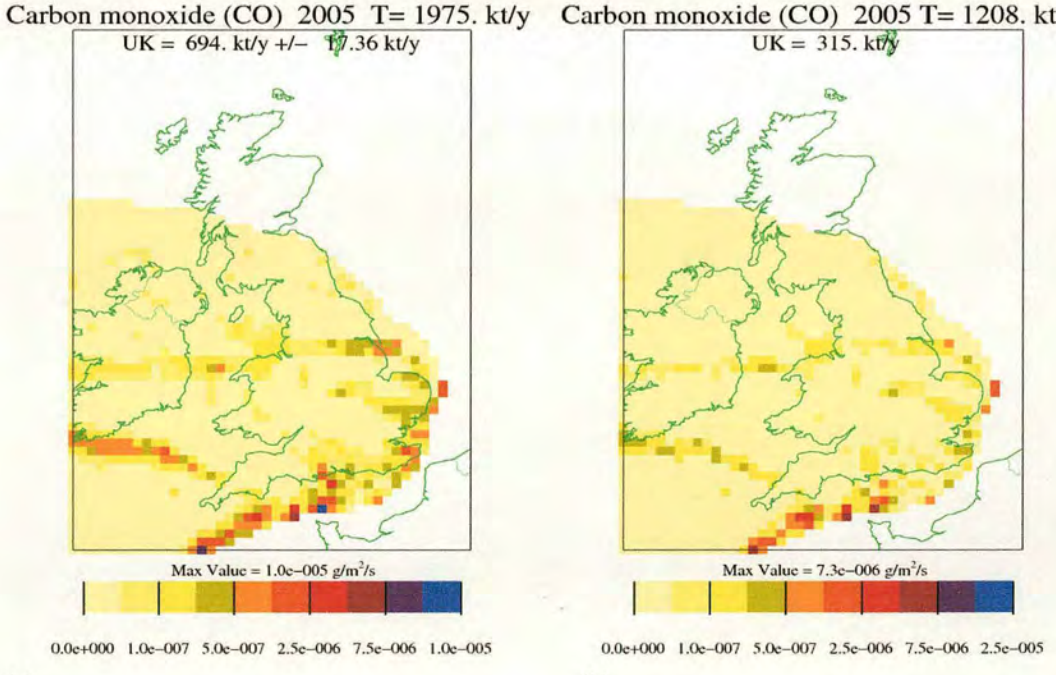

(a) (b)

Figure 151. CO emissions (g m^{-2} s^{-1}) for flight B118 at resolution 1×1 boxes and unrestricted domain. (b) Standard deviation of CO emissions for 3 maps produced at resolution 1×1 boxes and unrestricted domain.

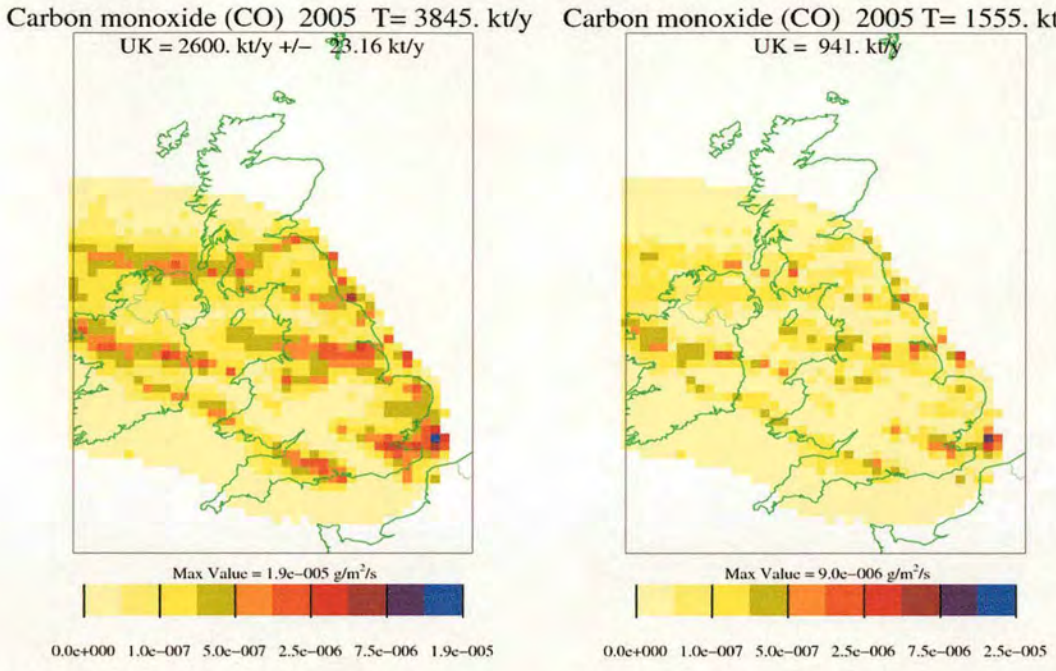

(a) (b)

Figure 152. CO emissions (g m^{-2} s^{-1}) for flight B119 at resolution 1×1 boxes and unrestricted domain. (b) Standard deviation of CO emissions for 3 maps produced at resolution 1×1 boxes and unrestricted domain.

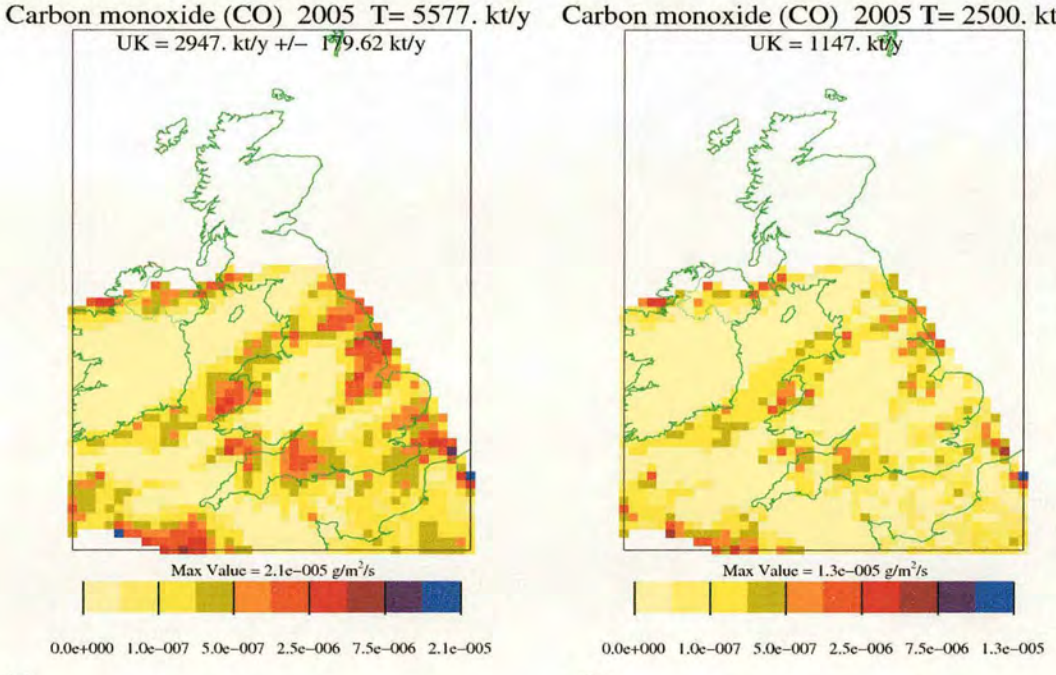

(a) (b)

Figure 153. CO emissions (g m^{-2} s^{-1}) for flight B126 at resolution 1×1 boxes and unrestricted domain. (b) Standard deviation of CO emissions for 3 maps produced at resolution 1×1 boxes and unrestricted domain.

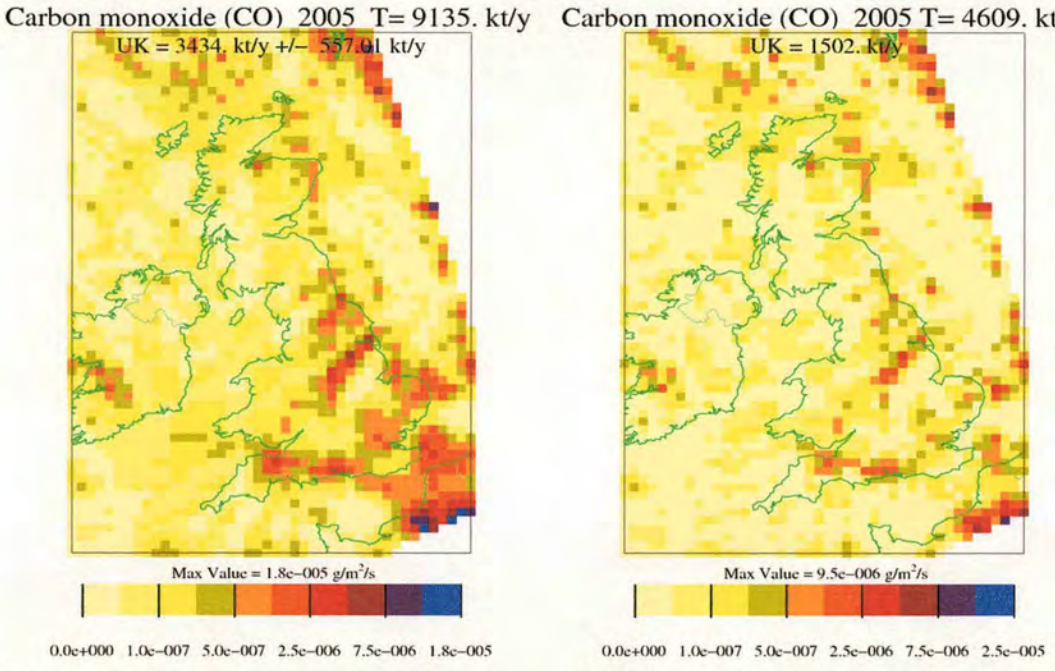

(a) (b)

Figure 154. CO emissions (g m^{-2} s^{-1}) for flight B130 at resolution 1×1 boxes and unrestricted domain. (b) Standard deviation of CO emissions for 3 maps produced at resolution 1×1 boxes and unrestricted domain.

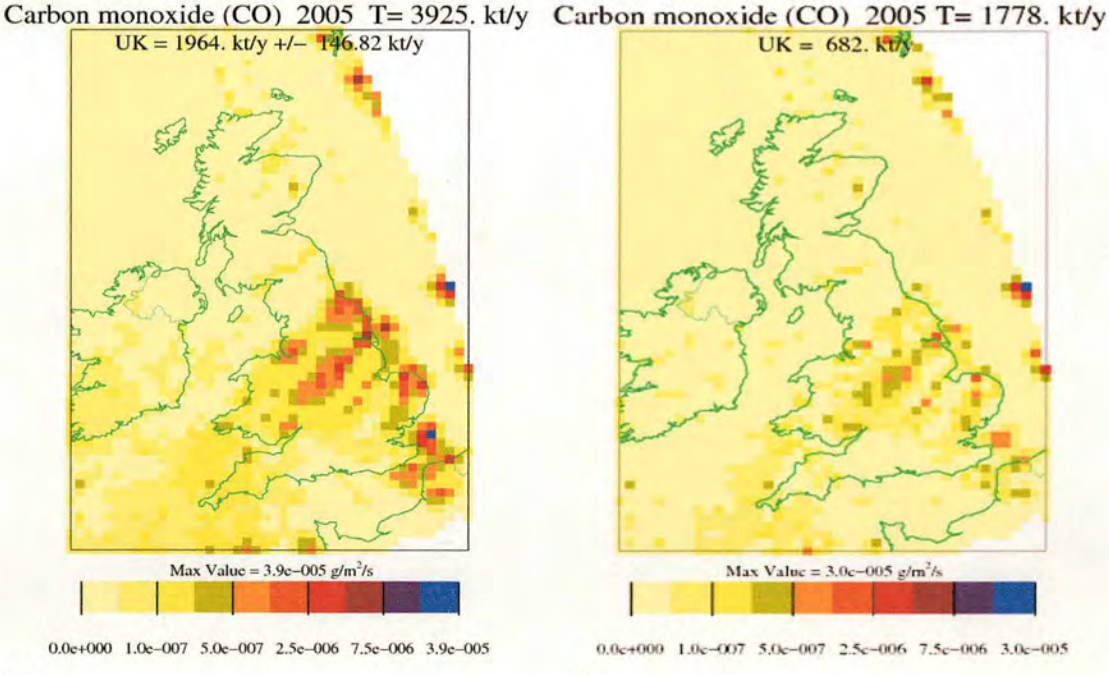

(a) (b)

Figure 155. CO emissions (g m^{-2} s^{-1}) for flight B132 at resolution 1×1 boxes and unrestricted domain. (b) Standard deviation of CO emissions for 3 maps produced at resolution 1×1 boxes and unrestricted domain.

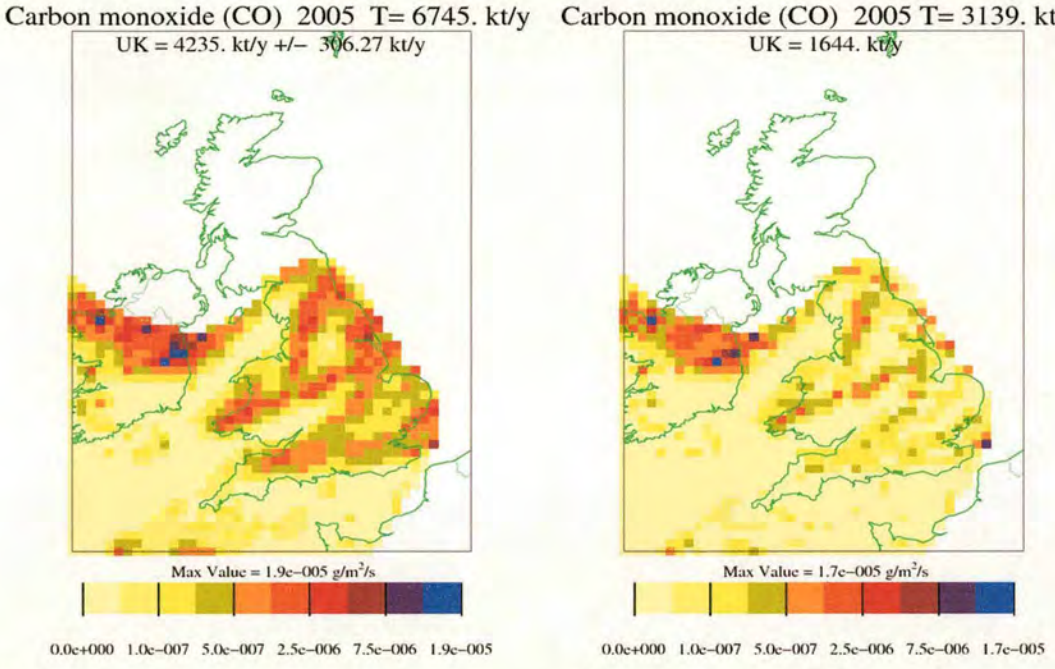

(a) (b)

Figure 156. CO emissions (g m^{-2} s^{-1}) for flight B134 at resolution 1×1 boxes and unrestricted domain. (b) Standard deviation of CO emissions for 3 maps produced at resolution 1×1 boxes and unrestricted domain.

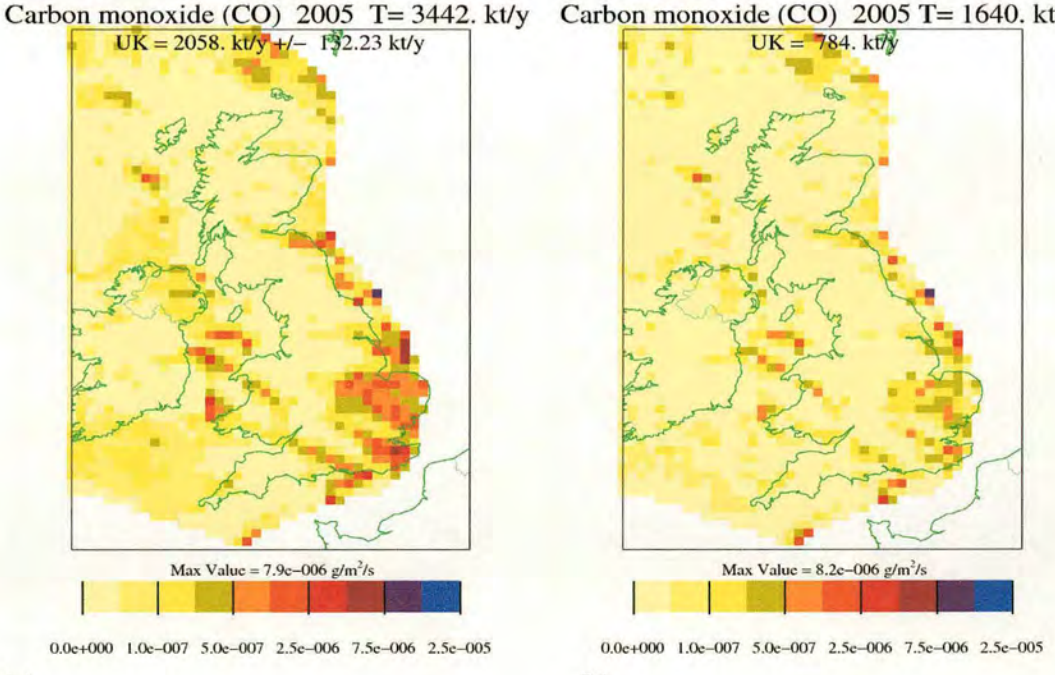

(a) (b)

Figure 157. CO emissions (g m^{-2} s^{-1}) for flight B136 at resolution 1×1 boxes and unrestricted domain. (b) Standard deviation of CO emissions for 3 maps produced at resolution 1×1 boxes and unrestricted domain.

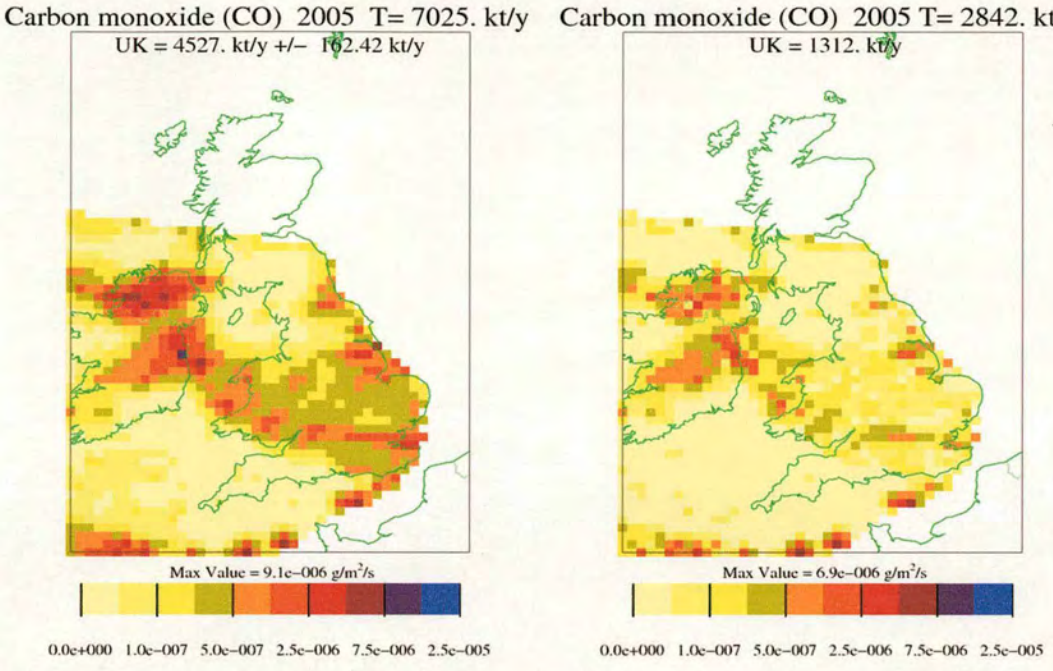

Figure 158. CO emissions (g m^{-2} s^{-1}) for flight B244 at resolution 1×1 boxes and unrestricted domain. (b) Standard deviation of CO emissions for 3 maps produced at resolution 1×1 boxes and unrestricted domain.

Appendix 2 NAME Inversion Emissions Maps for CO_2 for Individual Flights

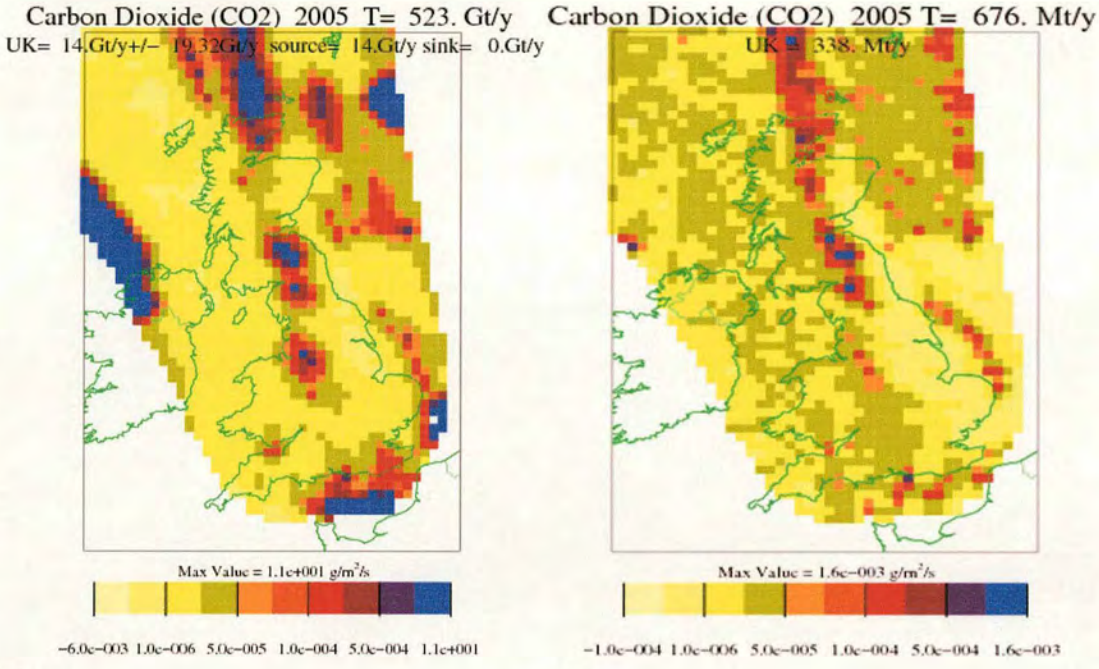

(a) (b)

Figure 159. (a) CO_2 emissions (g m^{-2} s^{-1}) for flight B92 at resolution 1×1 boxes and unrestricted domain. (b) Standard deviation of CO_2 emissions for 3 maps produced at resolution 1×1 boxes and unrestricted domain.

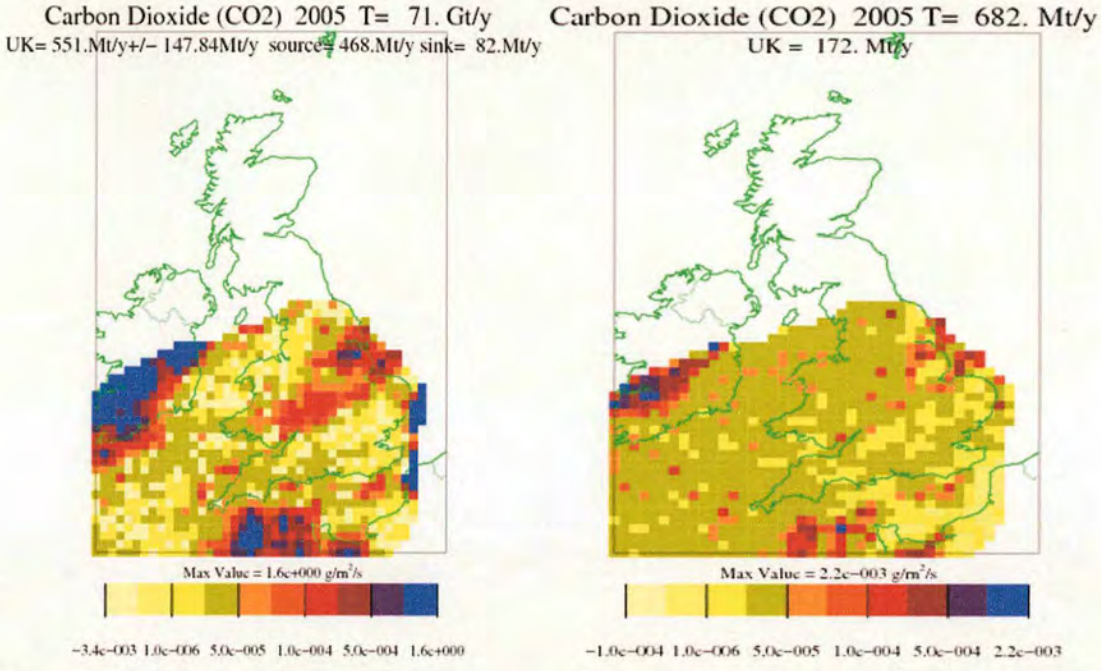

(a) (b)

Figure 160. (a) CO_2 emissions (g m^{-2} s^{-1}) for flight B97 at resolution 1×1 boxes and unrestricted domain. (b) Standard deviation of CO_2 emissions for 3 maps produced at resolution 1×1 boxes and unrestricted domain.

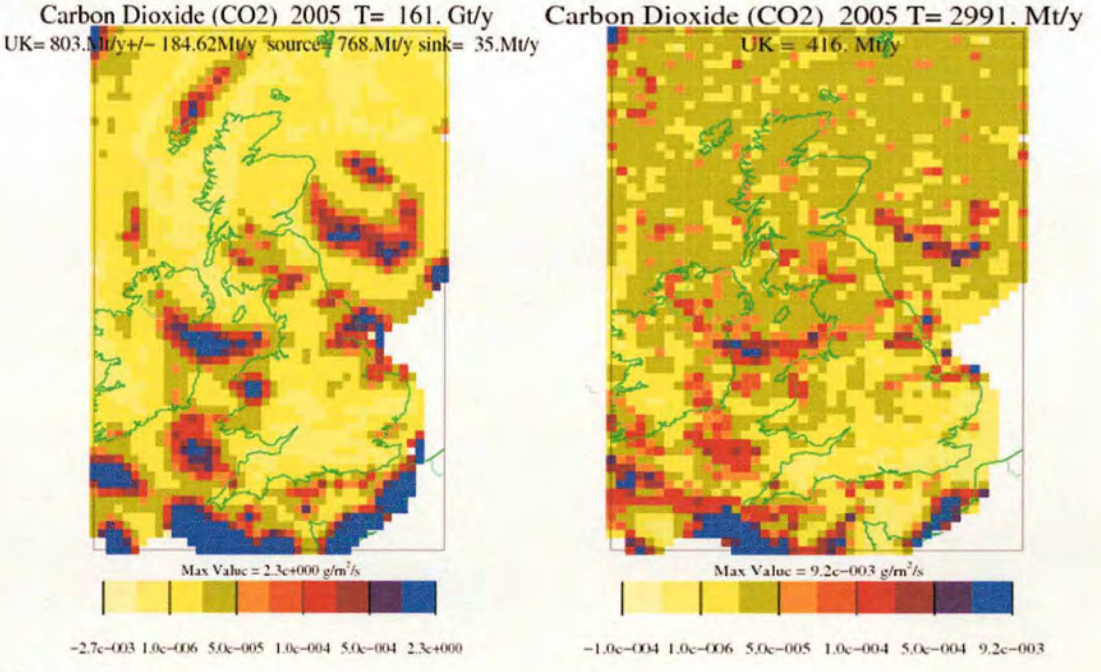

(a) (b)

Figure 161. CO_2 emissions (g m^{-2} s^{-1}) for flight B102 at resolution 1×1 boxes and unrestricted domain. (b) Standard deviation of CO_2 emissions for 3 maps produced at resolution 1×1 boxes and unrestricted domain.

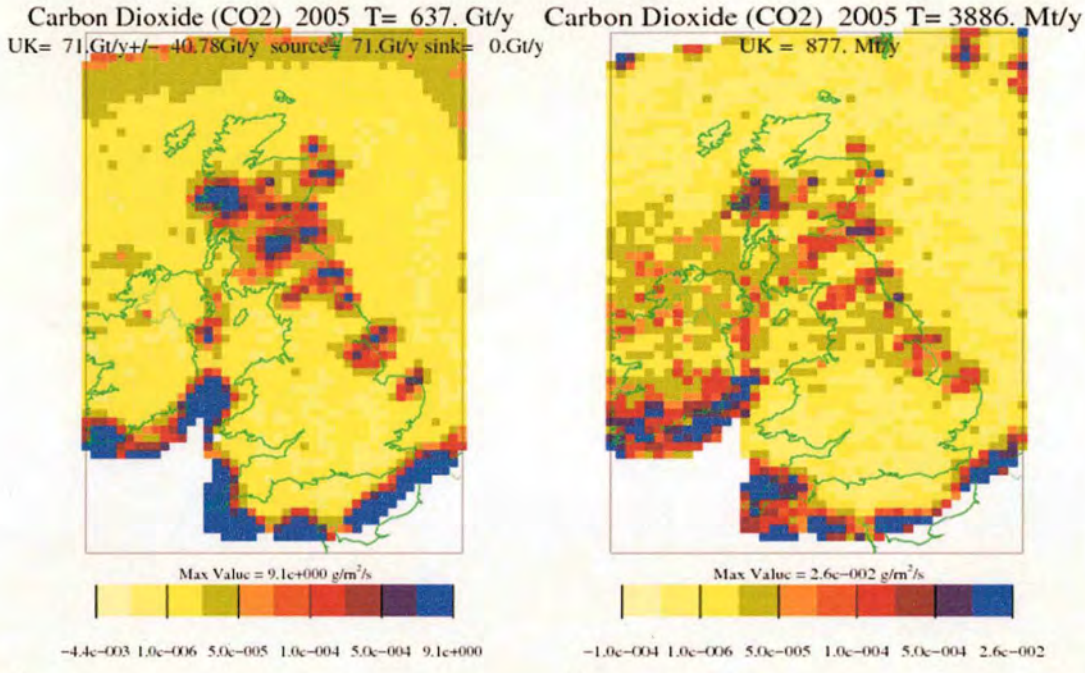

(a) (b)

Figure 162. CO_2 emissions (g m^{-2} s^{-1}) for flight B111 at resolution 1×1 boxes and unrestricted domain. (b) Standard deviation of CO_2 emissions for 3 maps produced at resolution 1×1 boxes and unrestricted domain.

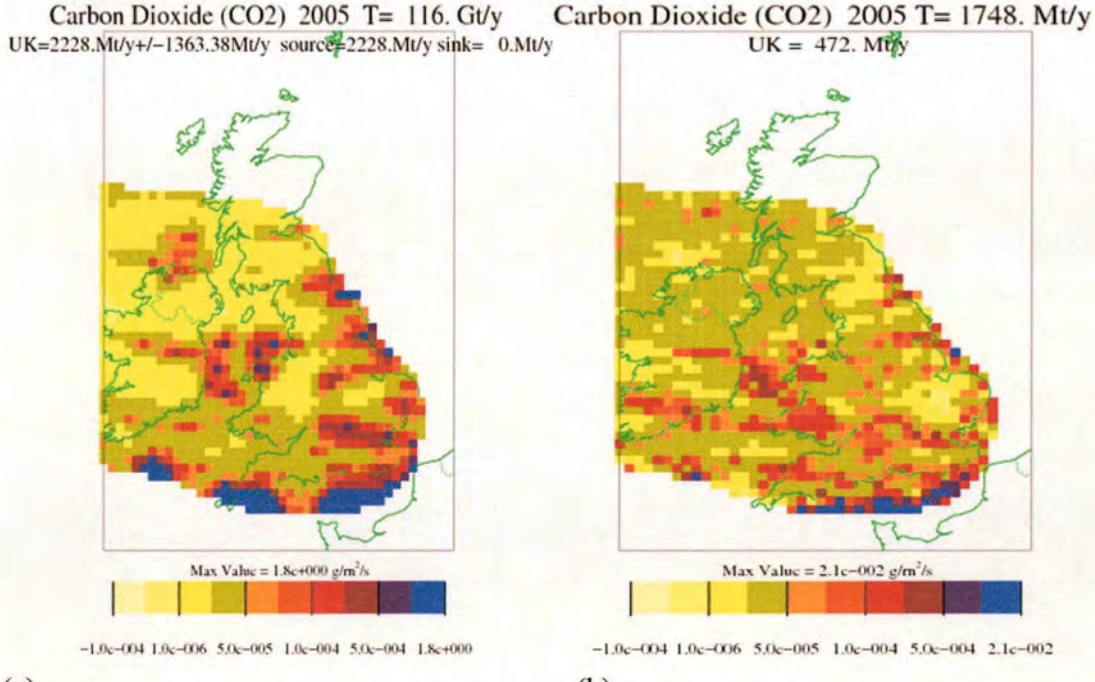

(a) (b)

Figure 163. CO_2 emissions (g m^{-2} s^{-1}) for flight B112 at resolution 1×1 boxes and unrestricted domain. (b) Standard deviation of CO_2 emissions for 3 maps produced at resolution 1×1 boxes and unrestricted domain.

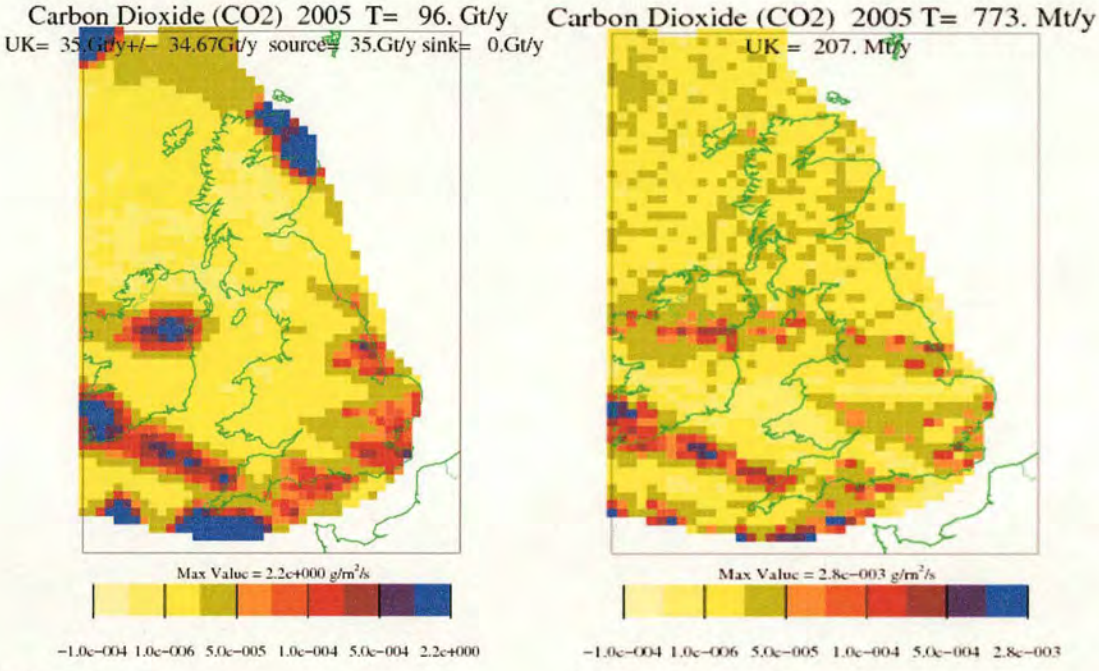

(a) (b)

Figure 164. CO_2 emissions (g m^{-2} s^{-1}) for flight B113 at resolution 1×1 boxes and unrestricted domain. (b) Standard deviation of CO_2 emissions for 3 maps produced at resolution 1×1 boxes and unrestricted domain.

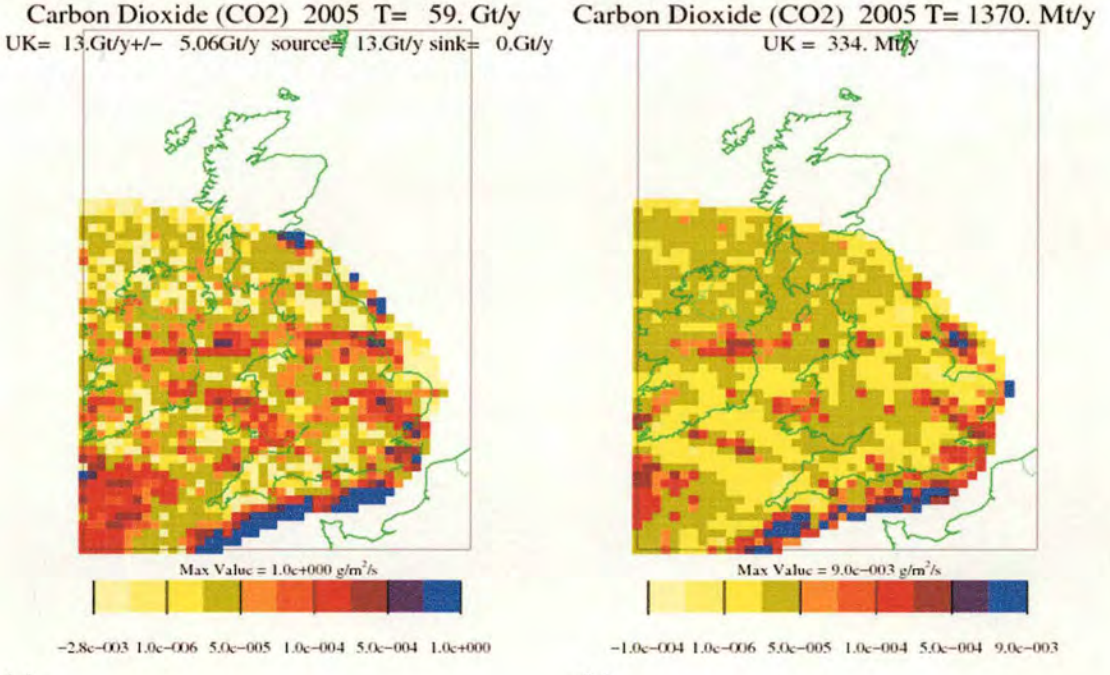

(a) (b)

Figure 165. CO_2 emissions (g m^{-2} s^{-1}) for flight B118 at resolution 1×1 boxes and unrestricted domain. (b) Standard deviation of CO_2 emissions for 3 maps produced at resolution 1×1 boxes and unrestricted domain.

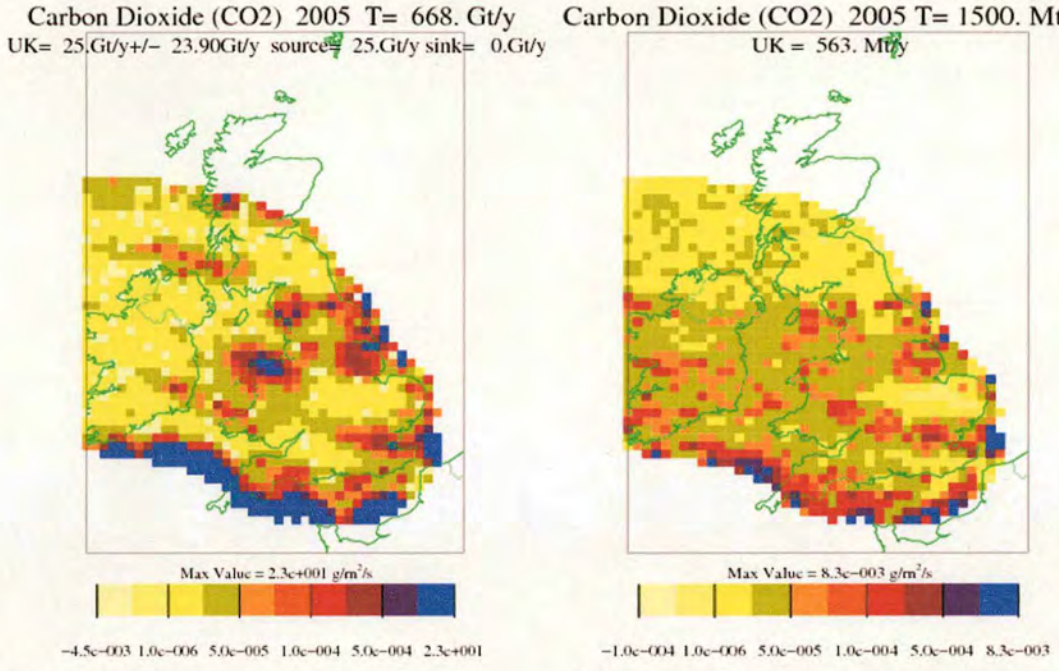

(a) (b)

Figure 166. CO_2 emissions (g m^{-2} s^{-1}) for flight B119 at resolution 1×1 boxes and unrestricted domain. (b) Standard deviation of CO_2 emissions for 3 maps produced at resolution 1×1 boxes and unrestricted domain.

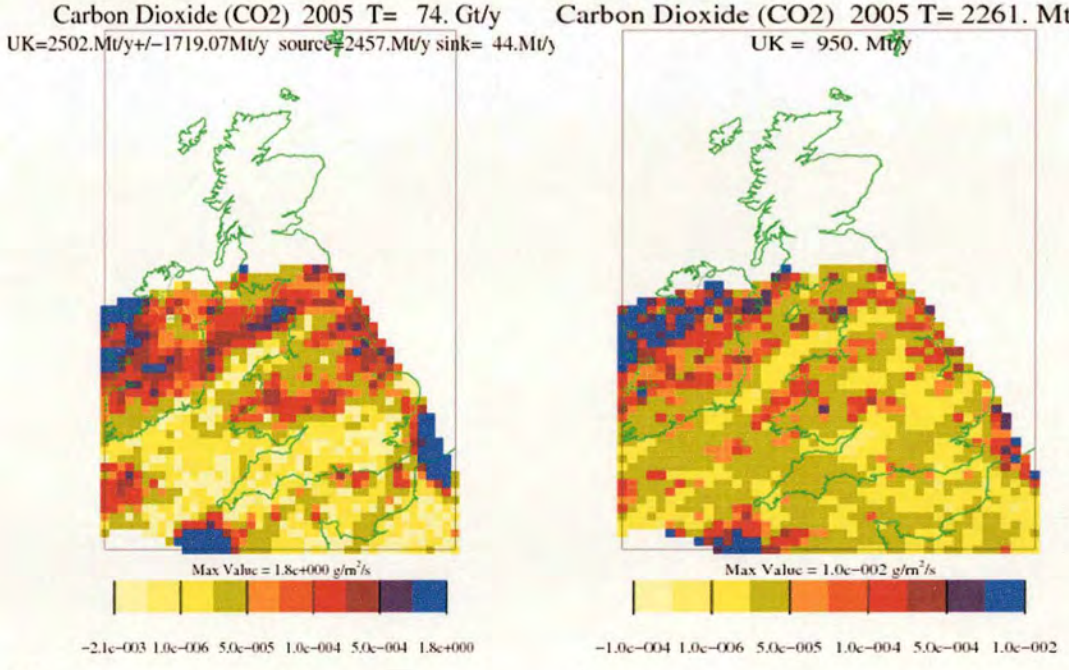

(a) (b)

Figure 167. CO_2 emissions (g m^{-2} s^{-1}) for flight B126 at resolution 1×1 boxes and unrestricted domain. (b) Standard deviation of CO_2 emissions for 3 maps produced at resolution 1×1 boxes and unrestricted domain.

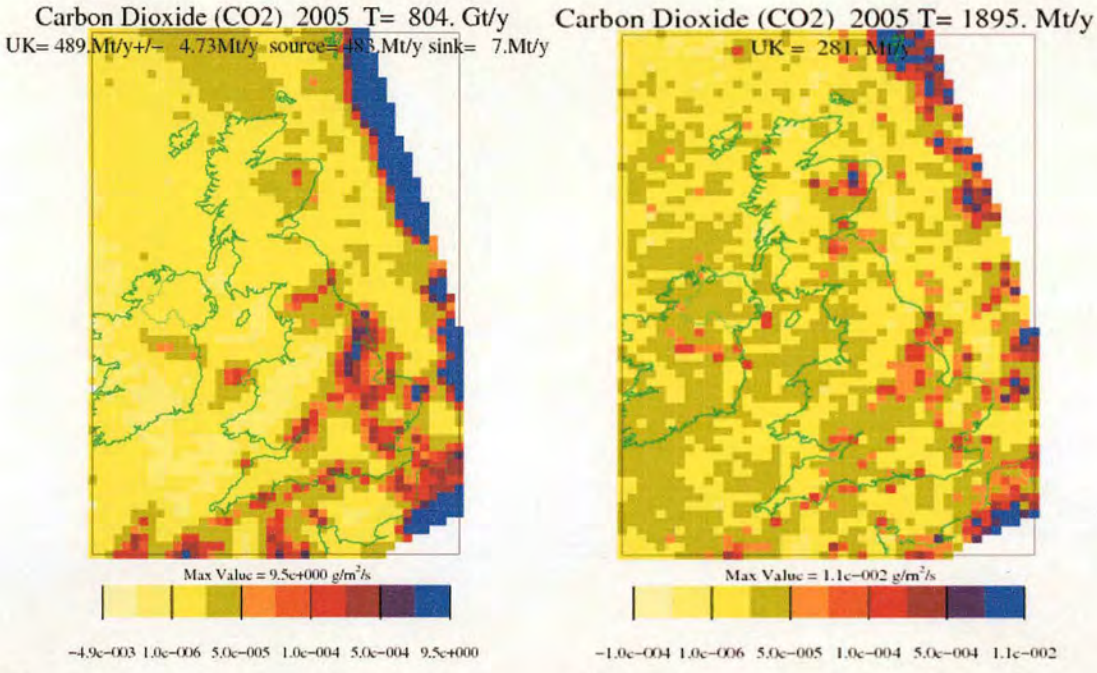

(a) (b)

Figure 168. CO_2 emissions (g m^{-2} s^{-1}) for flight B130 at resolution 1×1 boxes and unrestricted domain. (b) Standard deviation of CO_2 emissions for 3 maps produced at resolution 1×1 boxes and unrestricted domain.

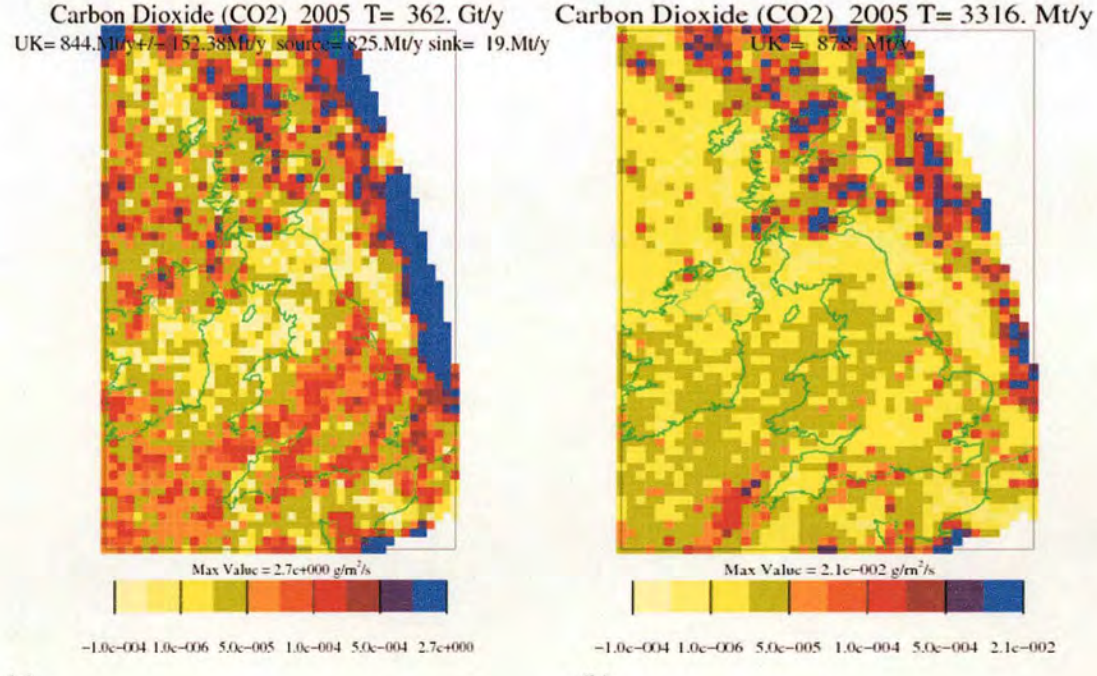

(a) (b)

Figure 169. CO_2 emissions (g m^{-2} s^{-1}) for flight B132 at resolution 1×1 boxes and unrestricted domain. (b) Standard deviation of CO_2 emissions for 3 maps produced at resolution 1×1 boxes and unrestricted domain.

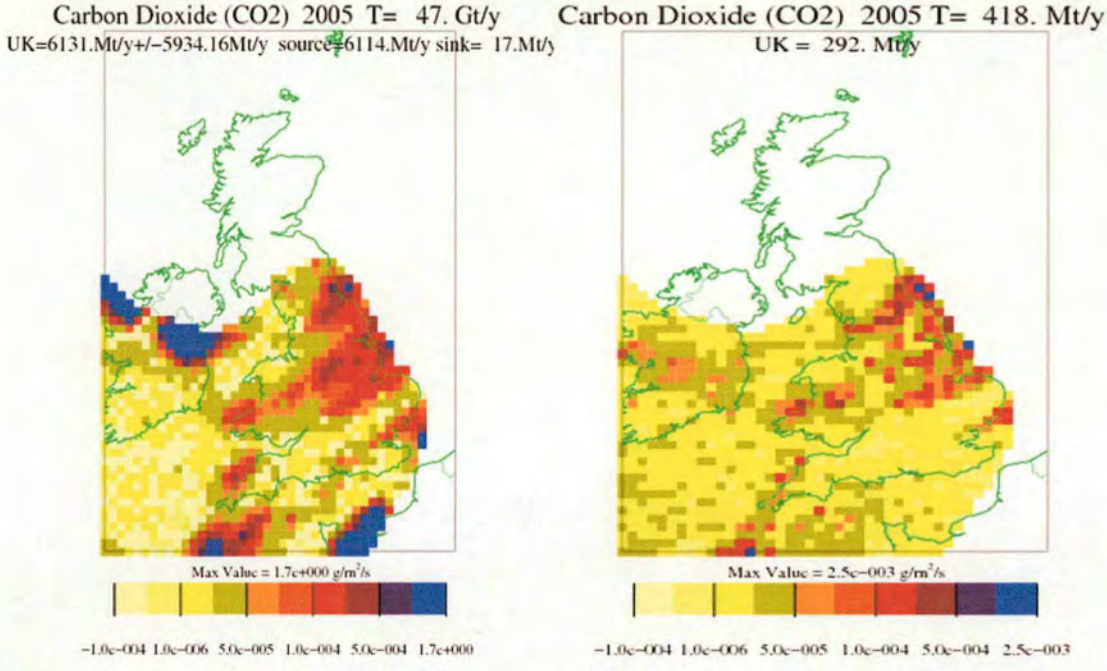

(a) (b)

Figure 170. CO_2 emissions (g m^{-2} s^{-1}) for flight B134 at resolution 1×1 boxes and unrestricted domain. (b) Standard deviation of CO_2 emissions for 3 maps produced at resolution 1×1 boxes and unrestricted domain.

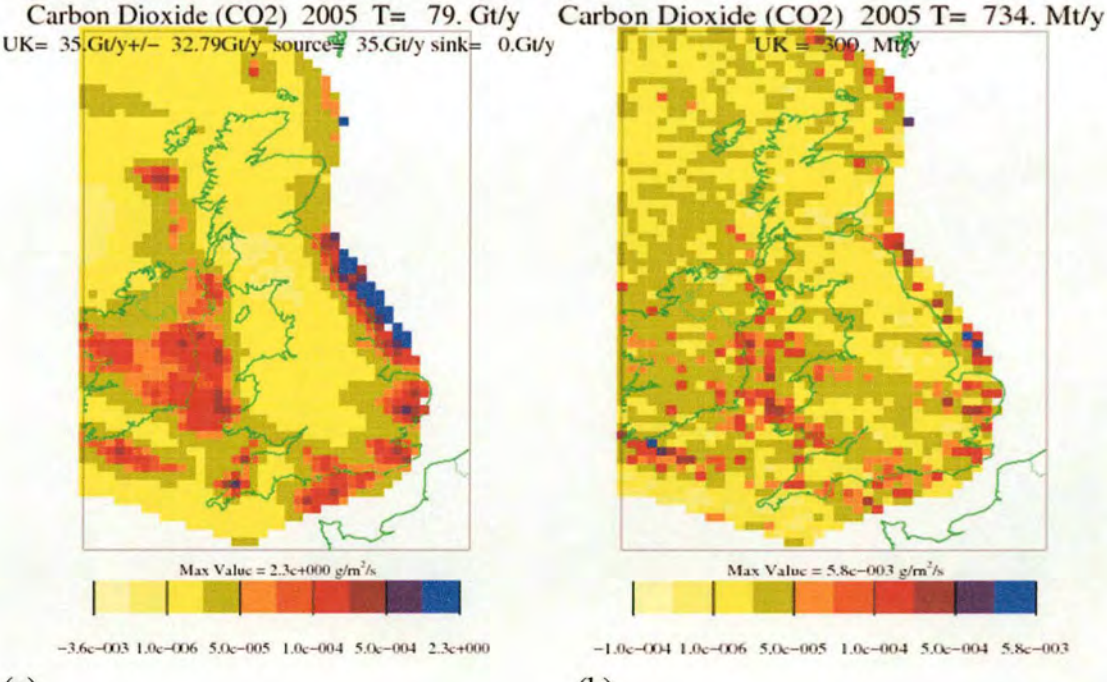

(a) (b)

Figure 171. CO_2 emissions (g m^{-2} s^{-1}) for flight B136 at resolution 1×1 boxes and unrestricted domain. (b) Standard deviation of CO_2 emissions for 3 maps produced at resolution 1×1 boxes and unrestricted domain.

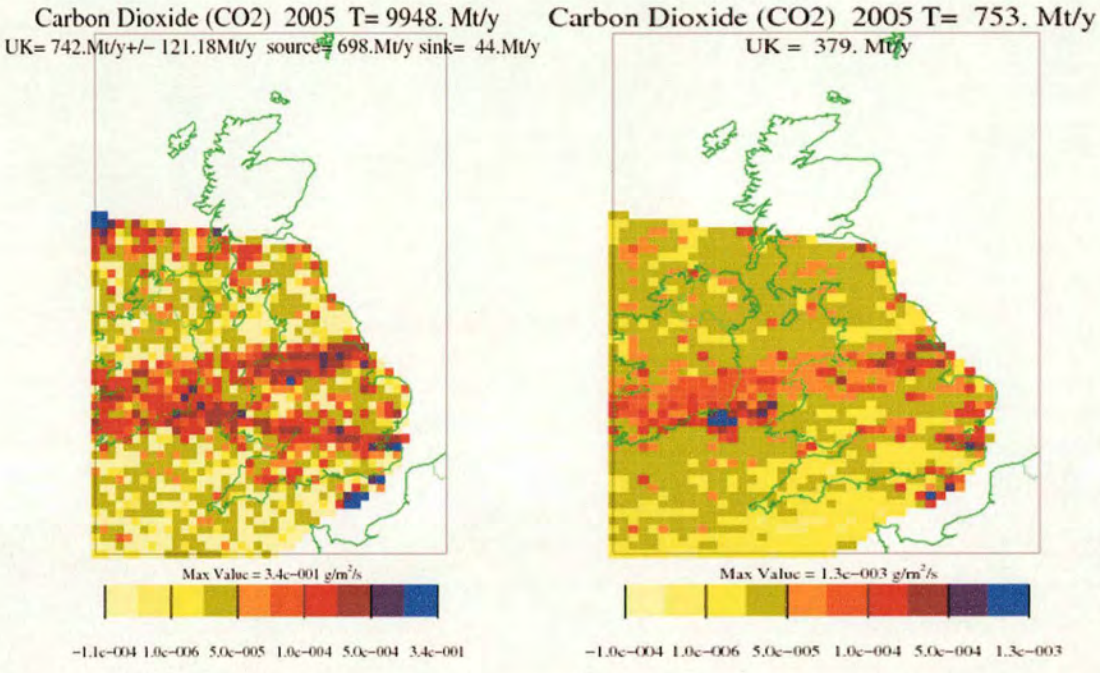

(a) (b)

Figure 172. CO_2 emissions (g m^{-2} s^{-1}) for flight B244 at resolution 1×1 boxes and unrestricted domain. (b) Standard deviation of CO_2 emissions for 3 maps produced at resolution 1×1 boxes and unrestricted domain.

Appendix 3 NAME Inversion Emissions Maps for CH_4 for Individual Flights

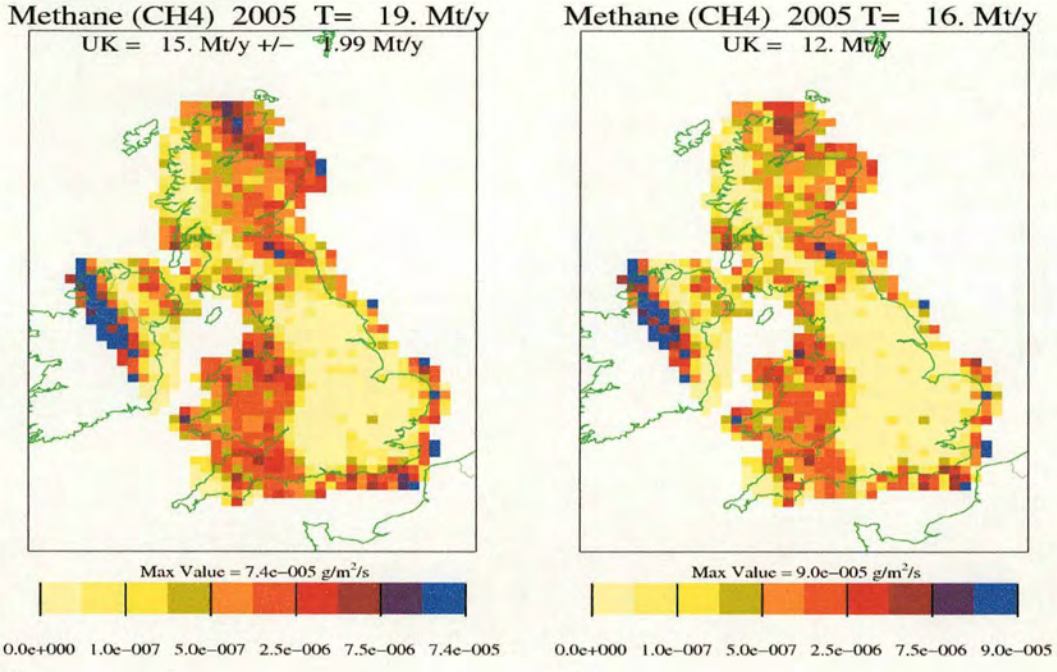

Figure 173. (a) CH_4 emissions (g m^{-2} s^{-1}) for flight B92 at resolution 1×1 boxes and restricted domain. (b) Standard deviation of CH_4 emissions for 3 maps produced at resolution 1×1 boxes and unrestricted domain.

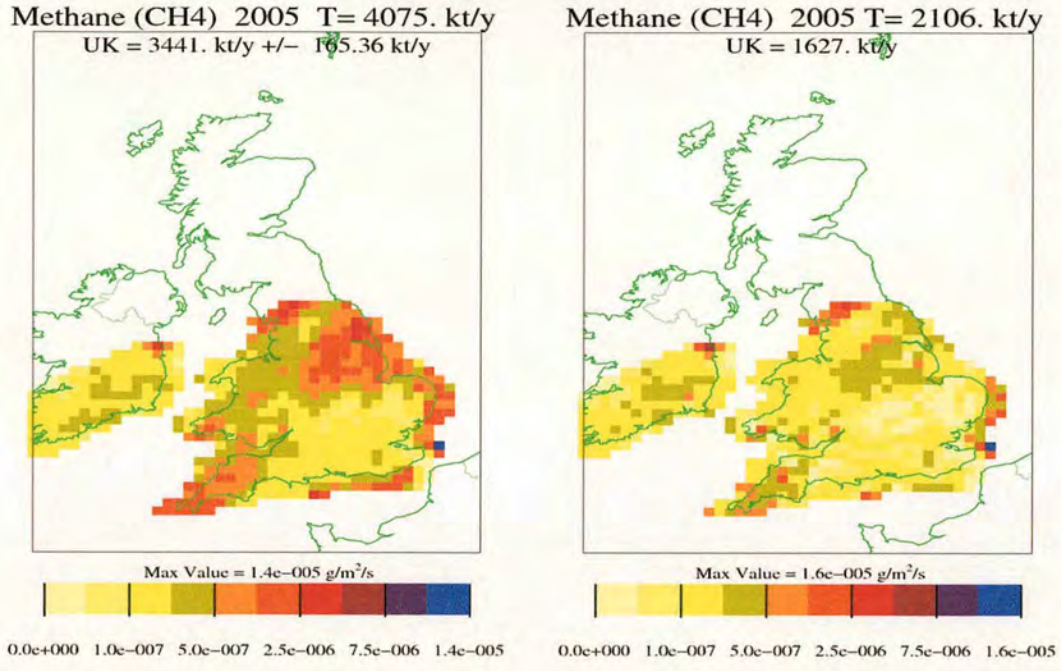

Figure 174. (a) CH_4 emissions (g m^{-2} s^{-1}) for flight B97 at resolution 1×1 boxes and restricted domain. (b) Standard deviation of CH_4 emissions for 3 maps produced at resolution 1×1 boxes and unrestricted domain.

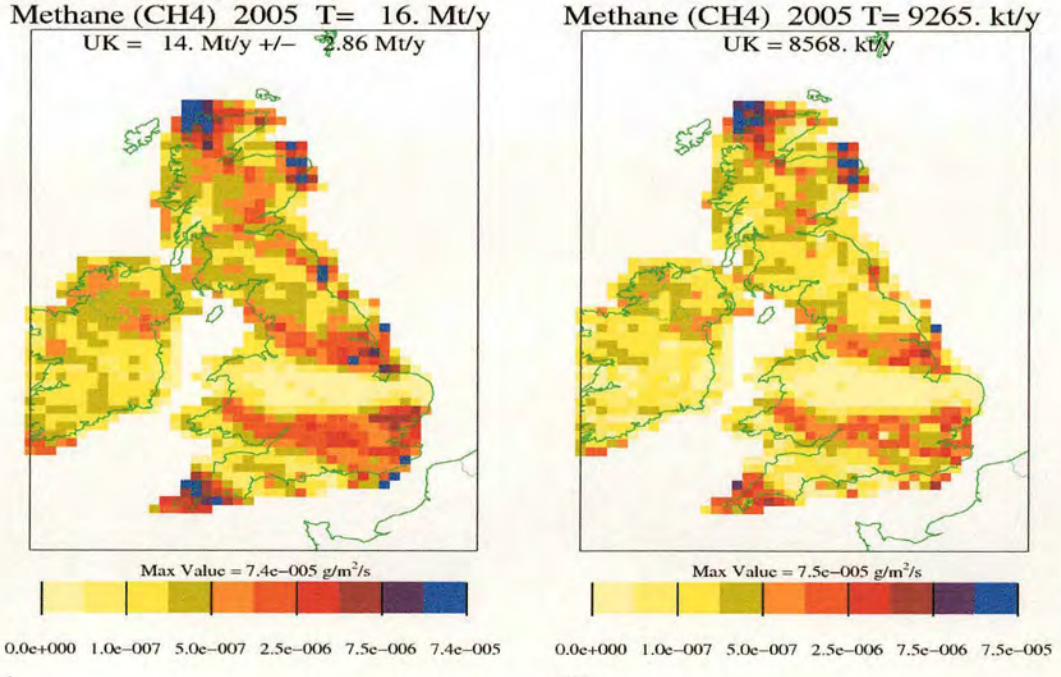

Figure 175. (a) CH_4 emissions (g m^{-2} s^{-1}) for flight B113 at resolution 1×1 boxes and restricted domain. (b) Standard deviation of CH_4 emissions for 3 maps produced at resolution 1×1 boxes and unrestricted domain.

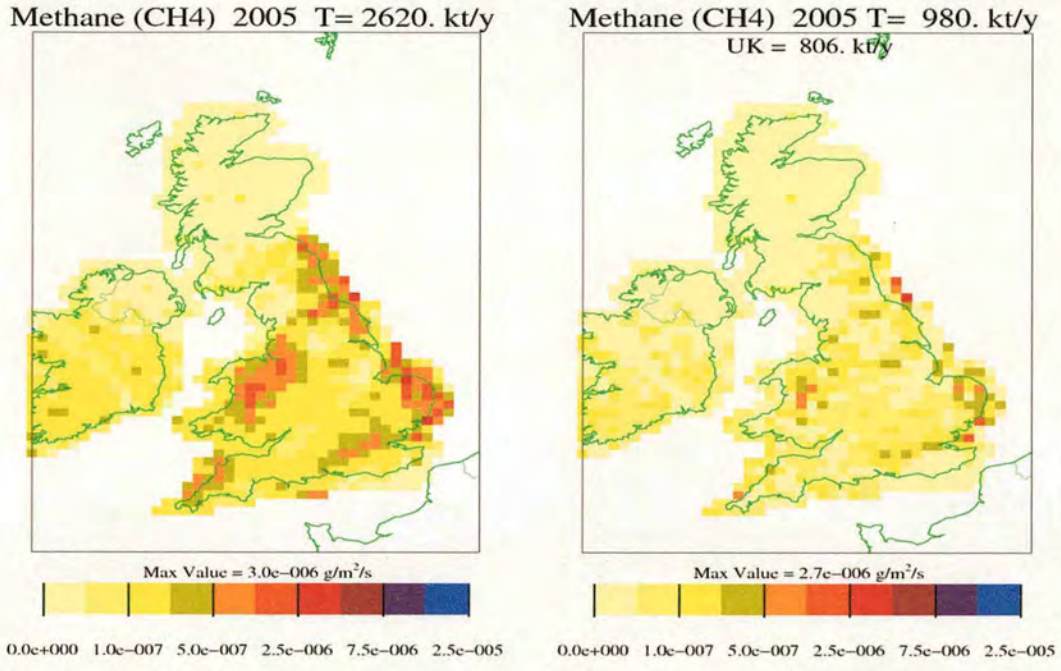

Figure 176. (a) CH_4 emissions (g m^{-2} s^{-1}) for flight B132 at resolution 1×1 boxes and restricted domain. (b) Standard deviation of CH_4 emissions for 3 maps produced at resolution 1×1 boxes and unrestricted domain.

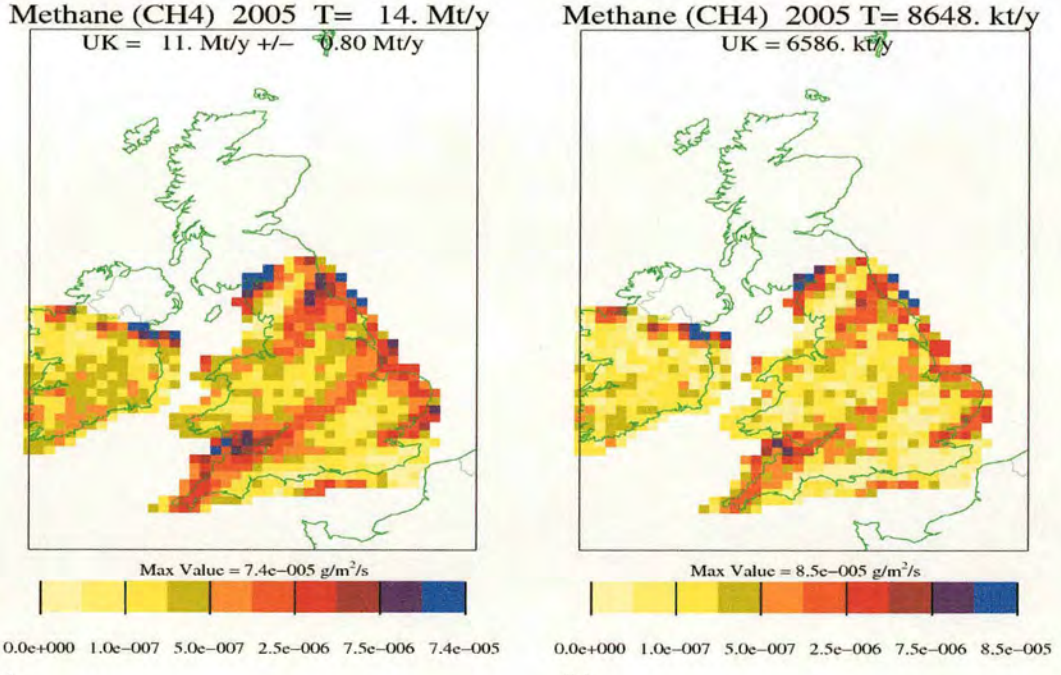

Figure 177. (a) CH_4 emissions (g m^{-2} s^{-1}) for flight B134 at resolution 1×1 boxes and restricted domain. (b) Standard deviation of CH_4 emissions for 3 maps produced at resolution 1×1 boxes and unrestricted domain.

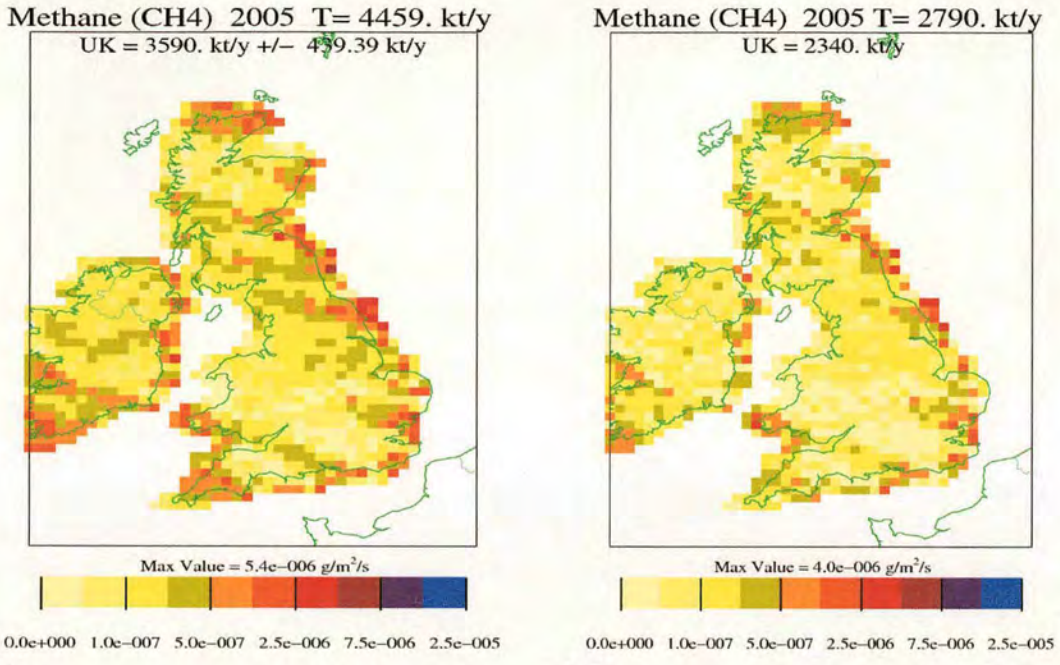

(a) (b)

Figure 178. (a) CH_4 emissions (g m^{-2} s^{-1}) for flight B136 at resolution 1×1 boxes and restricted domain. (b) Standard deviation of CH_4 emissions for 3 maps produced at resolution 1×1 boxes and unrestricted domain.

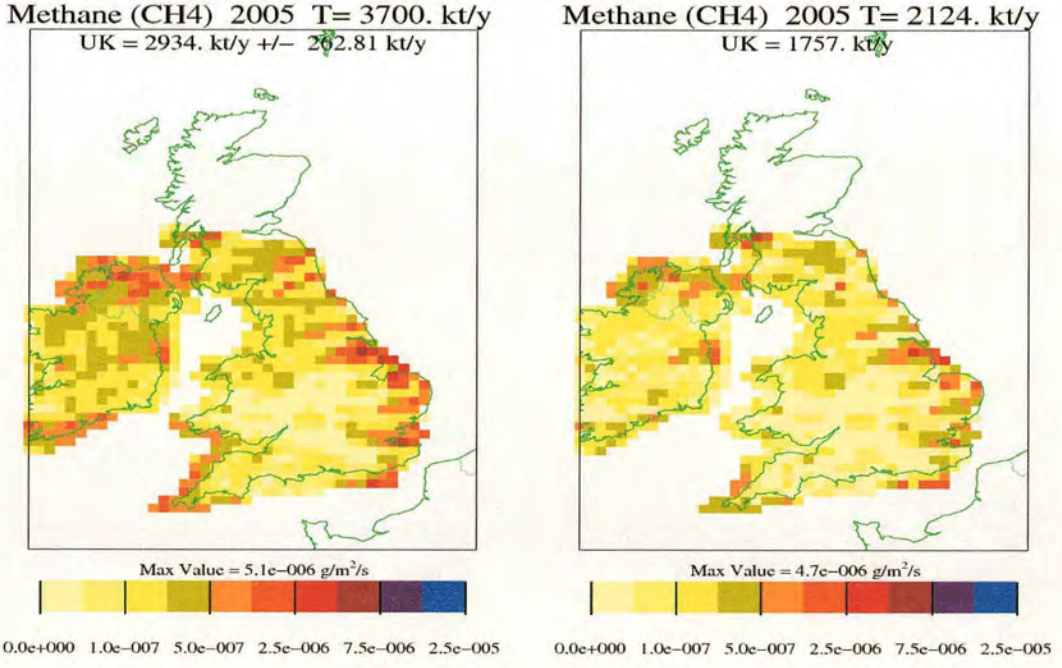

(a) (b)

Figure 179. (a) CH_4 emissions (g m^{-2} s^{-1}) for flight B244 at resolution 1×1 boxes and restricted domain. (b) Standard deviation of CH_4 emissions for 3 maps produced at resolution 1×1 boxes and unrestricted domain.

Appendix 4 NAME Inversion Emissions Maps for N_2O for Individual Flights

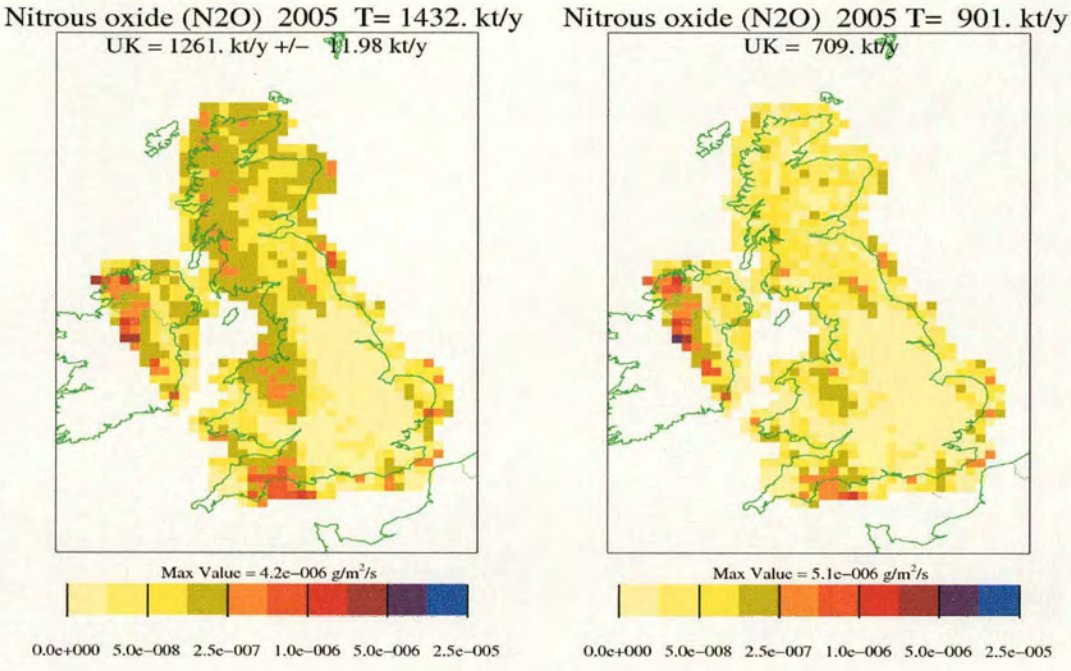

(a) (b)

Figure 180. (a) N_2O emissions (g m^{-2} s^{-1}) for flight B92 at resolution 1×1 boxes and unrestricted domain. (b) Standard deviation of N_2O emissions for 3 maps produced at resolution 1×1 boxes and unrestricted domain.

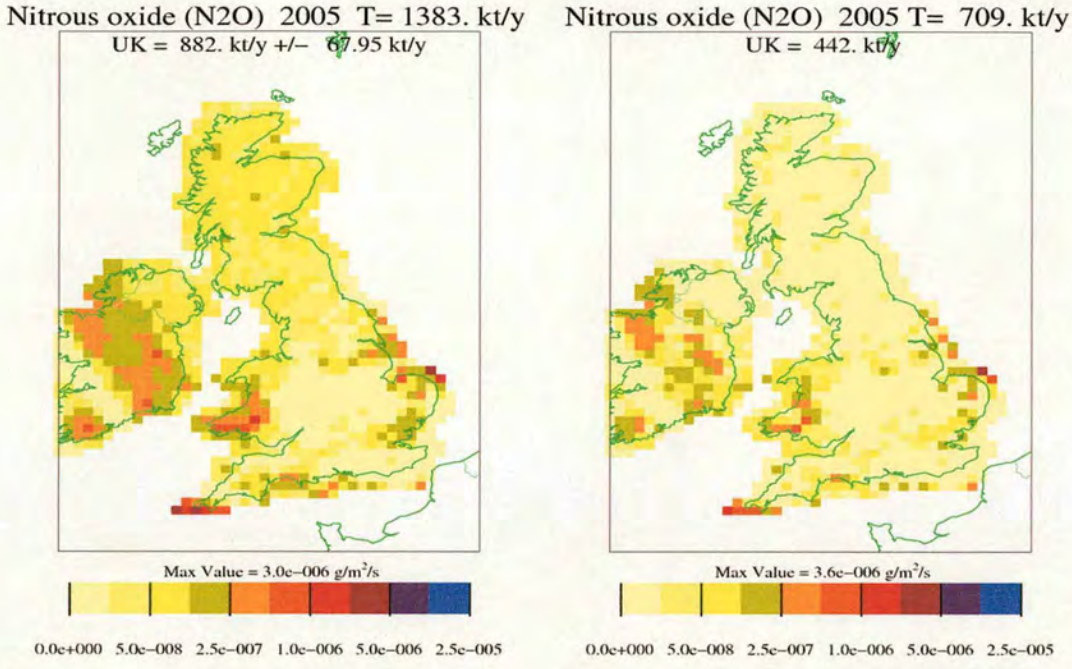

(a) (b)

Figure 181. (a) N_2O emissions (g m^{-2} s^{-1}) for flight B102 at resolution 1×1 boxes and unrestricted domain. (b) Standard deviation of N_2O emissions for 3 maps produced at resolution 1×1 boxes and unrestricted domain.

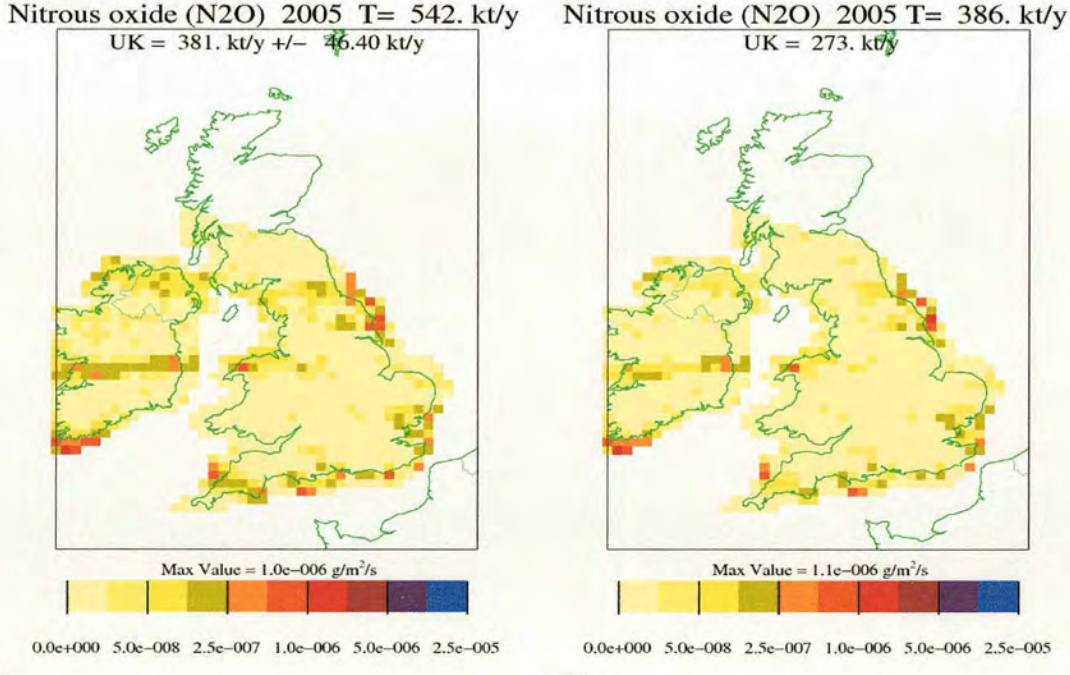

(a) (b)

Figure 182. (a) N_2O emissions (g m^{-2} s^{-1}) for flight B118 at resolution 1×1 boxes and unrestricted domain. (b) Standard deviation of N_2O emissions for 3 maps produced at resolution 1×1 boxes and unrestricted domain.

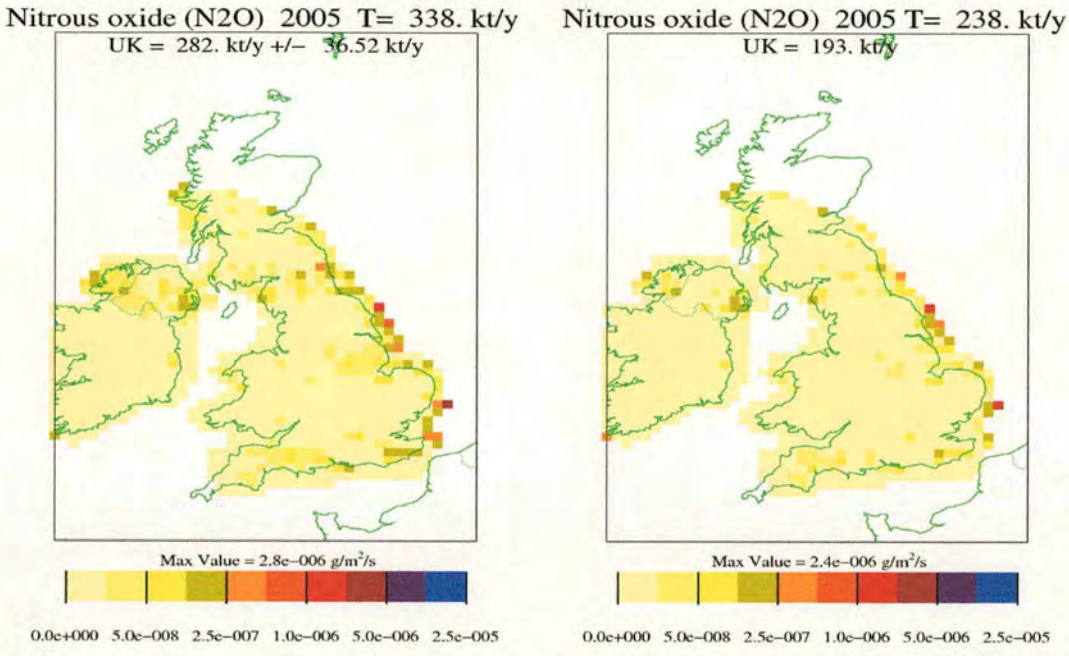

(a) (b)

Figure 183. (a) N_2O emissions (g m^{-2} s^{-1}) for flight B119 at resolution 1×1 boxes and unrestricted domain. (b) Standard deviation of N_2O emissions for 3 maps produced at resolution 1×1 boxes and unrestricted domain.

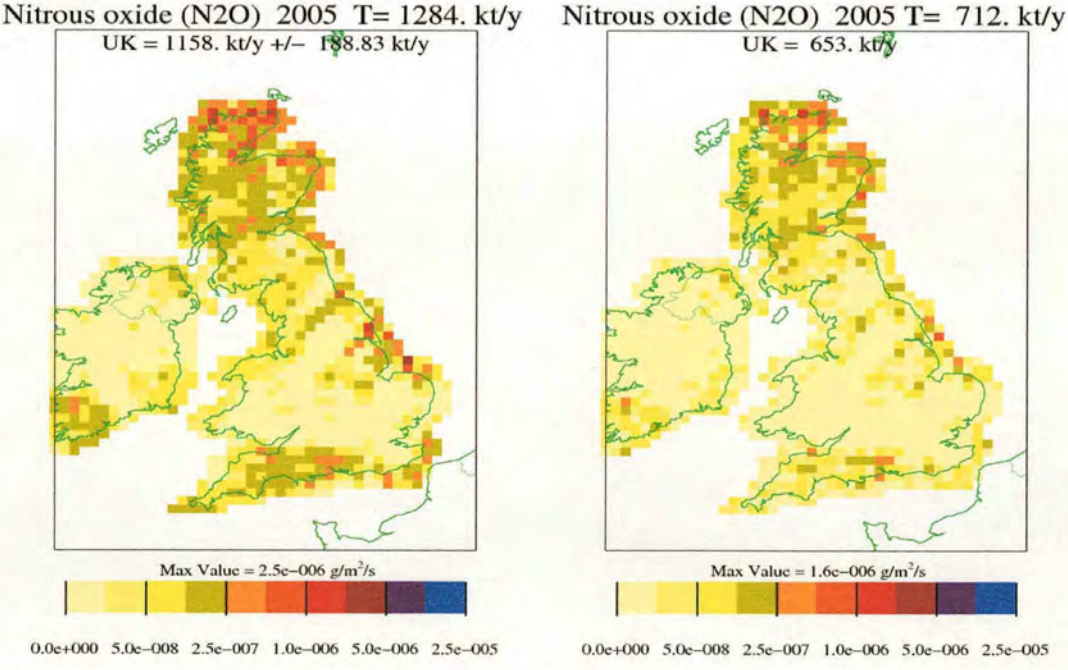

(a) (b)

Figure 184. (a) N_2O emissions (g m^{-2} s^{-1}) for flight B130 at resolution 1×1 boxes and unrestricted domain. (b) Standard deviation of N_2O emissions for 3 maps produced at resolution 1×1 boxes and unrestricted domain.

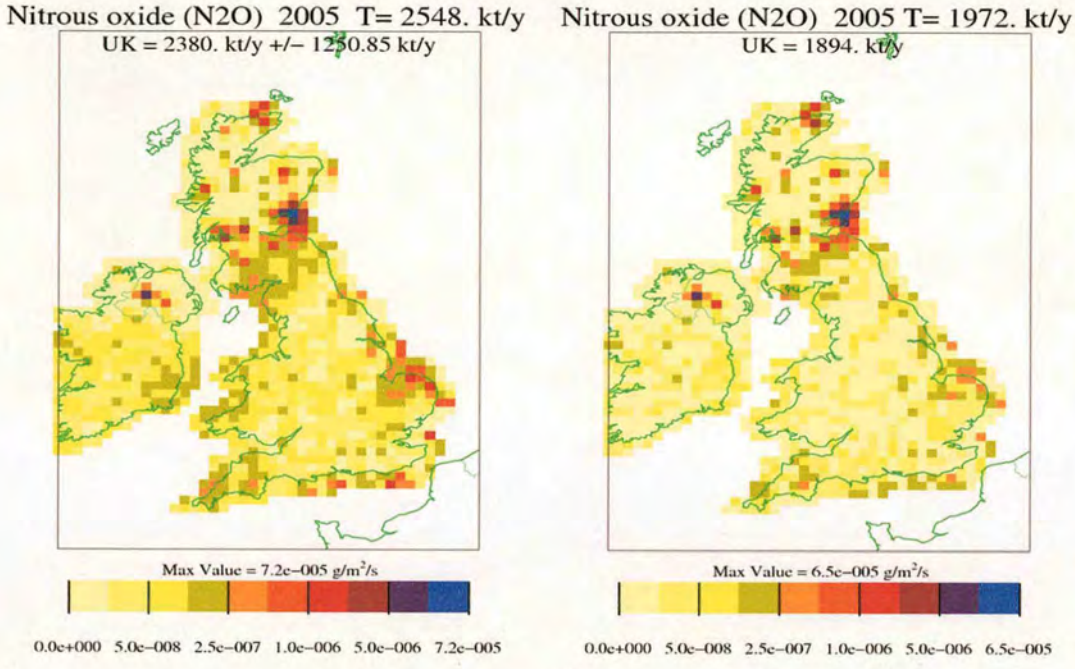

(a) (b)

Figure 185. (a) N_2O emissions (g m^{-2} s^{-1}) for flight B132 at resolution 1×1 boxes and unrestricted domain. (b) Standard deviation of N_2O emissions for 3 maps produced at resolution 1×1 boxes and unrestricted domain.

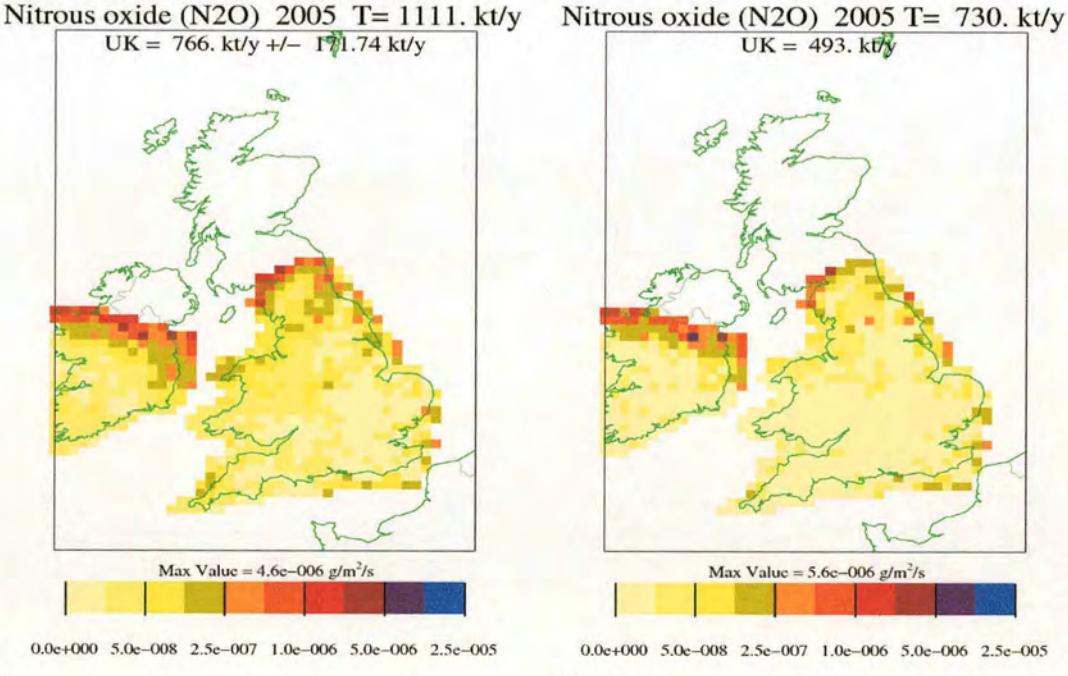

(a) (b)

Figure 186. (a) N_2O emissions (g m^{-2} s^{-1}) for flight B134 at resolution 1×1 boxes and unrestricted domain. (b) Standard deviation of N_2O emissions for 3 maps produced at resolution 1×1 boxes and unrestricted domain.

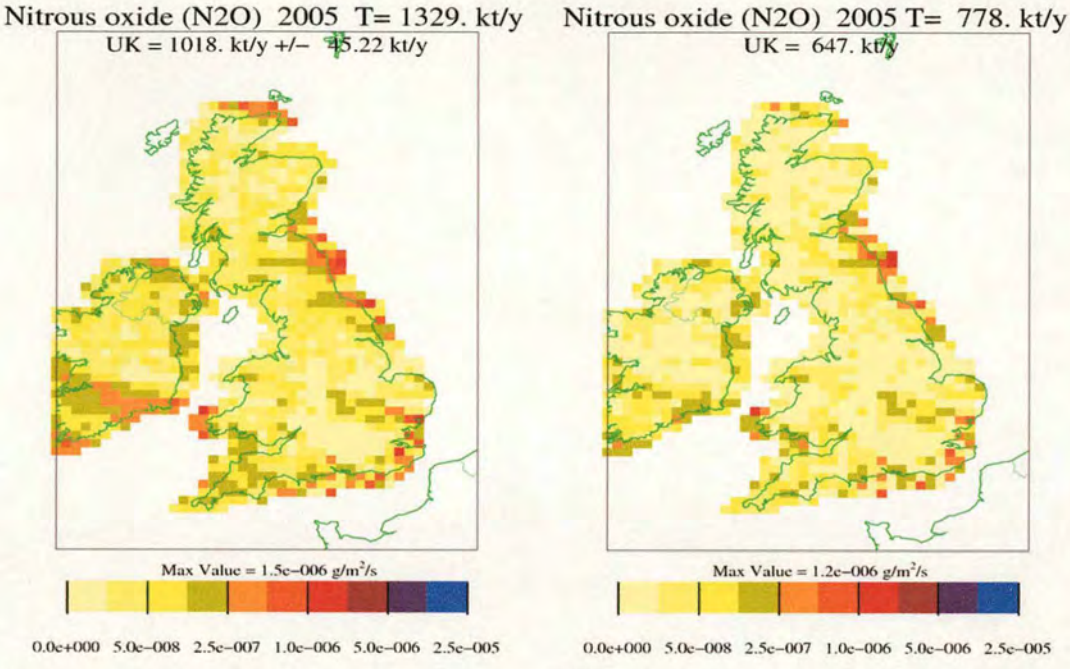

(a) (b)

Figure 187. (a) N_2O emissions (g m^{-2} s^{-1}) for flight B136 at resolution 1×1 boxes and unrestricted domain. (b) Standard deviation of N_2O emissions for 3 maps produced at resolution 1×1 boxes and unrestricted domain.

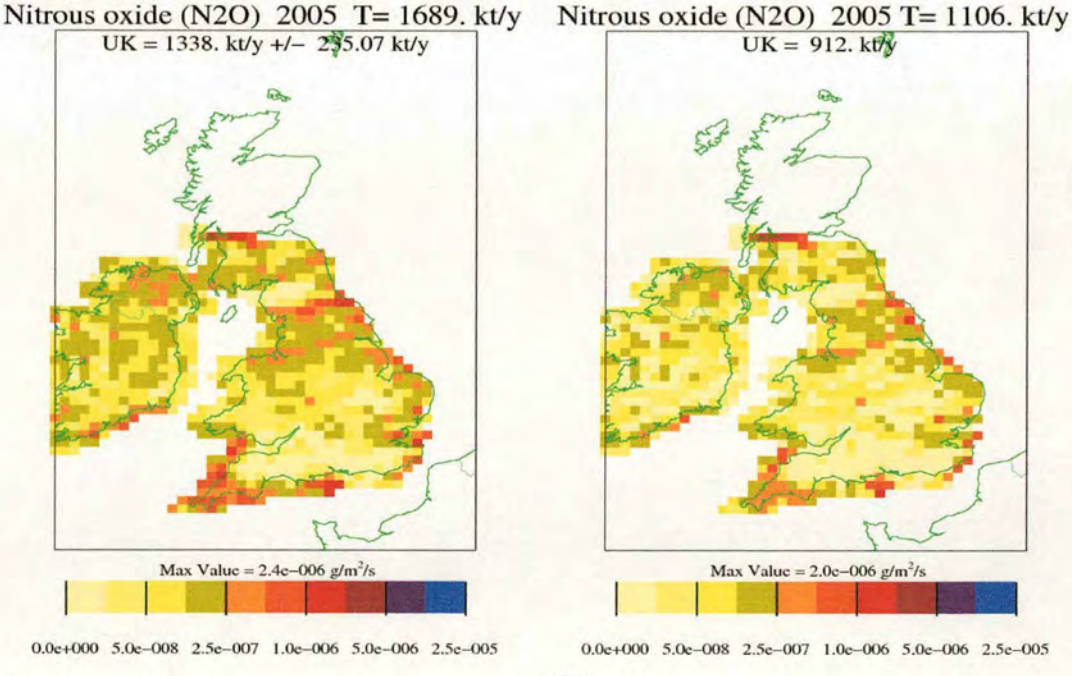

(a) (b)

Figure 188. (a) N_2O emissions (g m^{-2} s^{-1}) for flight B244 at resolution 1×1 boxes and unrestricted domain. (b) Standard deviation of N_2O emissions for 3 maps produced at resolution 1×1 boxes and unrestricted domain.

Appendix 5 NAME Inversion Emissions Maps for Halocarbons

Most maps shown use the unrestricted domain, however maps using the restricted domain are shown for some halocarbons where the unrestricted domain map is poor.

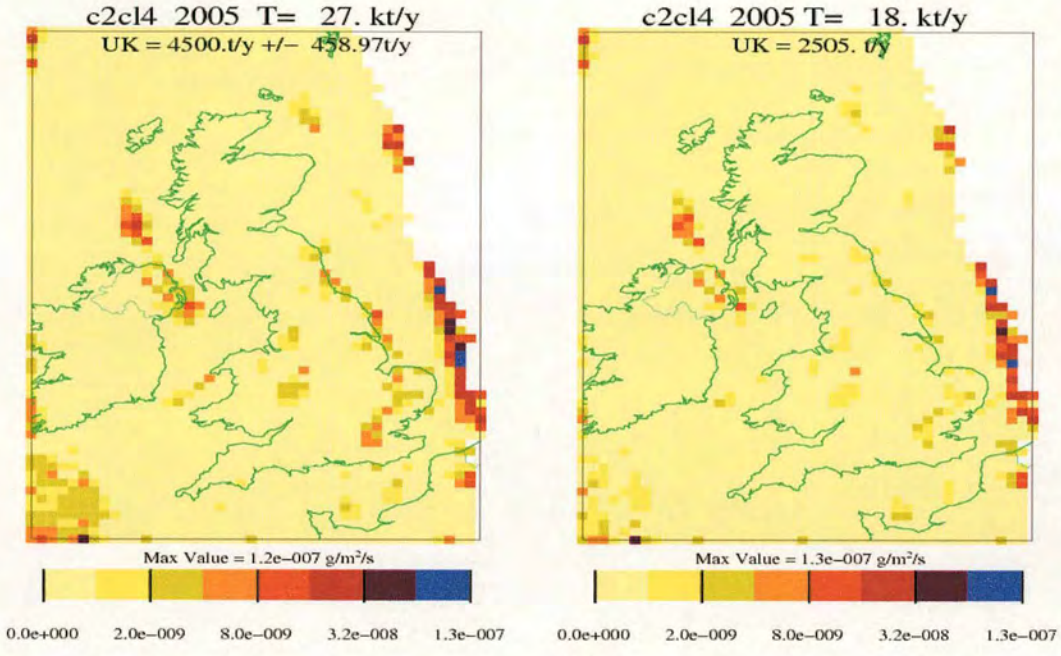

Figure 189. C_2Cl_4 emissions (g m^{-2} s^{-1}) for B92, B102, B111, B118 and B134. (a) 1×1 resolution emissions for unrestricted domain (b) 1×1 resolution standard deviation for 3 inversion solutions for unrestricted domain .

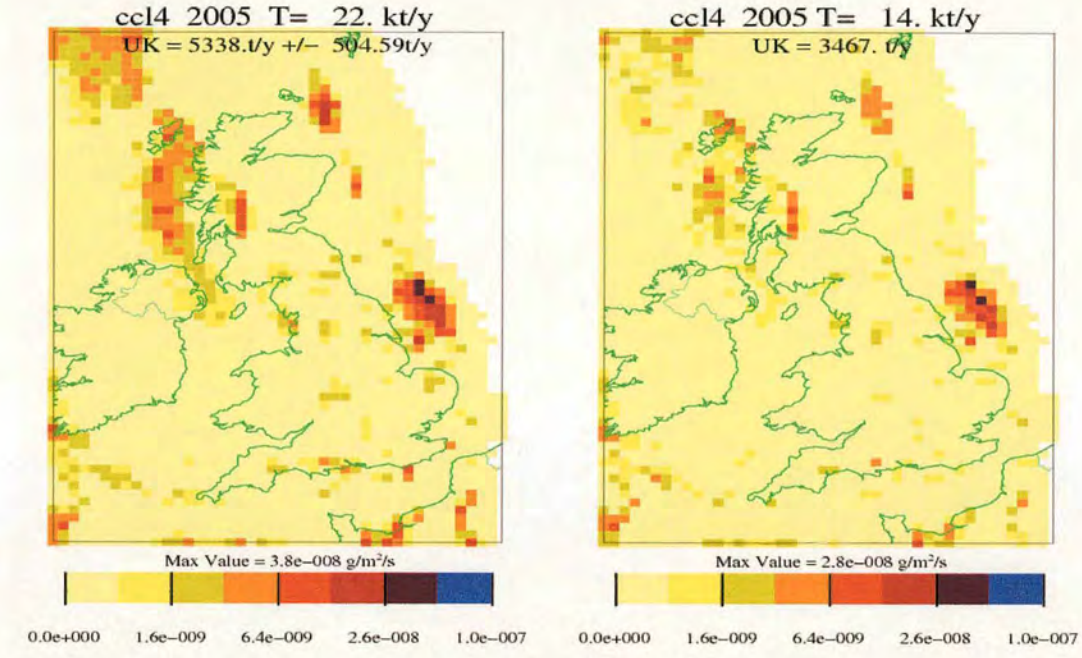

Figure 190. CCl_4 emissions (g m^{-2} s^{-1}) for B92, B102, B111, B118 and B134. (a) 1×1 resolution emissions for unrestricted domain (b) 1×1 resolution standard deviation for 3 inversion solutions for unrestricted domain.

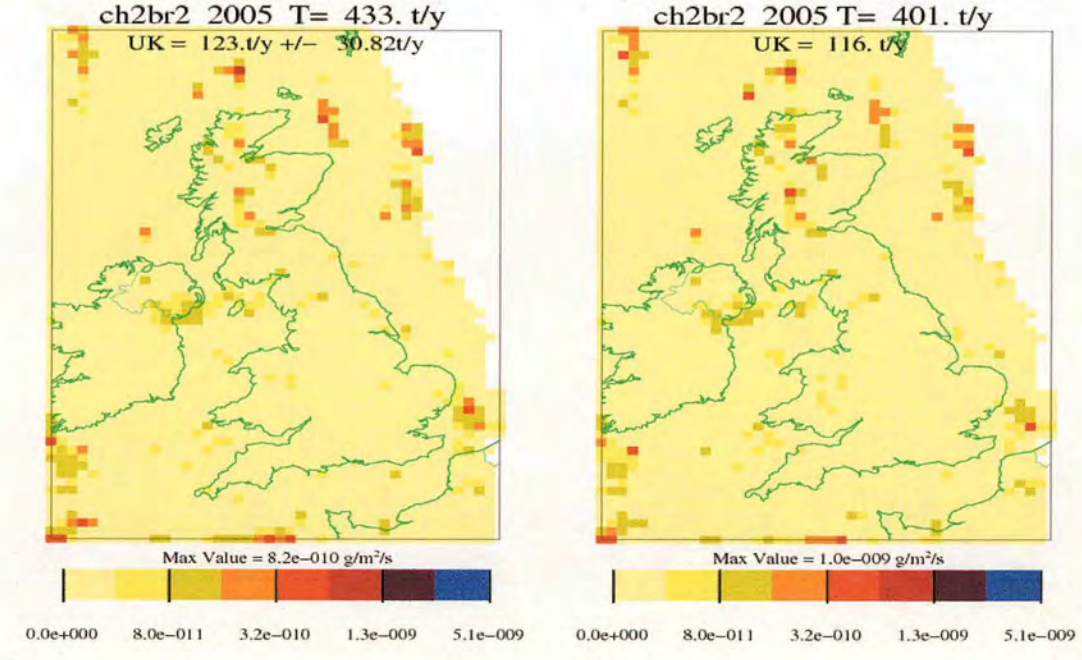

Figure 191. CH_2Br_2 emissions (g m^{-2} s^{-1}) for B92, B102, B111, B118 and B134. (a) 1×1 resolution emissions for unrestricted domain (b) 1×1 resolution standard deviation for 3 inversion solutions for unrestricted domain.

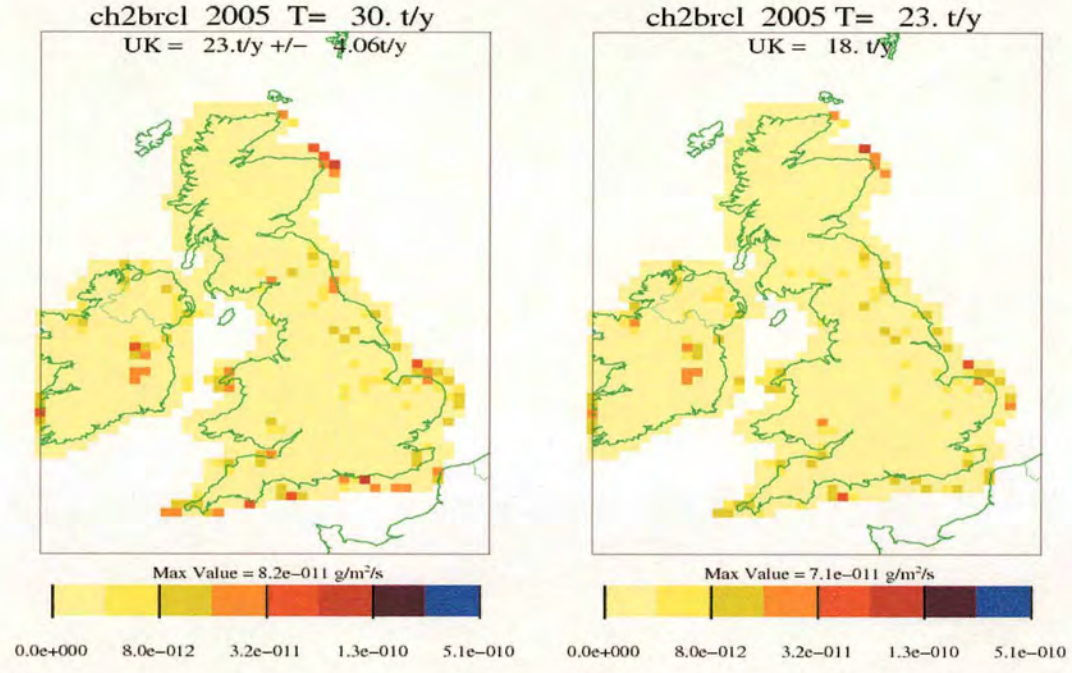

(a) (b)

Figure 192. CH_2BrCl emissions (g m^{-2} s^{-1}) for B92, B102, B111, B118 and B134. (a) 1×1 resolution emissions for restricted domain (b) 1×1 resolution standard deviation for 3 inversion solutions for restricted domain.

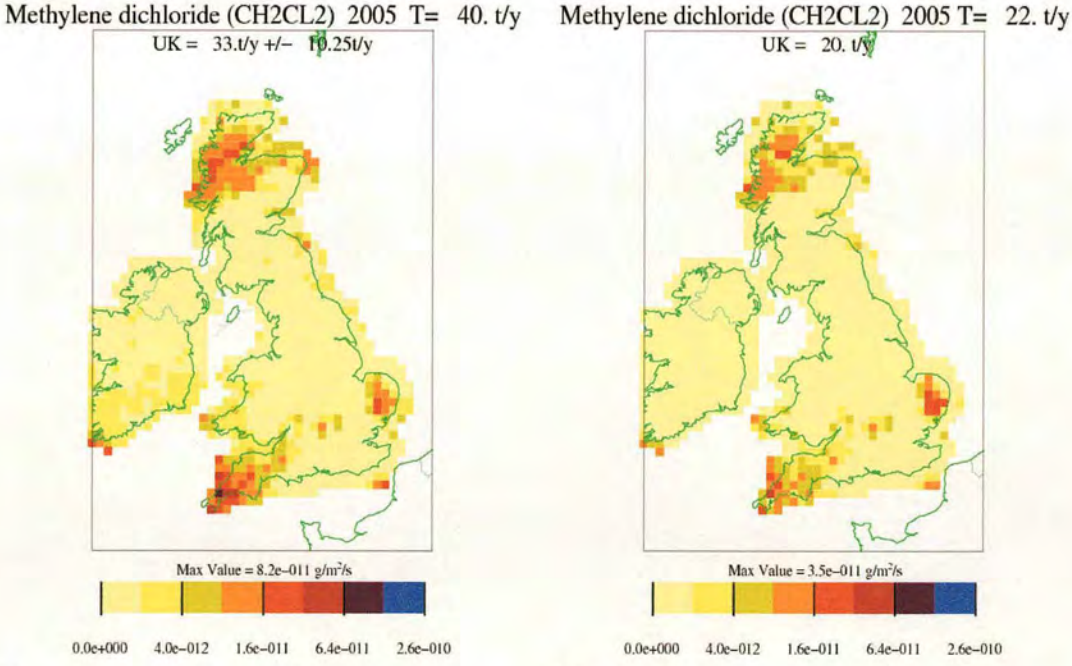

(a) (b)

Figure 193. CH_2Cl_2 emissions (g m^{-2} s^{-1}) for B92, B102, B111, B118 and B134. (a) 1×1 resolution emissions for restricted domain (b) 1×1 resolution standard deviation for 3 inversion solutions for restricted domain.

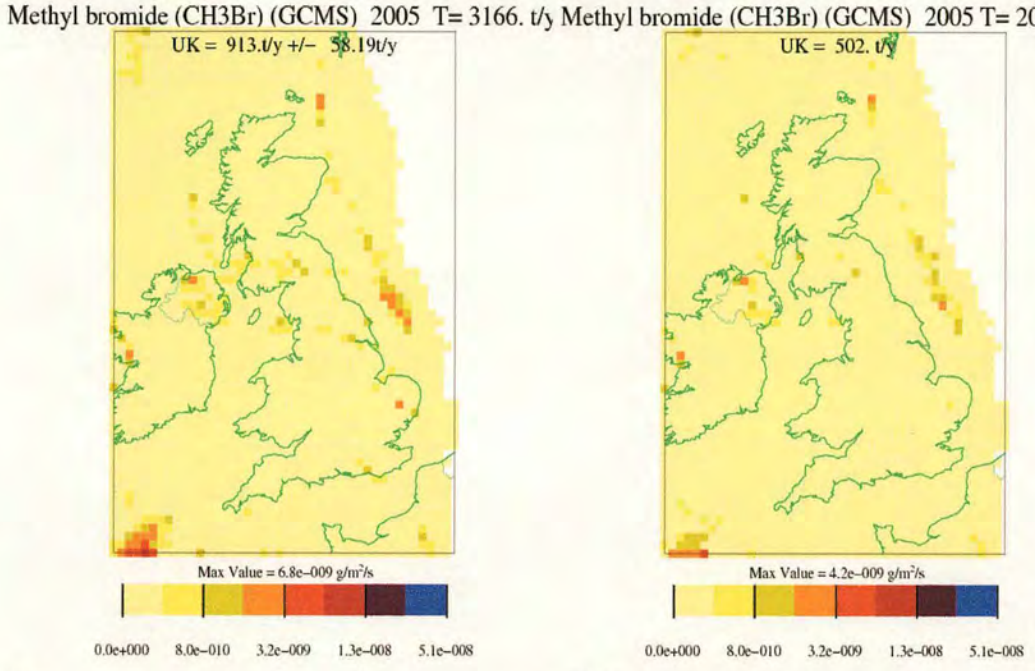

(a) (b)

Figure 194. CH_3Br emissions (g m^{-2} s^{-1}) for flights B92, B102, B111, B118 and B134. (a) 1×1 resolution emissions for unrestricted domain (b) 1×1 resolution standard deviation for 3 inversion solutions for unrestricted domain.

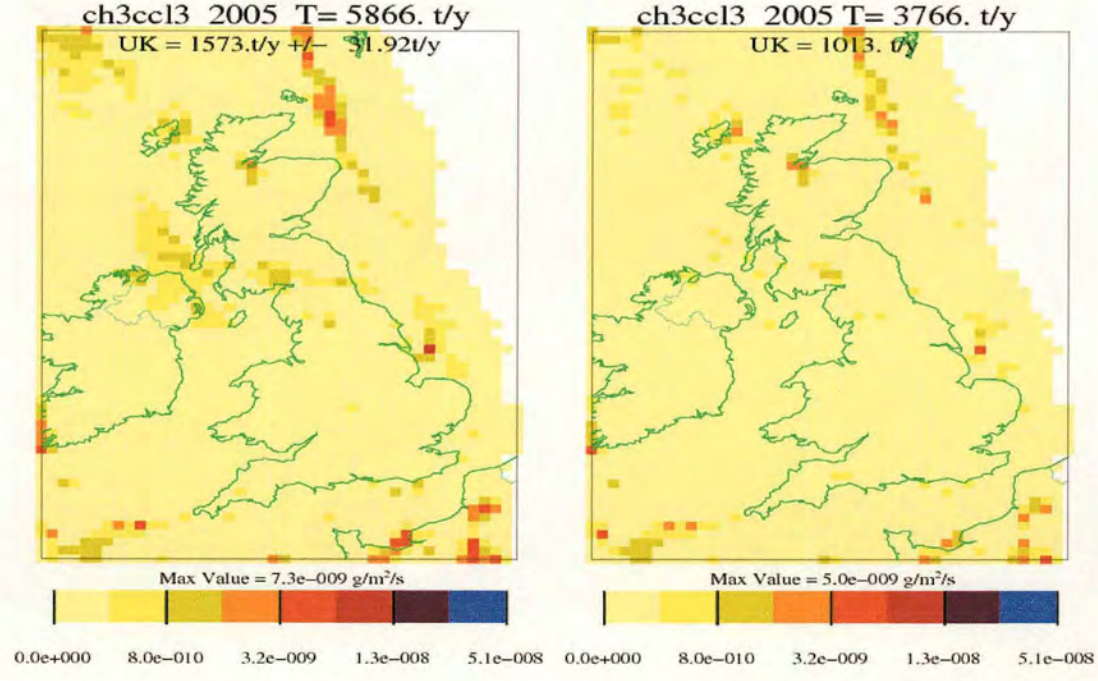

(a) (b)

Figure 195. CH_3CCl_3 emissions (g m^{-2} s^{-1}) for flights B92, B102, B111, B118 and B134. (a) 1×1 resolution emissions for unrestricted domain (b) 1×1 resolution standard deviation for 3 inversion solutions for unrestricted domain.

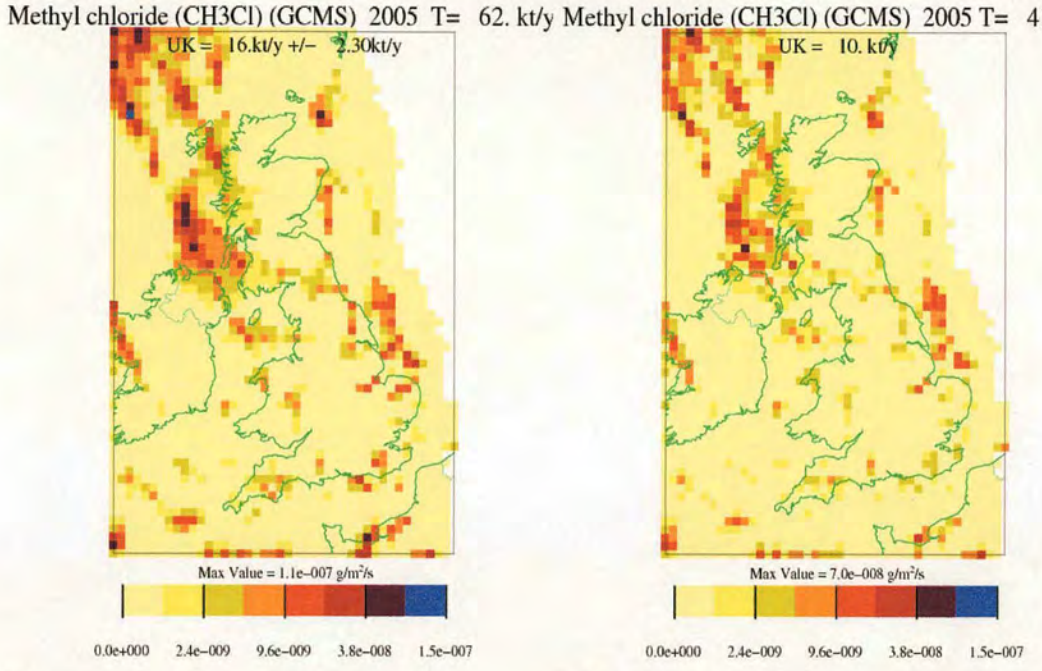

Figure 196. CH_3Cl emissions (g m^{-2} s^{-1}) for flights B92, B102, B111, B118 and B134. (a) 1×1 resolution emissions for unrestricted domain (b) 1×1 resolution standard deviation for 3 inversion solutions for unrestricted domain.

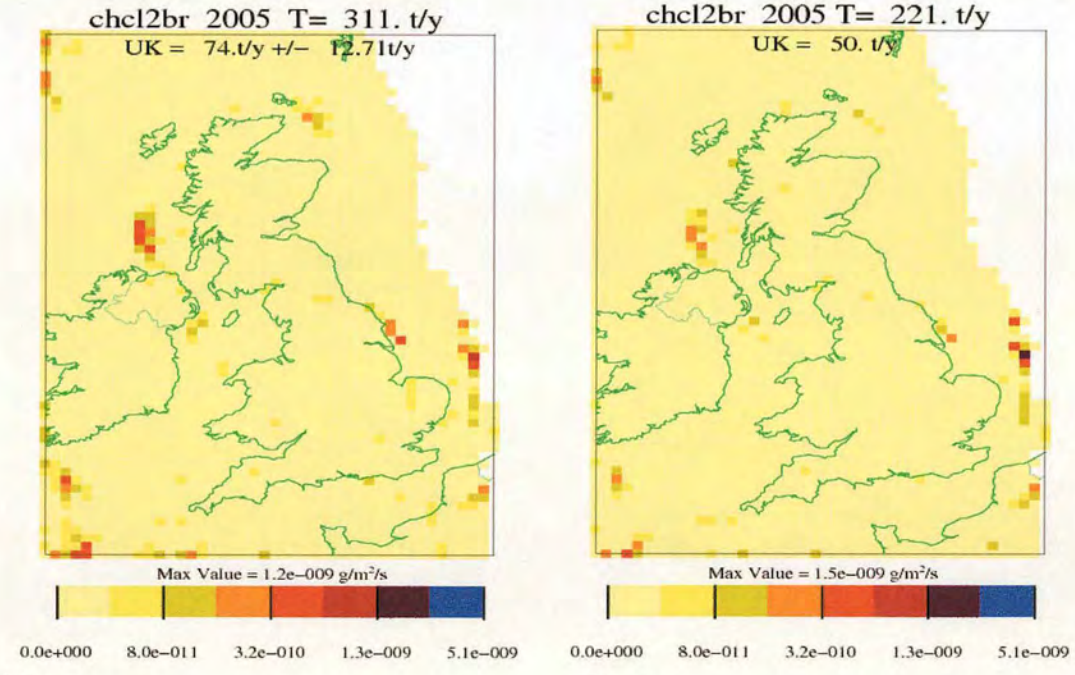

Figure 197. $CHCl_2Br$ emissions (g m^{-2} s^{-1}) for flights B92, B102, B111, B118 and B134. (a) 1×1 resolution emissions for unrestricted domain (b) 1×1 resolution standard deviation for 3 inversion solutions for unrestricted domain.

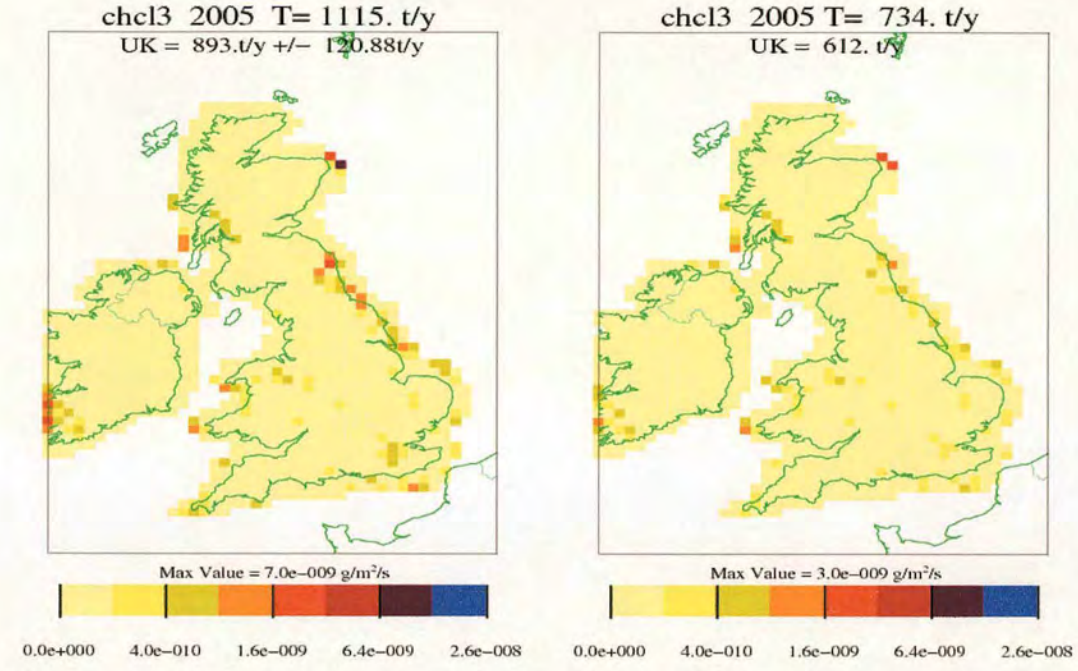

(a) (b)

Figure 198. $CHCl_3$ emissions (g m^{-2} s^{-1}) for flights B92, B102, B111, B118 and B134. (a) 1×1 resolution emissions for restricted domain (b) 1×1 resolution standard deviation for 3 inversion solutions for restricted domain.

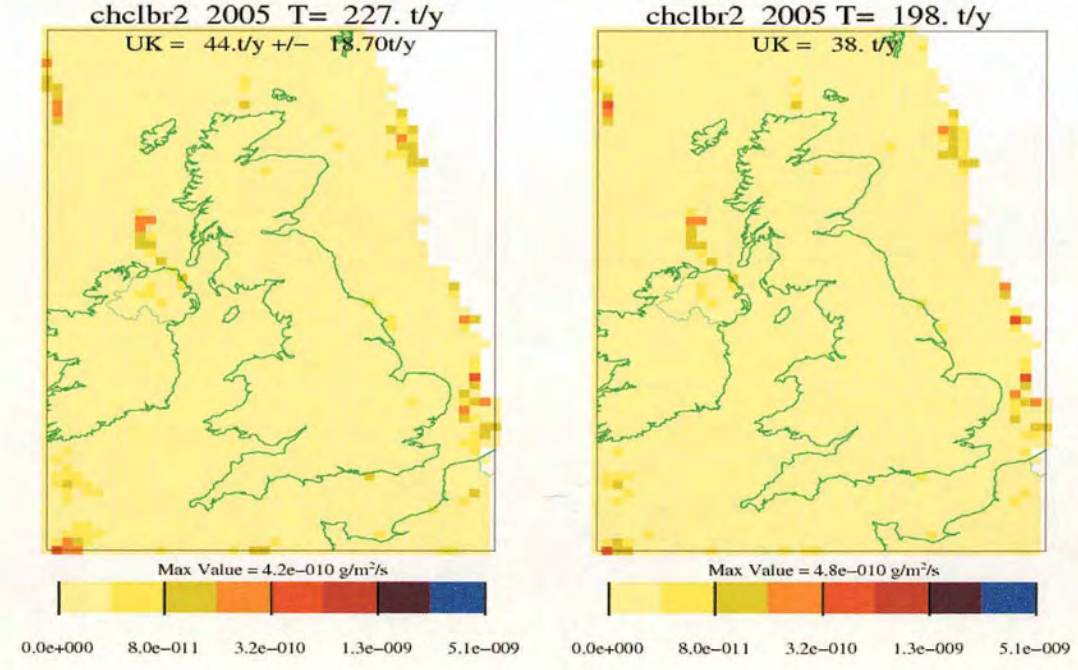

(a) (b)

Figure 199. $CHClBr_2$ emissions (g m^{-2} s^{-1}) for flights B92, B102, B111, B118 and B134. (a) 1×1 resolution emissions for unrestricted domain (b) 1×1 resolution standard deviation for 3 inversion solutions for unrestricted domain.

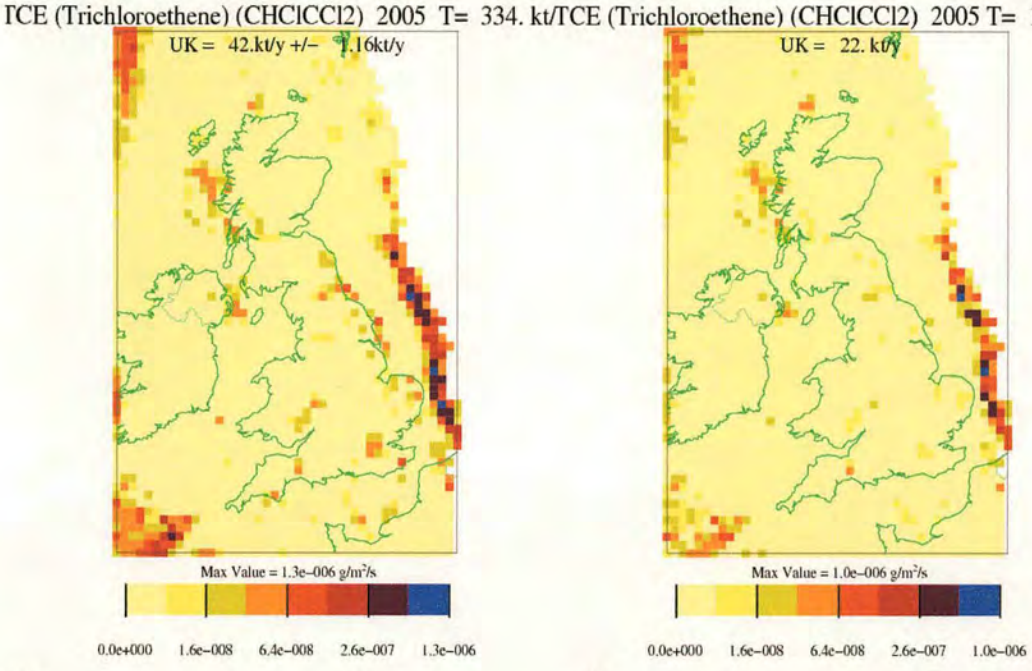

Figure 200. $CHClCCl_2$ emissions (g m^{-2} s^{-1}) for flights B92, B102, B111, B118 and B134. (a) 1×1 resolution emissions for unrestricted domain (b) 1×1 resolution standard deviation for 3 inversion solutions for unrestricted domain.

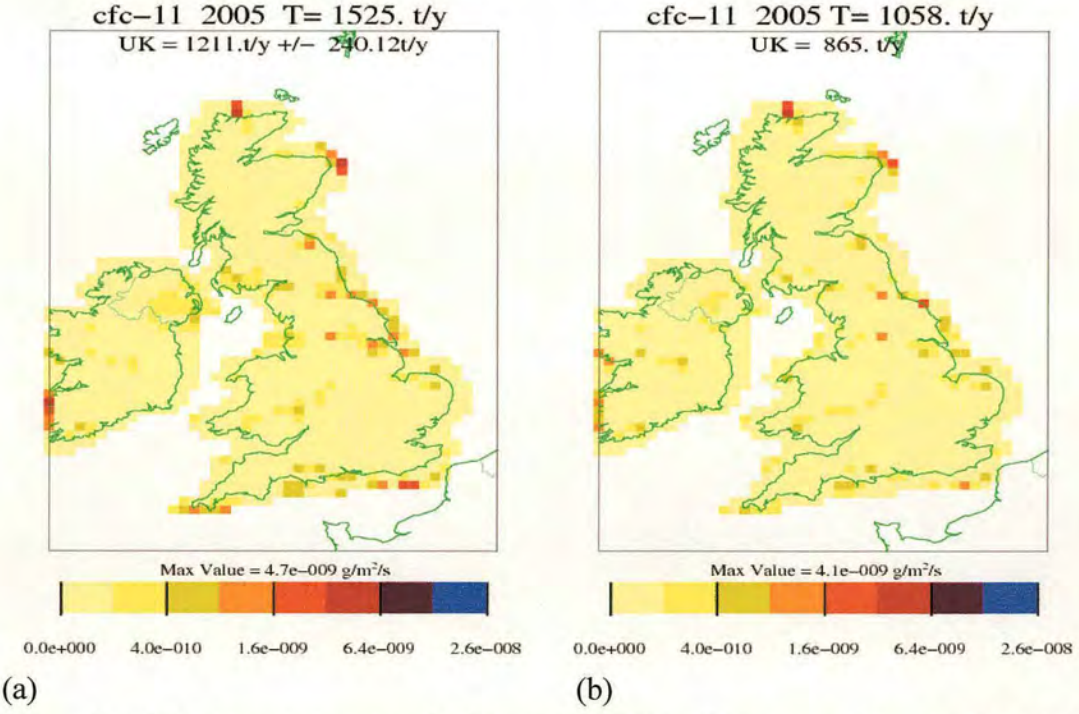

Figure 201. CFC-11 emissions (g m^{-2} s^{-1}) for flights B92, B102, B111, B118 and B134. (a) 1×1 resolution emissions for restricted domain (b) 1×1 resolution standard deviation for 3 inversion solutions for restricted domain.

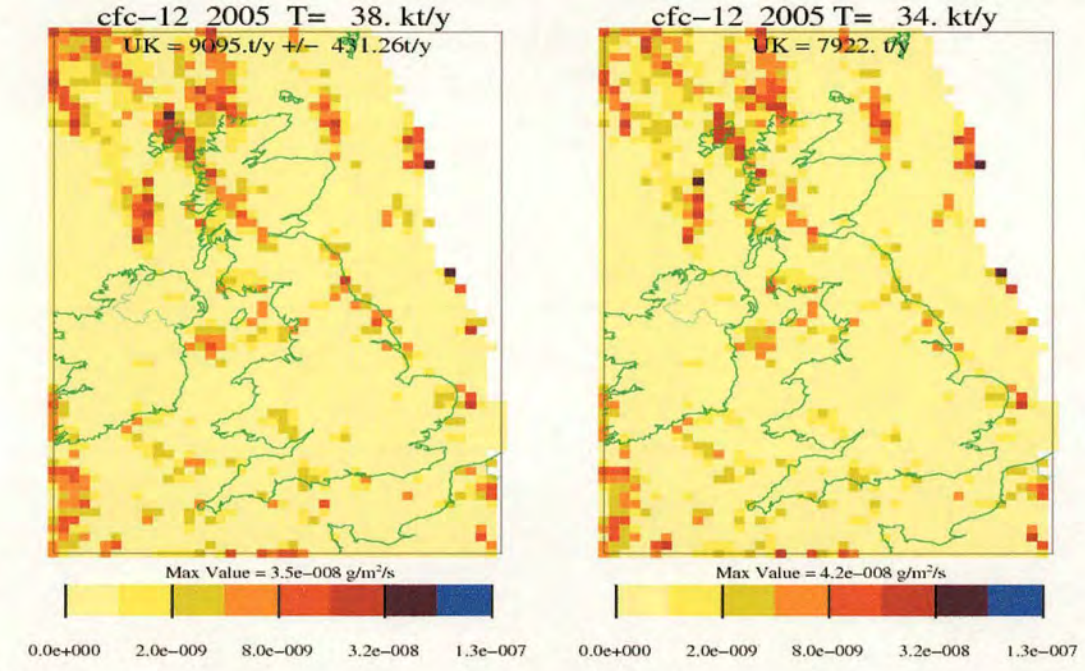

(a) (b)

Figure 202. CFC-12 emissions (g m^{-2} s^{-1}) for flights B92, B102, B111, B118 and B134. (a) 1×1 resolution emissions for unrestricted domain (b) 1×1 resolution standard deviation for 3 inversion solutions for unrestricted domain.

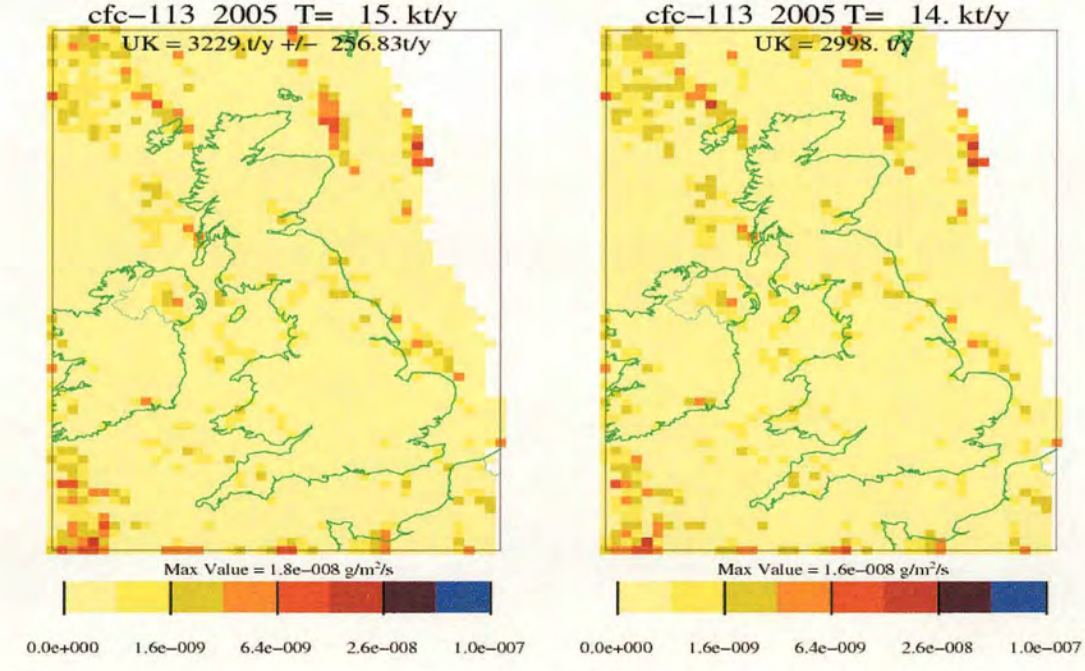

(a) (b)

Figure 203. CFC-113 emissions (g m^{-2} s^{-1}) for flights B92, B102, B111, B118 and B134. (a) 1×1 resolution emissions for unrestricted domain (b) 1×1 resolution standard deviation for 3 inversion solutions for unrestricted domain.

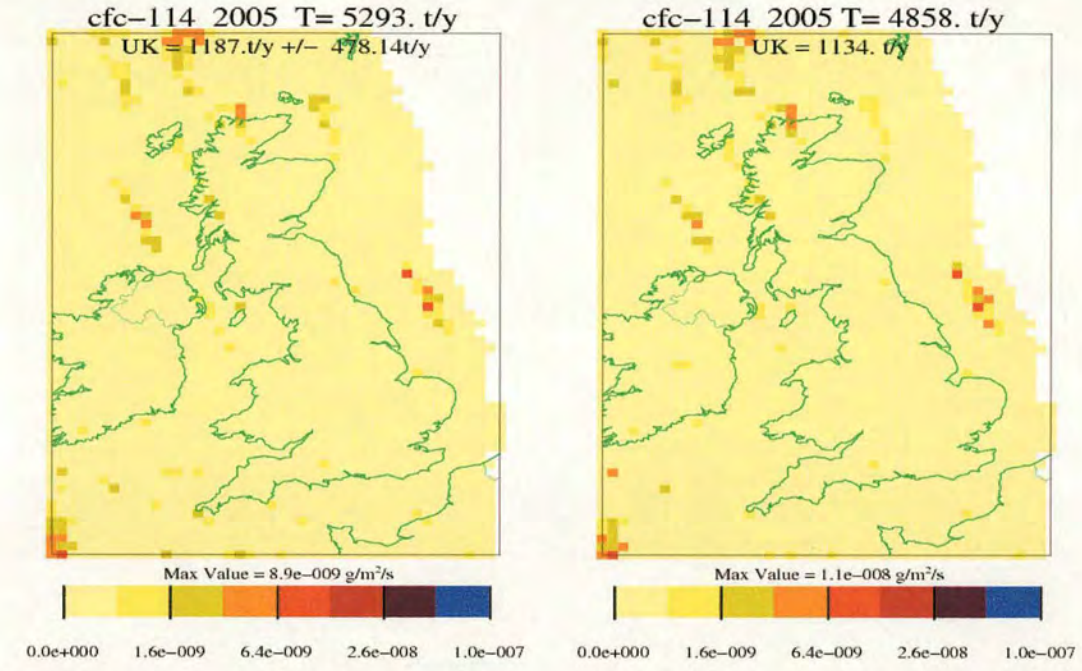

(a) (b)

Figure 204. CFC-114 emissions (g m^{-2} s^{-1}) for flights B92, B102, B111, B118 and B134. (a) 1×1 resolution emissions for unrestricted domain (b) 1×1 resolution standard deviation for 3 inversion solutions for unrestricted domain.

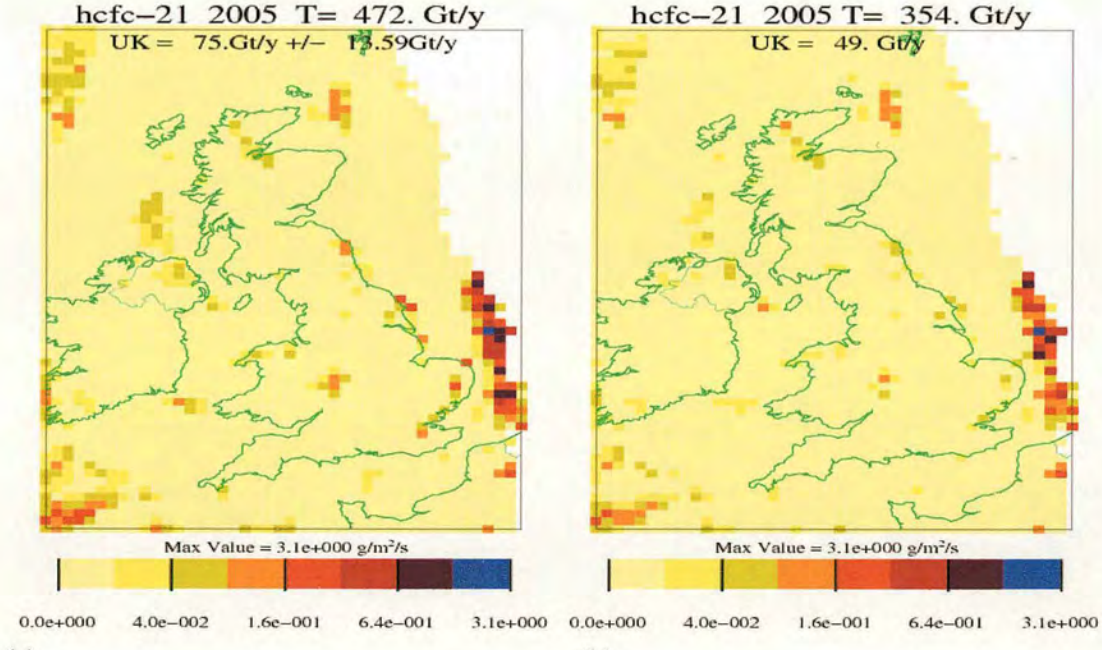

(a) (b)

Figure 205. HCFC-21 emissions (g m^{-2} s^{-1}) for flights B92, B102, B111, B118 and B134. (a) 1×1 resolution emissions for unrestricted domain (b) 1×1 resolution standard deviation for 3 inversion solutions for unrestricted domain. Should be in t/y not Gt/y scale should be multiplied by 10^{-9}.

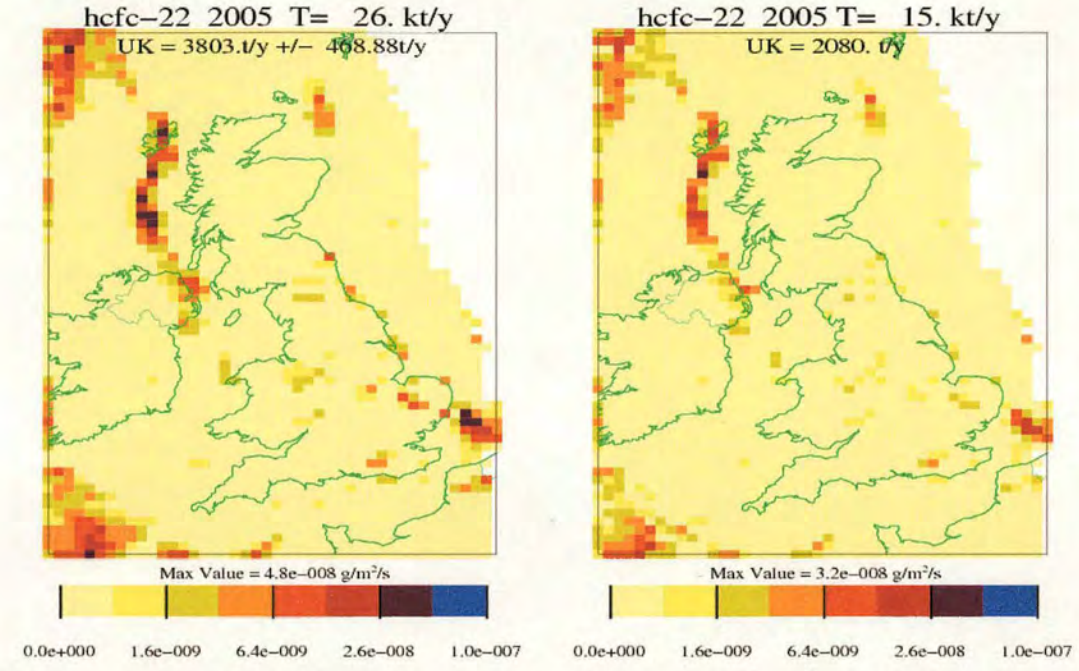

(a) (b)

Figure 206. HCFC-22 emissions (g m^{-2} s^{-1}) for flights B92, B102, B111, B118 and B134. (a) 1×1 resolution emissions for unrestricted domain (b) 1×1 resolution standard deviation for 3 inversion solutions for unrestricted domain.

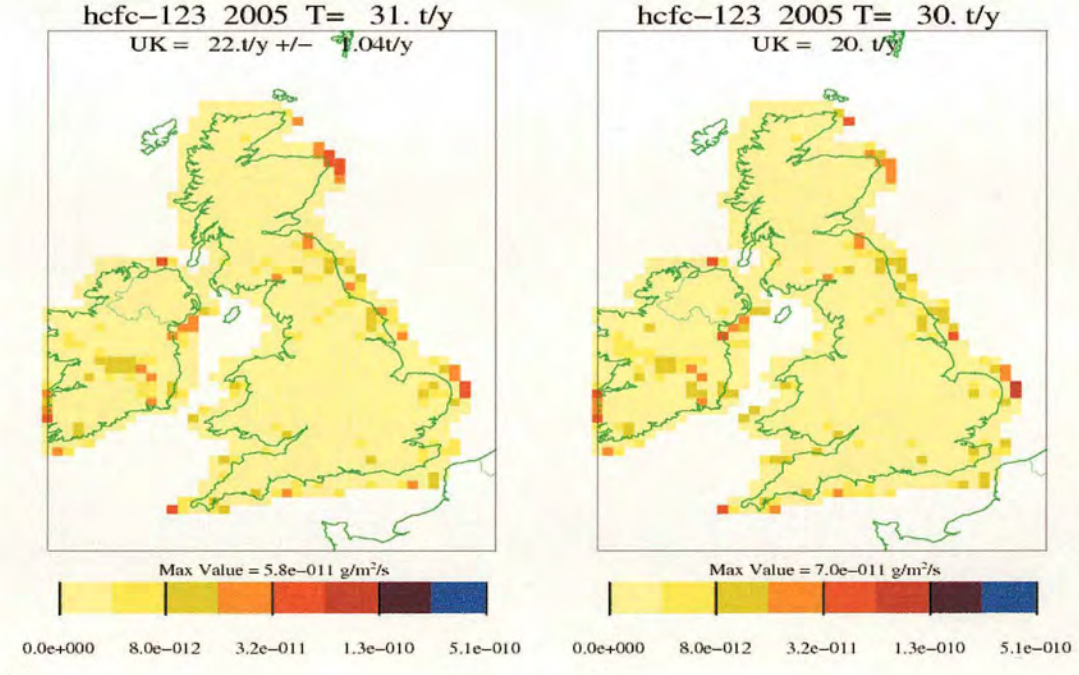

(a) (b)

Figure 207. HCFC-123 emissions (g m^{-2} s^{-1}) for flights B92, B102, B111, B118 and B134. (a) 1×1 resolution emissions for restricted domain (b) 1×1 resolution standard deviation for 3 inversion solutions for restricted domain.

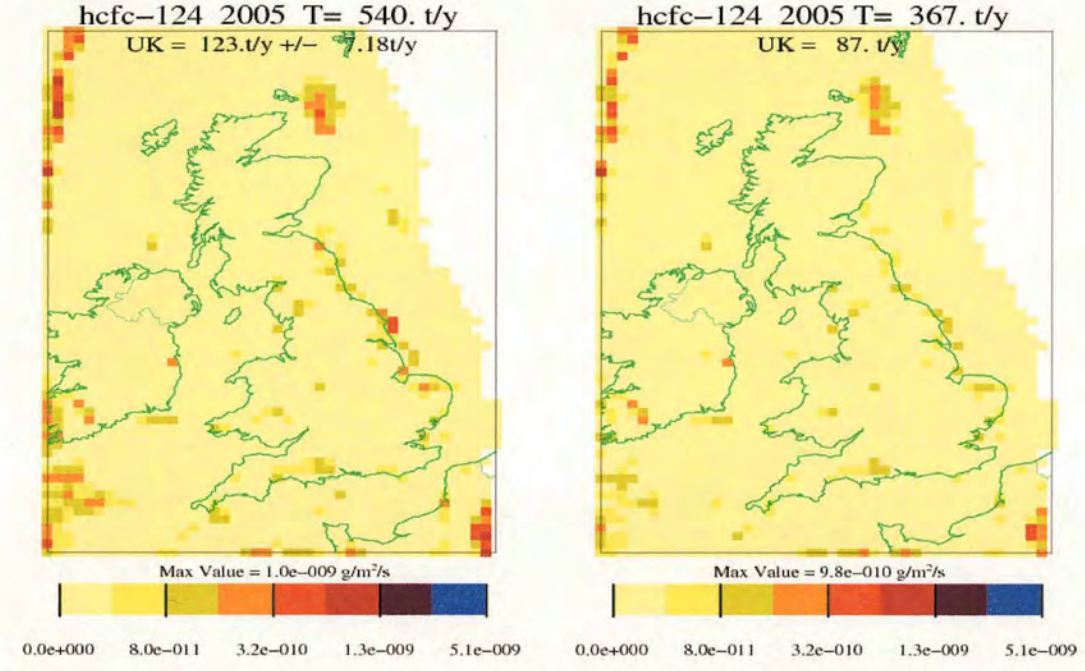

(a) (b)

Figure 208. HCFC-124 emissions (g m^{-2} s^{-1}) for flights B92, B102, B111, B118 and B134. (a) 1×1 resolution emissions for unrestricted domain (b) 1×1 resolution standard deviation for 3 inversion solutions for unrestricted domain.

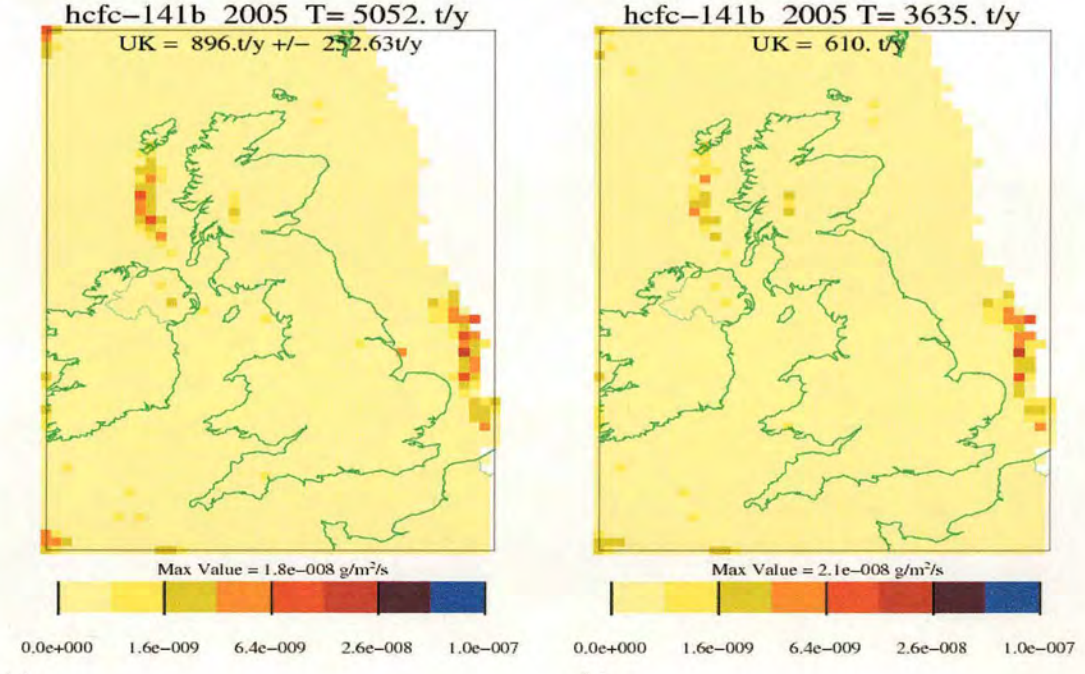

(a) (b)

Figure 209. HCFC-141b emissions (g m^{-2} s^{-1}) for flights B92, B102, B111, B118 and B134. (a) 1×1 resolution emissions for unrestricted domain (b) 1×1 resolution standard deviation for 3 inversion solutions for unrestricted domain.

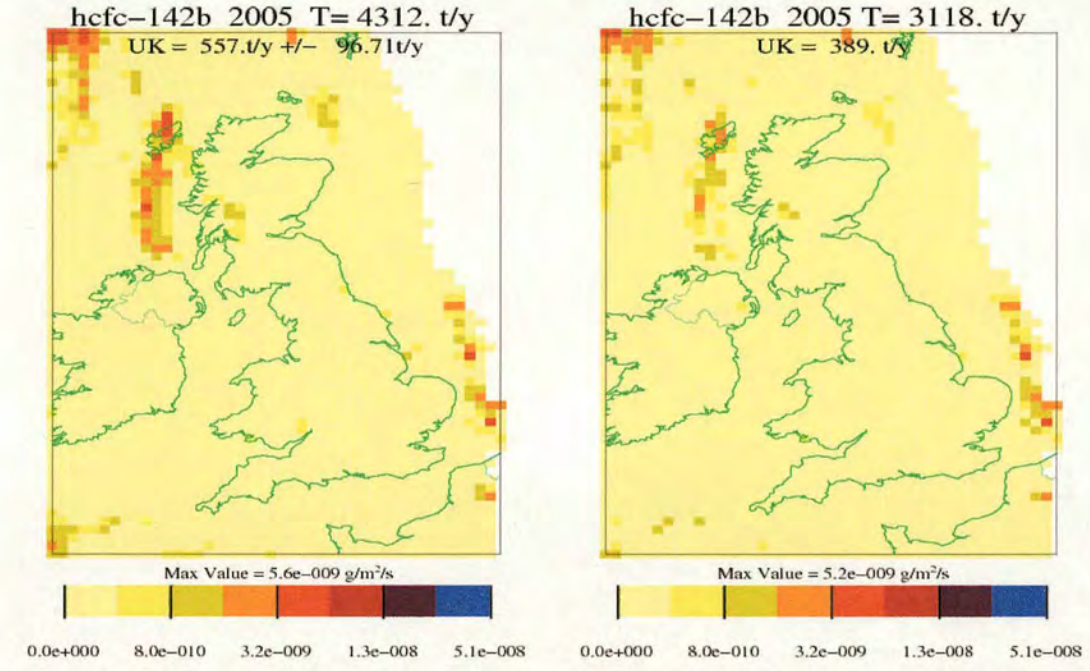

Figure 210. HCFC-142b emissions (g m^{-2} s^{-1}) for flights B92, B102, B111, B118 and B134. (a) 1×1 resolution emissions for unrestricted domain (b) 1×1 resolution standard deviation for 3 inversion solutions for unrestricted domain.

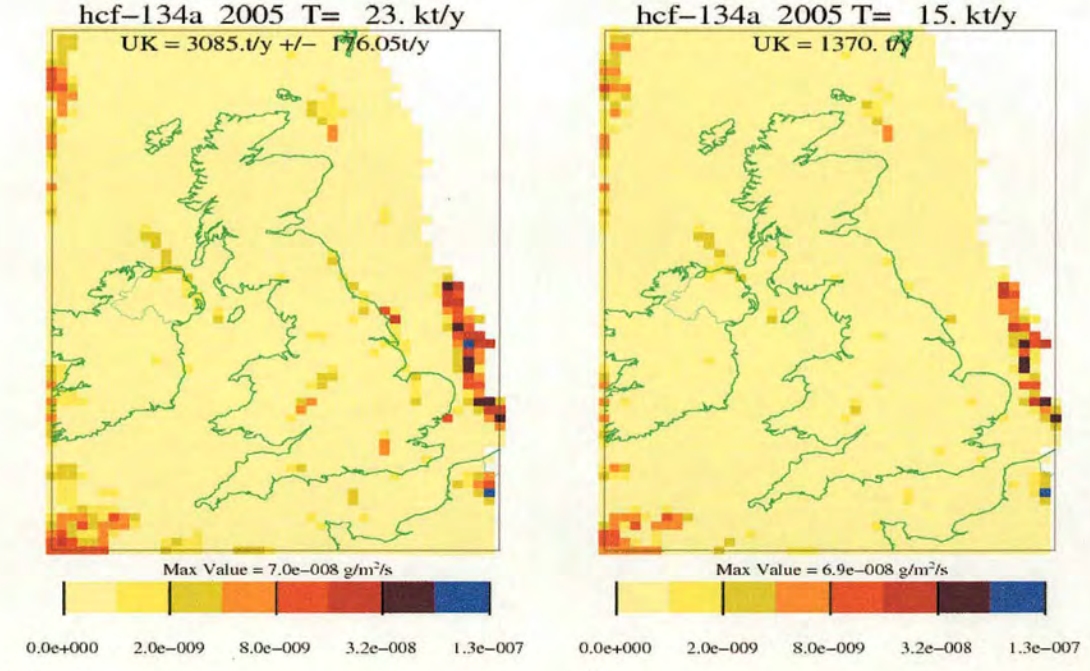

Figure 211. HCF-134a emissions (g m^{-2} s^{-1}) for flights B92, B102, B111, B118 and B134. (a) 1×1 resolution emissions for unrestricted domain (b) 1×1 resolution standard deviation for 3 inversion solutions for unrestricted domain.

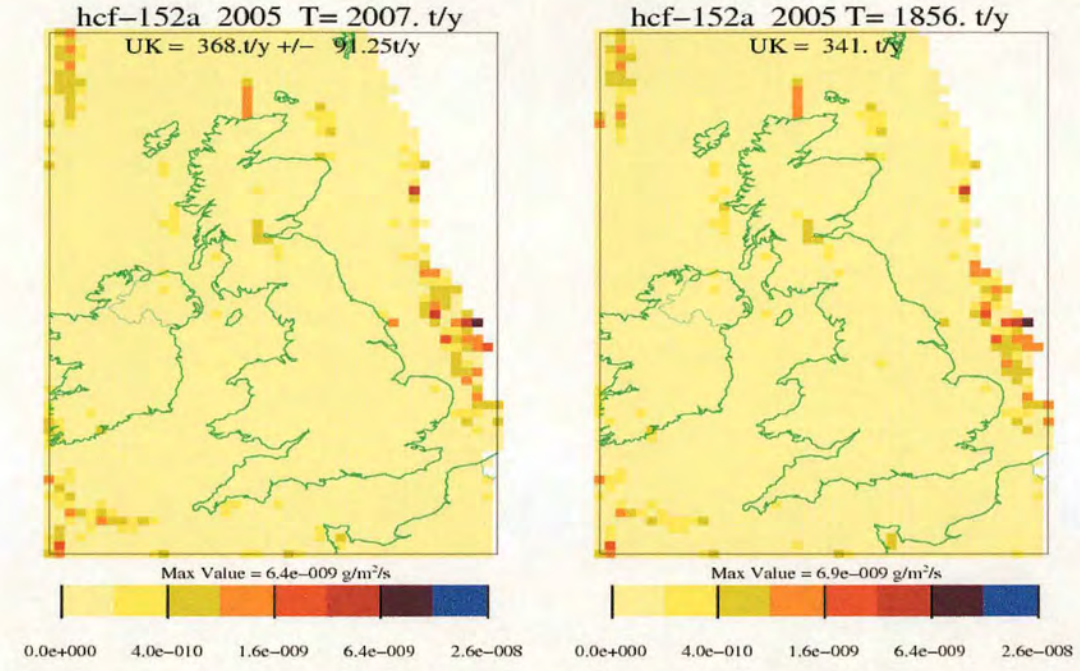

(a) (b)

Figure 212. HCF-152a emissions (g m^{-2} s^{-1}) for flights B92, B102, B111, B118 and B134. (a) 1×1 resolution emissions for unrestricted domain (b) 1×1 resolution standard deviation for 3 inversion solutions for unrestricted domain.

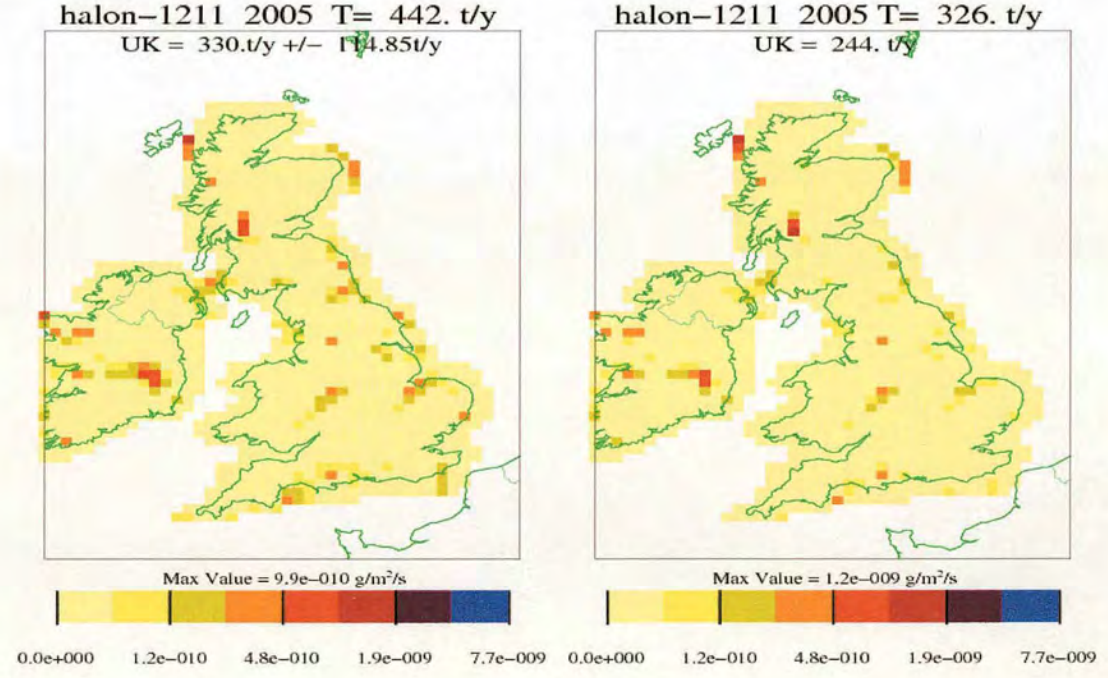

(a) (b)

Figure 213. Halon-1211 emissions (g m^{-2} s^{-1}) for flights B92, B102, B111, B118 and B134. (a) 1×1 resolution emissions for unrestricted domain (b) 1×1 resolution standard deviation for 3 inversion solutions for unrestricted domain.

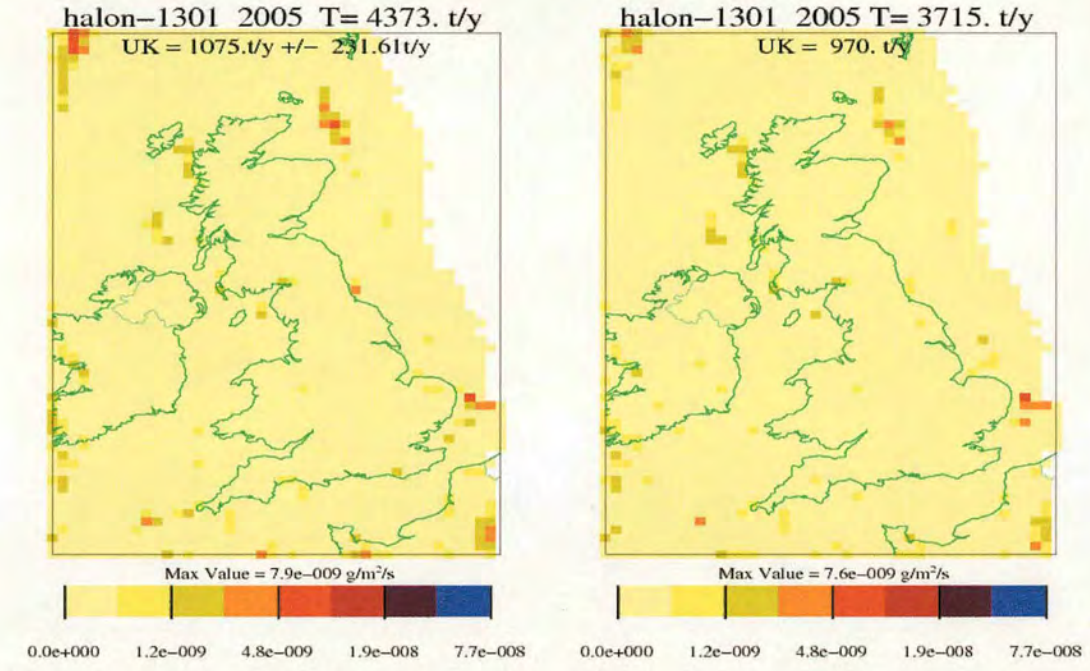

(a) (b)

Figure 214. Halon-1301 emissions (g m^{-2} s^{-1}) for flights B92, B102, B111, B118 and B134. (a) 1×1 resolution emissions for unrestricted domain (b) 1×1 resolution standard deviation for 3 inversion solutions for unrestricted domain.

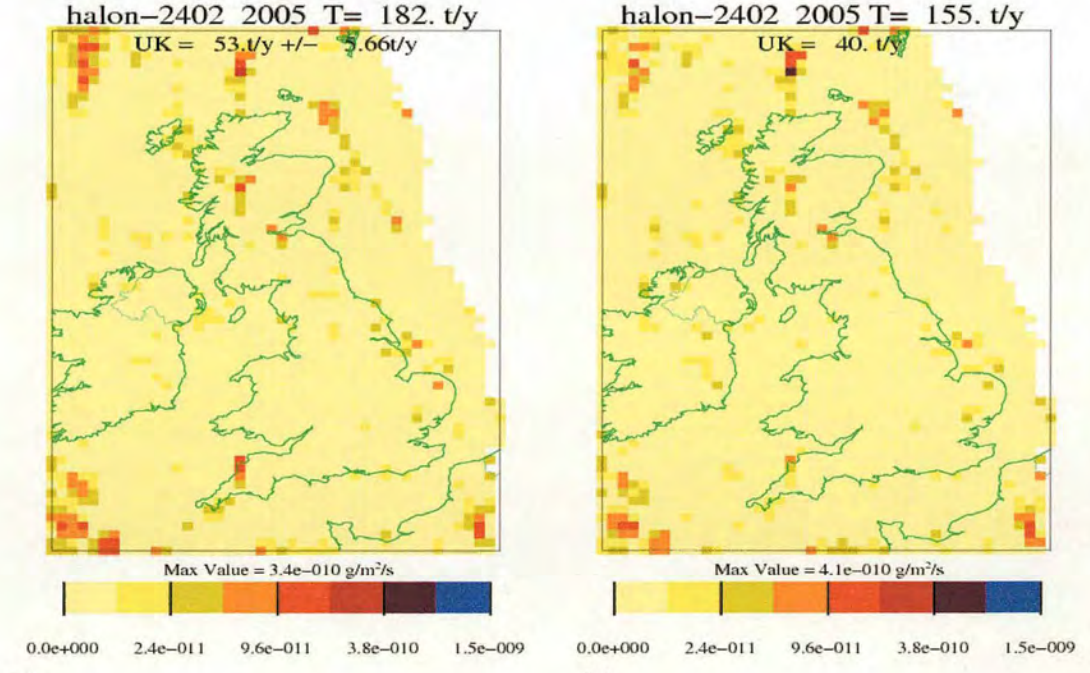

(a) (b)

Figure 215. Halon-2402 emissions (g m^{-2} s^{-1}) for flights B92, B102, B111, B118 and B134. (a) 1×1 resolution emissions for unrestricted domain (b) 1×1 resolution standard deviation for 3 inversion solutions for unrestricted domain.

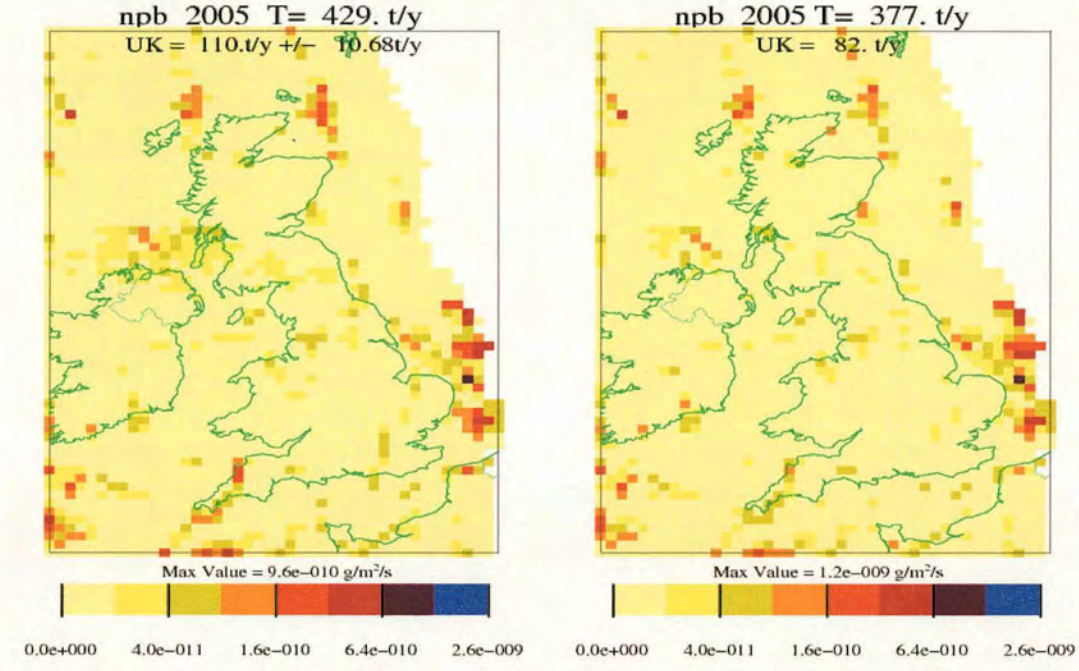

Figure 216. npb emissions (g m^{-2} s^{-1}) for flights B92, B102, B111, B118 and B134. (a) 1×1 resolution emissions for unrestricted domain (b) 1×1 resolution standard deviation for 3 inversion solutions for unrestricted domain.

Appendix 6 NAME Inversion Emissions Maps for Combined Flights

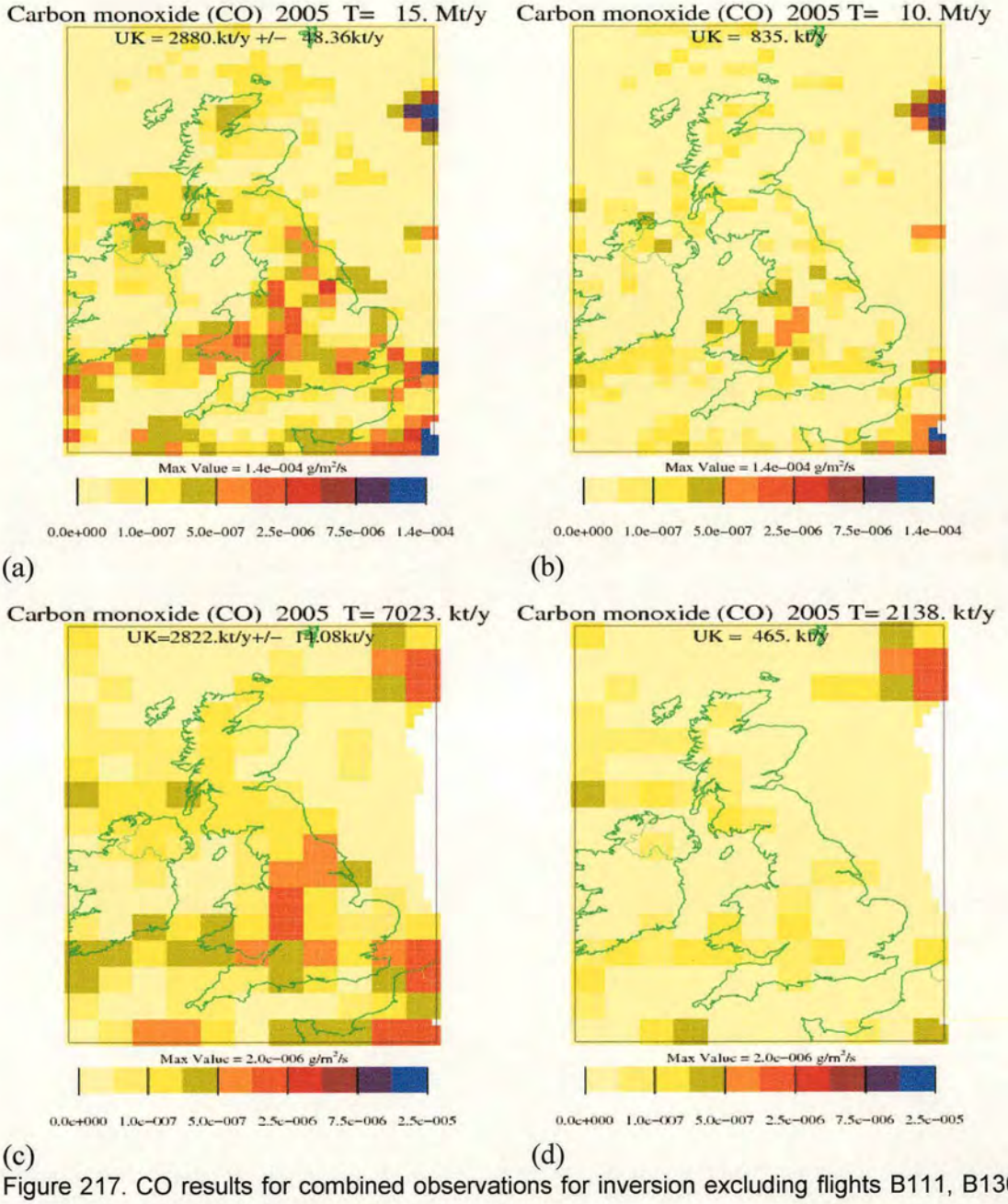

Figure 217. CO results for combined observations for inversion excluding flights B111, B130 and B247 (a) CO emissions (g m^{-2} s^{-1}), resolution 2×2 boxes, unrestricted domain. (b) Standard deviation of CO emissions, resolution 2×2 boxes, unrestricted domain. (c) CO emissions, resolution 4×4 boxes, unrestricted domain. (d) Standard deviation of CO emissions, resolution 4×4 boxes, unrestricted domain.

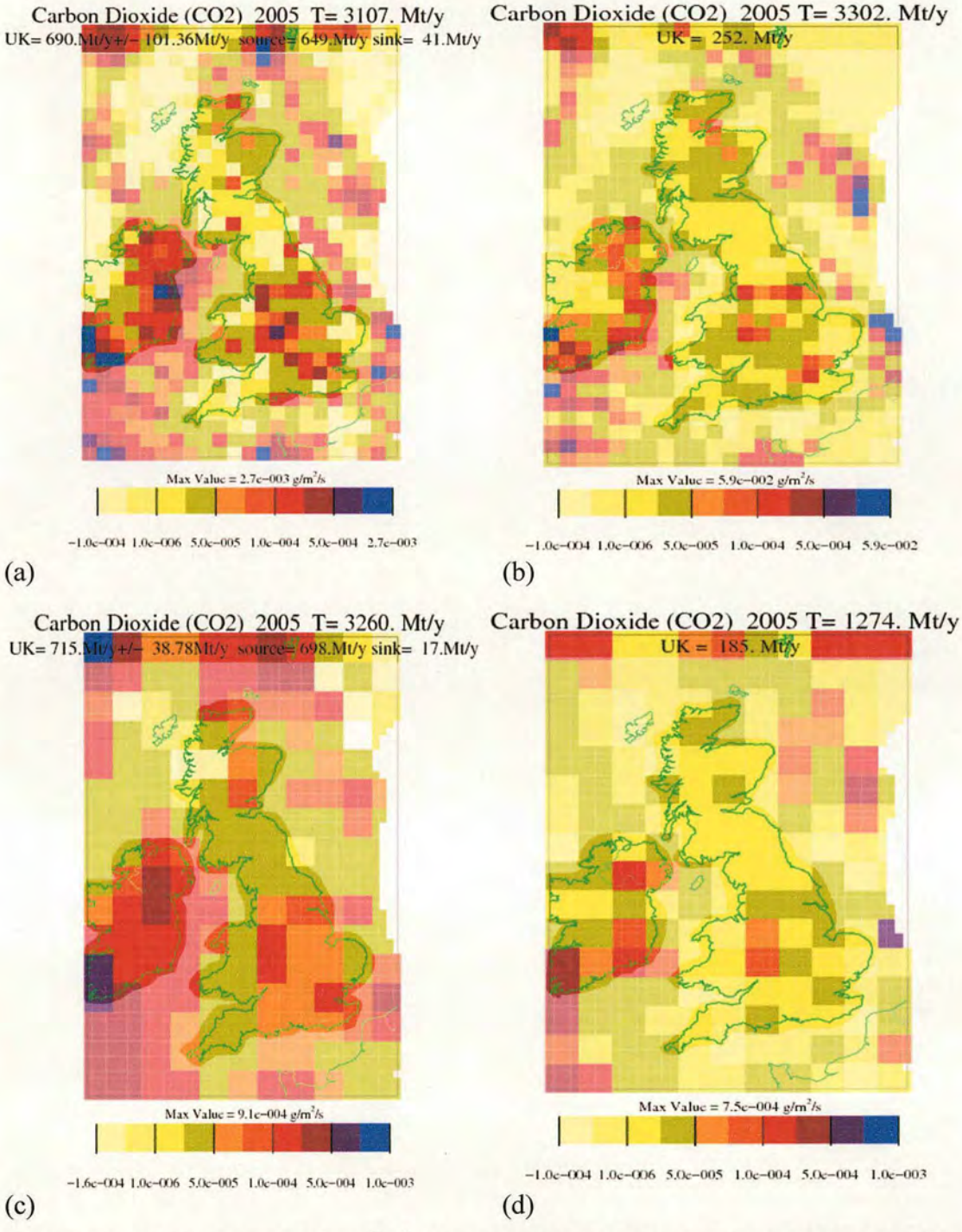

Figure 218. (a) CO_2 emissions (g m^{-2} s^{-1}) using combined observations for inversion excluding flights B111, B130 and B247, at resolution 2×2 boxes and unrestricted domain. (b) Standard deviation of CO2 emissions for 3 maps produced using combined observations excluding flights B111, B130 and B247, at resolution 2×2 boxes and unrestricted domain. (c) CO_2 emissions (g m^{-2} s^{-1}) using combined observations for inversion excluding flights B111, B130 and B247, at resolution 4×4 boxes and unrestricted domain. (d) Standard deviation of CO_2 emissions for 3 maps produced using combined observations excluding flights B111, B130 and B247, at resolution 4×4 boxes and unrestricted domain.

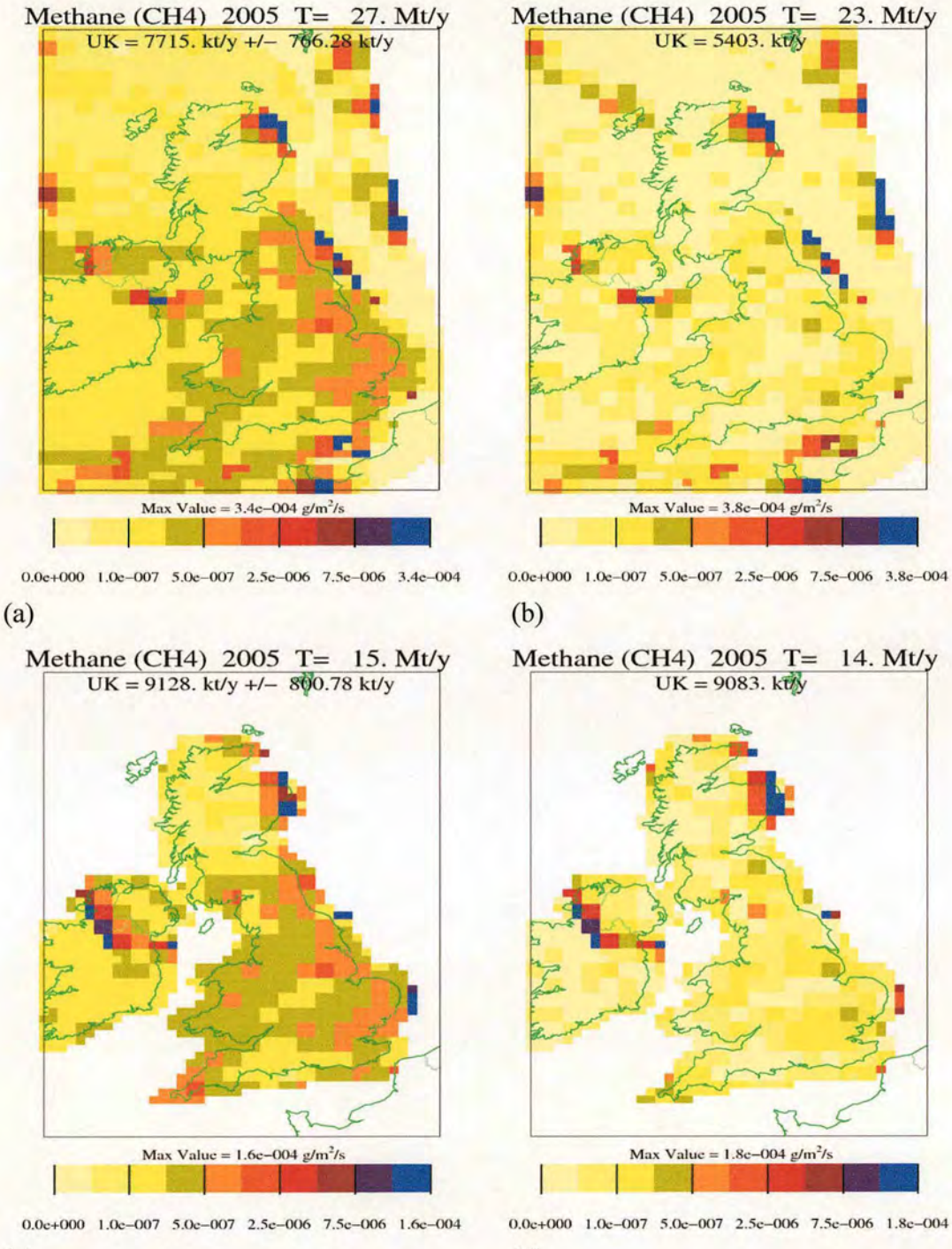

Figure 219. Using flights B92, B97, B113, B132, B134, B136, B244. (a) CH_4 emissions (g m^{-2} s^{-1}) using weighted average approach at resolution 2×2 grid boxes and with an unrestricted domain. (b) Standard deviation of CH_4 emissions for weighted average technique for resolution of 2×2 grid boxes and unrestricted domain (c) CH_4 emissions (g m^{-2} s^{-1}) for weighted average technique for resolution of 2×2 grid boxes and restricted domain. (d) Standard deviation of CH_4 emissions for weighted average technique for resolution of 2×2 grid boxes and restricted domain.

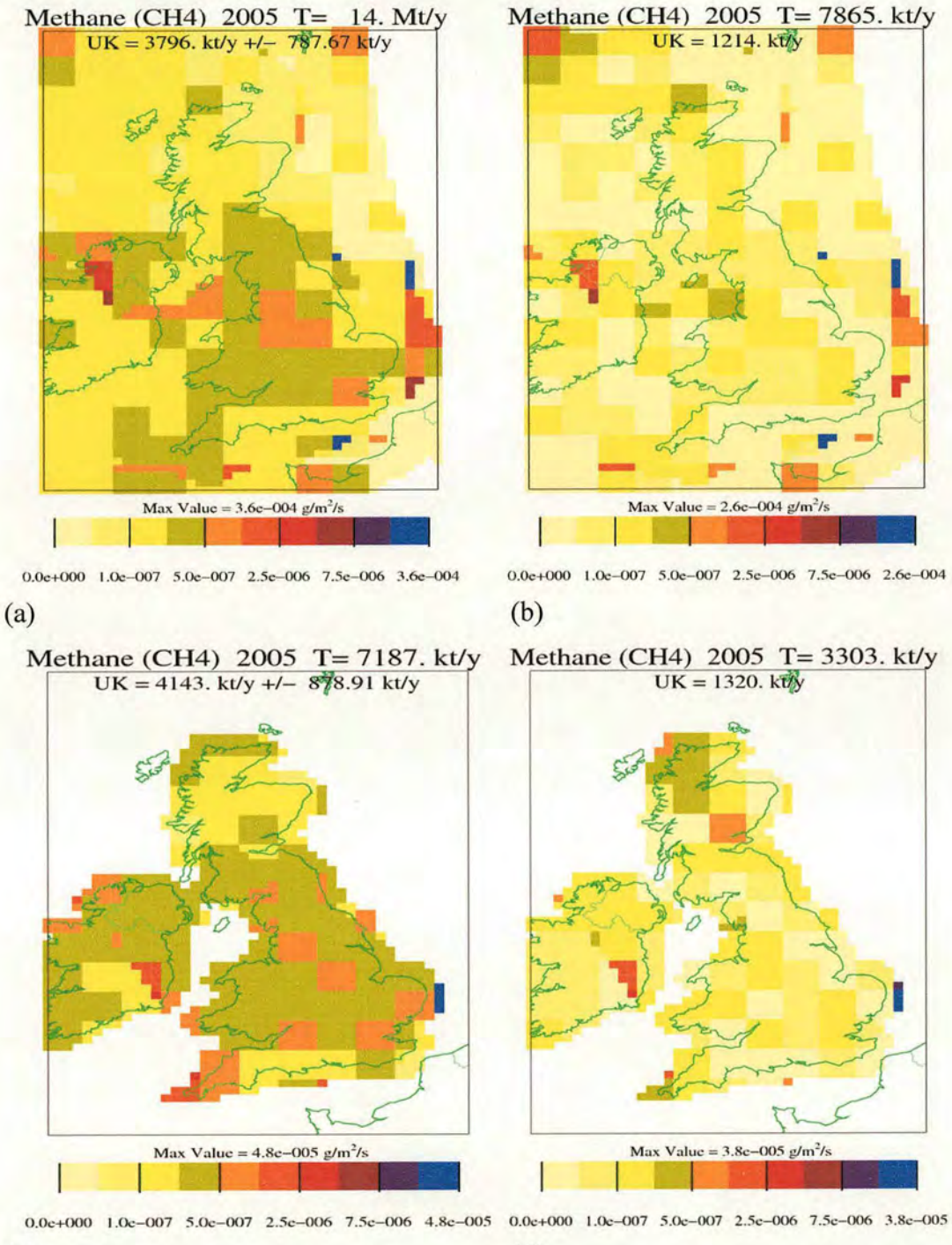

Figure 220. (a) CH_4 emissions (g m^{-2} s^{-1}) using weighted average approach at resolution 4×4 grid boxes and with an unrestricted domain. (b) Standard deviation of CH_4 emissions for weighted average technique for resolution of 4×4 grid boxes and unrestricted domain (c) CH_4 emissions (g m^{-2} s^{-1}) for weighted average technique for resolution of 4×4 grid boxes and restricted domain. (d) Standard deviation of CH_4 emissions for weighted average technique for resolution of 4×4 grid boxes and restricted domain.

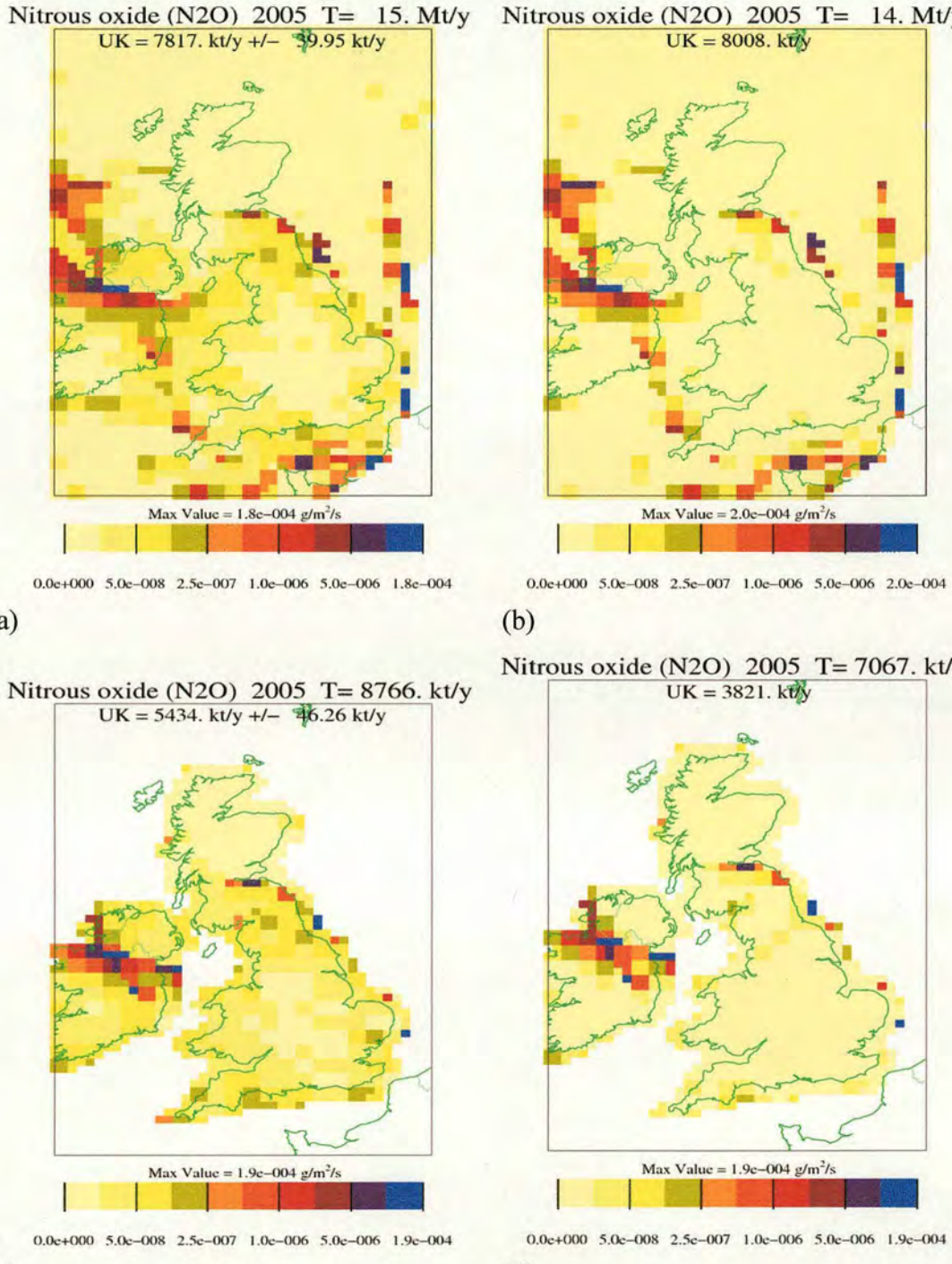

Figure 221. Using flights B92, B102, B118, B119, B134, B136, B244. (a) N_2O emissions (g m^{-2} s^{-1}) using weighted average approach at resolution 2×2 grid boxes and with an unrestricted domain. (b) Standard deviation of N_2O emissions for weighted average technique for resolution of 2×2 grid boxes and unrestricted domain (c) N_2O emissions (g m^{-2} s^{-1}) for weighted average technique for resolution of 2×2 grid boxes and restricted domain. (d) Standard deviation of N_2O emissions for weighted average technique for resolution of 2×2 grid boxes and restricted domain.

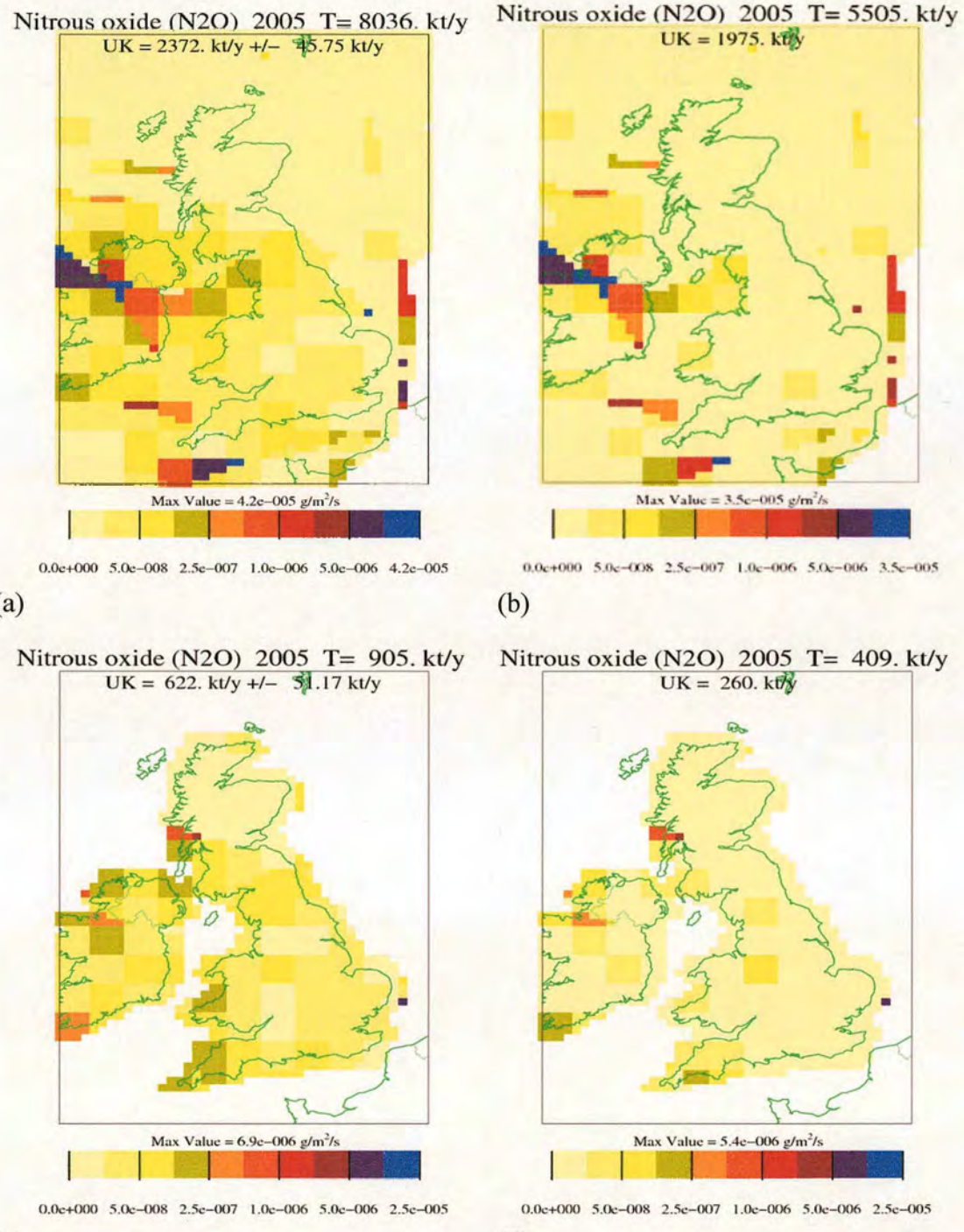

Figure 222. Using flights B92, B102, B118, B119, B134, B136, B244. (a) N_2O emissions (g m^{-2} s^{-1}) using weighted average approach at resolution 4×4 grid boxes and with an unrestricted domain. (b) Standard deviation of N_2O emissions for weighted average technique for resolution of 4×4 grid boxes and unrestricted domain (c) N_2O emissions (g m^{-2} s^{-1}) for weighted average technique for resolution of 4×4 grid boxes and restricted domain. (d) Standard deviation of N_2O emissions for weighted average technique for resolution of 4×4 grid boxes and restricted domain.

References

Alkezweeny, A.J., Powell, D.C., (1977). Estimation of transformation rate of SO_2 to SO_4 from atmospheric concentration data. *Atmospheric Environment*, 11, 179-182.

Anlauf, K.G., Fellin, P., Wiebe, H.A., (1982). The Nanticoke shoreline diffusion experiment, June 1978 IV. A. Oxidation of sulphur dioxide in a power plant plume. B. Ambient concentrations and transport of sulphur dioxide, particulate sulphate and nitrate, and ozone. *Atmospheric Environment*, 16, 455-466.

Baggott, S. L, Lelland, A., Passant, N., and Watterson (2004). Review of Carbon Emission Factors in the UK Greenhouse Gas Inventory. AEAT/ENV/R/2347

Baggott, S. L, Brown, L., Milne, Murrells, T. P., Passant, N., Thistlethwaite D, G., (2004) Greenhouse Gas Inventories for England, Scotland, Wales and Northern Ireland: 1990-2002. AEAT/ENV/R/1761

Baggott, S. L, Brown, L., Milne, R., Murrells, T. P., Passant, N., Thistlethwaite D, G., (2005) Greenhouse Gas Inventories for England, Scotland, Wales and Northern Ireland: 1990-2003. AEAT/ENV/R/2037

Baggott S, Cardenas L, Garnett E, Jackson J, Mobbs DC, Murrells T, Passant N, Thomson A, Watterson J, (2007) UK Greenhouse Gas Inventory, 1990 to 2005: Annual Report for submission under the Framework Convention on Climate Change AEAT/ENV/R/2500

Bamber, D. J., Clark, P. A., Glover, G. M., Healey, P. G., Kallend, A. S., Marsh, A. R., Tuck, A. F., and Vaughan, G., (1984) Aircraft sampling flights round the British Isles at low altitude: SO_2 oxidation and removal rates. *Atmospheric Environment*, 18, 1777-1790.

Barbante C. and Cairns W. (2002) The Role and Fate of Trace Elements in the Environment. *Journal de Physique Proceedings ERCA*, VOL 5, 125-141.

Bergamaschi, P., Krol1, M., Dentener, F., Vermeulen, A., Meinhardt, F., Graul, R., Ramonet, M., Peters, W., and Dlugokencky E. J., (2005) Inverse modelling of national and European CH_4 emissions using the atmospheric zoom model TM5. *Atmospheric Chemistry and Physics*, vol 5, p 2431.

Berger, A., (2002) Global Warming, *Journal De Physique IV Proceedings*.

Beswick K. M., Simpson T. W., Fowler D., Choularton T. W., Gallagher M. W., Hargreaves K. J., Sutton M. A., Kaye A. (1998) Methane Emissions on Large Scales. *Atmospheric Environment 32, 3283-3291.*

Bouwman, A. F., (1995) Compliation of a Global Inventory of Emissions of Nitrous Oxide. *PH.D Thesis for Landbouwuniversiteit Wageningen.*

Brost, R. A, Wyngaard, J. C., and Lenschow, D. H., (1982) Marine stratocumulus layers Part II: Turbulence budgets. *Journal of Atmospheric Science*, 39, 818-836.

Carson, D. J (1973). The development of a dry inversion-capped convectively unstable boundary layer. *Quart. J. Roy. Meteor. Soc.*, 99, 450-467.

Chou, W. W., Wofsy, S. C., Harriss, R. C., Lin, J. C., Gerbig, C., and Sachse, G. W., (2002) Net fluxes of CO_2 in Amazonia derived from aircraft observations. *Journal of Geophysical Research*, VOL 107, NO. D22, 4614, doi: 1029/2001JD001295.

Choularton T. W., Gallagher M. W., Bower K. N., Fowler D., Zahnister M. and Kaye A. (1995). Trace Gas Flux Measurements at the Landscape Scale using Boundary-Layer Budgets. *Philosophical Transactions of the Royal Society, London A 351, 357-369.*

Crutzen, P. J., (2002). An Overview on Atmospheric Chemistry, *Journal De Physique IV Proceedings.*

Cullen, M. J. P. (1993). The unified forecast/climate model. *Meteorological Magazone* (UK), 1449, 81-94

Dittenhoefer, A.C., De Pena, R.G., (1980). Sulphate aerosol production and growth in coal-operated power plant plumes. *Journal of Geophysical Research,* 85, 4499-4506.

Dacre, H., Gray, SL. L., and Belcher, S. E., (2007). A case study of boundary layer ventilation by convection and coastal processes. *Journal of Geophysical Research*, 112. D17106, doi:10.1029/2006JD007984.

Dolman, A. J., Noilhan2, J., Durand, P., Sarrat, C., Brut, A., Piguet, B., Butet, A., Jarosz, N., Brunet, Y., Loustau, D., Lamaud, E., Tolk, L., Ronda, R., Miglietta, F., Gioli, B., Magliulo, V., Esposito, M., Gerbig, C., Körner, S., Galdemard, P., Ramonet, M., Ciais, P., Neininger, B., Hutjes, R.W.A , Elbers, J. A., Macatangay, R., Schrems, O., Pérez-Landa, G., Sanz, M. J., Scholz, Y., Facon, G., Ceschia, E., and Beziat, P., (2006). CERES, the CarboEurope Regional Experiment Strategy. *Bulletin of the American Meteorological Society*, VOL 87, Issue 10, 1367–1379.

Donatelli, M., and Campbell, G. S., (1998) A simple model to estimate global solar radiation. *In: Proc. 5th ESA Congress*, Nitra, Slovak Republic, 2:133-134. (poster)

Donatelli, M., Campbell, G. S., Bellocchi, G., Acutis, M., Gommes, R., Michele Bernardi, M., Arjan Gijsman, A., Claudio O. Stöckle, C., Bechini, L., Ducco, G. and Petrassi, F., (2001) Global Radiation Estimate – RadEst 3.00. FAO – SDRN Agrometeorology Group, ISCI –Crop Science

Dore, C. J., Watterson, J. D., Murrells, T. P., Passant, N. R., Hobson, M.M., Baggott, S. L., Thistlethwaite, G., Goodwin, J. W. L., King, K. R., Adam, M., Walker, C., Downes, M. K., Coleman, P. J., Stewart, R. A., Wagner, A., Sturman, J., Conolly, C., Lawrence, H., Cumine, P. R., (2005) .UK Emissions of Air Pollutants 1970 to 2003.

Dore, C. J., Watterson, J. D., Murrells, T. P., Passant, N. R., Hobson, M.M., Baggott, S. L., Thistlethwaite, G., Goodwin, J. W. L., King, K. R., Adam, M., Walker, C., Downes, M. K., Coleman, P. J., Stewart, R. A., Wagner, A., Sturman, J., Conolly, C., Lawrence, H., Li, Y., Jackson, J., Bush, T., Grice, S., and Brophy N., (2006). UK Emissions of Air Pollutants 1970 to 2004

Eatough, D.J., Richter, B.E., Eatough, N.L., Hansen, L.D., (1981). Sulphur chemistry in smelter and power plant plumes in the Western U.S. *Atmospheric Environment* 15, 2241-2253.

Fang, C., and Moncrieff, J., B., (2001) The dependence of soil CO_2 efflux on temperature. *Soil Biology and Biochemistry*, 33, 155-165.

Forrest, J., Garber, R., Newman, L., (1979a). Formation of sulphate, ammonium and nitrate in an oil-fired power plant plume. *Atmospheric Environment*, 13, 1287-1297.

Forrest, J., Schwartz, S.E., Newman, L., (1979b). Conversion of sulphur dioxide to sulphate during the Da Vinci flights. *Atmospheric Environment*, 13, 157-167.

Forrest, J., Garber, R., Newman, I., (1981). Conversion rates in power plant plumes based on filter pack data: the coal-fires Cumberland plume. *Atmospheric Environment*, 13, 1287-1297.

Fournier N., Dore A. J., Vieno ., Weston K. J., Dragosits U., Sutton M. A., (2004) Modelling the Deposition of Atmospheric Oxidised Nitrogen and Sulphur to the United Kingdon using a Multi-Layer Long-Range Transport Model. *Atmospheric Environment*, 38, 683-69.

Fournier N., Pais V. A., Sutton M. A., Weston K. J., Dragosits U., Tany S. T., Aherne J., (2002) Parallelisation and Application of a Multi-Layer Atmospheric Transport Model to Quantify Dispersion and Deposition of Ammonia over the British Isles. *Environmental Pollution*, 116, 95-107.

Fowler D., Hargreaves K. J., Skiba U. and Bower K. N., (2000) Direct Measurement of the UK source strength of radiatively active gases. *Report for the UK Department of Environment.*

Fowler D., Skiba U., Bower K. N., Simpson T. W., Gallagher M.W., Choularton T. W., and Kaye A., (1999) Measurement of Greenhouse Gases at the UK Scale using Boundary Layer Budget Methods and Aircraft Sampling. *Proceeding of EUROTRAC Symposium 1998.*

Gallagher M. W., Choularton T. W., Bower K. N., Stromberg I. M., Beswick K. M., Fowler D., and Hargreaves K. J. (1994). Measurements of Methane Fluxes on the Landscape Scale from a Wetland Area in North Scotland. *Atmospheric Environment*, 28, 2421-2430.

Garber, R., Forrest, J., Newman, L., (1981). Conversion rates in power plant plumes based on filter pack data: the oil-fired Northport plume. *Atmospheric Environment*, 15, 2283-2292.

Gerbig, C., Lin, J. C., Wofsy, S. C., Daube, B. C., Andrews, A. E., Stephens, B. B., Bakwin, P. S., and Grainger, C. A., (2003). Toward constraining regional-scale fluxes of CO_2 with atmospheric observations over a continent: 1. Observed spatial variability from airborne platforms. *Journal of Geophysical Research*, VOL 108, NO. D24, 4756, doi: 1029/2002JD003018.

Gillani, N.V., Colby, J.A., Wilson, W.E., (1983). Gas to particle conversion of sulphur in power plant plumes - II. Parameterization of plume-cloud interactions. *Atmospheric Environment*, 17, 1753-1763.

Gillani, N.V., Husar, R.B., Husar, J.D., Patterson, D.E., Wilson, W.E., (1978). Project MISTT: kinetics of particulate sulphur formation in a power plant plume out to 300 km. *Atmospheric Environment*, 12, 589-598.

Gillani, N.V., Kohli, S., Wilson, W.E., (1981). Gas-to-particle conversion of sulphur in power plant plumes - I. Parametrization of the conversion rate for dry, moderately
polluted ambient conditions. *Atmospheric Environment*, 15, 2293-2313.

Gillani, N.V., Luria, M., Valente, R.J., Tanner, R.L., Imhoff, R.E., Meagher, J.F., (1998a). Loss rate of NO*y* from a power plant plume based on aircraft measurements. *Journal of Geophysical Research*, VOL 103, 22585-22592.

Gillani, N.V., Meagher, J.F., Valente, R.J., Imhoff, R.E., Tanner, R.L., Luria, M., (1998b). Relative production of ozone and nitrates in urban and rural power plant plumes1. Composite results based on data from 10 field measurement days. *Journal of Geophysical Research*, VOL 103, 22593-22615.

Gillani, N.V., Wilson, W.E., (1980). Formation and transport of ozone and aerosols in power plant plumes. *Annals of the New York Academy of Sciences*, 338, 276-296.

Gillani, N.V., Wilson, W.E., (1983). Gas to particle conversion of sulphur in power plant plumes - II. Observations of liquid-phase conversions. *Atmospheric Environment*, 17, 1739-1752.

Gimson, N. R., and Uliasz, M., (2003). The determination of agricultural methane emissions in New Zealand using inverse modelling techniques. *Atmospheric Environment*, 37, 3903-3912.

Grant, A. L., (1992) The structure of turbulence in the near-neutral atmospheric boundary layer. *Journal of Atmospheric Science*, 49, 226-239.

Hanna, S. R., (1982) Applications in air pollution modelling. In: *Atmospheric Turbulence and Air Pollution Modelling*, eds F. T. M Nieuwstadt and H. van Dop. D Reidle. Publishing Company, Dordrecht, Holland.

Hewitt, C. N., (2000), The atmospheric chemistry of sulphur and nitrogen in power station plumes. *Atmospheric Environment*, 35, 1155-1170.

Hegg, D.A., Hobbs, P.V., (1980), Measurements of gas-to-particle conversion in the plumes from five coal-fired electric power plants. *Atmospheric Environment*, 14, 99-116.

Hibberd, M. F., and Sawford B. L., (1994), A saline laboratory model of the planetary convective boundary layer. *Boundary-Layer Meteorology*, 69, 229-250.

Horvath, L., Nagy, Z., Weidinger, T., (1998). Estimation of dry deposition velocities of nitric oxide, sulphur dioxide, and ozone by the gradient method above short vegetation during the tract campaign. *Atmospheric Environment* 32, 1317-1322.

Husar, R.B., Patterson, D.E., Husar, J.D., Gillani, N.V., Wilson, W.E., (1978). Sulphur budget of a power plant plume. *Atmospheric Environment*, 12, 549-568.

IPCC, (2001), Climate Change Report

IPCC, (2007) A report of Working Group I of the Intergovernmental Panel on Climate Change. Summary for Policymakers.

Jackson, J., Li, Y., Passant, N., Glen Thistlethwaite, D, G., Thomson, A., and Cardenas, L., (2007) Greenhouse Gas Inventories for England, Scotland, Wales and Northern Ireland: 1990-2005

King, K., Sturman, J., and Passant, N., (2006) NAEI UK Emissions Mapping Methodology 2003.

Kirkpatrick, S., Gelatt., C. D., Vecchi, M. P., (1983) Optimization by Simulated Annealing, *Science*, 220, Number 4598, 671-680

Liebsch, E.J., De Pena, R.G., (1982). Sulphate aerosol production in coal-fired power plant plumes. *Atmospheric Environment*, 16, 1323-1331.

Lin, J. C., Gerbi, C., Wofsy, S. C., Andrews, A. E., Daube, B. C., Grainger, C. A., Stephens, B. B., Bakwin, P. S., and Hollinger D. Y., (2004) Measuring fluxes of trace gases at regional scales by Lagrangian observations: Application to the CO_2 Budget and Rectification Airborne (COBRA) study. *Journal of Geophysical Research*, VOL 109, D15304, doi:10.1029/2004JD004754.

Loubet. B., A Stochastic Langrangian model for short range ammonia dispersion and dry deposition. ITE Institute of Terrestrial Ecology, Edinburgh, INRA, Institut de la Recherche Agronomique, Paris, Final Report.

Luhar. A. K. and Britter R. E., (1989) A random walk model for dispersion in inhomogeneous turbulence in a convective boundary layer. *Atmospheric Environment*, 23, 1911-1924.

Luria, M., Olszyna, K.J., Meagher, J.F., (1983). The atmospheric oxidation of flue gases from a coal-fired power plant: a comparison between smog chamber and airborne plume sampling. *Journal of the Air Pollution Control Association* 483-487.

Malcolm A. l., Manning A. J., (2001) Testing the Skill of a Lagrangian Dispersion Model at Estimating Primary and Secondary Particulates. *Atmospheric Environment*, 5, 1677-1685.

Mamane, Y., Pueschel, R.F., (1980). Formation of sulphate particles in the plume of the Four Corners power plant. *Journal of Applied Meteorology*, 19, 779-790.

Manning, A. J., Ryall, D. B.,Derwent, R. G., Simmonds, P. G., and O'Doherty, S., (2003) Estimating European emissions of ozone-depleting and greenhouse gases using observations and a modeling back-attribution technique, *Journal of Geophysical Research*, VOL 108, D14, 4405.

Manning, A. J., and Derwent, R. G., (2006) Interpretation of long-term measurements of radiatively active trace gases and ozone depleting substances, Defra Contract: CPEG1 Quarterly Report.

Maryon, R. H., (1997) Determining cross-wind variance for low-frequency wind meander. *Atmospheric Environment*, 23, 1911-1924.

McGettigan, M., Connolly, N., Duffy, P. and O'Brien, P. (2007). Ireland's National Inventory Report 2007.

Meagher, J.F., Luria, M., (1982). Model calculations of the chemical processes occurring in the plume of a coal-"red power plant. *Atmospheric Environment*, 16, 183-195.

Meagher, J.F., Stockburger, L., Bonanno, R.J., Bailey, E.M., Luria, M., (1981). Atmospheric oxidation of flue gases from coal fired power plants - a comparison between conventional and scrubbed plumes. *Atmospheric Environment*, 15, 749-762.

Miller, D.F., Alkezweeny, A.J., (1980). Aerosol formation in urban plumes over Lake Michigan. *Annals of the New York Academy of Sciences*, 338, 219-232.

Milne, R., Mobbs, D. C., (2006) UK Emissions by Sources and Removals by Sinks due to Land Use, Land Use Change and Forestry Activities Report, April 2006 DEFRA Contract EPG 1/1/160 CEH No. C02275

Moller, D., (2002) Global Sulfur and Nitrogen Biogeochemical Cycles, *Journal De Physique IV Proceedings*

National Expert Group on Transboundary Air Pollution (NEGTAP) (2001). Tranboundary Air Pollution: Acidification, Eutrophication and Ground-Level Ozone. DEFRA Contract Report EPG 1/3/153.

O'Brien J. J., (1970) A note on the vertical structure of the eddy exchange coefficient in the planetary boundary layer. *Journal of Atmospheric Science*, 27, 1213-1215.

Pacyna J. M. (1994) Emissions of Pollutants and their Control. *Journal de Physique Proceedings of ERCA* Vol. I, 135-159

Parrish, D. D., (2004). Export of NO_y from the north American boundary layer: Reconciling aircraft observations and global model budgets. *Journal of Geophysical Research*, VOL 109, DO2313, doi:10.1029/2003JDOO4086.

Richards, L.W., Anderson, J.A., Blumenthal, D.L., Brandt, A.A., McDonald, J.A., Watus, N., Macias, E.S., Bhardwaja, P.S., (1981). The chemistry, aerosol physics, and optical properties of a western coal-fired power plant plume. *Atmospheric Environment*, 15, 2111.

Rivington, M., Bellocchi , G., Matthews, K. B., and Buchan, K., (2005). Evaluation of three model estimations of solar radiation at 24 UK stations. *Agricultural and Forest Meteorology*, 132, 228–243.

Ruimy, A., Jarvis, P. G., Baldocchi, D. D., and Saugier, B., (1995a) CO_2 fluxes over plant canopies and solar radiation: a review, *Advances in Ecological Research*, 26, 1-68.

Ryall D. B., Derwent R. G., Manning A. J., Simmonds P. G., Doherty S. O., (2001) Estimating Source Regions of European Emissions of Trace Gases from Observations at Mace Head. *Atmospheric Environment*, 35, 2507-2523.

Ryall D. B., Maryon R. H., (1998) Validation of the UK Met Office's NAME Model Against the ETEX Dataset. *Atmospheric Environment*, 32, 4265-4276.

Salway A. G., (2002) UK Greenhouse Gas Inventory 1990 – 2000. *Report for UK Department for Environment, Food and Rural Affairs.*

Salway, A. G., (1998) Treatment of Uncertainties for National Estimates of Greenhouse Gas Emissions. AEAT-2688

Sillman, S., (1999) The relation between ozone, NO_x and hydrocarbons in urban and polluted rural environments. *Atmospheric Environment*, 33, 1821-1845.

Singles R., (1996) Fine Resolution Modelling of Ammonia Dry Deposition over Great Britain. *PH.D Thesis for the University of Edinburgh.*

Singles R., Sutton M. A., Weston K. J., (1998) A Multi-Layer Model to Describe the Ammonia Transport and Deposition of Ammonia in Great Britain. *Atmospheric Environment*, 32, 393-399.

Skiba U., Sozanska M., Metcalfe S. and Fowler D., (2001) Spatially dissaggregated inventories of soil NO and N_2O emissions for Great Britain. *Water and Soil Pollution*, 1 109-118.

Springston, S. R., Kleiman, L. I., Brechtel, F., Lee, Y., Nunnermacker, L. J., and Wang, J., (2005) Chemical evolution of an isolated power plant plume during the TexAQS 2000 study. *Atmospheric Environment*, 39, 3431-3443.

Stull R. B., (1989) An Introduction to Boundary Layer Meteorology. *Kluwer Academic Publishers.*

Tarantola, A., (1988). Inverse Problem Theory: Methods for Data Fitting and Model Parameter Estimation. Elsevier, Amsterdam.

Thomson D.J., (1987) Criteria for the selection of stochastic models of particle trajectories in turbulent flows. *J. Fluid Mech.*, 180, 529-556

Ting, K.C., G. A. Giacomelli. (1987) Availability of Solar Photosynthetically Active Radiation. *Transactions of the ASAE.* 30(5):1453-1457.

Tsuang, B., Chen, C., Lin, C., Cheng, M., Tsai, Y., Chio, C., Pan, R., and Kuo, P., (2003). Quantification on the source/receptor relationship of primary pollutants and secondary aerosols by a Gaussian plume trajectory model: Part II. Case study. *Atmospheric Environment*, 37, 3993–4006.

Wratt, D. S., Grimson, N. R., Bailsford, G. W., Lassey, K. R., Bromley, A. M., and Bell, M. J., (2001) Estimating regional methane emissions from agriculture using aircraft measurements of concentration profiles. *Atmospheric Environment*, 35, 497-508.

Zak, B.D., (1981). Lagrangian measurements of sulphur dioxide to sulphate conversion rates. *Atmospheric Environment*, 15, 2583-2591.

Personal Communications

Dragosits, U, Centre for Ecology and Hydrology Edinburgh, Bush Estate, Penicuik, EH26 0QB

Harrison, M., Met Office, FitzRoy Road, Exeter, Devon, EX1 3PB

Manning, A., Met Office, FitzRoy Road, Exeter, Devon, EX1 3PB

O'Sullivan D, University of East Anglia, Norwich, NR4 7TJ UK

Skiba, U., Centre for Ecology and Hydrology Edinburgh, Bush Estate, Penicuik, EH26 0QB

Van Oijen, M., Centre for Ecology and Hydrology Edinburgh, Bush Estate, Penicuik, EH26 0QB

Webster, H., Met Office, FitzRoy Road, Exeter, Devon, EX1 3PB